Development of New Conjugated Polymers for Organic Photovoltaics

Ary Murad

Department of Chemistry

The University of Sheffield

Submitted to the University of Sheffield

In fulfilment of the requirements for the degree of

Doctor of Philosophy

2017

Declaration

I hereby declare that the research discussed has not been submitted, either entirely or partly, for this or any other degree. All the work presented in this thesis is the original work of the author, except where other sources have been acknowledged by references. This work was carried out at the University of Sheffield between October 2012 and February 2017.

Signature: Ary Murad

Date: 14/02/2017

Abstract

Polymer solar cells (PSCs) have received substantial consideration as clean and renewable energy sources due to their advantages such as solution-processing, low cost, lightweight and mechanically flexible devices. In the last few years, the power conversion efficiency of bulk heterojunction solar cells has increased dramatically reaching up to 10% recently.

This dissertation focuses on two types of conjugated polymers, thermocleavable polymers and donor-acceptor (D-A) polymers. Three novel thermocleavable polymers, **35**, **36** and **37** were prepared *via* the Stille polymerisation. **35** and **36** consisting of bithiophene and tetrathiophene as the donor units and secondary phthalate ester as the acceptor units. **37** contains fluorene flanked by thienyl groups as the donor units and secondary phthalate ester as the acceptor units. The optical band gaps (E_g) of the polymers are between 2.11 and 2.58 eV. After thermal treatment, the band gaps of the polymers have decreased to between 1.86 and 2.14 eV.

A series of D-A copolymers including benzothiadiazole dicarboxylic imide (**BTDI**) as acceptor units with different donor units were synthesised. Two different alkyl side chains (3,7-dimethyloctyl *vs* *n*-octyl) were anchored to the **BTDI** units in order to investigate the effect of these alkyl substituents on the solubility, molecular weights, optoelectronic properties, thermal and structural properties of the polymers. Four copolymers, **76**, **77**, **78** and **79** based on 2,7-fluorene or 2,7-dibenzosilole were synthesised *via* Suzuki polymerisation. Dibenzosilole-based polymers have slightly lower E_g relative to their fluorene-based analogues. Another four copolymers, **104**, **105**, **106** and **107** including 2,7-carbazole were also synthesised *via* Suzuki polymerisation. Two fluorine atoms were incorporated at the 3,6-positions of 2,7-carbazole units to investigate the impact of fluorine upon the optoelectronic properties, thermal and structural properties of the polymers. The E_g of fluorinated copolymers are slightly higher than non-fluorinated counterparts. Two copolymers, **109** and **110** containing 2,6-anthracene were also prepared through Suzuki polymerisation. Both polymers have low E_g of 1.66 eV.

A series of copolymers, **134**, **135**, **136** and **137** containing cyclopentadithiophene (**CPDT**) were prepared. **134** was prepared by Suzuki polymerisation, while the other three copolymers were prepared by direct arylation polymerisation. The E_g of the polymers are between 1.32 and 1.43 eV.

The final two alternating copolymers of dithienosilole (**DTS**), **144** and **145**, were prepared *via* Stille polymerisation. Both polymers have low E_g around 1.4 eV. Copolymers based on fluorene, dibenzosilole, carbazole and anthracene units have deep HOMO energy levels about –5.5 eV. However, the HOMO energy levels of the copolymers containing **CPDT** and **DTS** units are significantly shifted upward to around (–5.1 to –5.2 eV). The LUMO levels of the copolymers are between –3.4 and –3.5 eV. All polymers exhibit good thermal stability with decomposition temperatures surpassing 310 °C. Powder X-ray diffraction studies have shown that all polymers have an amorphous nature in solid state.

To my beloved wife Sozan Abdullah, my dear daughter
Elena Rahim and my family

Acknowledgments

First and foremost I would like to express my deepest gratitude to my supervisor Dr. Ahmed Iraqi. Thank you for your excellent guidance, advice and continuous motivation throughout my PhD research and writing of this thesis. He is extremely patient and very approachable. I am truly grateful for everything he has done for me throughout the course of my studies.

It is my great pleasure to acknowledge all the past and present members of Iraqi group; Hunan Yi, Ahmed Al-Azzawi and Omar Esmaeel for their helps during the lab. Special thanks to my best friend and colleague, Sulaiman Al-Isaee, for enormous support and he made every day in lab enjoyable.

I would like to thank Twyman group for generous support and contributions. I would also like to express my gratitude to all the staff and members in the chemistry department and all the members at the University of Sheffield.

I would like to thank my sponsorship Human Capacity Development Program (HCDP) in Kurdistan regional government of Iraq and also University of Sulaimani for their help and financial support.

Last but more important, I would like to thank my beloved wife Sozan Abdullah for her endless efforts and continuous encouragement through these challenging years and supporting me through stressful and difficult times. This work would not have been completed without her support. Thank you for sharing every happiness and sadness in every day in my life. I would like to thank my beloved mother, mother-in-law, brothers, sisters and little daughter Elena for their love, care and encouragement. I am also grateful to my brother-in-law Latif Abdullah. Thank you for your continuous support during the last five years.

Chapter 1 - Introduction 1

1.1. The electronic structure of conjugated polymers 1

1.2. Doping in conjugated polymers 2

1.3. Methods for preparation of conjugated polymers 4

1.3.1. The oxidative polymerisations 4

1.3.1.1. Electrochemical oxidative polymerisations 4

1.3.1.2. The chemical oxidative polymerisations 5

1.3.2. Transition metal catalysed cross-coupling polymerizations 7

1.3.2.1. Kumada-Corriu cross-coupling reactions 8

1.3.2.2. Negishi cross-coupling reactions 10

1.3.2.3. Stille cross-coupling reactions 11

1.3.2.4. The Suzuki-Miyaura reactions 13

1.3.2.5. Direct hetero (arylation) cross coupling reactions 16

1.3.3. Yamamoto coupling reactions 18

1.3.4. Condensation polymerisation methods 19

1.3.4.1. Wessling route 19

1.3.4.2. Gilch method 19

1.4. Applications of conjugated polymers 19

1.4.1. Organic light emitting diodes (OLEDs) 19

1.4.2. Organic Field Effect Transistors (OFETs) 21

1.4.3. Organic photovoltaics (OPVs) 22

1.5. Architecture of polymer solar cells 23

1.5.1. Single layer 23

1.5.2. Bilayer planar heterojunction 23

1.5.3. Bulk Heterojunction 24

1.6. Principle work of polymer solar cells 25

1.7. Characterisation of polymer solar cells 26

1.8. Designing conjugated polymers for photovoltaic applications 27

1.8.1. Optimisation of HOMO-LUMO energy levels and Optical Band Gaps 28
1.8.2. Strategies for Band Gap Tuning 29
1.9. Morphology 35
1.9.1. Choice of solvent(s) 36
1.9.2. Thermal annealing 37
1.9.3. Solvent annealing 39
1.9.4. Solvent additive 40
1.9.5. Blend composition 40
1.10. Novel Acceptor Materials 41
1.11. Aims and Objectives 43
References 49
Chapter 2 - Novel thermocleavable polymers based on phthalate esters ... 64
Abstract 64
2.1. Introduction 64
2.1.1. Wessling and Durham routes 64
2.1.2. Thermocleavable polymers 65
2.1.3. Dithiocarbamate precursor route 69
2.2. Synthesis of monomers 70
2.2.1. Synthesis of secondary phthalate ester monomers (6 and 8) 70
2.2.1.1. Synthesis of 3,6-dibromophthalic anhydride (2) 70
2.2.1.2. Synthesis of 3,6-dibromophthalic acid (3) 71
2.2.1.3. Synthesis of 2-undecanol (5) 72
2.2.1.4. Synthesis of 3,6-dibromo-bis(2-undecanyl) phthalate (6) 73
2.2.1.5. Synthesis of 3,6-bis(2-thienyl)-bis(2-undecanyl)phthalate (7) 75
2.2.1.6. Synthesis of 5,5'-dibromo-3,6-bis(2-thienyl)-bis(2-undecanyl)phthalate (8) 75
2.2.2. Synthesis of distannylated fluorene (29) 75
2.2.2.1. Synthesis of 2,7-dibromofluorene (27) 76

2.2.2.2. Synthesis of 9,9-dimethyl-2,7-dibromofluorene (28) 76

2.2.2.3. Synthesis of 9,9-dimethyl-2,7-bis(trimethylstannyl)fluorene (29) 77

2.2.3. Synthesis of 5,5'-bis(trimethylstannyl)-2,2'-bithiophene (34) 78

2.3. Preparation of the polymers 78

2.4. Molecular weights and yield of the polymers 80

2.5. Optical properties of the polymers 81

2.6. Thermal properties of the polymers 83

2.7. Powder X-ray diffraction (XRD) of the polymers 84

2.8. Conclusions 84

References 86

Chapter 3 - Fluorene/dibenzosilole-benzothiadiazole dicarboxylic imide alternating copolymers for photovoltaic applications 89

Abstract 89

3.1. Introduction 89

3.1.1. Conjugated polymers based on 2,1,3-benzothiadiazole and their derivatives 90

3.1.2. Fluorene based conjugated polymers 93

3.1.3. Dibenzosilole based conjugated polymers 96

3.2. Synthesis of monomers: 97

3.2.1. Synthesis of benzothiadiazole dicarboxylic imide (BTDI) monomers 97

3.2.1.1. Synthesis of 2,5-dibromothiophene (39) 98

3.2.1.2. Synthesis of 2,5-dibromo-3,4-dinitrothiophene (40) 98

3.2.1.3. Synthesis of 3',4'-dinitro-2,2':5',2"-terthiophene (41) 99

3.2.1.4. Synthesis of 3',4'-diamino-2,2':5,2"-terthiophene (42) 100

3.2.1.5. Synthesis of 4,6-bis(2-thienyl)-thieno[3,4-*c*][1,2,5]-thiadiazole (43) 101

3.2.1.6. Synthesis of 4,7-di(thien-2-yl)-2,1,3-benzothiadiazole-5,6-dimethyl ester (44) 101

3.2.1.7. Synthesis of 4,7-di(thien-2-yl)-2,1,3-benzothiadiazole-5,6-dicarboxylic acid (45) 102

3.2.1.8. Synthesis of 4,7-di(thien-2-yl)-2,1,3-benzothiadiazole-5,6-dicarboxylic anhydride (46) 103

3.2.1.9. Synthesis of 4,7-di(thien-2-yl)-2,1,3-benzothiadiazole-5,6-*N*-(3,7-dimethyloctyl)dicarboxylic imide (47) and 4,7-di(thien-2-yl)-2,1,3-benzothiadiazole-5,6-*N*-octyl-dicarboxylic imide (48) 104

3.2.1.10. Synthesis of 4,7-di(5-bromo-thien-2-yl)-2,1,3-benzothiadiazole-5,6-*N*-(3,7-dimethyloctyl)dicarboxylic imide (49) and 4,7-di(5-bromo-thien-2-yl)-2,1,3-benzothiadiazole-5,6-*N*-octyl-dicarboxylic imide (50) 106

3.2.1.11. Synthesis of 3,7-dimethyloctyl bromide (52) 106

3.2.1.12. Synthesis of *N*-(3,7-dimethyloctyl)phthalimide (53) 107

3.2.1.13. Synthesis of 3,7-dimethyl-1-octanamine (54) 107

3.2.2. Synthesis of diboronic ester of dibenzosilole (DBS) monomer (72) 109

3.2.2.1. Synthesis of 4,4'-dibromo-2,2'-dinitrobiphenyl (68) 109

3.2.2.2. Synthesis of 4,4'-dibromobiphenyl-2,2'-diamine (69) 110

3.2.2.3. Synthesis of 4,4'-dibromo-2,2'-diiodobiphenyl (70) 111

3.2.2.4. Synthesis of 2,7-dibromo-9,9-dioctyldibenzosilole (71) 112

3.2.2.5. Synthesis of 9,9-dioctyl-2,7-bis(4,4,5,5-tetramethyl-1,3,2-dioxaborolan-2-yl)-dibenzosilole (72) 112

3.3. Polymers synthesis 114

3.4. Molecular weights and yield of the polymers 114

3.5. Optical properties of the polymers 115

3.6. Electrochemical properties of the polymers 117

3.7. Thermal properties of the polymers 118

3.8. Powder X-ray diffraction (XRD) of the polymers 119

3.9. Conclusions 119

References 121

Chapter 4 - Influence of fluorine substitution upon the photovoltaic properties of carbazole-benzothiadiazole dicarboxylic imide alternate copolymers 124

Abstract 124

4.1. Introduction 124

4.1.1. Conjugated polymers based on 2,7-carbazole 126

4.1.2. The impact of fluorination on the efficiency of organic photovoltaics 127

4.2. Synthesis of 3,6-difluoro-substituted-2,7-carbazole monomer (89) 131

4.2.1. Synthesis of 1,4-dibromo-2-fluoro-5-nitrobenzene (81) 131

4.2.2. Synthesis of 4,4'-dibromo-5,5'-difluoro-2,2'-dinitrobiphenyl (82) 132

4.2.3. Synthesis of 4,4'-dibromo-5,5'-difluorobiphenyl-2,2'-diamine (83) 133

4.2.4. Synthesis of 3,6-difluoro-2,7-dibromo-*9H*-carbazole (84) 133

4.2.5. Synthesis of heptadecan-9-ol (86) 134

4.2.6. Synthesis of 9-heptadecane-*p*-toluenesulfonate (87) 134

4.2.7. Synthesis of 3,6-difluoro-*N*-9'-heptadecanyl-2,7-dibromocarbazole (88) ... 135

4.2.8. Synthesis of 3,6-difluoro-*N*-9'-heptadecanyl-2,7-bis(4,4,5,5-tetramethyl-1,3,2- dioxaborolan-2-yl)carbazole (89) 136

4.3. Polymers synthesis 137

4.4. Molecular weights and yield of the polymers 137

4.5. Optical properties of the polymers 138

4.6. Electrochemical properties of the polymers 140

4.7. Thermal properties of the polymers 141

4.8. Powder X-ray diffraction 142

4.9. Conclusions 143

References 145

Chapter 5 - Low band gap copolymers containing anthracene-benzothiadiazole dicarboxylic imide for photovoltaic applications 148

Abstract 148

5.1. Introduction 148

5.2. Polymers synthesis 152

5.3. Molecular weights and yield of the polymers 152

5.4. Optical properties of the polymers 153

5.5. Electrochemical properties of the polymers 154

5.6. Thermal properties of the polymers 156

5.7. Powder X-ray diffraction (XRD) of the polymers 156

5.8. Conclusions 157

References 159

Chapter 6 - Low band gap alternating copolymers based on cyclopentadithiophene-benzothiadiazole dicarboxylic imide for solar cell applications 160

Abstract 160

6.1. Introduction 160

6.2. Synthesis of cyclopentadithiophene (CPDT) monomers 163

6.2.1. Synthesis of bis(3-thienyl)methanol (113) 163

6.2.2. Synthesis of bis(2-iodo-3-thienyl)methanol (114) 164

6.2.3. Synthesis of bis(2-iodo-3-thienyl)ketone (115) 165

6.2.4. Synthesis of *4H*-cyclopenta[2,1-*b*:3,4-*b*']dithiophen-4-one (116) 166

6.2.5. Synthesis of *4H*-cyclopenta[2,1-*b*:3,4-*b*']dithiophene (117) 167

6.2.6. Synthesis of 4,4-bis(2-ethylhexyl)cyclopenta[2,1-*b*:3,4-*b*']dithiophene (118) and 4,4-dioctylcyclopenta[2,1-*b*:3,4-*b*']dithiophene (119) 168

6.2.7. Synthesis of 4,4-bis(2-ethylhexyl)-2,6-dibromocyclopenta[2,1-*b*:3,4-*b*']dithiophene (120) and 4,4-dioctyl-2,6-dibromocyclopenta[2,1-*b*:3,4-*b*']dithiophene (121) 168

6.2.8. Synthesis of 4,4-bis(2-ethylhexyl)-2,6-bis(4,4,5,5-tetramethyl-1,3,2-dioxaboralan-2-yl)cyclopenta[2,1-*b*:3,4-*b*']dithiophene (122) 168

6.3. Polymers synthesis 169

6.4. Molecular weights and yield of the polymers 170

6.5. Optical properties of the polymers 171

6.6. Electrochemical properties of the polymers 173

6.7. Thermal properties of the polymers 174

6.8. Powder X-ray diffraction of the polymers 175

6.9. Conclusions 176

References 178

Chapter 7 - Low band gap copolymers based on dithienosilole-benzothiadiazole dicarboxylic imide for photovoltaic applications 180

Abstract 180

7.1. Introduction 180

7.2. Synthesis of distannylated DTS (142) 183

7.2.1. Synthesis of 3,3',5,5'-tetrabromo-2,2'-bithiophene (138) 183

7.2.2. Synthesis of 3,3'-dibromo-2,2'-bithiophene (139) 183

7.2.3. Synthesis of 4,4-dioctyl-dithieno[3,2-*b*:2',3'-*d*]silole (140) 184

7.2.4. Synthesis of 4,4-dioctyl-2,6-dibromo-dithieno[3,2-*b*:2',3'-*d*]silole (141) ... 184

7.2.5. Synthesis of 4,4-dioctyl-2,6-bis(trimethylstannyl)-dithieno[3,2-*b*:2',3'-*d*]silole (142) 185

7.3. Polymers synthesis 185

7.4. Molecular weights and yield of the polymers 186

7.5. Optical properties of the polymers 187

7.6. Electrochemical properties of the polymers 188

7.7. Thermal properties of the polymers 190

7.8. Powder X-ray diffraction of the polymers 190

7.9 Conclusions 191

References 193

Chapter 8 - Conclusions and Future Work 195

8.1. Conclusions 195

8.2. Future Work 199

Chapter 9 - Experimental 202

9.1. General Procedures 202

9.1.1. Reagents and Solvents 202

9.1.2. Instrumentation 202
  9.1.2.1. Nuclear magnetic resonance (NMR) spectroscopy 202
  9.1.2.2. Elemental Analysis (EA) 202
  9.1.2.3. Mass Spectrometry 202
  9.1.2.4. Analytical Gel permeation chromatography (GPC) 203
  9.1.2.5. UV-visible (UV-vis) absorption spectroscopy 203
  9.1.2.6. Thermogravimetric analysis (TGA) 203
  9.1.2.7. Cyclic Voltammetry (CV) 203
  9.1.2.8. Powder X-ray diffraction (XRD) 203
  9.1.2.9. Infrared Absorption Spectroscopy (IR) 204
9.2. Synthetic procedures for the monomers 205
  9.2.1. Synthesis of 3,6-dibromophthalic anhydride (2) 205
  9.2.2. Synthesis of 3,6-dibromophthalic acid (3) 205
  9.2.3. Synthesis of 2-undecanol (5) 206
  9.2.4. Synthesis of 3,6-dibromo-bis(2-undecanyl) phthalate (6) 206
  9.2.5. Synthesis of 3,6-bis(2-thienyl)-bis(2-undecanyl)phthalate (7) 207
  9.2.6. Synthesis of 5,5′-dibromo-3,6-bis(2-thienyl)-bis(2-undecanyl)phthalate (8) 207
  9.2.7. Synthesis of 2,7-dibromofluorene (27) 208
  9.2.8. Synthesis of 9,9-dimethyl-2,7-dibromofluorene (28) 208
  9.2.9. Synthesis of 9,9-dimethyl-2,7-bis(trimethylstannyl)fluorene (29) 209
  9.2.10. Synthesis of 5,5'-bis(trimethylstannyl)-2,2'-bithiophene (34) 209
  9.2.11. Synthesis of 2,5-dibromothiophene (39) 210
  9.2.12. Synthesis of 2,5-dibromo-3,4-dinitrothiophene (40) 210
  9.2.13. Synthesis of 3′,4′-dinitro-2,2':5',2"-terthiophene (41) 211
  9.2.14. Synthesis of 3',4'-diamino-2,2':5,2"-terthiophene (42) 211
  9.2.15. Synthesis of 4,6-bis(2-thienyl)-thieno[3,4-*c*][1,2,5]-thiadiazole (43) 212

9.2.16. Synthesis of 4,7-di(thien-2-yl)-2,1,3-benzothiadiazole-5,6-dimethyl ester (44) 212

9.2.17. Synthesis of 4,7-di(thien-2-yl)-2,1,3-benzothiadiazole-5,6-dicarboxylic acid (45) 213

9.2.18. Synthesis of 4,7-di(thien-2-yl)-2,1,3-benzothiadiazole-5,6-dicarboxylic anhydride (46) 213

9.2.19. Synthesis of 4,7-di(thien-2-yl)-2,1,3-benzothiadiazole-5,6-*N*-(3,7-dimethyloctyl)dicarboxylic imide (47) 214

9.2.20. Synthesis of 4,7-di(thien-2-yl)-2,1,3-benzothiadiazole-5,6-*N*-octyl-dicarboxylic imide (48) 215

9.2.21. Synthesis of 4,7-di(5-bromo-thien-2-yl)-2,1,3-benzothiadiazole-5,6-*N*-(3,7-dimethyloctyl)dicarboxylic imide (49) 215

9.2.22. Synthesis of 4,7-di(5-bromo-thien-2-yl)-2,1,3-benzothiadiazole-5,6-*N*-octyl-dicarboxylic imide (50) 216

9.2.23. Synthesis of 3,7-dimethyloctyl bromide (52) 216

9.2.24. Synthesis of *N*-(3,7-dimethyloctyl)phthalimide (53) 217

9.2.25. Synthesis of 3,7-dimethyl-1-octanamine (54) 217

9.2.26. Synthesis of 4,4'-dibromo-2,2'-dinitrobiphenyl (68) 218

9.2.27. Synthesis of 4,4'-dibromobiphenyl-2,2'-diamine (69) 218

9.2.28. Synthesis of 4,4'-dibromo-2,2'-diiodobiphenyl (70) 219

9.2.29. Synthesis of 2,7-dibromo-9,9-dioctyldibenzosilole (71) 220

9.2.30. Synthesis of 9,9-dioctyl-2,7-bis(4,4,5,5-tetramethyl-1,3,2-dioxaborolan-2-yl)- dibenzosilole (72) 220

9.2.31. Synthesis of 1,4-dibromo-2-fluoro-5-nitrobenzene (81) 221

9.2.32. Synthesis of 4,4'-dibromo-5,5'-difluoro-2,2'-dinitrobiphenyl (82) 221

9.2.33. Synthesis of 4,4'-dibromo-5,5'-difluorobiphenyl-2,2'-diamine (83) 222

9.2.34. Synthesis of 3,6-difluoro-2,7-dibromo-9*H*-carbazole (84) 222

9.2.35. Synthesis of heptadecan-9-ol (86) 223

9.2.36. Synthesis of 9-heptadecane-*p*-toluenesulfonate (87) 223

9.2.37. Synthesis of 3,6-difluoro-*N*-9'-heptadecanyl-2,7-dibromocarbazole (88). 224

9.2.38. Synthesis of 3,6-difluoro-*N*-9'-heptadecanyl-2,7-bis(4,4,5,5-tetramethyl-1,3,2- dioxaborolan-2-yl)carbazole (89) 225

9.2.39. Synthesis of bis(3-thienyl)methanol (113) 225

9.2.40. Synthesis of bis(2-iodo-3-thienyl)methanol (114) 226

9.2.41. Synthesis of bis(2-iodo-3-thienyl)ketone (115) 226

9.2.42. Synthesis of *4H*-cyclopenta[2,1-*b*:3,4-*b*']dithiophen-4-one (116) 227

9.2.43. Synthesis of *4H*-cyclopenta[2,1-*b*:3,4-*b*']dithiophene (117) 227

9.2.44. Synthesis of 4,4-bis(2-ethylhexyl)cyclopenta[2,1-*b*:3,4-*b*']dithiophene (118) 228

9.2.45. Synthesis of 4,4-dioctylcyclopenta[2,1-*b*:3,4-*b*']dithiophene (119) 228

9.2.46. Synthesis of 4,4-bis(2-ethylhexyl)-2,6-dibromocyclopenta[2,1-*b*:3,4-*b*']dithiophene (120) 229

9.2.47. Synthesis of 4,4-dioctyl-2,6-dibromocyclopenta[2,1-*b*:3,4-*b*']dithiophene (121) 229

9.2.48. Synthesis of 4,4-bis(2-ethylhexyl)-2,6-bis(4,4,5,5-tetramethyl-1,3,2-dioxaboralan-2-yl)cyclopenta[2,1-*b*:3,4-*b*']dithiophene (122) 230

9.2.49. Synthesis of 3,3',5,5'-tetrabromo-2,2'-bithiophene (138) 230

9.2.50. Synthesis of 3,3'-dibromo-2,2'-bithiophene (139) 231

9.2.51. Synthesis of 4,4-dioctyl-dithieno[3,2-*b*:2',3'-*d*]silole (140) 231

9.2.52. Synthesis of 4,4-dioctyl-2,6-dibromo-dithieno[3,2-*b*:2',3'-*d*]silole (141) . 232

9.2.53. Synthesis of 4,4-dioctyl-2,6-bis(trimethylstannyl)-dithieno[3,2-*b*:2',3'-*d*]silole (142) 232

9.3. Other Monomers Used 234

9.3.1. 9,9-Dioctylfluorene-2,7-diboronic acid bis(1,3-propanediol) ester (75) 234

9.3.2. 9-(Heptadecan-9-yl)-2,7-bis(4,4,5,5-tetramethyl-1,3,2-dioxaborolan-2-yl)carbazole (103) 234

9.3.3. 9,10-Bis(4-(dodecyloxy)phenyl)-2,6-bis(4,4,5,5-tetramethyl-1,3,2-dioxaborolan-2-yl)anthracene (108) 234

9.4. Synthetic procedures for the polymers 235

9.4.1. Synthesis of poly[2,2'-bithiophene-*alt*-(3',6'-bis(2-undecanyl)phthalate)] (35) 235

9.4.2. Synthesis of poly[2,2'-bithiophene-*alt*-5,5-(3',6'-bis(2-thienyl)-bis(2-undecanyl)phthalate)] (36)........ 235

9.4.3. Synthesis of poly[9,9-dimethyl-2,7-fluorene-*alt*-5,5-(3',6'-bis(2-thienyl)-bis(2-undecanyl)phthalate)] (37) 236

9.4.4. Synthesis of poly[9,9-dioctyl-2,7-fluorene-*alt*-5,5-(4',7'-bis(2-thienyl)-2',1',3'-benzothiadiazole-5,6-*N*-(3,7-dimethyloctyl)dicarboxylic imide)] (76)...... 237

9.4.5. Synthesis of poly[9,9-dioctyl-2,7-fluorene-*alt*-5,5-(4',7'-bis(2-thienyl)-2',1',3'-benzothiadiazole-5,6-*N*-octyl-dicarboxylic imide)] (77) 238

9.4.6. Synthesis of poly[9,9-dioctyl-2,7-dibenzosilole-*alt*-5,5-(4',7'-bis(2-thienyl)-2',1',3'-benzothiadiazole-5,6-*N*-(3,7-dimethyloctyl)dicarboxylic imide)] (78)...... 238

9.4.7. Synthesis of poly[9,9-dioctyl-2,7-dibenzosilole-*alt*-5,5-(4',7'-bis(2-thienyl)-2',1',3'-benzothiadiazole-5,6-*N*-octyl-dicarboxylic imide)] (79) 239

9.4.8. Synthesis of poly[*N*-9'-heptadecanyl-2,7-carbazole-*alt*-5,5-(4',7'-bis(2-thienyl)-2',1',3'-benzothiadiazole-5,6-*N*-(3,7-dimethyloctyl)-dicarboxylic imide)] (104)........ 240

9.4.9. Synthesis of poly[*N*-9'-heptadecanyl-2,7-carbazole-*alt*-5,5-(4',7'-bis(2-thienyl)-2',1',3'-benzothiadiazole-5,6-*N*-octyl-dicarboxylic imide)] (105)........ 240

9.4.10. Synthesis of poly[*N*-9'-heptadecanyl-3,6-difluoro-2,7-carbazole-*alt*-5,5-(4',7'-bis(2-thienyl)-2',1',3'-benzothiadiazole-5,6-*N*-(3,7-dimethyloctyl)dicarboxylic imide)] (106)........ 241

9.4.11. Synthesis of poly[*N*-9'-heptadecanyl-3,6-difluoro-2,7-carbazole-*alt*-5,5-(4',7'-bis(2-thienyl)-2',1',3'-benzothiadiazole-5,6-*N*-octyl-dicarboxylic imide)] (107) 242

9.4.12. Synthesis of poly[9,10-bis(4-(dodecyloxy)phenyl)-2,6-anthracene-*alt*-5,5-(4',7'-bis(2-thienyl)-2',1',3'-benzothiadiazole-*N*-5,6-(3,7-dimethyloctyl)dicarboxylic imide)] (109)........ 242

9.4.13. Synthesis of poly[9,10-bis(4-(dodecyloxy)phenyl)-2,6-anthracene-*alt*-5,5-(4',7'-bis(2-thienyl)-2',1',3'-benzothiadiazole-5,6-*N*-octyl-dicarboxylic imide)] (110) 243

9.4.14. Synthesis of poly[4,4-bis(2-ethylhexyl)-2,6-cyclopenta[2,1-*b*:3,4-*b*']dithiophene-*alt*-5,5-(4',7'-bis(2-thienyl)-2',1',3'-benzothiadiazole-5,6-*N*-(3,7-dimethyloctyl) dicarboxylic imide)] (134) 244

9.4.14. Synthesis of poly[4,4-dioctyl-2,6-cyclopenta[2,1-*b*:3,4-*b*']dithiophene-*alt*-5,5-(4',7'-bis(2-thienyl)-2',1',3'-benzothiadiazole-5,6-*N*-(3,7-dimethyloctyl)-dicarboxylic imide)] (135) 244

9.4.16. Synthesis of poly[4,4-dioctyl-2,6-cyclopenta[2,1-*b*:3,4-*b*']dithiophene-*alt*-5,5-(4',7'-bis(2-thienyl)-2',1',3'-benzothiadiazole-5,6-*N*-octyl-dicarboxylic imide) (136) 245

9.4.17. Synthesis of poly[4,4-bis(2-ethylhexyl)-2,6-cyclopenta[2,1-*b*:3,4-*b*']dithiophene-*alt*-5,5-(4',7'-bis(2-thienyl)-2',1',3'-benzothiadiazole-5,6-*N*-octyl-dicarboxylic imide) (137) 246

9.4.18. Synthesis of poly[4,4-dioctyl-2,6-dithieno[3,2-*b*:2',3'-*d*]silole-*alt*-5,5-(4',7'-bis(2-thienyl)-2',1',3'-benzothiadiazole-5,6-*N*-(3,7-dimethyloctyl)-dicarboxylic imide) (144) 247

9.4.19. Synthesis of poly[4,4-dioctyl-2,6-dithieno[3,2-*b*:2',3'-*d*]silole-*alt*-5,5-(4',7'-bis(2-thienyl)-2',1',3'-benzothiadiazole-5,6-*N*-octyl-dicarboxylic imide) (145).... 247

References 249

Chapter 10 - Supporting Information.. 253

Glossary of Abbreviations and Terms

A

A	Electron acceptor
Acetone-d_6	Deutrated acetone
AM1.5	Air mass 1.5
ATR	Attenuated total reflectance

B

BHJ	Bulk heterojunction
bm	Broad multiplet (NMR)
bs	Broad singlet (NMR)
b	Broad (NMR)

C

^{13}C-NMR	Carbon Nuclear Magnetic Resonance Spectrometry
CB	Conduction band
$CDCl_3$	Deutrated chloroform
COD	1,5-Cyclooctadiene
CD_3SOCD_3	Deuterated dimethyl sulfoxide
CD_3COCD_3	Deuterated acetone
$CHCl_3$	Chloroform
$C_2D_2Cl_4$	Deutrated 1,1,2,2-tetrachloroethane

D

D	Electron donor
d	Doublet (NMR)
dd	Doublet of doublet (NMR)
DCM	Dichloromethane
DMF	*N*,*N*-Dimethylformamide
DMSO	Dimethyl sulfoxide
Dp	Degree of polymerisation

E

E_g	Optical band gap
E_g (elec)	Electrochemical bandgap
eV	Electron volt
EQE	External Quantum Efficiency
EI-MS	Electron Ionisation-Mass Spectrometry

F

FT-IR	Fourier Transform Infra-Red spectroscopy
FF	Fill factor

G

GPC	Gel Permeation Chromatography

H

^{1}H-NMR	Proton Nuclear Magnetic Resonance Spectrometry
HOMO	Highest Occupied Molecular Orbital
Hz	Hertz

I

IQE	Internal Quantum Efficiency

J

J_{sc}	Short circuit current density
J_{MPP}	Current at Maximum Power Point

K

KOAc	Potassium acetate

L

LUMO	Lowest Unoccupied Molecular Orbital

M

m	Multiplet (NMR)
M_n	Number Average Molecular Weight
M_w	Weight Average Molecular Weight
MOT	Molecular Orbital Theory
MEH-PPV	Poly[2-methoxy-5-(2-ethylhexyloxy)-1,4-phenylenevinylene]
MDMO-PPV	Poly[2-methoxy-5-(3',7'-dimethyloctyloxy)-1,4-phenylenevinylene]

N

NBS	*N*- Bromosuccinimide
$NiCl_2$(dppp)	Dichloro[1,3-bis(diphenylphosphino)propane]nickel
$NiCl_2$(dppe)	Dichloro[1,2-bis(diphenylphosphino)ethane]nickel
Ni(bipy)Cl_2	Dichloro(2,2'-bipyridyl)nickel
Ni$(COD)_2$	Bis(1,5-cyclooctadiene)nickel(0)

O

OSC	Organic Solar Cell
OPV	Organic Photovoltaic

P

PA	Polyacetylene
$PC_{61}BM$	[6,6]-phenyl-C_{61}-butyric acid methyl ester
$PC_{71}BM$	[6,6]-phenyl-C_{71}-butyric acid methyl ester
PDI	Polydispersity index
P3HT	Poly(3-hexylthiophene)
P3AT	Poly(3-alkylthiophene)
PCDTBT	Poly[*N*-9'-heptadecanyl-2,7-carbazole-*alt*-5,5'-(4',7'-di-2-thienyl-2',1',3'-benzothiadiazole)]
PF8DTBT	Poly[2,7-(9,9-dioctylfluorene)]-*alt*-5,5'-(4',7'-di-2-thienyl-2',1',3'-benzothiadiazole)]
PPP	Poly(*p*-phenylene)
PPV	Poly(*p*-phenylene vinylene)
PPy	Polypyrrole
PT	Polythiophene

PFu	Polyfuran
PEDOT:PSS	Poly(3,4-ethylenedioxythiophene)-polystyrenesulfonate
$Pd(PPh_3)_4$	Tetrakis(triphenylphosphino)palladium (0)
$Pd_2(dba)_3$	Tris(dibenzylideneacetone)dipalladium(0)
$Pd(PPh_3)_2Cl_2$	Bis(triphenylphosphine)palladium(II)dichloride
$Pd(OAc)_2$	Palladium(II) acetate
$Pd(dppf)Cl_2$	[1,1'-Bis(diphenylphosphino)ferrocene]palladium(II) dichloride
P(*o*-tol)$_3$	Tri(*o*-tolyl)phosphine
PPh_3	Triphenylphosphine
PSC	Polymer Solar Cell
PCE	Power Conversion Efficiency
R	
ROMP	Ring Opening Metathesis Polymerisation
S	
s	Singlet (NMR)
S cm^{-1}	Siemens per centimetre
T	
t	Triplet (NMR)
THF	Tetrahydrofuran
T_g	Glass transition temperature
T_d	Decomposition temperature (5% weight loss)
TGA	Thermogravimetric analysis
U	
UV/vis	Ultraviolet-visible Spectroscopy
V	
V_{oc}	Open circuit voltage
V	Volt
V_{MPP}	Voltage at Maximum Power Point

Chapter 1 - Introduction

1.1. The electronic structure of conjugated polymers

In order to understand the electronic configuration of conjugated polymers, it is better to compare the bond orientation and hybridisation of saturated polymers and conjugated polymers. Polyethylene (**PE**) and polyacetylene (**PA**) are selected as examples of saturated and conjugated polymers, respectively.

In **PE**, each carbon atom in the main chain is sp^3 hybridised and it is bonded with two neighbouring carbon atoms and two hydrogen atoms to form four sigma (σ) bonds. Therefore, each carbon atom utilises all four valence electrons and these electrons are strongly localised. As a result, **PE** is electrically insulating as there is no free electron in its backbone, which is responsible for conducting electricity. Consequently, the optical band gap (E_g) of **PE** is large around 8.0 eV and it is outside the optical spectrum[1]. However, in **PA**, each carbon atom is sp^2 hybridised and it is bonded to two neighbouring carbon atoms and one hydrogen atom to form three σ-bonds. The remaining unhybridised $2p_z$ orbital per carbon atom is perpendicular to the trigonal planar of the polymer backbone. Each unhybridised $2p_z$ orbital contains unpaired electron and overlap with adjacent $2p_z$ orbital to form π-bond and ultimately they are delocalised along the entire polymer backbone. This electronic delocalisation provides the semiconducting properties that permit the charge mobility along the conjugated polymer backbone[2].

The archetypal example of conjugated polymer is **PA** $(-CH-)_n$. If the carbon-carbon bonds in **PA** are equally long, the π-orbitals could be half-filled and it could possess a metallic behaviour. Peierls predicted that this structure is unstable. In **PA**, the backbone of the polymer has in fact alternating slightly longer single and slightly shorter double bonds[3]. It has two isomeric forms which are trans-polyacetylene (***t*-PA**) and cis-polyacetylene (***c*-PA**). Due to the Peierls theory each repeat unit in ***t*-PA** contains two carbon atoms $(-CH=CH-)_n$. As a result, the π-band in ***t*-PA** is divided into two sub-bands which are the filled π-band and empty π^*-band. The difference in energy between these bands is the band gap (E_g) and for the ***t*-PA** the value is 1.5 eV[4].

1.2. Doping in conjugated polymers

Conjugated polymers in the pristine state are neutral and usually semiconductors or insulator having low conductivities. Upon doping, charge carriers are created and move along the polymer chain. As a result, the conductivity significantly increases by several orders of magnitude[5]. For example, the conductivity of ***t*-PA** is lower than 10^{-5} S cm^{-1} in its undoped state. However, when it is doped with an oxidising agent[6] the conductivity reached a metallic regime ~ 10^3 S cm^{-1}.

Charge carriers can be generated *via* redox reactions. The doping in conjugated polymers can be achieved in a number of different ways for example photo, acid-base, charge injection and redox doping.

***t*-PA** is unique among the conjugated polymers because it has a degenerate ground state, i.e., two possible configurations (A and B phases) corresponding exactly to the identical total energy (**Figure 1.1**). The two phases are distinct from each other through interchanging the positions of single and double bonds[7]. As described above, each carbon atom in ***t*-PA** contains an unpaired electron in unhybridised $2p_z$ orbital. Neutral soliton (radical) is formed in pristine ***t*-PA** when each chain having an odd number of carbons[8]. The soliton is a domain wall between the two phases (A and B phases) along one chain in ***t*-PA** and is spreading over several carbon atoms (approximately seven) (**Figure 1.1**)[2].

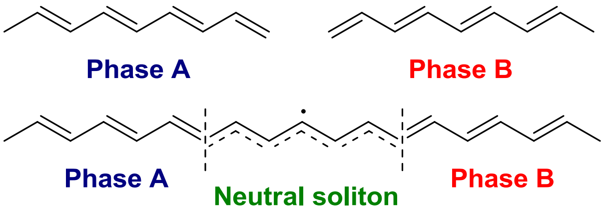

Figure 1.1: The schematic illustration of two degenerate ground state of the ***t*-PA** with domain boundary (neutral soliton) separates the two phases (A and B phases)

A new localised energy level at mid-gap appears for soliton with respect to the valence band (VB) and conduction band (CB) levels of the ***t*-PA**. If the soliton is neutral, the mid-gap is half-occupied. In the case of partially oxidised ***t*-PA** (p-type doping) a positively charged soliton is formed and the mid-gap is empty but when it is reduced partially (n-type doping) negatively charged soliton is created and the mid-gap contains two electrons. Soliton has charge-spin relationships since neutral soliton has a spin ½, however charged solitons are spinless (**Figure 1.2**)[9].

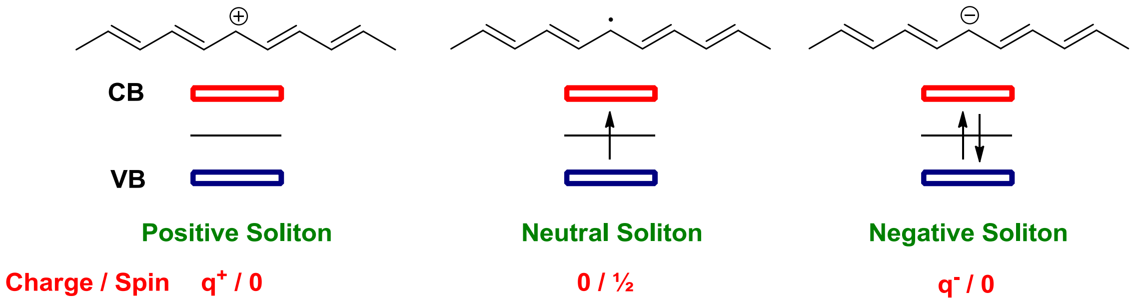

Figure 1.2: The schematic illustration of the chemical structures (upper), band structures, charges and spins (lower) for a positive, neutral and negative solitons in the ***t*-PA**

Unlike ***t*-PA**, the other conjugated polymers, for instance, ***c*-PA**, polypyrrole (**PPy**) and polythiophene (**PT**) possess two distinct resonance forms, aromatic and quinoid geometry which are not energetically equivalent. Quinoid resonance structure has a higher energy than the aromatic resonance form. These types of polymers are called nondegenerate ground state conjugated polymers[10]. In such polymers, radical cations (or radical anions) in p-type (or n-type) doping are the main charged excitations. For example, in p-type doping of **PPy** one electron is removed from the conjugated chain leads to the creation of a positively charged polaron (radical cation), which is associated with a quinoid-like segment spreading over about four pyrrole rings (**Figure 1.3**). Two new electronic states in the gap are formed in polarons. For doped **PPy**, these states are about 0.5 eV far from the band edges[11]. The lower state in a positive polaron contains an unpaired electron and it has a spin of ½. Second polaron is created by removing a second electron from the chain. The combination of two positive polarons causes the formation of energetically favourable dication species which is called positive bipolaron (**Figure 1.3**). In **PPy**, the bipolaron also spreads over four pyrrole rings similar to the polaron[11]. In the bipolaron the lower state is more upshifted from the VB and the higher state is more downshifted from the CB with respect to the polaron states and it is around 0.75 eV for **PPy**[11]. In positive bipolarons, those states are empty and are spinless. At higher doping level, the bipolaron states can overlap to form bipolaron bands.

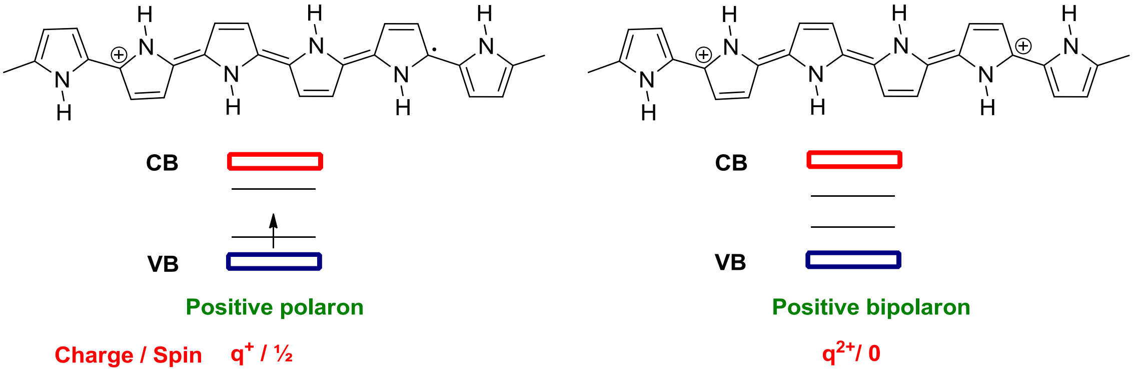

Figure 1.3: The schematic illustration of the chemical structures (upper), band structures, charges and spins (lower) for a positive polaron and positive bipolaron in **PPy**

1.3. Methods for preparation of conjugated polymers

Since the preparation of the first conjugated polymer, **PA** in 1977, numerous methods for synthesis of conjugated polymers have been developed. Generally, they can be classified into three main categories: The oxidative, metal catalysed cross-coupling and condensation polymerisation methods.

1.3.1. The oxidative polymerisations

The oxidative polymerisations are subdivided into two categories; electrochemical oxidative and chemical oxidative polymerisations.

1.3.1.1. Electrochemical oxidative polymerisations

This method is extensively used for the preparation of conjugated polymers such as **PPy** or **PT** from pyrrole or thiophene monomers respectively (**Scheme 1.1**)[12]. In the electrochemical oxidative polymerisation, the doped polymer film is directly deposited onto an electrode surface in a monomer solution which contains an electrolyte. The polymer film can be analysed by electrochemical methods[13]. For this type of polymerisation, an applied potential is required and it must be higher than the oxidation potential of the corresponding monomers. The polymerisation cannot be applied in large scale preparation of the polymers because of its limitation to the surface area of the electrode.

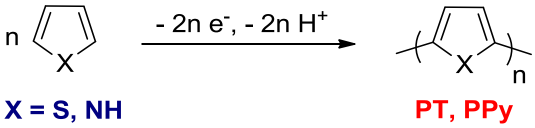

Scheme 1.1: Synthesis of **PT** or **PPy** by the electrochemical oxidative polymerisations

The mechanism of the electrochemical oxidative polymerisation is not known exactly and is a controversial subject but the generally agreed mechanism is Electrochemical-Chemical- Electrochemical [$E(CE)_n$] (**Scheme 1.2**). The first step involves the oxidation of the monomer to generate a radical cation[14]. This intermediate has three resonance forms (**1**, **2**, and **3**), while **2** is clearly the most stable[15]. Then, two radical cations are dimerised at *α*-positions *via* radical-radical coupling to form a dihydro dication dimer. The next step is release of two protons to form dimer and the driving force of this step is returning the aromaticity of the dimer. This dimer is further oxidised to generate dimeric radical cation and can attack another radical to form trimer after elimination of proton. These reactions repeat until the polymer is formed[16].

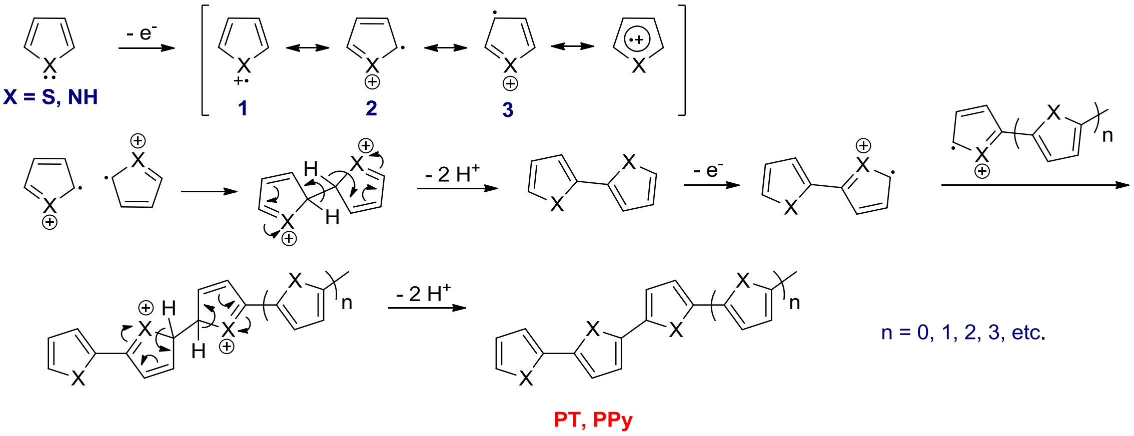

Scheme 1.2: The mechanism of electrochemical oxidative polymerisation for five membered heterocyclic monomers such as thiophene or pyrrole

1.3.1.2. The chemical oxidative polymerisations

Some conjugated polymers can be prepared by chemical oxidative polymerisations such as **PPy**, **PT** and their derivatives such as, poly(3-alkylthiophene)s (**P3ATs**) using oxidants such as anhydrous ferric chloride ($FeCl_3$) or ammonium persulfate [$(NH_4)_2S_2O_8$][17]. $FeCl_3$ has been widely used as an oxidizing agent in anhydrous chloroform. Yoshino and co-workers for the first time employed this type of polymerisation for the synthesis of five-membered heterocyclic conjugated polymers such as **PT** and its analogues **PPy** and polyfuran (**PFu**) from the thiophene, pyrrole and furan monomers respectively (**Scheme 1.3**)[18].

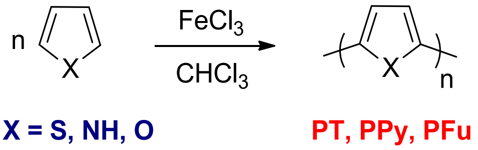

Scheme 1.3: The synthesis of **PT**, **PPy** and **PFu** by the chemical oxidative polymerisations

PT is insoluble and it has a lack of processability for optoelectronic applications. Introduction of flexible side chains into the backbone of **PT** dramatically increase the solubility of the resulting polymers, **P3ATs**. **P3ATs** with straight alkyl side chains (butyl or longer) are soluble and processable[17].

Since 3-substituted thiophene monomers are asymmetric, coupling in the 2- and 5-positions of two 3-alkylthiophene units leads to three distinct regiochemical diads (**Figure 1.4**). The first coupling is head-to-tail (HT), a second coupling is head-to-head (HH), and the last coupling is tail-to-tail (TT). Furthermore, when three 3-alkylthiophene monomers are linked together result is four possible triad regioisomers which are HT–HT, HT–HH, TT–HT and TT–HH (**Figure 1.4**).

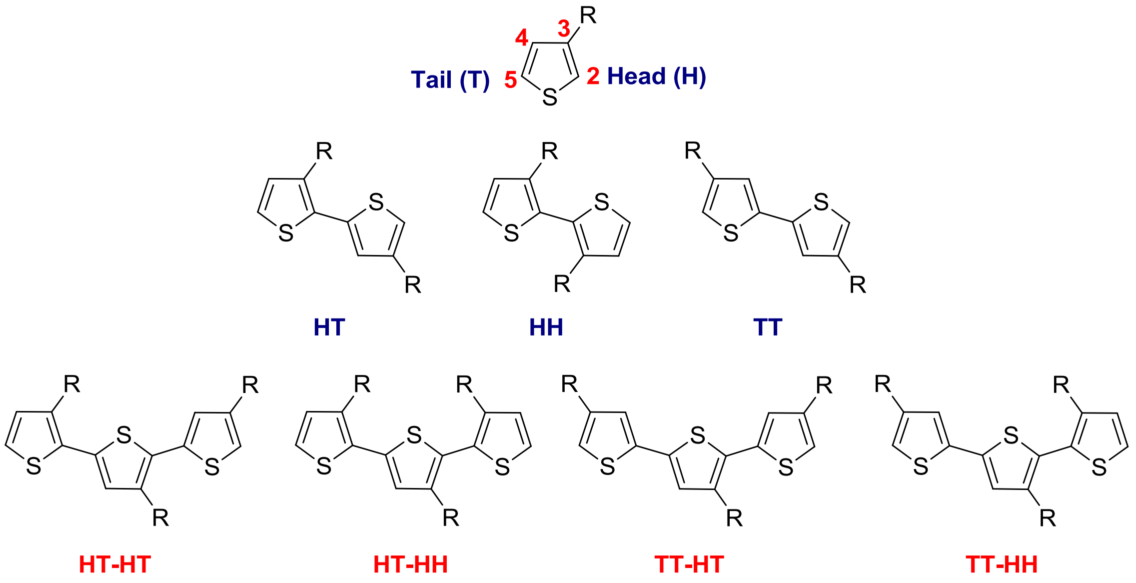

Figure 1.4: Possible regioisomeric couplings for 3-alkylthiophenes

The incorporation of HH diad configurations leads to twisting of the conjugated polymer chain, because of the increased steric hindrance between the solubilizing alkyl chains and the lone electron pairs of adjacent sp^2 sulfur atoms (**Figure 1.5**). **P3ATs** with a random mixture of HH linkages, TT linkages and HT linkages are referred to as regioirregular (**ri-P3ATs**) (**Figure 1.5**). However, **P3ATs** that consist of only HT arrangements are referred to as regioregular head-to-tail (**rr-P3ATs**) (**Figure 1.5**). As a result, **ri-P3ATs** have lower effective conjugation lengths and larger bandgaps when compared to **rr-P3ATs**[19].

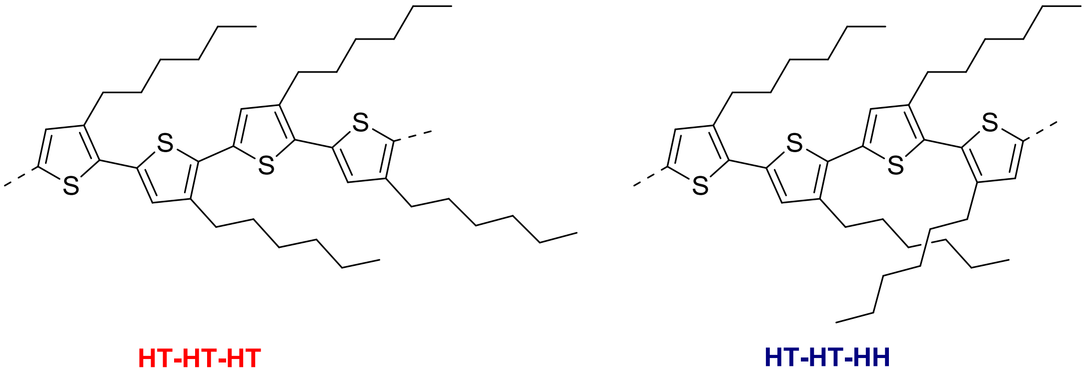

Figure 1.5: The schematic presentation of **rr-P3ATs** (left) and **ri-P3ATs** (right)

In general, high molecular weight polymers and excellent yields are achieved by chemical oxidative polymerisation with $FeCl_3$ as compared to the polymers synthesised by electrochemical oxidative polymerisation. The polymerization of 3-alkylthiophenes either by electrochemical or chemical oxidative method gives **ri-P3ATs** with approximately 60–80% HT-HT couplings[20]. Andersson *et al*. reported that the chemical oxidative polymerisation of a sterically hindered 3-(4-octylphenyl)thiophene by slow addition of $FeCl_3$ can provide regioregular poly[3-(4-octylphenyl)thiophene] (**POPT**) with up to 94% HT-HT couplings[21].

1.3.2. Transition metal catalysed cross-coupling polymerizations

Transition metal catalysed cross-coupling polymerizations between organohalides (Ar^1-X) and organometallic compounds (Ar^2-M) are powerful synthetic methods for Csp^2–Csp^2 bond formation[22]. Several conjugated polymers could be synthesised by these reactions. The four most commonly used metal catalysed cross coupling polymerisations are the Kumada-Corriu, Negishi, Stille and Suzuki, in which different nucleophilic reagents are used for example the aryl Grignard reagents, aryl zinc reagents, aryl stannanes and aryl boronic acids or esters respectively (**Scheme 1.4**). In these reactions palladium or nickel complexes are commonly used as catalysts. In addition, the metal catalysts which are used in these polymerisations are different, usually palladium based catalysts are used in Stille and Suzuki. However, nickel based catalysts are used in Kumada-Corriu. The polymers synthesized by these types of polymerisations are powders and in their neutral states.

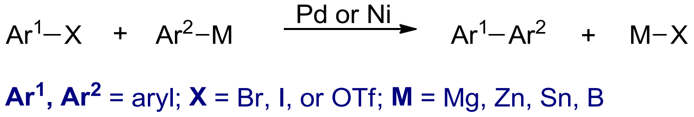

Scheme 1.4: The transition metal catalysed cross-coupling reactions

1.3.2.1. Kumada-Corriu cross-coupling reactions

In 1972, Corriu *et al*. and Kumada *et al*. independently reported the coupling between Grignard reagents and aryl halides using nickel complexes as catalysts (**Scheme 1.5**)[23,24]. They found that $NiCl_2$(dppp) is the most effective catalyst among all the nickel-phosphine complexes[24,25].

$$Ar^1\text{-}X \;+\; Ar^2MgX \xrightarrow{NiCl_2(dppp)} Ar^1\text{-}Ar^2 \;+\; MgX_2$$

Ar^1, Ar^2 = aryl; **X** = Br or Cl

Scheme 1.5: Kumada-Corriu cross-coupling reactions

The proposed catalytic cycle of the Kumada-Corriu reaction is depicted in scheme 1.6. First step is the reaction between dihalodiphosphinenickel(II) complex (**1**) with two equivalents of the Grignard reagent to form nickel(0) complex (**2**), which is the active catalyst in the catalytic cycle[23]. The second step is an oxidative addition of the active catalyst with an organohalide reagent to give halo(organo)nickel(II) complex (**3**). The third step is the transmetalation between **3** with the Grignard reagent to generate a new diorgano nickel(II) complex (**4**). In the final step, the latter complex undergoes the reductive elimination to form the coupled product (Ar^1-Ar^2) and concomitantly regenerate the L_2Ni(0) complex to complete the catalytic cycle[26].

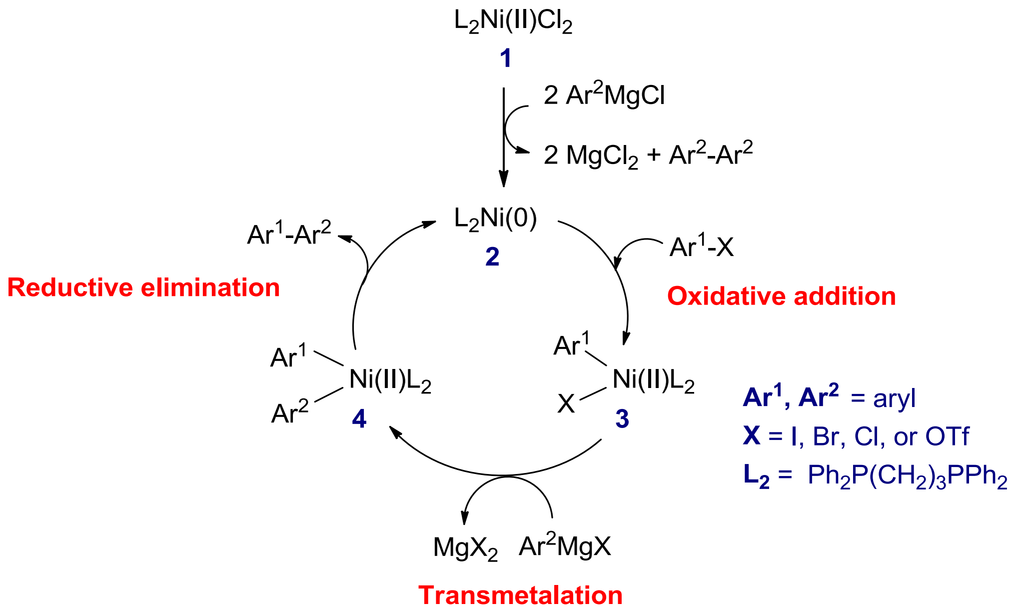

Scheme 1.6: The catalytic cycle of the Kumada-Corriu reaction

In 1980, the synthesis of **PT** was published by two research groups using Kumada-Corriu coupling reaction. The first group was Yamamoto which synthesised **PT** by treating 2,5-dibromothiophene (**1**) with magnesium metal in THF using Ni(bipy)Cl_2 as a catalyst

(**Scheme 1.7**)[27]. The second group was Lin and Dudek treating same starting material that was used by Yamamoto *et al.* in the presence of various transition metal acetylacetonate complexes, M(acac)$_n$ (**Scheme 1.7**)[28]. The **PT** prepared by these research groups had low molecular weights and they were insoluble even in THF. Soon after, Wudl *et al.* reported synthesis of **PT** by reacting 2,5-diiodothiophene (**2**) with magnesium metal in diethyl ether to form 2-iodo-5-iodomagnesiothiophene, which is the Grignard reagent intermediate[29]. This intermediate was separated and treated with hot anisole then Ni(dppp)Cl$_2$ added as a catalyst (**Scheme 1.7**).

The first chemical preparation of soluble **P3ATs** was synthesized by Elsenbaumer and co-workers *via* Kumada-Corriu coupling reaction[30]. 3-Alkylsubstituted-2,5-diiodothiophene (**3**) was treated with one equivalent of magnesium metal in THF (or 2MeTHF) as a solvent for the reaction to form the Grignard reagent (**Scheme 1.7**)[31]. Ni(dppp)Br$_2$ used as a catalyst and subsequently added to the resulting Grignard reagent to form soluble **P3ATs** with low number average molecular weight (M_n = 3000-8000 g mol^{-1}). The **P3ATs** prepared by this method contain only 50-80% HT-HT couplings and regioregularity cannot be controlled.

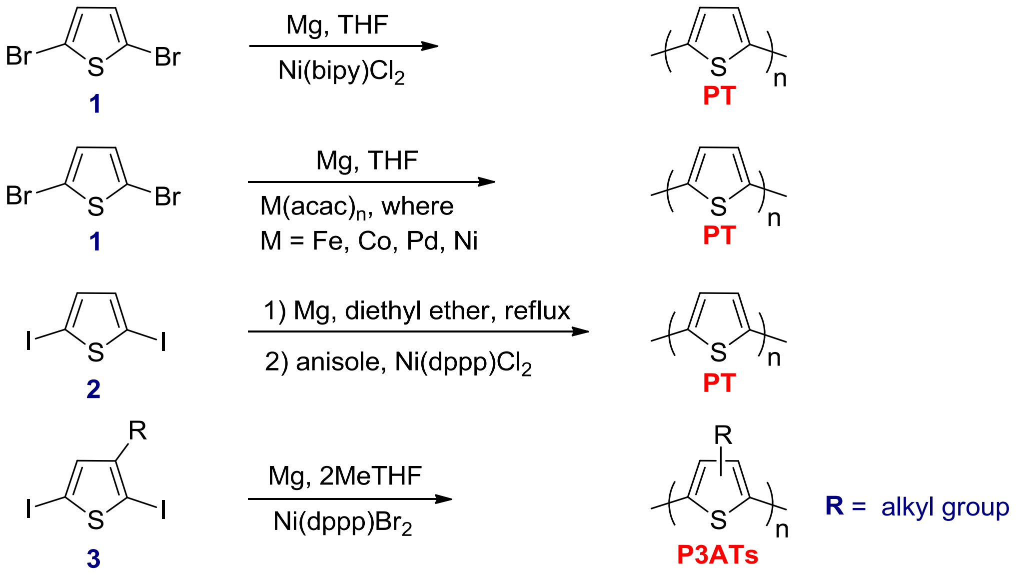

Scheme 1.7: The synthesis of **PT** and **P3ATs** by Kumada-Corriu coupling reaction

The first synthesis of **rr-P3ATs** was developed by McCullough and Lowe in 1992 (**Scheme 1.8**)[32]. This method starts with selective lithiation at the 5-position of 2-bromo-3-alkylthiophene (**1**) with lithium diisopropylamide (LDA) at cryogenic temperature to generate organolithium intermediate (**2**), which is stable at this temperature with only 1-2% of metal-halogen exchange[33]. This intermediate is changed to the organomagnesium intermediate (**3**) by the addition of magnesium bromide ethyl etherate (MgBr$_2$.OEt$_2$) and subsequently polymerised *in situ* using the Kumada-Corriu cross-coupling reaction by adding Ni(dppp)Cl_2 catalyst gave **rr-P3ATs** with almost 100% of HT–HT couplings[34].

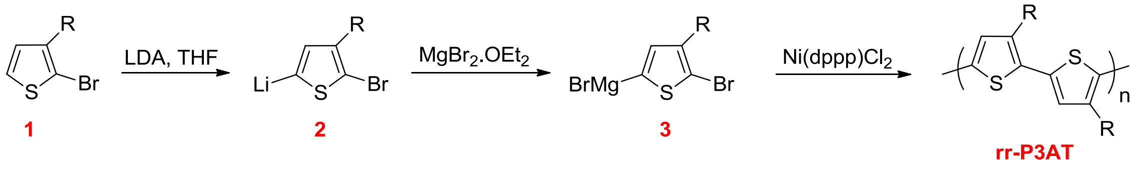

Scheme 1.8: The synthesis of **rr-P3ATs** by McCullough method

Later on, McCullough and co-workers have prepared **rr-P3ATs** *via* the Grignard metathesis (GRIM) method (**Scheme 1.9**)[35]. Treatment of 2,5-dibromo-3-alkylthiophene (**1**) with one equivalent of commercially available Grignard reagent resulted in a mixture of two regiochemical isomers (**2** and **3**) in a ratio of 85:15. This ratio was found independently of the type of the Grignard reagent, temperature and the reaction time used. The addition of Ni(dppp)Cl_2 as a catalyst to the above mixture yielded **rr-P3ATs** which contained more than 99% HT-HT couplings. This method does not require cryogenic temperature which is necessary in the McCullough method. Moreover, this method does not require the use of highly reactive metals and high molecular weight **rr-P3ATs** can be prepared in kilogram scale[36]. The reason provided for the regioregularity of the polymers obtained is that intermediates **2** and **3** are each involved separately in the growth of polymer chains which leads to selective formation of head-to-tail **P3ATs**.

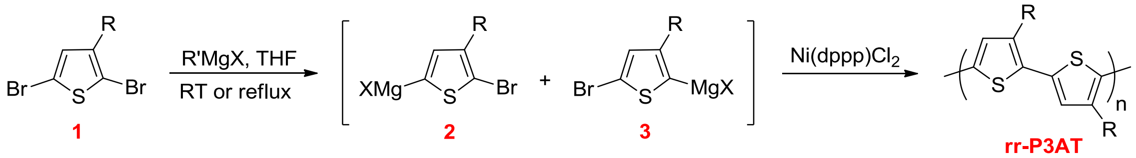

R = alkyl; **R'** = alkyl, or vinyl; **X** = Cl, or Br

Scheme 1.9: The synthesis of **rr-P3ATs** by the GRIM route

1.3.2.2. Negishi cross-coupling reactions

Negishi reported the first coupling between organozinc derivatives and organohalides by using Ni or Pd as the catalyst (**Scheme 1.10**)[37].

$$\mathrm{Ar^1X} \;+\; \mathrm{Ar^2ZnX'} \xrightarrow{\mathrm{PdL_n\ or\ NiL_n}} \mathrm{Ar^1\text{-}Ar^2} \;+\; \mathrm{ZnXX'}$$

Ar^1, Ar^2 = aryl; **X** = I, Br,Cl or OTf; **X'** = I, Br or Cl

Scheme 1.10: Negishi cross coupling reactions

Chen and Rieke reported the synthesis of **rr-P3ATs** *via* Negishi cross-coupling reaction (**Scheme 1.11**)[38]. In this method, 2,5-dibromo-3-alkylthiophene (**1**) was reacted with Rieke zinc (Zn*) at cryogenic temperature resulting in a mixture of the two regioisomers

(**2**) as the predominant intermediates and **3** in minor quantities. A regioselectivity was achieved as high as 97-98% at –78 °C for most cases. In addition, the ratio between these isomers depends less on the length of the alkyl chains[39]. These organozinc intermediates *in situ* undergo regioselective polymerization by adding catalytic amount of Ni(dppe)Cl_2 to afford the 97-98% head-to-tail **rr-P3ATs**. Whereas, use of a $Pd(PPh_3)_4$ as a catalyst under identical conditions yielded a totally **ri-P3ATs**.

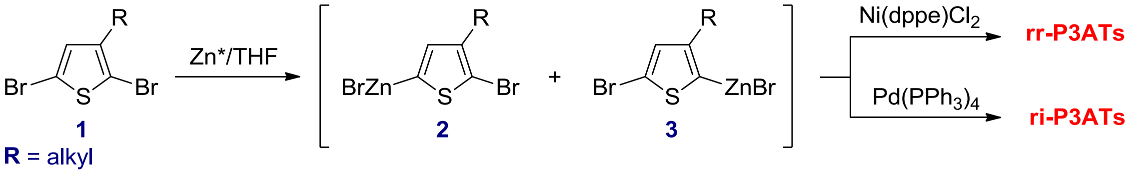

Scheme 1.11: Chen and Rieke method for synthesis of **rr-P3ATs** and **ri-P3ATs**

1.3.2.3. Stille cross-coupling reactions

The coupling reaction of organic electrophiles such as aryl halides or triflates and aryl stannanes catalysed by palladium is called the Stille coupling reaction and it is one of the most selective and powerful synthetic approaches to form Csp^2-Csp^2 bonds (**Scheme 1.12**)[40,41].

$$Ar^1X \quad + \quad Ar^2SnR_3 \quad \xrightarrow{Pd} \quad Ar^1\text{-}Ar^2 \quad + \quad XSnR_3$$

Ar^1, Ar^2 = aryl; **R** = methyl or butyl; **X** = I, Br or OTf

Scheme 1.12: The Stille cross coupling reactions

The advantages of the Stille reaction are that organotin reagents are readily prepared and are stable toward air and moisture and also the reaction is accomplished under neutral conditions. Moreover, they would tolerate different kinds of functional groups on both partners including ester or other sensitive groups such as nitrile and alcohol without any protection/deprotection strategies[42]. However, it has some disadvantages; organotin compounds and by-products are toxic materials[43,44].

A wide variety of different conjugated polymers with high molecular weights has been synthesised by using palladium catalysed Stille polycondensation between electron-rich distannane monomers and electron-deficient organodihalide monomers (**Scheme 1.13**)[40,45].

$$n\ XAr^1X \quad + \quad n\ R_3SnAr^2SnR_3 \quad \xrightarrow{Pd} \quad \left[Ar^1\text{-}Ar^2 \right]_n \quad + \quad 2n\ XSnR_3$$

Ar^1, Ar^2 = aryl; **R** = methyl or butyl; **X** = I or Br

Scheme 1.13: The Stille polycondensation

Iraqi and Barker have synthesised regioregular poly(3-hexylthiophene) (**rr-P3HT**) through the Stille polycondensation using 2-iodo-3-hexyl-5-*n*-butylstannylthiophene monomer (**2**) (**Scheme 1.14**)[46]. This monomer was synthesized by cryogenic lithiation of 2-iodo-3-hexylthiophene (**1**) at the 5-position using LDA and subsequently treated with tri-*n*-butyltin chloride. This monomer undergoes homopolymerization using variety solvents which resulted in **rr-P3HT** with greater than 96% HT-HT couplings.

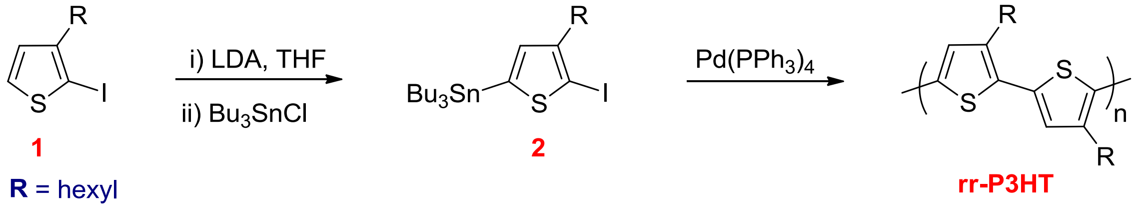

Scheme 1.14: The synthesis of **rr-P3HT** by Stille polycondensation

The generally accepted catalytic cycle for the Stille reaction is illustrated in scheme 1.15[41]. The reaction consists of four main steps. 1) Oxidative addition; 2) transmetallation; 3) trans to cis isomerisation; and finally 4) reductive elimination. The $Pd^{(0)}$ such as $Pd(PPh_3)_4$ and $Pd_2(dba)_3$ or $Pd^{(II)}$ for instance, $Pd(OAc)_2$ and $Pd(PPh_3)_2Cl_2$ are used as the catalysts. The $Pd^{(II)}$ is changed to $Pd^{(0)}L_2$ which is active catalyst by aryl stannane monomer and allowing access into the catalytic cycle. The first step is an oxidative addition of an organic electrophile (Ar^1X) to the $Pd^{(0)}L_2$ to form $Ar^1Pd^{(II)}L_2X$ intermediate. Espinet and Casado found that this complex is formed in the cis-configuration and after that it is isomerised to the more stable trans-configuration[47]. The mechanistic details of the transmetallation step was published by Espinet and Echavarren who proposed cyclic and open pathways[48]. In the cyclic pathway trans-$Ar^1Pd^{(II)}L_2X$ intermediate undergoes associative L-for-Ar^2 substitution through transition state (**TS1**) in which the Sn and Pd metals are bridged by X and Ar^2. As a result, T-shaped cis-$Ar^1Ar^2Pd^{(II)}L$ complex is formed after elimination of $XSnR_3$, from which the organic product (Ar^1-Ar^2) is generated and it is the final step which is called reductive elimination and the $Pd^{(0)}L_2$ catalyst is regenerated and re-enters the catalytic cycle[49]. The open pathway is favoured where no bridging ligands are available and in highly polar solvents and weakly coordinating anion (like triflate) which is readily substituted by the ligand or solvent[50]. In this pathway, X is replaced by coordinating solvent (S) or ligand (L) to form competitively cis- and trans-$Pd^{(II)}L_2Ar^1Ar^2$ complexes through transition state (**TS2**)[51]. Finally, the coupled product is formed.

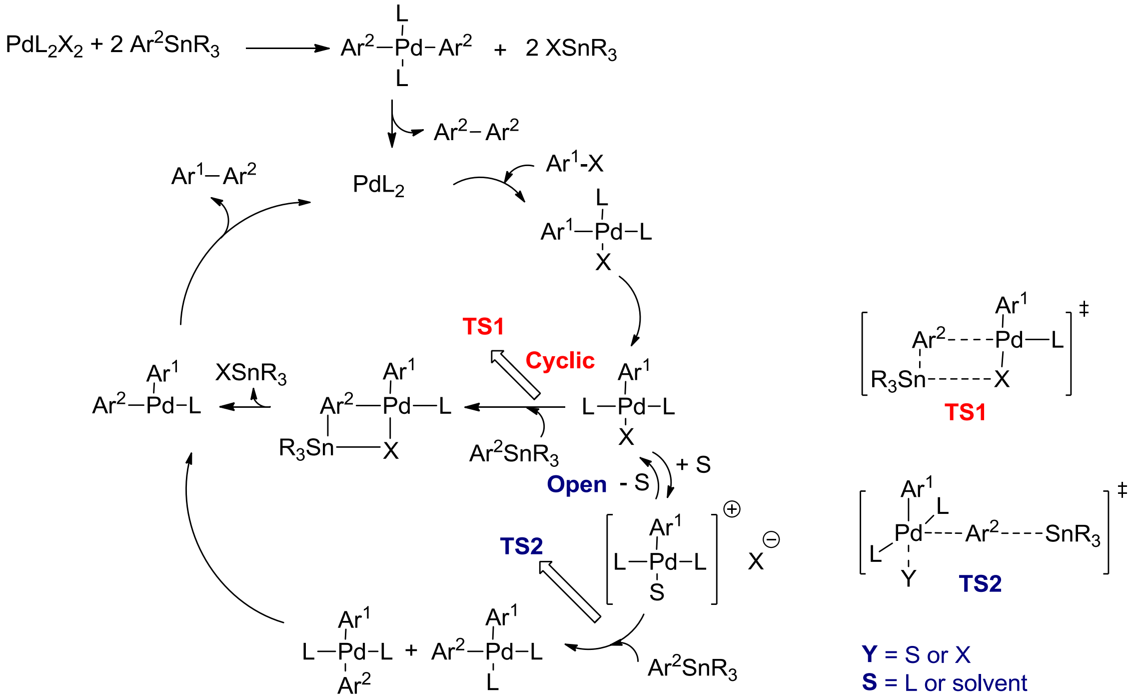

Scheme 1.15: The catalytic cycle of Stille cross-coupling reaction

1.3.2.4. The Suzuki-Miyaura reactions

The Suzuki-Miyaura reaction has become one of the most important and general methodologies for the construction of carbon-carbon bonds[52]. This reaction comprises of the coupling between different kinds of organic electrophiles such as halides or triflates and organoboronic acids or esters in the presence of base and palladium complexes (**Scheme 1.16**)[53].

$$\mathrm{Ar^1{-}X} \quad + \quad \mathrm{Ar^2{-}B(OR)_2} \quad \xrightarrow[\text{base}]{\text{Pd}} \quad \mathrm{Ar^1{-}Ar^2} \quad + \quad \mathrm{X{-}B(OR)_2}$$

Ar^1, Ar^2 = aryl; **X** = Br, I, or OTf; **R** = H or alkyl

Scheme 1.16: The Suzuki-Miyaura cross coupling reaction

The Suzuki-Miyaura reaction offers several advantages such as commercial availability of the reagents and mild reaction conditions. In addition, organoboron compounds are generally inert toward oxygen and water and thermally stable[54]. Moreover, they could tolerate various types of functional groups and by-products are non-toxic and can be easily handled and separated[55]. Therefore, this reaction is not only suitable for laboratories but also appropriate for large scale synthesis.

The Suzuki-Miyaura reaction has been used for preparing various types of conjugated polymers, for example, poly(arylene)s and their analogues. The Suzuki polycondensation (SPC) reaction is a step growth polymerisation between two different monomers in

(AA/BB approach) in which one of the aromatic monomer carrying two boronic acids (or esters) and the second monomer has two halogens (bromides or iodides) to form alternating copolymers[56]. The SPC could also use a bifunctional (AB) monomer in (AB approach) in which a monomer carries boronic acid (or ester) on the one side and the halogen on the other side to form homopolymers (**Scheme 1.17**)[56].

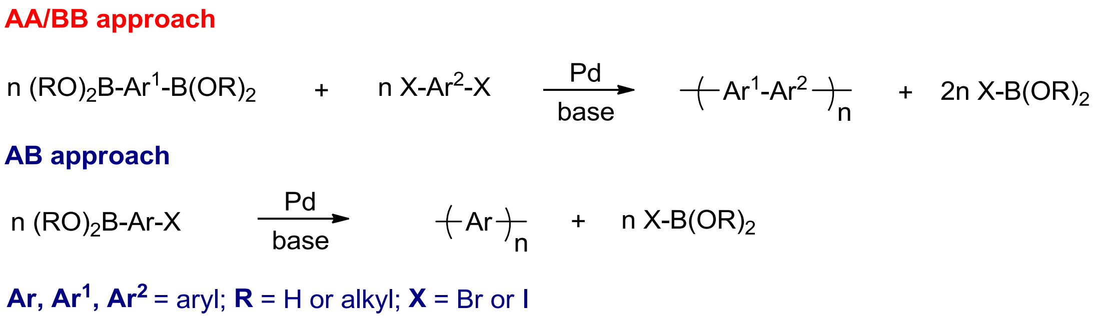

Scheme 1.17: The Suzuki polycondensation

Guillerez and Bidan reported the synthesis of a regioregular poly(3-octylthiophene) (**rr-P3OT**) through the SPC using 2-iodo-3-octyl-5-boronatothiophene monomer (**2**)[57]. Similar to Stille reaction, this monomer was obtained from 2-iodo-3-octylthiophene (**1**) by selective lithiation at 5-position at – 40 °C using LDA and subsequently treated with organoboron reagent. The polymerisation was carried out by coupling (**2**) using $Pd(OAc)_2$ as a catalyst yielded **rr-P3OT** which contained 96-97% HT-HT couplings (**Scheme 1.18**).

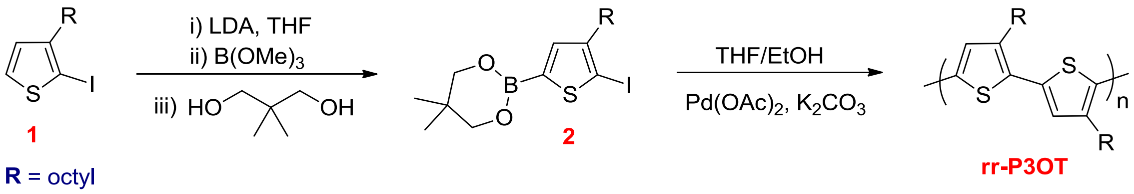

Scheme 1.18: The synthesis of **rr-P3OT** by the SPC

The catalytic cycle is similar to that of common cross-coupling reactions and widely accepted to occur in a sequence of three steps: 1) oxidative addition; 2) transmetalation, and 3) reductive elimination (**Scheme 1.19**)[54]. The oxidative addition of aryl halides (Ar^1X) to the Pd^0L_2 complex is the first step of the catalytic cycle[58]. In this step, palladium oxidises from oxidation state of (0) to (+2) to form $Ar^1Pd^{II}XL_2$ complex. This complex is formed in a square planar cis-configuration and afterward it isomerises to a more stable trans-configuration, which is the first isomerisation in the catalytic cycle[59]. These results were also confirmed theoretically by Braga and co-workers[60]. Although the oxidative addition and reductive elimination steps have been studied extensively experimentally and theoretically, the mechanism of these two steps is well understood and they are common in all transition metal catalysed cross-coupling reactions of organometallics. Less is known about the transmetallation step and it is different from one catalytic cycle to another[61]. This step is highly dependent on the type of organometallic reagent used or the reaction conditions for the couplings[62]. The base such as sodium hydroxide is required for the transmetalation step in the Suzuki-Miyaura cross-coupling reaction[63]. Two pathways are generally proposed for transmetalation (**Scheme 1.19**). In path A, the base reacts with an organoboronic acid to quaternise the boron atom and form a negatively charged boronate [$Ar^2B(OH)_3^-$] which increases the nucleophilicity of the aryl group on the boron atom, and it can undergo transmetalation with the $Ar^1Pd^{II}XL_2$ complex[54]. Alternatively, in path B, the halogen in $Ar^1Pd^{II}XL_2$ complex is replaced by a negatively charged base OH^- or OR^- depending on the type of the base used. Oxo-palladium(II) complexes ($Ar^1Pd^{II}OHL_2$) or ($Ar^1Pd^{II}ORL_2$) are formed and subsequently they can react with neutral organoboronic acids[64,65].

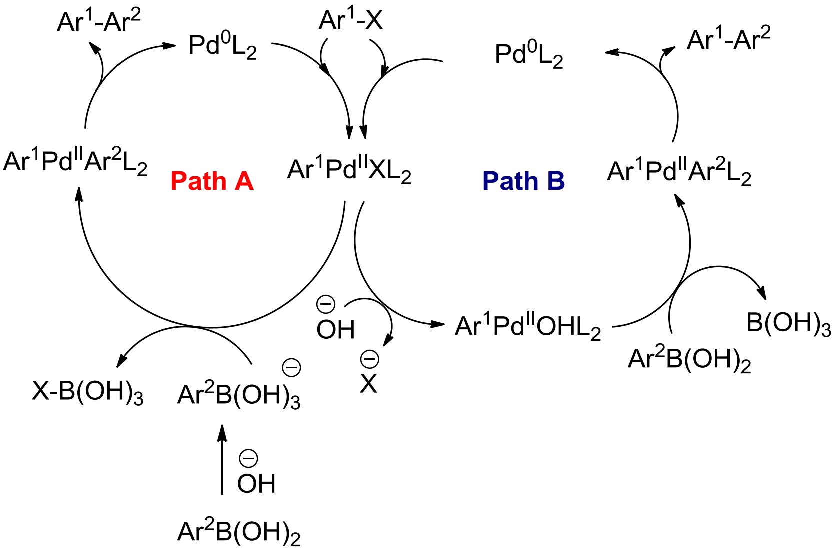

Scheme 1.19: The catalytic cycle of the Suzuki-Miyaura cross-coupling reaction

Hartwig *et al*. studied the kinetic of the transmetalation step in the Suzuki-Miyaura cross-coupling reaction[64]. They found that the rate of the transmetalation between boronate [$Ar^2B(OH)_3^-$] and $Ar^1Pd^{II}XL_2$ complex to be around four orders of magnitude slower than that between organoboronic acid and $Ar^1Pd^{II}OHL_2$. However, Electrospray ionization mass spectrometry (ESI-MS) was utilised by Aliprantis and Canary to detect the intermediates in the Suzuki-Miyaura coupling reaction[66]. In their studies two intermediates which are $[Ar^1Pd(PPh_3)_2Br]^+$ and $Ar^1PdAr^2(PPh_3)_2$ were consistently occurring but oxo-palladium intermediates such as $Ar^1PdOH(PPh_3)_2$ or $Ar^1PdOCH_3(PPh_3)_2$ were not observed.

The final step of the catalytic cycle is the reductive elimination and before this step the second isomerisation must take place[67]. $Ar^1Pd^{II}Ar^2L_2$ is formed in the trans-configuration as a result of transmetalation process. Therefore, it isomerises to cis-configuration and coupling product (Ar^1-Ar^2) is obtained and the palladium catalyst is reduced from the oxidation state of +2 to 0 and continues to the catalytic cycle.

1.3.2.5. Direct hetero (arylation) cross coupling reactions

The formation of carbon-carbon bonds between (hetero) aryl halides or pseudohalides and unfunctionalised (hetero) arenes to form hetero-hetero or biaryl molecules *via* palladium-catalysed direct hetero (arylation) has attracted significant attention (**Scheme 1.20**)[68].

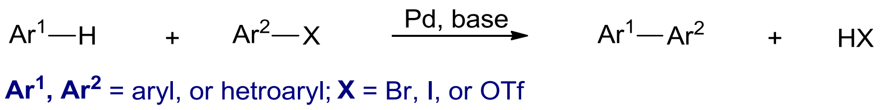

Scheme 1.20: The direct hetero (arylation) reaction

This novel reaction has recently emerged as an economically attractive and environmentally friendly alternative to traditional cross-coupling reactions[69]. These reactions as the latest developments in organic and polymer synthesis have numerous advantageous over conventional metal-catalysed cross-coupling reactions such as: 1) they do not require organometallic monomers, which are in some cases difficult to purify; 2) the byproduct is HX, which is less toxic than organotin compounds (Me_3SnX or Bu_3SnX) in the Stille reactions; 3) fewer synthetic steps; 4) lower cost and 5) in some cases higher yields[70].

P3AT was the first conjugated polymer synthesised by Lemaire and co-workers using direct heteroarylation polymerisation (DHAP)[71]. The dehydrohalogenative polycondensation of iodinated thiophene derivative (**1**) using $Pd(OAc)_2$ as a catalyst, K_2CO_3 base and stoichiometric amounts of tetra-*n*-butylammonium bromide (*n*-Bu_4NBr) gave **rr-P3AT** with low molecular weight (M_n ~ 3000 g mol^{-1}) (**Scheme 1.21**).

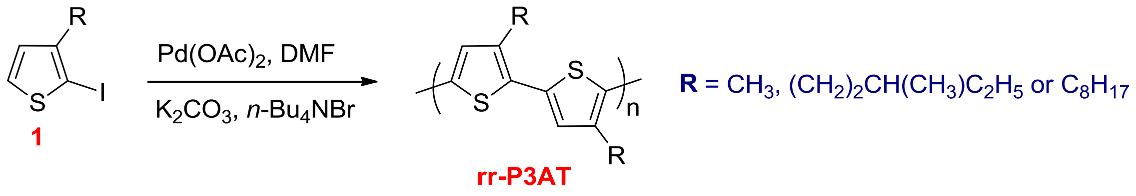

Scheme 1.21: The synthesis of **rr-P3AT** *via* DHAP

Ozawa and co-workers have synthesised higher molecular weight **P3HT** (M_n up to 30000 g mol^{-1}) with high regioregularity of 98% from 2-bromo-3-hexylthiophene (**1**) using Herrmann's catalyst and P(C_6H_4-*o*-NMe_2)$_3$ as a ligand (**Scheme 1.22**)[72].

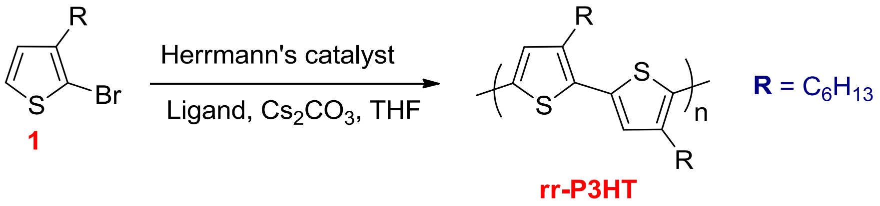

Scheme 1.22: The synthesis of **rr-P3HT** *via* DHAP

The mechanism of the Pd-catalysed direct arylation reaction has been studied experimentally and theoretically and several pathways have been proposed. Concerted Metallation-Deprotonation (CMD) is a more recent mechanistic pathway that has received much support[73,74,75]. The catalytic cycle for coupling of aryl halide (Ar^1-X) and arene (Ar^2-H) using Pd-phosphine catalytic system, stoichiometric amounts of pivalic acid as an additive and cesium carbonate base is depicted in scheme 1.23[76]. The first step in the catalytic cycle is the oxidative addition which is similar to that of Stille and Suzuki coupling reactions. In the second step, a halogen atom and one phosphine ligand are replaced by pivalate anion to form complex **1**. The pivalate anion functions as a proton shuttle in this complex which abstracts a proton from Ar^2-H and concurrently Pd-C bond is formed *via* transition state (**TS-1**)[77]. This transition state is transformed to biaryl palladium complex (**2**) and followed by exchange of the pivalic acid by phosphine ligand to create biaryl palladium diphosphine complex (**3**). Finally, the coupled product (Ar^1-Ar^2) is formed from the latter complex and the palladium catalyst is regenerated and re-enters the catalytic cycle.

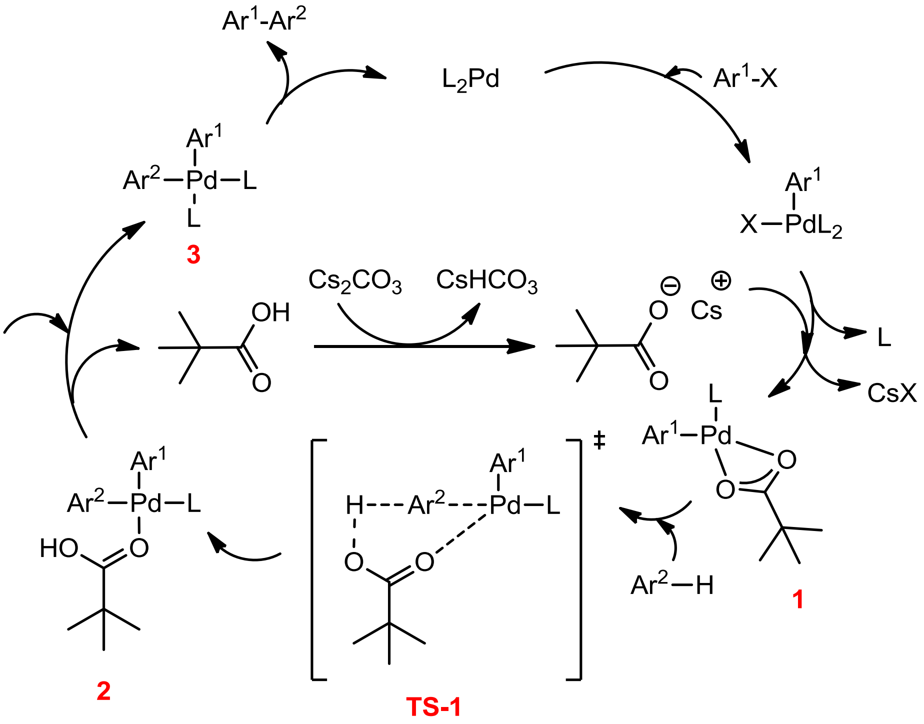

Ar^1, **Ar^2** = aryl; **X** = Br, I, or OTf**;** **L** = phosphine ligand

Scheme 1.23: The catalytic cycle of the DHAP

1.3.3. Yamamoto coupling reactions

A variety of conjugated polymers such as polyfluorenes, polyphenylenes, polycarbazoles and polythiophenes have been prepared by Yamamoto coupling reactions[78]. The reaction is carried out through dehalogenation polycondensation of dihalide monomer in the presence of zero-valent nickel complex such as $Ni(COD)_2$ as a catalyst and COD as a neutral ligand. Poly(*N*-alkyl-3,6-carbazole)s (**2**) were successfully synthesised by this method from *N*-alkyl-3,6-dibromocarbazoles (**1**) as starting materials (**Scheme 1.24**)[79].

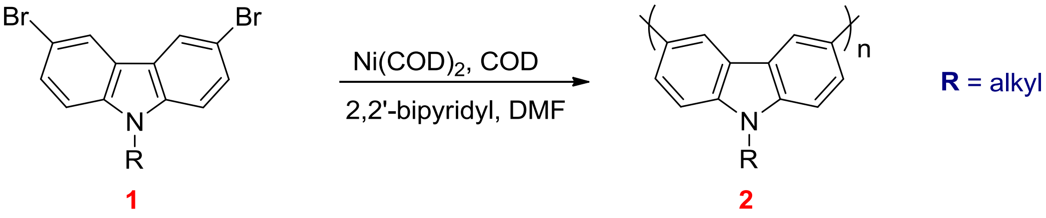

Scheme 1.24: The synthesis of polycarbazoles by Yamamoto reaction

The polymers which are prepared by this method have high molecular weights. The main drawbacks of the Yamamoto coupling reaction are that stoichiometric amounts of the catalyst must be used and the instability of the catalysts which are used.

1.3.4. Condensation polymerisation methods

These types of polymerisation are widely used for synthesising arylenevinylene polymers and copolymers. Poly(*p*-phenylene vinylene) (**PPV**) and its derivatives, Poly[2-methoxy-5-(2-ethylhexyloxy)-1,4-phenylenevinylene] (**MEH-PPV**) and Poly[2-methoxy-5-(3',7'-dimethyloctyloxy)-1,4-phenylenevinylene] (**MDMO-PPV**), can be prepared by condensation polymerisations. Wessling and Gilch are the two most common types for condensation polymerisations.

1.3.4.1. Wessling route

This route will be described in the chapter two.

1.3.4.2. Gilch method

Up to date, the ultimate versatile route for the synthesis of dialkoxy-substituted **PPV** derivatives is known as Gilch method. The most extensively studied **PPV** derivatives is **MEH-PPV** which has been synthesised by this method[80]. 1,4-Dihalo-2,5-dialkoxy-*p*-xylene (**1**) is polymerised with large excess of base such as potassium *tert*-butoxide (*t*-BuOK) in THF (**Scheme 1.25**).

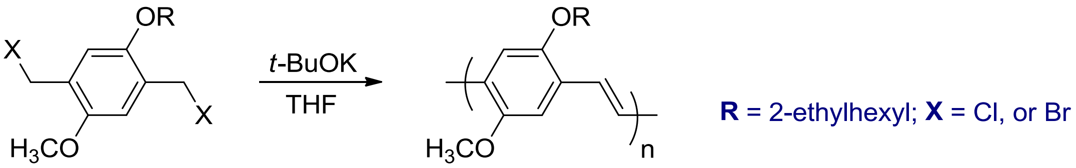

1

MEH-PPV

Scheme 1.25: Gilch method for preparation of **MEH-PPV**

1.4. Applications of conjugated polymers

Organic semiconducting materials are a promising alternate to inorganic semiconducting materials. The development of organic semiconductors has potential applications in optoelectronic devices like light-emitting diodes (LEDs)[81,82], field effect transistors (FETs)[83,84] and photovoltaics (PVs)[85,86].

1.4.1. Organic light emitting diodes (OLEDs)

Electroluminescence was discovered for anthracene by Pope *et al.* in 1963[87]. In 1987, Tang and VanSlyke demonstrated an effective electroluminescence in organic small molecules in a bilayer device with 1% external quantum efficiency[88]. In 1990, Burroughes *et al.* developed the first OLED using a semiconducting polymer, **PPV** which is called Polymer Light-Emitting Diode (PLED)[82]. The typical OLED comprises of one or more organic layers sandwiched between two electrodes[89]. A schematic illustration of a typical bilayer OLED is displayed in figure 1.6.

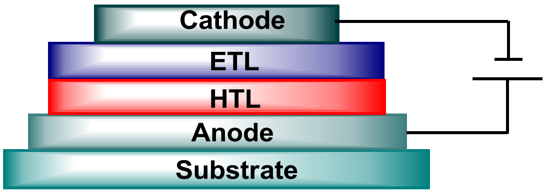

Figure 1.6: A typical bilayer OLED

Indium tin oxide (ITO), which is a transparent conducting oxide (TCO), coated on glass substrate or flexible polymer is frequently used as the anode and it has a high work function. Low work function metals like calcium, magnesium or aluminum are commonly utilised as the cathode[90]. One of the organic layers is a hole transport layer (HTL) and the other one is an electron transport layer (ETL), one of the two layers must be emissive. HTL has low ionisation potential (IP) but ETL has high electron affinity (EA). The operation process of two layer OLED[91] is illustrated in figure 1.7. When a forward voltage is applied across the device, electrons and holes are injected from the cathode and anode into the LUMO and HOMO of ETL and HTL, respectively. They are transported into the HTL/ETL interface and recombine to form excitons. Subsequently, they may decay radiatively to produce light emission[91].

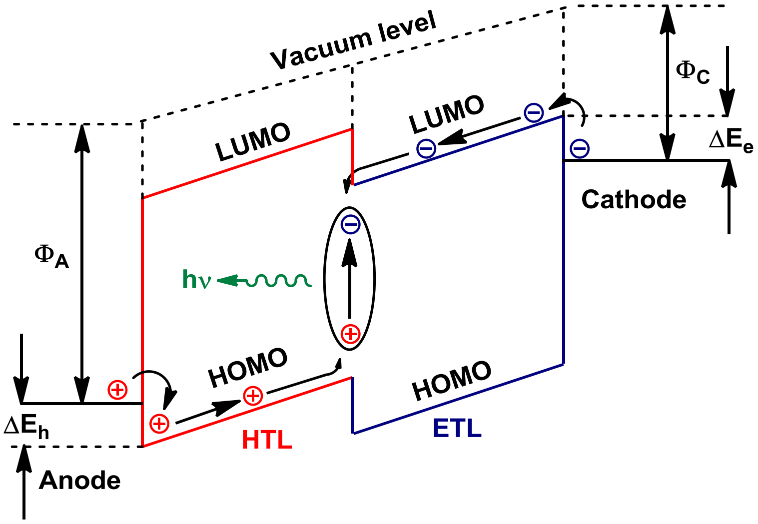

Figure 1.7: The Energy level diagram and the operation of two-layer OLED. Φ_c and Φ_A are abbreviations of the work functions of the cathode and anode electrodes, respectively. ΔE_e and ΔE_h are the electron and the hole injection barriers, respectively.

A variety of conjugated polymers has been investigated for light emitting diode applications such as poly(*p*-phenylene) (**PPP**)[92], polythiophenes (**PT**)s[93,94], polycarbazoles (**PCz**)s[95] and polyfluorenes (**PF**)s[96]. The colour of emission depends upon the band gap of the conjugated polymer light emitting materials, which emit light from ultraviolet to near infrared.

1.4.2. Organic Field Effect Transistors (OFETs)

Typical OFETs are composed of gate electrode, insulating layer, organic semiconducting layer, the source and drain electrodes (**Figure 1.8**)[97]. When a sufficient gate-source voltage (V_{GS}) is applied between gate and source electrodes, charge carriers are formed and accumulated at organic semiconducting/dielectric interface. As a result, a channel is generated and by applying a source-drain voltage (V_{SD}), these charges are transported and a current flows from source to drain electrode. This state of the OFET device is called on, while $V_{GS} = 0$, OFET is termed off[83].

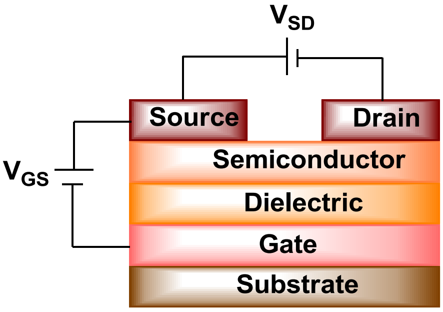

Figure 1.8: The OFET device configuration

The types of the charge carriers formed in OFETs depend on the sign of V_{GS}. When negative potential ($V_{GS} < 0$) is applied, the holes are generated and the type of organic semiconductor is called p-type. However, when positive voltage is biased ($V_{GS} > 0$) the electrons are formed and the type of organic semiconductor is designated as n-type. In addition, in a few cases organic semiconductors are able to transport both electrons and holes, which are considered as ambipolar[98].

Three kinds of π-conjugated materials have been used in OFETs such as small molecules[99], oligomers[100] and polymers[99]. They should have good stability, high charge carrier mobility and low cost for production and device fabrication.

Polythiophenes are frequently utilised in OFET devices. Unsubstituted polythiophene (**PT**) was used for the first time as semiconducting material in polymer field effect transistor (PFET) in 1986 by Ando and co-workers[101]. It showed a charge carrier mobility of 10^{-5} cm^2 V^{-1} s^{-1}. **rr-P3HT** showed significantly higher hole mobility compared to **ri-P3HT** (**Figure 1.5**)[102,103,104].

1.4.3. Organic photovoltaics (OPVs)

At present, most of the global energy consumption originates from fossil fuels[105]. Burning fossil fuels releases greenhouse gases such as CO_2 which has a harmful impact on the environment, causes air pollution, global warming and climate change[106]. In addition, the stock of these non-renewable energy sources is limited and cannot provide enough energy when the world’s population will increase. To solve these problems, renewable energy sources, for example hydropower, bioenergy, wind power, solar and geothermal energy have been developed in the past few decades. Harvesting solar energy and converting into electricity *via* photovoltaic (PV) technology is a promising solution to growing energy demand[107]. The power of the sunlight that strikes the surface of the earth amounts to 165000 terawatt (TW) per day and the energy of one hour is enough to provide the global energy consumption in an entire year[108,109,110].

The first inorganic crystalline silicon solar cell with efficiency of 6% was reported in 1954 by Chapin and co-workers[111]. Currently, single junction crystalline silicon solar cells dominate the photovoltaic technology and have reached efficiencies up to 25%[112,113]. The indirect band gap of silicon makes silicon-based solar cells necessitate relatively thick active layers to absorb sufficient sunlight[114]. In addition, high purity silicon crystals are required to avoid recombination losses during charge carriers transportation and collection. Furthermore, the manufacturing process requires high energy and combined with the high cost of silicon makes the silicon-based solar cell expensive. Therefore, silicon-based photovoltaics provide small amount of the global energy production.

Thus, alternative semiconducting materials have emerged during the last couple of decades in order to reduce the materials costs. Copper indium gallium diselenide (**CIGS**), cadmium telluride (**CdTe**), amorphous and nanocrystalline silicon (**a-Si** and **nc-Si**) are candidates for thin film photovoltaic devices. These inorganic materials are direct absorbers and they can absorb more photons than crystalline silicon[115]. Amorphous and nanocrystalline silicon delivered the power conversion efficiency (PCE) of 10.1%[116]. However, higher efficiencies of 16.5 and 21.5% have been reported for **CdTe** and **CIGS**, respectively[117,118]. Although, these kinds of solar cells have shown decent efficiencies, the material availability, toxicity (Cd, Te) and difficulties in controlling large scale uniform films are obstacles for widespread commercialisation.

Organic photovoltaic technology generally includes small molecules[119,120], conjugated polymers[121,122] and dye-sensitised[123,124] based solar cells. In particular, polymer photovoltaics have received substantial interest because of a number of reasons such as low cost, easy processability, mechanical flexibility, lightweight and large scale roll-to-roll (R2R) production[125,126,127]. In addition, the optoelectronic properties of the conjugated polymers could be adjusted by molecular design[128]. Furthermore, they have high absorption coefficients, therefore only 100-200 nm active layer thickness is required for adequate absorption of sunlight[129]. Although, PSCs have advanced very rapidly, their power conversion efficiencies and lifetime are still inferior compared to inorganic solar cells[130,131].

1.5. Architecture of polymer solar cells

1.5.1. Single layer

Single layer cells are the simplest device structure of organic photovoltaics containing only one organic layer between two electrodes (**Figure 1.10**)[132]. The anode is made of an ITO. The cathode is composed of a metal, for example calcium, magnesium or aluminium. The difference in the electrodes work function provides built-in electric field that is not high enough to overcome the exciton binding energy which is larger than 0.5 eV in conjugated polymers[133]. This energy is several orders of magnitude higher than that thermal energy, kT (300 K) = 0.026 eV and therefore, in such devices the electric fields are insufficient to separate the excitons into free electrons and holes[115]. **PPV** was used in single layer photovoltaic cells and provided very low external quantum efficiency (EQE) in the order of 1% and PCE lower than 0.1%[134].

1.5.2. Bilayer planar heterojunction

In a two layer planar heterojunction, acceptor and donor layers are sandwiched between the electrodes (**Figure 1.10**). The first two layer planar photovoltaic cell was developed by Tang, in which two different organic semiconductors, a donor (D) and an acceptor (A), embedded between a transparent ITO and a semitransparent metal electrode[135]. Tang's device achieved the PCE of about 1% under simulated air mass 2 (AM2) conditions. The overall improvement efficiency in bilayer devices is mainly due to the exciton dissociation at the D/A junction which is much more efficient than polymer/electrode junction in single layer devices[136,137].

The performance of bilayer devices is greatly restricted by the exciton diffusion length[138]. For most conjugated polymers, the exciton diffusion length is 4-20 nm[139,140,141]. Consequently, only the excitons that are produced near the D/A junction could be dissociated. The majority of excitons created far from the interface are lost by recombination, this leads to the low quantum efficiency and diminished the solar cell performance[142].

One of the major breakthroughs in the field of solar cell technology was the replacement of n-type material by Buckminsterfullerene (C_{60}) and its derivatives such as [6,6]-phenyl-C_{61}-butyric acid methyl ester (**$PC_{61}BM$**) and [6,6]-phenyl-C_{71}-butyric acid methyl ester (**$PC_{71}BM$**) in organic photovoltaic (OPV) devices (**Figure 1.9**).

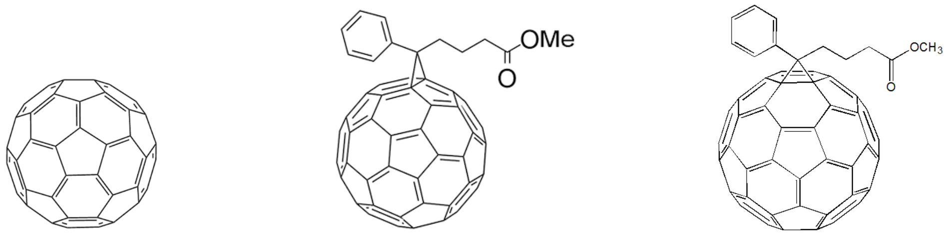

C_{60} $PC_{61}BM$ $PC_{71}BM$

Figure 1.9: The molecular structure of C_{60} and its derivatives

Fullerenes have become standard acceptors for organic solar cells due to their various advantages. First, they have deep-lying LUMO energy levels and therefore they possess high electron affinities[143]. Second, the triply degenerate C_{60} LUMO tends to reduce up to six electrons and stabilise the negative charge[144]. Third, ultrafast photoinduced electron transfer from conjugated polymers to C_{60} and its derivatives have been observed by Sariciftci *et al*. and Yoshino and co-workers independently on a time scale of (*ca*. 50 femtoseconds), which is significantly faster than any other competing photophysical methods that exist[145,146]. Finally, C_{60} derivatives also show very high electron mobilities[147].

The first bilayer heterojunction device based on conjugated polymer (**MEH-PPV**) and C_{60} reported by Sariciftci *et al*. in 1993 delivered only a PCE of 0.04% which was slightly improved compared to pristine **MEH-PPV** single layer based solar cells[148,149]. In order to overcome the exciton diffusion length limitation, a revolutionary development then came in the nineties with the introduction of bulk heterojunction (BHJ) architecture.

1.5.3. Bulk Heterojunction

This architecture was invented by Yu and co-workers in 1995, where the conjugated polymer and fullerene derivatives are blended together as the active layer of an OPV device, thus the distance that excitons migrate is dramatically reduced and concomitantly the D/A interfacial area significantly increased[150,151]. The photogenerated excitons are able to dissociate to free holes and electrons more efficiently compared to the previous architecture and thereby the efficiency of charge separation is improved leading to enhanced efficiency. Compared to the previous architecture where the A and D materials are consecutively placed on top of each other and can contact the cathode and anode electrodes selectively, the BHJ requires two channels for transporting electrons and holes to the electrodes. Thus, the D and A domains should form bicontinuous network with nanoscale morphology for efficient charge transport and collection after exciton dissociation[152]. Therefore, the BHJ devices are strongly affected by the nanomorphology of the photoactive layer (**Section 1.9**)[153].

The BHJ PSC device structure consists of several components as illustrated in figure 1.10[154]. A transparent positive electrode, typically ITO, coated on a glass substrate is commercially available. In addition, a buffer layer of poly(3,4-ethylenedioxythiophene)-polystyrenesulfonate (**PEDOT: PSS**) is placed between the ITO electrode and the photoactive layer[155]. This layer smoothens out the ITO surface and also facilitates the hole extraction[156]. The active layer is comprised of a blend of polymer D and fullerene A and coated on the top of the buffer layer. Finally, a negative electrode, such as Al, Mg or Ca employed as a cathode and evaporated. An electron transport layer (ETL) such as LiF is commonly inserted between the negative electrode and the photoactive layer[157].

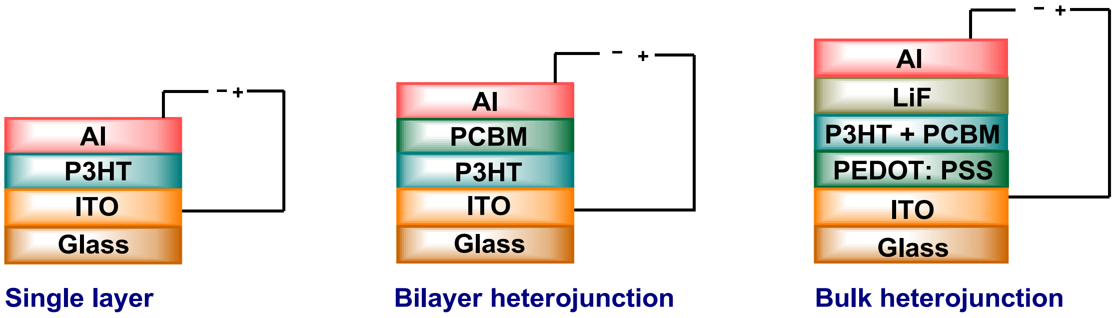

Figure 1.10: The polymer solar cell architectures

1.6. Principle work of polymer solar cells

Generally, four fundamental steps are involved in the process of charge generation from incident photons in polymer solar cells[158] (**Figure 1.11**): (a) upon the absorption of photons, electrons in the donor are promoted from the HOMO to the LUMO energy level and leaves holes in the HOMO, leading to the creation of excitons[159], (b) the excitons subsequently diffuse to the D/A interface[129], (c) the electrons are transported from the LUMO energy level of the D to the LUMO energy level of the A. The electrons and holes are on acceptor and donor phases, respectively, they are still strongly joined by coulomb attractions as a geminate pairs[160], and (d) dissociation of these geminate pairs into free holes and electrons and finally the holes and electrons migrate towards the anode and cathode electrodes through donor and acceptor domains and they are collected, respectively[161].

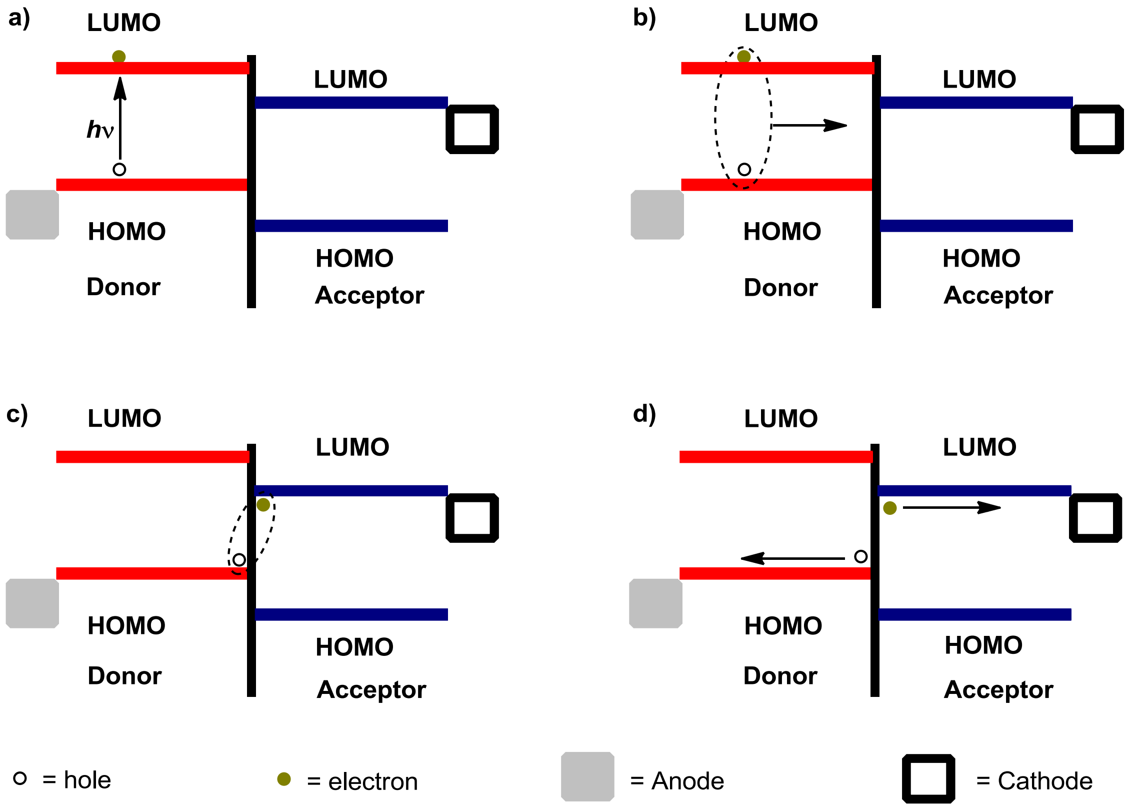

Figure 1.11: The schematic diagram for working principle of polymer solar cells

1.7. Characterisation of polymer solar cells

Typical current-voltage (*J*-*V*) characteristics for BHJ PSCs under illumination is shown in figure 1.12.

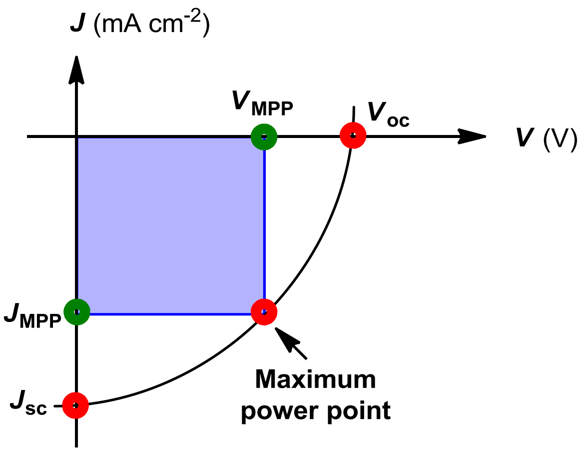

Figure 1.12: *J*-*V* curve for BHJ polymer photovoltaics

The most important performance parameters for the PSCs are short circuit current density (J_{sc}), open circuit voltage (V_{oc}), fill factor (FF) and power conversion efficiency (PCE). J_{sc} is the maximum current that a photovoltaic cell can generate under short circuit conditions. It is determined by the intersection of the graph with ordinate of the J-V curve at zero bias. V_{oc} is the maximum voltage that a photovoltaic device can produce. It is determined by the intersection of the graph in the abscissa of the J-V curve at which current is equal to zero under open circuit conditions. FF is calculated by the ratio between theoretically power outputs (V_{MPP} J_{MPP}) at maximum power point to the absolute power (V_{oc} J_{sc}) (**Equation 1.1**).

$$FF = \frac{P_{Max}}{V_{\mathrm{oc}} J_{\mathrm{sc}}} = \frac{V_{\mathrm{MPP}} J_{\mathrm{MPP}}}{V_{\mathrm{oc}} J_{\mathrm{sc}}} \quad \text{------} \quad (1.1)$$

The estimated PCE is the ratio of P_{out} to the P_{in}, where P_{out} and P_{in} are the power out and power of the incident light, respectively (**Equation 1.2**).

$$\mathrm{PCE} = \frac{P_{out}}{P_{in}} = \frac{FF\, V_{\mathrm{oc}} J_{\mathrm{sc}}}{P_{in}} \quad \text{------} \quad (1.2)$$

1.8. Designing conjugated polymers for photovoltaic applications

The first few polymers that were extensively studied for photovoltaic cells, are soluble **PPV** derivatives, for example, **MEH-PPV** developed by Wudl *et al.*[162] **MDMO-PPV** and **rr-P3HT**. The photovoltaic performance of **MEH-PPV: PC$_{61}$BM** composite showed about 1% efficiency, which was a major step of conjugated polymers for use in solar energy conversion[163]. In 2001, BHJ photovoltaic cell based on **MDMO-PPV: PC$_{61}$BM** blend achieved a benchmark PCE of 2.5%[164]. Wienk *et al.* fabricated a BHJ photovoltaic cell based on **MDMO-PPV** and **PC$_{71}$BM** that resulted in a higher PCE of 3% under AM1.5[165]. **PPV** derivatives have deep HOMO energy levels of –5.4 eV and as a result the BHJ devices can provide V_{oc} as high as 0.82 V. Further improvement for these polymers was limited because of relatively low hole mobility[166] and large band gap (*ca.* 2.0 eV) which restricted J_{sc} to 5-6 mA cm^{-2}. Therefore, the highest PCE reported for this system was 3.3% so far[167]. Benefitting from a lower E_g (*ca.* 1.9 eV) and good hole mobilities[102,168], **P3ATs** especially **rr-P3HT** have become one of the most representative organic photovoltaic polymer donors in the 2000s. In 2002, the BHJ solar cell based on **P3HT: PC$_{61}$BM** was fabricated and exhibited the maximum J_{sc} of 8.7 mA cm^{-2} which corresponded to very high external quantum efficiency (EQE) above 75% at the absorption peak. In addition, the internal quantum efficiency (IQE) close to 100% was reported for the same blend[169]. Due to extensive efforts of several groups all over the world, PCEs of around 4-5% have been reported with **P3HT: PC$_{61}$BM** blend[170,171,172,173].

The large E_g of **P3HT** (~ 1.9 eV) which can harvest only in the narrow range of the solar spectrum between 350-650 nm is one of the main factors that limits the OPV efficiency of **P3HT**, since the peak of photon flux density from the solar terrestrial radiation is positioned at ~ 1.77 eV (*ca.* 700 nm)[174,175]. In addition, it has a relatively high HOMO energy level that limits the V_{oc} to ~ 0.6 V for **P3HT: PC$_{61}$BM** based BHJ solar cells (**Figure 1.13**)[176,177].

1.8.1. Optimisation of HOMO-LUMO energy levels and Optical Band Gaps

In order to efficiently absorb solar energy, the absorption spectrum of polymer D should be optimally matched to the solar spectrum to maximise J_{sc} and hence the PCE[177,178]. Therefore, it is necessary to synthesise narrow E_g polymers with high extinction coefficients[178]. Two strategies can be used for reducing the E_g of the donor polymers. Firstly, the HOMO energy level of the D would be raised but inevitably results in decreases of V_{oc}. Since, it is demonstrated that the V_{oc} is proportional to the energy difference between the LUMO of the A and the HOMO of the D (**Figure 1.13**)[179,180,181]. Alternatively, the LUMO level of the polymer would be lowered but the ΔE_{LUMO}, which is difference between LUMO levels of polymer and fullerene, should be in the range of 0.3-0.5 eV that is higher than the exciton binding energy to provide efficient electron-hole pair dissociation at the polymer/fullerene interface and to promote charge carrier separation (**Figure 1.13**)[182,183,128]. However, this energy offset in **P3HT: PC$_{61}$BM** system is too large and results in lost energy[177].

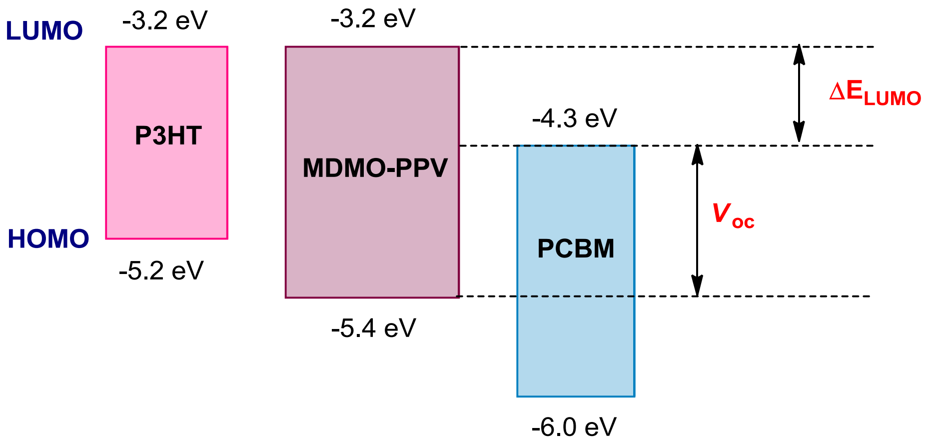

Figure 1.13: The band structures of **P3HT** and **MDMO-PPV** relative to **PCBM**

The LUMO energy level of an ideal polymer should be between –3.7 and –4.0 eV when **$PC_{61}BM$** is used as the acceptor (LUMO ~ –4.3 eV)[184]. In addition, the polymer must have good air stability with low-lying HOMO level which would help to exhibit a higher V_{oc} and a higher PCE in the BHJ photovoltaic device. Therefore, the HOMO level of the ideal polymer should be between –5.2 and –5.8 eV and the optimal band gap should be between 1.2 and 1.9 eV[184]. Furthermore, the ideal polymer should have a high hole mobility in order to increase J_{sc} and FF[160,185]. Moreover, the ideal polymer should have an appropriate solubility in organic solvents for solution processability with fullerene acceptor in fabrication of the BHJ photovoltaic devices. Finally, the ideal polymer should form an optimised morphology with fullerene acceptor in the active layer with a bicontinuous network on a nanoscale to enhance the J_{sc} and FF of the polymer solar cell device[186].

1.8.2. Strategies for Band Gap Tuning

Tuning the E_g, the LUMO and HOMO levels of polymer and fullerene derivatives are one of the significant parameters to achieve high efficiency organic photovoltaic cells. The E_g of the conjugated polymer is described as the energy difference between the LUMO and HOMO levels and influenced by several factors: bond length alternation energy (E^{BLA}), aromatic resonance energy (E^{res}), torsional angle energy (E^{θ}), substituents energy (E^{sub}), and intermolecular interactions energy (E^{int}) (**Equation 1.3**)[187,188].

$$E_g = E^{BLA} + E^{res} + E^{\theta} + E^{sub} + E^{int} \qquad \text{------} \quad (1.3)$$

These parameters are outlined in figure 1.14.

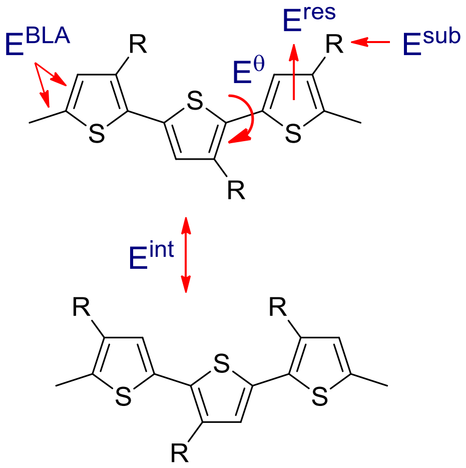

Figure 1.14: The parameters that affect the band gap of the polymer

$\mathbf{E^{BLA}}$ represents the major contribution to the band gap and it is the difference between single and double bond lengths[189]. Minimizing the BLA can be achieved by increasing the quinoid form along the conjugated polymer chain and consequently the E_g is reduced.

$\mathbf{E^{res}}$ is associated to the aromatic resonance energy of the conjugated polymers that contain aromatic monomers and it can be explained as the difference between the π-energy of the aromatic conjugated polymer and a structure with localised single and double bonds. Low E^{res} leads to a narrow band gap polymer[182].

$\mathbf{E^{\theta}}$ is related to the torsional angle (θ) between adjacent aromatic units and one useful strategy to minimise this angle is by increasing the planarity of the conjugated backbone. Planarisation can be achieved by reducing the steric hinderance between adjacent units. For example, **rr-P3ATs** adopt more planar structure and give a high delocalization of the π-electrons and as a result they have a low band gap. However, in **ri-P3ATs** the alkyl side chains twist the backbone and decrease the conjugation length and consequently increase the band gap (**Figure 1.5**)[190].

$\mathbf{E^{sub}}$ is the influence on the LUMO and HOMO levels of the polymer by substituents. These levels of the polymers could be altered by introducing electron donating (ED) or electron withdrawing (EW) substituents, respectively. ED substituents, such as alkyl or alkoxy groups elevate the HOMO level. However, EW substituents such as CN or NO_2 lower the LUMO level[175]. Raising the HOMO and lowering the LUMO levels leads to reducing the band gap of the polymer[191].

$\mathbf{E^{int}}$ is determined by intermolecular interactions between the polymer backbones. In the solid phase the chains are more ordered than in solution and consequently reducing the band gap[192].

One of the most efficient strategies to narrow the band gap is stabilising the quinoid structure of the conjugated polymer backbone. Polythiophene (**PT**) has a large band gap (~ 2 eV) because it has a pronounced single bond character between the thiophene repeating units and hence large $\mathbf{E^{BLA}}$[193]. One effective method to decrease the E_g of **PT** is the fusion of thiophene moiety at the 3,4-positions with another aromatic unit that has higher resonance energy ($\mathbf{E^{res}}$). For example, polyisothionaphthene (**PITN**) is formed by fusion of thiophene unit ($\mathbf{E^{res}}$ = 1.26 eV) with benzene ring ($\mathbf{E^{res}}$ = 1.56 eV), the benzene ring maintains the aromaticity and synchronously thiophene unit adopts a quinoid structure (**Figure 1.15**)[194,189]. Consequently, lower the E_g of the resulting **PITN** to 1.10 eV which is around 1.0 eV lower than the corresponding **PT**[195]. Other low band gap polymers such as Poly(thieno[3,4-*b*]pyrazine) (**PTP**) (E_g = 0.95 eV), and Poly(thieno[3,4-*b*]thiophene) (**PTT**) (E_g = 0.8−0.9 eV) were similarly synthesised by fusing thiophene with other heterocyclic rings such as pyrazine and thiophene, respectively (**Figure 1.15**)[196,197,198].

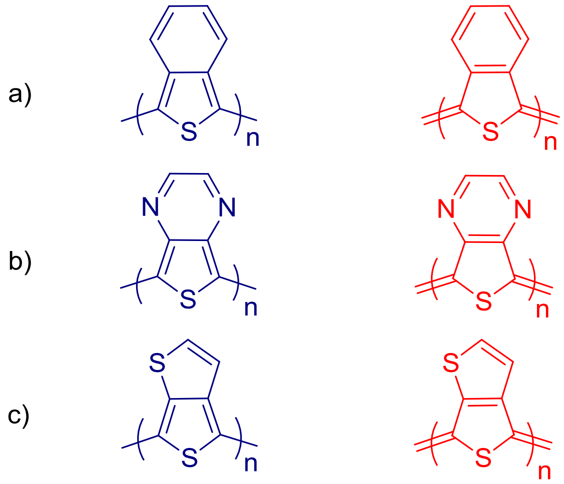

Figure 1.15: The structures of aromatic (left) and quinoid (right) forms a) **PITN** b) **PTP** and c) **PTT**

The most successful approach to reduce the E_g of the polymers is to design donor-acceptor (D-A) copolymers which contain D and A monomers[199,200,201]. The strong push–pull driving force facilitates electron delocalization through intramolecular charge transfer (ICT) from D monomer to A monomer[202]. Consequently, the double bond character is increased between the donor and acceptor units and reduces the $\mathbf{E^{BLA}}$, leading to narrow the band gap[203]. According to molecular orbital theory, the HOMO level of the D unit hybridises with the HOMO level of the A unit to produce two new HOMO energy levels in D-A copolymer[204]. Similarly, the LUMO level of the D moiety mixes with the LUMO level of the A moiety to generate two new LUMO energy levels in D-A copolymer. One of the two new HOMOs and LUMOs is higher in energy than the two initial HOMOs and LUMOs and the other one is lower than them. Hence, the higher HOMO of the D moiety and lower LUMO of the A moiety leads to reduce the optical band gap (**Figure 1.16**)[205].

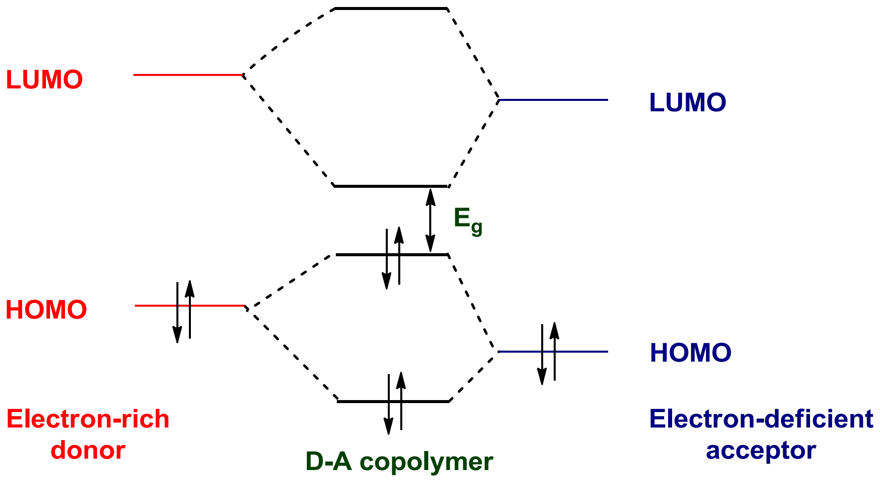

Figure 1.16: The orbital mixing between the D and the A moieties in D-A copolymer

By using this D-A approach, numerous new D-A copolymers have been developed for OPV applications with efficiencies near to or even higher than that of **P3HT** (**Table 1.1** and **Table 1.2**).

Yang and co-workers reported the **PBDTT-DTBT** copolymer containing benzo[1,2-*b*:4,5-*b'*]dithiophene (**BDT**) as a donor unit and dithienylbenzothiadiazole (**DTBT**) as an acceptor unit (**Table 1.1**)[206]. The **PBDTT-DTBT** has an E_g of 1.75 eV with a deep HOMO level of –5.31 eV. The **PBDTT-DTBT: $PC_{71}BM$** based devices exhibited a high PCE of 5.66%[206].

Yang *et al*. reported a first D-A copolymer based on alternating **BDT** as a donor building block and ester substituted thieno[3,4-*b*]thiophene (**TT**) as an acceptor moiety denoted as **PTB1** (**Table 1.1**)[207]. This copolymer was synthesised *via* Stille polymerisation and it has an E_g of 1.62 eV. The BHJ solar cells based on **PTB1: $PC_{61}BM$** showed a PCE of 4.76%. The PCE increased to 5.6% when **$PC_{71}BM$** used as the acceptor[207]. Using the same polymer backbone, the effects of substituents and chain lengths were further investigated. Yu and co-workers synthesised a series of **PTBs** (**Table 1.1**). **PTB3** was synthesised by replacing the alkoxy side chains on **BDT** moiety with alkyl chains[208]. The HOMO energy level of the resulting polymer lowered to –5.04 eV compared to –4.9 eV for **PTB1**. As a result, the V_{oc} for the polymer increased to 0.72 V and the blend of **PTB3: $PC_{61}BM$** showed a PCE of 5.85%. By the introduction of fluorine atom at the 3-position of **TT**, the new polymer (**PTB4**) synthesised with *n*-octyl side chain on the ester group and 2-ethylhexyloxy on **BDT** moiety. The HOMO energy level of the resultant polymer further lowered to –5.12 eV with respect to **PTB3**. Consequently, the V_{oc} is slightly enhanced to

0.74 V and the BHJ devices fabricated from **PTB4: PC$_{61}$BM** exhibited a higher PCE of 6.1%[208].

Table 1.1: Structures and photovoltaic performance of **PBDTT-DTBT**, **PTBs** and **PBDTTT-CF** copolymers in BHJ PSCs

Polymer	V_{oc} (V)	J_{sc} (mA cm^{-2})	FF (%)	PCE (%)	Ref.
PBDTT-DTBT 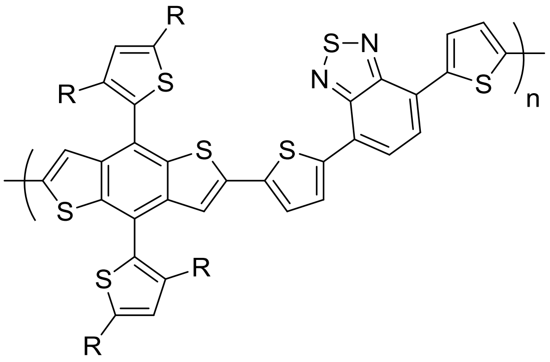 R = octyl	0.92	10.70	57.5	5.66	206
PTB1 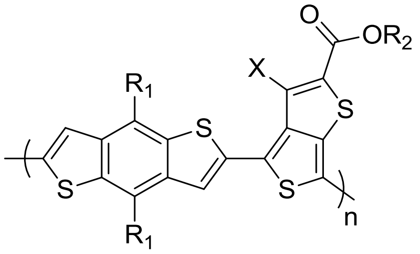 X = H, R$_1$ = octyloxy, R$_2$ = dodecyl	0.58	12.50	65.4	4.76	207
PTB3: X = H, R$_1$ = octyl, R$_2$ = 2-ethylhexyl	0.72	13.90	58.5	5.85	208
PTB4: X = F, R$_1$ = 2-ethylhexyloxy, R$_2$ = octyl	0.74	13.00	61.4	6.1	208
PTB7: X = F, R$_1$, R$_2$ = 2-ethylhexyl	0.74	14.50	68.9	7.4	209,210
PBDTTT-CF 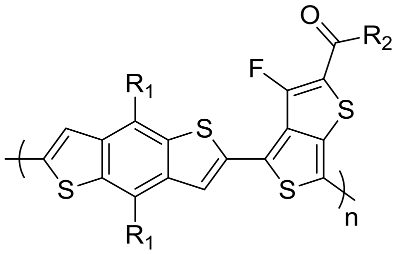 R$_1$ = 2-ethylhexyloxy, R$_2$ = heptyl	0.76	15.20	66.9	7.7	212

Yu *et al*. further developed **PTB7** using 2-ethylhexyl side chains on both **BDT** and **TT** moieties[209]. BHJ PSCs fabricated from **PTB7: $PC_{71}BM$** offered a very impressive PCE of 7.4%[209,210]. A similar polymer in the same series (**PBDTTT-CF**) reported by Li and co-workers in which the ester group on **TT** unit is replaced by a ketone group (**Table 1.1**)[211]. The higher PCE of 7.7% was obtained in devices based on **PBDTTT-CF: $PC_{71}BM$**[212].

Following these outstanding results for the **PBDTTT** copolymers, **BDT** unit copolymerised with another electron accepting unit, thieno[3,4-*c*]pyrrole-4,6-dione (**TPD**) to form **PBDTTPD** copolymers (**Table 1.2**). The first **PBDTTPD** copolymer was reported by Leclerc *et al.*[213]. They used straight alkyl chain on the **TPD** unit and branched alkoxy chains on **BDT** unit to enhance the solubility of the polymer, which was synthesised through Stille polymerisation. The resulting polymer exhibited an E_g of 1.80 eV, which is higher than that of **PBDTTT** copolymers. In addition, the **PBDTTPD** copolymers have lower HOMO energy levels than **PBDTTT** copolymers and consequently higher V_{oc} values could be expected. **PBDTTPD** blended with **$PC_{71}BM$** showed a PCE of 5.5%[213]. Soon after, Jen[214] and Frechet[215] groups have synthesised the same polymer but with higher M_n value of 33000 and 35000 g mol^{-1}, respectively than the previously reported polymer which has M_n value of 13000 g mol^{-1}. The polymer fabricated with **$PC_{71}BM$** in Jen group delivered a PCE of 4.1%[214]. Frechet group enhanced the PCE to 6.8% when the polymer blended with **$PC_{61}BM$**[215]. Xie *et al*. reported two **PBDTTPD** copolymers with two different alkoxy chains on **BDT** units and the same alkyl chain on **TPD** unit. **PBDTTPD1** and **PBDTTPD2** were synthesised with high M_n values of 43500 and 91100 g mol^{-1}, respectively and they have the same E_g of 1.84 eV (**Table 1.2**)[216]. BHJ solar cells of **PBDTTPD1** and **PBDTTPD2** with **$PC_{71}BM$** gave a PCE of 3.42 and 4.79%, respectively with V_{oc} values as high as 0.90 V[216]. Later on, a series of **PBDTTPD** copolymers was reported by Beaujuge *et al*. and they found that attaching 2-ethylhexyloxy chains on **BDT** unit and *n*-heptyl chain on **TPD** improved the performance of the polymer[217]. A remarkable PCE of 8.5% was achieved for **PBDTTPD**: **$PC_{71}BM$** blend (**Table 1.2**)[217].

Table 1.2: Structures and photovoltaic performance of **PBDTTPD** copolymers in BHJ PSCs

Polymer	V_{oc} (V)	J_{sc} (mA cm^{-2})	FF (%)	PCE (%)	Ref.
PBDTTPD 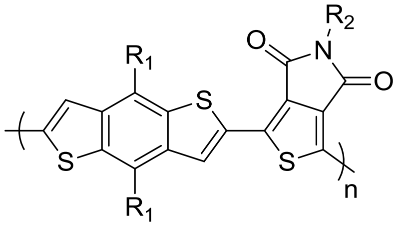 R$_1$ = 2-ethylhexyloxy, R$_2$ = octyl	0.85	9.81	66.0	5.5[a]	213
	0.84	9.80	49.5	4.1[b]	214
	0.85	11.50	68.0	6.8[c]	215
PBDTTPD1 R$_1$ = dodecyloxy, R$_2$ = 2-octyldodecyl	0.93	6.58	56.0	3.42[d]	216
PBDTTPD2 R$_1$ = 2-ethylhexyloxy, R$_2$ = 2-octyldodecyl	0.91	10.34	51.0	4.79[d]	216
PBDTTPD R$_1$ = 2-ethylhexyloxy, R$_2$ = heptyl	0.97	12.60	70.0	8.5[e]	217

[a] Leclerc *et al.*, [b] Jen group, [c] Frechet group, [d] Xie *et al.*, [e] Beaujuge *et al.*

1.9. Morphology

Even if the electron donor polymer has suitable optical and electronic properties, it must be blended with fullerene-based electron acceptor such as PCBM to form the active layer in BHJ structure. The overall efficiency of BHJ photovoltaic cells depends on the nanomorphology of the photoactive layer.

The degree of phase separation between the polymer and fullerene A is of paramount importance and ideal BHJ morphology has the domain sizes within the exciton diffusion length, which is on the orders of tens of nanometers[218]. If the domain sizes between the two components are too small, the transport of the free charge carrires will be strongly hindered due to the poorly conductive pathways for charge collection. As a result, free electrons and holes recombine before reaching their respective electrodes *via* bimolecular recombination[219]. This type of morphology is unfavorable and the PCE of the device could be low due to inefficient charge collection, which causes loss of J_{sc} and *FF*. In the case of large domains, few excitons are able to reach the polymer: fullerene interface and subsequently separate to free charge carriers. The performance of this type of morphology is limited due to insufficient exciton dissociation, which causes loss of J_{sc} and *FF* Therefore, to achieve the optimal nanomorphology of the photoactive layer controlling the degree of phase separation and feature size is essential during the fabrication of BHJ solar cells.

The nanomorphology of the photoactive layer can be affected by several processing parameters such as the choice of solvent(s) for spin casting film, thermal and solvent annealing, solvent additive and blend composition.

1.9.1. Choice of solvent(s)

The first important point is the choice of solvent(s) on the nanomorphology of polymer: PCBM film and the performance of the device. Shaheen *et al.* showed the impact of solvent on the morphology of the photoactive layer and device efficiency of the **MDMO-PPV: PC$_{61}$BM** blend film[164]. A PCE of only 0.9% was attained when toluene (TO) was used for casting the film, whereas the efficiency was dramatically increased to 2.5% when TO is replaced by chlorobenzene (CB). The size of the fullerene domains within the resulting films changes enormously with the choice of solvent[220]. For instance, Yang and co-workers observed that the size of PCBM clusters is less than 100 nm in CB-cast films, while in TO-cast films micrometre-sized PCBM-rich domains were observed[221]. Indeed, the solubility of PCBM in CB is higher than in TO. Liu and co-workers fabricated photovoltaic cells from blends of **MEH-PPV: C$_{60}$** with different solvents [CB, *o*-dichlorobenzene (DCB), xylene (XY), tetrahydrofuran (THF) and chloroform (CF)][222]. The authors claimed that the CB, DCB and XY solvents induce better contacts between the polymer and C_{60} molecules, resulted in larger J_{sc} and lower V_{oc} than using THF and CF solvents. Rispens *et al.* fabricated solar cells from **MDMO-PPV: PC$_{61}$BM** blends by changing the solvents from XY through CB to DCB and they compared the surface topology of the active layers[223]. They found that the phase separation was decreased from XY through CB to DCB. The PCE of 3% was obtained for a device made from CB with a significant improvement of J_{sc} and *FF*. The PCE of 6.1% reported for **PCDTBT** (**Scheme 4.2**) and **PC$_{71}$BM** photovoltaic cells prepared from DCB, which is higher than those devices processed from CF or CB[224]. This is probably due to DCB providing optimal phase separation relative to CF and CB solvents.

Some interesting results have been shown using mixed solvents. For example, a study on a blend of **PFDTBT** (**Scheme 3.3**) with **PC$_{61}$BM** fabricated by incorporating a small amount of CB in CF (CF: CB = 80: 1, v/v) showed a significantly enhanced J_{sc} compared with devices prepared from neat CF. However, a reduction in J_{sc} was exhibited when devices made from CF mixed with XY or TO[225]. Janssen and co-workers showed that the effect of mixed solvents on the nanomorphology of the active layers and the efficiencies of the photovoltaic devices containing low band gap polymer, **pBBTDPP2** (**Scheme 1.26**) blended with **PC$_{61}$BM**[226]. The device processed from CF: DCB (4:1, v/v) delivered the highest PCE of 3.2% than devices made from neat CF (1.1%) or DCB (2.9%). This is due to the large difference in boiling points and vapour pressures of the solvents, the evaporation rate of DCB is slow and allows the polymer to crystallise. In addition, the devices prepared from DCB alone and DCB: CF show small features less than 100 nm using atomic force microscopy (AFM) measurements of the blends, while devices processed from CF alone display large domains of several hundreds of nm. Similarly, Liu *et al.* used CF alone, DCB: CF (1:16 and 1: 4, v/v) for fabricating low band gap polymer, **pDPP** (**Scheme 1.26**) mixed with **PC$_{71}$BM**[227]. A low PCE of 1.05% was achieved when CF was used alone. The performance of the devices was significantly enhanced by gradually increasing the DCB content. The PCE was increased to 4.16% in the case of DCB: CF (1:16, v/v) and the highest PCE of 5.62% were obtained in DCB: CF (1:4, v/v). The higher performance is the result of higher J_{sc} due to improved crystallinity and morphology of **pDPP: PC$_{71}$BM** blends casting from mixed solvents.

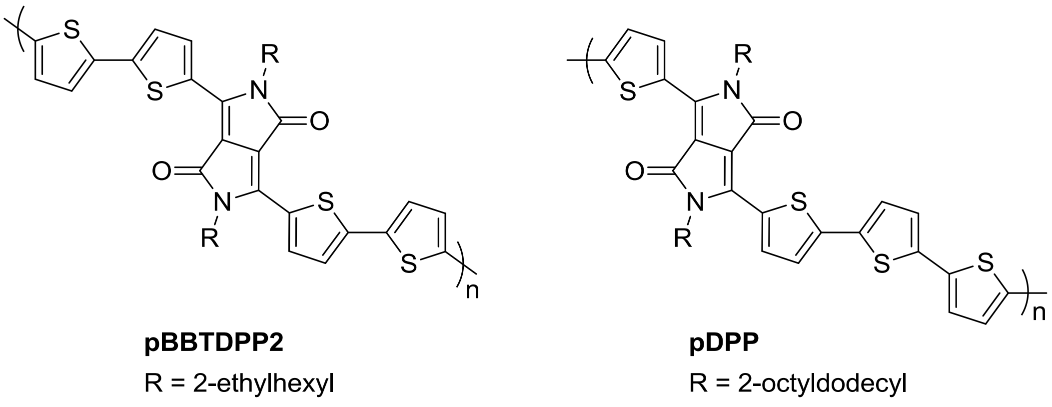

Scheme 1.26: Structures of **pBBTDPP2** and **pDPP**

1.9.2. Thermal annealing

Thermal annealing has proven to play an important role to control the nanomorphology of certain types of active layer materials. Dittmer and co-workers observed the effect of thermal treatment on **P3HT** blended with organic small molecule dye, *N,N'*-bis(1-

ethylpropyl)perylene-3,4:9,10-tetracarboxylic diimide (EP-PTC) (**Scheme 1.27**)[228]. The EQE was improved after annealing at 80 °C for one hour compared to non-annealed device. This improvement has been related to enhancement of the crystallinity of **P3HT** upon thermal annealing, which results in increased carrier mobility in the blend.

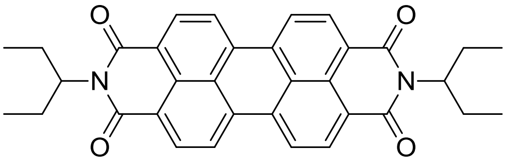

EP-PTC

Scheme 1.27: Structure of **EP-PTC**

Camaioni and co-workers reported that the efficiency of **P3HT: fulleropyrrolidine** solar cells could be increased by three to four folds under mild thermal treatment at 55 °C for 30 min[229]. Padinger *et al.* reported a postproduction treatment (after deposition of the cathode electrode) of **P3HT: PC$_{61}$BM** devices and the PCE of the device was improved to 3.5%[230]. Since then, extensive efforts have been devoted to optimising thermal annealing *via* carefully controlling temperature and time in order to improve the morphology of the photoactive layer and increase the efficiency of **P3HT: PC$_{61}$BM** devices and the PCEs around 5% were reported[171,173]. Chirvase *et al.* have studied the influence of thermal treatment on the nanomorphology and PCE of **P3HT: PC$_{61}$BM** devices[231]. They concluded that the absorption of **P3HT** is red-shifted in the blend films upon annealing the devices. Mihailetchi and co-workers also reported the similar phenomena[232]. The structural and optical properties of **P3HT: PC$_{61}$BM** composite have been investigated using grazing-incidence X-ray diffraction (GIXRD) measurements upon thermal annealing[233]. The **P3HT** backbone orientation became parallel to the substrate; however, their side chains were oriented perpendicular to the substrate after thermal annealing. In addition, upon thermal annealing fullerene molecules were redistributed and diffused into larger domains. Consequently, the absorption of **P3HT** is shifted to longer wavelengths due to increased crystallinity. A detailed investigation using transmission electron microscopy (TEM) and electron diffraction confirmed that upon thermal annealing of **P3HT: PC$_{61}$BM** blend films, the length of fibrillar crystals of **P3HT** phase was increased[234]. As a consequence, a large interfacial area was formed and the efficiency of charge generation was enhanced due to the improvement of charge transport for the blends upon annealing and yielding higher photovoltaic device efficiencies. Besides **P3HT: PC$_{61}$BM** blends, several other systems such as **PCPDTBT: PC$_{61}$BM**

(**Scheme 6.1**) and **PDTSBT: PC$_{71}$BM** (**Scheme 7.1**) have shown higher efficiencies after thermal annealing[235,236].

1.9.3. Solvent annealing

Solvent annealing (or slow growth) is another effective technique to alter the nanomorphology of the active layers. This is done by placing cast films in contact with solvents or their vapours in a partially closed container such as covered glass Petri dish, which slows the evaporation rate of the solvent[237,238,239]. Solvent annealing of **P3HT: PC$_{61}$BM** blends produce high degree of ordering of the **P3HT** chains, the crystallinity of the **P3HT** was improved and the polymer chains became self-organised[170]. As a result, the absorption of **P3HT** was shifted to lower energy region, and controlled phase separation[170]. Mihailetchi and co-workers reported that the hole mobility of **P3HT** was improved by 33-fold in **P3HT: PC$_{61}$BM** blend upon solvent annealing[240]. Li *et al.* have investigated the rate of solvent evaporation and thermal treatment on the device efficiency of **P3HT: PC$_{61}$BM** blends[170]. They found that the slow evaporation rate over 20 min period of the DCB solvent during film formation gave a PCE of 3.5%. If the evaporation time is reduced to 3 min this leads to a decrease in PCE to 2.80%. However, during fast solvent removing by heating the blend at 50 and 70 °C, the PCE was further dropped to 2.10 and 1.36%, respectively. In addition to solvent annealing, the device annealed at 110 °C for 20 min and the PCE increased to 4.37%. The improved PCE is attributed to high *FF* of 67.4% due to self-organisation of the **P3HT** chains, increased hole mobility and better balanced electron and hole transport. The effects of solvent annealing and thermal annealing on the polymer nanoscale crystallinity, absorption and the device performance of **P3HT: PC$_{71}$BM** blends have studied by Chu *et al.*[241]. Controlling the solvent-removal rate increased the molecular ordering of the **P3HT** in the blend films, as confirmed by GIXRD. The PCE of 3.80% was achieved for **P3HT: PC$_{71}$BM** after thermal annealing at 110 °C for slow grown film. The high efficiency is attributed to improved J_{sc} and *FF* due to enhanced absorption and higher charge carrier mobility, respectively. Shrotriya *et al.* have investigated the impact of self-organisation by controlling solvent-removal rate on the performance of **P3HT: PC$_{61}$BM** blends[242]. They found that the J_{sc} and *FF* were improved for slow growth process of the active layer. This enhancement is attributed to increased exciton generation and dissociation efficiency, enhanced carrier mobilities, and highly balanced charge transport.

1.9.4. Solvent additive

The utilisation of solvent additives is an alternative method to solvent and thermal annealing for controlling the nanomorphology of the photoactive layer in organic photovoltaic cells. Studies of the addition of additives to host solvent during film processing of the blend were first reported by Bazan group[243]. They demonstrated that the photoconductivity, carrier mobility and lifetime in **P3HT: $PC_{61}BM$** BHJ films were significantly increased by adding octanethiol (5% by volume) to the TO host solvent that resulted from enhanced structural order[243]. Peet *et al*. reported that after the addition of a few volume percentage of 1,8-octanedithiol (ODT) (2.5% by volume) into the **PCPDTBT: $PC_{71}BM$** system (**Scheme 6.1**), the photovoltaic device efficiency was almost doubled from 2.8 to 5.5%[244]. Soon after, Lee *et al*. showed a systematic study of the addition of 1,8-di(X)octanes (X = CN , SH, I , Br, Cl and CO_2CH_3) to CB host solvent for fabricating **PCPDTBT: $PC_{71}BM$** BHJ solar cells[245]. They found that 1,8-diiodooctane (DIO) was the best additive and the PCE of the solar cells was increased from 3.4 to 5.1%. They also demonstrated that alkanedithiols selectively dissolve the fullerene in the CB host solvent[245]. Since alkanedithiols have higher boiling points than CB, allowing the fullerene molecules to stay longer in the solution than the polymer during film processing[245]. Consequently, the morphology of thin films can be manipulated by selection of various additives and their concentrations to control the phase separation between donor and acceptor molecules[245].

Upon addition of the ODT to the **P3HT: $PC_{61}BM$** blend, the crystallinity of **P3HT** chains was increased[246]. In addition, higher hole mobility was achieved by adding octanethiol to the **P3HT: $PC_{61}BM$** composite[243]. However, no increase in hole mobility was observed using field effect transistor (FET) measurements for **PCPDTBT: $PC_{71}BM$** active layer by incorporating ODT[244]. Moreover, X-ray diffraction (XRD) data indicated that the **PCPDTBT: $PC_{71}BM$** films were amorphous with or without ODT processing[244]. Therefore, the increased device performance must result from the improved interpenetrating network, better percolation pathways for holes and electrons and also the electron mobility was significantly improved in the films when processed with ODT[247].

1.9.5. Blend composition

The blend composition of the polymer and fullerene compounds is an important parameter that influence the morphology and device performance of the system critically. In the case of **PPV** derivatives with **PCBM**, the best device performance was reported by taking a weight ratio of polymer: PCBM (1:4) to provide a suitable nanoscale phase separation between the two components, an efficient charge transport and a reduced recombination[164,248,249]. In contrast to the PPV-based devices, **P3HT: PCBM** composites require significantly lower fullerene contents for optimum photovoltaic cell efficiencies. Chirvase *et al*. have studied the influence of **P3HT: PCBM** weight ratio on the nanomorphology and the solar cell performance of **P3HT: PCBM** blends[231]. They found that the J_{sc} and EQE of the blends were significantly increased with decreasing the PCBM loading and the maximum values were attained at 50 wt% of **PCBM**. The highest PCE was achieved for device based on **P3HT: PCBM** blends (1:1, w/w). Ma *et al*. recorded a PCE of about 5% using **P3HT: PCBM** (1:0.8, w/w) active layer[173]. Shrotriya *et al*. have studied the impact of **P3HT: PCBM** weight ratio on the absorption spectra of films and the photovoltaic performance of **P3HT: PCBM** BHJ solar cells[250]. They confirmed that the absorption spectra of the films were blue-shifted about 63 and 80 nm when the amount of **PCBM** was 67 and 75 wt%, respectively. The maximum absorption wavelength for the blend was achieved with 50 wt% **PCBM**. They also found that the J_{sc} values were increased using lower amount of PCBM and the maximum value of 9.9 mA cm^{-2} was attained with **P3HT: PCBM** (1:1, w/w). The efficiency of 3.85% was obtained due to increased absorption in the low energy regions and better charge carrier transport in the **P3HT: PCBM** (1:1) composite.

1.10. Novel Acceptor Materials

As mentioned earlier, ΔE_{LUMO} would be lowered by upshifting the LUMO energy level of the fullerene in order to maximise the V_{oc} of **P3HT** based PSCs and hence increase the PCE of the device (**Figure 1.13**). Koster *et al*. have calculated the ultimate PCE of **P3HT: PC$_{61}$BM** BHJ solar cell versus ΔE_{LUMO} and band gap[183]. First, they studied the effect of lowering the ΔE_{LUMO} to 0.5 eV by raising the LUMO level of acceptor (i.e., the band gap of the **P3HT** unchanged) and the efficiency of 8.6% was predicted. This efficiency increase results from an increase of V_{oc} value. Second, the authors showed that by lowering the E_g of the **P3HT** to 1.5 eV by lowering its LUMO level (i.e., V_{oc} value unchanged) leading to an efficiency of 6.6%. This efficiency increase outcomes from enhanced the J_{sc} value. Finally, Koster and co-workers calculated the energy conversion efficiency of **P3HT: PC$_{61}$BM** BHJ solar cell to 10.8% for optimized ΔE_{LUMO}, band gap, layer thickness and high hole mobility[183].

Several novel fullerene derivatives have been developed and utilised as acceptors and tested in BHJ PSCs such as lutetium based endohedral fullerenes (**$Lu_3N@C_{80}$**), PC$_{60}$BM-bisadduct (**bisPC_{60}BM**), indene-C_{60} bisadduct (**$IC_{60}BA$**) and indene-C_{70} bisadduct (**$IC_{70}BA$**) (**Figure 1.17**)[251,252,253,254].

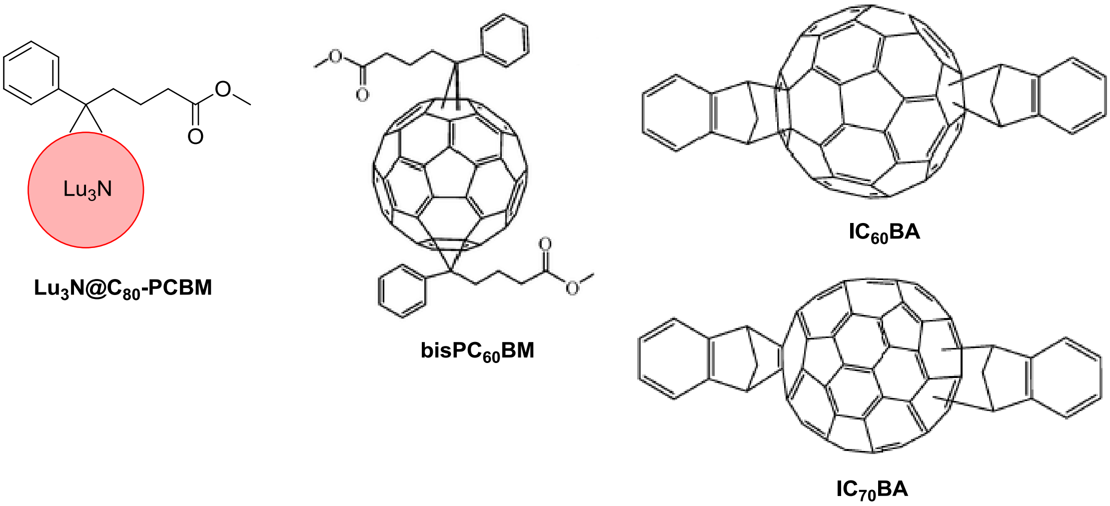

Figure 1.17: Structures of novel fullerene derivatives

In 2009, Ross *et al*. reported endohedral C_{80}-fullerene derivative (**$Lu_3N@C_{80}$-PCBM**)[251]. A PCE of **P3HT: $Lu_3N@C_{80}$-PCBM** BHJ solar cells reached 4.2% which is higher than that of **P3HT: $PC_{61}BM$** system (3.4%). Both devices had the same J_{sc} and *FF* but the former blend had a higher V_{oc} relative to the latter cell benefitting from a higher LUMO level of **$Lu_3N@C_{80}$-PCBM** than **$PC_{61}BM$**. Bisadduct analogue of PCBM (**bis$PC_{60}BM$**) has a higher LUMO energy level about 0.1 eV compared to **$PC_{61}BM$**. **P3HT: bis$PC_{60}BM$** based solar cell exhibited a higher PCE of 4.5% which is higher than that of **P3HT: $PC_{61}BM$** based solar cell (PCE of 3.8%)[252]. He *et al*. reported new bis-adduct fullerene derivative (**$IC_{60}BA$**) with stronger absorbance in the visible region compared to **$PC_{61}BM$** and the LUMO level of **$IC_{60}BA$** upshifted to –3.74 eV, which is higher than **$PC_{61}BM$**[253]. The photovoltaic devices including **P3HT: $IC_{60}BA$** showed an excellent PCE of 5.44% compared with **P3HT: $PC_{61}BM$** based polymer solar cells (PCE of 3.88%) under similar conditions. After device optimisation by the same group, the PCE of 6.5% was achieved for BHJ photovoltaic cells containing **P3HT: $IC_{60}BA$**[255]. He and co-workers further designed and synthesised new bis-adduct fullerene (**$IC_{70}BA$**) which displays stronger light absorption in the visible region than **$PC_{61}BM$**[254]. The LUMO level of **$IC_{70}BA$** is higher than that of **$PC_{61}BM$** and **$PC_{71}BM$**. Consequently, the V_{oc} and the PCE of the photovoltaic devices including **P3HT: $IC_{70}BA$** significantly improved (0.84 V, 5.64%) compared to **P3HT: $PC_{61}BM$** (0.59 V, 3.55%) and **P3HT: $PC_{71}BM$** (0.58 V, 3.96%) respectively. Sun *et al*. further optimised the devices based on **P3HT: $IC_{70}BA$** BHJ solar cells and the PCE reached 6.69%[256]. More importantly, Guo and co-workers further optimised the photovoltaic devices based on **P3HT: IC$_{70}$BA** blend and showed an impressive PCE of 7.40%[257].

1.11. Aims and Objectives

Polymer solar cells (PSCs) have received considerable attention as a renewable energy source because of their benefits such as lightweight, flexible devices, and solution processing[205]. The PCE of BHJ PSCs, where the photoactive layer involves a blend of donor and acceptor, has dramatically increased in the last few years. To achieve high PCEs with these devices, the conjugated polymer should have a deep HOMO level to increase V_{oc}, a low energy band gap in order to efficiently absorb the solar energy resulting in higher J_{sc}, a high absorption coefficient and a good hole mobility[258]. The most efficient strategy to construct low band gap polymers relies on the use of alternating D and A moieties along the backbone of conjugated polymers. Using this strategy, several kinds of D-A copolymers have shown excellent PCEs.

One of the aims of this project is to prepare novel conjugated polymers based on thermocleavable materials. Thermocleavable polymers have solubilising thermocleavable side chains such as branched alkyl chains which are attached to the conjugated polymer backbone through labile ester bonds. A thin film can be prepared from them by solution processing methods and after thermal annealing the solubilising groups are eliminated and the film becomes insoluble. Thermocleavable polymers have several advantages; firstly, they have a higher chromophore density as the nonconjugated side chains are removed after the thermal treatment. This makes these polymers possess more rigid structures and provides them with a better stability in BHJ PSCs. Secondly, the operational lifetime of the devices based on the films of these polymers for application in PSCs could be longer than those from devices based on polymers which have solubilising groups in the final film. Finally, low band gap polymers have been synthesised using this approach by donor-acceptor approach which could harvest large amounts of sunlight.

New phthalate-based thermocleavable polymers will be synthesised *via* the Stille polymerisation. **35** and **36** are two thermocleavable copolymers containing bithiophene or tetrathiophene as the donor units and secondary phthalate ester as the acceptor unit (**Scheme 1.28**). **37** is a thermocleavable copolymer which has a fluorene flanked by thienyl units as the donor building block and secondary phthalate ester as the acceptor moiety (**Scheme 1.28**). The impact of extending thiophene units and different donors will be investigated on the optical properties and molecular weight of the polymers. Upon thermal treatment, the soluble precursor polymers will be transformed into active phthalic anhydride polymers, upon cleavage of the ester groups into carboxyl groups followed by dehydration (**Scheme 1.28**). The resulting films will be completely insoluble. The photophysical and thermal properties of the polymers will be compared with each other as well as to the other thermocleavable polymers.

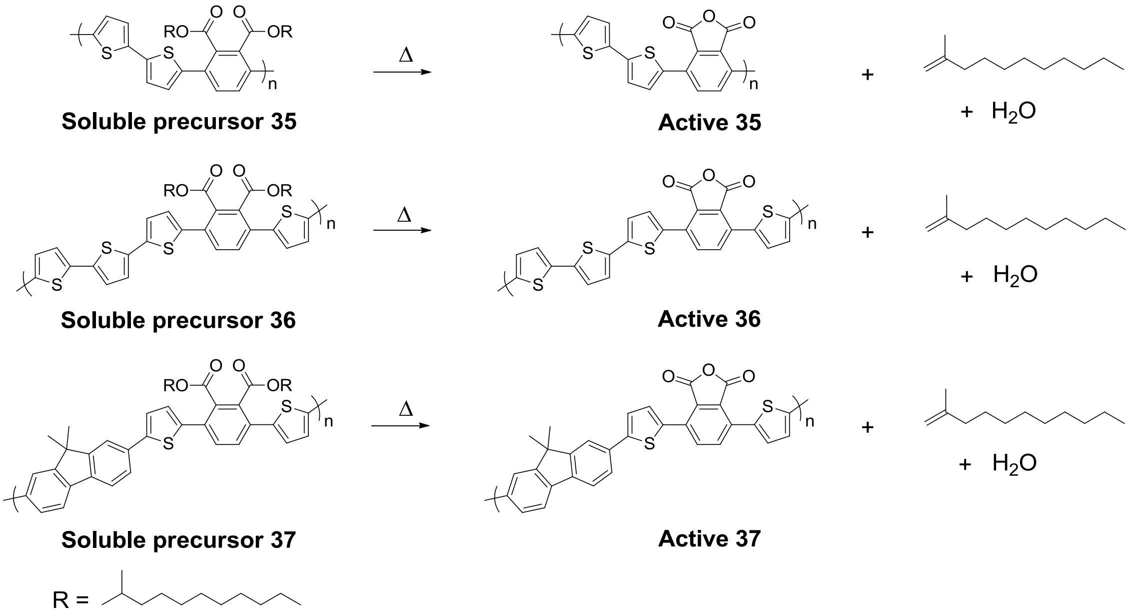

Scheme 1.28: Structures of **35**, **36** and **37** before and after thermal treatment

PFDTBT (**Scheme 3.3**) and **PDBSDTBT** (**Scheme 3.4**) are two fluorene/dibenzosilole-*alt*-benzothiadiazole donor-acceptor copolymers, which showed promising results in BHJ solar cells[225,259]. In order to prepare polymers with lower band gaps than these two polymers, new alternative polymers using benzothiadiazole dicarboxylic imide units will be targeted in this project.

The design and synthesis of fluorene/dibenzosilole-*alt*-benzothiadiazole dicarboxylic imide (**BTDI**) donor-acceptor copolymers, **76**, **77**, **78** and **79** will be undertaken (**Scheme 1.29**). All polymers will be synthesised *via* Suzuki polymerisation. The impact of attaching different substituents [3,7-dimethyloctyl (**DMO**) *vs* *n*-octyl] to the **BTDI** units upon the solubility, molecular weights, optical and electrochemical properties, thermal stability and structural properties of the resulting polymers will be studied. The photophysical and electronic properties of the polymers will be compared with each other and with those **PFDTBT**, **PDBSDTBT** and other analogues.

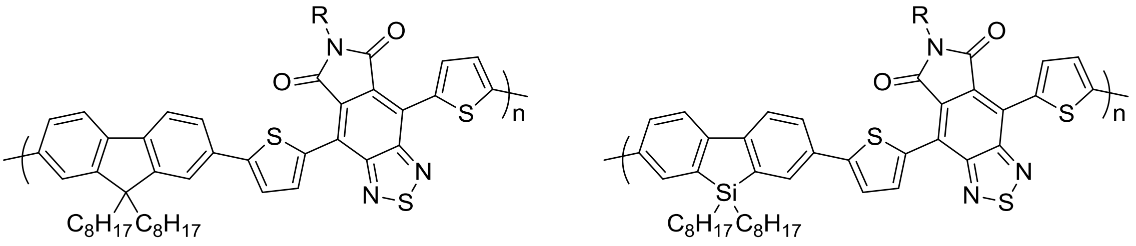

76: R = DMO
77: R = octyl

78: R = DMO
79: R = octyl

Scheme 1.29: Structures of **76**, **77**, **78** and **79**

PCDTBT (**Scheme 4.2**) is one of the most successful alternating copolymers containing 2,7-carbazole as the electron-rich moieties and benzothiadiazole as the electron-deficient moieties[260]. **PCDTBT** and **$PC_{71}BM$** in BHJ photovoltaic cells showed impressive PCE of 7.5%[263]. **O-PDFCDTBT** and **HD-PDFCDTBT** (**Scheme 4.4**) are two promising alternating D-A copolymers containing 3,6-difluoro-2,7-carbazole units and dioctyloxy substituted benzothiadiazole units[261,262]. **O-PDFCDTBT** and **HD-PDFCDTBT** blended with **$PC_{71}BM$** delivered power conversion efficiencies of 4.8 and 7.39%, respectively[261,262].

Inspired by these works, four new alternating copolymers, **104**, **105**, **106** and **107** will be designed and synthesised *via* Suzuki polymerisation (**Scheme 1.30**). The first and second copolymers contain 2,7-carbazole as the electron-rich moieties and **BTDI** as the electron-deficient moieties. Two distinct solubilising chains (3,7-dimethyloctyl *vs* *n*-octyl) attached to **BTDI** units to investigate the effects of these chains on molecular weights, optical and electrochemical properties, structural and thermal properties of the polymers. In addition, in the third and fourth copolymers two fluorine atoms are incorporated at 3,6-positions of 2,7-carbazole repeat units to investigate the influence of fluorination on the photophysical properties, the HOMO and LUMO energy levels, thermal properties and molecular ordering of the resulting polymers. The photophysical and electronic properties of the **104** and **105** will be compared with each other and with those **PCDTBT** and other analogues. In addition, the optical and electronic properties as well as molecular ordering of the **106** and **107** will be compared with each other and with those **O-PDFCDTBT**, **HD-PDFCDTBT** and other counterparts.

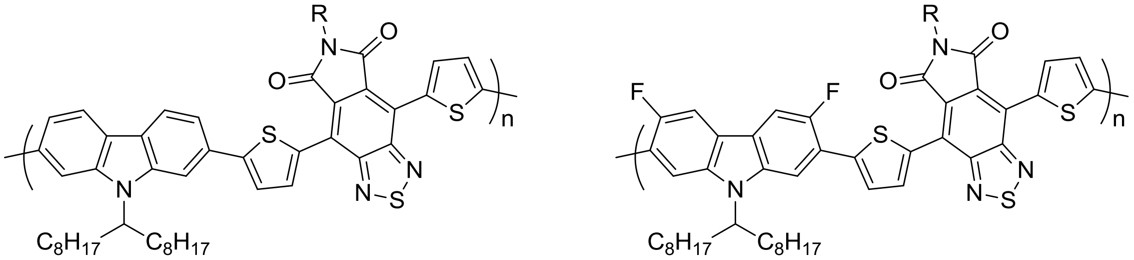

104: R = DMO
105: R = octyl

106: R = DMO
107: R = octyl

Scheme 1.30: Structures of **104**, **105**, **106** and **107**

PPATBT-8 and **PPAT2BT-8** (**Scheme 5.1**) are two promising alternating copolymers comprising 9,10-phenylanthracene flanked with two thienyl or bithienyl as the D units and dioctyloxy substituted benzothiadiazole as the A unit. These polymers were synthesised in the Iraqi group. **PPATBT-8** and **PPAT2BT-8** yielded the PCE of 3.92 and 4.17% in solar cell devices when mixed with **PC$_{71}$BM** as the acceptor, respectively[264]. Recently, anthracene-based copolymers delivered a remarkable PCE up to 8% in BHJ solar cells[265].

Inspired by these works, two new low band gap alternating copolymers, **109** and **110** will be designed and synthesised in this project (**Scheme 1.31**). The copolymers will be based on 2,6-linked anthracene as the electron-rich moieties and **BTDI** as the electron-deficient moieties. Two different alkyl chains will be anchored to the **BTDI** moieties in order to investigate the impact they have upon the molecular weights, optical and electrochemical properties, thermal stability and molecular ordering of the resulting polymers. The photophysical and electronic properties of the **109** and **110** will be compared with each other and with those of **PPATBT-8, PPAT2BT-8** and other counterparts.

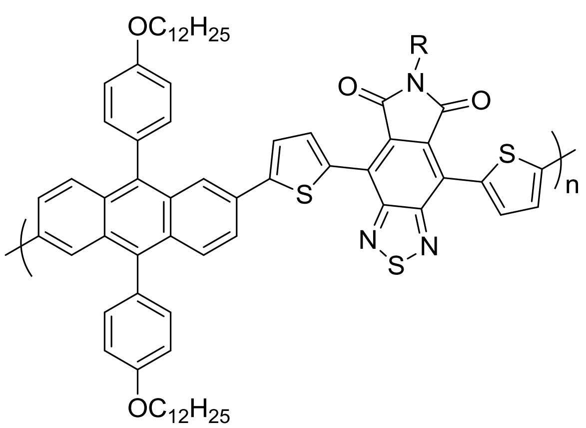

109: R = DMO
110: R = octyl

Scheme 1.31: Structures of **109** and **110**

Cyclopentadithiophene (**CPDT**) and dithienosilole (**DTS**) have attracted considerable attention as two promising donor building blocks for constructing low band gap D-A copolymers. **PCPDTBT** is one of the most popular low E_g D-A copolymers including **CPDT** as the strong D units and **BT** as the A units (**Scheme 6.1**). Photovoltaic devices comprise of **PCPDTBT: $PC_{71}BM$** blend achieved a high PCE of 5.5%[244]. CPDT-based copolymer showed an impressive PCE of 6.41% in BHJ solar cells[266].

Inspired by these works, a series of alternating copolymers comprising **CPDT** as the D moieties and **BTDI** as the A units will be designed and synthesised by different palladium catalysed cross coupling polymerisations. **134** will be synthesised by Suzuki polymerisation, while **135**, **136** and **137** will be synthesised by direct arylation polymerisation (**Scheme 1.32**). Two distinct side chains [2-ethylhexyl (**EH**) and *n*-octyl] will be anchored to the **CPDT** building blocks, whereas (3,7-dimethyloctyl and *n*-octyl**)** will be attached to **BTDI** moieties. The effects of these solubilising chains upon the solubility, molecular weights, optical properties, the HOMO and LUMO levels, thermal and structural properties of the polymers will be investigated. The photophysical and electronic properties of the polymers will be compared with each other as well as with those **PCPDTBT** and other polymer analogues.

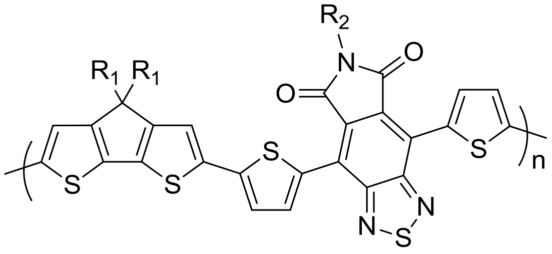

134: R_1 = EH, R_2 = DMO
135: R_1 = octyl, R_2 = DMO
136: R_1, R_2 = octyl
137: R_1 = EH, R_2 = octyl

Scheme 1.32: Structures of **134**, **135**, **136** and **137**

PDTSBT (**Scheme 7.1.**) is a low band gap copolymer including dithienosilole (**DTS**) as the strong D moiety and **BT** as the A unit. Photovoltaic devices based on **PDTSBT: $PC_{71}BM$** exhibited the high PCE of 5.1%[267]. DTS-based copolymers showed the remarkable PCE of 7.5% in BHJ solar cells[268].

Inspired by these works, two low band gap copolymers, **144** and **145** containing **DTS** as the D moieties and **BTDI** as the A units will be designed and synthesised *via* Stille polymerisation (**Scheme 1.33**). Two distinct solubilising chains will be attached to the

BTDI moieties in order to investigate the influences they have upon the solubility, molecular weights, optical and electrochemical properties, thermal stability and molecular ordering of the resulting polymers. The photophysical and electronic properties of the polymers will be compared with each other as well as with those **PDTSBT** and other polymer analogues.

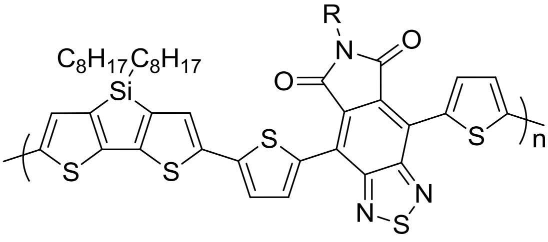

144: R = DMO
145: R = octyl

Scheme 1.33: Structures of **144** and **145**

References

1. W. R. Salaneck, R. H. Friend and J. L. Brédas, *Physics Reports*, 1999, **319**, 231-251.
2. A. J. Heeger, *Angewandte Chemie International Edition*, 2001, **40**, 2591-2611.
3. A. Moliton and R. C. Hiorns, *Polymer International*, 2004, **53**, 1397-1412.
4. A. Pron and P. Rannou, *Progress in Polymer Science*, 2002, **27**, 135-190.
5. A. G. MacDiarmid, *Angewandte Chemie International Edition*, 2001, **40**, 2581-2590.
6. C. K. Chiang, C. Fincher Jr, Y. W. Park, A. J. Heeger, H. Shirakawa, E. J. Louis, S. C. Gau and A. G. MacDiarmid, *Physical Review Letters*, 1977, **39**, 1098.
7. W. P. Su, J. Schrieffer and A. J. Heeger, *Physical Review Letters*, 1979, **42**, 1698.
8. J. Bredas, B. Themans, J. Andre, R. Chance and R. Silbey, *Synthetic Metals*, 1984, **9**, 265-274.
9. A. J. Heeger, S. Kivelson, J. Schrieffer and W.-P. Su, *Reviews of Modern Physics*, 1988, **60**, 781.
10. C. J. Brabec, V. Dyakonov, J. Parisi and N. S. Sariciftci, *Organic Photovoltaics: Concepts and Realization*, Springer Science & Business Media, 2013.
11. J. L. Bredas and G. B. Street, *Accounts of Chemical Research*, 1985, **18**, 309-315.
12. W. Feast, J. Tsibouklis, K. Pouwer, L. Groenendaal and E. Meijer, *Polymer*, 1996, **37**, 5017-5047.
13. Y. Wei, C. C. Chan, J. Tian, G. W. Jang and K. F. Hsueh, *Chemistry of Materials*, 1991, **3**, 888-897.
14. J. Heinze, B. A. Frontana-Uribe and S. Ludwigs, *Chemical Reviews*, 2010, **110**, 4724-4771.
15. R. Waltman and J. Bargon, *Canadian Journal of Chemistry*, 1986, **64**, 76-95.
16. T. Hayakawa, K. I. Fukukawa, M. Morishima, K. Takeuchi, M. Asai, S. Ando and M. Ueda, *Journal of Polymer Science Part A: Polymer Chemistry*, 2001, **39**, 2287-2295.
17. K. Yoshino, S. Nakajima and R.-i. Sugimoto, *Japanese Journal of Applied Physics*, 1987, **26**, L1038.
18. K. Yoshino, S. Hayashi and R.-i. Sugimoto, *Japanese Journal of Applied Physics*, 1984, **23**, L899.
19. Y.-J. Cheng, S.-H. Yang and C.-S. Hsu, *Chemical Reviews*, 2009, **109**, 5868-5923.

20. H. Mao, B. Xu and S. Holdcroft, *Macromolecules*, 1993, **26**, 1163-1169.

21. M. R. Andersson, D. Selse, M. Berggren, H. Järvinen, T. Hjertberg, O. Inganäs, O. Wennerström and J.-E. Österholm, *Macromolecules*, 1994, **27**, 6503-6506.

22. Y.-J. Cheng and T.-Y. Luh, *Journal of Organometallic Chemistry*, 2004, **689**, 4137-4148.

23. K. Tamao, K. Sumitani and M. Kumada, *Journal of the American Chemical Society*, 1972, **94**, 4374-4376.

24. M. Kumada, *Pure and Applied Chemistry*, 1980, **52**, 669-679.

25. K. Tamao, S. Kodama, I. Nakajima, M. Kumada, A. Minato and K. Suzuki, *Tetrahedron*, 1982, **38**, 3347-3354.

26. R. Jana, T. P. Pathak and M. S. Sigman, *Chemical Reviews*, 2011, **111**, 1417-1492.

27. T. Yamamoto, K. Sanechika and A. Yamamoto, *Journal of Polymer Science: Polymer Letters Edition*, 1980, **18**, 9-12.

28. J. W. P. Lin and L. P. Dudek, *Journal of Polymer Science: Polymer Chemistry Edition*, 1980, **18**, 2869-2873.

29. M. Kobayashi, J. Chen, T.-C. Chung, F. Moraes, A. Heeger and F. Wudl, *Synthetic Metals*, 1984, **9**, 77-86.

30. R. Elsenbaumer, K. Y. Jen and R. Oboodi, *Synthetic Metals*, 1986, **15**, 169-174.

31. R. Elsenbaumer, K. Jen, G. Miller and L. Shacklette, *Synthetic Metals*, 1987, **18**, 277-282.

32. R. D. McCullough and R. D. Lowe, *Journal of the Chemical Society, Chemical Communication*, 1992, 70-72.

33. R. D. McCullough, *Advanced Materials*, 1998, **10**, 93-116.

34. R. D. McCullough, R. D. Lowe, M. Jayaraman and D. L. Anderson, *The Journal of Organic Chemistry*, 1993, **58**, 904-912.

35. R. S. Loewe, S. M. Khersonsky and R. D. McCullough, *Advanced Materials*, 1999, **11**, 250-253.

36. R. S. Loewe, P. C. Ewbank, J. Liu, L. Zhai and R. D. McCullough, *Macromolecules*, 2001, **34**, 4324-4333.

37. E. Negishi, *Accounts of Chemical Research*, 1982, **15**, 340-348.

38. T. A. Chen and R. D. Rieke, *Journal of the American Chemical Society*, 1992, **114**, 10087-10088.

39. T.-A. Chen, X. Wu and R. D. Rieke, *Journal of the American Chemical Society*, 1995, **117**, 233-244.

40. B. Carsten, F. He, H. J. Son, T. Xu and L. Yu, *Chemical Reviews*, 2011, **111**, 1493-1528.
41. J. K. Stille, *Angewandte Chemie International Edition in English*, 1986, **25**, 508-524.
42. V. Farina and B. Krishnan, *Journal of the American Chemical Society*, 1991, **113**, 9585-9595.
43. J. Hassan, M. Sevignon, C. Gozzi, E. Schulz and M. Lemaire, *Chemical Reviews*, 2002, **102**, 1359-1470.
44. S. P. Stanforth, *Tetrahedron*, 1998, **54**, 263-303.
45. Z. Bao, W. K. Chan and L. Yu, *Journal of the American Chemical Society*, 1995, **117**, 12426-12435.
46. G. Barker, *Journal of Materials Chemistry*, 1998, **8**, 25-29.
47. A. L. Casado and P. Espinet, *Journal of the American Chemical Society*, 1998, **120**, 8978-8985.
48. P. Espinet and A. M. Echavarren, *Angewandte Chemie International Edition*, 2004, **43**, 4704-4734.
49. A. L. Casado, P. Espinet, A. M. Gallego and J. M. Martínez-Ilarduya, *Chemical Communications*, 2001, 339-340.
50. A. Nova, G. Ujaque, F. Maseras, A. Lledós and P. Espinet, *Journal of the American Chemical Society*, 2006, **128**, 14571-14578.
51. A. L. Casado, P. Espinet and A. M. Gallego, *Journal of the American Chemical Society*, 2000, **122**, 11771-11782.
52. A. Suzuki, *Journal of Organometallic Chemistry*, 1999, **576**, 147-168.
53. A. Suzuki, *Angewandte Chemie International Edition*, 2011, **50**, 6722-6737.
54. N. Miyaura, *Journal of Organometallic Chemistry*, 2002, **653**, 54-57.
55. N. Miyaura and A. Suzuki, *Chemical Reviews*, 1995, **95**, 2457-2483.
56. A. Schlüter, *Journal of Polymer Science Part A: Polymer Chemistry*, 2001, **39**, 1533-1556.
57. S. Guillerez and G. Bidan, *Synthetic Metals*, 1998, **93**, 123-126.
58. C. Amatore and A. Jutand, *Accounts of Chemical Research*, 2000, **33**, 314-321.
59. A. L. Casado and P. Espinet, *Organometallics*, 1998, **17**, 954-959.
60. A. A. Braga, G. Ujaque and F. Maseras, *Organometallics*, 2006, **25**, 3647-3658.
61. A. A. Braga, N. H. Morgon, G. Ujaque and F. Maseras, *Journal of the American Chemical Society*, 2005, **127**, 9298-9307.

62. A. A. Braga, N. H. Morgon, G. Ujaque, A. Lledós and F. Maseras, *Journal of Organometallic Chemistry*, 2006, **691**, 4459-4466.
63. K. Matos and J. A. Soderquist, *The Journal of Organic Chemistry*, 1998, **63**, 461-470.
64. B. P. Carrow and J. F. Hartwig, *Journal of the American Chemical Society*, 2011, **133**, 2116-2119.
65. R. Martin and S. L. Buchwald, *Accounts of Chemical Research*, 2008, **41**, 1461-1473.
66. A. O. Aliprantis and J. W. Canary, *Journal of the American Chemical Society*, 1994, **116**, 6985-6986.
67. L. Xue and Z. Lin, *Chemical Society Reviews*, 2010, **39**, 1692-1705.
68. P.-O. Morin, T. Bura, B. Sun, S. I. Gorelsky, Y. Li and M. Leclerc, *ACS Macro Letters*, 2014, **4**, 21-24.
69. A. Facchetti, L. Vaccaro and A. Marrocchi, *Angewandte Chemie International Edition*, 2012, **51**, 3520-3523.
70. S.-Y. Liu, M.-M. Shi, J.-C. Huang, Z.-N. Jin, X.-L. Hu, J.-Y. Pan, H.-Y. Li, A. K.-Y. Jen and H.-Z. Chen, *Journal of Materials Chemistry A*, 2013, **1**, 2795-2805.
71. M. Se, J. Papillon, E. Schulz and M. Lemaire, *Tetrahedron Letters*, 1999, **40**, 5873-5876.
72. Q. Wang, R. Takita, Y. Kikuzaki and F. Ozawa, *Journal of the American Chemical Society*, 2010, **132**, 11420-11421.
73. S. I. Gorelsky, D. Lapointe and K. Fagnou, *Journal of the American Chemical Society*, 2008, **130**, 10848-10849.
74. D. Lapointe and K. Fagnou, *Chemistry Letters*, 2010, **39**, 1118-1126.
75. L. Ackermann, *Chemical Reviews*, 2011, **111**, 1315-1345.
76. L. G. Mercier and M. Leclerc, *Accounts of Chemical Research*, 2013, **46**, 1597-1605.
77. M. Lafrance and K. Fagnou, *Journal of the American Chemical Society*, 2006, **128**, 16496-16497.
78. T. Yamamoto, A. Morita, T. Maruyama, Z. Zhou, T. Kanbara and K. Sanechika, *Polymer Journal*, 1990, **22**, 187-190.
79. Z.-B. Zhang, M. Fujiki, H.-Z. Tang, M. Motonaga and K. Torimitsu, *Macromolecules*, 2002, **35**, 1988-1990.
80. L. Akcelrud, *Progress in Polymer Science*, 2003, **28**, 875-962.

81. A. Kraft, A. C. Grimsdale and A. B. Holmes, *Angewandte Chemie International Edition in English*, 1998, **37**, 402-428.
82. J. Burroughes, D. Bradley, A. Brown, R. Marks, K. Mackay, R. Friend, P. Burns and A. Holmes, *Nature*, 1990, **347**, 539-541.
83. S. Allard, M. Forster, B. Souharce, H. Thiem and U. Scherf, *Angewandte Chemie International Edition*, 2008, **47**, 4070-4098.
84. H. Klauk, *Chemical Society Reviews*, 2010, **39**, 2643-2666.
85. C. J. Brabec, S. Gowrisanker, J. J. Halls, D. Laird, S. Jia and S. P. Williams, *Advanced Materials*, 2010, **22**, 3839-3856.
86. L. Lu, T. Zheng, Q. Wu, A. M. Schneider, D. Zhao and L. Yu, *Chemical Reviews*, 2015, **115**, 12666-12731.
87. M. Pope, H. Kallmann and P. Magnante, *The Journal of Chemical Physics*, 1963, **38**, 2042-2043.
88. C. W. Tang and S. A. VanSlyke, *Applied Physics Letters*, 1987, **51**, 913-915.
89. A. Brown, D. Bradley, J. Burroughes, R. Friend, N. Greenham, P. Burn, A. Holmes and A. Kraft, *Applied Physics Letters*, 1992, **61**, 2793-2795.
90. R. Friend, R. Gymer, A. Holmes, J. Burroughes, R. Marks, C. Taliani, D. Bradley, D. Dos Santos, J. Bredas and M. Lögdlund, *Nature*, 1999, **397**, 121-128.
91. L. Hung and C. Chen, *Materials Science and Engineering: R: Reports*, 2002, **39**, 143-222.
92. G. Grem, G. Leditzky, B. Ullrich and G. Leising, *Advanced Materials*, 1992, **4**, 36-37.
93. M. R. Andersson, M. Berggren, O. Inganäs, G. Gustafsson, J. Gustafsson-Carlberg, D. Selse, T. Hjertberg and O. Wennerström, *Macromolecules*, 1995, **28**, 7525-7529.
94. I. F. Perepichka, D. F. Perepichka, H. Meng and F. Wudl, *Advanced Materials*, 2005, **17**, 2281-2305.
95. J.-F. Morin and M. Leclerc, *Macromolecules*, 2002, **35**, 8413-8417.
96. A. Grice, D. Bradley, M. Bernius, M. Inbasekaran, W. Wu and E. Woo, *Applied Physics Letters*, 1998, **73**, 629-631.
97. C. D. Dimitrakopoulos and P. R. Malenfant, *Advanced Materials*, 2002, **14**, 99-117.
98. A. Facchetti, *Materials Today*, 2007, **10**, 28-37.
99. C. Wang, H. Dong, W. Hu, Y. Liu and D. Zhu, *Chemical Reviews*, 2011, **112**, 2208-2267.

100. G. Horowitz, *Advanced Materials*, 1998, **10**, 365-377.
101. A. Tsumura, H. Koezuka and T. Ando, *Applied Physics Letters*, 1986, **49**, 1210-1212.
102. Z. Bao, A. Dodabalapur and A. J. Lovinger, *Applied Physics Letters*, 1996, **69**, 4108-4110.
103. A. Assadi, C. Svensson, M. Willander and O. Inganäs, *Applied Physics Letters*, 1988, **53**, 195-197.
104. H. Sirringhaus, P. Brown, R. Friend, M. M. Nielsen, K. Bechgaard, B. Langeveld-Voss, A. Spiering, R. A. Janssen, E. Meijer and P. Herwig, *Nature*, 1999, **401**, 685-688.
105. N. S. Lewis and D. G. Nocera, *Proceedings of the National Academy of Sciences*, 2006, **103**, 15729-15735.
106. S. Solomon, G.-K. Plattner, R. Knutti and P. Friedlingstein, *Proceedings of the National Academy of Sciences*, 2009, pnas. 0812721106.
107. N. S. Lewis and G. Crabtree, Basic Research Needs for Solar Energy Utilization: Report of the Basic Energy Sciences Workshop on Solar Energy Utilization, 2005, 1-276.
108. R. E. Smalley, *Mrs Bulletin*, 2005, **30**, 412-417.
109. N. S. Lewis, *Science*, 2007, **315**, 798-801.
110. O. Morton, *Nature*, 2006, **443**, 19-22.
111. D. M. Chapin, C. Fuller and G. Pearson, *Journal of Applied Physics*, 1954, **25**, 676-677.
112. T. Ameri, G. Dennler, C. Lungenschmied and C. J. Brabec, *Energy & Environmental Science*, 2009, **2**, 347-363.
113. M. A. Green, K. Emery, Y. Hishikawa, W. Warta and E. D. Dunlop, *Progress in Photovoltaics: Research and Applications*, 2015, **23**, 1-9.
114. A. Shah, J. Meier, E. Vallat-Sauvain, C. Droz, U. Kroll, N. Wyrsch, J. Guillet and U. Graf, *Thin Solid Films*, 2002, **403**, 179-187.
115. B. Kippelen and J.-L. Brédas, *Energy & Environmental Science*, 2009, **2**, 251-261.
116. M. A. Green, K. Emery, Y. Hishikawa and W. Warta, *Progress in Photovoltaics: Research and Applications*, 2010, **18**, 346-352.
117. X. Wu, *Solar Energy*, 2004, **77**, 803-814.

118. J. Ward, K. Ramanathan, F. Hasoon, T. Coutts, J. Keane, M. Contreras, T. Moriarty and R. Noufi, *Progress in Photovoltaics: Research and Applications*, 2002, **10**, 41-46.

119. Y. Chen, X. Wan and G. Long, *Accounts of Chemical Research*, 2013, **46**, 2645-2655.

120. Y. Sun, G. C. Welch, W. L. Leong, C. J. Takacs, G. C. Bazan and A. J. Heeger, *Nature Materials*, 2012, **11**, 44-48.

121. J. C. Bijleveld, A. P. Zoombelt, S. G. Mathijssen, M. M. Wienk, M. Turbiez, D. M. de Leeuw and R. A. Janssen, *Journal of the American Chemical Society*, 2009, **131**, 16616-16617.

122. L. Cartwright, A. Iraqi, Y. Zhang, T. Wang and D. G. Lidzey, *RSC Advances*, 2015, **5**, 46386-46394.

123. M. Grätzel, *Nature*, 2001, **414**, 338-344.

124. Y. Bai, Y. Cao, J. Zhang, M. Wang, R. Li, P. Wang, S. M. Zakeeruddin and M. Grätzel, *Nature Materials*, 2008, **7**, 626-630.

125. F. C. Krebs, *Solar Energy Materials and Solar Cells*, 2009, **93**, 394-412.

126. F. C. Krebs, *Solar Energy Materials and Solar Cells*, 2009, **93**, 465-475.

127. F. C. Krebs, *Solar Energy Materials and Solar Cells*, 2009, **93**, 1636-1641.

128. M. C. Scharber, D. Mühlbacher, M. Koppe, P. Denk, C. Waldauf, A. J. Heeger and C. J. Brabec, *Advanced Materials*, 2006, **18**, 789-794.

129. J.-L. Brédas, J. E. Norton, J. Cornil and V. Coropceanu, *Accounts of Chemical Research*, 2009, **42**, 1691-1699.

130. M. Jørgensen, K. Norrman and F. C. Krebs, *Solar Energy Materials and Solar Cells*, 2008, **92**, 686-714.

131. M. Jørgensen, K. Norrman, S. A. Gevorgyan, T. Tromholt, B. Andreasen and F. C. Krebs, *Advanced Materials*, 2012, **24**, 580-612.

132. J. Nelson, *Current Opinion in Solid State and Materials Science*, 2002, **6**, 87-95.

133. C. J. Brabec, N. S. Sariciftci and J. C. Hummelen, *Advanced Functional Materials*, 2001, **11**, 15-26.

134. R. Marks, J. Halls, D. Bradley, R. Friend and A. Holmes, *Journal of Physics: Condensed Matter*, 1994, **6**, 1379.

135. C. W. Tang, *Applied Physics Letters*, 1986, **48**, 183-185.

136. P. W. Blom, V. D. Mihailetchi, L. J. A. Koster and D. E. Markov, *Advanced Materials*, 2007, **19**, 1551-1566.

137. H. Spanggaard and F. C. Krebs, *Solar Energy Materials and Solar Cells*, 2004, **83**, 125-146.

138. K. M. Coakley and M. D. McGehee, *Chemistry of Materials*, 2004, **16**, 4533-4542.

139. J. Halls, K. Pichler, R. Friend, S. Moratti and A. Holmes, *Applied Physics Letters*, 1996, **68**, 3120-3122.

140. T. J. Savenije, J. M. Warman and A. Goossens, *Chemical Physics Letters*, 1998, **287**, 148-153.

141. D. E. Markov, E. Amsterdam, P. W. Blom, A. B. Sieval and J. C. Hummelen, *The Journal of Physical Chemistry A*, 2005, **109**, 5266-5274.

142. S. Günes, H. Neugebauer and N. S. Sariciftci, *Chemical Reviews*, 2007, **107**, 1324-1338.

143. P. Allemand, A. Koch, F. Wudl, Y. Rubin, F. Diederich, M. Alvarez, S. Anz and R. Whetten, *Journal of the American Chemical Society*, 1991, **113**, 1050-1051.

144. N. Martín, L. Sánchez, B. Illescas and I. Pérez, *Chemical Reviews*, 1998, **98**, 2527-2548.

145. N. Sariciftci, L. Smilowitz, A. J. Heeger and F. Wudl, *Science*, 1992, **258**, 1474-1476.

146. S. Morita, A. A. Zakhidov and K. Yoshino, *Solid State Communications*, 1992, **82**, 249-252.

147. T. B. Singh, N. Marjanović, G. Matt, S. Günes, N. Sariciftci, A. M. Ramil, A. Andreev, H. Sitter, R. Schwödiauer and S. Bauer, *Organic Electronics*, 2005, **6**, 105-110.

148. N. Sariciftci, L. Smilowitz, A. Heeger and F. Wudl, *Synthetic Metals*, 1993, **59**, 333-352.

149. N. Sariciftci, D. Braun, C. Zhang, V. Srdanov, A. Heeger, G. Stucky and F. Wudl, *Applied Physics Letters*, 1993, **62**, 585-587.

150. G. Yu, J. Gao, J. C. Hummelen, F. Wudl and A. J. Heeger, *Science*, 1995, **270**, 1789.

151. H. Hoppe and N. S. Sariciftci, *Journal of Materials Research*, 2004, **19**, 1924-1945.

152. G. Dennler, M. C. Scharber and C. J. Brabec, *Advanced Materials*, 2009, **21**, 1323-1338.

153. R. Po, M. Maggini and N. Camaioni, *The Journal of Physical Chemistry C*, 2009, **114**, 695-706.

154. H. J. Son, B. Carsten, I. H. Jung and L. Yu, *Energy & Environmental Science*, 2012, **5**, 8158-8170.

155. L. Groenendaal, F. Jonas, D. Freitag, H. Pielartzik and J. R. Reynolds, *Advanced Materials*, 2000, **12**, 481-494.

156. S. Kirchmeyer and K. Reuter, *Journal of Materials Chemistry*, 2005, **15**, 2077-2088.

157. T. L. Benanti and D. Venkataraman, *Photosynthesis Research*, 2006, **87**, 73-81.

158. W. Cai, X. Gong and Y. Cao, *Solar Energy Materials and Solar Cells*, 2010, **94**, 114-127.

159. H. J. Son, F. He, B. Carsten and L. Yu, *Journal of Materials Chemistry*, 2011, **21**, 18934-18945.

160. B. C. Thompson and J. M. Frechet, *Angewandte Chemie International Edition*, 2008, **47**, 58-77.

161. N. Yeh and P. Yeh, *Renewable and Sustainable Energy Reviews*, 2013, **21**, 421-431.

162. Wudl, F.; Srdanov, G. In *US Patent 5189136 (1990) Chem*, Abstr, 1993; 255575.

163. V. Shrotriya, E. H.-E. Wu, G. Li, Y. Yao and Y. Yang, *Applied Physics Letters*, 2006, **88**, 064104.

164. S. E. Shaheen, C. J. Brabec, N. S. Sariciftci, F. Padinger, T. Fromherz and J. C. Hummelen, *Applied Physics Letters*, 2001, **78**, 841-843.

165. M. M. Wienk, J. M. Kroon, W. J. Verhees, J. Knol, J. C. Hummelen, P. A. van Hal and R. A. Janssen, *Angewandte Chemie*, 2003, **115**, 3493-3497.

166. C. Melzer, E. J. Koop, V. D. Mihailetchi and P. W. Blom, *Advanced Functional Materials*, 2004, **14**, 865-870.

167. C. J. Brabec, S. E. Shaheen, C. Winder, N. S. Sariciftci and P. Denk, *Applied Physics Letters*, 2002, **80**, 1288-1290.

168. H. Sirringhaus, N. Tessler and R. H. Friend, *Science*, 1998, **280**, 1741-1744.

169. P. Schilinsky, C. Waldauf and C. J. Brabec, *Applied Physics Letters*, 2002, **81**, 3885-3887.

170. G. Li, V. Shrotriya, J. Huang, Y. Yao, T. Moriarty, K. Emery and Y. Yang, *Nature Materials*, 2005, **4**, 864-868.

171. M. Reyes-Reyes, K. Kim and D. L. Carroll, *Applied Physics Letters*, 2005, **87**.

172. M. D. Irwin, D. B. Buchholz, A. W. Hains, R. P. Chang and T. J. Marks, *Proceedings of the National Academy of Sciences*, 2008, **105**, 2783-2787.

173. W. Ma, C. Yang, X. Gong, K. Lee and A. J. Heeger, *Advanced Functional Materials*, 2005, **15**, 1617-1622.

174. L. Dou, J. You, Z. Hong, Z. Xu, G. Li, R. A. Street and Y. Yang, *Advanced Materials*, 2013, **25**, 6642-6671.

175. B. C. Thompson, Y.-G. Kim, T. D. McCarley and J. R. Reynolds, *Journal of the American Chemical Society*, 2006, **128**, 12714-12725.

176. J. Hou, Z. a. Tan, Y. Yan, Y. He, C. Yang and Y. Li, *Journal of the American Chemical Society*, 2006, **128**, 4911-4916.

177. Y. Li, *Accounts of Chemical Research*, 2012, **45**, 723-733.

178. G. Li, R. Zhu and Y. Yang, *Nature Photonics*, 2012, **6**, 153-161.

179. C. J. Brabec, A. Cravino, D. Meissner, N. S. Sariciftci, T. Fromherz, M. T. Rispens, L. Sanchez and J. C. Hummelen, *Advanced Functional Materials*, 2001, **11**, 374-380.

180. F. B. Kooistra, J. Knol, F. Kastenberg, L. M. Popescu, W. J. Verhees, J. M. Kroon and J. C. Hummelen, *Organic Letters*, 2007, **9**, 551-554.

181. A. Gadisa, M. Svensson, M. R. Andersson and O. Inganäs, *Applied Physics Letters*, 2004, **84**, 1609-1611.

182. R. Kroon, M. Lenes, J. C. Hummelen, P. W. Blom and B. De Boer, *Polymer Reviews*, 2008, **48**, 531-582.

183. L. J. A. Koster, V. D. Mihailetchi and P. W. M. Blom, *Applied Physics Letters*, 2006, **88**, 093511.

184. N. Blouin, A. Michaud, D. Gendron, S. Wakim, E. Blair, R. Neagu-Plesu, M. Belletete, G. Durocher, Y. Tao and M. Leclerc, *Journal of the American Chemical Society*, 2008, **130**, 732-742.

185. X. Zhan and D. Zhu, *Polymer Chemistry*, 2010, **1**, 409-419.

186. M. T. Dang, L. Hirsch, G. Wantz and J. D. Wuest, *Chemical Reviews*, 2013, **113**, 3734-3765.

187. C. Winder and N. S. Sariciftci, *Journal of Materials Chemistry*, 2004, **14**, 1077-1086.

188. J. Roncali, *Macromolecular Rapid Communications*, 2007, **28**, 1761-1775.

189. J. Roncali, *Chemical Reviews*, 1997, **97**, 173-206.

190. I. Osaka and R. D. McCullough, *Accounts of Chemical Research*, 2008, **41**, 1202-1214.

191. E. Bundgaard and F. C. Krebs, *Solar Energy Materials and Solar Cells*, 2007, **91**, 954-985.

192. S. Ko, E. T. Hoke, L. Pandey, S. Hong, R. Mondal, C. Risko, Y. Yi, R. Noriega, M. D. McGehee and J.-L. Brédas, *Journal of the American Chemical Society*, 2012, **134**, 5222-5232.

193. H. Van Mullekom, J. Vekemans, E. Havinga and E. Meijer, *Materials Science and Engineering: R: Reports*, 2001, **32**, 1-40.

194. F. Wudl, M. Kobayashi and A. Heeger, *The Journal of Organic Chemistry*, 1984, **49**, 3382-3384.

195. N. Colaneri, M. Kobayashi, A. Heeger and F. Wudl, *Synthetic Metals*, 1986, **14**, 45-52.

196. M. Pomerantz, B. Chaloner-Gill, L. O. Harding, J. J. Tseng and W. J. Pomerantz, *Journal of the Chemical Society, Chemical Communications*, 1992, 1672-1673.

197. S. Y. Hong and D. S. Marynick, *Macromolecules*, 1992, **25**, 4652-4657.

198. G. A. Sotzing and K. Lee, *Macromolecules*, 2002, **35**, 7281-7286.

199. H. Zhou, L. Yang and W. You, *Macromolecules*, 2012, **45**, 607-632.

200. A. Ajayaghosh, *Chemical Society Reviews*, 2003, **32**, 181-191.

201. E. Havinga, W. Ten Hoeve and H. Wynberg, *Polymer Bulletin*, 1992, **29**, 119-126.

202. Y.-W. Su, S.-C. Lan and K.-H. Wei, *Materials Today*, 2012, **15**, 554-562.

203. Q. T. Zhang and J. M. Tour, *Journal of the American Chemical Society*, 1997, **119**, 5065-5066.

204. C. L. Chochos and S. A. Choulis, *Progress in Polymer Science*, 2011, **36**, 1326-1414.

205. C. Duan, F. Huang and Y. Cao, *Journal of Materials Chemistry*, 2012, **22**, 10416-10434.

206. L. Huo, J. Hou, S. Zhang, H. Y. Chen and Y. Yang, *Angewandte Chemie International Edition*, 2010, **49**, 1500-1503.

207. Y. Liang, Y. Wu, D. Feng, S.-T. Tsai, H.-J. Son, G. Li and L. Yu, *Journal of the American Chemical Society*, 2008, **131**, 56-57.

208. Y. Liang, D. Feng, Y. Wu, S.-T. Tsai, G. Li, C. Ray and L. Yu, *Journal of the American Chemical Society*, 2009, **131**, 7792-7799.

209. Y. Liang, Z. Xu, J. Xia, S. T. Tsai, Y. Wu, G. Li, C. Ray and L. Yu, *Advanced Materials*, 2010, **22**.

210. Y. Liang and L. Yu, *Accounts of Chemical Research*, 2010, **43**, 1227-1236.

211. J. Hou, H.-Y. Chen, S. Zhang, R. I. Chen, Y. Yang, Y. Wu and G. Li, *Journal of the American Chemical Society*, 2009, **131**, 15586-15587.

212. H.-Y. Chen, J. Hou, S. Zhang, Y. Liang, G. Yang, Y. Yang, L. Yu, Y. Wu and G. Li, *Nature Photonics*, 2009, **3**, 649-653.

213. Y. Zou, A. Najari, P. Berrouard, S. Beaupré, B. Réda Aïch, Y. Tao and M. Leclerc, *Journal of the American Chemical Society*, 2010, **132**, 5330-5331.

214. Y. Zhang, S. K. Hau, H.-L. Yip, Y. Sun, O. Acton and A. K.-Y. Jen, *Chemistry of Materials*, 2010, **22**, 2696-2698.

215. C. Piliego, T. W. Holcombe, J. D. Douglas, C. H. Woo, P. M. Beaujuge and J. M. Fréchet, *Journal of the American Chemical Society*, 2010, **132**, 7595-7597.

216. G. Zhang, Y. Fu, Q. Zhang and Z. Xie, *Chemical Communications*, 2010, **46**, 4997-4999.

217. C. Cabanetos, A. El Labban, J. A. Bartelt, J. D. Douglas, W. R. Mateker, J. M. Fréchet, M. D. McGehee and P. M. Beaujuge, *Journal of the American Chemical Society*, 2013, **135**, 4656-4659.

218. J. Peet, A. J. Heeger and G. C. Bazan, *Accounts of Chemical Research*, 2009, **42**, 1700-1708.

219. C. J. Brabec, M. Heeney, I. McCulloch and J. Nelson, *Chemical Society Reviews*, 2011, **40**, 1185-1199.

220. H. Hoppe, M. Niggemann, C. Winder, J. Kraut, R. Hiesgen, A. Hinsch, D. Meissner and N. S. Sariciftci, *Advanced Functional Materials*, 2004, **14**, 1005-1011.

221. X. Yang, J. K. van Duren, R. A. Janssen, M. A. Michels and J. Loos, *Macromolecules*, 2004, **37**, 2151-2158.

222. J. Liu, Y. Shi and Y. Yang, *Advanced Functional Materials*, 2001, **11**, 420.

223. M. T. Rispens, A. Meetsma, R. Rittberger, C. J. Brabec, N. S. Sariciftci and J. C. Hummelen, *Chemical Communications*, 2003, 2116-2118.

224. S. H. Park, A. Roy, S. Beaupre, S. Cho, N. Coates, J. S. Moon, D. Moses, M. Leclerc, K. Lee and A. J. Heeger, *Nature Photonics*, 2009, **3**, 297-302.

225. F. Zhang, K. G. Jespersen, C. Bjoerstroem, M. Svensson, M. R. Andersson, V. Sundström, K. Magnusson, E. Moons, A. Yartsev and O. Inganäs, *Advanced Functional Materials*, 2006, **16**, 667-674.

226. M. M. Wienk, M. Turbiez, J. Gilot and R. A. Janssen, *Advanced Materials*, 2008, **20**, 2556-2560.

227. F. Liu, Y. Gu, C. Wang, W. Zhao, D. Chen, A. L. Briseno and T. P. Russell, *Advanced Materials*, 2012, **24**, 3947-3951.

228. J. J. Dittmer, E. A. Marseglia and R. H. Friend, *Advanced Materials*, 2000, **12**, 1270-1274.

229. N. Camaioni, G. Ridolfi, G. Casalbore-Miceli, G. Possamai and M. Maggini, *Advanced Materials*, 2002, **14**, 1735-1738.

230. F. Padinger, R. S. Rittberger and N. S. Sariciftci, *Advanced Functional Materials*, 2003, **13**, 85-88.

231. D. Chirvase, J. Parisi, J. C. Hummelen and V. Dyakonov, *Nanotechnology*, 2004, **15**, 1317.

232. V. D. Mihailetchi, H. Xie, B. de Boer, L. A. Koster and P. W. Blom, *Advanced Functional Materials*, 2006, **16**, 699-708.

233. T. Erb, U. Zhokhavets, G. Gobsch, S. Raleva, B. Stühn, P. Schilinsky, C. Waldauf and C. J. Brabec, *Advanced Functional Materials*, 2005, **15**, 1193-1196.

234. X. Yang, J. Loos, S. C. Veenstra, W. J. Verhees, M. M. Wienk, J. M. Kroon, M. A. Michels and R. A. Janssen, *Nano Letters*, 2005, **5**, 579-583.

235. I. W. Hwang, C. Soci, D. Moses, Z. Zhu, D. Waller, R. Gaudiana, C. J. Brabec and A. J. Heeger, *Advanced Materials*, 2007, **19**, 2307-2312.

236. J. K. Park, J. Jo, J. H. Seo, J. S. Moon, Y. D. Park, K. Lee, A. J. Heeger and G. C. Bazan, *Advanced Materials*, 2011, **23**, 2430-2435.

237. Y. Zhao, Z. Xie, Y. Qu, Y. Geng and L. Wang, *Applied Physics Letters*, 2007, **90**, 043504.

238. S. Miller, G. Fanchini, Y.-Y. Lin, C. Li, C.-W. Chen, W.-F. Su and M. Chhowalla, *Journal of Materials Chemistry*, 2008, **18**, 306-312.

239. G. Li, Y. Yao, H. Yang, V. Shrotriya, G. Yang and Y. Yang, *Advanced Functional Materials*, 2007, **17**, 1636-1644.

240. V. D. Mihailetchi, H. Xie, B. de Boer, L. M. Popescu, J. C. Hummelen, P. W. Blom and L. J. A. Koster, *Applied Physics Letters*, 2006, **89**, 12107-12107.

241. C.-W. Chu, H. Yang, W.-J. Hou, J. Huang, G. Li and Y. Yang, *Applied Physics Letters*, 2008, **92**, 103306.

242. V. Shrotriya, Y. Yao, G. Li and Y. Yang, *Applied Physics Letters*, 2006, **89**, 063505.

243. J. Peet, C. Soci, R. Coffin, T. Nguyen, A. Mikhailovsky, D. Moses and G. C. Bazan, *Applied Physics Letters*, 2006, **89**, 252105.

244. J. Peet, J. Y. Kim, N. E. Coates, W. L. Ma, D. Moses, A. J. Heeger and G. C. Bazan, *Nature Materials*, 2007, **6**, 497-500.

245. J. K. Lee, W. L. Ma, C. J. Brabec, J. Yuen, J. S. Moon, J. Y. Kim, K. Lee, G. C. Bazan and A. J. Heeger, *Journal of the American Chemical Society*, 2008, **130**, 3619-3623.

246. Y. Yao, J. Hou, Z. Xu, G. Li and Y. Yang, *Advanced Functional Materials*, 2008, **18**, 1783-1789.

247. I.-W. Hwang, S. Cho, J. Y. Kim, K. Lee, N. E. Coates, D. Moses and A. J. Heeger, *Journal of Applied Physics*, 2008, **104**, 033706.

248. T. Martens, J. D'Haen, T. Munters, Z. Beelen, L. Goris, J. Manca, M. D'Olieslaeger, D. Vanderzande, L. De Schepper and R. Andriessen, *Synthetic Metals*, 2003, **138**, 243-247.

249. J. K. van Duren, X. Yang, J. Loos, C. W. Bulle-Lieuwma, A. B. Sieval, J. C. Hummelen and R. A. Janssen, *Advanced Functional Materials*, 2004, **14**, 425-434.

250. V. Shrotriya, J. Ouyang, R. J. Tseng, G. Li and Y. Yang, *Chemical Physics Letters*, 2005, **411**, 138-143.

251. R. B. Ross, C. M. Cardona, D. M. Guldi, S. G. Sankaranarayanan, M. O. Reese, N. Kopidakis, J. Peet, B. Walker, G. C. Bazan and E. Van Keuren, *Nature Materials*, 2009, **8**, 208-212.

252. M. Lenes, G. J. A. Wetzelaer, F. B. Kooistra, S. C. Veenstra, J. C. Hummelen and P. W. Blom, *Advanced Materials*, 2008, **20**, 2116-2119.

253. Y. He, H.-Y. Chen, J. Hou and Y. Li, *Journal of the American Chemical Society*, 2010, **132**, 1377-1382.

254. Y. He, G. Zhao, B. Peng and Y. Li, *Advanced Functional Materials*, 2010, **20**, 3383-3389.

255. G. Zhao, Y. He and Y. Li, *Advanced Materials*, 2010, **22**, 4355-4358.

256. Y. Sun, C. Cui, H. Wang and Y. Li, *Advanced Energy Materials*, 2011, **1**, 1058-1061.

257. X. Guo, C. Cui, M. Zhang, L. Huo, Y. Huang, J. Hou and Y. Li, *Energy & Environmental Science*, 2012, **5**, 7943-7949.

258. Z. G. Zhang and J. Wang, *Journal of Materials Chemistry*, 2012, **22**, 4178-4187.

259. E. Wang, L. Wang, L. Lan, C. Luo, W. Zhuang, J. Peng and Y. Cao, *Applied Physics Letters*, 2008, **92**, 33307-33307.

260. S. Beaupré and M. Leclerc, *Journal of Materials Chemistry A*, 2013, **1**, 11097-11105.

261. C. Du, W. Li, Y. Duan, C. Li, H. Dong, J. Zhu, W. Hu and Z. Bo, *Polymer Chemistry*, 2013, **4**, 2773-2782.

262. H. Wei, Y. H. Chao, C. Kang, C. Li, H. Lu, X. Gong, H. Dong, W. Hu, C. S. Hsu and Z. Bo, *Macromolecular Rapid Communications*, 2015, **36**, 84-89.

263. D. H. Wang, J. K. Kim, J. H. Seo, I. Park, B. H. Hong, J. H. Park and A. J. Heeger, *Angewandte Chemie International Edition*, 2013, **52**, 2874-2880.

264. A. Abdulaziz, *Chemical Communications*, 2013, **49**, 2252-2254.

265. J. W. Jung, F. Liu, T. P. Russell and W. H. Jo, *Advanced Energy Materials*, 2015, **5**.

266. Z. Li, S. W. Tsang, X. Du, L. Scoles, G. Robertson, Y. Zhang, F. Toll, Y. Tao, J. Lu and J. Ding, *Advanced Functional Materials*, 2011, **21**, 3331-3336.

267. J. Hou, H.-Y. Chen, S. Zhang, G. Li and Y. Yang, *Journal of the American Chemical Society*, 2008, **130**, 16144-16145.

268. T. Y. Chu, J. Lu, S. Beaupré, Y. Zhang, J. R. Pouliot, J. Zhou, A. Najari, M. Leclerc and Y. Tao, *Advanced Functional Materials*, 2012, **22**, 2345-2351.

Chapter 2 - Novel thermocleavable polymers based on phthalate esters

Abstract

Three novel phthalate-based thermocleavable copolymers, **35**, **36** and **37** have been designed and synthesised. **35** and **36** were prepared by copolymerising distannylated bithiophene without or with flanked thienyl groups as the electron-donor units with dibrominated secondary phthalate ester as the electron-acceptor units. **37** was prepared by copolymerising distannylated fluorene flanked by thienyl groups as the electron-donor moieties with dibrominated secondary phthalate ester as the electron-acceptor moieties. All polymers were prepared *via* the Stille polymerisation. The impact of two different electron-donor units on the solubility, molecular weights, and optical properties, thermal and structural properties of the resulting polymers was investigated. **37** has the highest number average molecular weight (M_n = 16400 g mol^{-1}). The polymers have E_g in the range of 2.11-2.58 eV. After thermal treatment, the E_g of the polymers are reduced by around 0.3-0.4 eV. TGA data show weight loss around 300 °C corresponding to the elimination of the secondary ester groups. After annealing, the soluble precursor polymers are transformed into active phthalic anhydride polymers and the resulting films are completely insoluble in all solvents. Powder XRD studies have shown that all polymers have an amorphous nature in the solid state.

2.1. Introduction

2.1.1. Wessling and Durham routes

A number of conjugated polymers were synthesised by a precursor route where thermal processing was utilised to remove the solubilising side chains from soluble saturated precursor intermediates to form the final conjugated polymer films. For example, poly(*p*-phenylene vinylene) (**PPV**) was synthesised *via* Wessling route (**Scheme 2.1a**)[1]. Treatment of the α,α'-dichloro-*p*-xylene (**1**) with tetrahydrothiophene in methanol affords bis-sulfonium salt (**2**) which subsequently reacts with sodium hydroxide to produce a quinodimethane intermediate (**3**). This intermediate undergoes polymerisation to form **4** which is a soluble precursor polymer. It could be cast on the substrate to form a thin film and finally the film is heated under vacuum to produce a high-quality **PPV** films. Later on, Gagnon *et al*. synthesised a **PPV** by the same method using dimethyl sulfide

[$(CH_3)_2S$] instead of tetrahydrothiophene[2]. Polyacetylene (**PA**) was synthesised using Durham route *via* ring opening metathesis polymerisation (**ROMP**) (**Scheme 2.1b**)[3,4].

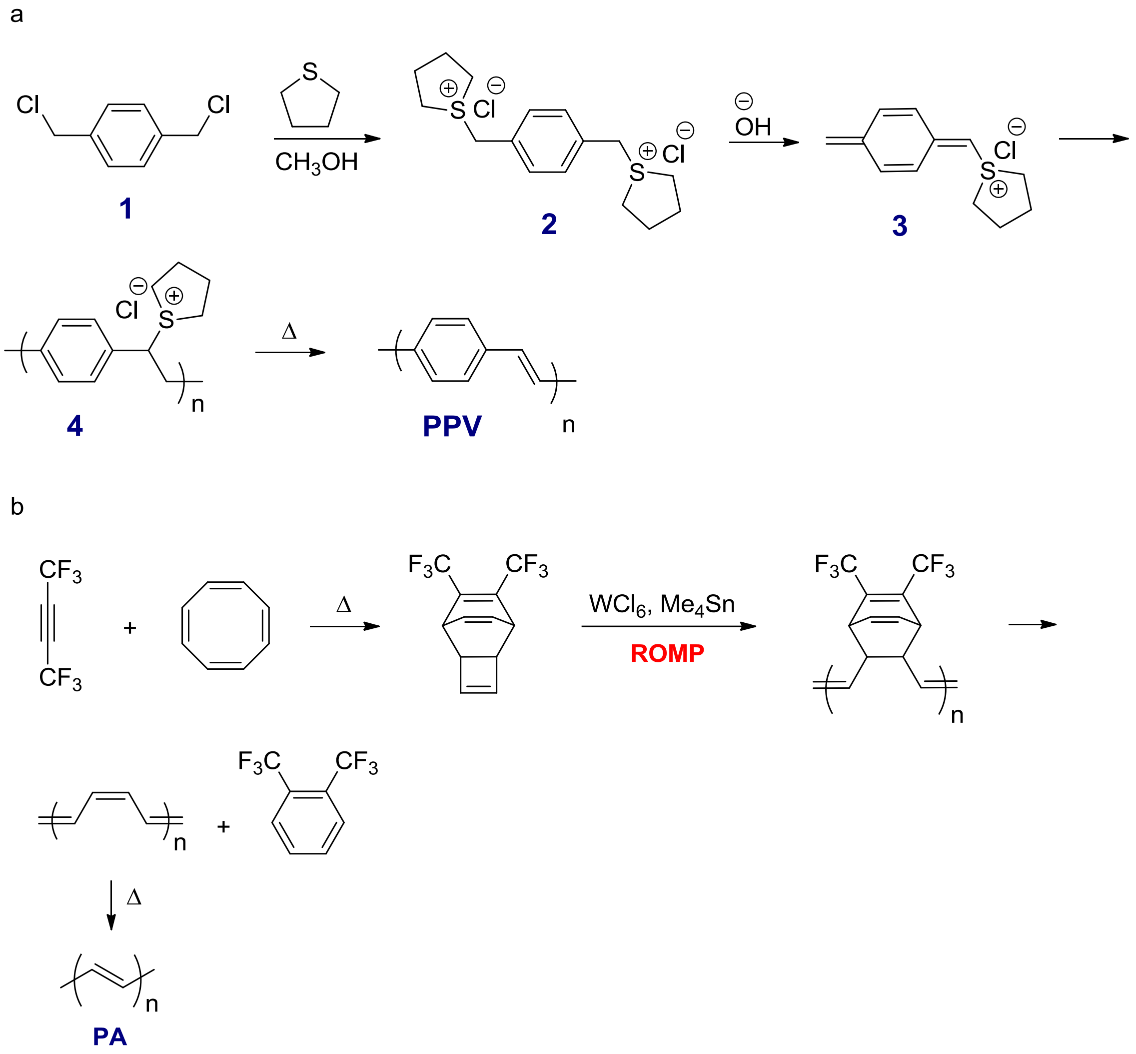

Scheme 2.1: a) The Wessling route for **PPV**; b) the Durham method for **PA**

2.1.2. Thermocleavable polymers

In the precursor route the conjugated polymer is formed after thermal treatment of a nonconjugated polymer precursor[5,6]. An alternative method to prepare polymers without solubilising substituents, relies on attaching thermocleavable side chains that provide solubility to the polymer and where an insoluble conjugated polymer is formed from the conjugated polymer backbone where the solubilising side chains are removed upon thermocleavage[7,8,9,10]. The final films which are formed in both methods are insoluble in all solvents and they have high chromophore density. The major difference between these two approaches is that the thermocleavable polymers can be processed in devices before the side chains are removed. In both routes a part of the material which forms the film is removed.

Unsubstituted conjugated polymers are rigid materials that are insoluble in common organic solvents. Therefore, solution processing is an important aspect for conjugated polymers to form films for optoelectronic applications. To make these materials soluble, the incorporation of solubilising side chains is required[11]. This is normally obtained by attaching long alkyl or alkoxy groups onto the polymer backbone[12]. For example, unsubstituted polythiophene (**PT**) is an insoluble material and by attaching the alkyl groups such as hexyl groups at the 3-positions of thiophene units it makes poly(3-hexylthiophene) (**P3HT**) soluble in common organic solvents. However, these solubilising groups are non-photoactive and therefore they do not participate in charge generation. As a result, they decrease the density of chromophores of the conjugated polymers[11]. In addition, after film formation the solubilising side chains are no longer required. Furthermore, they are responsible for softness of the material and are more likely lead to morphological changes and the resulting film is more susceptible for diffusing small molecules and constituents[13,14,15,16]. This is related to the instability of polymer photovoltaic cells due to photochemical reactions[17]. Therefore, more stable polymer solar cells can be achieved by a more rigid system. From this point of view, it is important to prepare bulk heterojunction organic photovoltaics *via* solution processing where the final active layer does not have side chains. The principle of thermocleavable materials realises this requirement. Thermocleavable materials have labile bonds between solubilising groups and the conjugated backbone. The most common thermocleavable materials contain carboxylic ester groups. These materials have solubilising groups such as branched alkyl chains that are attached to the conjugated backbone through labile ester bonds[18]. After thermal processing, these bonds are broken and volatile alkenes are eliminated and leaving the polymer material insoluble in organic solvents (**Scheme 2.2**)[19].

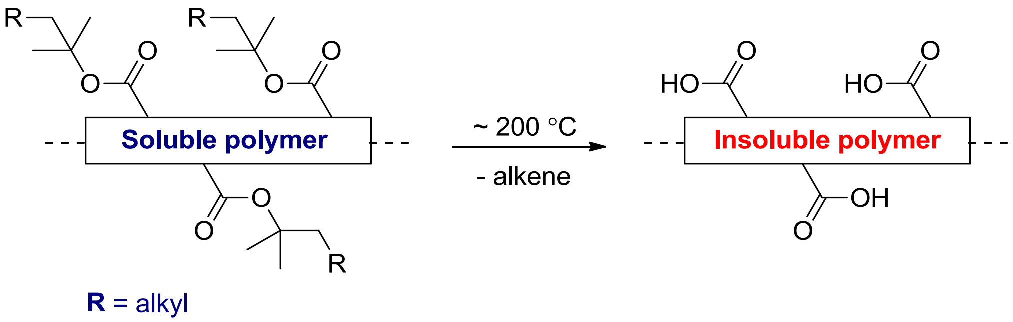

Scheme 2.2: The side chain removal by thermal treatment in thermocleavable polymers

As a result, these polymers have high density of chromophores, they are much more rigid and consequently they have more stable morphology. The glass transition temperature

(T_g) of the resulting polymers would be increased and therefore improve the thermal stability and photovoltaic properties of the devices[20,21,22].

BHJ photovoltaic cells containing poly(3-(2-methylhex-2-yl)-oxy-carbonyldithiophene (**P3MHOCT**) as donor and C_{60} as an acceptor show a very stable device with lifetime more than 10000 hours after elimination of solubilising groups upon thermal treatment[7,23]. This polymer is a soluble conjugated polymer which is transformed to a more rigid and insoluble poly-3-carboxydithiophene (**P3CT**) after elimination of 2-methylhexene upon heating the film around 200 °C[24]. **P3CT** is further transformed to polythiophene (**PT**) around 300 °C (**Scheme 2.3**), which was confirmed by ^{13}C labelling and solid-state NMR studies[25]. The chemical transformations can be seen visually during film annealing by changing colour from red to orange (transformation of **P3MHOCT** to **P3CT**) and then from orange to purple-red (transformation of **P3CT** to **PT**)[26]. The thermal properties for **P3MHOCT** were investigated by thermogravimetric analysis (**TGA**). Two different weight loss mechanisms can be seen from thermogravimetric data. The first weight loss about 200 °C corresponding to ester bond cleavage and the second loss peak is around 300 °C which belongs to decarboxylation[25]. BHJ devices based on **P3MHOCT: $PC_{61}BM$** (or **$PC_{71}BM$**) gave PCE in the range of 0.7-0.9%. When **P3MHOCT** was converted to **P3CT**, the device showed the poorest PCE in the range of 0.1-0.4%. Finally, the PCE was dramatically increased when **P3CT** is converted to **PT** and PCE of 0.6% was observed in the case of **$PC_{61}BM$** and up to 1.5% in the case of **$PC_{71}BM$**[26].

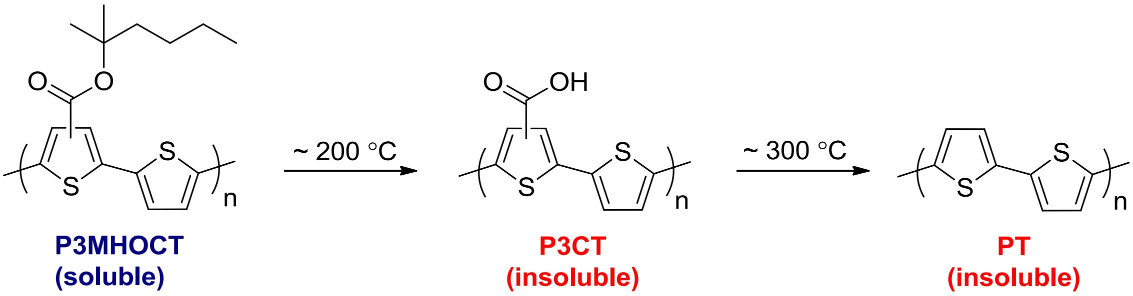

Scheme 2.3: The chemical changes of **P3MHOCT** into **P3CT** and then to **PT**[27]

A series of low band gap thermocleavable polymers were synthesised by copolymerising thienopyrazine as acceptor units and dialkoxy benzene (**1**), fluorene (**2**), thiophene (**3**) and cyclopentadithiophene (**4**) flanked by thienyl units as donor moieties (**Scheme 2.4**)[28]. Different ester groups are attached to the diphenyl substituted thienopyrazine units. The temperatures at which the ester groups eliminated were studied. The tertiary ester groups were observed to cleave at the lowest temperatures in the range of 220-240 °C leaving the carboxyl groups on the benzene rings of thienopyrazine (**Scheme 2.4**). However, the polymers which are bearing primary esters required the highest temperatures and lead to the decomposition of the polymers[29]. The BHJ devices fabricated from **polymer: PC$_{61}$BM** gave the best PCE of 1.21% for the copolymer containing **4** without thermocleavage. After thermal treatment at 225 °C, the PCE dropped to 0.64%.

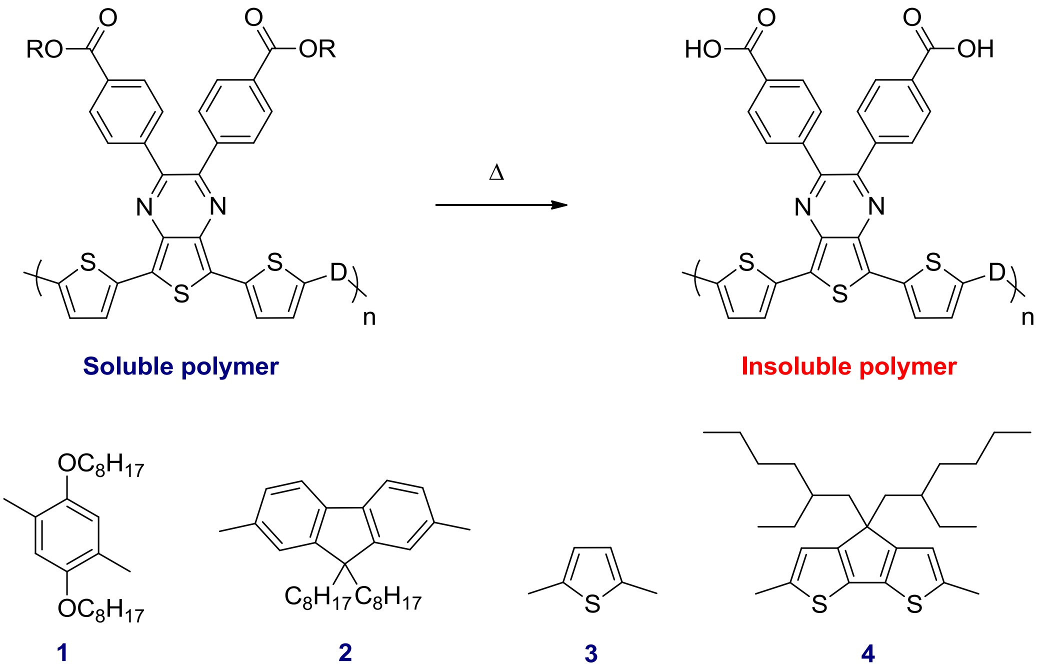

Scheme 2.4: Low band gap thermocleavable polymers including thienopyrazine and cleavage of ester groups upon thermal treatment

A new type of thermocleavable polymer including 2,1,3-benzothiadiazole (**BT**) and thiophene units was prepared by Helgesen *et al.* (**Scheme 2.5**)[30]. A photovoltaic performance of the **polymer: PC$_{61}$BM** as active layer was measured without thermal treatment and after annealing at 200 and 285 °C, respectively. Without annealing, the device showed a PCE of only 0.21% and after thermal treatment at 200 °C the PCE improved slightly to 0.24%. Finally, when the tertiary ester groups are thermocleaved after thermal treatment at 285 °C the PCE improved to 0.42%.

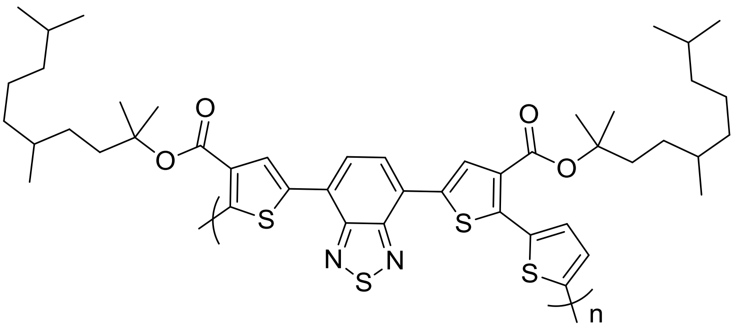

Scheme 2.5: The thermocleavable polymer based on **BT** and thiophene units

Helgesen and co-workers further developed and synthesised two new thermocleavable polymers (**T1** and **T2**) based on **BT** as acceptor units and cyclopentadithiophene (**CPDT**) flanked by thienyl groups as donor units (**Scheme 2.6**)[31]. Branched alkyl side chains attached to the 3-positions and 4-positions of thiophene units through labile ester bonds in **T1** and **T2** respectively. The positions of the alkyl chains had a major effect on the PCE of the resulting polymers. BHJ photovoltaic cells comprised of **T2: $PC_{71}BM$** delivered the highest PCE of 1.92% without annealing. In addition, the same device gave a PCE of 1.49% when the tertiary ester groups are thermocleaved after annealing at 265 °C. On the contrary, **T1: $PC_{61}BM$** gave a PCE of only 0.18%.

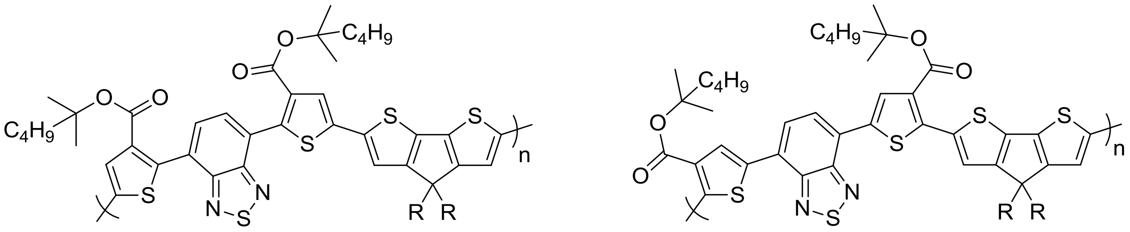

T1: R = 2-ethylhexyl (EH)

T2: R = EH

Scheme 2.6: The structures of **T1** and **T2**

2.1.3. Dithiocarbamate precursor route

Poly(thienylene vinylene) (**PTV**) and its derivatives could be prepared *via* dithiocarbamate precursor route (**Scheme 2.7**)[32,33]. In this route, dithiocarbamates are labile bonds and after thermal processing around 160 °C, these bonds are broken and yielded insoluble conjugated **PTV**. It was blended with **$PC_{61}BM$** and gave a PCE of 0.76% after thermocleavage[32].

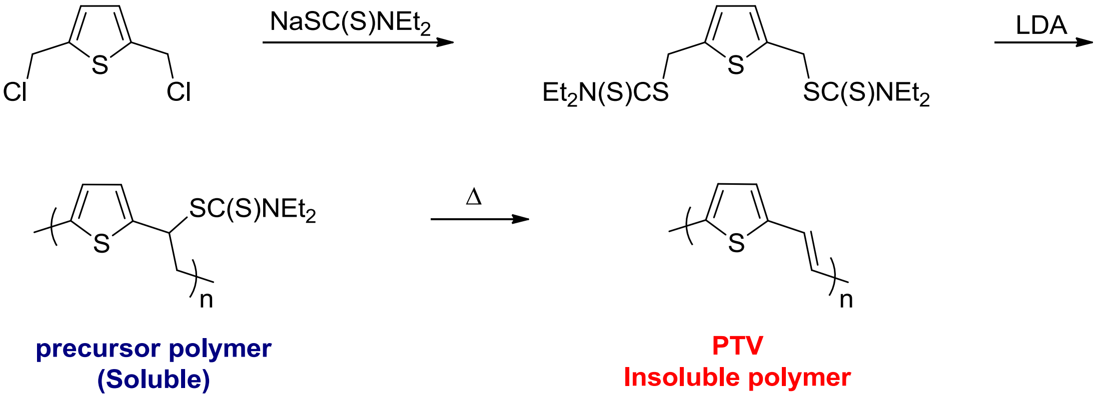

Scheme 2.7: The synthesis of **PTV** by dithiocarbamate precursor route

2.2. Synthesis of monomers

2.2.1. Synthesis of secondary phthalate ester monomers (6 and 8)

6 and **8** were synthesised through four and six steps starting from commercially available phthalic anhydride (**1**), respectively (**Scheme 2.8**). The different steps and their preparation are discussed below.

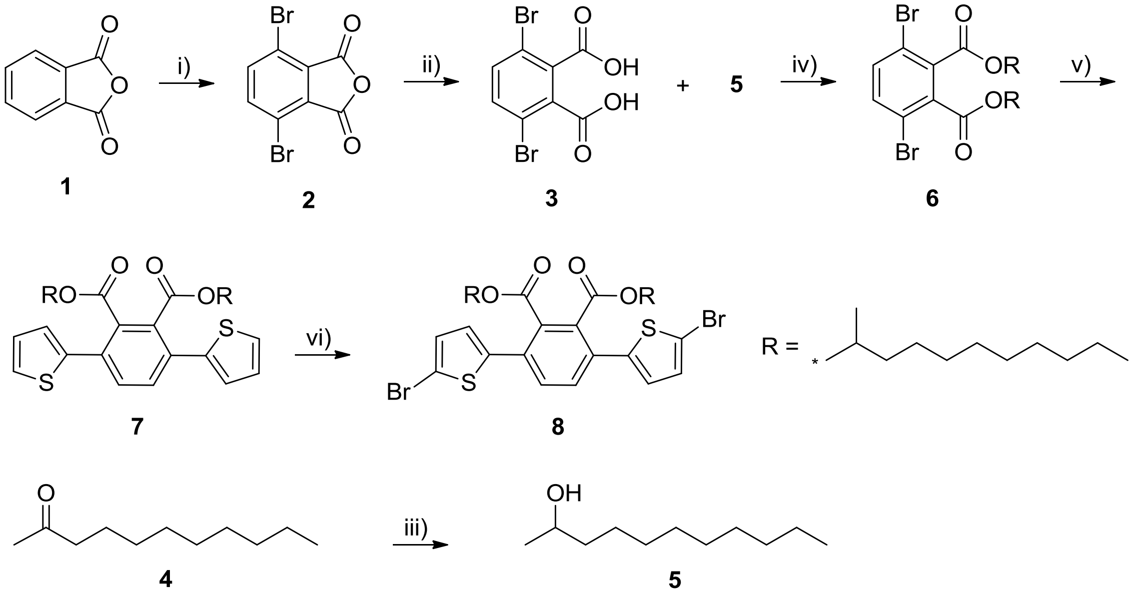

Scheme 2.8: The synthetic steps of the **6**and **8**

Reagents and conditions: i) Br_2, I_2, fuming H_2SO_4 (30% free SO_3), 60 °C, 24h; ii) H_2O, THF, reflux, 24h; iii) MeOH, $NaBH_4$, RT, 1h, HCl; iv) DCM, DMAP, $Sc(OTf)_3$, DIC, reflux, 24h; v) 2-(tributylstannyl)thiophene, toluene, $PdCl_2(PPh_3)_2$, 110 °C, 24h; vi) NBS, $CHCl_3$: HOAc (1:1, v/v), RT, 24h

2.2.1.1. Synthesis of 3,6-dibromophthalic anhydride (2)

2 was prepared by bromination of phthalic anhydride (**1**) using bromine and fuming sulfuric acid in the presence of small amount of iodine. It was obtained as white crystals in 22% yield (**Scheme 2.8**)[34].

The mechanism of the reaction is an electrophilic aromatic substitution (**Scheme 2.9**). In the first step, bromine reacts with fuming sulfuric acid to form $Br\text{-}Br^+\text{-}H$ which functions as an electrophile. In the second step, benzene functions as a nucleophile and attacks the electrophile to form a carbocation intermediate, which is stabilised by three resonance structures (**9**, **10** and **11**). In the third step, the carbocation is deprotonated by HSO_4^- to form 3-bromophthalic anhydride (**12**) which is subsequently brominated at the 6-position to give **2** and sulfuric acid regenerated as the catalyst.

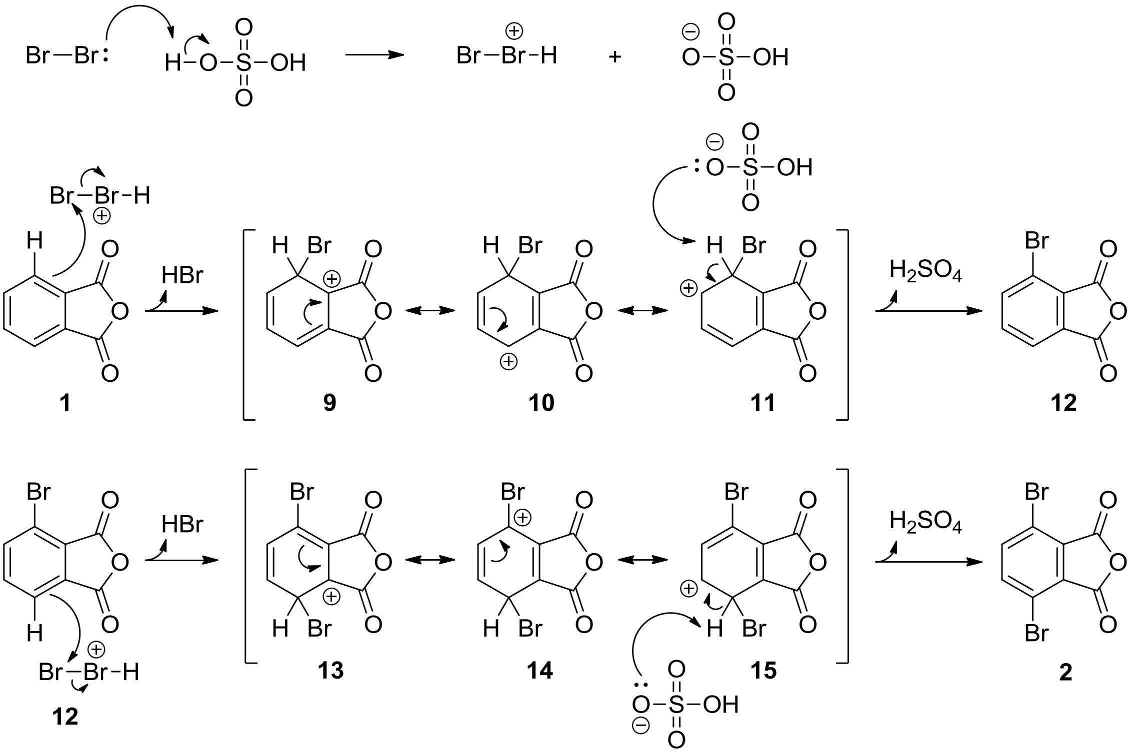

Scheme 2.9: The mechanism of bromination of phthalic anhydride (**1**)

The structure and purity of **2** were verified by variety of analytical tools. The ^{1}H NMR spectrum of **2** shows a singlet peak at 7.87 ppm with an integral of two protons. The mass spectrum of **2** displays the main integer signals at 304, 306 and 308 in a 1:2:1 ratio due to the existence of two isotopes of bromine (^{79}Br and ^{81}Br).

2.2.1.2. Synthesis of 3,6-dibromophthalic acid (3)

2 was hydrolysed in THF/water under reflux to yield **3** as a white solid in a yield of 94% (**Scheme 2.8**)[35].

The mechanism of hydrolysis of **2** is a type of addition-elimination process and consists of three core steps (**Scheme 2.10**). In the first step, water functions as a nucleophile and attacks a carbonyl group of **2** to form an intermediate (**16**). In the second step, the carbonyl group is regenerated when the leaving group is expelled to form an intermediate (**17**). This leaving group in the cyclic anhydride is an internal carboxylate anion. Finally, the latter intermediate is protonated to form the dicarboxylic acid product (**3**).

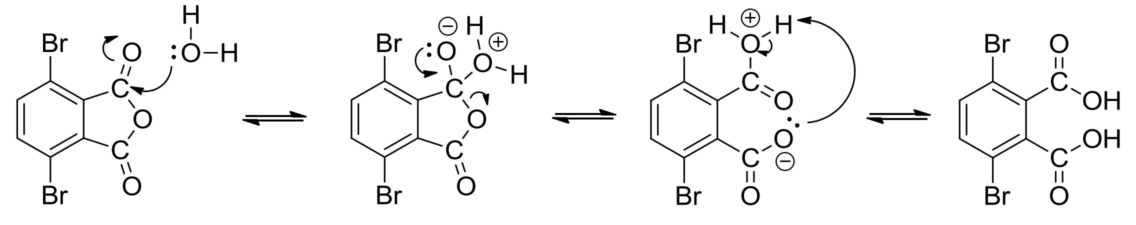
2 **16** **17** **3**

Scheme 2.10: The mechanism of hydrolysis of **2**

From the ^{1}H NMR spectrum of **3,** it is obvious that the hydrolysis was successful as a singlet peak at 8.06 ppm in **2** changes to 7.69 ppm in **3** in DMSO-d_6, which is integrated to two protons. In addition, a singlet peak at 14 ppm appears corresponding to the two protons of the carboxyl groups. The structure of **3** was further confirmed by the FT-IR spectroscopy. The FT-IR spectrum of **3** shows a broad peak around 2300-3500 cm^{-1}, which is representative of the O-H stretching vibration of carboxyl group. The ^{13}C NMR spectroscopy, mass spectrometry and elemental analysis are in agreement with the structure of **3**.

2.2.1.3. Synthesis of 2-undecanol (5)

The commercially available 2-undecanone (**4**) was reduced using sodium borohydride (NaBH$_4$) as a reducing agent in methanol and gave **5** as a colourless oil in an excellent yield of 94% (**Scheme 2.8**)[36].

The mechanism of the reaction comprises of two steps (**Scheme 2.11**). In the first step, sodium borohydride delivers a hydride ion to the carbonyl group of 2-undecanone (**4**) to form a negatively charged tetrahedral intermediate (**18**). In the second step, this intermediate is protonated to form a secondary alcohol product (**5**).

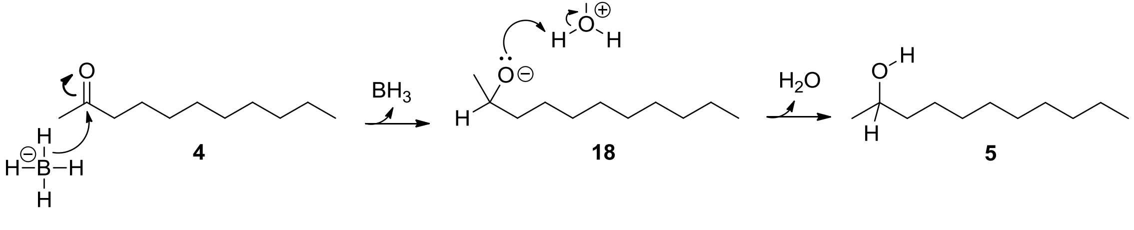
4 **18** **5**

Scheme 2.11: The mechanism of formation of **5**

The ^{1}H NMR spectrum of **5** showed a multiplet peak in the range of 3.75–3.86 ppm for one proton on the C2 and it exhibits a triplet peak at 0.90 ppm for three protons of the terminal methyl group. Furthermore, it shows another multiplet and doublet in the range of 1.24–1.54 and 1.20 ppm, respectively for the methylene and methyl protons. The structure and purity of the **5** further confirmed by the ^{13}C NMR and FT-IR spectroscopy.

The ^{13}C NMR spectrum of **5** displays eleven peaks for eleven environmentally different carbon atoms. The FT-IR spectrum of **5** shows a broad band in the range of 3200-3500 cm^{-1} for the O-H stretching vibration.

2.2.1.4. Synthesis of 3,6-dibromo-bis(2-undecanyl) phthalate (6)

6 was prepared by a Steglich esterification reaction between dicarboxylic acid compound (**3**) and a secondary alcohol substance (**5**). The reaction was performed in the presence of *N,N′*-diisopropylcarbodiimide (DIC), 4-(dimethylamino)pyridine (DMAP) and a catalytic amount of scandium triflate [$Sc(OTf)_3$] in anhydrous dichloromethane and gave **6** as a colorless oily material in 31% yield (**Scheme 2.8**)[37].

The mechanism of the Steglich esterification is illustrated in scheme 2.12. DIC is a coupling reagent which functions as a nucleophile and can deprotonate the carboxyl group of **3** to form a carboxylate anion intermediate (**19**). This intermediate acts as a nucleophile and attacks to the protonated DIC to generate an O-acylisourea intermediate (**20**). This intermediate is protonated by alcohol (**5**) to form a new intermediate (**21**). DMAP is a base which functions as a catalyst and acyl transfer reagent. It attacks the carbonyl group of **21** to form an intermediate (**22**). The carbonyl group is reformed to form intermediate (**23**) and subsequently diisopropylurea (DIPU) is isolated as a by-product of the reaction. The alkoxide ion attacks to the carbonyl group of the latter intermediate to generate negatively charged tetrahedral intermediate (**24**). Finally, **6** is produced and DMAP is regenerated as a catalyst.

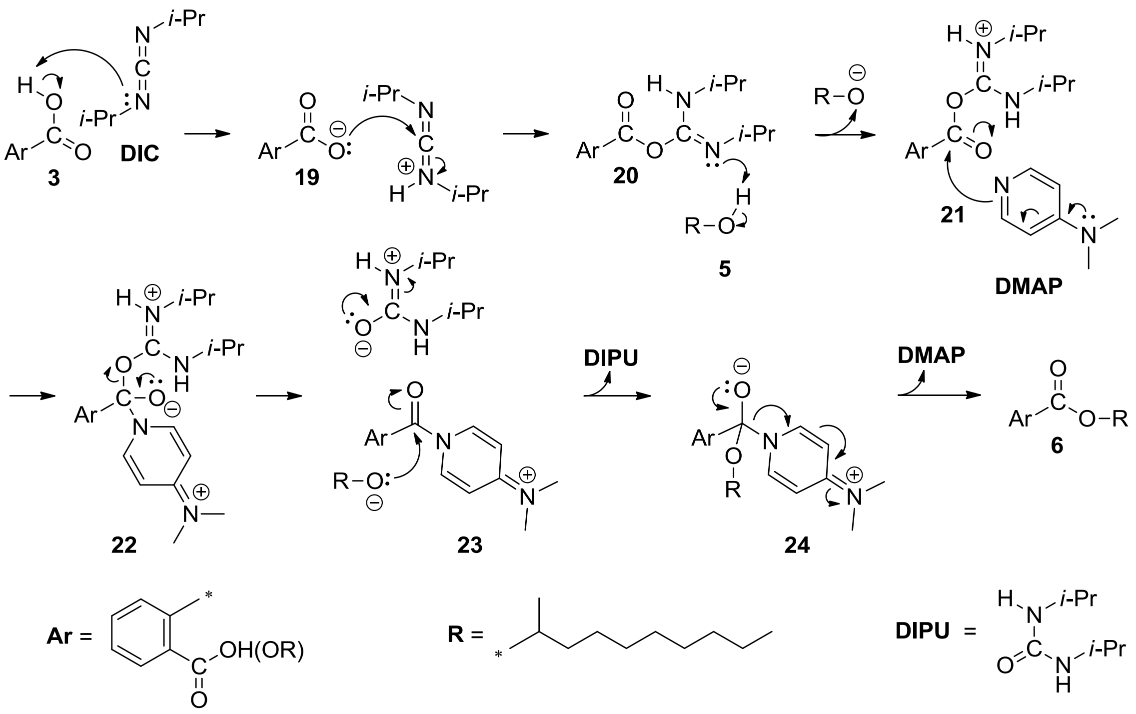

Scheme 2.12: Mechanism of the synthesis of **6**

Scandium triflate functions as a catalyst and coordinates with the oxygen of the carbonyl group of the intermediate (**23**) in the mechanism to form a highly reactive intermediate (**25**) (**Scheme 2.13**)[38].

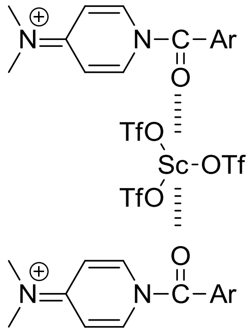

25

Scheme 2.13: Formation of the intermediate **25**

The ^{1}H NMR spectrum of **6** shows a singlet peak at 7.49 ppm corresponding to the protons on the benzene ring. A sextet can be seen in the range of 5.10-5.20 ppm, which is indicative of the protons neighbouring to the ester functional groups. These protons are more deshielded because of the ester groups. It also displays the expected number of protons in the aliphatic region.

2.2.1.5. Synthesis of 3,6-bis(2-thienyl)-bis(2-undecanyl)phthalate (7)

6 can undergo the Stille coupling reaction with 2-(tributylstannyl)thiophene using $Pd(PPh_3)_2Cl_2$ as a catalyst in toluene to yield **7** as white crystals in 74% yield (**Scheme 2.8**)[39]. The mechanism of the reaction is similar to that of the Stille reaction described in the introduction chapter.

From the ^1H NMR spectrum of **7**, the peaks corresponding to thiophene protons can be visualised as three doublets of doublets at 7.06, 7.12 and 7.37 ppm and a singlet peak at 7.52 ppm for the two protons on the benzene ring. It also displays the expected number of protons in the aliphatic region.

2.2.1.6. Synthesis of 5,5'-dibromo-3,6-bis(2-thienyl)-bis(2-undecanyl)phthalate (8)

7 was brominated using two equivalents of NBS in a mixture of chloroform/acetic acid in the dark to obtain **8** as white crystals in 77% yield (**Scheme 2.8**)[40]. The mechanism of the reaction is similar to that for the synthesis of **2** as shown in scheme 2.9.

The ^1H NMR spectroscopy was utilised to characterise the **8**. ^1H NMR spectrum of **8** shows a singlet and two doublets at 7.46, 7.02 and 6.86 ppm, respectively in the aromatic region. It also displays the expected number of protons in the aliphatic region. The structure and purity of the **8** were verified by the ^{13}C NMR spectroscopy, the elemental analysis and mass spectrometry, which are in agreement with the proposed structure.

2.2.2. Synthesis of distannylated fluorene (29)

29 was synthesised through three steps starting from commercially available fluorene (**26**) (**Scheme 2.14**). The different steps in its preparation are discussed below.

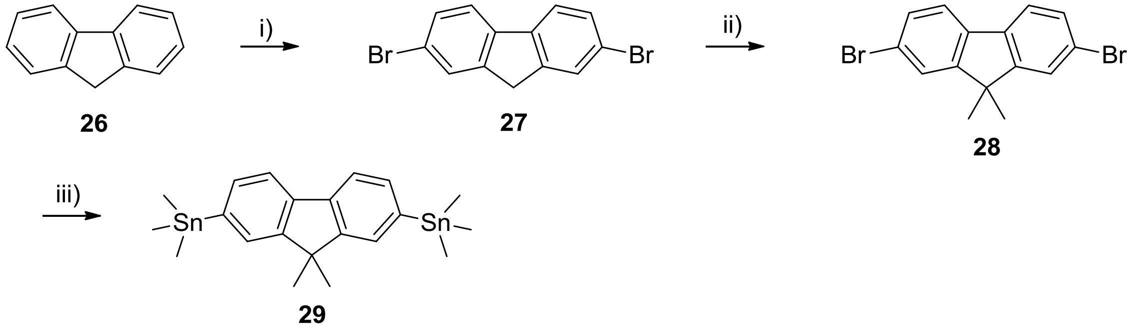

Scheme 2.14: The synthetic steps of the **29**

Reagents and conditions: i) Br_2, $CHCl_3$, RT, 24h; ii) KOH, KI, DMSO, CH_3I, RT, 24h; iii) *n*-BuLi, Et_2O, -78 °C, TMEDA, $(CH_3)_3SnCl$, RT, overnight

2.2.2.1. Synthesis of 2,7-dibromofluorene (27)

Fluorene (**26**) was brominated using bromine in chloroform to give **27** as white crystals in good yield of 77% (**Scheme 2.14**)[41]. The bromination was accomplished in the dark in order to prevent bromination of the methylene protons. The mechanism of the reaction is similar to that for the synthesis of **2** as shown in scheme 2.9.

The ^{1}H NMR spectrum for **27** shows a singlet peak at 3.89 ppm corresponding to the protons at the 9-position of the fluorene. It also displays the expected number of protons in the aromatic region.

2.2.2.2. Synthesis of 9,9-dimethyl-2,7-dibromofluorene (28)

27 was alkylated at the 9-position using iodomethane and small catalytic amount of potassium iodide under basic conditions in DMSO to yield **28** as pale yellow crystals in 97% yield (**Scheme 2.14**)[42].

The mechanism of the reaction is a bimolecular nucleophilic substitution (S_N2) (**Scheme 2.15**). Two protons at C-9 of **27** are acidic, which are deprotonated by a hydroxide ion to generate the carbanion intermediate (**30**). This intermediate functions as a nucleophile and attacks the methyl group of iodomethane *via* S_N2 mechanism to give the intermediate (**31**) and iodide ion as a leaving group. The second methylation of **31** gave **28**.

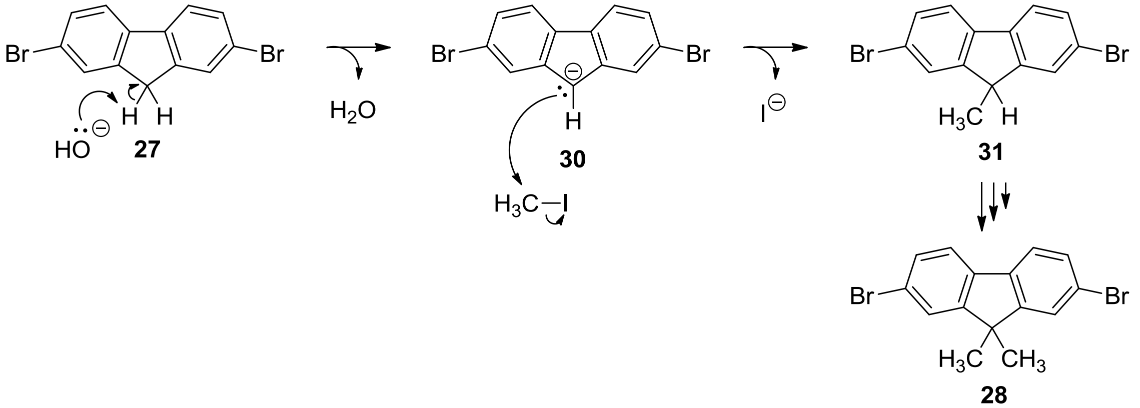

Scheme 2.15: The mechanism of the alkylation of **27**

The ^{1}H NMR studies on **28** shows the disappearance of the singlet peak at 3.89 ppm for the two protons at the 9-position of the **27** and the appearance of a singlet peak at 1.48 ppm for the six protons of the methyl groups. It also displays a multiplet and a doublet of doublet at 7.53-7.61 and 7.48 ppm corresponding to six aromatic protons. The structure and purity of **28** were further confirmed by the ^{13}C NMR spectroscopy, mass spectrometry and elemental analysis, which are in agreement with the proposed structure.

2.2.2.3. Synthesis of 9,9-dimethyl-2,7-bis(trimethylstannyl)fluorene (29)

28 was lithiated selectively at 2,7-positions using two equivalents of *n*-butyllithium (*n*-BuLi) and tetramethylethylenediamine (TMEDA) in anhydrous diethyl ether at –78 °C, which was subsequently treated with trimethyltin chloride (Me_3SnCl) to yield **29** as white crystals in 62% yield (**Scheme 2.14**)[43]. TMEDA is a bidentate ligand which forms a complex with *n*-BuLi at –78 °C and enhance the reactivity of *n*-BuLi (**Scheme 2.16**)[44].

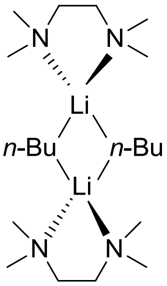

Scheme 2.16: The complex formation between *n*-BuLi and TMEDA

The mechanism of the reaction consists of two steps (**Scheme 2.17**). In the first step, **28** was lithiated selectively at the 2,7-positions to form dilithiated intermediate (**32**). In the second step, this intermediate is reacted with trimethyltin chloride to afford the distannylated product (**29**).

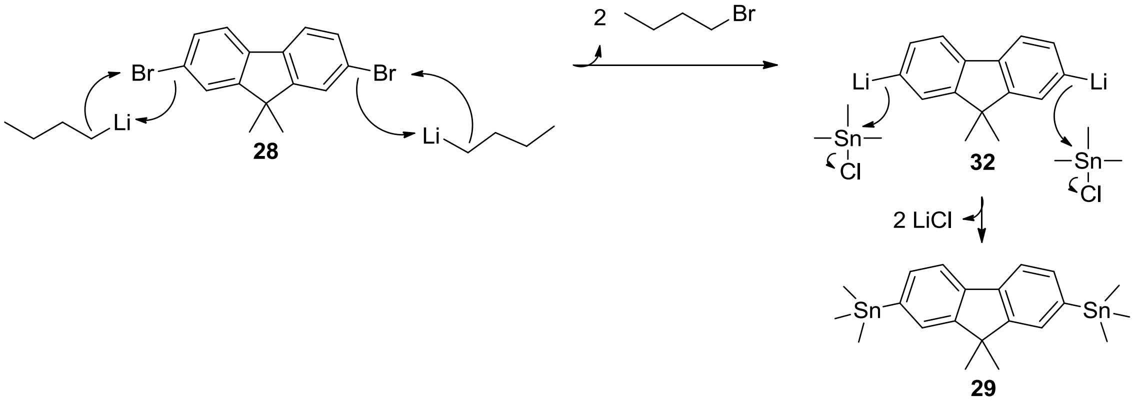

Scheme 2.17: Mechanism of the stannylation of **28**

From the ^{1}H NMR spectrum of **29,** a singlet peak is observed at 0.35 ppm, with an integration of eighteen protons, which indicated that the stannylation reaction was successful. Further evidence of the presence of the trimethylstannyl groups was given on analysis of the ^{13}C NMR spectrum of **29**. It shows a peak at –7.5 ppm which belongs to the methyl carbons for the trimethylstannyl group. The mass spectrum of **29** displays multi main integer masses at 501, 503, 505, 507, 509 and 511 as anticipated due to the presence of three most abundant tin isotopes (^{116}Sn,^{118}Sn and ^{120}Sn). Moreover, it shows a peak at $m/z = 520$, corresponding to the mass of the molecular ion $[M]^+$ of **29**.

2.2.3. Synthesis of 5,5'-bis(trimethylstannyl)-2,2'-bithiophene (34)

Commercially available 2,2'-bithiophene (**33**) was lithiated selectively at 5,5'-positions using two equivalents of *n*-BuLi in anhydrous THF at –78 °C, which was subsequently treated with trimethyltin chloride (Me_3SnCl) to obtain **34** as pale green crystals in 71% yield (**Scheme 2.18**)[45]. The mechanism of the reaction is similar to that for the synthesis of **29** as shown in the previous scheme.

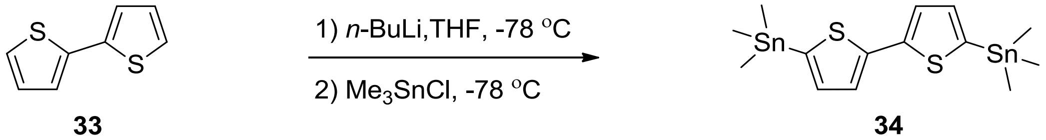

Scheme 2.18: The synthesis of **34**

The ^1H NMR spectrum of **34** shows a singlet peak at 0.40 ppm, which relates to eighteen protons of the methyl groups. In the aromatic region, two doublets can be seen at 7.10 and 7.29 ppm, which relate to four protons of the thiophene rings. Furthermore, two small peaks, which are satellite signals, also appear in the aromatic region due to the three isotopes of tin.

2.3. Preparation of the polymers

In this section, the synthesis of three novel thermocleavable copolymers, **35**, **36** and **37** is described. **35** and **36** were prepared *via* the Stille coupling polymerisation between distannylated bithiophene (**34**) with dibrominated compounds (**6** and **8**), respectively (**Scheme 2.19**). **37** was prepared *via* the Stille coupling polymerisation between distannylated fluorene (**29**) and dibrominated monomer (**8**) under the same experimental conditions (**Scheme 2.19**). The polymerisations were performed using $Pd(OAc)_2/P(o\text{-}tol)_3$ catalyst in anhydrous toluene. All polymerisations were left for 48 hours. The solutions became viscous and turned green without formation of polymer precipitates for **35** and **37**, while large amounts of red precipitates formed for **36** as the reactions proceeded. The polymers were then dissolved in chloroform and an ammonia solution added and the mixture stirred overnight to remove the Pd metal catalyst residues by forming $Pd(NH_3)_4(OH)_2$ soluble complexes. The polymers were obtained by precipitation from methanol followed by filtration. The polymers purified *via* Soxhlet extraction with methanol, acetone, hexane and finally toluene. The methanol and acetone fractions removed the small molecules, oligomers and impurities in the case of **35** and **37**. The hexane fractions of **35** and **37** were subsequently collected and concentrated *in vacuo*, reprecipitated in methanol followed by filtration to yield the purified polymers. However, **36** was collected in the toluene fraction.

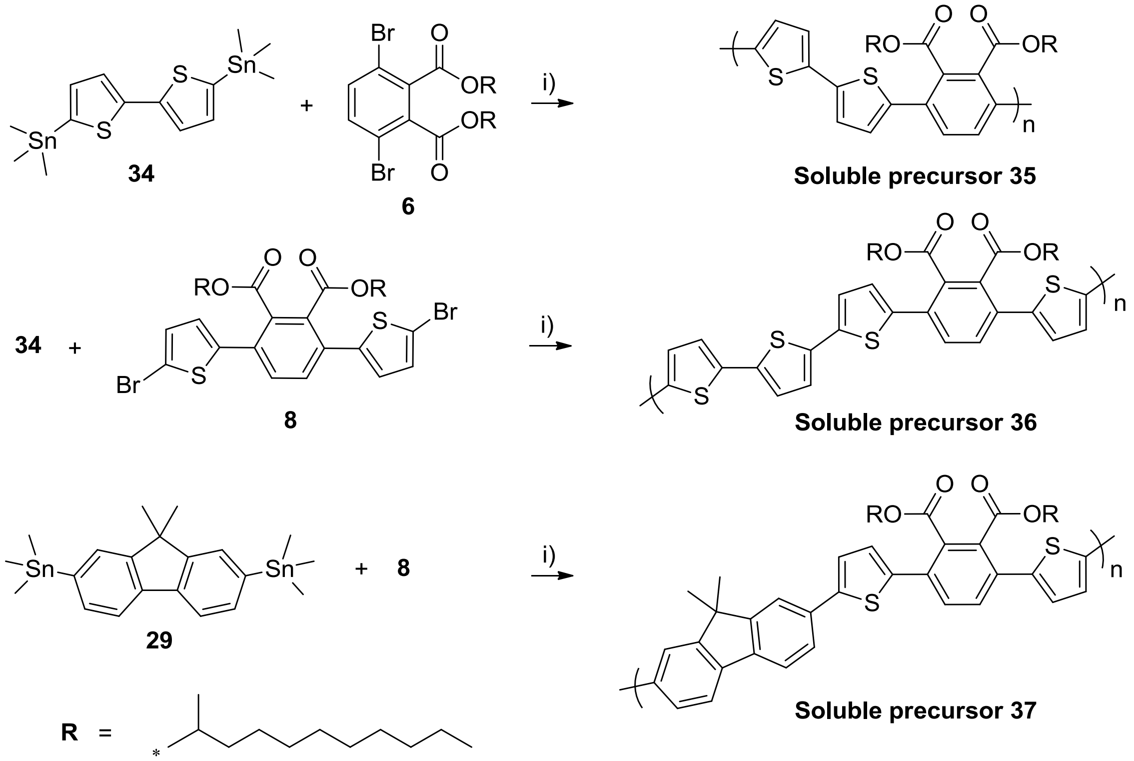

Scheme 2.19: Synthesis of soluble precursor polymers, **35**, **36** and **37** *via* the Stille polymerisation

Reagents and conditions: i) anhydrous toluene, $Pd(OAc)_2$, $P(o\text{-}tol)_3$, 100 °C, 48h

Upon thermal treatment around 300 °C for 1 hour, the soluble precursor polymers were transformed into active phthalic anhydride polymers upon cleavage of the ester groups into carboxyl groups followed by dehydration (**Scheme 2.20**). The resulting polymer films were completely insoluble.

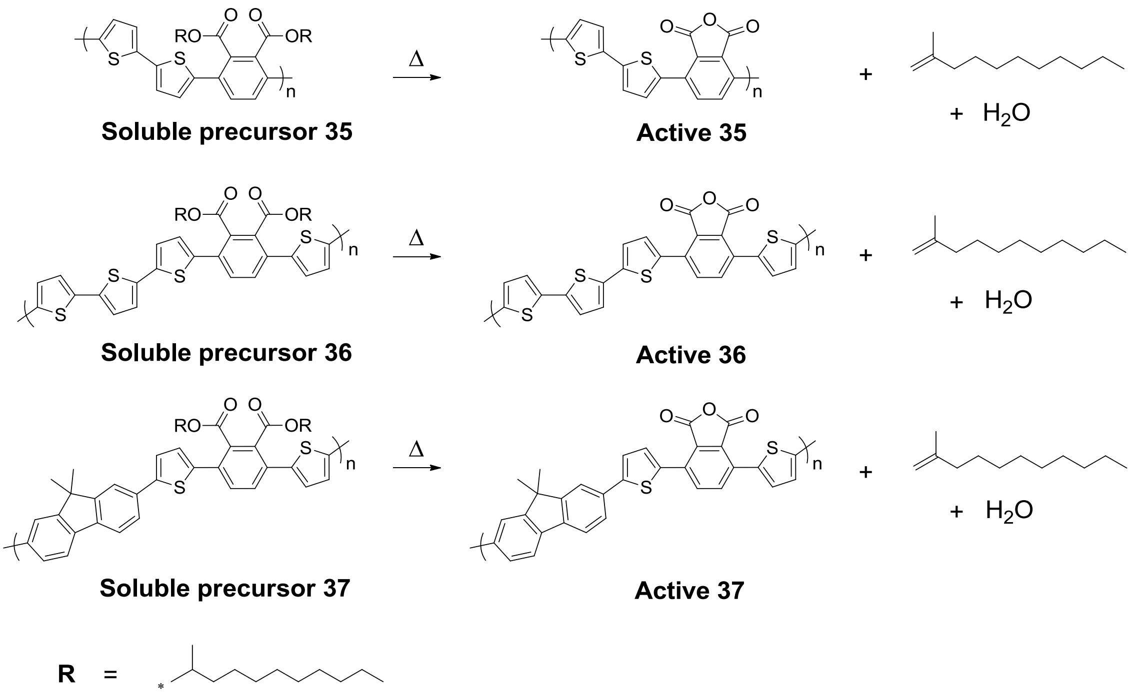

Scheme 2.20: The chemical transformations of the polymers after annealing around 300 °C for 1h

2.4. Molecular weights and yield of the polymers

Molecular weights of the polymers were measured by gel permeation chromatography (GPC) using chloroform at 40 °C relative to polystyrene standards (**Table 2.1**). **35** was extracted in the hexane fraction, while **36** was extracted in the toluene fraction and they have comparable M_n values. The latter polymer was prepared in 87% yield which was more than twice the yield obtained for the former polymer. The results indicate that altering bithiophene unit as a donor unit in **35** for tetrathiophene unit in **36** has a substantial influence on the solubility and yields of the polymers, while it has a negligible impact on the M_n values of the polymers. This may arise from the fact that **36** has two extra thiophene units in the backbone of the polymer which make the polymer more conjugated and more rigid relative to **35**. The third copolymer, **37** was synthesised in a moderate yield which was higher than that of **35** but lower than that of **36**. Even though, it was extracted in the hexane fraction, it has the highest M_n value among all polymers prepared. The results indicate that substituting bithiophene unit in **36** for fluorene unit in **37** has a negative effect on the solubility and yield of the polymer, however, the M_n value of the resulting polymer is significantly increased. This could be due to more aggregation in **36** with more intermolecular interactions relative to **37**.

Table 2.1: The percentage yield, number and weight average molecular weights with polydispersity indexes of **35**, **36** and **37**

Polymer	% yield	Hexane fraction M_n (g mol^{-1})	Hexane fraction M_w (g mol^{-1})	Hexane fraction PDI	Toluene fraction M_n (g mol^{-1})	Toluene fraction M_w (g mol^{-1})	Toluene fraction PDI
35	39	9600	13500	1.3			
36	87				9500	14300	1.5
37	64	16400	30300	1.8			

2.5. Optical properties of the polymers

The absorption spectra of the polymers in chloroform solutions and in thin-films are exhibited in figure 2.1a and figure 2.1b. The optical properties of the polymers are summarised in table 2.2. In solutions, the absorption of **35** and **37** display similar absorption maxima at 397 and 398 nm, respectively. However, the absorption maxima of **36** is red-shifted by more than 65 nm in solution relative to those **35** and **37** analogues. This could be related to the extended four thiophene segments in **36** which makes the polymer backbone more rigid and with a more planar structure relative to **35** and **37**. This is consistent with the solubility of the polymers. Compared to **37**, **36** contains a tetrathiophene as a donor building block which has a stronger electron-donating ability than a fluorene unit flanked by two thiophenes and thereby improving the π-electron delocalisation along the polymer main chain. In thin films, the absorption spectra of the polymers show red-shifted absorption maxima by 10 to 28 nm relative to their absorption in solutions. This could be attributed to stronger interchain π-π stacking and more coplanar structures in the solid state. The optical band gaps (E_g) of **35**, **36** and **37** are 2.19, 2.11 and 2.58 eV, respectively. The absorption spectra of the polymers upon thermal treatment of the films are illustrated in figure 2.2. Upon thermal treatment of the films, the absorption maxima of **35**, **36** and **37** are shifted to longer wavelengths at 498, 491 and 411 nm, respectively. **35** show quite strong bathochromic shift absorption maxima by more than 70 nm relative to its thin-film before thermocleavage. The E_g of **35**, **36** and **37** are reduced to 1.86, 1.89 and 2.14 eV, respectively. Upon annealing, the soluble precursor polymers are transformed into active phthalic anhydride polymers, upon cleavage of the ester groups into carboxyl groups followed by dehydration (**Scheme 2.20**). Reducing the band gaps of the polymers could be explained by the fact that the polymer backbones are changed into more rigid and more coplanar structures after annealing. Furthermore, the anhydride unit formed after annealing is a stronger electron acceptor than the original diester functional unit which leads to stronger intramolecular charge transfer along the polymer backbones and consequently lower the E_g of the polymers. The molar absorptivity (ε) of the **36** is significantly higher than **35** and **37** (**Table 2.2**). This could be attributed to **36** having the highest absorption maxima of about 464 nm in solution which is red-shifted by more than 65 nm compared to **35** and **37** (**Table 2.2**).

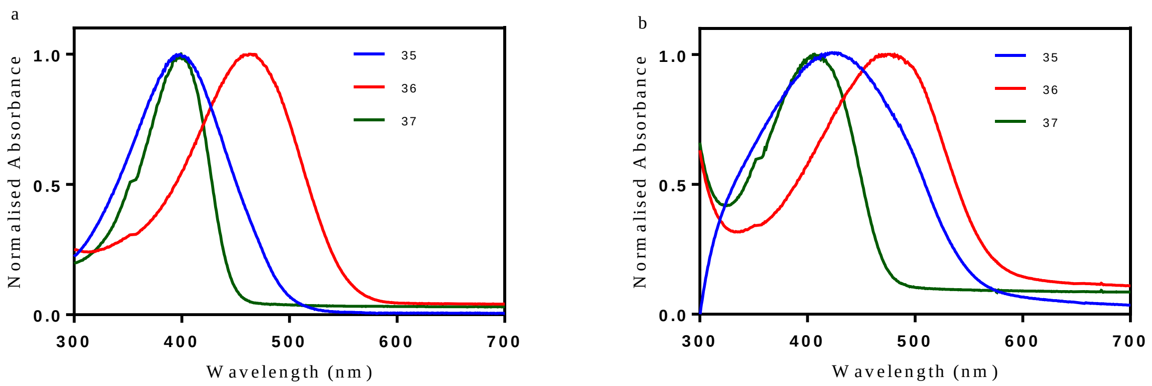

Figure 2.1: Normalised UV-vis absorption spectra of **35**, **36** and **37** in a) chloroform solutions; and b) thin films

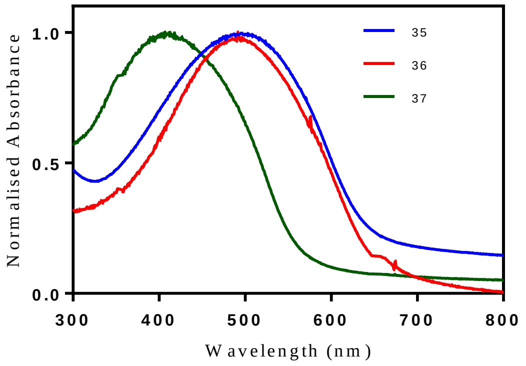

Figure 2.2: Normalised UV-vis absorption spectra of **35**, **36** and **37** after thermal treatment around 300 °C for 1h

Table 2.2: UV-vis data and optical band gaps of the polymers

Polymer	ε (M^{-1} cm^{-1})	Solution	Film			Film after thermal treatment around 300 °C		
		λ_{max} (nm)	λ_{max} (nm)	λ_{onset} (nm)	E_g (eV)	λ_{max} (nm)	λ_{onset} (nm)	E_g (eV)
35	16800	397	425	564	2.19	498	666	1.86
36	59900	464	475	585	2.11	491	656	1.89
37	37500	398	408	480	2.58	411	579	2.14

The E_g of **37** is much higher than a thermocleavable polymer reported in the literature based on a fluorene unit flanked by thienyl units as donor unit and thienopyrazine as an acceptor unit due to the thienopyrazine being a stronger electron-acceptor than the phthalate ester monomer (**Scheme 2.4**)[28]. The band gaps of the reported polymers (**T1** and **T2**) are 2.03 and 1.66 eV, respectively which are lower than those of **35**, **36** and **37** because the **CPDT** units on those polymers has stronger electron-donating ability than fluorene or bithiophene units as well as the **BT** unit is a stronger electron acceptor than the phthalate ester monomer (**Scheme 2.6**)[31]. Therefore, the overlap of the orbitals between **CPDT** and **BT** units in **T1** and **T2** are stronger than the fluorene or bithiophene units with phthalate ester moieties in **35**, **36** and **37**. As a result, the π-electron delocalisation along the conjugated polymer backbones in **T1** and **T2** is increased and lead to lower band gaps. After thermal treatment at 300 °C for 10 minutes, the E_g of **T1** is significantly reduced to 1.73 eV, while it has a negligible impact on the band gap of **T2**. The band gaps of **T1** and **T2** are also lower than **35**, **36** and **37** after thermal treatment.

2.6. Thermal properties of the polymers

The thermal properties of the polymers were studied by TGA (**Figure 2.3**). TGA for the polymers indicates two different weight loss peaks. The first weight loss peaks are around 300 °C corresponding to thermocleavage of the secondary phthalate ester groups into carboxyl groups followed by dehydration and conversion of the soluble precursor polymers into active phthalic anhydride polymers (**Scheme 2.20**). The secondary esters are cleaved significantly at higher temperatures than tertiary esters as reported in previous literature[29]. The second weight loss peaks are about 500 °C corresponding to the decomposition of the conjugated polymer backbone.

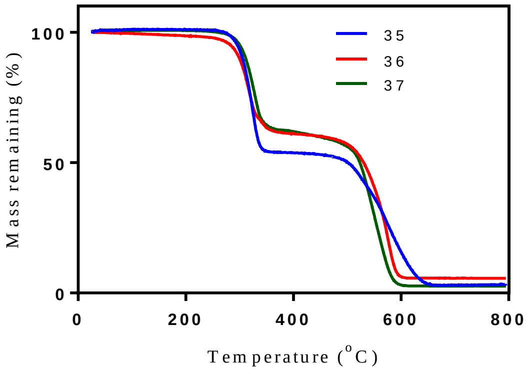

Figure 2.3: TGA of **35**, **36** and **37**

2.7. Powder X-ray diffraction (XRD) of the polymers

The structural properties of the polymers were studied by powder XRD in the solid state (**Figure 2.4**). The XRD of the **35**, **36** and **37** show diffraction peaks at 20°, 20.3° and 18.5° corresponding to the π-π stacking distance of 4.43, 4.36 and 4.79 Å, respectively. The results show that all polymers have an amorphous nature.

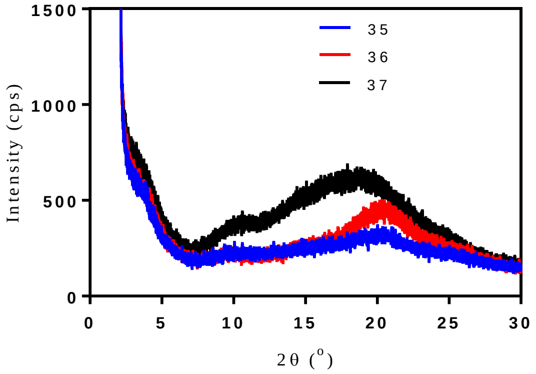

Figure 2.4: The powder XRD of **35**, **36** and **37**

2.8. Conclusions

In summary, three novel phthalate-based thermocleavable copolymers were synthesised by the Stille polymerisation. **35** and **36** are two thermocleavable copolymers including bithiophene or tetrathiophene as the donor units and secondary phthalate esters as the acceptor units. **37** copolymer has a fluorene flanked by thienyl units as a donor moiety and secondary phthalate ester as the acceptor building block. The impact of the different donor units was investigated on the solubility, molecular weights, optical and structural properties of the resulting polymers. **36** was synthesised in 87% yield which was significantly higher than **35** (39% yield). **37** was synthesised in 64% yield. **36** and **35** have comparable M_n values around 9500 g mol^{-1}, despite the fact that the former polymer was extracted in toluene fraction, while the latter polymer was extracted in hexane fraction. **37** has the highest M_n value among all polymers prepared (M_n = 16400 g mol^{-1}), however, it was extracted in the hexane fraction. In solutions, the absorption spectrum of **36** shows red-shifted absorption maxima more than 65 nm relative to **35** and **37** which display similar absorption maxima (397 *vs* 398 nm). This is probably due to **36** having tetrathiophene segments as the donor repeat units which makes the polymer backbone adopt more coplanar structure relative to **35** and **37**. In thin films, the absorption spectra of the polymers show red-shifted absorption maxima relative to their absorption in solutions. **35** and **36** have comparable optical band gaps of around 2.1 eV which is significantly lower than **37** (2.58 eV). Upon thermal treatment of the films, the absorption maxima of the polymers are shifted to longer wavelengths, **35** show quite strong bathochromic shift absorption maxima more than 70 nm relative to its thin-film before thermocleavage. Upon thermocleavage, the E_g of the polymer are reduced to around 1.8 eV for **35** and **36** and 2.14 eV for **37**. TGA analysis confirmed that the solubilising secondary ester groups on soluble precursor polymers are changed to carboxyl groups followed by dehydration into active phthalic anhydride polymers around 300 °C. The powder XRD of the polymers show diffraction peaks around 20° for **35** and **36** and 18.5° for **37** corresponding to the π-π stacking distance of about 4.0 Å. All polymers have an amorphous nature.

References

1. R. Wessling, Journal of Polymer Science: Polymer Symposia, Wiley Online Library: 1985, **72**, 55-66.

2. D. Gagnon, J. Capistran, F. Karasz, R. Lenz and S. Antoun, *Polymer*, 1987, **28**, 567-573.

3. W. J. Feast and J. N. Winter, *Journal of the Chemical Society, Chemical Communications*, 1985, 202-203.
4. D. Bott, C. Brown, C. Chai, N. Walker, W. Feast, P. Foot, P. Calvert, N. Billingham and R. Friend, *Synthetic Metals*, 1986, **14**, 245-269.
5. S. Günes, H. Neugebauer, N. S. Sariciftci, F. Banishoeib, A. Henckens, T. Cleij, L. Lutsen and D. Vanderzande, *Solar Energy Materials and Solar Cells*, 2006, **90**, 2815-2828.
6. F. Banishoeib, P. Adriaensens, S. Berson, S. Guillerez, O. Douheret, J. Manca, S. Fourier, T. Cleij, L. Lutsen and D. Vanderzande, *Solar Energy Materials and Solar Cells*, 2007, **91**, 1026-1034.
7. J. Liu, E. N. Kadnikova, Y. Liu, M. D. McGehee and J. M. Fréchet, *Journal of the American Chemical Society*, 2004, **126**, 9486-9487.
8. X. Han, X. Chen and S. Holdcroft, *Advanced Materials*, 2007, **19**, 1697-1702.
9. T. J. Gordon, J. Yu, C. Yang and S. Holdcroft, *Chemistry of Materials*, 2007, **19**, 2155-2161.
10. C. Edder, P. B. Armstrong, K. B. Prado and J. M. Fréchet, *Chemical Communications*, 2006, 1965-1967.
11. M. Helgesen, R. Søndergaard and F. C. Krebs, *Journal of Materials Chemistry*, 2010, **20**, 36-60.
12. K. Yoshino, S. Nakajima and R.-i. Sugimoto, *Japanese Journal of Applied Physics*, 1987, **26**, L1038.
13. K. Norrman, N. Larsen and F. C. Krebs, *Solar Energy Materials and Solar Cells*, 2006, **90**, 2793-2814.
14. K. Norrman and F. C. Krebs, *Solar Energy Materials and Solar Cells*, 2006, **90**, 213-227.
15. K. Norrman, S. A. Gevorgyan and F. C. Krebs, *ACS Applied Materials & Interfaces*, 2008, **1**, 102-112.
16. M. Lira-Cantu, K. Norrman, J. W. Andreasen and F. C. Krebs, *Chemistry of Materials*, 2006, **18**, 5684-5690.

17. M. Manceau, A. Rivaton, J.-L. Gardette, S. Guillerez and N. Lemaître, *Polymer Degradation and Stability*, 2009, **94**, 898-907.

18. O. Hagemann, M. Bjerring, N. C. Nielsen and F. C. Krebs, *Solar Energy Materials and Solar Cells*, 2008, **92**, 1327-1335.

19. M. Bjerring, J. S. Nielsen, A. Siu, N. C. Nielsen and F. C. Krebs, *Solar Energy Materials and Solar Cells*, 2008, **92**, 772-784.

20. F. C. Krebs and H. Spanggaard, *Chemistry of Materials*, 2005, **17**, 5235-5237.

21. E. Katz, S. Gevorgyan, M. Orynbayev and F. C. Krebs, *The European Physical Journal Applied Physics*, 2006, **36**, 307-311.

22. S. Bertho, G. Janssen, T. J. Cleij, B. Conings, W. Moons, A. Gadisa, J. D'Haen, E. Goovaerts, L. Lutsen and J. Manca, *Solar Energy Materials and Solar Cells*, 2008, **92**, 753-760.

23. F. C. Krebs and K. Norrman, *Progress in Photovoltaics: Research and Applications*, 2007, **15**, 697-712.

24. J. Liu, E. N. Kadnikova, Y. Liu, M. D. McGehee and J. M. J. Frechet, *Journal of the American Chemical Society*, 2004, **126**, 9486-9487.

25. M. Bjerring, J. S. Nielsen, N. C. Nielsen and F. C. Krebs, *Macromolecules*, 2007, **40**, 6012-6013.

26. S. A. Gevorgyan and F. C. Krebs, *Chemistry of Materials*, 2008, **20**, 4386-4390.

27. T. Tromholt, S. A. Gevorgyan, M. Jørgensen, F. C. Krebs and K. O. Sylvester-Hvid, *ACS Applied Materials & Interfaces*, 2009, **1**, 2768-2777.

28. M. Helgesen and F. C. Krebs, *Macromolecules*, 2010, **43**, 1253-1260.

29. M. H. Petersen, S. A. Gevorgyan and F. C. Krebs, *Macromolecules*, 2008, **41**, 8986-8994.

30. M. Helgesen, S. A. Gevorgyan, F. C. Krebs and R. A. J. Janssen, *Chemistry of Materials*, 2009, **21**, 4669-4675.

31. M. Helgesen, M. Bjerring, N. C. Nielsen and F. C. Krebs, *Chemistry of Materials*, 2010, **22**, 5617-5624.

32. F. Banishoeib, A. Henckens, S. Fourier, G. Vanhooyland, M. Breselge, J. Manca, T. Cleij, L. Lutsen, D. Vanderzande and H. Neugebauer, *Thin Solid Films*, 2008, **516**, 3978-3988.

33. C. Girotto, D. Cheyns, T. Aernouts, F. Banishoeib, L. Lutsen, T. J. Cleij, D. Vanderzande, J. Genoe, J. Poortmans and P. Heremans, *Organic Electronics*, 2008, **9**, 740-746.

34. X. Guo, F. S. Kim, S. A. Jenekhe and M. D. Watson, *Journal of the American Chemical Society*, 2009, **131**, 7206-7207.
35. N. Eleya, T. Patonay, A. Villinger and P. Langer, *Helvetica Chimica Acta*, 2013, **96**, 408-413.
36. D. Albanese, M. Benaglia, D. Landini, A. Maia, V. Lupi and M. Penso, *Industrial & Engineering Chemistry Research*, 2002, **41**, 4928-4935.
37. M. Helgesen, M. Bjerring, N. C. Nielsen and F. C. Krebs, *Chemistry of Materials*, **22**, 5617-5624.
38. H. Zhao, A. Pendri and R. B. Greenwald, *The Journal of Organic Chemistry*, 1998, **63**, 7559-7562.
39. J. Y. Lee, S. M. Lee, K. W. Song and D. K. Moon, *European Polymer Journal*, 2012, **48**, 532-540.
40. J. Y. Lee, K. W. Song, J. R. Ku, T. H. Sung and D. K. Moon, *Solar Energy Materials and Solar Cells*, 2011, **95**, 3377-3384.
41. Q. Li, H. Guo, L. Ma, W. Wu, Y. Liu and J. Zhao, *Journal of Materials Chemistry*, 2012, **22**, 5319-5329.
42. V. Singh, S. Wang and E. T. Kool, *Journal of the American Chemical Society*, 2013, **135**, 6184-6191.
43. P. Chen, R. A. Lalancette and F. Jäkle, *Journal of the American Chemical Society*, 2011, **133**, 8802-8805.
44. S. T. Chadwick, A. Ramirez, L. Gupta and D. B. Collum, *Journal of the American Chemical Society*, 2007, **129**, 2259-2268.
45. D. S. Chung, J. W. Park, S.-O. Kim, K. Heo, C. E. Park, M. Ree, Y.-H. Kim and S.-K. Kwon, *Chemistry of Materials*, 2009, **21**, 5499-5507.

Chapter 3 - Fluorene/dibenzosilole-benzothiadiazole dicarboxylic imide alternating copolymers for photovoltaic applications

Abstract

Four donor-acceptor copolymers, **76**, **77**, **78** and **79** based on alternating 2,7-fluorene or 2,7-dibenzosilole flanked by thienyl units as electron-donor moieties and benzothiadiazole dicarboxylic imide (**BTDI**) as electron-accepting units have been designed and synthesised for photovoltaic applications. All polymers were synthesised in good yields *via* Suzuki polymerisation. The impact of attaching two different alkyl chains (3,7-dimethyloctyl *vs* *n*-octyl) to the **BTDI** units upon the solubility, molecular weights, optical and electrochemical properties, thermal and structural properties of the resulting polymers was investigated. **77** has the highest number average molecular weight (M_n = 24900 g mol^{-1}) among all polymers prepared. Dibenzosilole-based polymers have slightly lower optical band gaps relative to their fluorene-based analogues. All polymers displayed deep-lying HOMO levels. Their HOMO energy levels are unaffected by the nature of either the alkyl substituents or the donor moieties. Similarly, the LUMO levels are almost identical for all polymers. All polymers exhibit excellent thermal stability with T_d exceeding 350 °C. Powder XRD studies have shown that all polymers have an amorphous nature in the solid state.

3.1. Introduction

Solution processable polymer solar cells (PSCs) have received substantial consideration as a renewable energy source due to their benefits for example, flexible devices, light weight, low costs and easy fabrication[1,2,3,4]. The most successful method to build the active layer of PSCs is based on the bulk heterojunction (BHJ) architecture[5,6]. The photoactive layer is comprised of a phase separated blend of a polymer donor and a fullerene acceptor. To achieve high power conversion efficiencies (PCEs) with these devices, the conjugated polymer should have a low-lying HOMO level to obtain high open circuit voltage (V_{oc}) value, a low optical band gap to ensure high short circuit current density (J_{sc}) value, a high absorption coefficient and a good hole mobility[7,8]. The most efficient strategy to construct narrow band gap polymers relies on the use of alternating donor (D) and acceptor (A) moieties along the backbone of conjugated polymers. Using this strategy, several kinds of D-A copolymers have shown excellent PCEs and reaching up to 10% recently[9]. A range of electron-donating monomers have been successfully developed for use in this area such as fluorene, carbazole, dibenzosilole (**DBS**), anthracene, cyclopentadithiophene (**CPDT**), dithienosilole (**DTS**), and benzodithiophene (**BDT**). Meanwhile, many types of electron-accepting building blocks such as benzothiadiazole (**BT**), diketopyrrolopyrrole (**DPP**), quinoxaline (**Q**) and thienopyrroledione (**TPD**) have been used in D-A copolymers.

3.1.1. Conjugated polymers based on 2,1,3-benzothiadiazole and their derivatives

One of the most studied electron-accepting (A) heterocycle is the benzothiadiazole moiety[10]. Two types of comonomers have been developed for photovoltaic materials. The first one is the use of 2,1,3-benzothiadiazole (**BT**) which can be copolymerised with a variety of electron-donating (D) moieties to construct push-pull narrow band gap conjugated polymers for BHJ photovoltaic cells (**Scheme 3.1**)[11,12]. The second comonomer is the 4,7-di-2-thienyl-2,1,3-benzothiadiazole (**DTBT**) where there are two flanking thienyl units between the **BT** moiety and the electron-donating unit (**Scheme 3.1**)[13,14,15]. The advantages of these two thiophene spacers are to reduce the steric hindrance so that the resulting D-A copolymers adopt more planar structures[16]. In addition, these polymers possess higher charge carrier (usually hole) mobility and low band gaps[17]. However, the copolymers based on **DTBT** units have poor solubilities, consequently, low molecular weights. The donor units must contain solubilising groups of sufficient bulk to enable processability of the polymers[18]. To address this issue, 5,6-positions of the **BT** unit can be used for anchoring either electron-releasing or electron-accepting substituents in order to increase solubility, molecular weights and tuning the HOMO and LUMO levels of the resulting copolymers[19,20]. By attaching alkoxy chains on these positions, two weaker electron-accepting units called 5,6-dialkoxy-2,1,3-benzothiadiazole **(OR)$_2$BT** and 4,7-di-2-thienyl-5,6-dialkoxy-2,1,3-benzothiadiazole [**DT(OR)$_2$BT**] emerged (**Scheme 3.1**)[21]. Polymers containing these new acceptor repeat units have higher solubilities than polymers containing unsubstituted **BT**. However, by adding two electron-withdrawing substituents such as fluorine atoms, another new acceptor unit of 4,7-di-2-thienyl-5,6-difluoro-2,1,3-benzothiadiazole (**DTffBT**) emerged (**Scheme 3.1**)[22]. This fluorinated **BT** monomer is stronger electron-acceptor unit than **BT** with deeper HOMO and LUMO energy levels which lead to higher V_{oc} value compared to **DTBT** analogue. Several copolymers with high PCEs were reported based on **DTffBT**[22]. Recently, a new acceptor moiety 4,7-di-2-thienyl-2,1,3-benzothiadiazole-5,6-

N-alkyl-dicarboxylic imide (**DTBTDI**) which consists of the dicarboxylic imide group fused to the **BT** unit has been developed (**Scheme 3.1**)[20,23,24]. This acceptor has been shown as a stronger electron-deficient unit compared to both **DTBT** and **DTffBT** analogues.

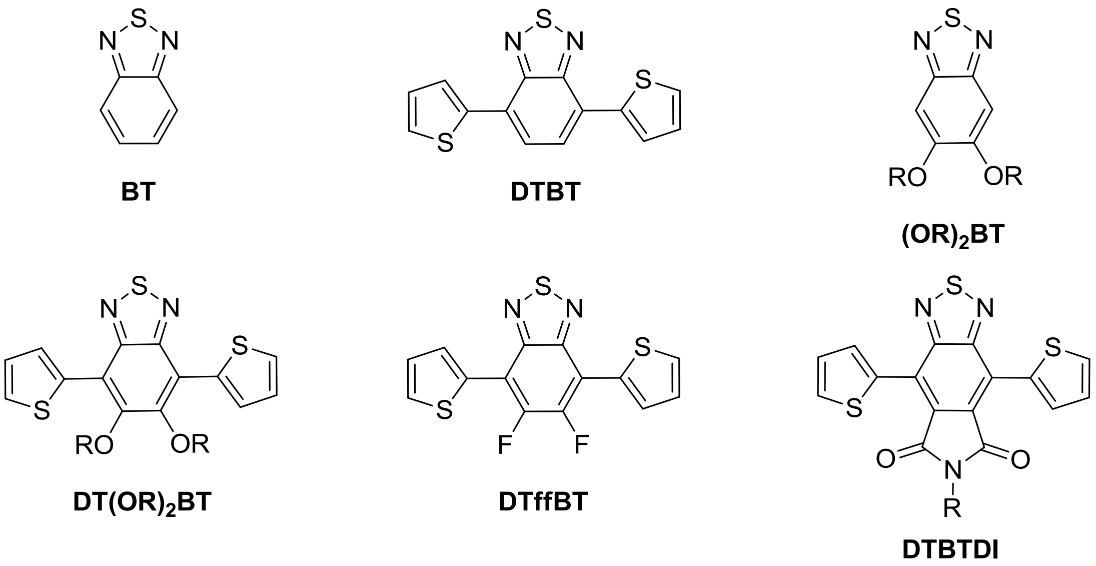

Scheme 3.1: Structures of benzothiadiazole and their derivatives

In 2013, Wang *et al.* synthesised two novel copolymers based on **DTBTDI** and benzodithiophene units which were used for solar cell applications (**Scheme 3.2**)[23]. These polymers were prepared by the Stille polymerisation between dibrominated **DTBTDI** and distannylated benzodithiophene monomers. Both **PDI-BDTT** and **PDI-BDTO** polymers have the same side chain on the acceptor unit and different side chains attached to the 4,8-positions of benzodithiophene units. The M_n values of **PDI-BDTO** and **PDI-BDTT** are 44000 and 29000 g mol^{-1}, respectively. In solutions, the **PDI-BDTT** is red-shifted (λ_{max} = 670 nm) compared to **PDI-BDTO** (λ_{max} = 632 nm), which can be attributed to the two dimensional conjugated thienyl groups in the former polymer. In thin-films, both polymers display bathochromic shifts (λ_{max} = 692 nm for **PDI-BDTT** and λ_{max} = 654 nm for **PDI-BDTO** respectively) relative to their absorption in solutions. The optical band gap (E_g) of the **PDI-BDTT** and **PDI-BDTO** are 1.55 and 1.54 eV respectively. The HOMO levels determined from the onset of oxidation by cyclic voltammetry are estimated at –5.51 eV for **PDI-BDTT** and –5.44 eV for **PDI-BDTO**. The deep-lying HOMO energy level and red-shifted absorption spectra for **PDI-BDTT** are beneficial to achieve high V_{oc} and high J_{sc} values for BHJ PSCs. The solar cell based on a **PDI-BDTT: PC$_{71}$BM** delivered an impressive PCE of 5.19%. In contrast, under the same experimental conditions, **PDI-BDTO: PC$_{71}$BM** showed a lower PCE of 2.10%[23].

More recently, Li *et al.* synthesised two other polymers based on the same acceptor, with benzodithiophene and dithienyl fluorene (**DTF**) as donors units (**Scheme 3.2**)[24]. The polymers **P(BTI-B)** and **P(BTI-F)** were synthesised by the Stille polymerisation between dibrominated **DTBTDI** and distannylated **BDT** and **DTF** units. In solutions, **P(BTI-B)** is red-shifted by 50 nm compared to **P(BTI-F)**. **P(BTI-B)** has an E_g of 1.68 eV, which is smaller than **P(BTI-F)**, since the **BDT** unit has stronger donating ability than fluorene unit. The HOMO energy level of **P(BTI-F)** is deeper than that of **P(BTI-B)**, which can be attributed to the weaker donating ability of fluorene. However, both polymers have similar LUMO energy levels. BHJ photovoltaic cells fabricated from **P(BTI-B): $PC_{61}BM$** and **P(BTI-F): $PC_{61}BM$** offered a PCE of 3.42 and 1.61%, respectively. The deep-positioned HOMO energy level for **P(BTI-F)** is advantageous for achieving a high V_{oc} of 1.11 eV. However, The J_{sc} for **P(BTI-B)** is more than twice relative to that of **P(BTI-F)** (9.8 *vs* 4.0 mA cm^{-2}) due to a smaller band gap and a higher hole mobility.

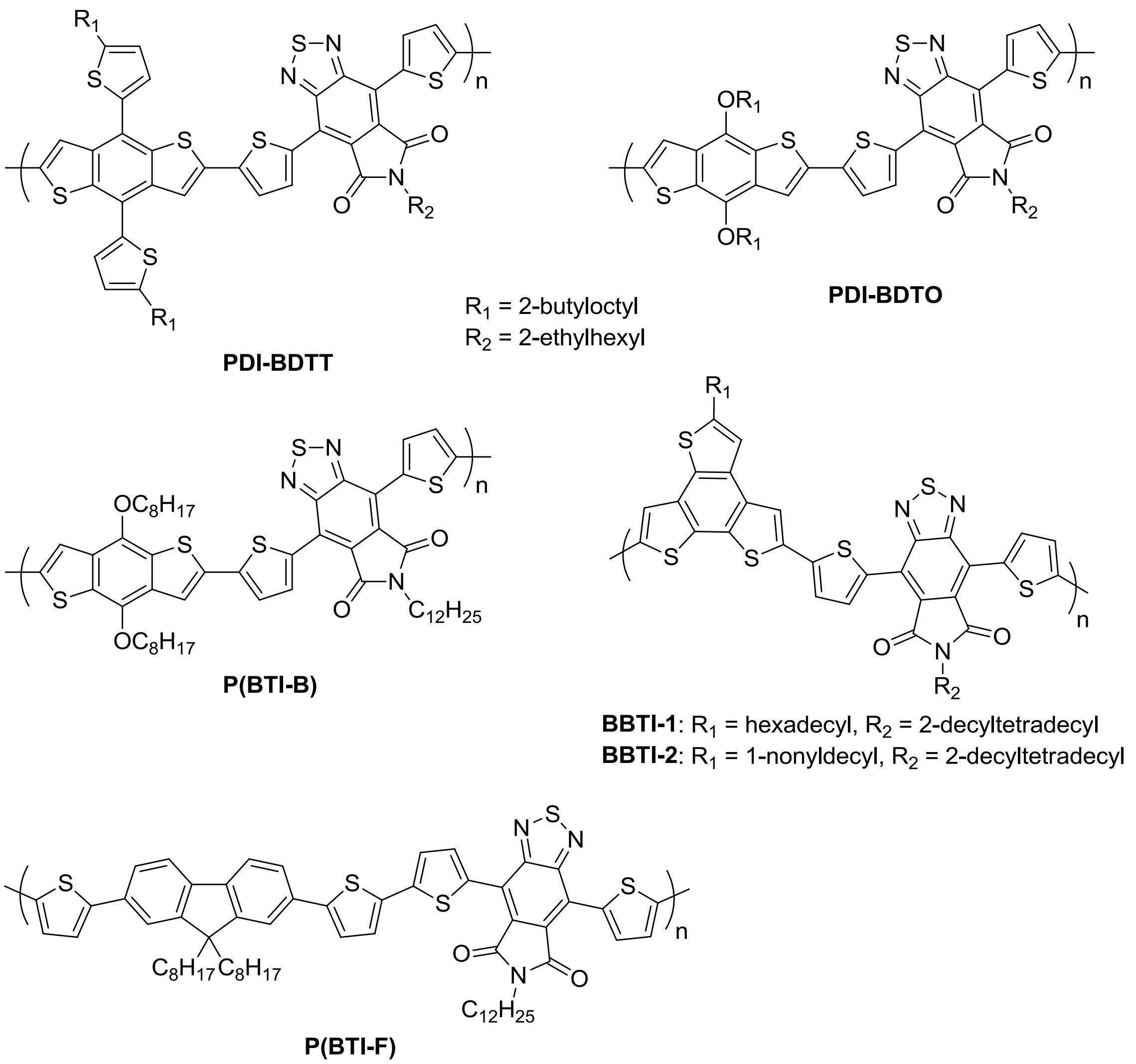

Scheme 3.2: The D-A copolymers based on **BTDI** as the acceptor units with different donor building blocks

Lately, Nielsen and co-workers prepared two novel copolymers based on the same acceptor and benzotrithiophene (**BTT**) as donor unit (**Scheme 3.2**)[20]. The polymers, **BBTI-1** and **BBTI-2**, were prepared by microwave Stille coupling polymerisation between dibrominated **DTBTDI** with distannylated **BTT**. The M_n values for the **BBTI-1** and **BBTI-2** are 64000 and 75000 g mol^{-1}, respectively. In solutions, **BBTI-1** is slightly red-shifted relative to **BBTI-2** (λ_{max} 705 *vs* 700 nm). In films, both polymers display bathochromic shifts compared to their absorption in solutions. **BBTI-1** and **BBTI-2** have the HOMO levels of –5.2 and –5.3 eV, respectively. The BHJ photovoltaic cells including **BBTI-1**: **PC$_{71}$BM** gave a remarkable PCE of 8.3%. However, **BBTI-2**: **PC$_{71}$BM** delivered a lower PCE of 6%.

3.1.2. Fluorene based conjugated polymers

Polyfluorene (**PF**) and their derivatives belong to the class of materials with fused ring aromatic systems, which are rigid and provide coplanar backbone. **PF** derivatives generally possess low HOMO energy levels around –5.5 eV, which makes them thermally and chemically stable. Due to their good solubility and high photoluminescence efficiency, conjugated polymers containing fluorene units have been widely investigated as blue emissive materials for OLED applications.

Fluorene unit is one of the promising donor building blocks for solar cell applications because of the low HOMO energy levels and acceptable hole mobilities of **PF** derivatives which provide high V_{oc} values and moderate J_{sc} values in organic photovoltaic (OPV) devices. However, **PFs** have large band gaps (2.8-3.0 eV) which are not suitable for efficient OPVs. This problem can be addressed by incorporating acceptor units into polymer backbones to generate alternating D-A copolymers, which lower the band gaps to efficiently harvest sunlight.

The D-A copolymers based on fluorene as the donor units with various acceptor units such as **DTBT**[18], quinoxaline (**Q**)[25], thienopyrazine (**TP**)[26] and pyrazinoquinoxaline (**PQ**)[27] have been reported (**Scheme 3.3**). The poly[2,7-(9-(2'-ethylhexyl)-9-hexyl-fluorene)-*alt*-5,5'-(4',7'-di-2-thienyl-2',1',3'-benzothiadiazole)] (**PFDTBT**) was the first D-A copolymer synthesised by Suzuki polymerisation published by Andersson *et al.* with an optical band gap (~1.9 eV) and a number average molecular weight (M_n) of 4800 g mol^{-1} with poor solubility (**Scheme 3.3**)[18]. The photovoltaic performance of the resulting polymer was 2.2% when blended with **PC$_{61}$BM** as the electron acceptor. The **PFDTBT**-based polymers show significant V_{oc} around 1.0 V, benefiting from low-lying HOMO level around –5.5 eV. A similar polymer **PF8DTBT** with two *n*-octyl chains in the 9-position of fluorene units exhibited a slightly higher PCE of 2.84% by using chloroform/chlorobenzene as a mixed solvent for casting the active layer (**Scheme 3.3**)[28]. Slooff *et al.* reported the same polymer backbone with two *n*-decyl chains on the fluorene moiety, **PF10DTBT** (**Scheme 3.3**)[15]. The PCE of 4.2% was obtained for **PF10DTBT: $PC_{61}BM$** based photovoltaic cell. Later on, linear alkyl chains substituted with 3,7-dimethyloctyl side chains (**DMO**) to generate a new polymer, **BisDMO-PFDTBT** (**Scheme 3.3**)[14]. The **BisDMO-PFDTBT** was used in photovoltaic cell with **$PC_{71}BM$** as the acceptor, showed higher PCE of 4.5%.

Iraqi *et al*. designed and synthesised four copolymers based on 2,7-fluorene and **BT** with or without octyloxy substituents[29]. In addition, two flanked thiophene or selenophene units are incorporated between donor and acceptor moieties (**Scheme 3.3**). All polymers were prepared by Suzuki polymerisation. The **PFDSeBT** and **PFDTBT** have E_g of 1.86 eV. However, the E_g of **PFDSeBT-8** and **PFDTBT-8** are 1.87 and 1.98 eV, respectively. They have comparable HOMO energy levels, while the LUMO levels of the polymers with selenophene spacers are higher about 0.2 eV than those with thiophene spacers. In addition, the LUMO energy levels of the polymers with octyloxy chains are higher by about 0.15 eV than those without octyloxy chains. This is attributed to the **$(OR)_2BT$** unit is a weaker electron acceptor than the **BT** unit. The polymers were fabricated with **$PC_{71}BM$** in BHJ devices gave PCE between 3.45 and 5.41%. **PFDTBT: $PC_{71}BM$** gave the highest PCE of 5.41%.

Iraqi and co-workers further reported a novel copolymer **PFDT2BT-8** based on 2,7-fluorene with **$(OR)_2BT$**[30]. In addition, two bithiophene units as spacers are inserted between donor and acceptor moieties (**Scheme 3.3**). **PFDT2BT-8** was synthesised by Suzuki polymerisation and it possesses an E_g of 1.86 eV. It exhibited high hole mobility measured by FET and also remarkable EQE of 74% at 510 nm. BHJ devices based on **PFDT2BT-8: $PC_{71}BM$** gave an impressive PCE of 6.20%.

Recently, **PFDTTBT-8** was developed and synthesised by Iraqi *et al.* using two thieno[3,2-*b*]thiophene (**TT**) units as spacers between 2,7-fluorene and **$(OR)_2BT$** (**Scheme 3.3**)[31]. The E_g of **PFDTTBT-8** is 1.94 eV, which is slightly higher than **PFDT2BT-8** analogue. The HOMO energy level of **PFDTTBT-8** is comparable to its **PFDT2BT-8** counterpart, while it has higher LUMO energy level. **PFDTTBT-8: $PC_{71}BM$** gave a PCE of 4.43%.

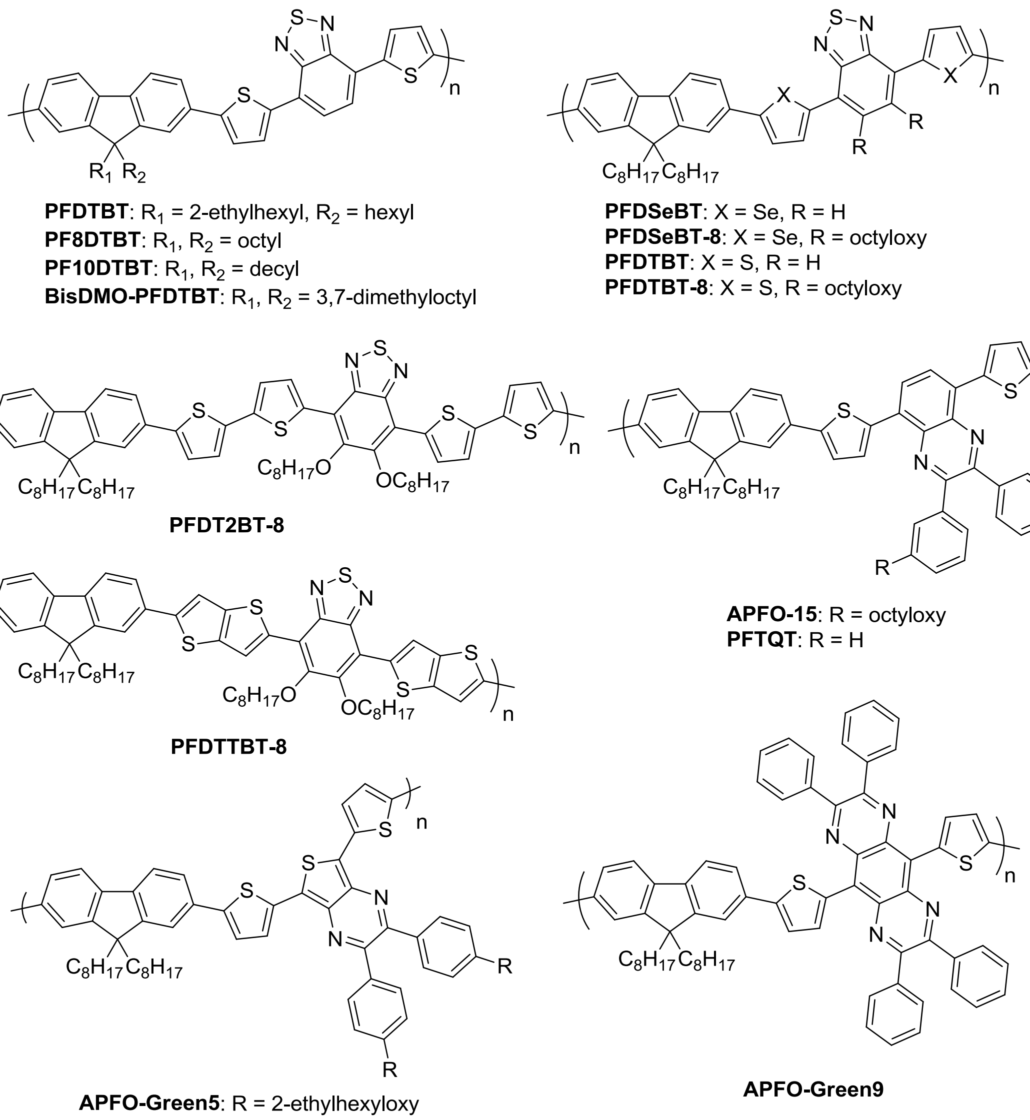

Scheme 3.3: Alternating copolymers containing fluorene units and various acceptor units

Gadisa and co-workers reported an alternating D-A copolymer, poly[2,7-(9,9-dioctylfluorene)-*alt*-5,5-{5',8'-di-2-thienyl-2',3'-bis-(3''-octyloxyphenyl)}-quinoxaline] (**APFO-15**) based on fluorene as a donor unit and dithienylquinoxaline (**TQT**) as acceptor unit (**Scheme 3.3**)[25]. It has deep-positioned HOMO energy level of –6.3 eV. The E_g of **APFO-15** is slightly higher relative to **PFDTBT** counterpart, since the quinoid character in **BT** is higher than the quinoxaline moiety[32]. The BHJ PSCs based on **APFO-15: PC$_{61}$BM** showed a PCE of 3.7%. Kitazawa *et al.* reported the same polymer backbone, poly[2,7-(9,9-dioctylfluorene)-*alt*-5,5-(5',8'-di-2-thienyl-2',3'-diphenylquinoxaline)] (**PFTQT**) but without octyloxy groups on the phenyl rings of the quinoxaline unit (**Scheme 3.3**)[33]. They found that using chloroform/chlorobenzene in a ratio (2/3, v/v) as a co-solvent for fabricating the active layer has a strong influence on the morphology of the BHJ material. As a result, J_{sc} significantly increased but both V_{oc} and *FF* remain almost constant. The **PFTQT: PC$_{71}$BM** gave a higher PCE of 5.5%.

By replacing the benzothiadiazole and quinoxaline by thienopyrazine (**TP**) unit a new D-A copolymer, **APFO-Green5** reported by Zhang and co-workers (**Scheme 3.3**)[26]. It has a high molecular weight (M_n = 40000 g mol^{-1}) and possesses a much lower E_g of 1.5 eV compared to D-A copolymers containing benzothiadiazole and quinoxaline units, since the **TP** increase the π-electron delocalisation along the conjugated polymer backbone due to it adopts the quinoid structure by maintaining the aromaticity of pyrazine units[32]. **APFO-Green5** devices fabricated with **PC$_{61}$BM** delivered a moderate PCE of 2.2%.

To further lower the band gap, **TP** unit was replaced by pyrazinoquinoxaline (**PQ**) unit and yielded **APFO-Green9** which has an E_g of 1.4 eV (**Scheme 3.3**)[27]. The PSCs based on **APFO-Green9: PC$_{71}$BM** achieved a PCE of 2.3%.

3.1.3. Dibenzosilole based conjugated polymers

Upon introduction of a silicon atom instead of a methylene bridge in fluorene, another promising donor unit dibenzosilole (**DBS**) has emerged. Leclerc *et al.* were the first research group to prepare a D-A copolymer, poly[9,9-dioctyl-2,7-dibenzosilole-*alt*-5,5-(4',7'-di-2-thienyl-2',1',3'-benzothiadiazole)] (**PDBSDTBT**) based on **DBS** and **DTBT** for photovoltaic applications (**Scheme 3.4**)[34]. It was synthesised by the Suzuki polymerisation with an E_g of 1.85 eV and a M_n of 15000 g mol^{-1}. The photovoltaic performance of this polymer with **PC$_{61}$BM** as the acceptor delivered a PCE of 1.6%. Soon after, Cao *et al.* independently reported a higher PCE of 5.4% for the same polymer using 4-fold higher M_n (79000 g mol^{-1})[35]. The improved performance of **PDBSDTBT** compared to **PFDTBT** analogue was due to higher hole mobility measured by FET and broader absorption spectrum. In addition, the C-Si bond in **DBS** unit is longer than C-C bond in fluorene unit. Consequently, **DBS** units create less steric hindrance compared to their fluorene counterparts and therefore a better π-π stacking between polymer chains is expected[36].

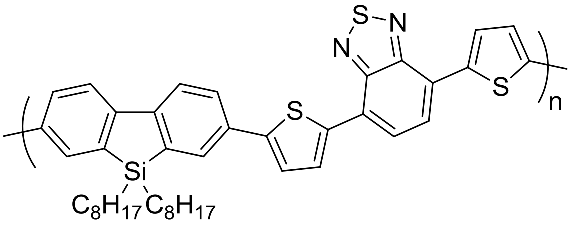

PDBSDTBT

Scheme 3.4: The structure of **PDBSDTBT**

3.2. Synthesis of monomers:

3.2.1. Synthesis of benzothiadiazole dicarboxylic imide (BTDI) monomers

49 and **50** are **BTDI** monomers for the preparation of the target polymers in this chapter. **49** and **50** were synthesised through several steps starting from commercially available thiophene (**38**) (**Scheme 3.5**). The different steps in their preparation are discussed below.

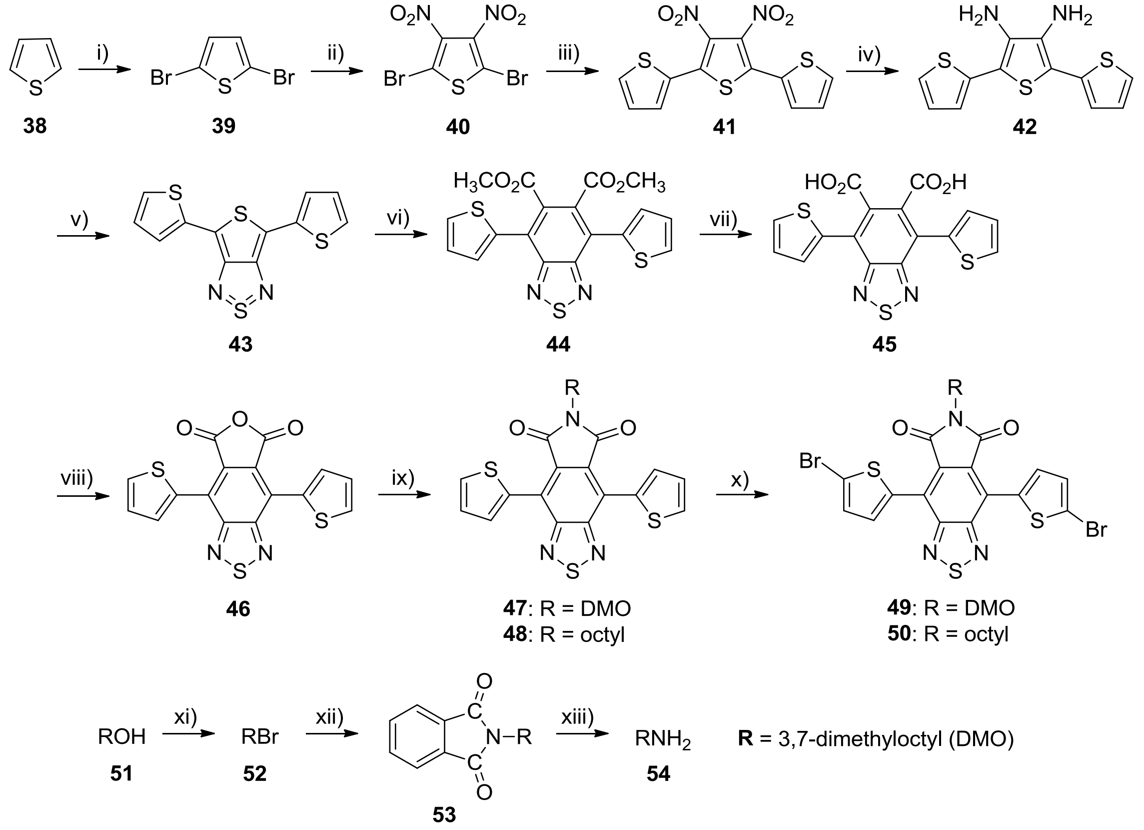

Scheme 3.5: Synthetic steps of the **BTDI** monomers

Reagents and conditions: i) NBS, DMF, –15 °C, RT, overnight; ii) fuming H_2SO_4 (20% free SO_3), conc. H_2SO_4, conc. HNO_3, 20 °C, 20-30 °C, 3h; iii) 2-(tributylstannyl)thiophene, anhydrous toluene, $PdCl_2(PPh_3)_2$, 115 °C, 24h; iv) anhydrous $SnCl_2$, HCl (35%), ethanol, 30 °C, 24h, NaOH (25%); v) PhNSO, TMSCl, anhydrous pyridine, 3h, RT, HCl (1.0 N); vi) dimethyl acetylenedicarboxylate, anhydrous xylene, reflux 24h; vii) aqueous NaOH, ethanol, reflux 24h, HCl (35%); viii) anhydrous Ac_2O, anhydrous xylene, 130 °C, 6h; ix) HOAc (100%), 100 °C overnight, Ac_2O, 100 °C, 6h; x) NBS, THF, RT, overnight; xi) DCM, PPh_3, NBS, RT, 90 min; xii) potassium phthalimide, anhydrous DMF, 90 °C, 17h, KOH; xiii) hydrazine hydrate (51%), methanol, reflux, HCl (5.0 M), reflux, 1h

3.2.1.1. Synthesis of 2,5-dibromothiophene (39)

Thiophene (**38**) was selectively brominated at 2,5-positions using two equivalents of *N*-bromosuccinimide (NBS) in DMF in the dark gave **39** as a yellow oily product in a high yield of 82% (**Scheme 3.5**)[37].

The mechanism of the reaction is an electrophilic aromatic substitution and consists of two main steps (**Scheme 3.6**). In the first step, the thiophene (**38**) functions as a nucleophile and attacks the electrophilic bromine of NBS to form a carbocation intermediate, which is stabilised by three resonance structures (**55**, **56** and **57**). In the second step, the carbocation is deprotonated by succinimide anion to form 2-bromothiophene intermediate (**58**) which was then brominated at C-5 to give **39**.

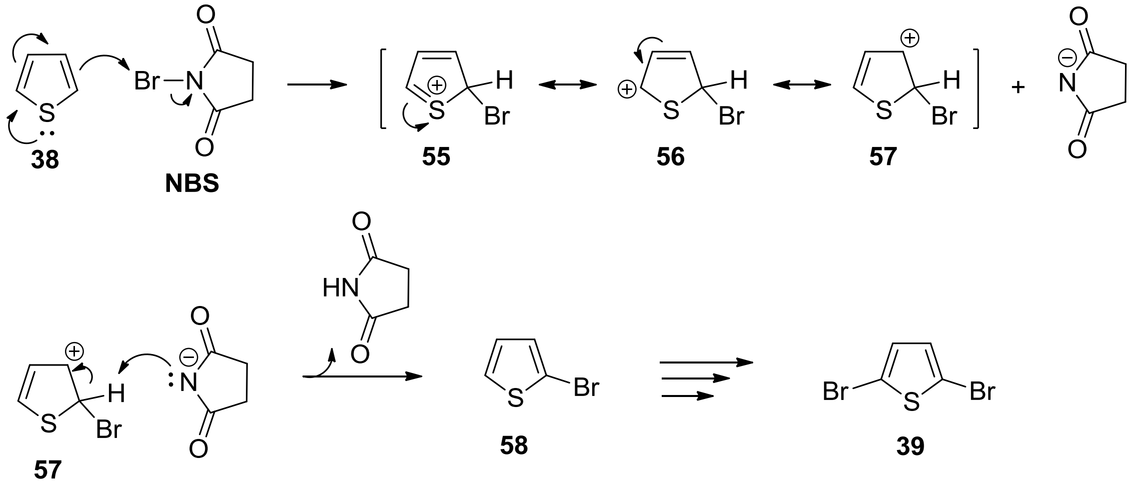

Scheme 3.6: The mechanism of bromination of thiophene (**38**) by NBS

The structure and purity of **39** were approved by the ^{1}H NMR spectroscopy. The ^{1}H NMR spectrum of **39** shows a singlet peak at 6.87 ppm equivalent to the two protons.

3.2.1.2. Synthesis of 2,5-dibromo-3,4-dinitrothiophene (40)

40 was readily prepared through the nitration reaction of **39** with concentrated nitric acid, concentrated sulfuric acid and fuming sulfuric acid (**Scheme 3.5**)[38]. The first nitration takes place at 3-position of 2,5-dibromothiophene (**39**) to form 2,5-dibromo-3-nitrothiophene (**60**). A nitro group functions as an electron withdrawing group and deactivates the **60** towards the second nitration. Therefore, the second nitration at the 4-position of the **60** needs vigorous conditions. Fuming sulfuric acid is required to form **40** in a high yield. Furthermore, extending the reaction time for three hours is necessary at 20–30 °C to accomplish the reaction. Otherwise, a mixture of mono- and dinitro-compounds is formed[39].

The method and order of addition of the acids in the nitration of **39** can play a crucial role. In our work, **40** was synthesised in an excellent yield of 91% by adding concentrated nitric acid dropwise to a mixture of **39**, concentrated sulfuric acid and fuming sulfuric acid (20% free SO_3)[38]. On the other hand, nitration gave only 50% yield by adding **39** to the mixture of fuming sulfuric acid, concentrated sulfuric acid and fuming nitric acid[39,40].

The mechanism of the nitration reaction comprises of three distinct steps (**Scheme 3.7**)[41]. In the first step, the hydroxyl group of nitric acid is protonated by the sulfuric acid; subsequently a molecule of water is expelled to form a nitronium ion (NO_2^+) electrophile. In the second step, **39** functions as a nucleophile, attacks the NO_2^+ to form an arenium ion intermediate (**59**). Then, in the third step, HSO_4^- deprotonates **59** to form intermediate **60** and H_2SO_4 is regenerated as a catalyst. Finally, **40** is formed from the latter intermediate by the same mechanism.

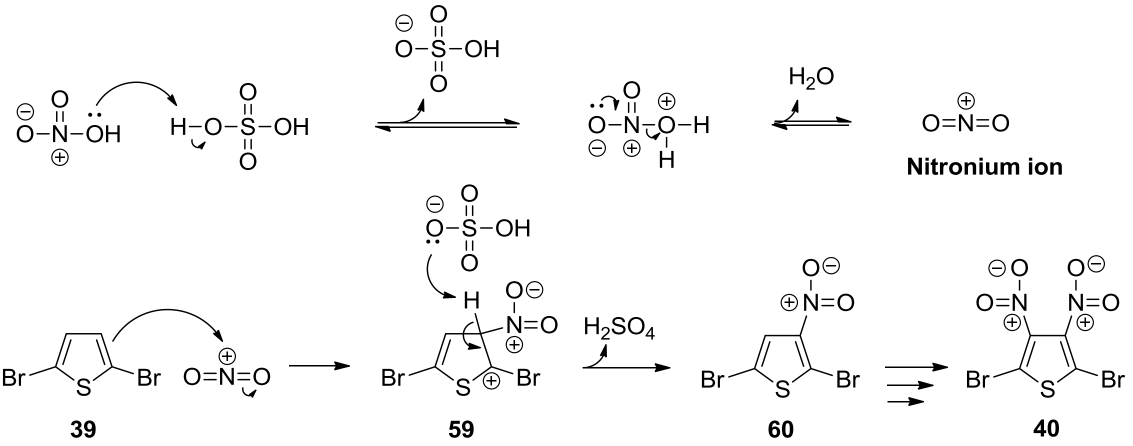

Scheme 3.7: The mechanism of nitration of **39**

40 does not contain a hydrogen atom; therefore, ^{13}C NMR spectroscopy is a fundamental method for initial characterisation. The ^{13}C NMR spectrum of the **40** shows two signals at 113.4 and 140.7 ppm for the two chemically different environments of carbon atoms. The FT-IR spectrum of the **40** exhibits two peaks at 1345 and 1535 cm^{-1} for symmetric and asymmetric stretching vibrations of the nitro groups respectively.

3.2.1.3. Synthesis of 3',4'-dinitro-2,2':5',2''-terthiophene (41)

41 was synthesised using the Stille coupling reaction between **40** and 2-(tributylstannyl)thiophene in the presence of $PdCl_2(PPh_3)_2$ as a catalyst in anhydrous toluene at 115 °C (**Scheme 3.5**)[42]. It was obtained as orange crystals in an excellent yield of 90%. The mechanism of the reaction is similar to that of the Stille reaction described in the introduction chapter.

41 was characterised by several techniques such as the ^{1}H NMR spectroscopy and mass spectrometry. The ^{1}H NMR spectrum of **41** shows three doublet of doublet at 7.62, 7.56 and 7.19 ppm for six protons on the thiophene rings. In addition, mass spectrum of **41** shows a peak at 338 corresponding to the mass of the molecular ion $[M]^+$ of **41**.

3.2.1.4. Synthesis of 3',4'-diamino-2,2':5,2''-terthiophene (42)

42 was obtained by a reduction reaction of **41** using excess anhydrous tin (II) chloride ($SnCl_2$) as a common reducing agent in the presence of a mixture of HCl in ethanol to ensure the reaction was accomplished (**Scheme 3.5**)[43]. **42** was achieved as a brown solid in an excellent yield of 97%.

The mechanism of the reduction of the nitro group by tin(II) chloride is performed by single electron transfer (SET) (**Scheme 3.8**). In the first step one electron is transferred from the tin(II) chloride to the oxygen atom of the nitro group and a radical anion is formed and then protonated. After the protonation takes place, a second electron is transfered to the nitrogen. Then, a second proton is added, followed by loss of water the nitroso intermediate (**61**) is formed. The second intermediate which is hydroxylamine (**62**) is formed by the same sequence. Finally, the N-O bond is broken by adding another two electrons to give anions of the products which are protonated to give **42**.

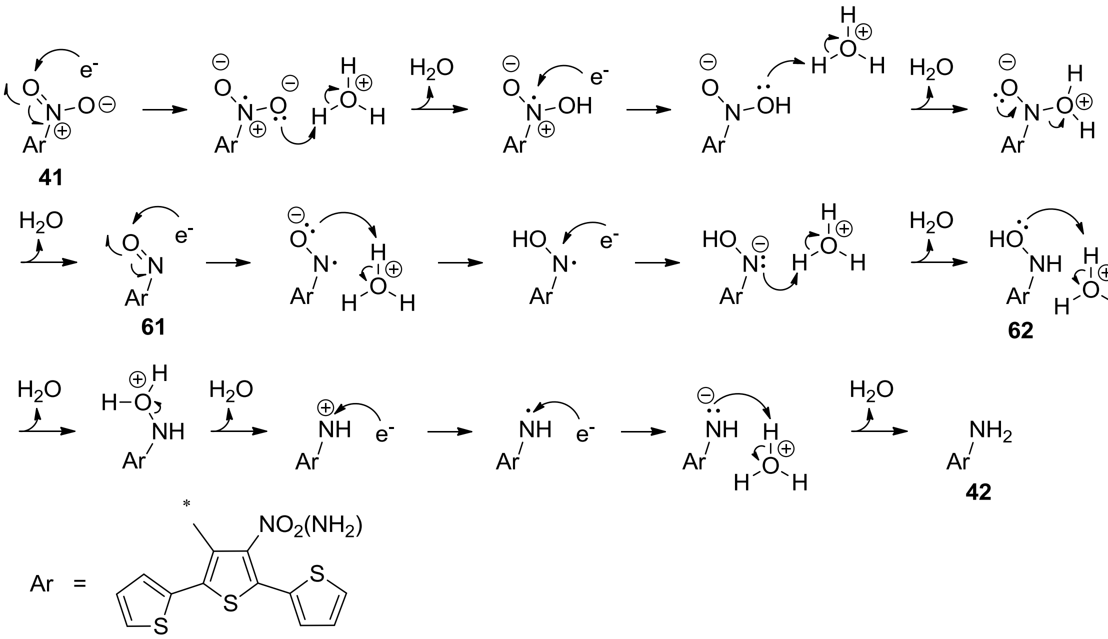

Scheme 3.8: The mechanism of reduction of nitro groups by tin(II) chloride to form **42**

Tin is oxidised from oxidation state of + II to + IV by loss of two electrons and in the same time nitrogen is reduced from the oxidation state of + V to – III by gaining eight electrons. Therefore, four equivalents of the tin(II) chloride are required to reduce each nitro group.

The ^1H NMR spectrum of **42** shows a doublet and a multiplet at 7.30 and 7.09-7.14 ppm respectively for six protons on the thiophene rings. In addition, it also displays a broad singlet at 3.76 ppm corresponding to four protons of the amino groups. The FT-IR spectrum of **42** shows two peaks at 3298 and 3371 cm^{-1} for symmetric and asymmetric N-H stretching vibrations for the amino groups. Moreover, N-H bending is observed at 1615 cm^{-1}. The mass spectrum of **42** exhibits a peak at $m/z = 278$ corresponding to the mass of the molecular ion $[M]^+$ of **42**.

3.2.1.5. Synthesis of 4,6-bis(2-thienyl)-thieno[3,4-*c*][1,2,5]-thiadiazole (43)

43 was synthesised by reaction of **42** with *N*-thionyl aniline (PhNSO) and trimethylsilyl chloride (TMSCl) in anhydrous pyridine to afford blue crystals in an excellent yield of 93% (**Scheme 3.5**)

The ^1H NMR spectrum of the **43** shows three doublet of doublet at 7.59, 7.34 and 7.12 ppm for six protons on the thiophene rings. Furthermore, a broad band at 3.76 ppm for amino protons disappears which is good evidence that the cyclisation reaction was successful. The structure of **43** was further confirmed by the FT-IR spectroscopy. The FT-IR spectrum of **43** indicated that the two peaks at 3298 and 3371 cm^{-1} for symmetric and asymmetric N-H stretching vibrations for the amine groups disappear.

3.2.1.6. Synthesis of 4,7-di(thien-2-yl)-2,1,3-benzothiadiazole-5,6-dimethyl ester (44)

44 was obtained using the Diels-Alder reaction between **43** and dimethyl acetylenedicarboxylate in anhydrous xylene at reflux[23]. It was obtained in an excellent yield of 94% as yellow crystals (**Scheme 3.5**).

The Diels-Alder reaction is one type of pericyclic reactions named as a $[4\pi + 2\pi]$ cycloaddition because the reaction involves two different π-systems, for instance, **43** is an electron-rich heterocyclic conjugated diene, whereas the dimethyl acetylenedicarboxylate functions as an electron-deficient dienophile because it bears two electron-withdrawing ester groups conjugated to the acetylene unit.

The mechanism of the reaction involves the formation of bridged bicyclic intermediate (**63**) (**Scheme 3.9**). **44** is formed from this intermediate by heating through loss of sulfur atom to construct heterocyclic six-membered ring benzothiadiazole. Four π-bonds are broken in dimethyl acetylenedicarboxylate and **43**. Simultaneously, two new σ-bonds and two new π-bonds are formed in **44**.

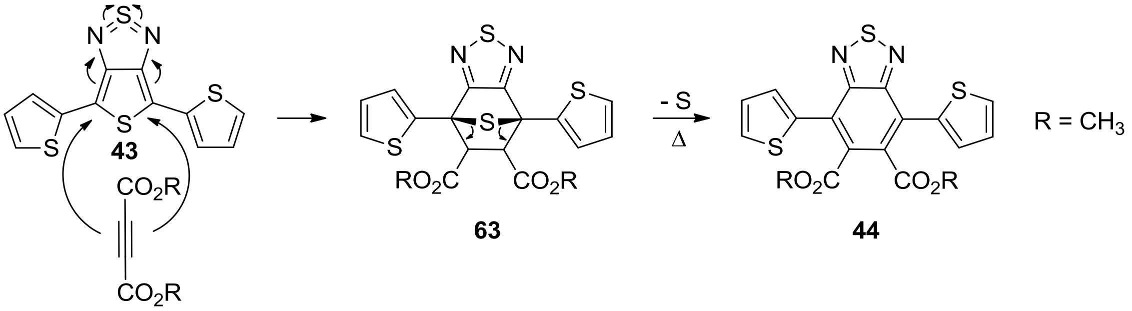

Scheme 3.9: The mechanism of the formation of **44** using the Diels-Alder reaction

The structure and purity of **44** were assessed by the ^{1}H NMR, ^{13}C NMR and FT-IR spectroscopy. The ^{1}H NMR spectrum of **44** displays four different proton environments, three in the aromatic region and one in the aliphatic region. It shows three doublets of doublets at 7.62, 7.44 and 7.22 ppm corresponding to six protons on the thiophene rings. The singlet peak at 3.78 ppm integrating to six protons denotes the presence of methyl protons and they are more deshielded in comparison to standard methyl protons (~ 0.9 ppm). The ^{13}C NMR spectrum of **44** displays nine different carbon environments, seven of which are in the aromatic region and a peak at 168.1 ppm with a high chemical shift belong to the ester groups. Moreover, the peak at 53.1 ppm can be assigned for methyl carbons. The FT-IR spectrum of **44** shows a peak at 1730 cm^{-1} corresponding to the ester groups.

3.2.1.7. Synthesis of 4,7-di(thien-2-yl)-2,1,3-benzothiadiazole-5,6-dicarboxylic acid (45)

45 was synthesised upon hydrolysis of **44** under basic conditions in ethanol under reflux followed by acidification (**Scheme 3.5**)[20]. It was obtained as a yellow solid in a yield of 85%.

The mechanism of an ester hydrolysis under basic conditions is an example of nucleophilic acyl substitution and follows four steps (**Scheme 3.10**). In the first step, the hydroxide ion acts as a nucleophile and attacks the carbonyl group of **44** to generate a negatively charged tetrahedral intermediate (**64**). In the second step, the carbonyl group is reformed by leaving the methoxide anion (CH_3O^-) and the carboxylic acid intermediate (**65**) is formed. A carboxylate anion (**66**) and methanol are generated by deprotonating the carboxylic acid by the methoxide anion in the third step. The final step is an acidification of the carboxylate anion (**66**) to form **45**.

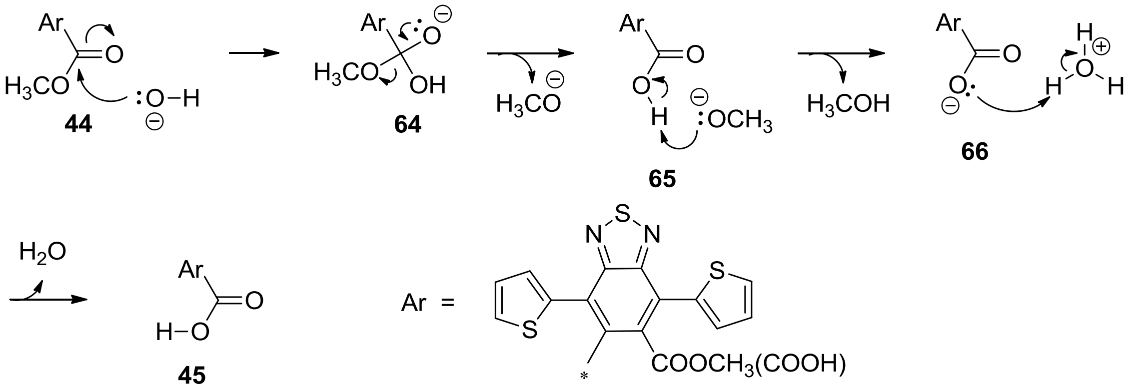

Scheme 3.10: The mechanism of the hydrolysis of **44** under basic conditions

The ^{1}H NMR spectrum of **45** displays three doublets of doublets at 7.86, 7.47 and 7.25 ppm corresponding to six protons on the thiophene rings. Furthermore, the singlet peak at 3.78 ppm for methyl protons in the ^{1}H NMR spectrum of **44** disappears, which is a good indication for the success of the reaction. The structure of **45** further confirmed by the FT-IR spectroscopy. The FT-IR spectrum of **45** shows the broad peak in the range of 2600-3300 cm^{-1} corresponding to stretching vibration of OH of carboxyl group and meanwhile the peak at 1730 cm^{-1} disappears for the ester group.

3.2.1.8. Synthesis of 4,7-di(thien-2-yl)-2,1,3-benzothiadiazole-5,6-dicarboxylic anhydride (46)

45 underwent intramolecular ring closure in the presence of acetic anhydride and anhydrous xylene at 130 °C to afford **46** as a red solid in an excellent yield of 97% (**Scheme 3.5**)[45]. The mechanism of a dehydration reaction of **45** is shown in scheme 3.11.

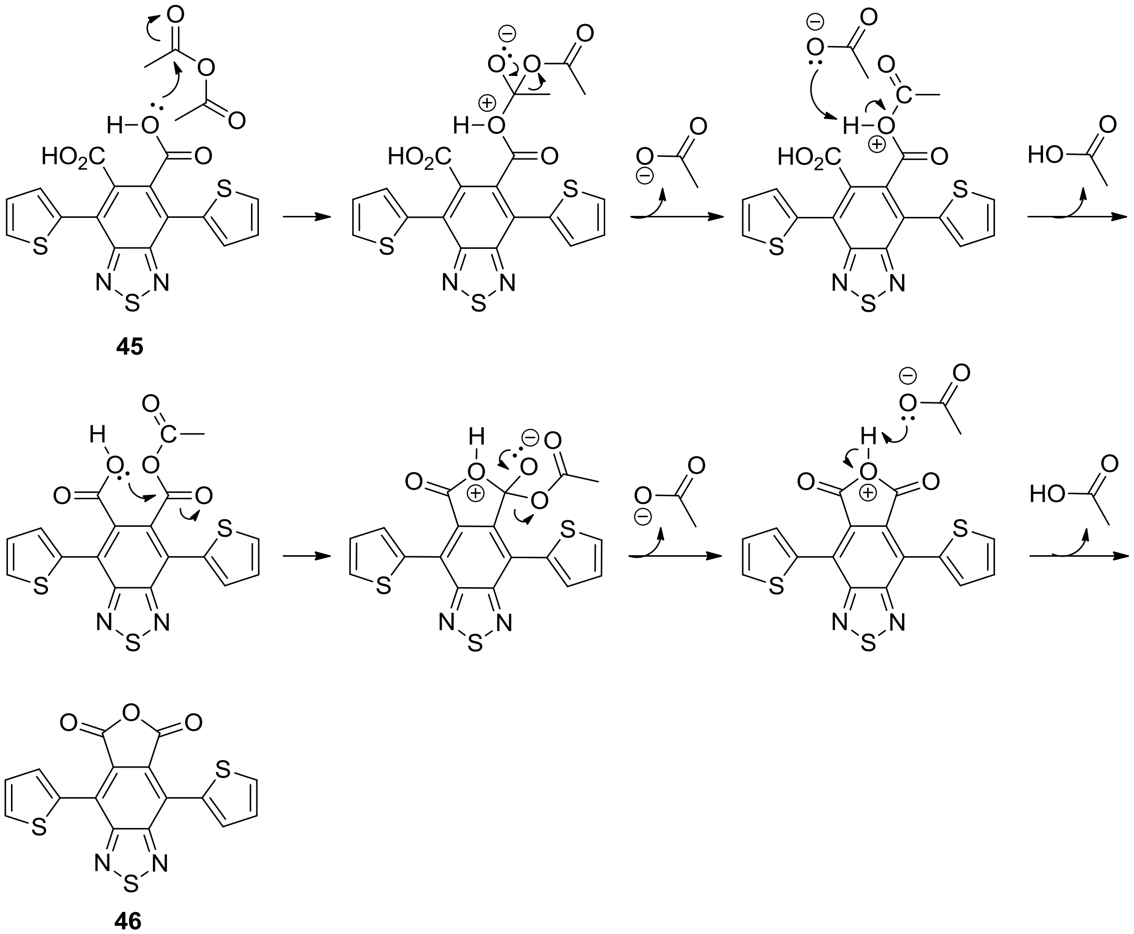

Scheme 3.11: The mechanism of the dehydration reaction of **45**

The ^{1}H NMR spectrum of **46** displays three doublets of doublets at 8.11, 7.82 and 7.33 ppm corresponding to six protons on the thiophene rings. The structure of **46** was further confirmed by the FT-IR spectroscopy. The FT-IR spectrum of **46** shows two peaks at 1765 and 1808 cm^{-1} corresponding to symmetrical and asymmetrical stretching vibrations for the anhydride functional group.

3.2.1.9. Synthesis of 4,7-di(thien-2-yl)-2,1,3-benzothiadiazole-5,6-*N*-(3,7-dimethyloctyl)dicarboxylic imide (47) and 4,7-di(thien-2-yl)-2,1,3-benzothiadiazole-5,6-*N*-octyl-dicarboxylic imide (48)

46 was reacted with 3,7-dimethyl-1-octanamine (**54**) and 1-octanamine in the presence of acetic acid and acetic anhydride to yield imide functionalised monomers (**47** and **48**) as orange solids in 84 and 93% yield, respectively (**Scheme 3.5**)[45]. The mechanism of the formation of **47** and **48** is outlined in scheme 3.12.

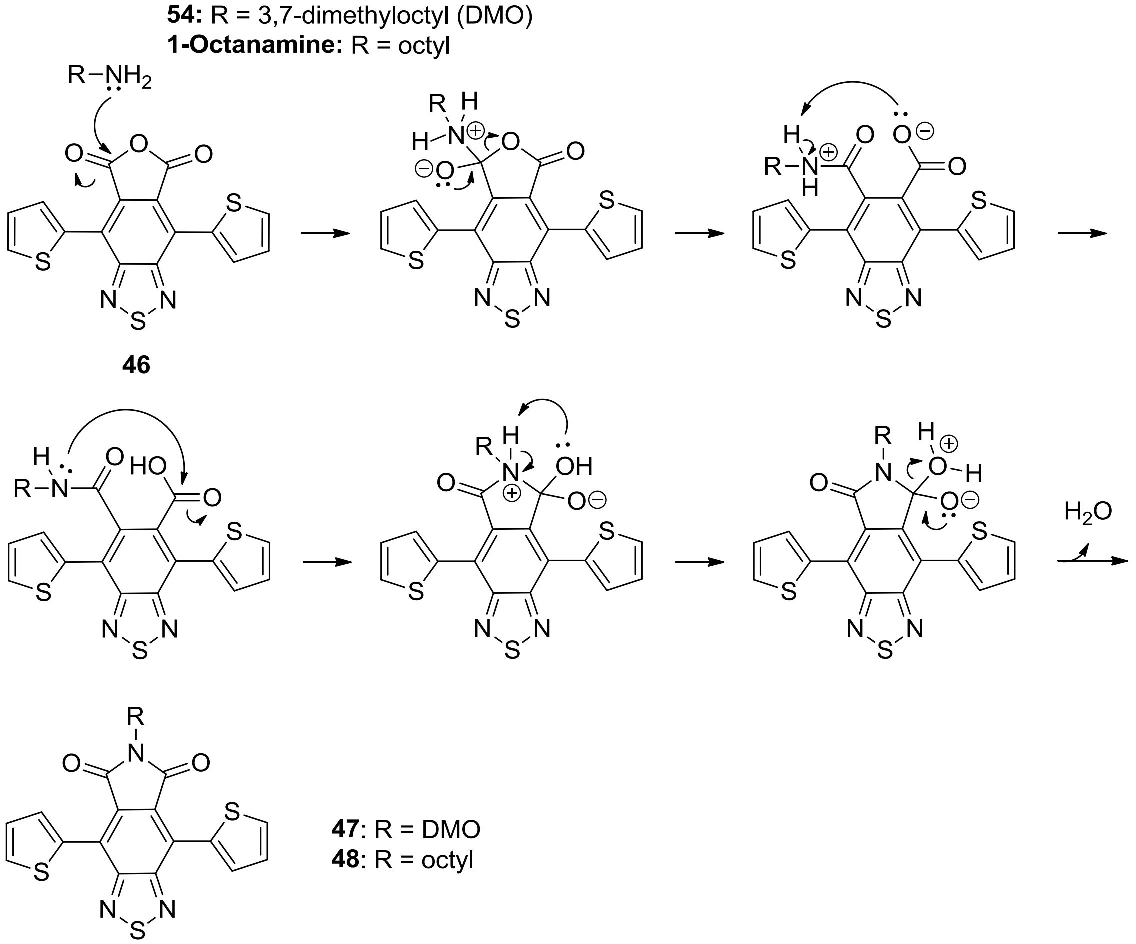

Scheme 3.12: The mechanism of the formation of **47** and **48**

47 and **48** were characterised by the ^{1}H NMR spectroscopy. The ^{1}H NMR spectra for both monomers show three doublets of doublets at 7.91, 7.73 and 7.30 ppm corresponding to six protons on the thiophene rings. Moreover, they exhibit the expected number of protons of the alkyl chains in the aliphatic region. The structures and purities of both monomers further confirmed by the ^{13}C NMR spectroscopy. The ^{13}C NMR spectra for both monomers show seven peaks for seven carbons in the aromatic region and one peak for carbon for imide functional group at 165.7 ppm and ten peaks for ten carbons for **47** and eight peaks for eight carbons for **48** in the aliphatic region, respectively. The FT-IR spectra show two peaks at 1751 and 1804 cm^{-1} for **47**, 1754 and 1808 cm^{-1} for **48**, which are representative of symmetric and asymmetric stretching vibrations for imide functional group.

3.2.1.10. Synthesis of 4,7-di(5-bromo-thien-2-yl)-2,1,3-benzothiadiazole-5,6-*N*-(3,7-dimethyloctyl)dicarboxylic imide (49) and 4,7-di(5-bromo-thien-2-yl)-2,1,3-benzothiadiazole-5,6-*N*-octyl-dicarboxylic imide (50)

47 and **48** were selectively brominated at 5,5'-positions using NBS in THF and gave **49** and **50** as red solids in excellent yields of 98 and 96%, respectively (**Scheme 3.5**)[20].

In order to selectively brominate the thiophene units at the 5,5'-positions for similar monomers, the reactions are usually performed using two equivalents of NBS to avoid multi-brominations, which often afford mixtures that are difficult to separate. However, for the bromination of **47** and **48** five equivalents of NBS were needed. This situation might be due to the strong electron-withdrawing character of the **BTDI** unit, which reduces the reactivity of the thiophene units towards the electrophilic attack. Fortunately, according to all characterisations there was no indication for tri- and tetrabrominated by-products. The mechanism of the reaction is similar to the bromination of thiophene (**38**) as illustrated in scheme 3.6.

The structures and purities of both monomers were approved by the ^{1}H NMR spectroscopy. The ^{1}H NMR spectra for both monomers exhibit two doublets at 7.80 and 7.24 ppm corresponding to four protons on the thiophene rings and expected number of protons of the alkyl chains in the aliphatic regions.

3.2.1.11. Synthesis of 3,7-dimethyloctyl bromide (52)

The commercially available 3,7-dimethyl-1-octanol (**51**) was reacted with triphenylphosphine (Ph_3P) and NBS in dichloromethane to yield **52** as a colourless oil in 73% yield (**Scheme 3.5**)[46]. The mechanism of the reaction is presented in scheme 3.13 and proceeds *via* a bimolecular nucleophilic substitution (S_N2) reaction.

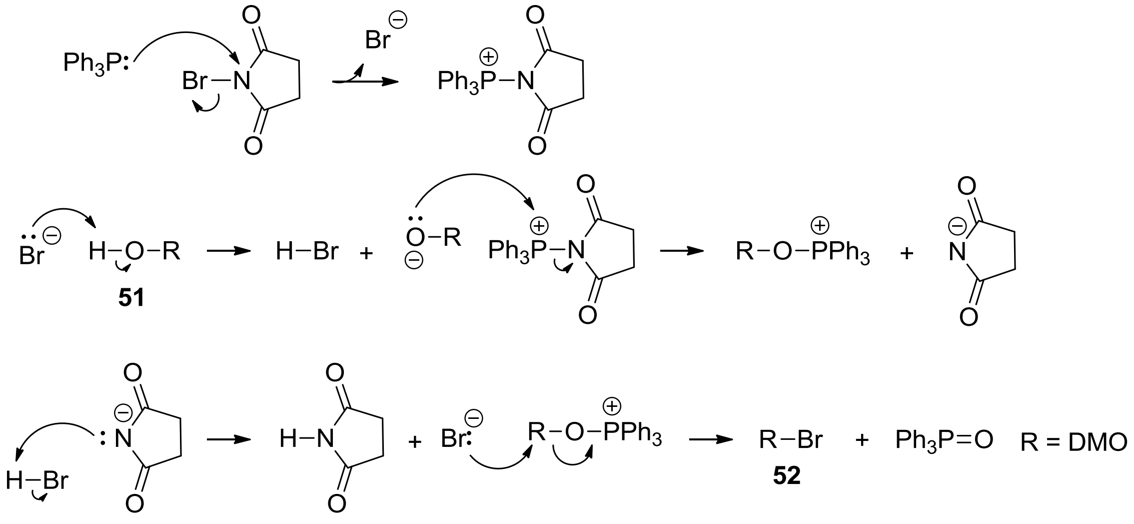

Scheme 3.13: The mechanism of bromination of **51**

52 was characterised by the ^{1}H NMR and ^{13}C NMR spectroscopy. The ^{1}H NMR spectrum of **52** shows expected number of protons. The ^{13}C NMR spectrum of **52** shows ten peaks for ten different carbon environments.

3.2.1.12. Synthesis of *N*-(3,7-dimethyloctyl)phthalimide (53)

52 was reacted with potassium phthalimide in anhydrous DMF to give **53** as colourless oil in an excellent yield of 91% (**Scheme 3.5**)[47]. The mechanism of the reaction proceeds *via* a S$_N$2 as outlined in scheme 3.14.

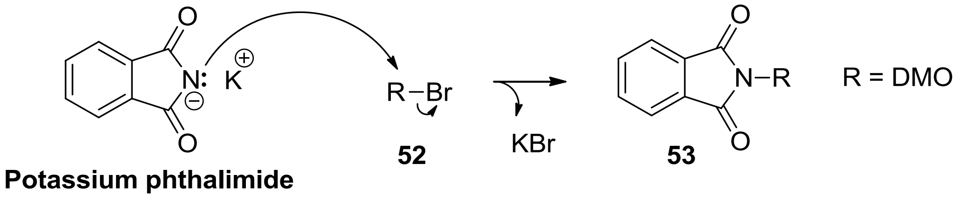

Scheme 3.14: The mechanism of formation of **53**

The structure and purity of **53** were confirmed by the ^{1}H NMR spectroscopy. The ^{1}H NMR spectrum of **53** exhibits two doublets of doublets at 7.85 and 7.72 ppm corresponding to the protons on the benzene ring. Meanwhile, it shows a series of multiplet and doublets in the aliphatic region, which are attributed to the protons of the 3,7-dimethyloctyl chain.

3.2.1.13. Synthesis of 3,7-dimethyl-1-octanamine (54)

54 was obtained from **53** using hydrazine hydrate (NH_2NH_2) in methanol as brown oil in 86% yield by Gabriel synthesis (**Scheme 3.5**)[48]. The mechanism of the reaction is depicted in scheme 3.15.

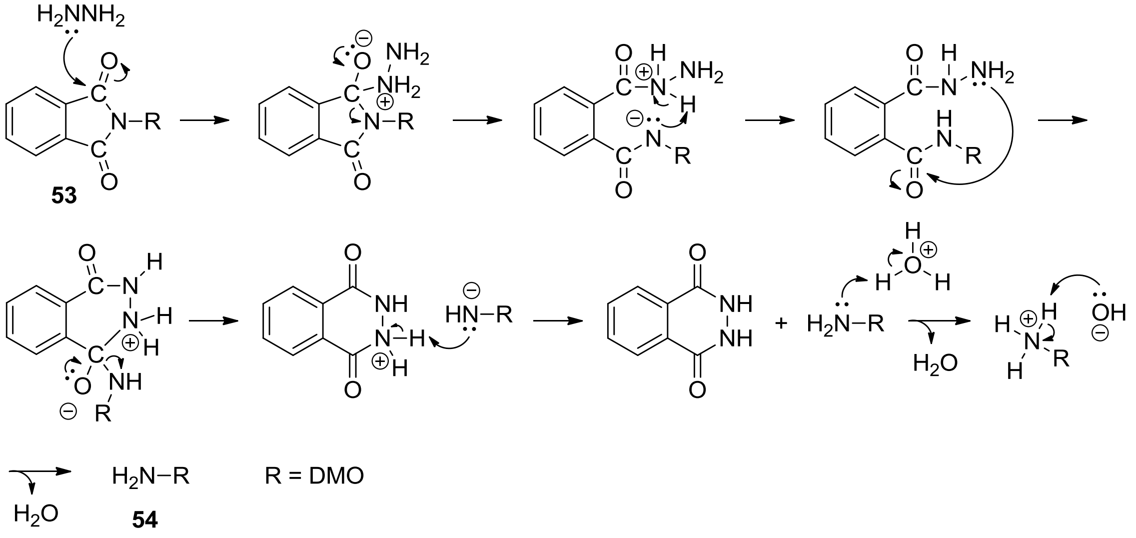

Scheme 3.15: The mechanism of the formation of **54** by Gabriel synthesis using hydrazine hydrate

The structure of **54** was approved by the ^{1}H NMR and ^{13}C NMR spectroscopy. The two doublets of doublets at 7.85 and 7.72 ppm, which were attributed to four protons of **53** disappear in the ^{1}H NMR spectrum of **54**, it is good evidence that the reaction was successful. Moreover, it shows the expected number of protons in the aliphatic region for the 3,7-dimethyloctyl chain. The ^{13}C NMR spectrum of **54** shows ten peaks for ten different carbons in the aliphatic region and meanwhile three peaks for three different carbons in the aromatic region and carbon of the imide group for **53** disappear.

3.2.2. Synthesis of diboronic ester of dibenzosilole (DBS) monomer (72)

72 is a **DBS** monomer for the preparation of the target polymers in this chapter. It was synthesised through five steps starting from the commercially available 2,5-dibromonitrobenzene (**67**) (**Scheme 3.16**). The different steps in its preparation are discussed below.

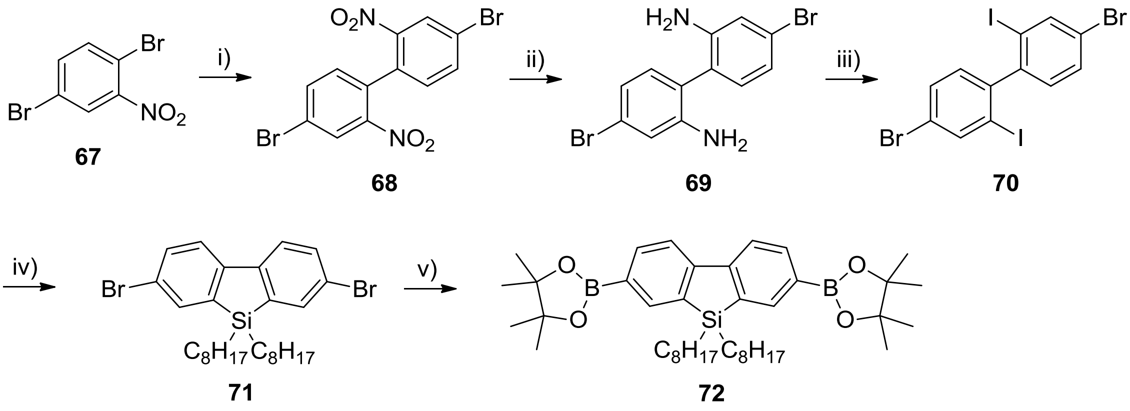

Scheme 3.16: Synthetic steps of the **DBS** monomer (**72**)

Reagents and conditions: i) Cu, DMF, 125 °C, 3h; ii) Sn, HCl (32%), ethanol, 3h, reflux, NaOH (20%); iii) HCl (32%), acetonitrile, $NaNO_2$, 0 °C, –5 to –10 °C, KI, 0 °C, –10 to –15 °C, RT, 80 °C, 20h, $Na_2S_2O_3$; iv) anhydrous THF, –78 °C, *n*-BuLi, 3h, dichlorodioctylsilane, RT, overnight; v) bis(pinacolato)diboron, $PdCl_2$(dppf), KOAc, anhydrous DMF, 100 °C, 48h

3.2.2.1. Synthesis of 4,4'-dibromo-2,2'-dinitrobiphenyl (68)

68 was prepared by the Ullmann coupling reaction using **67** and copper powder in anhydrous DMF and it was obtained as yellow crystals in an excellent yield of 90% (**Scheme 3.16**)[49].

The mechanism of the Ullmann coupling reaction comprises of two steps (**Scheme 3.17**). In the first step, copper acts as a nucleophile and attacks to the C-Br bond which is ortho to the nitro group to form an intermediate (**73**). The second step is coupling between **73** and a second molecule of the starting material to obtain the **68**.

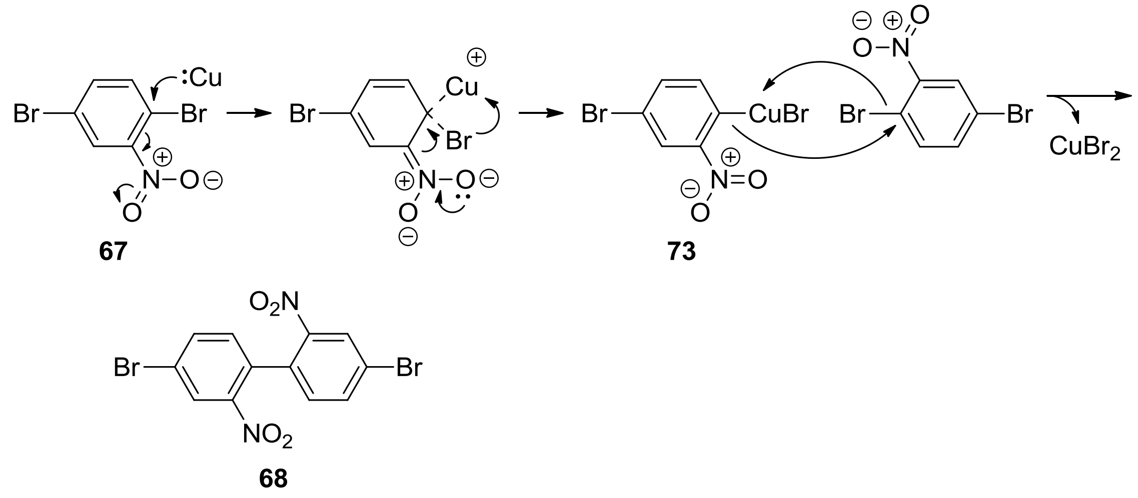

Scheme 3.17: The mechanism of the formation of **68** using Ullmann coupling reaction

The ^{1}H NMR spectrum of **68** shows a doublet, a doublet of doublet and another doublet at 8.40, 7.85 and 7.18 ppm, respectively corresponding to six protons on the biphenyl ring. The FT-IR spectrum of **68** exhibits two peaks at 1332 and 1556 cm^{-1} for symmetric and asymmetric stretching vibrations of the nitro groups.

3.2.2.2. Synthesis of 4,4'-dibromobiphenyl-2,2'-diamine (69)

68 was reduced using tin metal in ethanol under acidic medium to obtain **69** as brown crystals in a yield of 70% (**Scheme 3.16**)[50].

The reduction of nitro groups consists of two steps (**Scheme 3.18**). In the first step, **68** was reacted with Sn and HCl to generate protonated amine intermediate (**74**). In the second step, this intermediate was treated with sodium hydroxide to release the free amine (**69**).

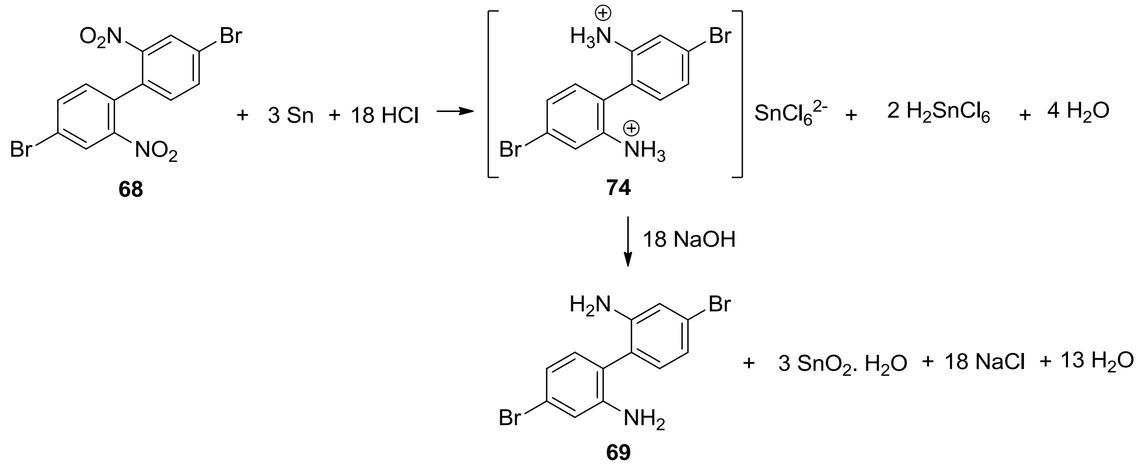

Scheme 3.18: The reduction of **68**

The structure of **69** was assessed by the ^{1}H NMR, ^{13}C NMR and FT-IR spectroscopy. The ^{1}H NMR spectrum of **69** shows a new broad singlet peak at 3.59 ppm corresponding to four protons of the amino groups. The ^{13}C NMR spectrum of **69** displays six peaks for six different carbons. The FT-IR spectrum of **69** shows two new peaks at 3280 and 3393 cm^{-1} for the symmetric and asymmetric stretching vibrations for the amino groups. Meanwhile, the two peaks at 1332 and 1556 cm^{-1} for symmetric and asymmetric stretching vibrations for the nitro groups of **68** disappear.

3.2.2.3. Synthesis of 4,4'-dibromo-2,2'-diiodobiphenyl (70)

69 was reacted with a mixture of aqueous sodium nitrite and HCl in acetonitrile which was subsequently treated with aqueous potassium iodide to give **70** *via* the Sandmeyer type reaction as white crystals in a yield of 51% (**Scheme 3.16**)[51].

The mechanism of the reaction proceeded through formation of the diazonium ion intermediate from the primary amine (**69**) and subsequently treating with aqueous potassium iodide to generate **70** (**Scheme 3.19**).

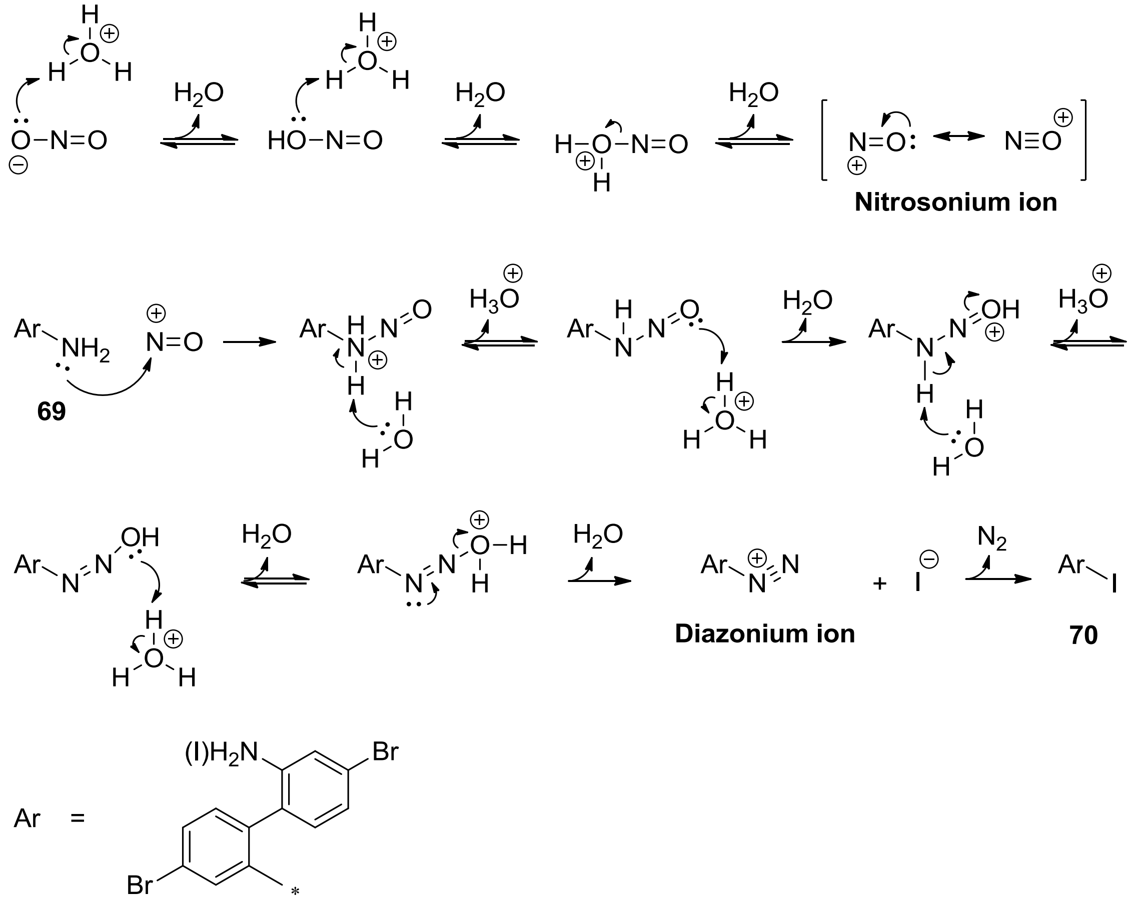

Scheme 3.19: The mechanism of formation of **70**

The structure of **70** was assessed by the ^{1}H NMR and FT-IR spectroscopy. The ^{1}H NMR spectrum of **70** shows a doublet, a doublet of doublet and another doublet at 8.11, 7.57 and 7.05 ppm, respectively corresponding to six protons on the biphenyl ring.

Furthermore, a broad singlet peak at 3.59 ppm of **69** disappears, which is a good evidence for success of the reaction. The FT-IR spectrum of **70** shows that the two peaks at 3280 and 3393 cm^{-1} for the symmetric and asymmetric stretching vibrations for the amino groups of **69** disappear.

3.2.2.4. Synthesis of 2,7-dibromo-9,9-dioctyldibenzosilole (71)

70 was reacted with *n*-BuLi in anhydrous THF and subsequently treated with dichlorodioctylsilane [$(C_8H_{17})_2SiCl_2$] to obtain **71** as colourless oil in 90% yield (**Scheme 3.16**)[52].

The mechanism of the reaction is outlined in scheme 3.20. **70** was selectively lithiated at 2,2'-positions using two equivalents of *n*-BuLi and then reacted with two equivalents of dichlorodioctylsilane to form **71**.

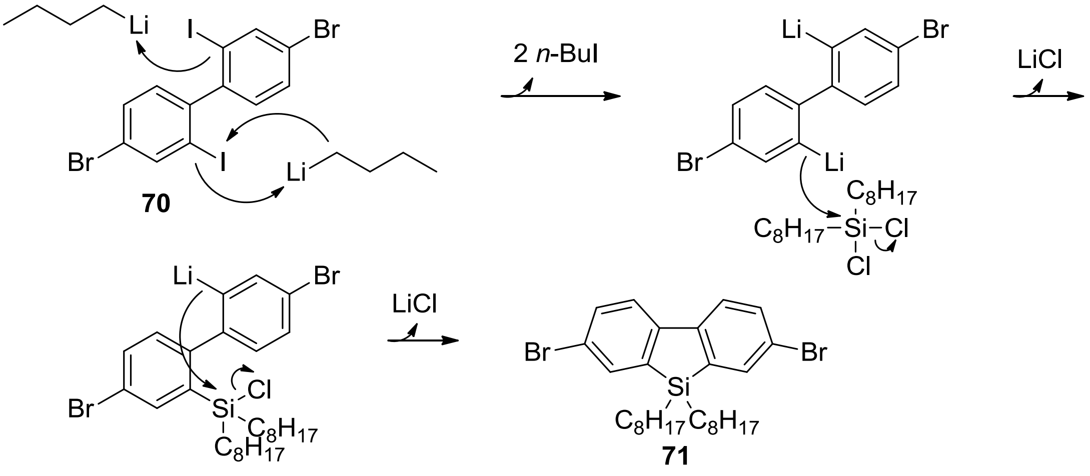

Scheme 3.20: The mechanism of formation of **71**

The ^1H NMR spectrum of **71** shows two doublets and a doublet of doublet at 7.70, 7.65 and 7.55 ppm respectively corresponding to six protons on the benzene rings. In addition, it displays a multiplet and triplet in the aliphatic region for the octyl chain protons. The structure of **71** was further confirmed by the ^{13}C NMR spectroscopy. The ^{13}C NMR spectrum of **71** exhibits six peaks for six different carbons in the aromatic region and eight peaks for eight carbons of the *n*-octyl chains in the aliphatic region.

3.2.2.5. Synthesis of 9,9-dioctyl-2,7-bis(4,4,5,5-tetramethyl-1,3,2-dioxaborolan-2-yl)-dibenzosilole (72)

71 was reacted with excess of bis(pinacolato)diboron, potassium acetate base and $PdCl_2$(dppf) catalyst in anhydrous DMF which yielded **72** as brown crystals in 53% yield

(**Scheme 3.16**)[53]. The mechanism of the reaction is similar to that of the Suzuki reaction described in the introduction chapter.

The structure of **72** was approved by the ^{1}H NMR spectroscopy and mass spectrometry. The ^{1}H NMR spectrum of **72** shows a singlet peak at 1.39 ppm, which belongs to twenty four protons of methyl groups of boronic ester. It also displays an expected number of protons in the aromatic and aliphatic regions. The mass spectrum of **72** shows a peak at 658.5 corresponding to the mass of the molecular ion $[M]^+$ of **72**.

3.3. Polymers synthesis

In this chapter, the synthesis of four alternating D-A copolymers, **76**, **77**, **78** and **79** is described. The polymers were prepared by the Suzuki polymerisation between bis-boronate esters (**75** and **72**) with dibromides (**49** and **50**), respectively (**Scheme 3.21**). The polymerisations were performed using Pd(OAc)$_2$/P(*o*-tol)$_3$ catalyst, NaHCO$_3$ base in anhydrous THF. All polymerisations were left for 21-30 hours with large amounts of purple precipitates forming as the reactions proceeded. The polymers were obtained and purified as described in chapter 2. The structures of the **76**, **77**, **78** and **79** were verified by the ^{1}H NMR spectroscopy, FT-IR spectroscopy and elemental analysis.

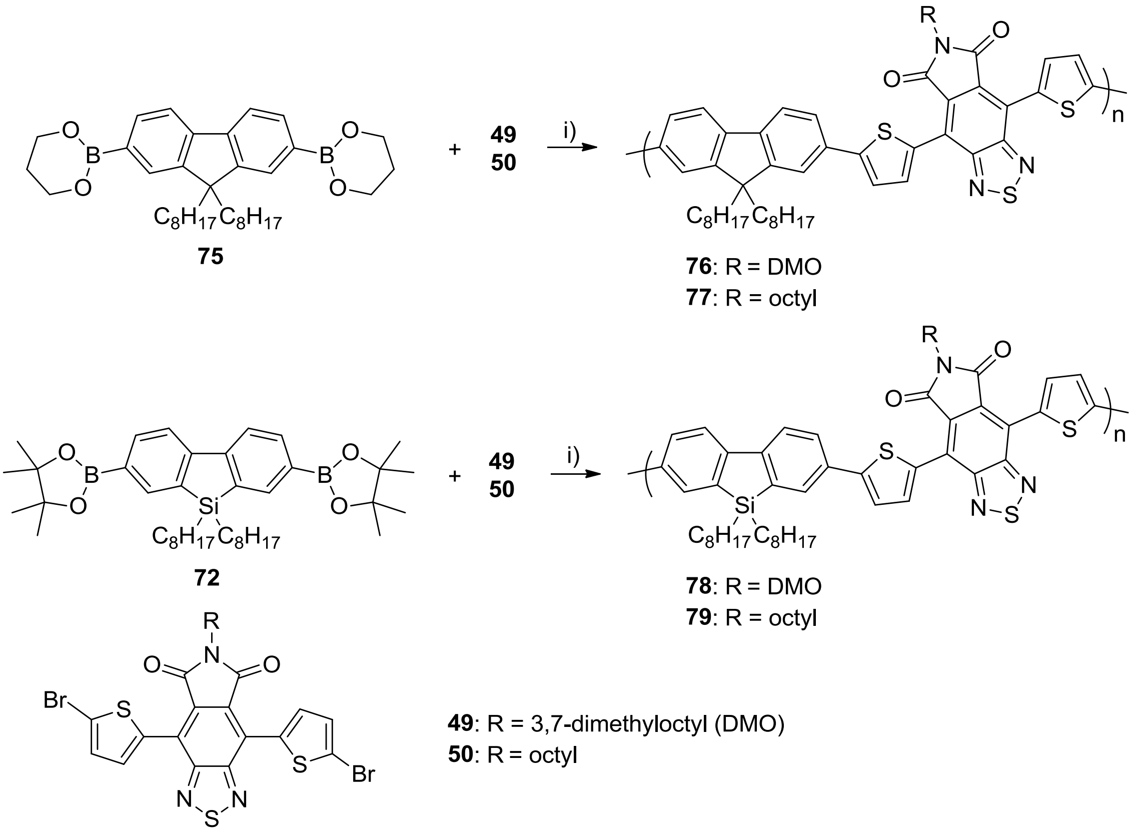

Scheme 3.21: The synthesis of **76**, **77**, **78** and **79** *via* Suzuki polymerisation

Reagents and conditions: i) anhydrous THF, NaHCO$_3$, Pd(OAc)$_2$, P(*o*-tol)$_3$, 90 °C, 21-30h

3.4. Molecular weights and yield of the polymers

Molecular weights of the polymers were measured by GPC using chloroform at 40 °C relative to polystyrene standards (**Table 3.1**). Substituting 3,7-dimethyloctyl chains in **76** for octyl chains in **77** on the **BTDI** building blocks results in a polymer with lower M_n values for the toluene fractions of the polymers. However, **77** afforded another fraction in chloroform of a higher M_n value that was not soluble in toluene while **76** did not provide chloroform fraction. The results indicate that a higher solubility of the polymer with 3,7-dimethyloctyl chains as a result of the branching of its substituents. The toluene fractions of the dibenzosilole-based polymers (**78** and **79**) have similar M_n values. However, **79** has a lower M_n value to that of **78** for the chloroform fractions. This could be attributed to the effect of the branched chains in **78** which provides it with a greater solubility and allows it to provide higher molecular weight fractions. Polymers with *n*-octyl chains provided lower yields compared to those with branched chains. Moreover, the yield of fluorene-based polymers is higher relative to dibenzosilole-based polymers (**Table 3.1**). This could be due to more aggregation in dibenzosilole-based polymers with more intermolecular interactions relative to fluorene-based polymers.

Table 3.1: The percentage yield, weight and number average molecular weights with polydispersity indexes of **76**, **77**, **78** and **79**

Polymer	% yield	Toluene fraction			Chloroform fraction		
		M_n (g mol^{-1})	M_w (g mol^{-1})	PDI	M_n (g mol^{-1})	M_w (g mol^{-1})	PDI
76	85	16000	33000	2.0			
77	78	11200	29100	2.5	24900	74400	2.9
78	68	9400	19400	2.0	20000	44900	2.2
79	59	10000	26200	2.6	16100	38700	2.4

3.5. Optical properties of the polymers

The normalised UV-vis absorption spectra of all polymers in chloroform solutions and in thin-films are shown in figure 3.1. The optical properties of these polymers are summarised in table 3.2. All polymers show two absorption bands at short and long wavelengths. The peak at shorter wavelengths could be related to π-π* transition. However, the other band at lower energy is related to the intramolecular charge transfer (ICT) between donor (D) and acceptor (A) units. The band gap (E_g) of the polymers are assessed from the absorption onsets in thin-films. In solutions, all polymers display comparable absorption maxima. In thin-films, the absorption spectra of the polymers show red-shifted absorption maxima by 22-34 nm relative to their absorption in solutions. This could be explained by stronger intermolecular π-π interaction and a more planar structure in the solid state. Compared with fluorene-based polymers, dibenzosilole-based polymers have broader absorption bands and therefore lower E_g values. A change of alkyl chains on **BTDI** units from 3,7-dimethyloctyl chains to *n*-octyl chains has a negligible impact on the E_g of the resulting polymers. **77** is red-shifted relative to its **76** analogue; this may arise from the fact that the former polymer has a higher molecular weight than the latter polymer.

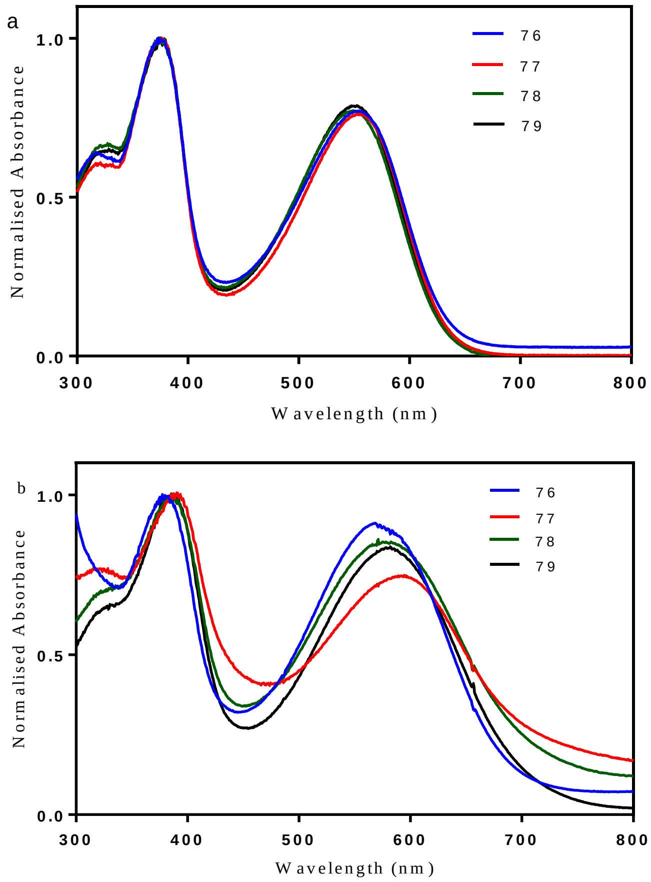

Figure 3.1: Normalised UV-vis absorption spectra of **76**, **77**, **78** and **79** in a) chloroform solutions; and b) thin films

Table 3.2: The UV-vis data and optical band gaps of the polymers

Polymer	ε	solution	Film		
	$(M^{-1}\ cm^{-1})$	λ_{max} (nm)	λ_{max} (nm)	λ_{onset} (nm)	E_g (eV)
76	26200	550	572	685	1.81
77	22900	551	585	696	1.78
78	35500	550	576	700	1.77
79	34900	550	578	697	1.77

76 and **77** have lower E_g relative to **P(BTI-F)** (**Scheme 3.2**) which has two extra thiophene spacers between fluorene and **DTBTDI** units. The latter polymer is blue-shifted around 10-25 nm relative to the former polymers. As expected, **76** and **77** have lower E_g values around 0.1 eV compared with that of **PFDTBT** (**Scheme 3.3**) due to the stronger electron-accepting strength of the **BTDI** building blocks than **BT** unit[18]. Similarly, **78** and **79** have lower E_g relative to **PDBSDTBT** analogue (**Scheme 3.4**)[35]. The absorption coefficients (ε) of the dibenzosilole-based polymers are higher than fluorene-based polymers (**Table 3.2**). This indicates that all things been equal, the dibenzosilole polymers should lead to more efficient OPV devices.

3.6. Electrochemical properties of the polymers

Cyclic voltammetry was used to study the electrochemical properties of the polymers. The LUMO and HOMO levels of all polymers calculated from the onsets of reduction and oxidation potentials, respectively (**Figure 3.2** and **Table 3.3**). The onsets were determined from cyclic voltammograms on drop cast polymer films on Pt electrode as working electrode in Bu_4NClO_4/CH_3CN (0.1 M) *vs* Ag/Ag^+ reference electrode. All polymers show the same HOMO energy levels. The results indicate that switching from fluorene to **DBS** moiety does not alter the HOMO levels of the resulting polymers. The HOMO level is dominated by the nature of the donor unit and that both fluorene and **DBS** units are weak electron donors of comparable strength. All polymers display low-lying HOMO energy levels which are beneficial for the chemical stability of polymers in oxygen and should lead to higher V_{oc} values of the fabricated OPV devices including these polymers as donor materials. All polymers have nearly identical LUMO energy levels, as all polymers have the same **BTDI** acceptor units which control the LUMO levels in these materials. Furthermore, anchoring different alkyl chains on **BTDI** units has little impact on the LUMO levels of the resulting polymers.

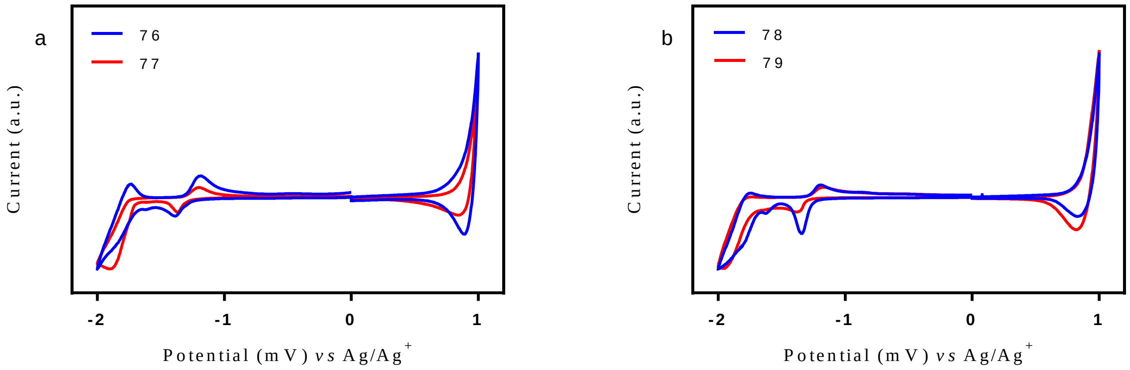

Figure 3.2: Cyclic voltammograms of a) **76** and **77**; b) **78** and **79** on Pt electrode in Bu_4NClO_4/CH_3CN at 100 mV/s

Table 3.3: Thermal and electrochemical properties of the polymers

Polymer	T_d (°C)	$E_{ox}{}^0$ (V)	HOMO (eV)	$E_{red}{}^0$ (V)	LUMO (eV)	$E_{g\,(elec)}$ (eV)
76	409	0.87	-5.59	1.27	-3.44	2.15
77	367	0.87	-5.59	1.27	-3.44	2.15
78	438	0.87	-5.59	1.25	-3.46	2.12
79	359	0.87	-5.59	1.29	-3.42	2.16

All polymers have comparable HOMO levels relative to **P(BTI-F)** (**Scheme 3.2**), which has a HOMO level of –5.60 eV[24]. This indicates that the incorporation of two extra thiophene spacers between fluorene and **DTBTDI** units has negligible effect on the HOMO levels of the resulting polymers. However, all polymers have deeper HOMO levels compared to those of **PDI-BDTT**, **PDI-BDTO**, **BBTI-1** and **BBTI-2** (**Scheme 3.2**). This could be attributed to fluorene and **DBS** units being weaker electron donors than **BDT** and **BTT** units[23,20].The LUMO levels of the polymers are higher than those of **PFDTBT** and **PDBSDTBT** (**Scheme 3.3** and **Scheme 3.4**) (–3.8 eV), which are related to the stronger electron accepting ability of **BTDI** moiety than **BT** unit[18,35].

3.7. Thermal properties of the polymers

The thermal properties of the polymers were studied by TGA (**Figure 3.3** and **Table 3.3**). All polymers show high thermal stability with T_d up to 350 °C. The thermal stability of the polymers with *n*-octyl chains on **BTDI** moiety is significantly lower than those with 3,7-dimethyloctyl chains. The results show that the thermal properties of the polymers are mostly affected by the size of the alkyl chains anchored to the **BTDI** units as well as by the type of the donor building blocks.

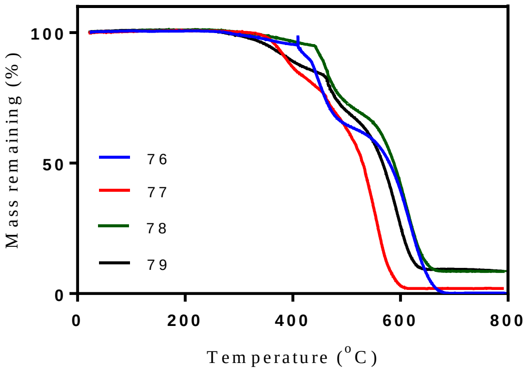

Figure 3.3: TGA of **76**, **77**, **78** and **79**

3.8. Powder X-ray diffraction (XRD) of the polymers

The structural properties of the polymers were investigated by powder XRD in solid state (**Figure 3.4**). The XRD of the **76**, **77**, **78** and **79** show diffraction peaks at 20.0, 20.5, 19.7 and 20.3° corresponding to the π-π stacking distance of 4.43, 4.32, 4.5 and 4.36 Å, respectively. The results show that all polymers have an amorphous nature. It is also worth noting that the peaks for the polymers containing *n*-octyl chains are more pronounced which indicates more aggregation than those polymers including 3,7-dimethyloctyl chains as also indicated by their lower solubility.

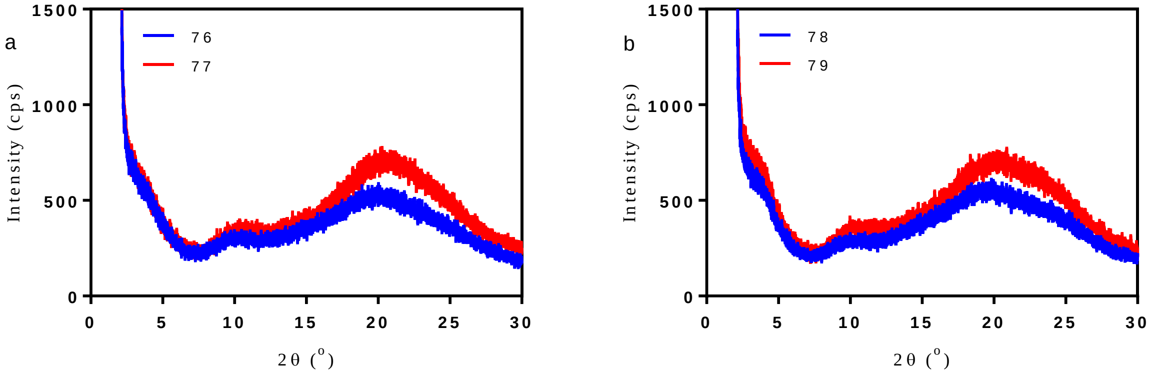

Figure 3.4: Powder XRD of a) **76** and **77**; b) **78** and **79**

3.9. Conclusions

In summary, four fluorene and dibenzosilole-based copolymers were prepared by copolymerising 2,7-fluorene and 2,7-dibenzosilole (**DBS**) with both **49** and **50** and yielded **76**, **77**, **78** and **79**, respectively. All polymers exhibit good solubility in common organic solvents. Changing the alkyl chains on **BTDI** moieties has a substantial influence on the solubility of the polymers. The use of 3,7-dimethyloctyl side groups on **BTDI** units in the fluorene-based polymers afforded **76** in high yield, however, the polymer was extracted in the toluene fraction due to its high solubility. The use of *n*-octyl side groups on **BTDI** units yielded **77** which has a lower solubility. In addition to the toluene fraction, another fraction from chloroform which has a higher molecular weight was obtained. However, in the case of dibenzosilole-based copolymers, linear octyl side chains have a negative impact on the molecular weight and the solubility of the resulting polymer. In solutions, all polymers show similar absorption maxima. In thin-films, the absorption spectra of the polymers display bathochromic shift absorption maxima relative to their absorption in solutions. The optical band gaps of the fluorene-based copolymers are slightly higher than those of dibenzosilole-based copolymers. The band gaps of the fluorene-based polymers are slightly changed by substituting 3,7-dimethyloctyl chains with *n*-octyl chains on **BTDI** units, while the band gaps of dibenzosilole-based polymers are the same. Upon varying fluorene to **DBS** unit**,** the HOMO levels of the resulting polymers do not change. This is due to the HOMO energy levels are controlled by the nature of the donor units, both fluorene and **DBS** units are weak electron-donors of similar strength. All polymers show deep-lying HOMO energy levels of –5.59 eV, which are advantageous for the chemical stability, and this would lead to higher V_{oc} values using these polymers as electron-donating materials in the BHJ devices. All polymers have almost the same LUMO levels and have the same **BTDI** acceptor units which dominate the LUMO levels in these materials. Moreover, attaching different alkyl chains on **BTDI** units has small impact on the LUMO energy levels of the resulting polymers. All polymers illustrate excellent thermal stability with T_d exceeding 350 °C. The polymers based on branched 3,7-dimethyloctyl chains have higher thermal stability than those polymers based on *n*-octyl chains. The thermal stability of the polymers is dependent upon the type of the alkyl substituents attached to the acceptor moieties. The powder X-ray diffraction studies of the polymers show diffraction peaks around 20.0^o corresponding to the π-π stacking distance of about 4.0 Å. All polymers have the amorphous nature. The photovoltaic properties of these materials are currently under investigation in BHJ solar cells with fullerene derivatives.

References

1. S. Günes, H. Neugebauer and N. S. Sariciftci, *Chemical Reviews*, 2007, **107**, 1324-1338.
2. B. C. Thompson and J. M. Frechet, *Angewandte Chemie International Edition*, 2008, **47**, 58-77.
3. Y.-J. Cheng, S.-H. Yang and C.-S. Hsu, *Chemical Reviews*, 2009, **109**, 5868-5923.
4. C. Duan, F. Huang and Y. Cao, *Journal of Materials Chemistry*, 2012, **22**, 10416-10434.
5. G. Yu, J. Gao, J. C. Hummelen, F. Wudl and A. J. Heeger, *Science*, 1995, **270**, 1789.
6. G. Yu and A. J. Heeger, *Journal of Applied Physics*, 1995, **78**, 4510-4515.
7. Y. Li, *Accounts of Chemical Research*, 2012, **45**, 723-733.
8. Z. G. Zhang and J. Wang, *Journal of Materials Chemistry*, 2012, **22**, 4178-4187.
9. S. Zhang, L. Ye and J. Hou, *Advanced Energy Materials*, 2016.
10. J. Chen and Y. Cao, *Accounts of Chemical Research*, 2009, **42**, 1709-1718.
11. J. Hou, H.-Y. Chen, S. Zhang, G. Li and Y. Yang, *Journal of the American Chemical Society*, 2008, **130**, 16144-16145.
12. Z. Zhu, D. Waller, R. Gaudiana, M. Morana, D. Mühlbacher, M. Scharber and C. Brabec, *Macromolecules*, 2007, **40**, 1981-1986.
13. L. Huo, H.-Y. Chen, J. Hou, T. L. Chen and Y. Yang, *Chemical Communications*, 2009, 5570-5572.
14. M. H. Chen, J. Hou, Z. Hong, G. Yang, S. Sista, L. M. Chen and Y. Yang, *Advanced Materials*, 2009, **21**, 4238-4242.
15. L. Slooff, S. Veenstra, J. Kroon, D. Moet, J. Sweelssen and M. Koetse, *Applied Physics Letters*, 2007, **90**, 143506.
16. P.-L. T. Boudreault, A. Najari and M. Leclerc, *Chemistry of Materials*, 2010, **23**, 456-469.
17. H. Zhou, L. Yang and W. You, *Macromolecules*, 2012, **45**, 607-632.
18. M. Svensson, F. Zhang, O. Inganäs and M. Andersson, *Synthetic Metals*, 2003, **135**, 137-138.
19. P. Zhou, Z.-G. Zhang, Y. Li, X. Chen and J. Qin, *Chemistry of Materials*, 2014, **26**, 3495-3501.
20. C. B. Nielsen, R. S. Ashraf, N. D. Treat, B. C. Schroeder, J. E. Donaghey, A. J. White, N. Stingelin and I. McCulloch, *Advanced Materials*, 2015, **27**, 948-953.

21. H. Yi, S. Al-Faifi, A. Iraqi, D. C. Watters, J. Kingsley and D. G. Lidzey, *Journal of Materials Chemistry*, 2011, **21**, 13649-13656.
22. H. Zhou, L. Yang, A. C. Stuart, S. C. Price, S. Liu and W. You, *Angewandte Chemie*, 2011, **123**, 3051-3054.
23. L. Wang, D. Cai, Q. Zheng, C. Tang, S.-C. Chen and Z. Yin, *ACS Macro Letters*, 2013, **2**, 605-608.
24. H. Li, *Journal of Materials Chemistry*, 2014, **2**, 17925-17933.
25. A. Gadisa, W. Mammo, L. M. Andersson, S. Admassie, F. Zhang, M. R. Andersson and O. Inganäs, *Advanced Functional Materials*, 2007, **17**, 3836-3842.
26. F. Zhang, W. Mammo, L. M. Andersson, S. Admassie, M. R. Andersson and O. Inganäs, *Advanced Materials*, 2006, **18**, 2169-2173.
27. F. Zhang, J. Bijleveld, E. Perzon, K. Tvingstedt, S. Barrau, O. Inganäs and M. R. Andersson, *Journal of Materials Chemistry*, 2008, **18**, 5468-5474.
28. F. Zhang, K. G. Jespersen, C. Bjoerstroem, M. Svensson, M. R. Andersson, V. Sundström, K. Magnusson, E. Moons, A. Yartsev and O. Inganäs, *Advanced Functional Materials*, 2006, **16**, 667-674.
29. A. A. Alghamdi, D. C. Watters, H. Yi, S. Al-Faifi, M. S. Almeataq, D. Coles, J. Kingsley, D. G. Lidzey and A. Iraqi, *Journal of Materials Chemistry A*, 2013, **1**, 5165-5171.
30. D. C. Watters, H. Yi, A. J. Pearson, J. Kingsley, A. Iraqi and D. Lidzey, *Macromolecular Rapid Communications*, 2013, **34**, 1157-1162.
31. A. J. Pearson, D. C. Watters, H. Yi, M. S. Sarjadi, L. X. Reynolds, P. P. Marchisio, J. Kingsley, S. A. Haque, A. Iraqi and D. G. Lidzey, *RSC Advances*, 2014, **4**, 43142-43149.
32. C.-H. Chen, C.-H. Hsieh, M. Dubosc, Y.-J. Cheng and C.-S. Hsu, *Macromolecules*, 2009, **43**, 697-708.
33. D. Kitazawa, N. Watanabe, S. Yamamoto and J. Tsukamoto, *Applied Physics Letters*, 2009, **95**, 3701.
34. P. L. T. Boudreault, A. Michaud and M. Leclerc, *Macromolecular Rapid Communications*, 2007, **28**, 2176-2179.
35. E. Wang, L. Wang, L. Lan, C. Luo, W. Zhuang, J. Peng and Y. Cao, *Applied Physics Letters*, 2008, **92**, 33307-33307.
36. H. Y. Chen, J. Hou, A. E. Hayden, H. Yang, K. Houk and Y. Yang, *Advanced Materials*, 2010, **22**, 371-375.

37. S. Ponomarenko, A. Muzafarov, O. Borshchev, E. Vodopyanov, N. Demchenko and V. Myakushev, *Russian Chemical Bulletin*, 2005, **54**, 684-690.

38. L. Wen and S. C. Rasmussen, *Journal of Chemical Crystallography*, 2007, **37**, 387-398.

39. D. D. Kenning, K. A. Mitchell, T. R. Calhoun, M. R. Funfar, D. J. Sattler and S. C. Rasmussen, *The Journal of Organic Chemistry*, 2002, **67**, 9073-9076.

40. L. E. McNamara, N. Liyanage, A. Peddapuram, J. S. Murphy, J. H. Delcamp and N. I. Hammer, *The Journal of Organic Chemistry*, 2015, **81**, 32-42.

41. P. M. Esteves, J. W. de M. Carneiro, S. P. Cardoso, A. G. Barbosa, K. K. Laali, G. Rasul, G. S. Prakash and G. A. Olah, *Journal of the American Chemical Society*, 2003, **125**, 4836-4849.

42. R. L. Schwiderski and S. C. Rasmussen, *The Journal of Organic Chemistry*, 2013, **78**, 5453-5462.

43. H. Hailu, B. Atsbeha, S. Admassie, W. Mammo, V. Raju and Y. Chebude, *Bulletin of the Chemical Society of Ethiopia*, 2011, **25**.

44. M. R. Delgado, V. Hernandez, J. L. Navarrete, S. Tanaka and Y. Yamashita, *Journal of Physical Chemistry B*, 2004, **108**, 2516-2526.

45. L. Lan, Z. Chen, Y. Li, L. Ying, F. Huang and Y. Cao, *Polymer Chemistry*, 2015, **6**, 7558-7569.

46. Y. Matsueda, S. Xu and E.-i. Negishi, *Tetrahedron Letters*, 2015, **56**, 3346-3348.

47. A. Thomson, S. O’Connor, B. Knuckley and C. P. Causey, *Bioorganic & Medicinal Chemistry*, 2014, **22**, 4602-4608.

48. W. Yue, Y. Zhao, S. Shao, H. Tian, Z. Xie, Y. Geng and F. Wang, *Journal of Materials Chemistry*, 2009, **19**, 2199-2206.

49. G. Lu, H. Usta, C. Risko, L. Wang, A. Facchetti, M. A. Ratner and T. J. Marks, *Journal of the American Chemical Society*, 2008, **130**, 7670-7685.

50. J. Yang, N. Sun, J. Huang, Q. Li, Q. Peng, X. Tang, Y. Dong, D. Ma and Z. Li, *Journal of Materials Chemistry C*, 2015, **3**, 2624-2631.

51. C. W. Keyworth, K. L. Chan, J. G. Labram, T. D. Anthopoulos, S. E. Watkins, M. McKiernan, A. J. White, A. B. Holmes and C. K. Williams, *Journal of Materials Chemistry*, 2011, **21**, 11800-11814.

52. H. Usta, G. Lu, A. Facchetti and T. J. Marks, *Journal of the American Chemical Society*, 2006, **128**, 9034-9035.

53. K. L. Chan, M. J. McKiernan, C. R. Towns and A. B. Holmes, *Journal of the American Chemical Society*, 2005, **127**, 7662-7663.

Chapter 4 - Influence of fluorine substitution upon the photovoltaic properties of carbazole-benzothiadiazole dicarboxylic imide alternate copolymers

Abstract

Four novel donor-acceptor copolymers, **104**, **105**, **106** and **107**, were designed and synthesised *via* Suzuki polymerisation. The first two copolymers including 2,7-carbazole flanked by thienyl moieties as the electron donor unit and benzothiadiazole dicarboxylic imide (**BTDI**) as electron acceptor units. In the last two copolymers, two fluorine atoms were incorporated at 3,6-positions of 2,7-carbazole to investigate the impact of fluorine upon the optoelectronic properties, structural and thermal properties of the resulting polymers. **107** possesses the highest number average molecular weight (M_n = 24200 g mol^{-1}) among all polymers synthesised. **104**, **105** show identical optical band gaps of 1.76 eV. However, the optical band gaps of fluorinated copolymers are slightly higher than non-fluorinated counterparts. All polymers have deep-lying HOMO levels. Changing the alkyl chain substituents on **BTDI** moieties from linear *n*-octyl to branched 3,7-dimethyloctyl groups as well as substituting the two hydrogen atoms at 3,6-positions of carbazole unit by fluorine atoms has negligible impact on the HOMO levels of the polymers. Similarly, the LUMO energy levels are almost comparable for all polymers. Thermogravimetric analysis (TGA) have shown that all polymers have good thermal stability and also confirmed that the fluorinated copolymers have higher thermal stability relative to those non-fluorinated analogues. Powder XRD studies proved that all polymers have an amorphous nature in the solid state.

4.1. Introduction

Carbazole is a fused-ring aromatic system, in which two benzene rings are fused in the center by a pyrrole ring (**Figure 4.1**). It is one of the most extensively utilised donor repeat units for optoelectronic applications, for example OLEDs[1], OFETs[2,3] and solar cells[4]. It is structurally analogous to fluorene, but the carbon at 9-position of fluorene is substituted by nitrogen atom. Relative to fluorene, carbazole is a more electron rich unit due to its lone-pair of electrons on the nitrogen atom, which is involved in the aromatic system. In addition, carbazole derivatives have fully aromatic properties and they are able to form stable radical cations[5]. Furthermore, they have relatively high charge carrier mobilities and they show good photochemical and thermal stabilities[5]. Moreover, the nitrogen atom in the carbazole unit is easily functionalised with different alkyl chains for enhancing solubility of the resulting polymers[6]. Fluorene easily undergoes oxidation at the 9-position to ketone, while the nitrogen atom at the 9-position of carbazole prevents oxidation under electrochemical conditions[7].

Carbazole moiety can be linked through the 3,6-positions or 2,7-positions (**Figure 4.1**). Coupling of carbazole units through the 3,6-positions limits the π-conjugation of the resulting materials because a large amount of twisting along the polymer backbone. However, connecting carbazole units *via* the 2,7-positions provides a greater degree of conjugation because the repeat units adopt a more planar structure[8,9]. However, cyclic voltammetry studies revealed that these types of polymers undergo irreversible oxidation and therefore they are less stable under electrolytic conditions. This is due to the nitrogen atom activating the 3,6-positions of carbazole[10]. As a result, side reactions can easily occur and cross-linked polymers are formed. The mechanism of the reaction has been proposed by Zotti *et al.* (**Scheme 4.1**)[11].

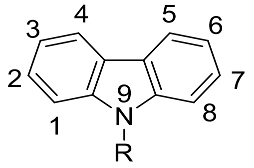

Figure 4.1: The structure of carbazole unit

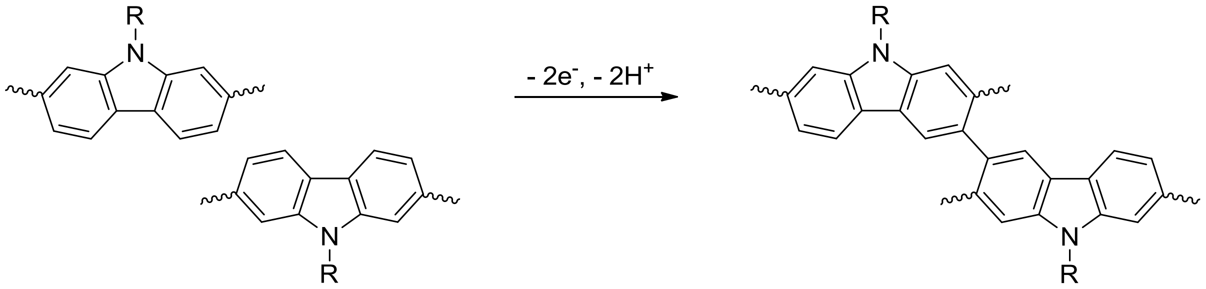

Scheme 4.1: The cross-linking of polymers at 3,6-positions of 2,7-linked carbazole

Iraqi *et al.* protected the 3,6-positions of 2,7-linked carbazole polymers by substituting hydrogen atoms with either methyl groups or fluorine atoms[10,12]. They found that the resulting polymers have higher electrolytic stability relative to those non-substituted analogues.

4.1.1. Conjugated polymers based on 2,7-carbazole

Similar to fluorene, carbazole-based homopolymers usually have large band gaps therefore they are not suitable candidate for BHJ photovoltaic cells[4]. The band gap of polycarbazoles can be lowered by copolymerising 2,7-carbazole moieties with a variety of acceptor units through alternating donor-acceptor (D-A) strategy. Based on this strategy, a variety of high photovoltaic performance carbazole copolymers has been developed. The most successful D-A copolymer is poly[*N*-9'-heptadecanyl-2,7-carbazole-*alt*-5,5-(4',7'-di-2-thienyl-2',1',3'-benzothiadiazole)] (**PCDTBT**) based on 2,7-carbazole flanked by thienyl units as electron-rich moiety and **BT** as an acceptor unit which was developed by Leclerc group (**Scheme 4.2**)[13]. The **PCDTBT** was synthesised *via* Suzuki polymerisation. The photovoltaic devices based on **PCDTBT: PC$_{61}$BM** showed a PCE of 3.6%[13]. Leclerc and co-workers further optimised the devices based on **PCDTBT** and the photovoltaic performance up to 5.7% was recorded[14,15]. Later on, many research groups improved the efficiency of **PCDTBT** up to 6.79% by inserting different layers such as a titanium oxide (TiO_x), conjugated polyelectrolyte, and alcohol/water soluble conjugated polymer between the active layer and top aluminium electrode (Al)[16,17,18]. Recently, PCE of 7.5% was reported for **PCDTBT: PC$_{71}$BM**[19]. Zhou *et al.* reported the same polymer backbone **PCDTBT** based on 2,7-carbazole with bulkier side chain delivered a PCE of 3.05%[20].

Leclerc *et al.* reported a new copolymers including 2,7-carbazole and a 2,1,3-benzooxadiazole (**BO**) by substituting sulfur atom in **BT** unit by oxygen atom (**Scheme 4.2**)[21]. **PCDTBO: PC$_{61}$BM** BHJ solar cell delivered a moderate PCE of 2.4%.

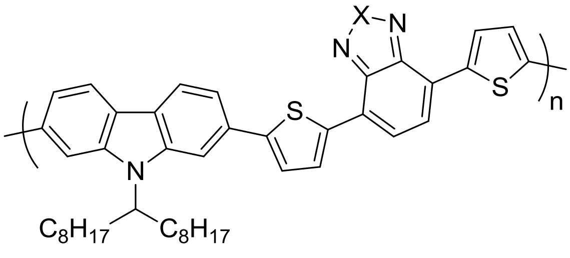

PCDTBT: X = S
PCDTBO: X = O
PCDTTAZ: X = N-R, R = dodecyl

Scheme 4.2: The structures of copolymers containing 2,7-carbazole flanked by thienyl units and different acceptor units

Cao and co-workers synthesised another D-A copolymer, **PCDTTAZ** based on 2,7-carbazole and 2-alkyl-2',1',3'-benzotriazole (**TAZ**) as acceptor moiety (**Scheme 4.2**)[22].

The BHJ solar cells fabricated from **PCDTTAZ: $PC_{61}BM$** as active layer delivered a PCE of 2.75%.

Zhang *et al.* reported **HXS-1** copolymer including 2,7-carbazole and 5,6-dialkoxy-2,1,3-benzothiadiazole [**$(OR)_2BT$**] as an acceptor (**Scheme 4.3**)[23]. **HXS-1** blended with **$PC_{71}BM$** exhibited a PCE of 5.4%. Iraqi *et al.* designed and synthesised three copolymers, **PCDTBT-8** and **PCDT2BT-8** and **PCDTBT** based on 2,7-carbazole flanked by thienyl or bithienyl units as donor units and **BT** or **$(OR)_2BT$** as acceptor moieties (**Scheme 4.3**)[24]. **PCDTBT** blended with **$PC_{71}BM$** delivered the highest PCE of 4.30%. Iraqi and co-workers synthesised four copolymers based on 2,7-carbazole flanked by thienyl or selenophenyl units as donor units and **BT** or **$(OR)_2BT$** as acceptor moieties (**Scheme 4.3**)[25]. **PCDTBT** fabricated with **$PC_{71}BM$** in BHJ devices gave the highest PCE of 5.10%. Recently, **PCDT2BT-8** and **PCDTTBT-8** were synthesised by Iraqi *et al.* using bithiophene and thieno[3,2-*b*]thiophene (**TT**) units as spacers between 2,7-carbazole and **$(OR)_2BT$** (**Scheme 4.3**)[26]. The BHJ solar cell based on **PCDT2BT-8: $PC_{71}BM$** as active layer gave a PCE of 4.12%. However, **PCDTTBT-8: $PC_{71}BM$** gave a higher PCE of 4.5%.

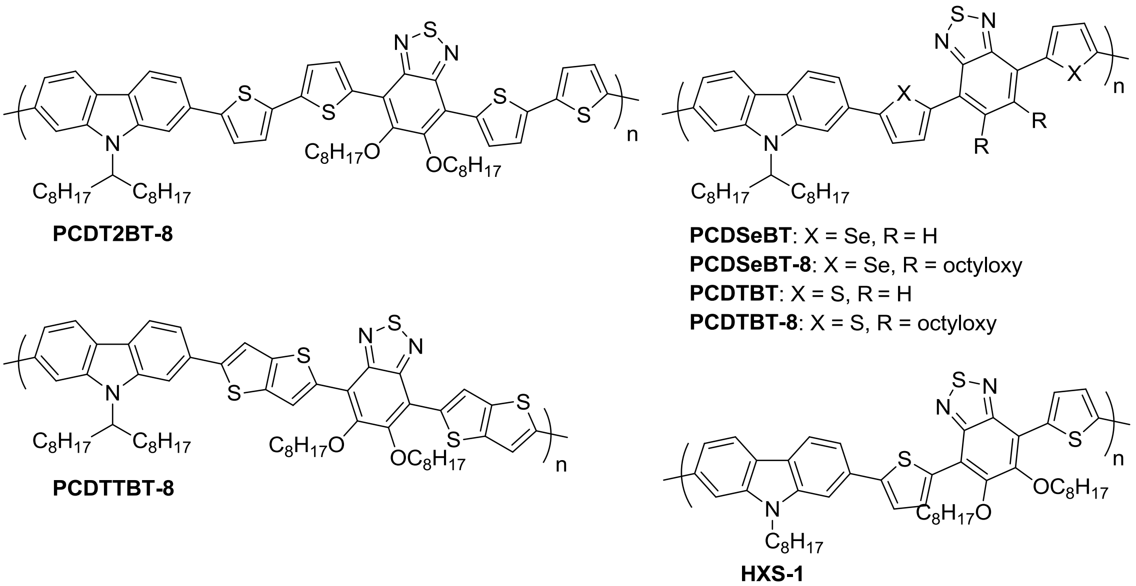

Scheme 4.3: The structures of alternating copolymers including 2,7-carbazole units, benzothiadiazole and dialkoxy benzothiadiazole moieties

4.1.2. The impact of fluorination on the efficiency of organic photovoltaics

Although the physical and electronic properties of conjugated polymers are dominated by the selection of D and A units in the main chain of D-A copolymers, substituents such as fluorine atom can be used for fine tuning these properties. Fluorine is the most electronegative atom in the periodic table and it has small size. Incorporating fluorine atoms onto the polymer backbone could be lower the HOMO energy level without introducing much steric effects[27]. The low-lying HOMO energy levels of fluorinated polymers can provide high V_{oc} values in PSCs[28]. You and co-workers have designed and synthesised a new acceptor unit, 4,7-di-2-thienyl-5,6-difluoro-2,1,3-benzothiadiazole (**DTffBT**) (**Scheme 3.1**)[29]. It was copolymerised with benzodithiophene (**BDT**) to build a **PBDT-DTffBT** copolymer (**Scheme 4.4**). To study the influence of fluorine atoms on the efficiency of PSCs, they prepared **PBDT-DTBT** without fluorine atoms. **PBDT-DTffBT** has E_g of 1.7 eV, which is similar to that of **PBDT-DTBT**. However, the LUMO and HOMO levels of **PBDT-DTffBT** are lower relative to those of its non-fluorinated analogue. The **PBDT-DTffBT** was fabricated into solar cell devices with **$PC_{61}BM$** offered an impressive PCE of 7.2%. In contrast, the non-fluorinated counterpart only exhibited a PCE of 5.0%.

You *et al.* further developed another new acceptor unit based on **TAZ** by replacing two hydrogen atoms at 5,6-positions of **TAZ** with two fluorine atoms to build a **FTAZ**[27]. It was copolymerised with a **BDT** to generate a novel **PBDT-FTAZ** copolymer (**Scheme 4.4**). Moreover, they prepared **PBDT-HTAZ** copolymer without fluorine atoms to investigate the impact of fluorine atoms on the performance of the devices. BHJ photovoltaic devices composed of **PBDT-FTAZ** and **$PC_{61}BM$** as active layer delivered a remarkable PCE of 7.1%. On the other hand, **PBDT-HTAZ** showed only a PCE of 4.36%.

In 2013, Wang *et al.* reported three copolymers based on **BDT** and **DTffBT** with different solubilising chains, **$PBDT_{TEH}$-DT_{H}ffBT**, **$PBDT_{TEH}$-DT_{EH}ffBT** and **$PBDT_{HDO}$-DT_{H}ffBT** (**Scheme 4.4**)[30]. **$PBDT_{TEH}$-DT_{H}ffBT** and **$PBDT_{TEH}$-DT_{EH}ffBT** blended with **$PC_{71}BM$** delivered the PCE of 4.46 and 6.20%, respectively. On the other hand, **$PBDT_{HDO}$-DT_{H}ffBT** offered an unprecedentedly high PCE of 8.30%.

Peng *et al.* developed a new acceptor moiety based on **DTBT** by substituting one hydrogen atom at 5-position of **BT** with fluorine atom to construct **DTfBT**[31]. It was copolymerised with alkylthienyl substituted **BDT** to form **PBDT-DTfBT** (**Scheme 4.4**). The BHJ solar cell based on **PBDT-DTfBT: $PC_{71}BM$** showed a high PCE of 6.21%.

Jen and co-workers reported a **PCPDTFBT** copolymer including cyclopentadithiophene (**CPDT**) and partially fluorinated **BT** (**FBT**) (**Scheme 4.4**)[32]. In parallel, they synthesised non-fluorinated **PCPDTBT** counterpart to examine the effect of fluorine on the photovoltaic efficiency of the device. The **PCPDTFBT: $PC_{71}BM$** delivered much higher

PCE than **PCPDTBT** (5.51 *vs* 2.75%). Nehr *et al*. independently reported the same copolymers **PCPDTFBT** and **PCPDTBT**. **PCPDTFBT** and **PCPDTBT** fabricated with **$PC_{71}BM$** delivered a PCE of 6.16 and 3.59% respectively[33].

For all of the highly efficient copolymers mentioned above fluorine was incorporated on the acceptor units. Bo and co-workers inserted fluorine atoms on the donor unit[34]. They reported a novel copolymer, **O-PDFCDTBT** based on 3,6-difluoro-2,7-carbazole flanked by thienyl units and **$(OR)_2BT$** (**Scheme 4.4**). The copolymer had a low molecular weight (M_n = 9100 g mol^{-1}) due to its limited solubility. The BHJ solar cell based on **O-PDFCDTBT: $PC_{71}BM$** as active layer showed a PCE of 4.8%. They replaced the *n*-octyl side chains on carbazole units by 2-hexyldecyl side chains (**HD**) so as to increase the solubility and molecular weight of the resulting polymer (**Scheme 4.4**)[35]. The new copolymer, **HD-PDFCDTBT** was synthesised with a M_n as high as 38000 g mol^{-1}. The **HD-PDFCDTBT** showed much higher hole mobility than **O-PDFCDTBT** probably due to higher molecular weight of the former polymer. **HD-PDFCDTBT** blended with **$PC_{71}BM$** delivered a high PCE of 7.39%.

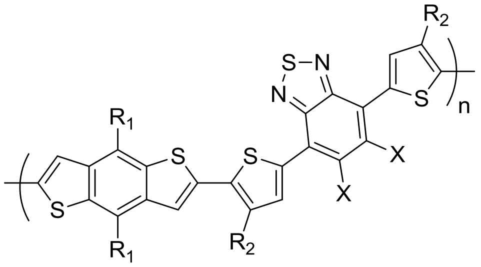

PBDT-DTBT: X = H, R_1 = 3-butylnonyl, R_2 = 2-ethylhexyl
PBDT-DTffBT: X = F, R_1 = 3-butylnonyl, R_2 = 2-ethylhexyl
PBDT$_{HDO}$-DT$_{H}$ffBT: X = F, R_1 = 2-hexyldecyloxy, R_2 = hexyl

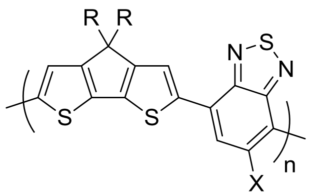

PCPDTBT: X = H, R = 2-ethylhexyl
PCPDTFBT: X = F, R = 2-ethylhexyl

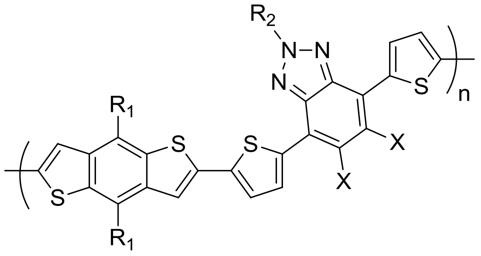

PBDT-HTAZ: X = H, R_1 = 3-butylnonyl, R_2 = 2-butyloctyl
PBDT-FTAZ: X = F, R_1 = 3-butylnonyl, R_2 = 2-butyloctyl

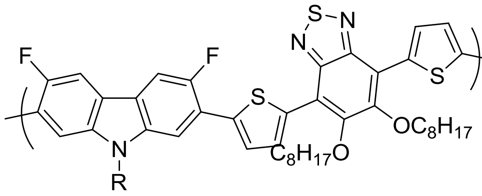

O-PDFCDTBT: R = octyl
HD-PDFCDTBT: R = 2-hexyldecyl

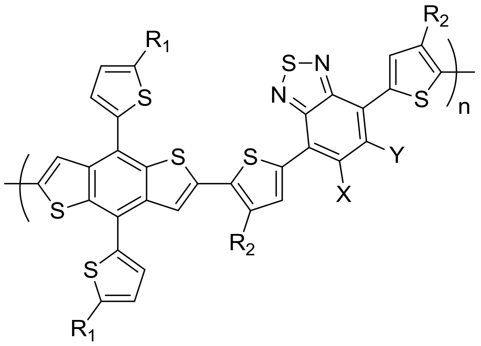

PBDT-DTfBT: X = H, Y = F, R_1 = dodecyl, R_2 = octyl
PBDT$_{TEH}$-DT$_{EH}$ffBT: X, Y = F, R_1, R_2 = 2-ethylhexyl
PBDT$_{TEH}$-DT$_{H}$ffBT: X, Y = F, R_1 = 2-ethylhexyl, R_2 = hexyl

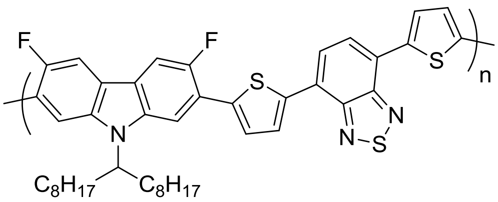

PCffDTBT

Scheme 4.4: The structures of fluorinated copolymers and their analogues

4.2. Synthesis of 3,6-difluoro-substituted-2,7-carbazole monomer (89)

89 is a key monomer for the preparation of the target polymers in this chapter. It was synthesised through eight steps starting from commercially available 1,4-dibromo-2-fluorobenzene (**80**) (**Scheme 4.5**). The different steps in its preparation are discussed below.

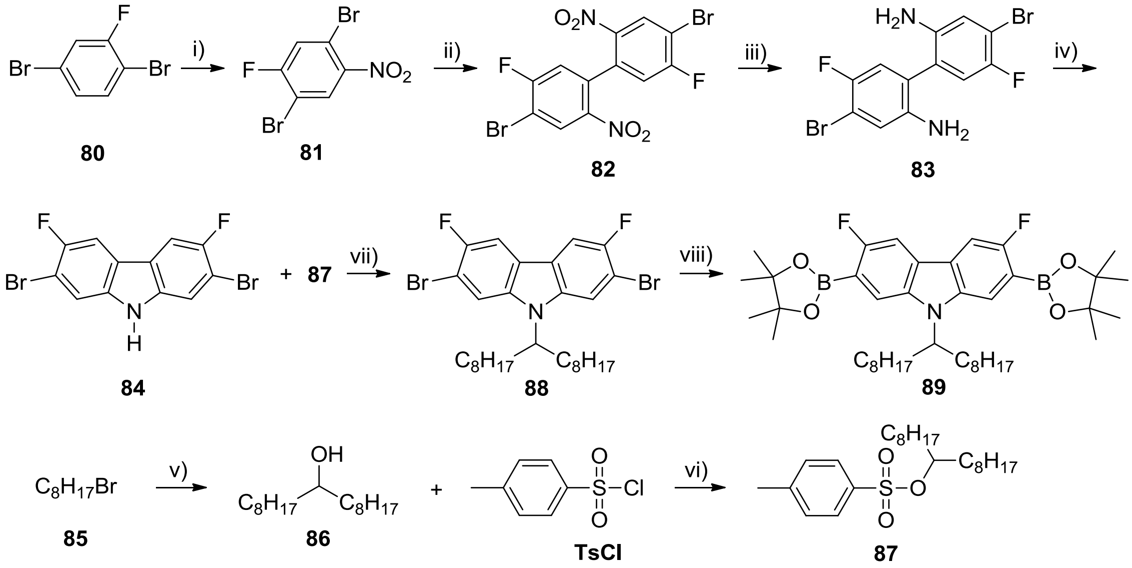

Scheme 4.5: The synthetic steps of the **89**

Reagents and conditions: i) TFA, TFAA, NH_4NO_3, DCM, 0 °C; ii) Cu powder, DMF, 120 °C, 3h; iii) Sn, HCl, EtOH, reflux, 3h; iv) H_3PO_4, 190 °C, 24h; v) Mg, THF, ethyl formate; vi) Et_3N, $Me_3N.HCl$, DCM; vii) KOH, DMSO, THF, 45 °C, overnight; viii) bis(pinacolato)diboron, KOAc, anhydrous DMF, Pd(dppf)Cl_2, 100 °C, 48h

4.2.1. Synthesis of 1,4-dibromo-2-fluoro-5-nitrobenzene (81)

81 was synthesised by nitration of **80**[34]. The reaction was performed between **80** and ammonium nitrate as a nitrating agent in the presence of trifluoroacetic acid (TFA) and trifluoroacetic anhydride (TFAA) in dichloromethane and yielded **81** as yellow crystals in an excellent yield of 85% (**Scheme 4.5**).

The mechanism of the reaction is an electrophilic aromatic substitution and comprises of three steps (**Scheme 4.6**). In the first step, nitrate ion (NO_3^-) reacts with TFAA to form nitronium ion (NO_2^+), which is an electrophile. In the second step, **80** functions as a nucleophile and attacks to the NO_2^+ to form a sigma complex, which is stabilised by three resonance structures (**90**, **91** and **92**). In the third step, the aromaticity of the benzene ring is restored by deprotonation of the sigma complex to form the **81**.

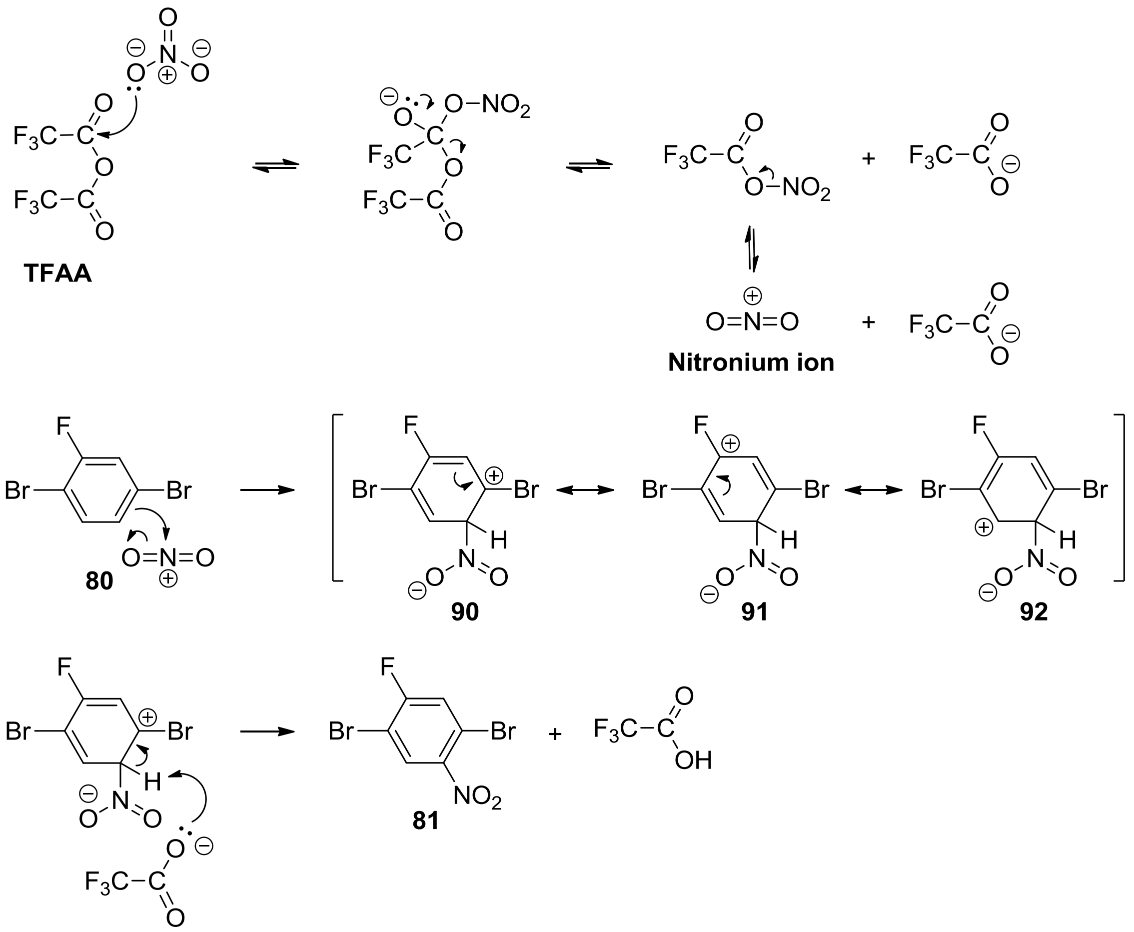

Scheme 4.6: The mechanism of nitration reaction to form **81**

The structure of **81** was verified by the ^{1}H NMR and ^{19}F NMR spectroscopy. The ^{1}H NMR spectrum of **81** shows two doublets at 8.20 and 7.55 ppm corresponding to the aromatic protons. The ^{19}F NMR spectrum of **81** exhibits a triplet at –97.2 ppm for a fluorine atom.

4.2.2. Synthesis of 4,4'-dibromo-5,5'-difluoro-2,2'-dinitrobiphenyl (82)

82 was prepared by the Ullmann coupling reaction of **81** using copper powder in anhydrous DMF and obtained as yellow crystals in 76% yield (**Scheme 4.5**)[36]. The mechanism of the reaction is similar to that for the synthesis of **68** as shown in scheme 3.17.

The structure of **82** was approved by the ^{1}H NMR, and ^{19}F NMR spectroscopy. The ^{1}H NMR spectrum of **82** displays two doublets at 8.57 and 7.09 ppm, which belong to aromatic protons. The ^{19}F NMR spectrum of **82** exhibits a triplet at –95.9 ppm for two chemically equivalent fluorine atoms.

4.2.3. Synthesis of 4,4'-dibromo-5,5'-difluorobiphenyl-2,2'-diamine (83)

82 was reduced using tin powder under acidic conditions in ethanol to obtain **83** as a brown solid in a yield of 81% (**Scheme 4.5**)[37]. The mechanism of reaction is similar to that for the synthesis of **69** as shown in scheme 3.18.

The structure of **83** was assessed by the ^1H NMR, and ^{19}F NMR spectroscopy. The ^1H NMR spectrum of **83** shows two doublets at 6.99 and 6.90 ppm, which belong to the aromatic protons. It also displays a broad singlet peak at 3.74 ppm corresponding to protons of amino groups. The ^{19}F NMR spectrum of **83** exhibits a triplet at –121.2 ppm for two chemically equivalent fluorine atoms.

4.2.4. Synthesis of 3,6-difluoro-2,7-dibromo-*9H*-carbazole (84)

84 was prepared in 79% yield by reacting **83** with concentrated phosphoric acid (**Scheme 4.5**)[38].

The mechanism of the reaction involves three steps (**Scheme 4.7**). In the first step, one of the amino groups of **83** is protonated by phosphoric acid, followed by the leaving of an ammonia molecule following intramolecular attack of the second amino group on the carbon bearing it; leading to ring closure to form protonated intermediate (**93**). Finally, this intermediate is deprotonated by $H_2PO_4^-$ to yield **84** and regenerates the phosphoric acid as a catalyst.

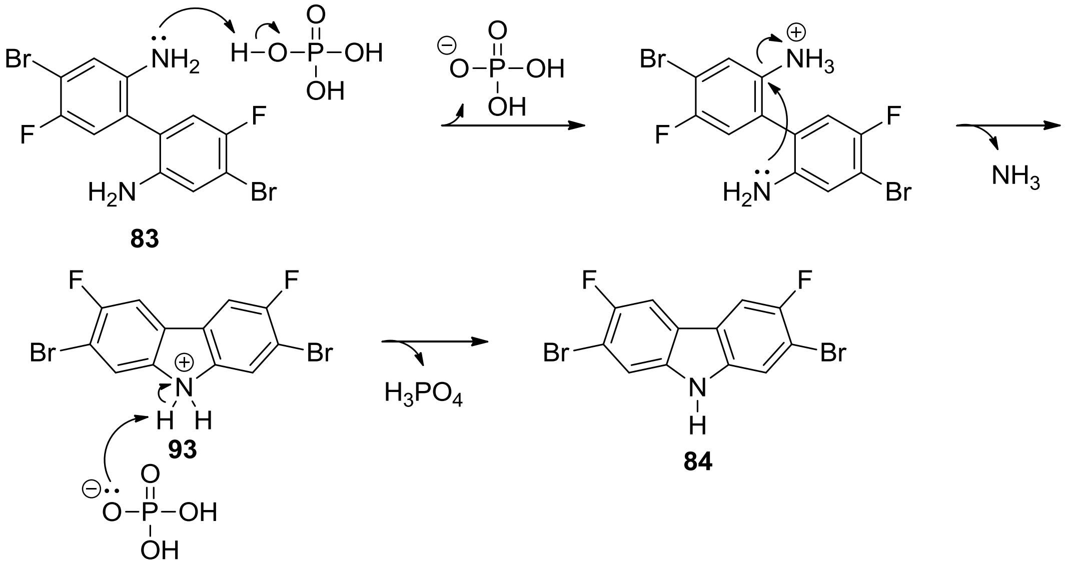

Scheme 4.7: The mechanism of formation of **84**

The structure of **84** was verified by the ^1H NMR spectroscopy. The ^1H NMR spectrum of **84** in acetone-d_6 displays two doublets at 8.09 and 7.85 ppm, which belong to aromatic protons. It also displays a new broad singlet peak at 10.67 ppm, which attributes to a proton on nitrogen atom of carbazole. Meanwhile, a broad singlet peak at 3.74 ppm for protons of amino groups in the ^{1}H NMR spectrum of **83** disappears.

4.2.5. Synthesis of heptadecan-9-ol (86)

86 was synthesised through two steps starting from commercially available 1-bromooctane (**85**)[39]. In the first step, **85** was reacted with magnesium metal in anhydrous THF to form *n*-octylmagnesium bromide (**94**), which is the Grignard reagent. In the next step, the Grignard reagent was treated with ethyl formate (**95**) to obtain **86** as white solid in an excellent yield of 99% (**Scheme 4.5**).

The mechanism of the reaction consists of four steps (**Scheme 4.8**). In the first step, the Grignard reagent (**94**) acts as a nucleophile and attacks the carbonyl group of **95** to yield a negatively charged tetrahedral intermediate (**96**). In the second step, the carbonyl group is reformed upon the leaving of the ethoxide anion to form an aldehyde intermediate (**97**). In the third step, the second molecule of the Grignard reagent attacks the carbonyl group of **97** to generate a new alkoxide intermediate (**98**). Finally, the latter intermediate is protonated by an acid to give **86**, which is a secondary alcohol.

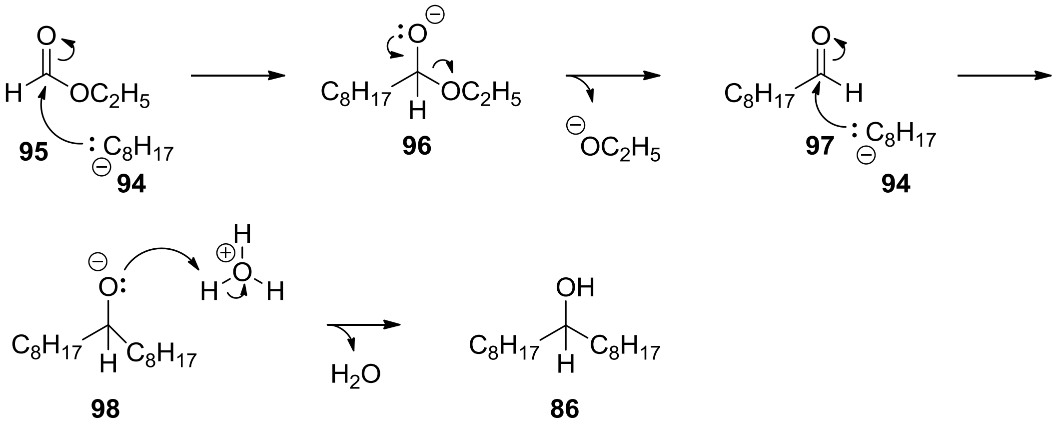

Scheme 4.8: The mechanism of formation of **86**

The structure of **86** was approved by the ^{1}H NMR and ^{13}C NMR spectroscopy. The ^{1}H NMR spectrum of **86** shows the expected number of protons. The ^{13}C NMR spectrum of **86** displays nine peaks for nine environmentally different carbon atoms.

4.2.6. Synthesis of 9-heptadecane-*p*-toluenesulfonate (87)

Tosylation reaction between **86** and *p*-toluenesulfonyl chloride (TsCl) in the presence of trimethylammonium monohydrochloride and triethyl amine in dichloromethane yielded **87** as white crystals in 89% yield (**Scheme 4.5**)[40].

The mechanism of the reaction is suggested by Yoshida and co-workers (**Scheme 4.9**)[41]. In the beginning, triethylamine was reacted with trimethylammonium monohydrochloride to generate trimethylamine because trimethylamine is less basic than triethylamine (pK_b: 9.81 *vs* 11.01), respectively. The trimethyl amine functions as a nucleophile and attacks the sulfur atom of TsCl to form an intermediate (**99**), which is a strong tosylating reagent. This intermediate subsequently reacted with **86** to generate tosylate compound (**87**).

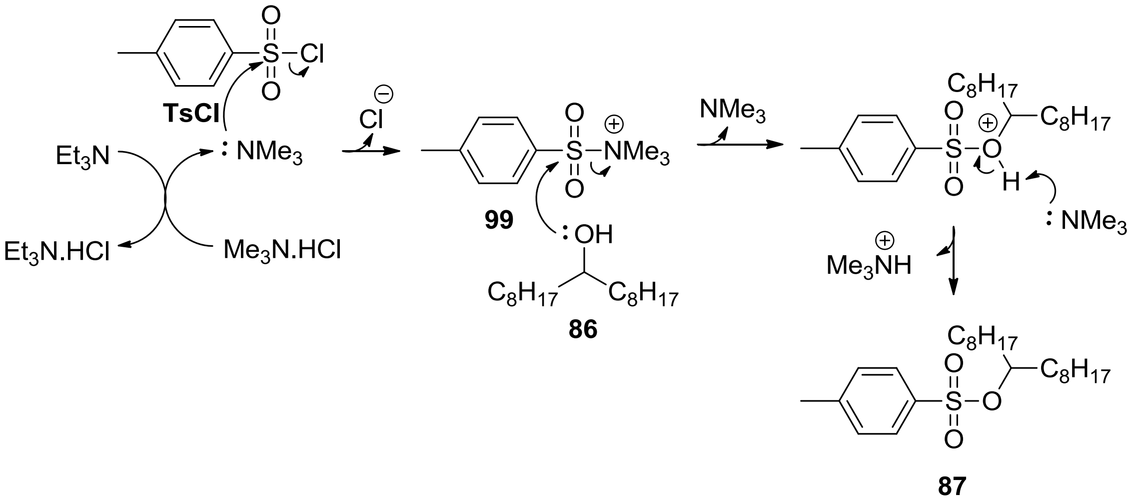

Scheme 4.9: The mechanism of the formation of **87**

The structure of **87** was approved by the ^1H NMR and FT-IR spectroscopy. The ^1H NMR spectrum of **87** shows two doublet of doublets at 7.81 and 7.34 ppm which belong to the protons of tosylate ring. It also displays a singlet at 2.47 ppm corresponding to the methyl protons. In addition, it shows expected number of protons of alkyl chains. The FT-IR spectrum of **87** shows a new peak at 1354 cm^{-1} which belongs to S-O stretching vibration. Meanwhile, the broad peak for O-H stretching vibration of **86** disappears.

4.2.7. Synthesis of 3,6-difluoro-*N*-9'-heptadecanyl-2,7-dibromocarbazole (88)

The alkylation reaction between **84** and **87** under basic conditions in anhydrous DMSO/THF as a co-solvent yielded **88** as white crystals in 76% yield (**Scheme 4.5**)[42].

The mechanism of the reaction includes two steps (**Scheme 4.10**). In the first step, **84** is deprotonated by the hydroxide ion to form a negative charge on the nitrogen atom, which functions as a nucleophile. In the second step, the nucleophile attacks **87** to generate **88** through a bimolecular nucleophilic substitution (S_N2) mechanism. The *p*-toluenesulfonate is a very good leaving group as it is stabilised through three resonance structures (**100**, **101** and **102**).

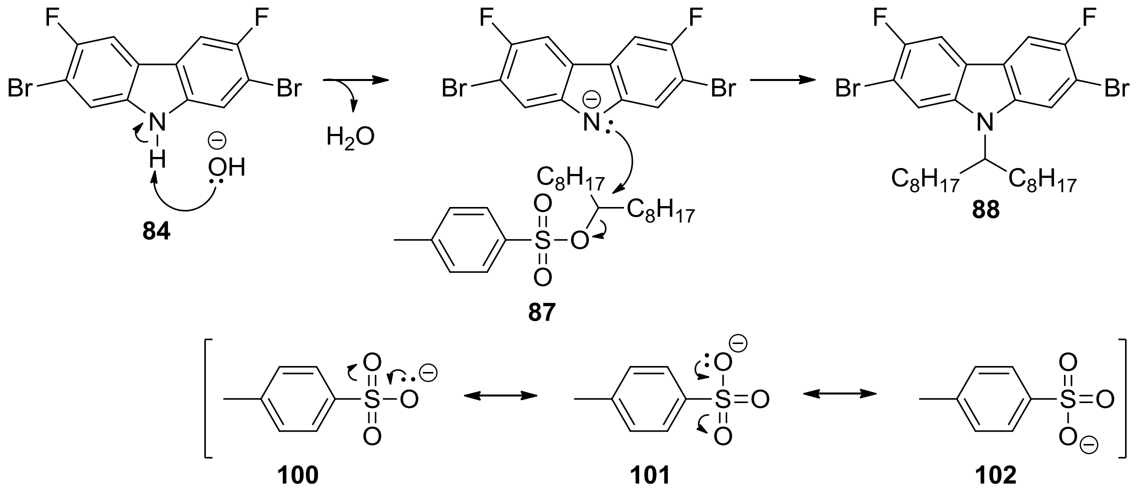

Scheme 4.10: The mechanism of the formation of **88**

The structure of **88** was verified by the ^{1}H NMR spectroscopy and mass spectrometry. The ^{1}H NMR spectrum of **88** shows a broad multiplet and doublet at 7.83-7.69 and 7.58 ppm respectively corresponding to the aromatic protons. It also displays a series of multiples and triplet in the aliphatic region for alkyl chain protons. The mass spectrum of **88** shows a main integer peak at 599.1 corresponding to the mass of the molecular ion $[M]^+$ of **88**.

4.2.8. Synthesis of 3,6-difluoro-*N*-9'-heptadecanyl-2,7-bis(4,4,5,5-tetramethyl-1,3,2-dioxaborolan-2-yl)carbazole (89)

88 reacted with excess of bis(pinacolato)diboron, potassium acetate base and $PdCl_2$(dppf) catalyst in anhydrous DMF to afford **89** as brown crystals in 69% yield (**Scheme 4.5**)[43]. The mechanism of the reaction is similar to that of the Suzuki coupling reaction described in the introduction chapter.

The structure of **89** was approved by the ^{1}H NMR spectroscopy and mass spectrometry. The ^{1}H NMR spectrum of **89** shows a singlet peak at 1.43 ppm, which belongs to twenty four protons of methyl groups of boronic ester. Furthermore, it displays expected number of protons in the aromatic and aliphatic regions. The mass spectrum of **89** exhibits a peak at 693.5 corresponding to the mass of the molecular ion $[M]^+$ of **89**.

4.3. Polymers synthesis

The synthesis of the four target alternating D-A copolymers, **104**, **105**, **106** and **107** is described in this section. The polymers were prepared by the Suzuki polymerisation between bis-boronate esters (**103** and **89**) with dibromides (**49** and **50**), respectively (**Scheme 4.11**). The polymerisations were performed using $Pd(OAc)_2/P(o\text{-tol})_3$ catalyst, $NaHCO_3$ base in anhydrous THF. All polymerisations were left running between 24 and 48 hours with large amounts of purple precipitates forming as the reactions proceeded. The polymers were obtained and purified as described in chapter 2. The structures of **104**, **105**, **106** and **107** were confirmed by the ^1H NMR spectroscopy, FT-IR spectroscopy and elemental analysis.

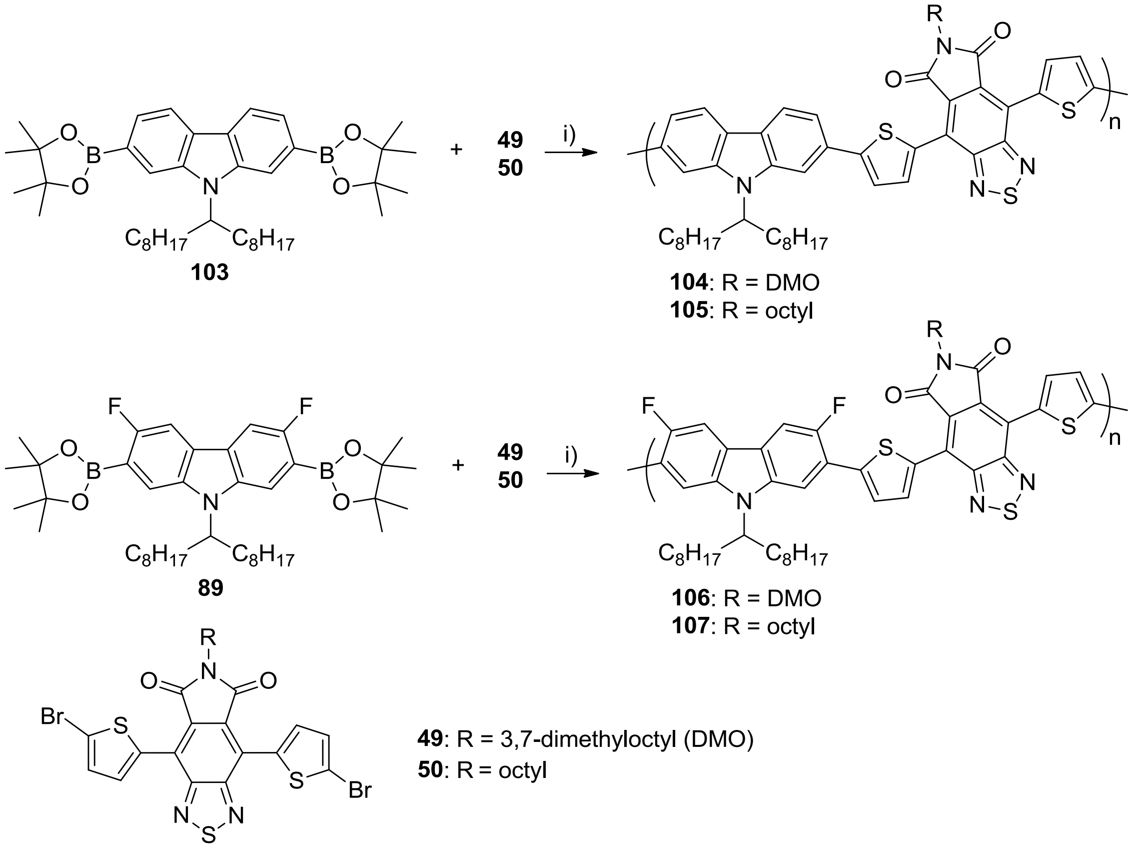

Scheme 4.11: The synthesis of **104**, **105**, **106** and **107** *via* Suzuki polymerisation

Reagents and conditions: i) anhydrous THF, $NaHCO_3$, $Pd(OAc)_2$, $P(o\text{-tol})_3$, 90 °C, 24-48h

4.4. Molecular weights and yield of the polymers

Molecular weights of the polymers were estimated by GPC using chloroform at 40 °C using polystyrene as calibration standard (**Table 4.1**). Substituting 3,7-dimethyloctyl chains in **104** by linear *n*-octyl chains on the **BTDI** unit yielded **105**. This polymer afforded a chloroform fraction which has a higher M_n value relative to **104**. Changing 3,7-

dimethyloctyl chains in fluorinated copolymer **106** with *n*-octyl chains in **107** on the **BTDI** moieties results in a polymer with lower M_n values for the toluene fractions of the polymers. However, **107** afforded another fraction in chloroform of a higher M_n value that was not soluble in toluene while **106** did not provide chloroform fraction. The results indicate that a higher solubility of the polymers with 3,7-dimethyloctyl chains as a result of the branching of its substituents. Fluorinated copolymers have lower molecular weights than those non-fluorinated analogues in toluene fraction. In contrary, **107** has the highest M_n value in chloroform fraction among all polymers prepared. All polymers synthesised in good yield in the range of 68-98%.

Table 4.1: The percentage yield, weight and number average molecular weights with polydispersity indexes of **104**, **105**, **106** and **107**

Polymer	% yield	Toluene fraction			Chloroform fraction		
		M_n (g mol^{-1})	M_w (g mol^{-1})	PDI	M_n (g mol^{-1})	M_w (g mol^{-1})	PDI
104	73	12200	30400	2.4			
105	86				20500	65300	3.1
106	98	8700	16300	1.8			
107	68	8200	18400	2.2	24200	46300	1.9

4.5. Optical properties of the polymers

The normalised UV-vis absorption spectra of all polymers were investigated in chloroform solutions and in thin-films (**Figure 4.2** and **Table 4.2**). In solutions, the absorption of the polymers is not affected by the nature of substituents on **BTDI** units and both polymers with *n*-octyl and 3,7-dimethyloctyl substituents display similar absorption maxima (557 nm for **104** *vs* 561 nm for **105** and also the same absorption maxima of 536 nm for both **106** and **107**). This indicates that these substituents have a minimal effect on the conformation of polymer chains in solutions. In both solutions and films the fluorinated polymers are blue-shifted relative to those non-fluorinated analogues. This increase in the band gap of the fluorinated polymers could be explained by the fact that there is a decrease in the intramolecular charge transfer along polymer backbones upon substitution of the carbazole repeat units with electron withdrawing substituents. In thin-films, the absorption spectra of the polymers show a red-shift of absorption bands by 27-32 nm relative to their absorption in solutions. This could be attributed to stronger interchain π-π stacking and more coplanar structures in the solid state. The band gap (E_g)

of the polymers are estimated from the absorption onsets in thin-films. The E_g of the **104** and **105** are comparable. However, the E_g of the **106** and **107** are 1.78 and 1.81 eV, respectively which are slightly higher than non-fluorinated counterparts. The results indicate that a change of alkyl chains on **BTDI** units from 3,7-dimethyloctyl chains to *n*-octyl chains does not have any impact on the E_g of the **104** and **105**, while it has a little impact on the E_g of the fluorinated polymers.

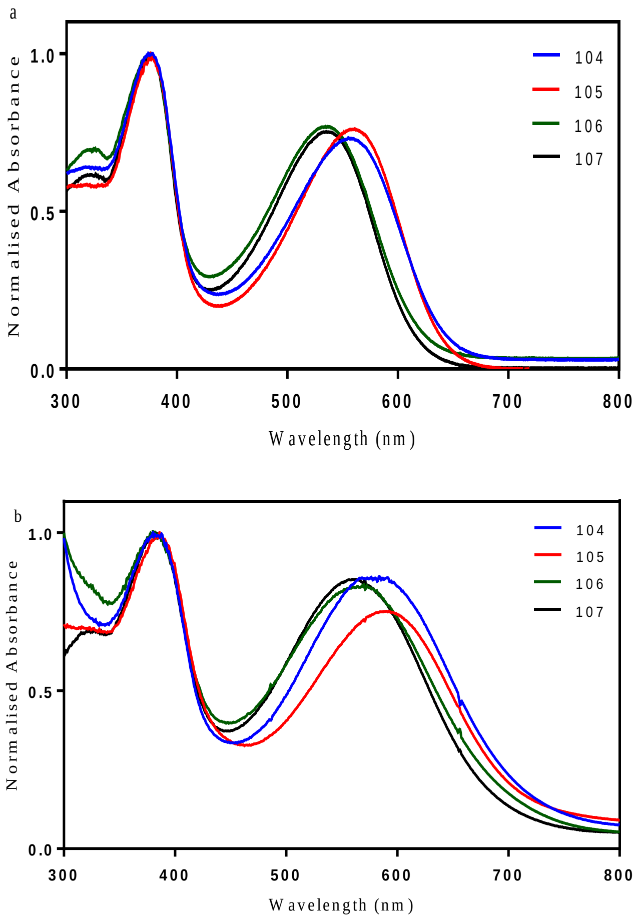

Figure 4.2: Normalised UV-vis absorption spectra of **104**, **105**, **106** and **107** in a) chloroform solutions; and b) thin-films

Table 4.2: Uv-vis data and optical band gaps of the polymers

Polymer	ε (M^{-1} cm^{-1})	solution	Film		
		λ_{max} (nm)	λ_{max} (nm)	λ_{onset} (nm)	E_g (eV)
104	31900	557	583	701	1.76
105	29100	561	588	702	1.76
106	31400	536	568	693	1.78
107	21800	536	561	684	1.81

As anticipated, the **104** and **105** have lower E_g values around 0.1 eV relative to those **PCDTBT** analogue (**Scheme 4.2**) because of the **BTDI** moiety is a stronger acceptor than **BT** unit[13]. **PCffDTBT** synthesised in Iraqi group has an E_g of 1.82 eV (**Scheme 4.4**) which is slightly higher than **106** and **107**[44]. The E_g of **O-PDFCDTBT** is 1.75 eV (**Scheme 4.4**) which is slightly lower than **106** and **107**. The absorption coefficient (ε) of the **104** is comparable with fluorinated analogue. On the other hand, **107** has lower absorption coefficient than non-fluorinated counterpart which may arise from larger E_g (**Table 4.2**).

4.6. Electrochemical properties of the polymers

Cyclic voltammetry was used to study the electrochemical properties of the polymers. All polymers display one oxidation wave and two reduction waves at similar potentials. The LUMO and HOMO levels of all polymers calculated from the onsets of reduction and oxidation potentials, respectively (**Figure 4.3** and **Table 4.3**). The onsets were determined from cyclic voltammograms on drop cast polymer films on Pt electrode as working electrode in Bu_4NClO_4/CH_3CN (0.1 M) *vs* Ag/Ag^+ reference electrode. The HOMO energy levels of all polymers are comparable. The results indicate that the fluorine substituents at the 3,6-positions of 2,7-carbazole units as well as changing the alkyl chains on **BTDI** units have no impact on the HOMO levels of the resulting polymers. This phenomenon was also observed on other polymers described by Bo and co-workers[34]. However, it is well known that the fluorine substitution can lower the HOMO level of the polymer as reported in previous literature reports[29,32,45]. All polymers display deep-lying HOMO levels which are advantageous for the chemical stability of polymers in oxygen and higher V_{oc} values could be expected of the fabricated OPV devices based on these polymers as donor materials. The LUMO energy levels of all polymers are comparable because the LUMO energy levels of these materials are dominated by the same **BTDI** acceptor building blocks. In addition, further anchoring different alkyl chains on **BTDI** units has little effect on the LUMO energy levels of the polymers.

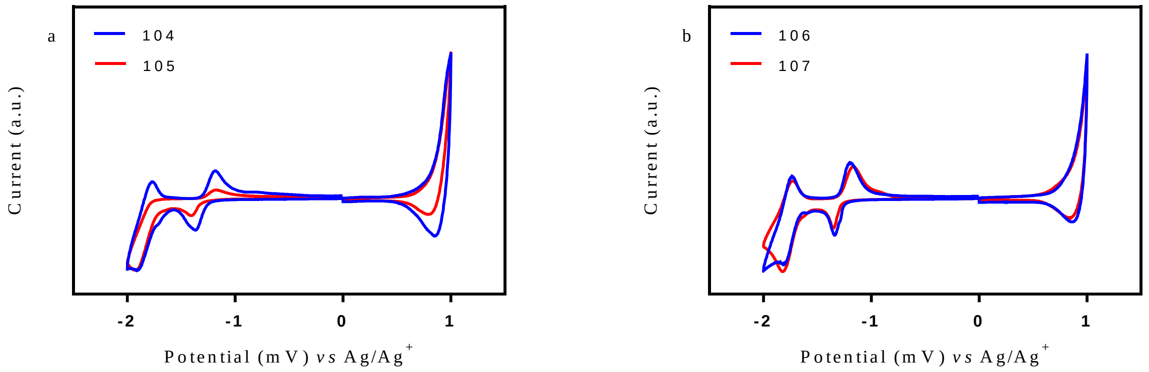

Figure 4.3: Cyclic voltammograms of a) **104** and **105**; b) **106** and **107** on Pt electrode in Bu_4NClO_4/CH_3CN at 100 mV/s

Table 4.3: Thermal and electrochemical properties of the polymers

Polymer	T_d (°C)	E_{ox}^{0} (V)	HOMO (eV)	E_{red}^{0} (V)	LUMO (eV)	$E_{g\,(elec)}$ (eV)
104	381	0.84	–5.56	1.23	–3.48	2.08
105	359	0.83	–5.55	1.30	–3.41	2.14
106	392	0.84	–5.56	1.23	–3.48	2.08
107	371	0.86	–5.56	1.26	–3.45	2.12

All polymers have deeper HOMO levels relative to those **O-PDFCDTBT**, **HD-PDFCDTBT** and **PCffDTBT** analogues (**Scheme 4.4**)[34,35,44]. The HOMO levels of all polymers are comparable to the HOMO level of **PCDTBT** prepared in Leclerc group (*ca.* –5.5 eV) (**Scheme 4.2**)[13], while deeper than the one synthesised in Iraqi group (–5.35 eV)[24]. The LUMO levels of all polymers are comparable to the LUMO energy level of **PCDTBT** prepared in Iraqi group (–3.42 eV)[24], whereas they are higher than LUMO energy level of **PCDTBT** synthesised in Leclerc group (*ca.* –3.6 eV)[13].

4.7. Thermal properties of the polymers

The thermal properties of the polymers were studied by TGA (**Figure 4.4** and **Table 4.3**). All polymers show high thermal stability with T_d up to 350 °C. The thermal stability of both fluorinated and non-fluorinated polymers with branched 3,7-dimethyloctyl side chain on **BTDI** moiety is higher than those with linear *n*-octyl side chain analogues. It can be seen that fluorinated polymers possess higher thermal stability than those non-fluorinated counterparts. This is consistent with previous literatures that exhibit the fluorination at the 3,6-positions of carbazole units increases the thermal stability of the resulting polymers[34,35].

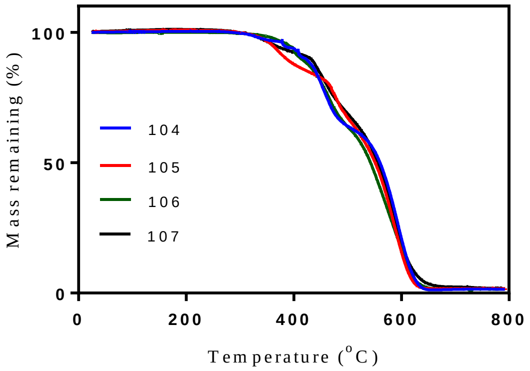

Figure 4.4: TGA of **104**, **105**, **106** and **107**

4.8. Powder X-ray diffraction

The structural properties of the polymers were studied by powder X-ray diffraction (XRD) in the solid state (**Figure 4.5**). The XRD of **104**, **105**, **106** and **107** show diffraction peaks at 20.2, 19.7, 19.9 and 20.8° corresponding to the π-π stacking distance of 4.39, 4.50, 4.45 and 4.26 Å, respectively. The results show that all polymers have an amorphous nature. The powder XRD of **106** and **107** are comparable to **PCffDTBT** prepared in Iraqi group (**Scheme 4.4**)[44]. The results indicate that adding fluorine atoms on the 3,6-positions of carbazole units do not have substantial influence on the crystallinity of the resulting polymers. However, **O-PDFCDTBT** showed a sharp peak at 5.36° corresponding to distance of 16.5 Å between conjugated polymer backbones separated by solubilising alkyl chains (**Scheme 4.4**)[34]. In **O-PDFCDTBT**, the less bulky linear *n*-octyl chains on the carbazole units adopt more coplanar structure than **106** and **107**, with bulky branched chains (C17).

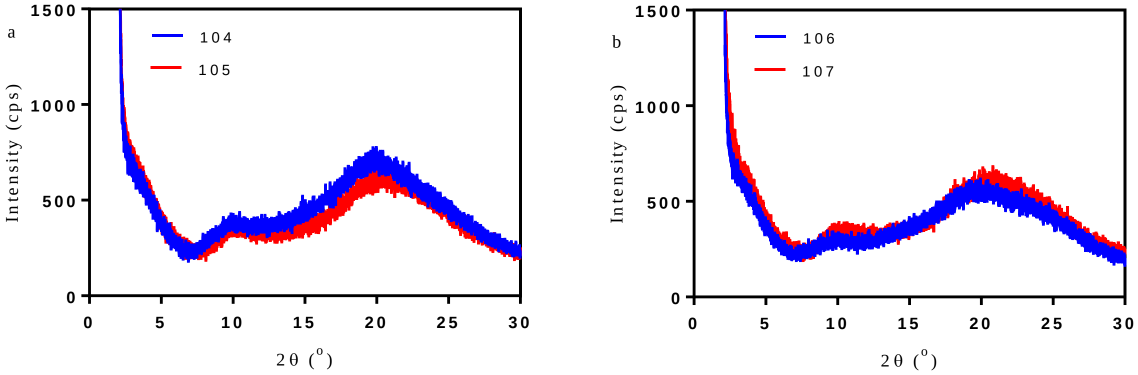

Figure 4.5: Powder XRD of a) **104** and **105**; b) **106** and **107**

4.9. Conclusions

In summary, four novel alternating copolymers including 2,7-linked carbazole units or 3,6-difluoro-2,7-linked carbazole moieties flanked by thienyl units as electron donor units and benzothiadiazole dicarboxylic imide (**BTDI**) as electron acceptor units, were synthesised *via* Suzuki polymerisation and yielded the polymers, **104**, **105**, **106** and **107**. All polymers were prepared in good yields and possess excellent solubility in common organic solvents. Two distinct side chains (linear *n*-octyl *vs* branched 3,7-dimethyloctyl) were attached to the **BTDI** units to investigate the effect of these substituents on the solubility, molecular weights, optical and electrochemical properties, thermal and structural properties of the resulting polymers. Two distinct classes of materials were also prepared amongst this series of polymers to investigate the influence of fluorine substitution on the solubility, molecular weight, optoelectronic, thermal and structural properties of the resulting polymers. The first class had hydrogen atoms at the 3,6-positions of their 2,7-linked carbazole repeat units while the second class had fluorine atoms at the 3,6-positions of their 2,7-linked carbazole repeat units. Changing the alkyl chains on **BTDI** units had an important effect on the solubility of the resulting polymers. The use of branched 3,7-dimethyloctyl chains on **BTDI** units in the carbazole-based polymers afforded **104** in 73% yield, however, the polymer was extracted in the toluene fraction due to its high solubility. The use of linear *n*-octyl chains on **BTDI** units yielded **105** which has a lower solubility. As a result, the polymer was extracted in chloroform fraction and has a higher M_n value relative to **104**. However, in the case of fluorinated copolymers, linear octyl chains had a negative impact on the molecular weight for the toluene fractions of the polymers. Although, **107** afforded another fraction in chloroform which has the highest M_n value among all polymers prepared. The E_g of the fluorinated polymers are slightly changed by replacing 3,7-dimethyloctyl chains with *n*-octyl chains on **BTDI** units, while the band gaps of the non-fluorinated polymers are comparable. The band gaps of the fluorinated polymers are slightly higher relative to those non-fluorinated analogues. The HOMO levels of all polymers are similar. Anchoring different alkyl chains on **BTDI** units as well as substituting two hydrogen atoms at the 3,6-positions of the carbazole repeat units by two fluorine atoms have no impact on the HOMO levels of the polymers. All polymers show low-lying HOMO energy levels which are beneficial for the chemical stability of polymers in oxygen and high V_{oc} values could be anticipated for the BHJ photovoltaic cells including these polymers as donor materials and fullerene as acceptor materials. The LUMO levels of the polymers are comparable due to the fact that the LUMO levels of these materials are controlled by the same **BTDI** acceptor moieties. In addition, attaching different alkyl substituents on **BTDI** units has little influence on the LUMO energy levels of the polymers. All polymers demonstrate good thermal stability with decomposition temperatures exceeding 350 °C. The thermal stability of the polymers with linear *n*-octyl side chains is lower than those counterparts with branched 3,7-dimethyloctyl side chains on **BTDI** moieties. In addition, the fluorinated polymers have higher thermal stability than those non-fluorinated analogues. The powder XRD of the polymers show diffraction peaks around 20.0° corresponding to the π-π stacking distance of about 4.0 Å. All polymers have the amorphous nature. The photovoltaic properties of these materials are currently under investigation in BHJ solar cells with fullerene derivatives.

References

1. H. Yi, A. Iraqi, M. Stevenson, C. J. Elliott and D. G. Lidzey, *Macromolecular Rapid Communications*, 2007, **28**, 1155-1160.
2. S. Wakim, N. Blouin, E. Gingras, Y. Tao and M. Leclerc, *Macromolecular Rapid Communications*, 2007, **28**, 1798-1803.
3. N. Drolet, J. F. Morin, N. Leclerc, S. Wakim, Y. Tao and M. Leclerc, *Advanced Functional Materials*, 2005, **15**, 1671-1682.
4. J. Li, F. Dierschke, J. Wu, A. C. Grimsdale and K. Müllen, *Journal of Materials Chemistry*, 2006, **16**, 96-100.
5. L. Bian, E. Zhu, J. Tang, W. Tang and F. Zhang, *Progress in Polymer Science*, 2012, **37**, 1292-1331.
6. N. Blouin and M. Leclerc, *Accounts of Chemical Research*, 2008, **41**, 1110-1119.
7. Y.-J. Cheng, S.-H. Yang and C.-S. Hsu, *Chemical Reviews*, 2009, **109**, 5868-5923.
8. A. Iraqi and I. Wataru, *Chemistry of Materials*, 2004, **16**, 442-448.
9. W. Tang, T. Lin, L. Ke and Z. k. Chen, *Journal of Polymer Science Part A: Polymer Chemistry*, 2008, **46**, 7725-7738.
10. A. Iraqi, D. F. Pickup and H. Yi, *Chemistry of Materials*, 2006, **18**, 1007-1015.
11. G. Zotti, G. Schiavon, S. Zecchin, J.-F. Morin and M. Leclerc, *Macromolecules*, 2002, **35**, 2122-2128.
12. H. Kun, H. Yi, R. G. Johnson and A. Iraqi, *Polymers for Advanced Technologies*, 2008, **19**, 299-307.
13. N. Blouin, A. Michaud and M. Leclerc, *Advanced Materials*, 2007, **19**, 2295-2300.
14. S. Wakim, S. Beaupré, N. Blouin, B.-R. Aich, S. Rodman, R. Gaudiana, Y. Tao and M. Leclerc, *Journal of Materials Chemistry*, 2009, **19**, 5351-5358.
15. T.-Y. Chu, S. Alem, P. G. Verly, S. Wakim, J. Lu, Y. Tao, S. Beaupre, M. Leclerc, F. Belanger and D. Desilets, *Applied Physics Letters*, 2009, **95**, 63304.
16. S. H. Park, A. Roy, S. Beaupre, S. Cho, N. Coates, J. S. Moon, D. Moses, M. Leclerc, K. Lee and A. J. Heeger, *Nature Photonics*, 2009, **3**, 297-302.
17. J. H. Seo, A. Gutacker, Y. Sun, H. Wu, F. Huang, Y. Cao, U. Scherf, A. J. Heeger and G. C. Bazan, *Journal of the American Chemical Society*, 2011, **133**, 8416-8419.

18. Z. He, C. Zhong, X. Huang, W. Y. Wong, H. Wu, L. Chen, S. Su and Y. Cao, *Advanced Materials*, 2011, **23**, 4636-4643.
19. D. H. Wang, J. K. Kim, J. H. Seo, I. Park, B. H. Hong, J. H. Park and A. J. Heeger, *Angewandte Chemie International Edition*, 2013, **52**, 2874-2880.
20. E. Zhou, J. Cong, S. Yamakawa, Q. Wei, M. Nakamura, K. Tajima, C. Yang and K. Hashimoto, *Macromolecules*, 2010, **43**, 2873-2879.
21. N. Blouin, A. Michaud, D. Gendron, S. Wakim, E. Blair, R. Neagu-Plesu, M. Belletete, G. Durocher, Y. Tao and M. Leclerc, *Journal of the American Chemical Society*, 2008, **130**, 732-742.
22. L. Zhang, C. He, J. Chen, P. Yuan, L. Huang, C. Zhang, W. Cai, Z. Liu and Y. Cao, *Macromolecules,* 2010, **43**, 9771-9778.
23. R. Qin, W. Li, C. Li, C. Du, C. Veit, H.-F. Schleiermacher, M. Andersson, Z. Bo, Z. Liu and O. Inganas, *Journal of the American Chemical Society*, 2009, **131**, 14612-14613.
24. H. Yi, S. Al-Faifi, A. Iraqi, D. C. Watters, J. Kingsley and D. G. Lidzey, *Journal of Materials Chemistry*, 2011, **21**, 13649-13656.
25. A. A. Alghamdi, D. C. Watters, H. Yi, S. Al-Faifi, M. S. Almeataq, D. Coles, J. Kingsley, D. G. Lidzey and A. Iraqi, *Journal of Materials Chemistry A*, 2013, **1**, 5165-5171.
26. A. J. Pearson, D. C. Watters, H. Yi, M. S. Sarjadi, L. X. Reynolds, P. P. Marchisio, J. Kingsley, S. A. Haque, A. Iraqi and D. G. Lidzey, *RSC Advances*, 2014, **4**, 43142-43149.
27. S. C. Price, A. C. Stuart, L. Yang, H. Zhou and W. You, *Journal of the American Chemical Society*, 2011, **133**, 4625-4631.
28. S. Wen, C. Wang, P. Ma, Y.-X. Zhao, C. Li and S. Ruan, *Journal of Materials Chemistry A*, 2015, **3**, 13794-13800.
29. H. Zhou, L. Yang, A. C. Stuart, S. C. Price, S. Liu and W. You, *Angewandte Chemie*, 2011, **123**, 3051-3054.
30. N. Wang, Z. Chen, W. Wei and Z. Jiang, *Journal of the American Chemical Society*, 2013, **135**, 17060-17068.
31. Q. Peng, X. Liu, D. Su, G. Fu, J. Xu and L. Dai, *Advanced Materials*, 2011, **23**, 4554-4558.
32. Y. Zhang, J. Zou, C.-C. Cheuh, H.-L. Yip and A. K.-Y. Jen, *Macromolecules*, 2012, **45**, 5427-5435.

33. S. Albrecht, S. Janietz, W. Schindler, J. Frisch, J. Kurpiers, J. Kniepert, S. Inal, P. Pingel, K. Fostiropoulos and N. Koch, *Journal of the American Chemical Society*, 2012, **134**, 14932-14944.
34. C. Du, W. Li, Y. Duan, C. Li, H. Dong, J. Zhu, W. Hu and Z. Bo, *Polymer Chemistry*, 2013, **4**, 2773-2782.
35. H. Wei, Y. H. Chao, C. Kang, C. Li, H. Lu, X. Gong, H. Dong, W. Hu, C. S. Hsu and Z. Bo, *Macromolecular Rapid Communications*, 2015, **36**, 84-89.
36. P. K. Kundu, A. Lerner, K. Kučanda, G. Leitus and R. Klajn, *Journal of the American Chemical Society*, 2014, **136**, 11276-11279.
37. M. Nakamura, K. Yamabuki, T. Oishi and K. Onimura, *Polymer Journal*, 2014, **46**, 94-103.
38. M. Sonntag and P. Strohriegl, *Chemistry of Materials*, 2004, **16**, 4736-4742.
39. A. Saeki, S. Yoshikawa, M. Tsuji, Y. Koizumi, M. Ide, C. Vijayakumar and S. Seki, *Journal of the American Chemical Society*, 2012, **134**, 19035-19042.
40. W. Bao, M. Reddy Billa, K. Kassireddy, M. Haro, M. J. Kelly, S. P. Kitney, M. S. Al Kalifah, P. Wei, D. Dong and M. O'Neill, *Liquid Crystals*, 2010, **37**, 1289-1303.
41. Y. Yoshida, Y. Sakakura, N. Aso, S. Okada and Y. Tanabe, *Tetrahedron*, 1999, **55**, 2183-2192.
42. E. Zhou, S. Yamakawa, K. Tajima, C. Yang and K. Hashimoto, *Chemistry of Materials*, 2009, **21**, 4055-4061.
43. J. Jo, C. Chi, S. Höger, G. Wegner and D. Y. Yoon, *Chemistry–A European Journal*, 2004, **10**, 2681-2688.
44. L. Cartwright, H. Yi and A. Iraqi, *New Journal of Chemistry*, 2016.
45. L. Cartwright, A. Iraqi, Y. Zhang, T. Wang and D. G. Lidzey, *RSC Advances*, 2015, **5**, 46386-46394.

Chapter 5 - Low band gap copolymers containing anthracene-benzothiadiazole dicarboxylic imide for photovoltaic applications

Abstract

Two novel low band gap D-A copolymers, **109** and **110** were synthesised by copolymerising bis-boronate ester of 9,10-phenylsubstituted anthracene flanked by thienyl groups as electron-donor units with benzothiadiazole dicarboxylic imide (**BTDI**) as electron-accepting units. Both polymers were synthesised in excellent yields *via* Suzuki polymerisation. Two different solubilising alkyl chains were anchored to the **BTDI** units in order to investigate the impact they have upon the solubility, molecular weights, optical and electrochemical properties, structural properties and thermal stability of the resulting polymers. Both polymers have comparable molecular weights and have low E_g of 1.66 eV. Both polymers have low-lying HOMO levels about –5.5 eV as well as similar LUMO energy levels of –3.56 eV. **109** and **110** show good thermal stability with decomposition temperatures at 354 and 313 °C, respectively. Powder X-ray diffraction studies have shown that both polymers have an amorphous nature in the solid state.

5.1. Introduction

Anthracene is one of the interesting building blocks as an electron donor unit. Anthracene-based polymers have strong intermolecular interactions because of the planar and rigid structure of the anthracene unit[1]. Anthracene has been used as the donor unit to construct medium band gap donor-acceptor (D-A) copolymers for photovoltaic applications[2]. Anthracene has a weak electron-donating ability, therefore anthracene-based D-A copolymers should have low-lying HOMO levels, which are beneficial to obtain high V_{oc} values in BHJ PSCs[3]. In addition, anthracene would be incorporated into the conjugated polymer chains through its 2,6-positions or 9,10-positions[4,5,1]. Polymerising anthracene through its 2,6-positions provides the 9,10-positions for attaching different solubilising side chains for better processability of the resulting polymers[2]. Anthracene and its derivatives have been widely applied in PLEDs[6] and FETs[7], while few reports have been published for anthracene in PSCs[8].

Sonar *et al.* synthesised a D-A copolymer, **PDPP-FAF** by copolymerising diketopyrrolopyrrole (**DPP**) with 2,6-linked anthracene and two furan units as spacers between donor and acceptor units (**Scheme 5.1**)[9]. BHJ PSCs based on **PDPP-FAF: PC$_{71}$BM** gave a PCE of 2.5%.

Iraqi and co-workers developed three alternating copolymers, **PPATBT**, **PPATBT-8** and **PPAT2BT-8**, comprising 9,10-phenylanthracene as donor units and various benzothiadiazole (**BT**) as acceptor units (**Scheme 5.1**)[4]. **PPATBT**, **PPATBT-8**, and **PPAT2BT-8** have E_g of 1.84, 1.96 and 1.86 eV, respectively. The photovoltaic performance of **PPATBT** was less than 2% because of its poor solubility. However, **PPATBT-8** and **PPAT2BT-8** yielded the PCE of 3.92 and 4.17% when mixed with **PC$_{71}$BM** as the acceptor, respectively.

Iraqi *et al*. reported three new copolymers, **PTATffBT**, **PTATBT-8** and **PTAT2BT-8**. The copolymers were synthesised by Suzuki polymerisation between 2,6-linked anthracene and various benzothiadiazole acceptor units (**Scheme 5.1**)[10]. Anthracene was functionalised with triisopropylsilylacetylene (TIPS) at its 9,10-positions. The E_g of the polymers are in the range of 1.81-1.92 eV. The **PTATffBT** has the deep-lying HOMO but high-lying LUMO energy levels compared to its **PTATBT-8** and **PTAT2BT-8** analogues. BHJ solar cell based on **PTATBT-8**: **PC$_{71}$BM** gave a PCE of 2.36%. On the contrary, **PTAT2BT-8** fabricated with **PC$_{71}$BM** yielded a higher PCE of 3.15%.

Anthracene functionalised at 9,10-positions with dodecyloxy, dodecylthienyl and dodecylphenyl side chains were copolymerised through 2,6-positions with **BT** bearing dodecyloxy and octyloxy substituents yielded **POA12OTBT**, **PTA12OTBT**, **PBA12OTBT**, **POA8OTBT**, **PTA8OTBT** and **PBA8OTBT**, respectively (**Scheme 5.1**)[8]. The E_g of the two dimensional (2D) conjugated polymers with thienyl and phenyl chains on anthracene unit are comparable (*ca*. 1.85 eV), which are much lower than those copolymers with dodecyloxy chains on the anthracene unit (*ca*. 2.13 eV). The 2D-conjugated polymers have deeper HOMO energy levels relative to those with dodecyloxy chains. Therefore, the V_{oc} values of the former polymers are higher than the latter polymers. The hole mobilities of **POA12OTBT** and **POA8OTBT** are lower than the polymers with aromatic side group analogues. As a result, J_{sc} values of the latter polymers are higher than the former polymers. **POA8OTBT** and **POA12OTBT** fabricated with **PC$_{71}$BM** delivered a PCE of 1.82 and 2.26%, respectively. However, 2D-conjugated polymers gave PCE higher than 3% under the same experimental conditions. **PBA8OTBT** yielded the highest PCE of 4.34%.

Recently, Jo *et al*. reported four alternating copolymers, **PTADTBT**, **PTADTFBT**, **PTADTDFBT** and **PTADTBTO** (**Scheme 5.1**)[2]. The copolymers were synthesised by Stille polymerisation between 9,10-thienylanthracene (**TA**) and **BT** with different substituents at 5,6-positions. The E_g of the polymers is in the range of 1.8-2.1 eV and **PTADTBTO** has the highest E_g among all polymers prepared. The polymers have HOMO levels between –5.38 and –5.55 eV, while the **PTADTDFBT** has the deepest HOMO energy level. The LUMO energy levels of **PTADTBT**, **PTADTFBT** and **PTADTDFBT** are comparable around –3.6 eV but **PTADTBTO** has the highest LUMO level of –3.28 eV. **PTADTBTO** blended with **PC$_{71}$BM** gave PCE of 4.64%. However, **PTADTBT** and **PTADTFBT** blended with **PC$_{71}$BM** delivered the PCE of 6.92 and 7.27%, respectively. **PTADTDFBT** delivered the highest PCE up to 8%.

Very recently, Jo and co-workers further developed two novel D-A copolymers, **PTATDPP** and **PTAFDPP** based on 9,10-thienyl substituted anthracene and **DPP**, respectively (**Scheme 5.1**)[11]. **PTATDPP** and **PTAFDPP** have the same E_g of 1.61 eV. They have high degree of crystallinity as confirmed by X-ray diffraction (XRD) studies. As a consequence, **PTATDPP** and **PTAFDPP** have high hole mobilities measured by FETs. **PTAFDPP** fabricated with **PC$_{71}$BM** gave a PCE of 5.22%. On the other hand, **PTATDPP: PC$_{71}$BM** delivered much higher PCE up to 7% under the same experimental conditions.

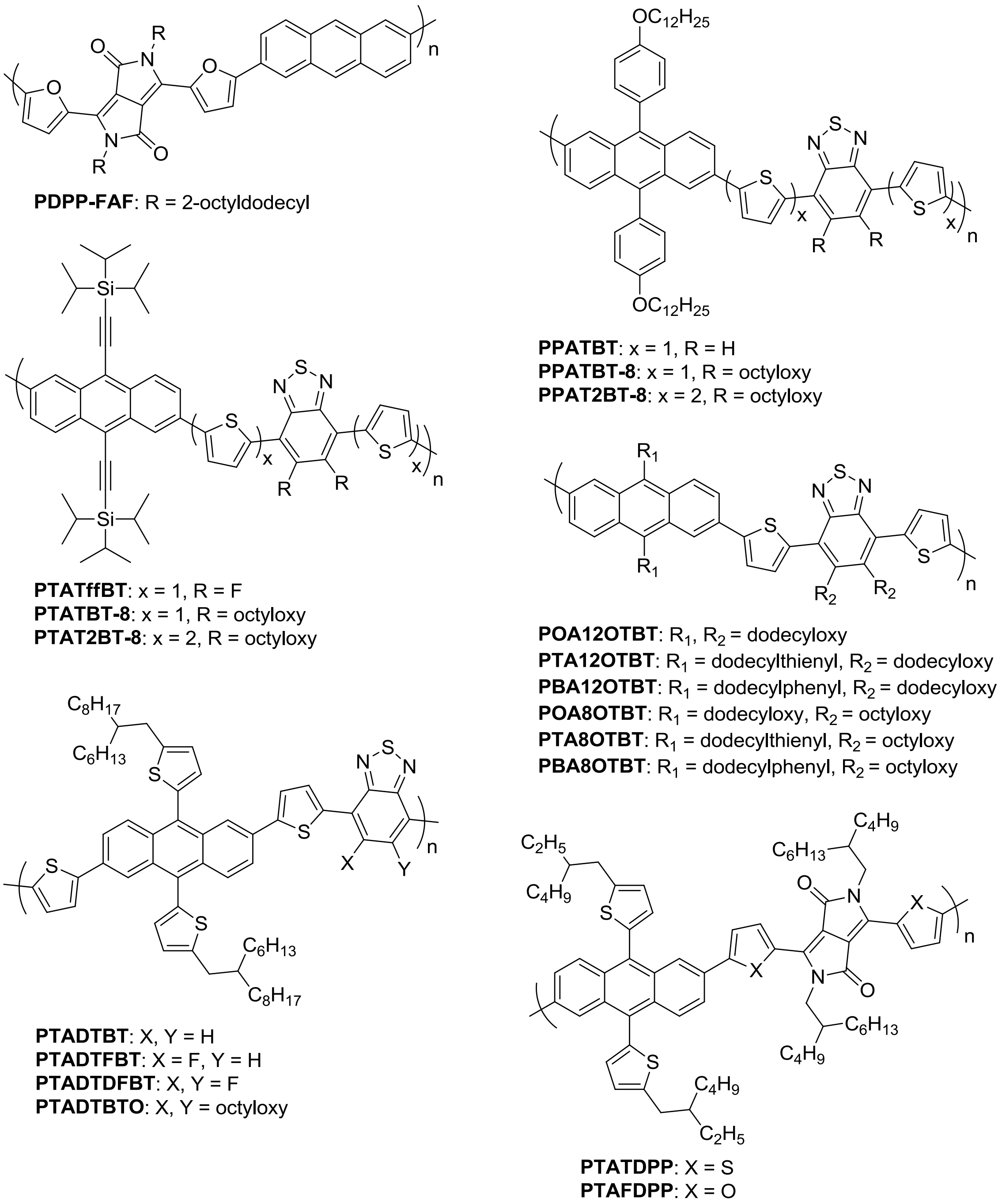

PDPP-FAF: R = 2-octyldodecyl

PPATBT: x = 1, R = H
PPATBT-8: x = 1, R = octyloxy
PPAT2BT-8: x = 2, R = octyloxy

PTATffBT: x = 1, R = F
PTATBT-8: x = 1, R = octyloxy
PTAT2BT-8: x = 2, R = octyloxy

POA12OTBT: R_1, R_2 = dodecyloxy
PTA12OTBT: R_1 = dodecylthienyl, R_2 = dodecyloxy
PBA12OTBT: R_1 = dodecylphenyl, R_2 = dodecyloxy
POA8OTBT: R_1 = dodecyloxy, R_2 = octyloxy
PTA8OTBT: R_1 = dodecylthienyl, R_2 = octyloxy
PBA8OTBT: R_1 = dodecylphenyl, R_2 = octyloxy

PTADTBT: X, Y = H
PTADTFBT: X = F, Y = H
PTADTDFBT: X, Y = F
PTADTBTO: X, Y = octyloxy

PTATDPP: X = S
PTAFDPP: X = O

Scheme 5.1: The D-A copolymers based on anthracene with different acceptor units.

5.2. Polymers synthesis

In this chapter, the preparation and characterisation of two alternating copolymers, **109** and **110** is presented. The polymers were synthesised *via* the Suzuki polymerisation between the diboronic ester of 2,6-linked anthracene (**108**) and dibrominated **BTDI** monomers (**49** and **50**), respectively (**Scheme 5.2**). The polymerisations were performed with $Pd(OAc)_2/P(o\text{-tol})_3$ catalyst, $NaHCO_3$ base in anhydrous THF. Both polymerisations were left for 23-24 hours with large amounts of purple precipitates forming as the reactions proceeded. The polymers were obtained and purified as described in chapter 2. The structures of **109** and **110** were confirmed by the ^{1}H NMR spectroscopy, FT-IR spectroscopy and elemental analysis.

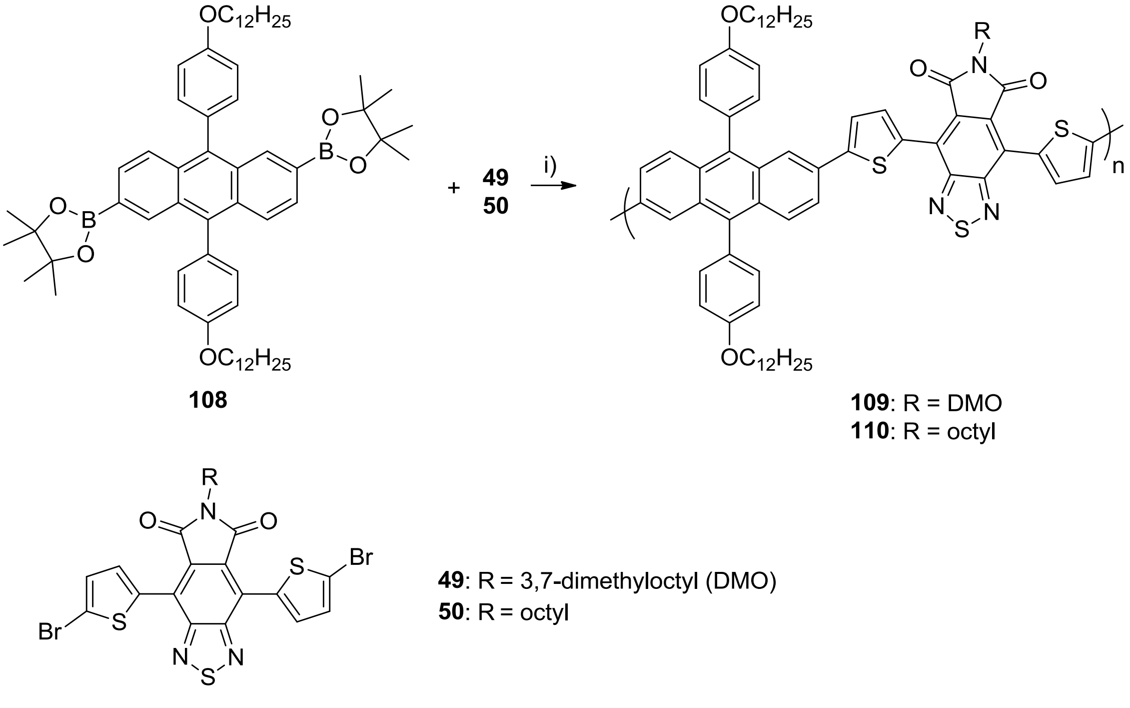

108

109: R = DMO
110: R = octyl

49: R = 3,7-dimethyloctyl (DMO)
50: R = octyl

Scheme 5.2: The Synthesis of **109** and **110** *via* Suzuki polymerisation

Reagents and conditions: i) anhydrous THF, $NaHCO_3$, $Pd(OAc)_2$, $P(o\text{-tol})_3$, 90 °C, 23-24h

5.3. Molecular weights and yield of the polymers

Molecular weights of the polymers were measured by GPC in chloroform solution at 40 °C relative to polystyrene standards (**Table 5.1**). Both polymers were synthesised in excellent yields and the number average molecular weight (M_n) of toluene and chloroform fractions are comparable. The M_n for the toluene fractions of the polymers are relatively low. However, the M_n for the chloroform fractions of the polymers are almost twice than those of the toluene fractions. The results indicate that anchoring different chains (*n*-octyl *vs* 3,7-dimethyloctyl) on the imide functionality of the **BTDI** building blocks provides polymers with similar processability and has a negligible impact on the M_n values of the resulting polymers.

Table 5.1: The percentage yield, number and weight average molecular weights with polydispersity indexes of **109** and **110**

Polymer	% yield	Toluene fraction			Chloroform fraction		
		M_n (g mol^{-1})	M_w (g mol^{-1})	PDI	M_n (g mol^{-1})	M_w (g mol^{-1})	PDI
109	97	6700	12600	1.8	12700	22400	1.7
110	97	6000	11000	1.8	12500	27400	2.1

5.4. Optical properties of the polymers

The normalised UV-vis absorption spectra of the polymers in chloroform solutions and in thin-films are shown in figure 5.1. The optical properties of these polymers are summarised in table 5.2. **109** and **110** display absorption maxima at 540 and 535 nm in solutions with shoulder absorption bands at 632 and 635 nm, respectively. The shoulder absorption bands may arise from π-π intermolecular interactions between the polymer chains and their aggregation in solutions. As compared to chloroform solutions, the absorption maxima in film states are slightly red shifted (5-11 nm) with stronger shoulder absorption bands at 660 nm for both **109** and **110**. This result indicates that both polymers show more pronounced aggregation in the solid state with formation of more coplanar structures in thin films. The E_g of the polymers are assessed from the absorption onsets in thin-films. Both polymers have comparable E_g value of 1.66 eV. The UV-Vis absorption spectra revealed that attaching different chains on the imide functionality of the **BTDI** units has not substantial influence on the optical properties of the polymers.

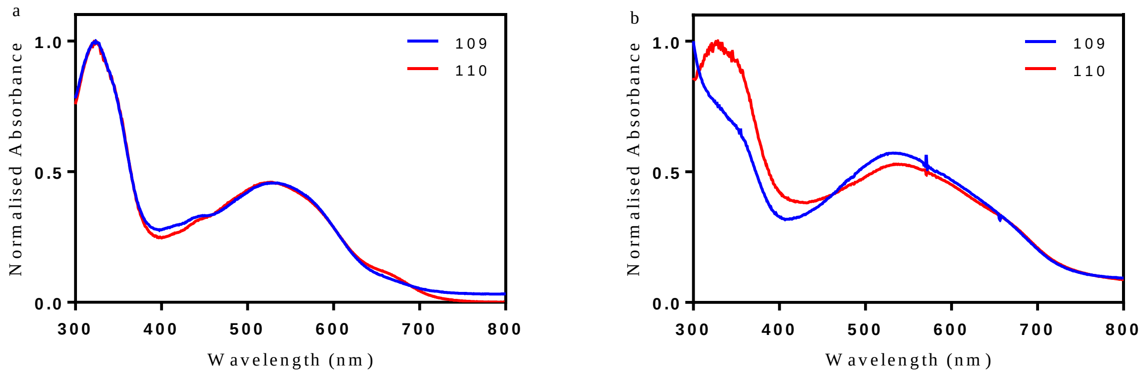

Figure 5.1: Normalised UV-vis absorption spectra of **109** and **110** in a) chloroform solutions; and b) thin films

Table 5.2: The UV-vis data and optical band gaps of the polymers

Polymer	ε (M^{-1} cm^{-1})	solution	Film		
		λ_{max} (nm)	λ_{max} (nm)	λ_{onset} (nm)	E_g (eV)
109	24300	540	545	744	1.66
110	34000	535	546	744	1.66

The absorption maxima and E_g of **109** and **110** are comparable with **PTATDPP** and **PTAFDPP** analogues (**Scheme 5.1**)[11]. The E_g of **109** and **110** are significantly lower than those **PPATBT**, **PPATBT-8** and **PPAT2BT-8** counterparts (**Scheme 5.1**)[4]. This may arise from the stronger electron withdrawing capability of **BTDI** units than **BT** and **(OR)$_2$BT** moieties, consequently lowering the LUMO energy levels of BTDI-based polymers. The E_g of **109** and **110** are significantly lower than that of fluorene-, dibenzosilole- and carbazole-based polymers, which are mentioned in chapters 3 and 4 of this thesis. This is probably due to anthracene-based two dimensional conjugated polymers have stronger and broader absorption bands[12]. The absorption coefficient (ε) of the **110** is significantly higher than **109** despite the fact that they have comparable M_n values and band gaps.

5.5. Electrochemical properties of the polymers

Cyclic voltammetry was used to study the electrochemical properties of the polymers. The LUMO and HOMO levels of the polymers calculated from the onsets of reduction and oxidation potentials, respectively (**Figure 5.2** and **Table 5.3**). The onsets were determined from cyclic voltammograms on drop cast polymer films on Pt electrode as working electrode in Bu_4NClO_4/CH_3CN (0.1 M) *vs* Ag/Ag^+ reference electrode. **109** shows a reversible oxidation peak, while **110** displays an irreversible oxidation peak. Both polymers show one reversible reduction peak at higher potential and one irreversible reduction peak at the lower potential. The HOMO levels of both polymers are comparable. The HOMO energy level is dominated by the nature of the donor unit and as both polymers have the same anthracene donor unit. Both polymers show deep-lying HOMO energy levels which are beneficial for the chemical stability of the polymers in oxygen and should lead to higher V_{oc} values when fabricated in BHJ solar cells as donor materials to fullerene derivatives as acceptor materials. The LUMO levels of both polymers are similar, as both polymers have the same **BTDI** acceptor units which control the LUMO energy levels in these materials. Substituting 3,7-dimethyloctyl chain with *n*-octyl chain on the imide functionality of the **BTDI** units does not have a major effect on the electrochemical properties of the polymers.

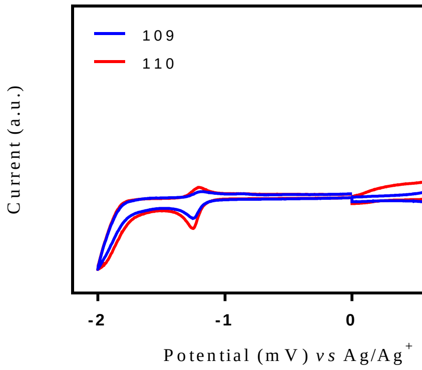

Figure 5.2: Cyclic voltammograms of **109** and **110** on Pt electrode in Bu_4NClO_4/CH_3CN at 100 mV/s

Table 5.3: Thermal and electrochemical properties of the polymers

Polymer	T_d (°C)	$E_{ox}{}^0$ (V)	HOMO (eV)	$E_{red}{}^0$ (V)	LUMO (eV)	$E_{g\,(elec)}$ (eV)
109	354	0.79	–5.51	1.15	–3.56	1.95
110	313	0.81	–5.53	1.15	–3.56	1.97

The HOMO energy levels of **109** and **110** are slightly lower than those of **PPATBT** and **PPATBT-8**, whereas they are significantly deeper than **PPAT2BT-8** analogues (**Scheme 5.1**)[4]. The shallower HOMO energy level of **PPAT2BT-8** is mainly due to flanking bithiophene units between anthracene unit and **$(OR)_2$BT** unit which increase the intramolecular charge transfer along its polymer backbone. **109** and **110** have very low-lying LUMO energy levels relative to those **PPATBT**, **PPATBT-8** and **PPAT2BT-8** counterparts[4]. This could be explained by the stronger electron-withdrawing ability of **BTDI** unit than **BT** and **$(OR)_2$BT** moieties. The HOMO energy levels of **109** and **110** are similar to the fluorene-, dibenzosilole- and carbazole-based polymers, while the LUMO energy levels are slightly lower than those counterparts as mentioned in chapters 3 and 4. These results are highly promising as to the photovoltaic properties of these two polymers in BHJ solar cells with fullerene derivatives.

5.6. Thermal properties of the polymers

The thermal properties of the polymers were studied by TGA. **109** and **110** exhibit excellent thermal stability with T_d at 354 and 313 °C, respectively (**Figure 5.3** and **Table 5.3**). The thermal stability of **110** is significantly lower than that of **109**. It is worth noting that the thermal properties of the polymers essentially depend on the type of the alkyl chains anchored to the imide functionality on the **BTDI** units.

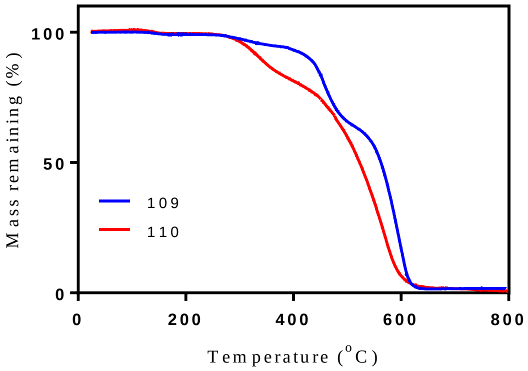

Figure 5.3: TGA of **109** and **110**

The thermal stability of the polymers is significantly lower than that of fluorene-, dibenzosilole- and carbazole-based polymers as described in chapters 3 and 4. However, both polymers have thermal stability windows that are well within those used in solar cell applications and should be stable for such use.

5.7. Powder X-ray diffraction (XRD) of the polymers

The structural properties of the polymers were studied by powder XRD in the solid state (**Figure 5.4**). **109** and **110** exhibit a similar diffraction patent with a broad diffraction peak at an angle of 20.0°, corresponding to the π-π stacking distances between polymer chains of 4.43 Å. This result shows that both polymers have an amorphous nature which are similar to analogous anthracene-based polymers, **PTATPD(O)**, **PTATPD(DMO)** and **PTATPD(BP)** (**Scheme 5.3**)[13].

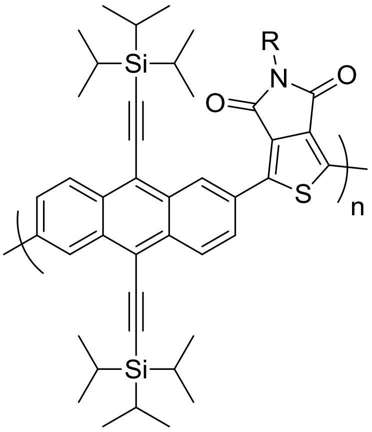

PTATPD(O): R = *n*-octyl
PTATPD(DMO): R = 3,7-dimethyloctyl (DMO)
PTATPD(BP): R = 4-butylphenyl (BP)

Scheme 5.3: Structures of **PTATPD** copolymers

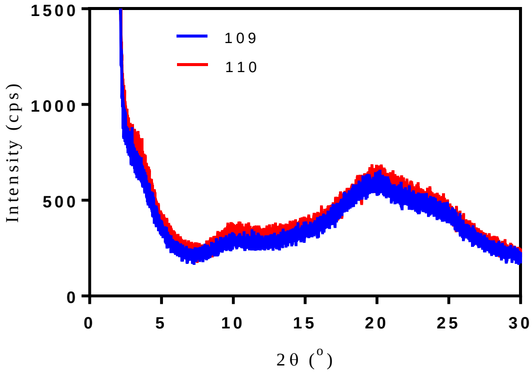

Figure 5.4: Powder XRD of **109** and **110**

5.8. Conclusions

In summary, two low band gap alternating copolymers comprising of 2,6-linked anthracene moieties flanked by thienyl units as electron donor units and benzothiadiazole dicarboxylic imide (**BTDI**) as electron acceptor units were synthesised through Suzuki polymerisation, and yielded **109** and **110**. Both polymers were prepared in excellent yields and show good solubility in common organic solvents. Both polymers have comparable M_n values for both toluene and chloroform fractions. The M_n of the toluene fractions of the polymers are about 6000 g mol^{-1} which are relatively low. However, the M_n of the chloroform fractions of the polymers are higher than 12000 g mol^{-1}. Both polymers show absorption maxima around 540 nm in chloroform solutions with shoulder absorption bands about 635 nm. The shoulder absorption peak could be attributed to intermolecular interactions between the polymer chains and a certain degree of their aggregation in solutions. In thin-films, the absorption spectra of the polymers show slightly bathochromic shift absorption maxima with stronger shoulder at 660 nm relative to their absorption in solutions. This is related to those polymers adopting a more planar structure in thin-films. The band gap of the polymers are low (E_g = 1.66 eV) which are beneficial to obtain high J_{sc} values in BHJ solar cells. The HOMO levels of both polymers are comparable because the HOMO energy level is controlled by the nature of the donor unit and both polymers have the same anthracene donor units. Both polymers show low-lying HOMO energy levels of about –5.5 eV which are useful for the chemical stability of the polymers in oxygen, and should lead to high V_{oc} values when fabricated in BHJ solar cells as donor materials to fullerene derivatives as acceptor materials. The LUMO energy levels of both polymers are similar, as both polymers have the same **BTDI** acceptor units which dominate the LUMO levels in these materials. Both polymers show good thermal stability with degradation temperature surpass 310 °C. Attaching different solubilising chains (3,7-dimethyloctyl *vs* *n*-octyl) on **BTDI** moieties has a significant impact on the thermal properties of the polymers, for example, the **110** has lower thermal stability than **109**. However, they have little impact on the molecular weights and optoelectronic properties of the polymers. The powder XRD of the polymers show diffraction peaks at 20.0° corresponding to the π-π stacking distance of 4.43 Å. Both polymers have the amorphous nature in the solid state. The photovoltaic properties of these materials are currently under investigation in BHJ solar cells with fullerene derivatives.

References

1. X. Gong, C. Li, Z. Lu, G. Li, Q. Mei, T. Fang and Z. Bo, *Macromolecular Rapid Communications*, 2013, **34**, 1163-1168.
2. J. W. Jung, F. Liu, T. P. Russell and W. H. Jo, *Advanced Energy Materials*, 2015, **5**.
3. H. Zhou, L. Yang, S. Stoneking and W. You, *ACS Applied Materials & Interfaces*, 2010, **2**, 1377-1383.
4. A. Abdulaziz, *Chemical Communications*, 2013, **49**, 2252-2254.
5. D. SungáChung, D. HoonáLee, N. SungáCho and C. EonáPark, *Chemical Communications*, 2010, **46**, 1863-1865.
6. H.-Y. Chen, C.-T. Chen and C.-T. Chen, *Macromolecules*, 2010, **43**, 3613-3623.
7. J. Y. Back, T. K. An, Y. R. Cheon, H. Cha, J. Jang, Y. Kim, Y. Baek, D. S. Chung, S.-K. Kwon and C. E. Park, *ACS Applied Materials & Interfaces*, 2015, **7**, 351-358.
8. C. Liu, W. Cai, X. Guan, C. Duan, Q. Xue, L. Ying, F. Huang and Y. Cao, *Polymer Chemistry*, 2013, **4**, 3949-3958.
9. P. Sonar, S. P. Singh, E. L. Williams, Y. Li, M. S. Soh and A. Dodabalapur, *Journal of Materials Chemistry*, 2012, **22**, 4425-4435.
10. L. Cartwright, L. J. Taylor, H. Yi, A. Iraqi, Y. Zhang, N. W. Scarratt, T. Wang and D. G. Lidzey, *RSC Advances*, 2015, **5**, 101607-101615.
11. J. W. Jung and W. H. Jo, *Polymer Chemistry*, 2015, **6**, 4013-4019.
12. Y. Li and Y. Zou, *Advanced Materials*, 2008, **20**, 2952-2958.
13. L. Cartwright, T. J. Neal, N. J. Rutland and A. Iraqi, *Polymers for Advanced Technologies*, 2016, **27**, 525-531.

Chapter 6 - Low band gap alternating copolymers based on cyclopentadithiophene-benzothiadiazole dicarboxylic imide for solar cell applications

Abstract

A series of alternating copolymers containing cyclopentadithiophene (**CPDT**) flanked by thienyl moieties as electron-donor units and benzothiadiazole dicarboxylic imide (**BTDI**) as electron-acceptor units were designed and synthesised for solar cell applications. Different solubilising side chains, including 2-ethylhexyl chains and *n*-octyl chains were attached to **CPDT** units, whereas 3,7-dimethyloctyl chains and *n*-octyl chains were anchored to the **BTDI** moieties. The impact of these substituents on the solubility, molecular weights, optical and electrochemical properties, thermal and structural properties of the resulting polymers was investigated. **134** was synthesised *via* Suzuki polymerisation, whereas **135**, **136** and **137** were prepared through direct arylation polymerisation. **135** has the highest number average molecular weight (M_n = 17400 g mol^{-1}) among all polymers prepared. The **135** and **136** which have *n*-octyl substituents on their **CPDT** units have comparable optical band gaps (E_g ~ 1.3 eV) which are around 0.1 eV lower than **134** and **137** analogues which have 2-ethylhexyl substituents on their **CPDT** units. The polymers have their HOMO levels between –5.10 and –5.22 eV with **134** having the deepest HOMO energy level. The LUMO levels of the polymers are between –3.4 and –3.5 eV. All polymers exhibit good thermal stability with decomposition temperatures surpassing 350 °C. Powder XRD studies have shown that all polymers have the amorphous nature in solid state.

6.1. Introduction

Cyclopenta[2,1-*b*:3,4-*b*']dithiophene (**CPDT**) derivatives are analogous materials to fluorene derivatives, where two thiophenes rather than two phenyl groups are bridged by a carbon atom. These materials have attracted considerable attention. The **CPDT** unit has a much stronger electron-donating ability than fluorene and hence has stronger orbital mixing with electron-deficient moieties. In addition, donor-acceptor (D-A) copolymers based on the **CPDT** have higher planarity, lower optical band gaps, which offer enhanced conjugation and stronger intermolecular interactions resulting in high charge carrier mobilities. One of the most promising D-A low band gap (E_g) copolymers containing the

CPDT unit is poly[2,6-(4,4-bis(2-ethylhexyl)-4*H*-cyclopenta[2,1-*b*:3,4-*b*']dithiophene)-*alt*-2,1,3-benzothiadiazole] (**PCPDTBT) (Scheme 6.1**)[1]. **PCPDTBT** is an alternating copolymer comprising of the **CPDT** as the donor moiety and 2,1,3-benzothiadiazole (**BT**) as an acceptor unit which was first synthesised using Stille polymerisation by Brabec *et al.* and used in photovoltaic cells[1]. It has an E_g around 1.4 eV with a broad absorption up to 850 nm[2,3]. **PCPDTBT** fabricated with **PC$_{71}$BM** achieved a PCE of 3.5%[2]. Bazan and Heeger groups further optimised devices based on **PCPDTBT: PC$_{71}$BM** and the photovoltaic performance up to 5.5% was recorded[4,5]. Brabec *et al.* reported a high hole mobility for **PCPDTBT** of 0.02 cm^2 V^{-1} s^{-1}.[6] Zhang and co-workers synthesised **PCPDTBT** with *n*-hexyldecyl chains on the **CPDT** unit and FET devices based on this polymer showed a higher hole mobility of 0.17 cm^2 V^{-1} s^{-1} due to enhanced solubility and increased packing order[7]. Recently, a hole mobility as high as 3.3 cm^2 V^{-1} s^{-1} based on the same polymer have been achieved by Tsao *et al.*[8]. A series of D-A copolymers were synthesised based on the **CPDT** as the donor building blocks and different acceptor moieties instead of **BT**. For instance, Janssen group synthesised a new low band gap copolymers, **PCPDTBO** by copolymerising **CPDT** unit with 2,1,3-benzoxadiazole (**BO**) as an electron acceptor unit (**Scheme 6.1**)[9]. **PCPDTBO: PC$_{61}$BM** BHJ solar cell gave a PCE of 2.5%. **PCPDTDTBT** synthesised by copolymerising **CPDT** flanked by thienyl units as the donor unit with **BT** as the acceptor unit (**Scheme 6.1**)[10]. BHJ solar cells based on **PCPDTDTBT: PC$_{61}$BM** showed the PCE of 2.1%.

Li *et al.* synthesised a new copolymer, **PCPDTDTBTz** by copolymerising **CPDT** flanked by thienyl units as the electron donor unit with 2,2'-bithiazole (**BTz**) as an electron acceptor unit (**Scheme 6.1**)[11]. **PCPDTDTBTz: PC$_{61}$BM** BHJ photovoltaic cells delivered a PCE of 3%. Li and co-workers further synthesised two copolymers, **PCPDT$_{H}$DT$_{H}$Tz** and **PCPDT$_{H}$DT$_{EH}$Tz** based on **CPDT** flanked by thienyl units as the donor units and 1,2,4,5-tetrazine (**Tz**) as an acceptor unit (**Scheme 6.1**)[12,13]. **PCPDT$_{H}$DT$_{H}$Tz** has a molecular weight almost twice than its **PCPDT$_{H}$DT$_{EH}$Tz** analogue due to less steric hindrance from the linear side chains. **PCPDT$_{H}$DT$_{H}$Tz** fabricated with **PC$_{71}$BM** in BHJ solar cell gave a high PCE of 5.53%. However, **PCPDT$_{H}$DT$_{EH}$Tz** delivered lower PCE of 3.89%.

Alternating copolymers including **CPDT** as the strong donor units and thieno[3,4-*c*]pyrrole-4,6-dione (**TPD**) as the acceptor units have been reported by several groups[14,15,16]. **PCPDT$_{Oc}$TPD$_{Dd}$** was synthesised by Guo *et al. via* Stille polymerisation (**Scheme 6.1**)[14]. **PCPDT$_{Oc}$TPD$_{Dd}$: PC$_{71}$BM** exhibited the PCE higher than 3%. Soon after, Li *et al.* reported **PCPDT$_{H}$TPD$_{Oc}$** with *n*-hexyl chains on **CPDT** units and *n*-octyl chains on the **TPD** units (**Scheme 6.1**)[16]. **PCPDT$_{H}$TPD$_{Oc}$** blended with **PC$_{71}$BM** in BHJ photovoltaic cell gave an impressive PCE of 6.41%.

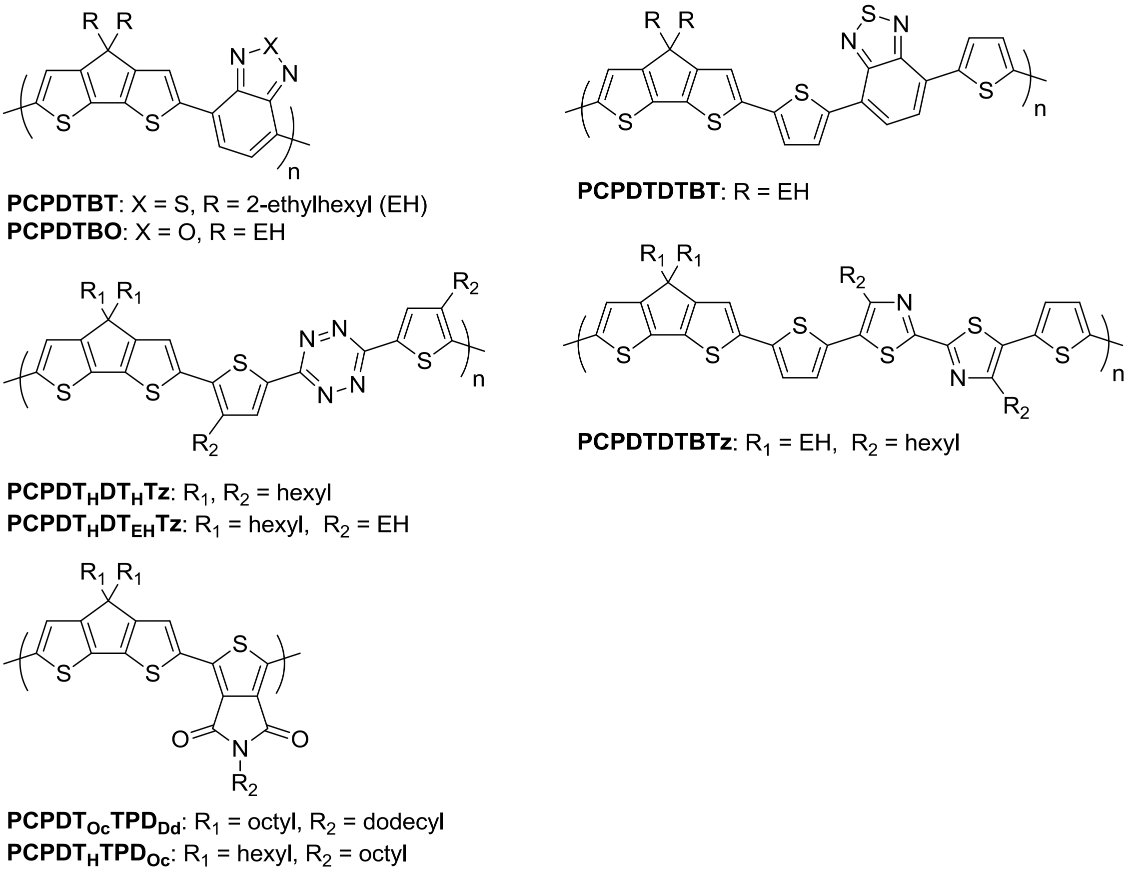

PCPDTBT: X = S, R = 2-ethylhexyl (EH)
PCPDTBO: X = O, R = EH

PCPDTDTBT: R = EH

PCPDT$_{H}$DT$_{H}$Tz: R_1, R_2 = hexyl
PCPDT$_{H}$DT$_{EH}$Tz: R_1 = hexyl, R_2 = EH

PCPDTDTBTz: R_1 = EH, R_2 = hexyl

PCPDT$_{Oc}$TPD$_{Dd}$: R_1 = octyl, R_2 = dodecyl
PCPDT$_{H}$TPD$_{Oc}$: R_1 = hexyl, R_2 = octyl

Scheme 6.1: The D-A copolymers based on **CPDT** units with different acceptor units

6.2. Synthesis of cyclopentadithiophene (CPDT) monomers

120, **121** and **122** are **CPDT** monomers for the preparation of the target polymers in this chapter. **120** and **121** were synthesised through seven steps, while **122** was prepared *via* eight steps starting from commercially available 3-bromothiophene (**111**) and thiophene-3-carboxaldehyde (**112**) (**Scheme 6.2**). The different steps in their preparation are discussed below.

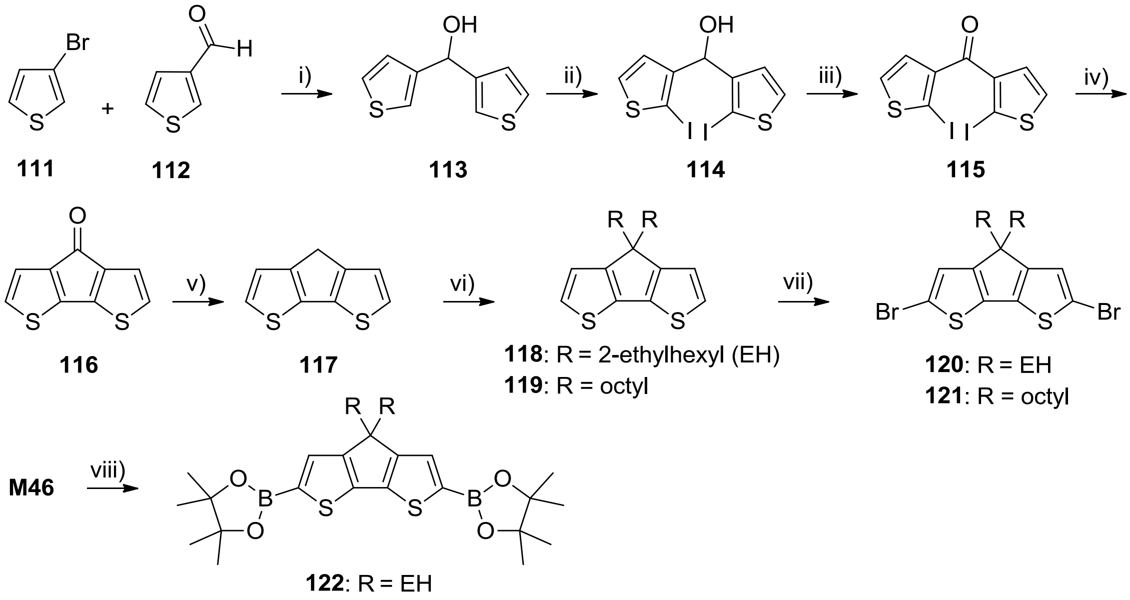

Scheme 6.2: The synthetic steps of the **CPDT** monomers

Reagents and conditions: i) *n*-BuLi, anhydrous Et_2O, −78 °C; ii) *n*-BuLi, anhydrous Et_2O, −78 °C, I_2; iii) PCC, CH_2Cl_2, RT, 24h; iv) Cu, anhydrous DMF, reflux, 150 °C, 22h; v) triethylene glycol, KOH, hydrazine hydrate, 180 °C, 17h; vi) KOH, KI, anhydrous DMSO, R-Br, RT, 24h; vii) NBS, DMF, RT, 24h; viii) bis(pinacolato)diboron, $PdCl_2$(dppf), KOAc, anhydrous DMF, 80 °C, 48h

6.2.1. Synthesis of bis(3-thienyl)methanol (113)

111 was lithiated selectively at the 3-position at –78 °C and subsequently treated with **112** to obtain **113** as a yellow oil in 85% yield (**Scheme 6.2**)[17].

The mechanism of the reaction consists of three steps (**Scheme 6.3**). In the first step, **111** was reacted with *n*-BuLi to generate organolithium intermediate (**123**) through halogen-metal exchange. This intermediate functions as a nucleophile which attacks the carbonyl group of **112** to form alkoxide intermediate (**124**). Finally, the alkoxide ion is protonated using aqueous ammonium chloride to form **113**, which is a secondary alcohol.

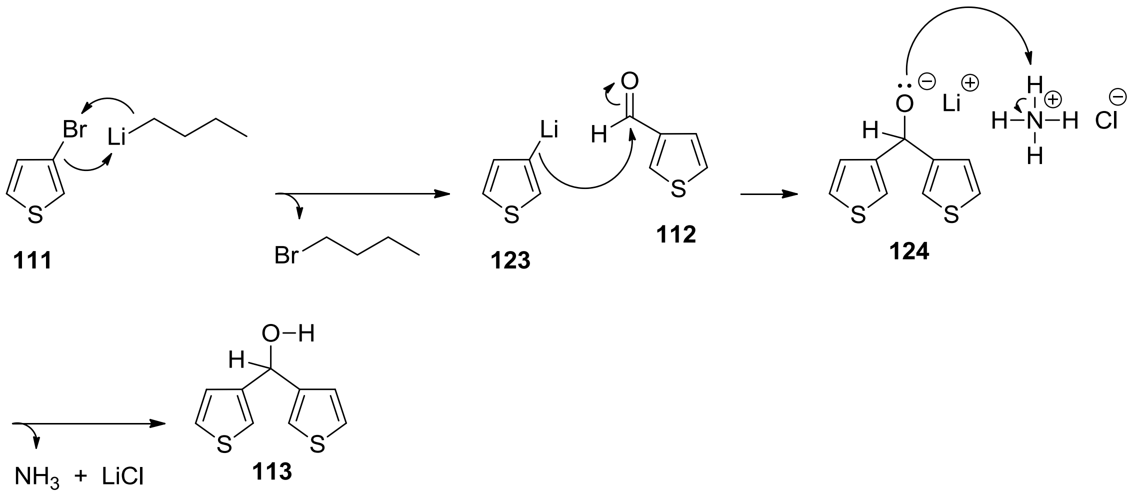

Scheme 6.3: The mechanism for synthesis of 113

The structure and purity of **113** were verified by the ^{1}H NMR, ^{13}C NMR and FT-IR spectroscopy. The ^{1}H NMR spectrum of **113** shows a doublet of doublet, a multiplet and another doublet of doublet at 7.32, 7.25-7.23 and 7.07 ppm respectively corresponding to thiophene protons. It also shows two doublets at 5.99 and 2.22 ppm, which belong to proton of hydroxyl group and a proton attached to the carbon that bears the hydroxyl group, respectively. The ^{13}C NMR spectrum of **113** is in accordance with literature and shows four carbon atoms in the aromatic region for thiophene rings and one carbon atom in the aliphatic region at 73.0 ppm for the carbon that bears the hydroxyl group. The FT-IR spectrum of **113** shows a broad peak at 3131-3507 cm^{-1}, which is representative of O-H stretching vibration.

6.2.2. Synthesis of bis(2-iodo-3-thienyl)methanol (114)

113 was lithiated selectively at 2,2'-positions and subsequently reacted with iodine to yield **114** as cream coloured crystals in 79% yield (**Scheme 6.2**)[18].

The mechanism of the iodination reaction suggested by Brzezinski and Reynolds includes three steps (**Scheme 6.4**)[19]. First, **113** was reacted with three equivalents of *n*-BuLi to lithiate regioselectively the 2,2'-positions of thiophene rings and also hydroxyl group to yield the trilithiated intermediate (**125**). This intermediate subsequently reacts with three equivalents of iodine to generate a hypoiodite intermediate (**126**). Finally, **114** is obtained by hydrolysis of the latter intermediate by aqueous sodium thiosulfate.

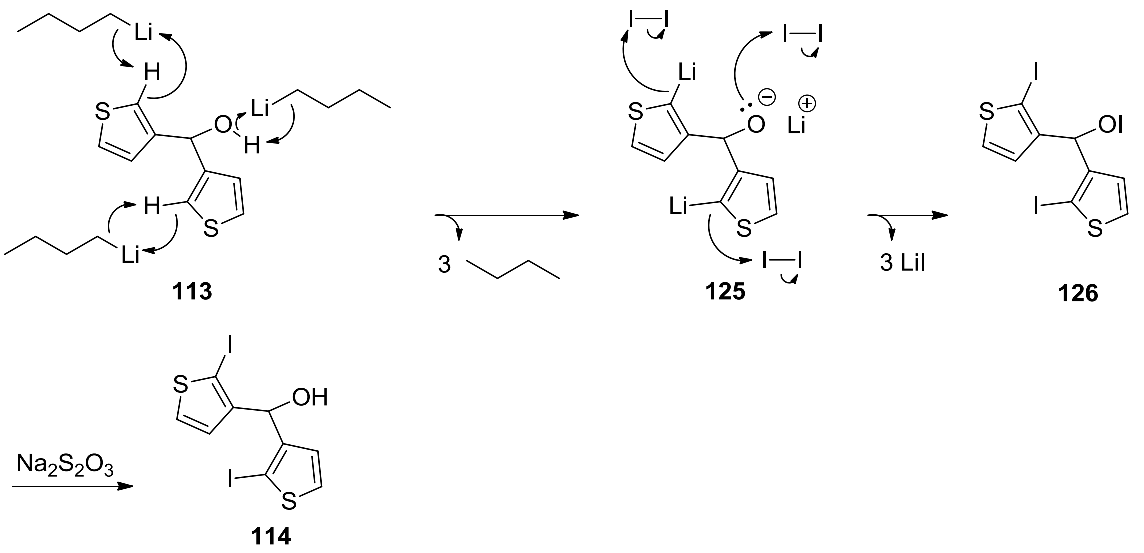

Scheme 6.4: The mechanism of iodination reaction of **113**

114 was characterised by several analytical tools. From the ^{1}H NMR spectrum of **114**, the peaks corresponding to thiophene protons can be visualised as a doublet of doublet and a doublet at 7.46 and 6.96 ppm, respectively. It also shows two doublets in the aliphatic region. The mass spectrum of **114** shows a peak at 447.8 indicating the mass of the molecular ion $[M]^+$ for **114**. The structure and purity of **114** was further confirmed by the ^{13}C NMR and FT-IR spectroscopy.

6.2.3. Synthesis of bis(2-iodo-3-thienyl)ketone (115)

114 was oxidised by pyridinium chlorochromate (PCC) as an oxidising agent in dichloromethane at room temperature to obtain **115** as yellow crystals in 97% yield (**Scheme 6.2**)[20].

The mechanism of the oxidation reaction is depicted in scheme 6.5. The oxygen atom of **114** acts as a nucleophile and attacks the chromium (6+) in PCC, followed by proton transfer and subsequent removal of chloride ion to give a chromate ester intermediate (**127**). This intermediate undergoes a bimolecular elimination (E_2) reaction by removing proton to form **115** and chromium (4+).

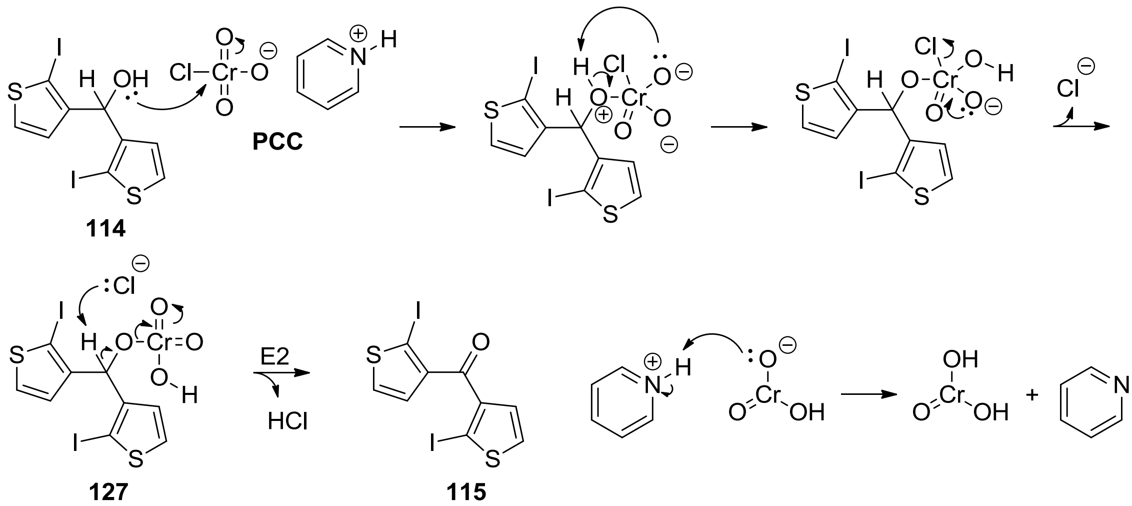

Scheme 6.5: The mechanism of oxidation reaction of **114**

The ^{1}H NMR, ^{13}C NMR and FT-IR spectroscopy were used to characterise **115**. From the ^{1}H NMR spectrum of **115**, it is confirmed that the oxidation reaction was successful as the two doublets at 5.80 and 2.26 ppm in the ^{1}H NMR spectrum of **114** are no longer present. It also shows two doublets at 7.49 and 7.08 ppm for thiophene protons, respectively. The ^{13}C NMR spectrum of **115** displays fours peaks in the aromatic region for thiophene carbons and also a peak at 185.5 ppm for a carbon of ketone group. Meanwhile, a peak at 72.0 ppm for alcohol carbon in the ^{13}C NMR spectrum of **114** disappears. The FT-IR spectrum of **115** shows a new peak at 1648 cm^{-1} corresponding to carbonyl stretching vibration. Meanwhile, the broad peak for O-H stretching vibration of **114** also disappears.

6.2.4. Synthesis of *4H*-cyclopenta[2,1-*b*:3,4-*b*']dithiophen-4-one (116)

116 was prepared by the Ullmann coupling reaction between **115** with copper powder in anhydrous DMF and it was obtained as purple crystals in 98% yield (**Scheme 6.2**)[21]. The mechanism of the reaction is performed through intramolecular ring closure, which is similar to that for the synthesis of **68** as shown in scheme 3.17.

The ^{1}H NMR spectroscopy and mass spectrometry were implemented to characterise the structure of **116**. The ^{1}H NMR spectrum of **116** displays two doublets at 7.06 and 7.01 ppm corresponding to thiophene protons. The mass spectrum of **116** displays a peak at 192 indicating the mass of the molecular ion [M]$^+$ of **116**.

6.2.5. Synthesis of *4H*-cyclopenta[2,1-*b*:3,4-*b*']dithiophene (117)

116 was reduced to **117** using hydrazine hydrate (NH_2NH_2) in triethylene glycol under basic conditions and it was obtained as white crystals in 80% yield by Wolff-Kishner reduction (**Scheme 6.2**)[22].

The mechanism of the reaction contains a number of steps (**Scheme 6.6**). In the beginning, a hydrazine hydrate molecule functions as a nucleophile and attacks the carbonyl group of **116** to form an intermediate (**128**). This intermediate is protonated twice and followed by loss of water molecule to form a hydrazone intermediate (**129**). In the next step, the hydrazone intermediate is deprotonated by hydroxide ion to form a resonance stabilised intermediates (**130** and **131**) which is protonated and then deprotonated to form a diimide anion intermediate (**132**). Carbanion intermediate (**133**) is generated by leaving nitrogen gas from **132**. Finally, **133** is protonated to give the **117**.

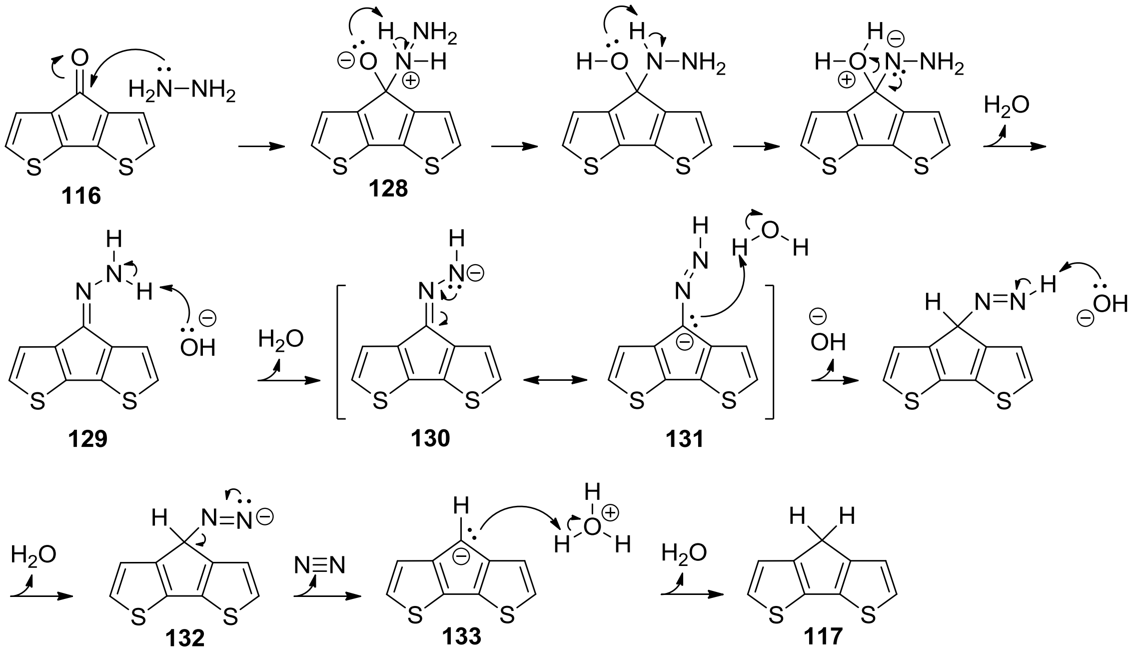

Scheme 6.6: The mechanism of reduction reaction of **116**

The ^1H NMR and ^{13}C NMR spectroscopy used to characterise **117**. From the ^1H NMR spectrum of **117**, it is obvious that the reduction reaction was successful as a new singlet peak at 3.56 ppm appears integrating for two protons, which is indicative of methylene protons. It also displays two doublets at 7.20 and 7.11 ppm for thiophene protons, respectively. The ^{13}C NMR spectrum of **117** displays a new peak at 32.0 ppm corresponding to the methylene carbon. Meanwhile, a peak at 183.0 ppm, which belongs to the carbon of the ketone group of **116** disappears in the spectrum of **117**.

6.2.6. Synthesis of 4,4-bis(2-ethylhexyl)cyclopenta[2,1-*b*:3,4-*b*']dithiophene (118) and 4,4-dioctylcyclopenta[2,1-*b*:3,4-*b*']dithiophene (119)

117 was alkylated under basic conditions with 2-ethylhexyl bromide or 1-bromooctane (**85**) using small catalytic amount of potassium iodide in anhydrous DMSO and gave **118** and **119** as yellow oil in 89 and 91% yield, respectively (**Scheme 6.2**)[23]. The mechanism of the reaction is similar to that for the synthesis of **28** as shown in scheme 2.15.

The ^{1}H NMR and ^{13}C NMR spectroscopy were implemented to characterise the structure of **118** and **119**. From the ^{1}H NMR spectra of both monomers, it is clear that the alkylation reactions were successful as a singlet peak at 3.56 ppm for methylene protons of **117** disappear. They also show the expected protons in the aromatic and aliphatic regions. A new peak at 53.0 ppm can be seen in the ^{13}C NMR spectra for **118** and **119**. Meanwhile, a peak at 32.0 ppm for **117** is no longer present in the ^{13}C NMR spectra of both monomers.

6.2.7. Synthesis of 4,4-bis(2-ethylhexyl)-2,6-dibromocyclopenta[2,1-*b*:3,4-*b*']dithiophene (120) and 4,4-dioctyl-2,6-dibromocyclopenta[2,1-*b*:3,4-*b*']dithiophene (121)

118 and **119** were brominated regioselectively at the 2,6-positions with two equivalents of NBS in DMF and yielded **120** and **121** as yellow oil in 88 and 87% yield, respectively (**Scheme 6.2**)[24]. The mechanism of reaction is similar to that for the synthesis of **39** as shown in scheme 3.6.

120 and **121** were characterised by several analytical tools. From the ^{1}H NMR spectra for **120** and **121**, the peak corresponding to thiophene protons can be visualised as triplet and singlet at 6.95 and 6.94 ppm, respectively. In addition, they show a series of multiplet and triplets for methylene and methyl protons. The ^{13}C NMR spectra for both monomers are in agreement with literature[24]. The mass spectra for both monomers display peaks at 560.1, which are indicative of the masses of the molecular ions $[M]^+$ of both monomers.

6.2.8. Synthesis of 4,4-bis(2-ethylhexyl)-2,6-bis(4,4,5,5-tetramethyl-1,3,2-dioxaboralan-2-yl)cyclopenta[2,1-*b*:3,4-*b*']dithiophene (122)

120 was reacted with excess of bis(pinacolato)diboron, potassium acetate as a base and $PdCl_2$(dppf) as a catalyst in anhydrous DMF to yield **122** as a red sticky oil in 57% yield (**Scheme 6.2**)[25]. The mechanism of the reaction is similar to that of the Suzuki coupling reaction described in the introduction chapter.

122 was sticky oily material and it was used for the Suzuki polymerisation without further purification. The purification for **122** was problematic by column chromatography because the diboronic ester degrades upon attempted chromatographic purification and transforms to **118**. Attempts at recrystallising **122** from methanol after passing methanol through a basic alumina column to remove acidic protons were also unsuccessful. According to the ^{1}H NMR and ^{13}C NMR spectroscopy, **122** is not pure and contains traces of monoboronic ester and traces of unreacted starting material (**120**).

6.3. Polymers synthesis

In this part, the preparations of four low band gap copolymers either through Suzuki or direct arylation polymerisations are discussed. **134** was synthesised *via* Suzuki polymerisation between diboronic ester of **CPDT** monomer (**122**) and dibrominated **BTDI** monomer (**49**) (**Scheme 6.7**). A direct arylation polymerisation as a new synthetic method was used to prepare the other three copolymers based on **CPDT** units. One of the advantages of the direct arylation polymerisation is that it requires less synthetic steps compared to Suzuki and Stille polymerisations[26]. It eliminates the need to prepare boronic ester and stannylated monomeric compounds, which are sometimes challenging to purify from their by-products as in the case for **122**. It also avoids the use of toxic compounds especially tin compounds[27]. **135**, **136** and **137** were synthesised successfully through direct arylation polymerisation using $Pd_2(dba)_3.CHCl_3/P(o\text{-}MeOPh)_3$ catalyst, caesium carbonate base and pivalic acid in anhydrous toluene: DMF as a co-solvent (**Scheme 6.7**). **121** was copolymerised with both **47** and **48** to form **135** and **136**, respectively. **137** was obtained by copolymerising **120** with **48**. All polymerisations were left running between 17 and 96 hours with large amounts of dark green precipitates forming as the reactions proceeded. The polymers were obtained and purified as described in chapter 2. The structures of the **134**, **135**, **136** and **137** were confirmed by the ^{1}H NMR spectroscopy, FT-IR spectroscopy and elemental analysis.

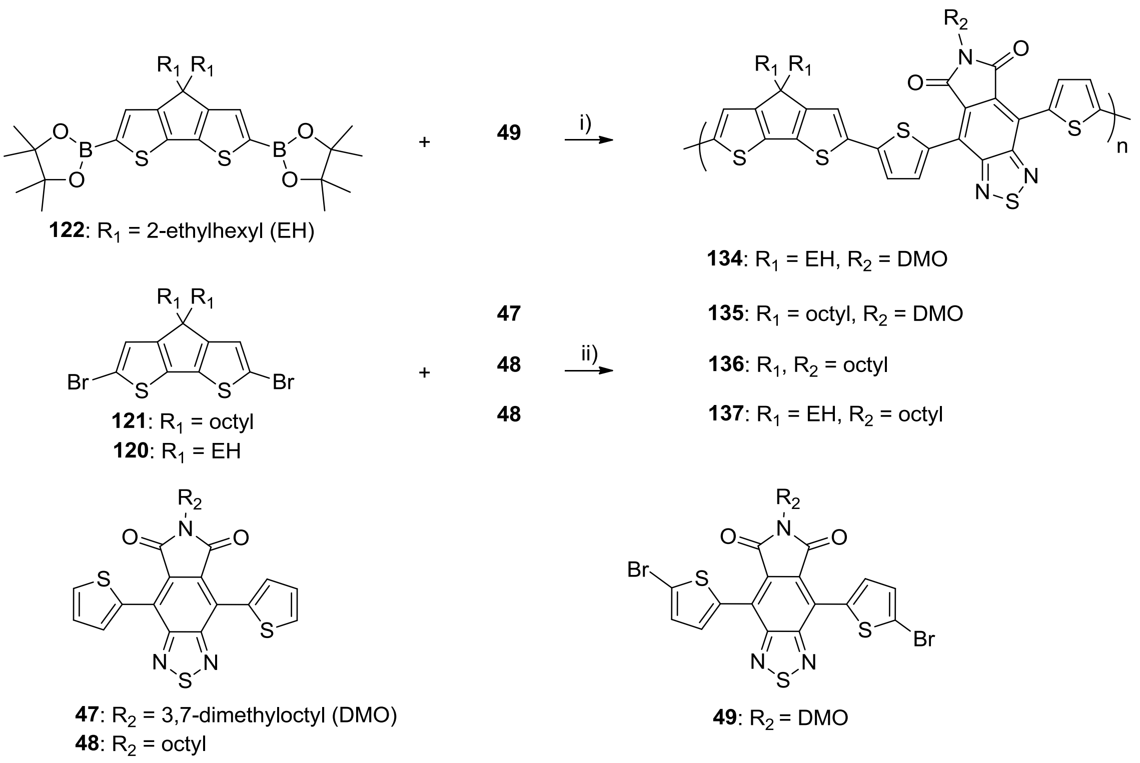

Scheme 6.7: The synthesis of **134**, **135**, **136** and **137**

Reagents and conditions: i) anhydrous THF, $NaHCO_3$, $Pd(OAc)_2$, P(*o*-tol)$_3$, 90 °C, 48h; ii) $Pd_2(dba)_3.CHCl_3$, P(*o*-MeOPh)$_3$, PivOH, Cs_2CO_3, anhydrous toluene: anhydrous DMF (10:1, v/v), 115 °C, 17-96h

6.4. Molecular weights and yield of the polymers

Molecular weights of the polymers were measured by GPC in chloroform solution at 40 °C relative to polystyrene standards (**Table 6.1**). Although, the polymerisation of **134** was performed for 48 hours, it was synthesised in very low yield (< 10%) and with a low number average molecular weight (M_n ~ 5000 g mol^{-1}). There are several factors that would lead to the low M_n value and low yield of this polymer. One of the main reasons is probably due to severe steric hindrance between two branched alkyl chains (2-ethylhexyl and 3,7-dimethyloctyl) on **CPDT** and **BTDI** repeat units respectively. The second reason is that the bis-boronic ester monomer (**122**) contains some impurities such as unreacted staring material and monoboronic ester, since **122** was used for polymerisation without further purification. Since the monomer was unstable, it was difficult to purify by column chromatography. Finally, the polymer contains too much solubilising side chains. It is well known that both steric hindrance and impurities disrupt the effective conjugation length (ECL) and lead to low molecular weight polymers. **135** and **136** were synthesised twice under the same experimental conditions but with different reaction times. Substituting 3,7-dimethyloctyl chains in **135** for *n*-octyl chains in **136** on the **BTDI** units which leads to lower M_n values for the toluene fractions of the polymers in the first polymerisation. However, in the second polymerisation, by extending the reaction time, the M_n value of the former polymer increased slightly, while M_n value of the latter polymer increased significantly for the toluene fractions. In addition, **135** afforded another fraction in chloroform of a higher M_n value. The higher molecular weight polymers could be obtained by prolonging the polymerisation times as well as by substituting *n*-octyl chains to 3,7-dimethyloctyl chains on the **BTDI** building blocks. Furthermore, replacing *n*-octyl chains in **136** by 2-ethylhexyl chains in **137** on the **CPDT** moieties results in a polymer with the higher M_n value for toluene fractions. Moreover, **137** has the highest M_n value for toluene fractions among all polymers prepared. This could be attributed to the effect of the branched chains in both **135** and **137** which provide greater solubilities and higher molecular weight fractions. The yields of the direct arylation polymerisation were high between 72 and 95% and **135** has the highest yield.

Table 6.1: The percentage yield, reaction time, weight and number average molecular weights with polydispersity indexes of **134**, **135**, **136**, and **137**

Polymer	% yield	Time (h)	Toluene fraction		
			M_n (g mol^{-1})	M_w (g mol^{-1})	PDI
134	8	48	5200	10100	1.9
135	95	17	7800	18100	2.3
135*	86	72	10000	30900	3.0
136	72	51	4900	20800	4.2
136	76	96	9100	18300	2.0
137	72	96	15900	29700	1.8

*Chloroform fraction: M_n = 17400 g mol^{-1}, M_w = 61400 g mol^{-1} and PDI = 3.5

6.5. Optical properties of the polymers

The UV-vis absorption spectra of all polymers were investigated in chloroform solutions and in thin-films (**Figure 6.1** and **Table 6.2**). In solutions, **135**, **136** and **137** display comparable absorption maxima which are red-shifted around 40 nm relative to those of **134** analogue probably as a result of the low molecular weight of the latter polymer. In thin-films, the absorption spectra of the polymers show quite strong bathochromic shift absorption maxima between 29 and 86 nm relative to their absorption in solutions. This could be explained by stronger intermolecular π-π interaction and more planar structures in the solid state. The E_g of the polymers are estimated from the absorption onsets in thin-films. **135** and **136** have comparable E_g (*ca.* 1.3 eV) which are around 0.1 eV lower than those of **134** and **137** analogues. The results indicate that substituting 2-ethylhexyl chains by *n*-octyl chains on **CPDT** units would lead to lower E_g of the polymers, while changing 3,7-dimethyloctyl chains by *n*-octyl chains on **BTDI** moieties has a minimal effect on the E_g of the polymers. These polymers are good candidates as donor materials fabricated with fullerene derivatives as top BHJ cell in tandem solar cells due to their low optical band gaps[28].

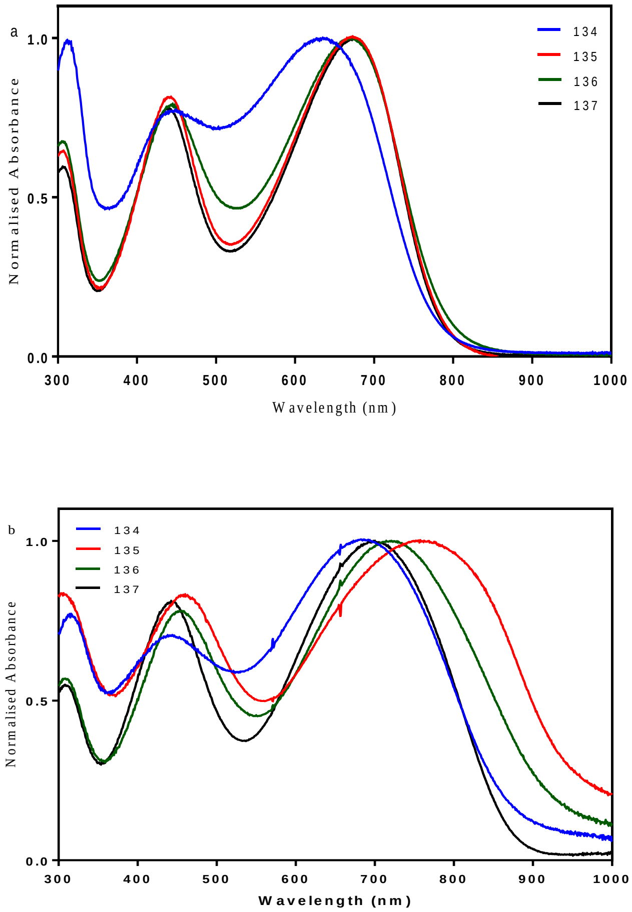

Figure 6.1: Normalised UV-vis absorption spectra of **134**, **135**, **136** and **137** in a) chloroform solutions; and b) thin films

Table 6.2: The Uv-vis data and optical band gaps of the polymers

Polymer	ε	solution	Film		
	(M^{-1} cm^{-1})	λ_{max} (nm)	λ_{max} (nm)	λ_{onset} (nm)	E_g (eV)
134	28200	635	686	865	1.43
135	37500	673	759	936	1.32
136	27500	672	724	922	1.34
137	28400	675	704	873	1.42

The E_g values of **134** and **137** are comparable to **PCPDTBT** analogue (**Scheme 6.1**)[1]. However, **135** and **136** have lower E_g values around 0.1 eV relative to **PCPDTBT** counterpart. The E_g of the polymers are significantly lower than those thienopyrroledione-, bithiazole- and tetrazine-based polymers because the **BTDI** unit is stronger acceptor than those units (**Scheme 6.1**)[14,15,16,11,12,13]. Compared to the polymers based on fluorene, dibenzosilole, carbazole and anthracene, which mentioned in chapters 3, 4 and 5, the polymers have lower E_g. This may arise from the fact that **CPDT** units have stronger electron-donating abilities than those donor moieties, therefore adopt more planar structure with stronger interchain interactions along the polymer backbone. **134** and **137** have comparable absorption coefficients (ε) and their coefficients are slightly higher than **136**. **135** has the highest absorption coefficient among all polymers prepared. This could be attributed to the **135** having the highest absorption maxima of about 759 nm in solid state and it is red-shifted by more than 80 nm compared to solution among all polymers (**Table 6.2**).

6.6. Electrochemical properties of the polymers

Cyclic voltammetry was used to study the electrochemical properties of the polymers. The LUMO and HOMO levels of the polymers calculated from the onsets of reduction and oxidation potentials, respectively (**Figure 6.2** and **Table 6.3**). The onsets were determined from cyclic voltammograms on drop cast polymer films on Pt electrode as working electrode in Bu_4NClO_4/CH_3CN (0.1 M) *vs* Ag/Ag^+ reference electrode. The HOMO levels of **135** and **137** are –5.20 and –5.22 eV, respectively which are deeper than **134** and **136**. The LUMO energy levels of **135** and **136** are higher than **134** and **137**. The HOMO and LUMO levels of the polymers are not significantly affected by different substituents attached to the **CPDT** and **BTDI** units.

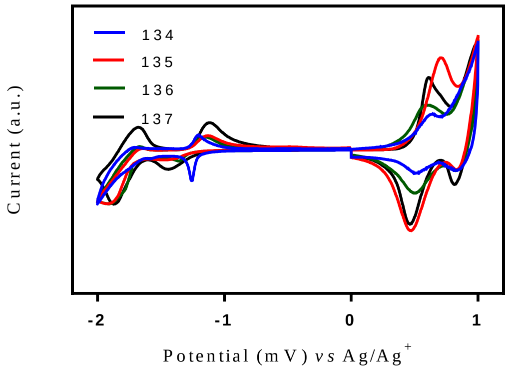

Figure 6.2: Cyclic voltammograms of **134**, **135**, **136** and **137** on Pt electrode in Bu_4NClO_4/CH_3CN at 100 mV/s

Table 6.3: Thermal and electrochemical properties of the polymers

Polymer	T_d (°C)	$E_{ox}{}^0$ (V)	HOMO (eV)	$E_{red}{}^0$ (V)	LUMO (eV)	$E_{g\,(elec)}$ (eV)
134	378	0.44	–5.15	1.19	–3.52	1.63
135	419	0.49	–5.20	1.24	–3.47	1.73
136	402	0.39	–5.10	1.27	–3.44	1.66
137	377	0.51	–5.22	1.17	–3.54	1.68

The HOMO levels of the polymers are higher around 0.1 to 0.2 eV, while the LUMO energy levels are almost identical relative to its **PCPDTBT** analogue (**Scheme 6.1**)[2]. The HOMO levels of the polymers are shallower than the HOMO level of **PCPDTTPD** (–5.43 eV), while their LUMO energy levels are lower than the LUMO energy level of **PCPDTTPD** (–3.25 eV) (**Scheme 6.1**)[15]. The HOMO levels of the polymers are significantly shifted upward compared to the fluorene-, dibenzosilole-, carbazole- and anthracene-based polymers, which were mentioned in chapters 3, 4 and 5. This could be attributed to the **CPDT** unit being a stronger donor compared to those donor units. However, their LUMO energy levels are comparable to those polymers because the LUMO level is dominated by the **BTDI** acceptor unit.

6.7. Thermal properties of the polymers

Thermal properties of the polymers were studied by TGA (**Figure 6.3** and **Table 6.3**). All polymers show high thermal stability with decomposition temperatures up to 370 °C. It is interesting to note that the thermal stability of the polymers with linear *n*-octyl chains on **CPDT** repeat units is higher than those polymers with branched 2-ethylhexyl chains. In addition, the thermal stability of the **134** and **137** is not affected by the nature of substituents on **BTDI** units, while changing the 3,7-dimethyloctyl chains in **135** to *n*-octyl chains in **136** on the acceptor moieties has a negative impact on the thermal stability of the polymers. It was tentatively hypothesized that the polymers with *n*-octyl chains are more planar than those with 2-ethylhexyl chains; therefore they might need higher temperature to decompose. Moreover, the differences in thermal stability of the polymers is probably due to different molecular weight of the polymers.

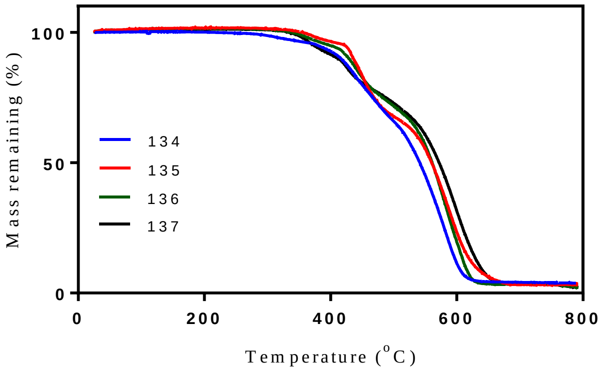

Figure 6.3: TGA of **134**, **135**, **136** and **137**

6.8. Powder X-ray diffraction of the polymers

The structural properties of the **135**, **136** and **137** were investigated by powder X-ray diffraction (XRD) in solid state (**Figure 6.4**). However, **134** was not studied by powder XRD because the amount obtained from the polymerisation was not enough to undertake measurements. The XRD of **135**, **136** and **137** show diffraction peaks at 24.7, 24.5 and 24.4° corresponding to the π-π stacking distance of 3.60, 3.62 and 3.64 Å, respectively. The results show that all polymers have an amorphous nature. Similarly, **PCPDTBT** did not show crystallinity as studied by XRD as reported in previous literature report[29].

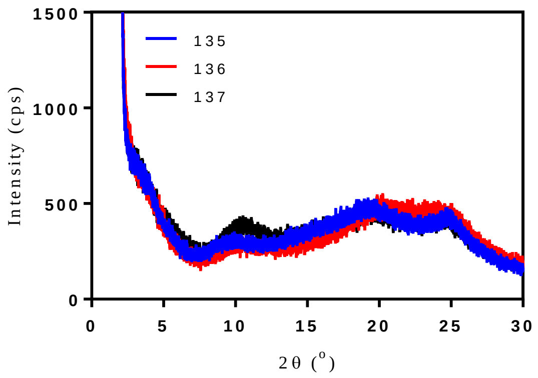

Figure 6.4: Powder XRD of **135**, **136** and **137**

6.9. Conclusions

In summary, four novel low band gap alternating copolymers including cyclopentadithiophene (**CPDT**) flanked by thienyl units as electron donor moieties and benzothiadiazole dicarboxylic imide (**BTDI**) as electron acceptor units were synthesised *via* two different palladium catalysed cross coupling polymerisations. **134** was prepared by copolymerising the diboronic ester of **CPDT** (**122**) with dibrominated **BTDI** (**49**) *via* Suzuki polymerisation. The yield of the polymerisation was too low (< 10%) and the polymer has a low M_n value around 5000 g mol^{-1}. To circumvent these problems, direct arylation polymerisation as a new alternative preparation method was utilised to prepare the **135**, **136** and **137**. All polymers were synthesised in good yields and they have excellent solubility in common organic solvents. Two distinct side chains (*n*-octyl *vs* 2-ethylhexyl) were attached to the **CPDT** units as well as two different side chains (*n*-octyl *vs* 3,7-dimethyloctyl) were anchored to the **BTDI** units to investigate the effect of these substituents on the solubility, molecular weights, optical and electrochemical properties, thermal and structural properties of the resulting polymers. Changing 3,7-dimethyloctyl chains on the **BTDI** units in **135** for *n*-octyl chains in **136** as well as prolonging the polymerisation times had a significant effect on the solubility and also on the M_n values of the resulting polymers. **135** provided a toluene fraction which has a M_n value of 10000 g mol^{-1}. In addition to the toluene fraction, another fraction from chloroform was obtained which has a higher M_n value of 17400 g mol^{-1}. However, **136** was extracted in the toluene fraction which has the M_n value of 9100 g mol^{-1}. Moreover, substituting *n*-octyl chains in **136** for 2-ethylhexyl chains in **137** on the **CPDT** units leads to a polymer with higher M_n value of 15900 g mol^{-1} for the toluene fraction. The polymers with one branched chains on either **CPDT** or **BTDI** units can provide greater solubilities and higher molecular weight fractions. In solutions, the polymers which were synthesised by direct arylation polymerisation show comparable absorption maxima and display bathochromic shift around 40 nm relative to **134**. In thin-films, the absorption spectra of the polymers show red-shifted absorption maxima by 29-86 nm relative to their absorption in solutions. The optical band gaps of the polymers with *n*-octyl chains on the **CPDT** units are about 1.3 eV which are about 0.1 eV lower than those analogues with 2-ethylhexyl chains. However, substituting 3,7-dimethyloctyl chains by *n*-octyl chains on **BTDI** units has little influence on the E_g of the polymers. The low band gap of these polymers is beneficial to achieve high J_{sc} values in BHJ solar cells. These polymers could also be used along with higher band gap conjugated polymers as top cells in tandem solar cells. The HOMO energy levels of the polymers are between –5.10 and –5.22 eV. The LUMO energy levels of the polymers are between –3.44 and –3.54 eV. Both the LUMO and HOMO levels of the polymers are affected around 0.1 eV by attaching different substituents on both **CPDT** and **BTDI** repeat units as well as changing the types of polymerisations. All polymers display good thermal stability with T_d exceeding 370 °C. The polymers based on *n*-octyl chains on **CPDT** units have higher thermal stability than those polymers with 2-ethylhexyl chains on **CPDT** units. The powder XRD of the polymers show diffraction peaks around 24.0° corresponding to the π-π stacking distance of about 3.60 Å. All polymers have an amorphous nature. The photovoltaic properties of these materials are currently under investigation both in traditional BHJ solar cells as well as in tandem solar cells.

References

1. D. Mühlbacher, M. Scharber, M. Morana, Z. Zhu, D. Waller, R. Gaudiana and C. Brabec, *Advanced Materials*, 2006, **18**, 2884-2889.
2. Z. Zhu, D. Waller, R. Gaudiana, M. Morana, D. Mühlbacher, M. Scharber and C. Brabec, *Macromolecules*, 2007, **40**, 1981-1986.
3. C. Soci, I. W. Hwang, D. Moses, Z. Zhu, D. Waller, R. Gaudiana, C. J. Brabec and A. J. Heeger, *Advanced Functional Materials*, 2007, **17**, 632-636.
4. J. Peet, J. Y. Kim, N. E. Coates, W. L. Ma, D. Moses, A. J. Heeger and G. C. Bazan, *Nature Materials*, 2007, **6**, 497-500.
5. J. K. Lee, W. L. Ma, C. J. Brabec, J. Yuen, J. S. Moon, J. Y. Kim, K. Lee, G. C. Bazan and A. J. Heeger, *Journal of the American Chemical Society*, 2008, **130**, 3619-3623.
6. M. Morana, M. Wegscheider, A. Bonanni, N. Kopidakis, S. Shaheen, M. Scharber, Z. Zhu, D. Waller, R. Gaudiana and C. Brabec, *Advanced Functional Materials*, 2008, **18**, 1757-1766.
7. M. Zhang, H. N. Tsao, W. Pisula, C. Yang, A. K. Mishra and K. Müllen, *Journal of the American Chemical Society*, 2007, **129**, 3472-3473.
8. H. N. Tsao, D. M. Cho, I. Park, M. R. Hansen, A. Mavrinskiy, D. Y. Yoon, R. Graf, W. Pisula, H. W. Spiess and K. Müllen, *Journal of the American Chemical Society*, 2011, **133**, 2605-2612.
9. J. C. Bijleveld, M. Shahid, J. Gilot, M. M. Wienk and R. A. Janssen, *Advanced Functional Materials*, 2009, **19**, 3262-3270.
10. A. J. Moulé, A. Tsami, T. W. Bünnagel, M. Forster, N. M. Kronenberg, M. Scharber, M. Koppe, M. Morana, C. J. Brabec and K. Meerholz, *Chemistry of Materials*, 2008, **20**, 4045-4050.
11. K.-C. Li, J.-H. Huang, Y.-C. Hsu, P.-J. Huang, C.-W. Chu, J.-T. s. Lin, K.-H. Wei and H.-C. Lin, *Macromolecules*, 2009, **42**, 3681-3693.
12. Z. Li, J. Ding, N. Song, J. Lu and Y. Tao, *Journal of the American Chemical Society*, 2010, **132**, 13160-13161.
13. Z. Li, J. Ding, N. Song, X. Du, J. Zhou, J. Lu and Y. Tao, *Chemistry of Materials*, 2011, **23**, 1977-1984.
14. X. Guo, H. Xin, F. S. Kim, A. D. Liyanage, S. A. Jenekhe and M. D. Watson, *Macromolecules*, 2010, **44**, 269-277.

15. Y. Zhang, J. Zou, H.-L. Yip, Y. Sun, J. A. Davies, K.-S. Chen, O. Acton and A. K.-Y. Jen, *Journal of Materials Chemistry*, 2011, **21**, 3895-3902.
16. Z. Li, S. W. Tsang, X. Du, L. Scoles, G. Robertson, Y. Zhang, F. Toll, Y. Tao, J. Lu and J. Ding, *Advanced Functional Materials*, 2011, **21**, 3331-3336.
17. G. L. Gibson, T. M. McCormick and D. S. Seferos, *Journal of the American Chemical Society*, 2011, **134**, 539-547.
18. C.-H. Chen, C.-H. Hsieh, M. Dubosc, Y.-J. Cheng and C.-S. Hsu, *Macromolecules*, 2009, **43**, 697-708.
19. J. Z. Brzezinski and J. R. Reynolds, *Synthesis*, 2002, **8**, 1053-1056.
20. B. Pal, W.-C. Yen, J.-S. Yang, C.-Y. Chao, Y.-C. Hung, S.-T. Lin, C.-H. Chuang, C.-W. Chen and W.-F. Su, *Macromolecules*, 2008, **41**, 6664-6671.
21. W. C. Yen, B. Pal, J. S. Yang, Y. C. Hung, S. T. Lin, C. Y. Chao and W. F. Su, *Journal of Polymer Science Part A: Polymer Chemistry*, 2009, **47**, 5044-5056.
22. R. Li, J. Liu, N. Cai, M. Zhang and P. Wang, *The Journal of Physical Chemistry B*, 2010, **114**, 4461-4464.
23. P. Coppo, D. C. Cupertino, S. G. Yeates and M. L. Turner, *Macromolecules*, 2003, **36**, 2705-2711.
24. A. P. Zoombelt, S. G. Mathijssen, M. G. Turbiez, M. M. Wienk and R. A. Janssen, *Journal of Materials Chemistry*, 2010, **20**, 2240-2246.
25. C.-Y. Yu and C.-Y. Wu, *Dyes and Pigments*, 2014, **106**, 81-86.
26. J.-R. Pouliot, B. Sun, M. Leduc, A. Najari, Y. Li and M. Leclerc, *Polymer Chemistry*, 2015, **6**, 278-282.
27. M. Wakioka, Y. Kitano and F. Ozawa, *Macromolecules*, 2013, **46**, 370-374.
28. T. Ameri, G. Dennler, C. Lungenschmied and C. J. Brabec, *Energy & Environmental Science*, 2009, **2**, 347-363.
29. H. Y. Chen, J. Hou, A. E. Hayden, H. Yang, K. Houk and Y. Yang, *Advanced Materials*, 2010, **22**, 371-375.

Chapter 7 - Low band gap copolymers based on dithienosilole-benzothiadiazole dicarboxylic imide for photovoltaic applications

Abstract

Two alternating copolymers of dithienosilole (**DTS**) flanked by thienyl units as electron-donor moieties and benzothiadiazole dicarboxylic imide (**BTDI**) as electron-acceptor units were designed and synthesised for photovoltaic applications. Two distinct solubilising side chains including 3,7-dimethyloctyl chains and *n*-octyl chains were anchored to the **BTDI** moieties. The impact of these substituents on the solubility, molecular weights, optical and electrochemical properties, thermal and structural properties of the resulting polymers was investigated. **144** and **145** were synthesised *via* Stille polymerisation. The number average molecular weight of **144** and **145** are 14600 and 5700 g mol^{-1}, respectively. Both polymers have comparable optical band gaps around 1.4 eV. The HOMO levels of the polymers are comparable around –5.2 eV. **145** and **145** have lowest unoccupied molecular orbital (LUMO) levels at –3.56 and –3.45 eV, respectively. They exhibit good thermal stability with decomposition temperatures surpassing 350 °C. Powder XRD studies have shown that both polymers have an amorphous nature in the solid state.

7.1. Introduction

Dithieno[3,2-*b*:2',3'-*d*]silole (**DTS**) is a promising donor unit for constructing low band gap D-A conjugated polymers. Replacing the bridging carbon atom in the cyclopentadithiophene (**CPDT**) unit with a silicon atom, a new donor moiety, **DTS**, has been developed. The C-Si bond in the **DTS** unit is longer than the C-C bond in the **CPDT** unit which could reduce the steric hindrance between the solubilising side chains and the conjugated polymer backbone. As a result, this leads to stronger π-π stacking between polymer chains and thereby improved crystallinity and charge carrier mobility of the DTS-based polymers[1]. Yang and co-workers reported the first alternating copolymer, **PDTSBT** based on **DTS** as a donor unit and **BT** as an acceptor unit (**Scheme 7.1**)[2]. It has 3-fold higher hole mobility than that for **PCPDTBT** analogue. Photovoltaic devices based on **PDTSBT: PC$_{71}$BM** delivered a high PCE of 5.1%[2]. Bazan *et al.* reported a similar copolymer, **PDTSBT12** with *n*-dodecyl chains on the silicon atom (**Scheme 7.1**)[3]. It was synthesised by microwave-assisted Stille polymerisation with high number average molecular weight (M_n = 34000 g mol^{-1}). **PDTSBT12** fabricated with **PC$_{71}$BM** achieved higher PCE of 5.9%. Yang *et al.* further reported three copolymers, **PDTS$_H$DTBT**, **PDTS$_{EH}$DTBT** and **PDTS$_{12}$DTBT** using **DTBT** as an acceptor unit (**Scheme 7.1**)[4]. The first polymer showed limited solubility in common organic solvents and could not be fabricated in BHJ solar cell. **PDTS$_{EH}$DTBT** blended with **PC$_{71}$BM** in BHJ solar cell gave the PCE of 2.95%, while, **PDTS$_{12}$DTBT** delivered a higher PCE of 3.43% with higher J_{sc} and *FF* values. This is probably due to less steric hindrance for *n*-dodecyl chains than 2-ethylhexyl chains. These polymers have higher performance compared to **PCPDTDTBT** analogue[5].

Tao *et al.* designed and synthesised a new copolymer, **PDTSTPD** using thieno[3,4-*c*]pyrrole-4,6-dione (**TPD**) as the acceptor unit (**Scheme 7.1**)[6]. **PDTSTPD** fabricated with **PC$_{71}$BM** exhibited a very impressive PCE of 7.3%. Soon after, they reported a PCE of 7.5% for higher molecular weight polymer (M_n = 31000 g mol^{-1})[7]. The higher PCE could be attributed to higher hole mobility, lower series resistance and larger *FF* for higher molecular weight polymers. **PDTSTPD** has higher PCE relative to its **PCPDTTPD** analogue[8,9].

Li and co-workers developed a new copolymer, **PDTSDTBTz** using 2,2'-bithiazole (**BTz**) as an acceptor with two flanking thiophene units between **BTz** and **DTS** units (**Scheme 7.1**)[10]. **PDTSDTBTz** blended with **PC$_{71}$BM** gave a PCE of 2.86%. Li *et al.* further developed another two copolymers, **PDTSDTTTz-3** and **PDTSDTTTz-4** using more rigid and more coplanar geometry thiazolo[5,4-*d*]thiazole (**TTz**) acceptor unit (**Scheme 7.1**)[11]. The positions of the solubilising side chains on the flanking thiophene units between **TTz** and **DTS** were changed. **PDTSDTTTz-3** has higher hole mobility relative to its **PDTSDTBTz** analogue due to increased backbone planarity and stronger intermolecular interactions. **PDTSDTTTz-3** blended with **PC$_{71}$BM** delivered the PCE of 5.59%. **PDTSDTTTz-4** has a higher hole mobility compared to its **PDTSDTTTz-3** analogue due to it adopts a more planar structure. **PDTSDTTTz-4: PC$_{71}$BM** showed a higher PCE of 5.88% with a remarkable *FF* of 71.6%.

The **DTS** was copolymerised with naphtho(2,3-*c*)thiophene-4,9-dione (**NTDO**) acceptor to form a new copolymer, **PDTSNTDO** (**Scheme 7.1**)[12]. **PDTSNTDO: PC$_{71}$BM** gave the PCE of 5.21%.

PDTSDTTAZ and **PDTSTAZ** were synthesised *via* Stille polymerisation between **DTS** and 2-alkyl-2,1,3-benzotriazole (**TAZ**) acceptor unit with and without thiophene spacers, respectively (**Scheme 7.1**)[13]. Flanking two thiophene units between donor and acceptor units decrease the steric hindrance and thereby improve the planarity of the polymer backbone. **PDTSDTTAZ** fabricated with **PC$_{71}$BM** in BHJ solar cell exhibited a higher PCE compared to its **PDTSTAZ** analogue (3.80 *vs* 1.64%), respectively.

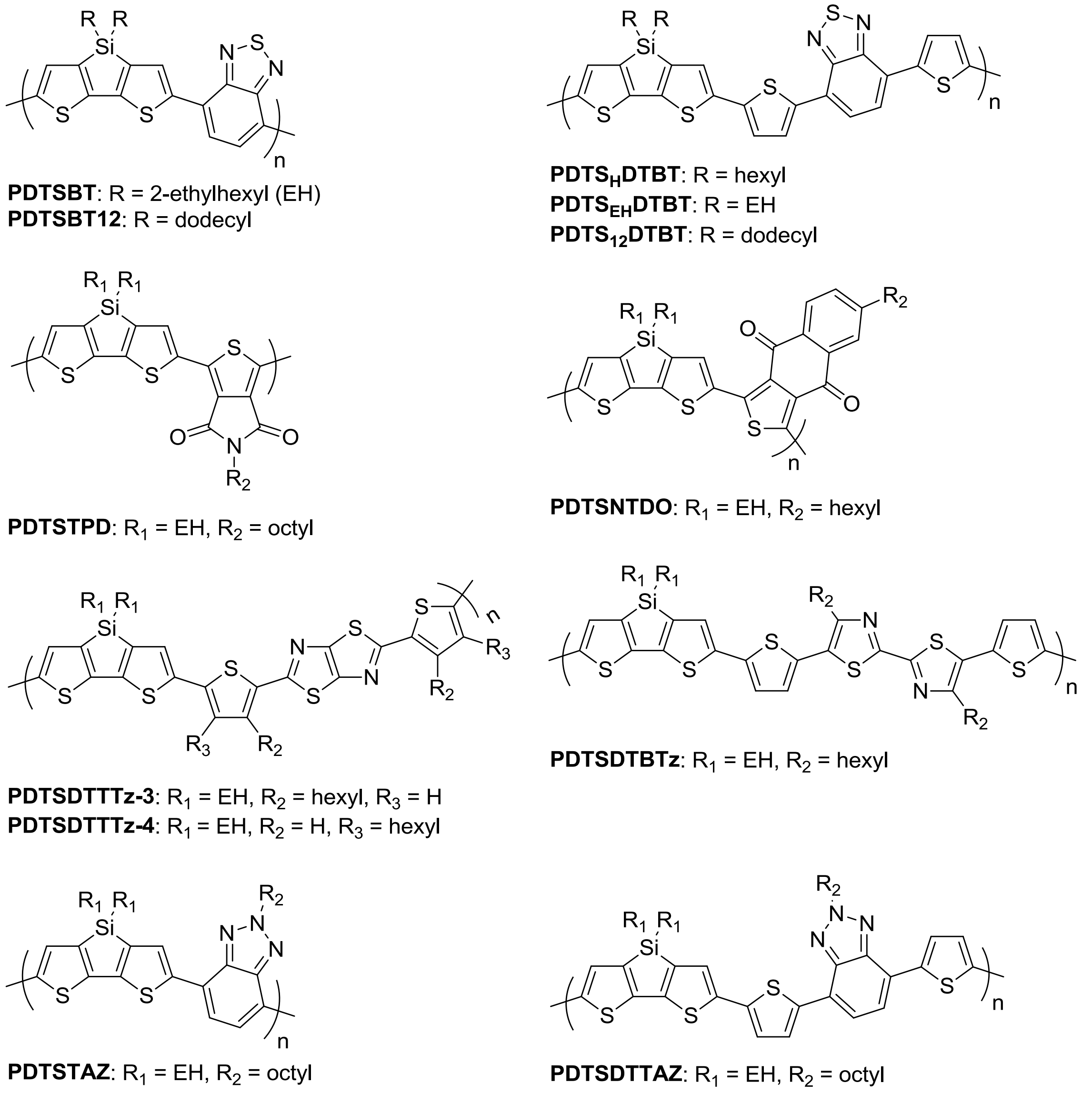

PDTSBT: R = 2-ethylhexyl (EH)
PDTSBT12: R = dodecyl

PDTS$_{H}$DTBT: R = hexyl
PDTS$_{EH}$DTBT: R = EH
PDTS$_{12}$DTBT: R = dodecyl

PDTSTPD: R_1 = EH, R_2 = octyl

PDTSNTDO: R_1 = EH, R_2 = hexyl

PDTSDTTTz-3: R_1 = EH, R_2 = hexyl, R_3 = H
PDTSDTTTz-4: R_1 = EH, R_2 = H, R_3 = hexyl

PDTSDTBTz: R_1 = EH, R_2 = hexyl

PDTSTAZ: R_1 = EH, R_2 = octyl

PDTSDTTAZ: R_1 = EH, R_2 = octyl

Scheme 7.1: The D-A copolymers based on **DTS** units with different acceptor units

7.2. Synthesis of distannylated DTS (142)

142 is a key monomer for the preparation of the target polymers in this chapter. It was synthesised through five steps starting from commercially available 2,2'-bithiophene (**33**) (**Scheme 7.2**). The different steps in its preparation are discussed below.

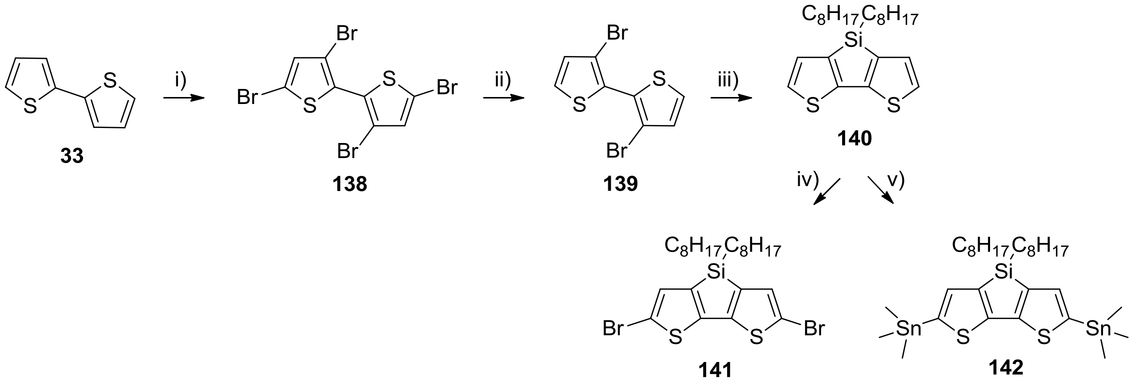

Scheme 7.2: The synthetic steps of **142**

Reagents and conditions: i) Br_2, $CHCl_3$, HOAc, 0 °C, 3h, 70 °C, 24h ; ii) Zn powder, ethanol, H_2O, HOAc, HCl (3.0 M), reflux, 2h; iii) *n*-BuLi, anhydrous (Et_2O/THF), –78 °C, 3h, $(C_8H_{17})_2SiCl_2$, anhydrous THF, –78 °C, 5h, RT, overnight; iv) NBS, DMF, RT, 10 min; v) *n*-BuLi, anhydrous *n*-hexane, TMEDA, 0 °C, 3h, $(CH_3)_3SnCl$, 0 °C, 3h, RT, overnight

7.2.1. Synthesis of 3,3',5,5'-tetrabromo-2,2'-bithiophene (138)

33 was brominated regioselectively at 3,3',5,5'-positions using bromine in chloroform/acetic acid as a co-solvent and gave **138** as green crystals in 75% yield (**Scheme 7.2**)[14]. The mechanism of the reaction is similar to that for the synthesis of **39** as illustrated in scheme 3.6.

138 was characterised by several analytical tools. From the ^1H NMR spectrum of **138**, the peak corresponding to thiophene protons can be seen as a singlet at 7.07 ppm. The ^{13}C NMR spectrum of **138** shows four peaks for four chemically different environments of carbons of thiophenes. The mass spectrum of **138** displays a peak at 481.6, which is indicative of the mass of the molecular ion $[M]^+$ of **138**. The structure and purity of **138** was further confirmed by the FT-IR spectroscopy and elemental analysis.

7.2.2. Synthesis of 3,3'-dibromo-2,2'-bithiophene (139)

138 was dehalogenated selectively at 5,5'-positions using zinc powder in ethanol and a mixture of water and HCl to obtain **139** as white crystals in 69% yield (**Scheme 7.2**)[15].

The reaction proceeds through two steps as outlined in scheme 7.3. In the first step, two equivalents of zinc metal are reacted with two bromines at 5,5'-positions of **138** to generate organozinc intermediate (**143**). This intermediate is highly polarised like a Grignard reagent, carbon atoms at 5,5'-positions have partially negative charges and function as nucleophiles which abstract two protons from water molecules to form **139**.

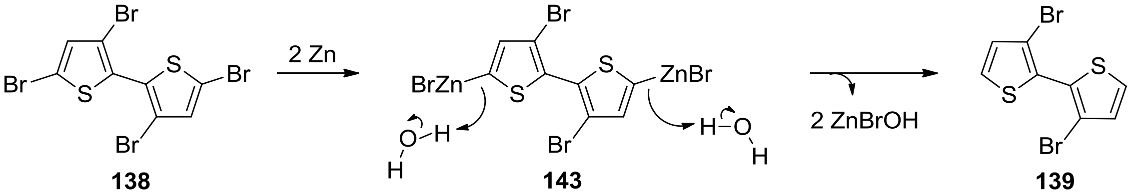

138 **143** **139**

Scheme 7.3: The mechanism of dehalogenation of **138**

^{1}H NMR and ^{13}C NMR spectroscopy were implemented to characterise the structure of **139**. From the ^{1}H NMR spectrum of **139**, it is obvious that the reduction reaction was successful as two doublets at 7.43 and 7.10 ppm can be seen, integrating for four protons on the thiophene rings. Meanwhile, the singlet peak disappears for **138**. The ^{13}C NMR spectrum of **139** is in agreement with the literature[16].

7.2.3. Synthesis of 4,4-dioctyl-dithieno[3,2-*b*:2',3'-*d*]silole (140)

139 was lithiated selectively at 3,3'-positions using two equivalents of *n*-BuLi in anhydrous diethyl ether/THF co-solvent at –78 °C which was subsequently reacted with dioctyldichlorosilane to yield **140** as a yellow oil in 60% yield (**Scheme 7.2**)[17]. The mechanism of the reaction is similar to that for the synthesis of **71** as illustrated in scheme 3.20.

^{1}H NMR spectrum of **140** displays two doublets at 7.21 and 7.07 ppm corresponding to four protons on the thiophene rings. It also displays three multiplets at 1.47-1.35, 1.34-1.17 and 0.98-0.84 ppm integrating for thirty four protons of the *n*-octyl chains. The ^{13}C NMR spectrum of **140** exhibits four peaks for carbons of thiophene rings and eight peaks for carbons of *n*-octyl chains. The FT-IR spectrum of **140** shows three new peaks at 2854, 2918, and 2953 cm^{-1} for C-H stretching vibrations of the alkyl chains.

7.2.4. Synthesis of 4,4-dioctyl-2,6-dibromo-dithieno[3,2-*b*:2',3'-*d*]silole (141)

140 was brominated selectively at 2,6-positions using two equivalents of NBS in DMF and gave **141** as yellow oil in 56% yield (**Scheme 7.2**)[18]. **141** was used in direct arylation polymerisation with **47** and **48** to prepare the target polymers but unfortunately the polymerisations were not successful. The mechanism of the reaction is similar to that for the synthesis of **39** as shown in scheme 3.6.

^{1}H NMR and ^{13}C NMR spectroscopy were implemented to characterise the structure of **141**. From the ^{1}H NMR spectrum of **141**, it is clear that the bromination reaction was successful as a singlet peak at 7.01 ppm can be seen, integrating for two protons of thiophenes. The ^{13}C NMR spectrum of **141** is in agreement with the literature[19].

7.2.5. Synthesis of 4,4-dioctyl-2,6-bis(trimethylstannyl)-dithieno[3,2-*b*:2',3'-*d*]silole (142)

140 was lithiated selectively at 2,6-positions using two equivalents of *n*-BuLi and TMEDA at 0 °C in anhydrous *n*-hexane which was subsequently reacted with two equivalents of trimethyltin chloride and gave distannylated monomer (**142**) as green sticky oil in 81% yield (**Scheme 7.2**)[20]. The mechanism of the reaction is similar to that for the synthesis of **29** as shown in scheme 2.17.

The structure and purity of **142** were assessed using ^{1}H NMR spectroscopy. A singlet peak can be seen at 0.40 ppm, integrating for eighteen protons, which indicates that the stannylation reaction was successful. In addition, it shows a singlet peak at 7.10 ppm for protons of thiophenes. Moreover, it displays the expected number of protons in the aliphatic region. Further evidence of the presence of the trimethylstannyl groups was given on analysis of the ^{13}C NMR spectrum of **142**; there is a peak at –8.0 ppm corresponding to the methyl carbons for the trimethylstannyl group.

7.3. Polymers synthesis

In this chapter, the synthesis of two alternating copolymers, **144** and **145** is described. Both polymers were prepared by Stille coupling polymerisation between distannylated **DTS** monomer (**142**) with dibrominated **BTDI** monomers (**49** and **50**), respectively using $Pd(OAc)_2/P(o\text{-tol})_3$ catalyst in anhydrous toluene (**Scheme 7.4**). Both polymerisations were left running for 72 hours with large amounts of dark blue precipitates forming as the reactions proceeded. The polymers were obtained and cleaned as described in chapter 2. The structures of the **144** and **145** were confirmed by the ^{1}H NMR spectroscopy, FT-IR spectroscopy and elemental analysis.

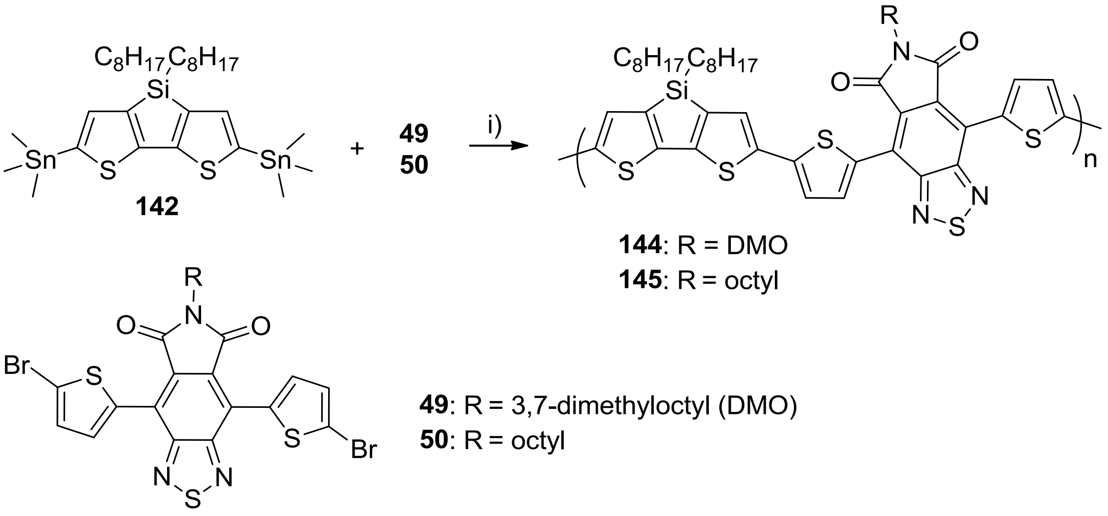

Scheme 7.4: The synthesis of **144** and **145** *via* Stille polymerisation

Reagents and conditions: i) Pd(OAc)$_2$, P(*o*-tol)$_3$, anhydrous toluene, 110 °C, 72h

7.4. Molecular weights and yield of the polymers

Molecular weights of the polymers were measured by GPC in chloroform solution at 40 °C relative to polystyrene standards (**Table 7.1**). Both polymers were synthesised under the same experimental conditions. Substituting 3,7-dimethyloctyl chains in **144** for *n*-octyl chains in **145** on the **BTDI** units which leads to a polymer with slightly lower M_n values for the toluene fractions of the polymers. In addition, **144** afforded another fraction in chloroform of a higher M_n value. The results indicate that the **145** has limited solubility because *n*-octyl chains were attached on both **DTS** and **BTDI** units, therefore providing a relatively low molecular weight polymer. **144** was prepared in excellent yield and it has significantly higher molecular weights than **145**, especially its chloroform fraction. This could be explained by the higher solubility of the **144**, which allows the polymerisation reaction to proceed further before precipitation of the growing polymer out of solution.

Table 7.1: The percentage yield, weight and number average molecular weights with polydispersity indexes of **144** and **145**

Polymer	% yield	Toluene fraction			Chloroform fraction		
		M_n (g mol^{-1})	M_w (g mol^{-1})	PDI	M_n (g mol^{-1})	M_w (g mol^{-1})	PDI
144	92	6200	20600	3.2	14600	79900	5.4
145	57	5700	14000	2.4			

7.5. Optical properties of the polymers

The normalised UV-vis absorption spectra of the polymers in chloroform solutions and in thin films are shown in figure 7.1. The optical properties of the polymers are summarised in table 7.2. In both solutions and thin films, the absorption maxima of **144** are red-shifted compared to **145**. This may arise from the fact that the former polymer having higher molecular weight than the latter polymer. In thin films, absorption peaks for both **144** and **145** show bathochromic shift compared to their absorption in solutions with absorption maxima of 689 and 670 nm, respectively. This could be attributed to the more aggregated configurations and a more planar structure in solid state. The E_g of the polymers are assessed from the absorption onsets in thin-films. The E_g of both polymers are comparable about 1.4 eV. A change of alkyl chains on **BTDI** units from 3,7-dimethyloctyl chains to *n*-octyl chains has a negligible impact on the E_g of the resulting polymers.

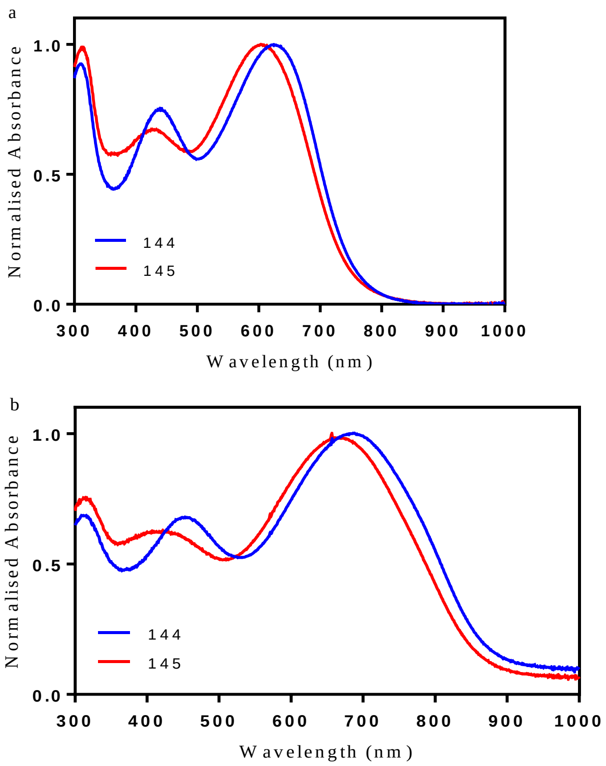

Figure 7.1: Normalised UV-vis absorption spectra of **144** and **145** in a) chloroform solutions; and b) thin films

Table 7.2: The Uv-vis data and optical band gaps of the polymers

Polymer	ε	solution	Film		
	(M^{-1} cm^{-1})	λ_{max} (nm)	λ_{max} (nm)	λ_{onset} (nm)	E_g (eV)
144	32300	627	689	873	1.42
145	23400	613	670	863	1.43

The E_g of both polymers are slightly lower than **PDTSBT** which is 1.45 eV (**Scheme 7.1**)[2]. As expected, the E_g of both polymers are lower than those **PDTS$_{EH}$DTBT** and **PDTS$_{12}$DTBT** counterparts which are 1.53 and 1.51 eV, respectively (**Scheme 7.1**)[4]. This can be explained by the stronger electron-accepting strength of the **BTDI** unit than **BT** unit. The E_g of both polymers are significantly lower than those **PDTSDTBTz**, **PDTSDTTTz-3**, **PDTSDTTTz-4** and **PDTSTPD** analogues which are 1.85, 1.81, 1.76 and 1.73 eV, respectively (**Scheme 7.1**)[10,11,6]. Similarly, The E_g of both polymers are significantly lower than those **PDTSDTTAZ**, **PDTSTAZ** and **PDTSNTDO** which are 1.81, 1.78 and 1.65 eV, respectively (**Scheme 7.1**)[13,12]. This is due to the **BTDI** moiety is a stronger electron acceptor than bithiazole, thiazolothiazole, thienopyrroledione, benzotriazole and napthothiophenedione units. Compared to the polymers based on fluorene, dibenzosilole, carbazole and anthracene, which were mentioned in chapters 3, 4 and 5, the polymers have lower E_g. This may arise from the fact that the **DTS** unit has stronger electron-donating ability than those donor moieties. Therefore, this new class of polymers adopt more planar structures with stronger intrachain charge transfer along the polymer backbone. **144** and **145** have comparable E_g values to the **134** and **137**, while their E_g values are around 0.1 eV higher than **135** and **136** mentioned in chapter 6 (**Scheme 6.7** and **Table 6.2**). This could be due to the fact that both **DTS** and **CPDT** units are strong electron donors with comparable strength. The absorption coefficient (ε) of **144** is significantly higher than **145**. This is probably due to the higher molecular weight and red-shifted absorption maxima of the former polymer.

7.6. Electrochemical properties of the polymers

Cyclic voltammetry was used to study the electrochemical properties of the polymers. The LUMO and HOMO levels of the polymers calculated from the onsets of reduction and oxidation potentials, respectively (**Figure 7.2** and **Table 7.3**). The onsets were determined from cyclic voltammograms on drop cast polymer films on Pt electrode as working electrode in Bu_4NClO_4/CH_3CN (0.1 M) *vs* Ag/Ag^+ reference electrode. The HOMO levels of **144** and **145** are comparable, while the LUMO energy level of the former polymer is lower than the latter polymer. The results indicate that attaching different side chains on **BTDI** units has negligible impact on the HOMO levels of the polymers but the LUMO levels of the polymers are affected by about 0.1 eV. The HOMO energy level is dominated by the nature of the donor unit and both polymers have the same **DTS** donor unit.

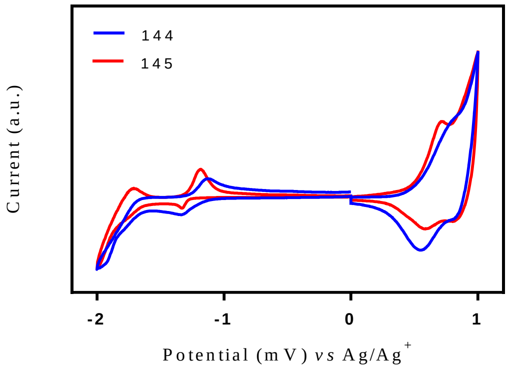

Figure 7.2: Cyclic voltammograms of **144** and **145** on Pt electrode in Bu_4NClO_4/CH_3CN at 100 mV/s

Table 7.3: Thermal and electrochemical properties of the polymers

Polymer	T_d (°C)	$E_{ox}{}^0$ (V)	HOMO (eV)	$E_{red}{}^0$ (V)	LUMO (eV)	$E_{g\ (elec)}$ (eV)
144	357	0.50	–5.21	1.15	–3.56	1.65
145	394	0.52	–5.23	1.26	–3.45	1.78

The HOMO levels of the polymers are slightly deeper than **PDTSDTBTz** which is –5.18 eV[10]. The HOMO energy levels of both polymers are deeper relative to those **PDTSBT**, **PDTS$_{EH}$DTBT**, **PDTS$_{12}$DTBT** and **PDTSDTTTz-4** analogues which are –5.05, –4.99, –5.02 and –5.04 eV, respectively[2,4,11]. Their LUMO energy levels are lower compared to those **PDTSBT**, **PDTS$_{EH}$DTBT**, **PDTS$_{12}$DTBT** and **PDTSDTTTz-4** analogues which are –3.27, –3.17, –3.19 and –3.41 eV, respectively[2,4,11]. Furthermore, the LUMO levels of the polymers are considerably lower than **PDTSTAZ** and **PDTSDTTAZ** which are –2.76 and –2.81 eV, respectively[13]. This could be ascribed by the stronger electron-accepting ability of **BTDI** unit than benzothiadiazole, dithienylbenzothiadiazole, thiazolothiazole, benzotriazole and dithienylbenzotriazole units. However, they have shallower HOMO and LUMO energy levels compared to **PDTSTPD** counterpart[6]. The HOMO levels of the polymers are significantly shifted upward compared to the fluorene-, dibenzosilole-, carbazole- and anthracene-based polymers, which were mentioned in chapters 3,4 and 5. This could be attributed to stronger electron-donating ability of **DTS** unit compared to those donor units. However, the LUMO energy levels are comparable because the LUMO level is controlled by the **BTDI** acceptor moiety. The HOMO and LUMO levels of both polymers are comparable to **135** and **137**, while their HOMO and LUMO levels are deeper than **134** and **136**, mentioned in chapter 6 (**Scheme 6.7** and **Table 6.3**).

7.7. Thermal properties of the polymers

Thermal properties of the polymers were studied by TGA (**Figure 7.3** and **Table 7.3**). The decomposition temperatures of the **144** and **145** are at 357 and 394 °C, respectively. The TGA results revealed that the thermal stability of the polymers is significantly affected by the nature of the substituents on the **BTDI** moieties. Thermal properties of **144** and **145** are significantly higher than **PDTSDTTTz-4** and **PDTSNTDO** with decomposition temperatures at 317 and 321 °C, respectively[11,12]. **145** has higher thermal stability than **PDTSDTBTz** and **PDTSTAZ** with decomposition temperatures at 368 and 388 °C, respectively, while **144** has less stability than those polymers[10,13]. Both polymers have less thermal stability than **PDTSDTTAZ** with decomposition temperatures at 415 °C[13]. The difference in thermal stabilities of the polymers could be related to different side chains on **DTS** units and different acceptor units.

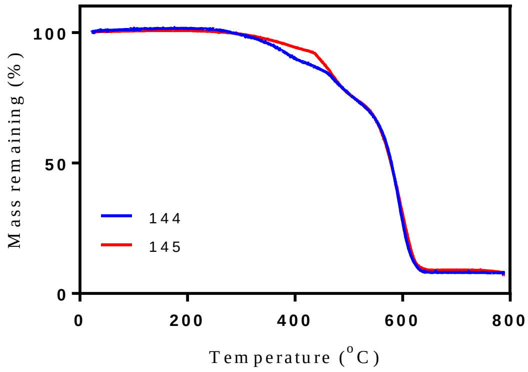

Figure 7.3: TGA of **144** and **145**

7.8. Powder X-ray diffraction of the polymers

The structural properties of the **144** and **145** were investigated by powder X-ray diffraction (XRD) in the solid state (**Figure 7.4**). The XRD of **144** and **145** show diffraction peaks at 24.6 and 24.9° corresponding to the π-π stacking distance of 3.61 and 3.57 Å, respectively. The results show that both polymers have an amorphous nature. The powder XRD of the polymers are comparable to **PDTSDTBTz**[10]. However, the **PDTSBT** showed crystallinity as reported in previous literature report[1].

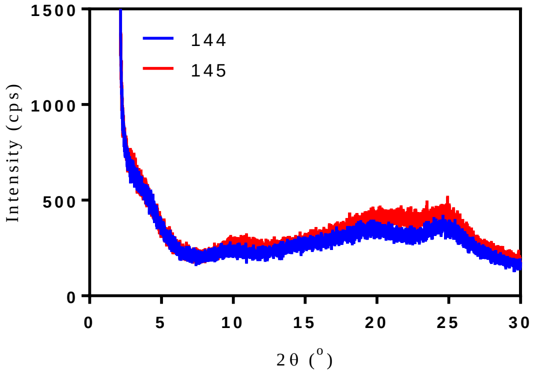

Figure 7.4: Powder XRD of **144** and **145**

7.9 Conclusions

In summary, two novel low band gap alternating copolymers including dithienosilole (**DTS**) flanked by thienyl units as electron donor moieties and benzothiadiazole dicarboxylic imide (**BTDI**) as electron acceptor segments were synthesised by Stille polymerisation. Distannylated **DTS** monomer (**142**) was copolymerised with dibrominated **BTDI** monomers (**49** and **50**) to prepare **144** and **145**, in 92 and 57% yield respectively. Two distinct side chains (*n*-octyl *vs* 3,7-dimethyloctyl) were attached to the **BTDI** units to investigate the effect of these substituents on the solubility, molecular weights, optical and electrochemical properties, thermal and structural properties of the resulting polymers. Replacing 3,7-dimethyloctyl chains in **144** for *n*-octyl chains in **145** on the **BTDI** units has a negative impact on the solubility and molecular weights of the polymers. **145** was separated using Soxhlet extraction and its toluene fraction has a low M_n value (5700 g mol^{-1}) due to its limited solubility. Soxhlet extraction of **144** provided two fractions; a toluene fraction which has a slightly higher M_n value to that of **145**, in addition to another fraction from chloroform with a M_n value more than twice higher. In both solution and thin-film, absorption maxima of **145** are blue-shifted relative to those of **144**. In thin-films, the absorption spectra of both polymers display bathochromic shift absorption maxima relative to their absorption in solutions. Both polymers have comparable optical band gaps around 1.4 eV. The HOMO levels of the polymers are comparable. The LUMO levels of the **144** and **145** are –3.56 and –3.45 eV, respectively. Anchoring different alkyl chains on **BTDI** units has little impact on the band gaps and the HOMO levels of the polymers, while the LUMO energy levels are affected by about 0.1 eV. **144** and **145** have good thermal stability with decomposition temperatures at 357 and 394 °C, respectively. The thermal properties of the polymers are significantly affected by changing substituents on imide functionality of **BTDI** units. The powder XRD studies of the polymers show diffraction peaks around 24.0° corresponding to the π-π stacking distance of about 3.6 Å. Both polymers have an amorphous nature. The photovoltaic properties of these materials are currently under investigation both in regular bulk heterojunction solar cells and in tandem solar cells.

References

1. H. Y. Chen, J. Hou, A. E. Hayden, H. Yang, K. Houk and Y. Yang, *Advanced Materials*, 2010, **22**, 371-375.
2. J. Hou, H.-Y. Chen, S. Zhang, G. Li and Y. Yang, *Journal of the American Chemical Society*, 2008, **130**, 16144-16145.
3. R. C. Coffin, J. Peet, J. Rogers and G. C. Bazan, *Nature Chemistry*, 2009, **1**, 657-661.
4. L. Huo, H.-Y. Chen, J. Hou, T. L. Chen and Y. Yang, *Chemical Communications*, 2009, 5570-5572.
5. A. J. Moulé, A. Tsami, T. W. Bünnagel, M. Forster, N. M. Kronenberg, M. Scharber, M. Koppe, M. Morana, C. J. Brabec and K. Meerholz, *Chemistry of Materials*, 2008, **20**, 4045-4050.
6. T.-Y. Chu, J. Lu, S. Beaupré, Y. Zhang, J.-R. Pouliot, S. Wakim, J. Zhou, M. Leclerc, Z. Li and J. Ding, *Journal of the American Chemical Society*, 2011, **133**, 4250-4253.
7. T. Y. Chu, J. Lu, S. Beaupré, Y. Zhang, J. R. Pouliot, J. Zhou, A. Najari, M. Leclerc and Y. Tao, *Advanced Functional Materials*, 2012, **22**, 2345-2351.
8. X. Guo, H. Xin, F. S. Kim, A. D. Liyanage, S. A. Jenekhe and M. D. Watson, *Macromolecules*, 2010, **44**, 269-277.
9. Z. Li, S. W. Tsang, X. Du, L. Scoles, G. Robertson, Y. Zhang, F. Toll, Y. Tao, J. Lu and J. Ding, *Advanced Functional Materials*, 2011, **21**, 3331-3336.
10. M. Zhang, H. Fan, X. Guo, Y. He, Z. Zhang, J. Min, J. Zhang, G. Zhao, X. Zhan and Y. Li, *Macromolecules*, 2010, **43**, 5706-5712.
11. Z.-G. Zhang, J. Min, S. Zhang, J. Zhang, M. Zhang and Y. Li, *Chemical Communications*, 2011, **47**, 9474-9476.
12. C. Cui, X. Fan, M. Zhang, J. Zhang, J. Min and Y. Li, *Chemical Communications*, 2011, **47**, 11345-11347.
13. J. Min, Z.-G. Zhang, S. Zhang, M. Zhang, J. Zhang and Y. Li, *Macromolecules*, 2011, **44**, 7632-7638.
14. E. Khor, S. C. Ng, H. C. Li and S. KHOR, *Heterocycles*, 1991, **32**, 1805-1812.
15. J. A. Letizia, M. R. Salata, C. M. Tribout, A. Facchetti, M. A. Ratner and T. J. Marks, *Journal of the American Chemical Society*, 2008, **130**, 9679-9694.
16. H. Usta, G. Lu, A. Facchetti and T. J. Marks, *Journal of the American Chemical Society*, 2006, **128**, 9034-9035.

17. P. M. Beaujuge, H. N. Tsao, M. R. Hansen, C. M. Amb, C. Risko, J. Subbiah, K. R. Choudhury, A. Mavrinskiy, W. Pisula and J.-L. Brédas, *Journal of the American Chemical Society*, 2012, **134**, 8944-8957.
18. R. Grisorio, G. P. Suranna, P. Mastrorilli, G. Allegretta, A. Loiudice, A. Rizzo, G. Gigli, K. Manoli, M. Magliulo and L. Torsi, *Journal of Polymer Science Part A: Polymer Chemistry*, 2013, **51**, 4860-4872.
19. P. M. Beaujuge, W. Pisula, H. N. Tsao, S. Ellinger, K. Müllen and J. R. Reynolds, *Journal of the American Chemical Society*, 2009, **131**, 7514-7515.
20. H. Medlej, H. Awada, M. Abbas, G. Wantz, A. Bousquet, E. Grelet, K. Hariri, T. Hamieh, R. C. Hiorns and C. Dagron-Lartigau, *European Polymer Journal*, 2013, **49**, 4176-4188.

Chapter 8 - Conclusions and Future Work

8.1. Conclusions

A series of donor-acceptor (D-A) thermocleavable conjugated polymers was successfully synthesised. Three thermocleavable polymers, **35**, **36** and **37** consisting of electron-rich bithiophene or fluorene as the donor units and electron-deficient secondary phthalate esters as the acceptor units were synthesised *via* the Stille coupling polymerisation (**Scheme 8.1**). The secondary solubilising phthalate ester groups are thermocleavable about 300 °C through elimination of volatile alkenes and change to carboxyl groups followed by dehydration to lead to rigid polymers with phthalic anhydride repeating units (**Scheme 8.1**). The optical band gaps of **35** and **36** are 2.19 and 2.11 eV, respectively and their band gaps are significantly lower than that of **37** (2.58 eV). The optical band gaps of **35**, **36** and **37** are lowered to 1.86, 1.89 and 2.14 eV, respectively upon their thermal treatment in the solid state. While the thermocleavage process takes place at relatively high temperature, these polymers show promise for use in bulk heterojunction photovoltaic cells as well as in FET applications.

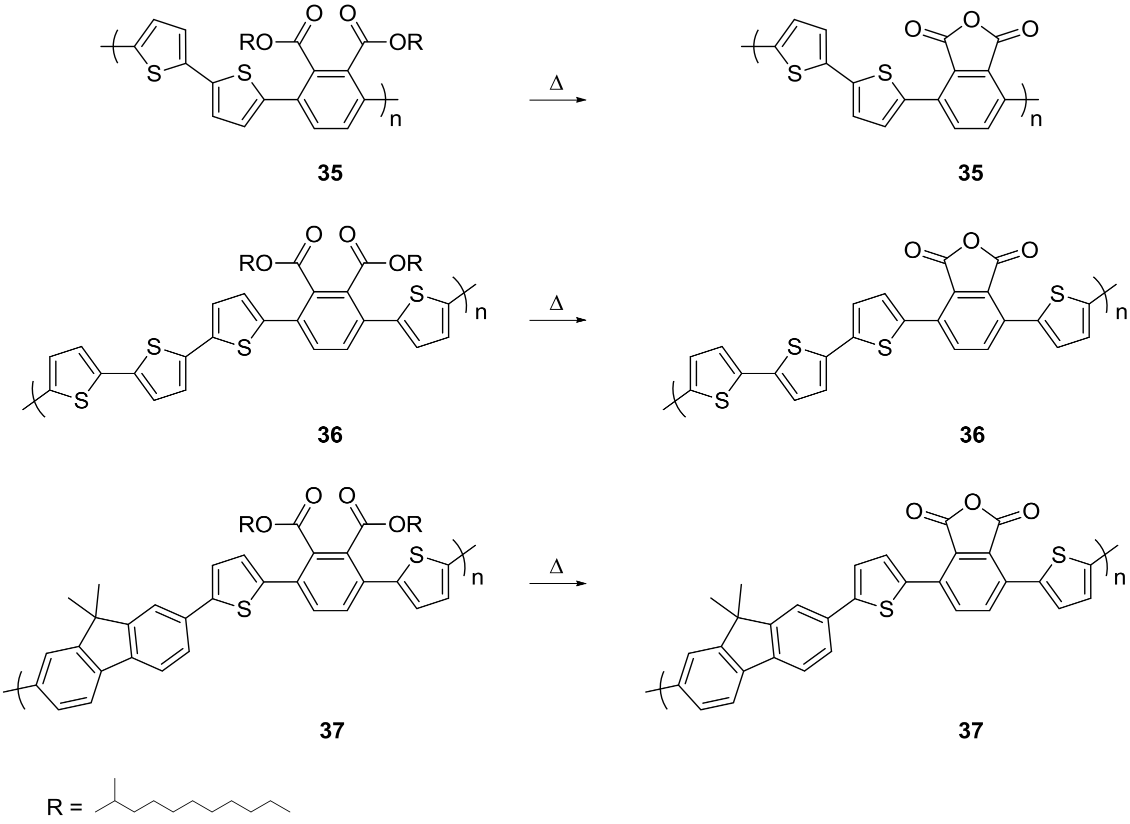

Scheme 8.1: Structures of thermocleavable polymers, **35**, **36** and **37** before and after thermal treatment

A series of D-A polymers based on benzothiadiazole dicarboxylic imide (**BTDI**) as the electron acceptor units alternating with various donor segments were synthesised. Two different alkyl solubilising groups including 3,7-dimethyloctyl chains (**DMO**) and *n*-octyl chains were attached to the **BTDI** units to investigate the effect of these substituents on the solubility, molecular weights, optoelectronic properties, thermal and structural properties of the resulting polymers.

Fluorene and dibenzosilole flanked by thienyl units as the electron-donating moieties were copolymerised with **BTDI** units *via* Suzuki polymerisation and yielded the polymers, **76**, **77**, **78** and **79** respectively (**Scheme 8.2**). The optical band gaps of **76**, **77**, **78** and **79** are 1.81, 1.78 and 1.77 eV respectively. The optical and electrochemical properties of these polymers show promise for application in bulk heterojunction solar cells.

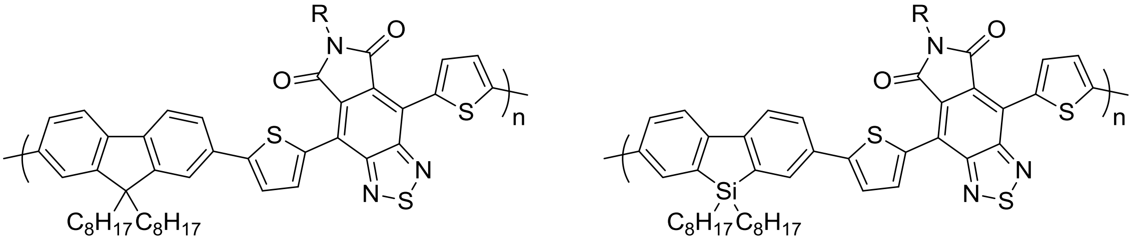

76: R = DMO
77: R = octyl

78: R = DMO
79: R = octyl

Scheme 8.2: Structures of polymers, **76**, **77**, **78** and **79**

Four novel alternating copolymers, **104**, **105**, **106** and **107** were prepared *via* Suzuki polymerisation (**Scheme 8.3**). The polymers are based on 2,7-linked carbazole units or 3,6-difluoro-2,7-linked carbazole moieties flanked by thienyl units as donor units alternating with **BTDI** moieties along the polymer backbones. Two fluorine atoms were anchored to the 3,6-positions of the 2,7-linked carbazole repeat units to investigate the effect of fluorination on the solubility, molecular weight, optoelectronic properties, thermal and structural properties of the resulting polymers. The optical band gaps of **106** and **107** are 1.78 and 1.81 eV, respectively which are slightly higher relative to those non-fluorinated analogues (1.76 eV). The optical and electrochemical properties of these polymers show promise for application in bulk heterojunction solar cells.

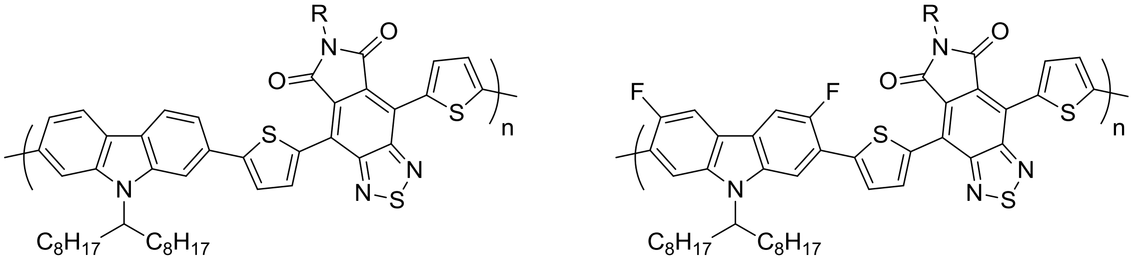

104: R = DMO
105: R = octyl

106: R = DMO
107: R = octyl

Scheme 8.3: Structures of polymers, **104**,**105**,**106** and **107**

The copolymers including fluorene, dibenzosilole and carbazole units have optical band gaps around 1.7-1.8 eV. To further reduce the band gap of the polymers, 9,10-phenylsubstituted-2,6-linked anthracene units flanked by thienyl groups as electron donor units were copolymerised with **BTDI** units through Suzuki polymerisation yielded **109** and **110** (**Scheme 8.4**). Both polymers have low optical band gaps of 1.66 eV. They have a good overlap between their absorption spectrum and that of the solar spectrum which should be beneficial to obtain high J_{sc} values and hence could provide BHJ solar cell devices with enhanced photovoltaic performance.

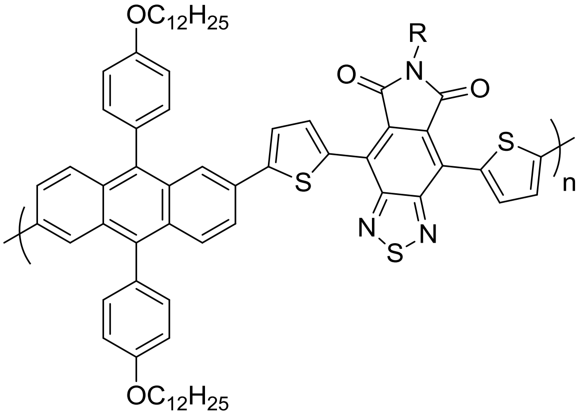

109: R = DMO
110: R = octyl

Scheme 8.4: Structures of polymers, **109** and **110**

A series of novel low band gap copolymers consisting of electron-rich cyclopentadithiophene (**CPDT**) flanked by thienyl units as donor segments and **BTDI** units were synthesised *via* two different palladium catalysed cross coupling polymerisations. **134** was prepared by Suzuki polymerisation (**Scheme 8.5**). However, **135**, **136** and **137** were synthesised through direct arylation polymerisation as a new alternative preparation method (**Scheme 8.5**). Two different solubilising side chains [*n*-octyl *vs* 2-ethylhexyl (**EH**)] were attached to the **CPDT** units to investigate the effect of these substituents on the solubility, molecular weights, optical and electrochemical properties, thermal and structural properties of the resulting polymers. The optical band gaps of **135**, **136** are around 1.3 eV which around 0.1 eV lower than those **134** and **137** analogues.

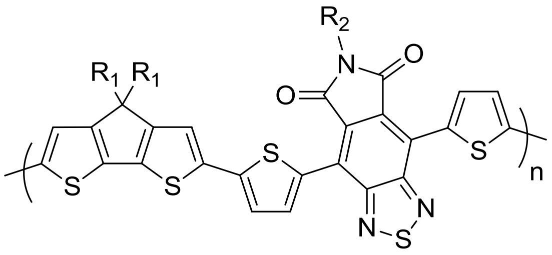

134: R_1 = EH, R_2 = DMO
135: R_1 = octyl, R_2 = DMO
136: R_1, R_2 = octyl
137: R_1 = EH, R_2 = octyl

Scheme 8.5: Structures of polymers, **134**, **135**,**136** and **137**

Alternatively, two novel low band gap copolymers, **144** and **145**, which contain dithienosilole (**DTS**) rather than cyclopentadithiophene (**CPDT**) flanked by thienyl units as electron-donating units and **BTDI** units were also synthesised *via* Stille coupling polymerisation (**Scheme 8.6**). Both polymers have comparable optical band gaps around 1.4 eV. The narrow band gaps of the polymers including **CPDT** and **DTS** are beneficial to achieve high J_{sc} values in BHJ solar cells. These polymers could be used either on their own in traditional BHJ solar cells. They could also be used along with higher band gap conjugated polymers as top cells in tandem solar cells.

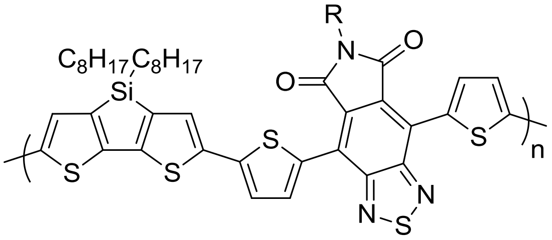

144: R = DMO
145: R = octyl

Scheme 8.6: Structures of polymers, **144** and **145**

The copolymers based on fluorene, dibenzosilole, carbazole and anthracene as the donor units and **BTDI** as the acceptor units have low-lying HOMO energy levels about –5.5 eV. They have advantageous for the chemical stability in air and high V_{oc} values could be anticipated when these polymers will be fabricated in BHJ solar cells as donor materials to fullerene derivatives as acceptor materials. However, the HOMO energy levels of the polymers containing **CPDT** and **DTS** as the donor units and **BTDI** as the acceptor units are significantly shifted upward between –5.10 and –5.23 eV. This is due to the **CPDT** and **DTS** are stronger donor units compared to fluorene, dibenzosilole, carbazole and anthracene donor units. The LUMO levels of all polymers are between –3.41 and –3.56 eV. This is due to the fact that all polymers have the same **BTDI** acceptor units which can dominate the LUMO energy levels in these materials. Anchoring different alkyl chains on **BTDI** units has little impact on the band gaps and the HOMO levels of the polymers, while the LUMO levels are affected about 0.1 eV.

All polymers have good thermal stability with T_d exceeding 310 °C. The good thermal stability of all polymers is desirable for the fabrication of polymer solar cell applications.

The powder XRD of the polymers show diffraction peaks between 18.5 and 24.7° corresponding to the π-π stacking distance in the range of 4.79 and 3.6 Å. All polymers have an amorphous nature in the solid state.

8.2. Future Work

Conjugated polymers with fluorene, dibenzosilole, carbazole and anthracene donor units have been synthesised in this work for application in photovoltaic cells. These polymers are promising candidates as new materials for application in this area because of several reasons. First, they have E_g between 1.6 and 1.8 eV which optimally match the solar spectrum, since the peak of photon flux density from the solar terrestrial radiation is positioned about 1.77 eV. As a result, the materials developed should provide solar cells with high J_{sc} values and hence potentially high power conversion efficiencies. Second, they have deep HOMO energy levels which are useful properties for stability of the polymers in air and also a prerequisite to provide solar cells with high V_{oc} values when these polymers are used as donor materials in blends with PCBM derivatives as acceptor materials in bulk heterojunction photovoltaic cells. Third, the LUMO energy levels of the polymers are compatible with those of fullerene derivatives to provide efficient electron transfer in bulk heterojunction photovoltaic cells. Fourth, all polymers possess relatively high molecular weights that would provide good hole mobilities when they will be tested in field effect transistor devices. Finally, all polymers show good thermal properties which can be used as stable polymers for photovoltaic applications. These polymers will be investigated in bulk heterojunction solar cells as electron donor materials with fullerene derivatives. The photovoltaic properties of these devices will be investigated in collaboration with the Department of Physics and Astronomy in University of Sheffield.

Cyclopentadithiophene and dithienosilole-based polymers are good candidates for solar cell applications due to their narrow optical band gaps which cover most of the solar cell spectrum. This is advantageous to achieve high J_{sc} value in BHJ solar cells. These polymers could also be used along with higher band gap conjugated polymers as top cells in tandem solar cells. Future investigations should include careful investigations on the use of these materials in these applications in collaboration with the Department of Physics and Astronomy in University of Sheffield.

Alternative classes of donor-acceptor conjugated polymers based on the **BTDI** units as the acceptor units should also be targeted. New conjugated polymers with several donor moieties such as 3,3'-bis(alkoxy)-2,2'-bithiophene, 3,3'-bis(alkyl)-2,2'-bithiophene and 3,6-bis(alkyl)thieno[3,2-*b*]thiophene (**Scheme 8.7**) are expected to provide low energy band gap materials in view of the electron rich properties of bithiophene and thienothiophene repeat units. A judicious choice of substituents attached to the electron donor moieties should also provide the opportunity to address the morphology of blends between these materials and fullerene derivatives in BHJ solar cells which is a crucial element in the efficiency of devices.

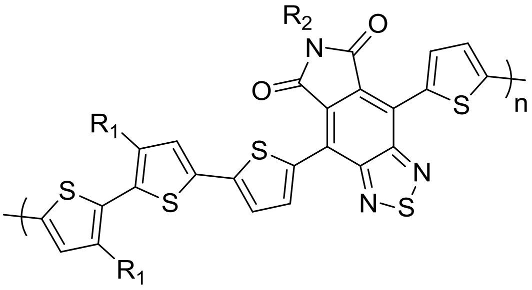

PBTDTBTDI-8,DMO: R_1 = octyl, R_2 = 3,7-dimethyloctyl (DMO)
PBTDTBTDI-EH,8: R_1 = 2-ethylhexyl (EH), R_2 = octyl

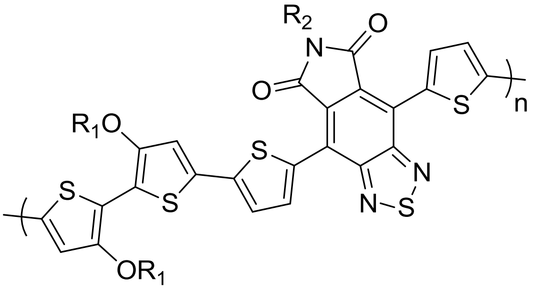

PBTODTBTDI-8,DMO: R_1 = octyl, R_2 = DMO
PBTODTBTDI-EH,8: R_1 = EH, R_2 = octyl

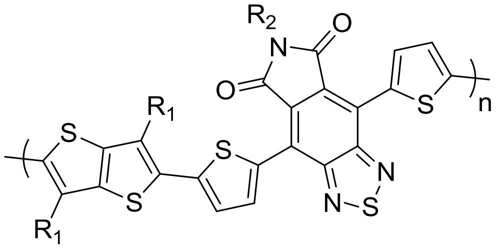

PTTDTBTDI-8,DMO: R_1 = octyl, R_2 = DMO
PTTDTBTDI-EH,8: R_1 = EH, R_2 = octyl

Scheme 8.7: Alternating copolymers based on **BTDI** and different donor units

Chapter 9 - Experimental

9.1. General Procedures

9.1.1. Reagents and Solvents

All chemicals and reagents obtained from suppliers. Most of the reactions were carried out under argon. Anhydrous solvents used for the reactions obtained from Grubbs solvent purification system within the University of Sheffield Chemistry Department.

9.1.2. Instrumentation

9.1.2.1. Nuclear magnetic resonance (NMR) spectroscopy

All ^{1}H NMR and ^{13}C NMR spectra for the monomers measured either with a Bruker Avance AV 3HD 400 (400 MHz) spectrometer in deuterated chloroform ($CDCl_3$), deuterated acetone (CD_3COCD_3) or deuterated dimethyl sulfoxide (CD_3SOCD_3) as the solvents at room temperature. The ^{1}H NMR spectra for the polymers were measured with Bruker AV 3HD 500 (500 MHz) in deuterated 1,1,2,2-tetrachloroethane ($C_2D_2Cl_4$) as the solvent at 100 °C. The chemical shifts were measured in parts per million (ppm). The NMR splitting patterns are described using the following abbreviations: s = singlet, d = doublet, dd = doublet of doublet, t = triplet, qt = quartet, m = multiplet, bs = broad singlet, bd = broad doublet, bm = broad multiplet and the coupling constants (*J*) are calculated in Hertz (Hz). The ^{1}H NMR and ^{13}C NMR spectra were analysed using Bruker TopSpin 3.2 software.

9.1.2.2. Elemental Analysis (EA)

Elemental analysis (CHN) was performed by either the Perkin Elmer 2400 CHNS/O Series II Elemental Analyser or Vario MICRO Cube CHN/S Elemental Analyser for CHN analysis. Anion analysis (Br, I and S) was performed by the Schöniger oxygen flask combustion method.

9.1.2.3. Mass Spectrometry

Mass spectra for the monomers were recorded on Agilent 7200 accurate mass Q-TOF GC-MS spectrometer. Helium is used as a carrier gas in rate of (1.2 mL min^{-1}), the injection volume is (1.0 μL) and the concentration of measured sample is (5 mg mL^{-1}) in $CHCl_3$ solvent. The temperature program is between 60 to 320 °C at 10 °C min^{-1}. Mass spectra for the monomers were obtained by the electron ionization method (EI).

9.1.2.4. Analytical Gel permeation chromatography (GPC)

GPC measurements accomplished by Viscotek GPC Max, a waters 410 instrument with a differential refractive index detector, two Polymer Labs PLgel 5µ Mixed C (7.5 × 300 mm) columns and a guard (7.5 × 50 mm). Molecular weights for the polymers were determined by preparing polymer solutions (2.5 mg mL^{-1}) using HPLC grade $CHCl_3$. The columns were thermostated at 40 °C using $CHCl_3$.

9.1.2.5. UV-visible (UV-vis) absorption spectroscopy

UV-vis absorption spectra were measured by SPECORD S600 UV/visible Spectrophotometer at room temperature. The absorbance of the polymers was measured in $CHCl_3$ solution using quartz cuvettes (light path length = 10 mm) and blank quartz cuvettes including $CHCl_3$ was used as a reference. The polymers were coated on quartz substrates from $CHCl_3$ solutions (1 mg mL^{-1}) and blank quartz substrate was used as a reference.

9.1.2.6. Thermogravimetric analysis (TGA)

TGA measurements were recorded by Perkin Elmer (Pyris 1) thermogravimetric Analyser. Platinum pans was used as sample holder and the weight of the measured samples was about (3 mg).

9.1.2.7. Cyclic Voltammetry (CV)

Cyclic voltammograms were measured using a Model 263A Potentiostat/Galvanostat-Princeton Applied Research. A standard three electrode system was used based on a Pt disk working electrode, a silver wire reference electrode (Ag/Ag^+) inserted in (0.01 M) $AgNO_3$ solution in acetonitrile and put it in the electrolyte solution and a Pt wire counter electrode was purged with argon atmosphere during all measurements at room temperature. Tetrabutylammonium perchlorate in acetonitrile (Bu_4NClO_4/CH_3CN) (0.1 M) was used as the electrolyte. Polymer thin films were drop cast onto the Pt disk from polymer solutions in CH_3Cl (1 mg mL^{-1}) and dried under nitrogen prior to measurement. Ferrocene (Fc/Fc^+) was used as a reference redox system

9.1.2.8. Powder X-ray diffraction (XRD)

Powder XRD for the polymers was measured by Bruker D8 ADVANCE X-ray powder diffractometer.

9.1.2.9. Infrared Absorption Spectroscopy (IR)

Infrared absorption spectra recorded on ATR Perkin Elmer Rx/FT-IR system and Nicolet Model 205 FT-IR spectrometer.

9.2. Synthetic procedures for the monomers

9.2.1. Synthesis of 3,6-dibromophthalic anhydride (2)

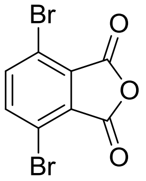

Phthalic anhydride (**1**) (80.00 g, 540.10 mmol), oleum (125 mL, 30% free SO_3), bromine (104.00 g, 650.78 mmol) and iodine (0.51 g, 2.00 mmol) added into a flask and stirred at 60 °C for 24h. The mixture cooled to RT, DCM added and the whole mixture was carefully diluted with deionised water. Subsequently, the mixture was filtered and extracted with DCM. The organic phase dried over $MgSO_4$ and the solvent concentrated to yield a product which recrystallised from acetic acid (100%) to afford **2** as white crystals (36.00 g, 118 mmol, 22% yield)[1].

^1H NMR ($CDCl_3$, δ): 7.87 (s, 2H). ^{13}C NMR ($CDCl_3$, δ): 158.9, 141.3, 131.1, 119.9. FT-IR (cm^{-1}): 3580, 3092, 2699, 2575, 2159, 2056, 1928, 1804, 1845, 1585, 1450, 1380, 1214, 1130, 1093. EI-MS (*m/z*): 306 $[M]^+$. EA (%) calculated for $C_8H_2Br_2O_3$: C, 31.41; H, 0.66; Br, 52.24. Found: C, 31.58; H, 0.64; Br, 50.10.

9.2.2. Synthesis of 3,6-dibromophthalic acid (3)

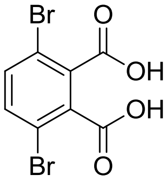

2 (20.00 g, 65.37 mmol) dissolved in THF (200 mL) in a flask, to this mixture deionised water (40 mL) added and refluxed for 24h. After cooling the reaction flask to RT, THF removed and deionised water added to the mixture and extracted with Et_2O. The organic phase dried over $MgSO_4$, and filtered. The solvent concentrated to yield **3** as a white powder (20.00 g, 62 mmol, 94% yield)[2].

^1H NMR (CD_3SOCD_3, δ): 7.69 (s, 2H), 14.00 (s, 2H). ^{13}C NMR (CD_3SOCD_3, δ): 166.8, 136.5, 135.6, 118.4. FT-IR (cm^{-1}): broad (3500-2300), 2160, 2056, 1929, 1771, 1760, 1551, 1451, 1358, 1216, 1131, 1093. EI-MS (*m/z*): 324 $[M]^+$. EA (%) calculated for $C_8H_4Br_2O_4$: C, 29.66; H, 1.24; Br, 49.34. Found: C, 29.87; H, 1.19; Br, 49.07.

9.2.3. Synthesis of 2-undecanol (5)

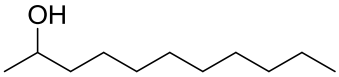

2-Undecanone (**4**) (44.93 g, 263.83 mmol) dissolved in methanol (300 mL) in a flask and the mixture cooled to 0 °C for 10 minutes. To this mixture, Sodium borohydride (10.00 g, 264.34 mmol) added slowly. The contents stirred at RT for 1h. Subsequently, HCl added dropwise to quench the reaction. A white precipitate was formed and filtrated. Deionised water added to the filtrate and extracted with ethyl acetate. The organic phase dried over $MgSO_4$ and filtered. The solvent concentrated to yield the product which purified by column chromatography (70:30, petroleum ether: ethyl acetate) to afford **5** as colourless oil (42.84 g, 249 mmol, 94% yield)[3].

^{1}H NMR ($CDCl_3$, δ): 3.75-3.86 (m, 1H), 1.24-1.54 (m, 17H), 1.20 (d, 3H, J = 6.0 Hz), 0.90 (t, 3H, J = 7.0 Hz). ^{13}C NMR ($CDCl_3$, δ): 68.2, 39.3, 31.9, 29.6, 29.6, 29.5, 29.3, 25.7, 23.4, 22.7, 14.1. FT-IR (cm^{-1}): broad (3200-3500), 2922, 2853, 2958, 1465, 1395, 1085. EI-MS (m/z): 157.3 $[M-CH_3]^+$. EA (%) calculated for $C_{11}H_{24}O$: C, 76.68; H, 14.04. Found: C, 75.29; H, 13.69.

9.2.4. Synthesis of 3,6-dibromo-bis(2-undecanyl) phthalate (6)

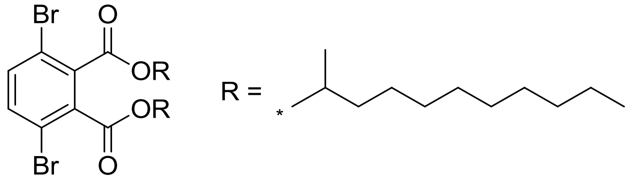

3 (10.00 g, 30.87 mmol), 4-(dimethylamino)pyridine (8.29 g, 67.85 mmol), scandium triflate (1.51 g, 3.06 mmol) and **5** (11.69 g, 67.89 mmol) added to a flask. The reaction flask was purged with three vacuum/argon cycles followed by adding anhydrous DCM (250 mL), and the mixture stirred at RT for 30 min. *N,N′*-diisopropylcarbodiimide (8.56 g, 67.89 mmol) added dropwise to the mixture and the contents stirred and refluxed for 24h. After cooling the flask to RT, the reaction contents filtered and washed with DCM. The filtrate was combined and the solvent concentrated to yield the product which purified by chromatography (80:20, petroleum ether: ethyl acetate) to afford **6** as colourless oil (6.00 g, 9.5 mmol, 31% yield)[4].

^{1}H NMR ($CDCl_3$, δ): 7.49 (s, 2H), 5.10-5.20 (sextet, 2H), 1.68-1.83 (m, 4H), 1.54-1.65 (m, 4H), 1.38 (d, 6H, J = 6.00 Hz), 1.20-1.35 (m, 24H), 0.89 (t, 6H, J = 7.00 Hz). ^{13}C NMR ($CDCl_3$, δ): 164.9, 135.8, 135.2, 118.9, 74.3, 35.7, 31.9, 29.6, 29.5, 29.3, 25.4, 25.3, 25.3, 22.7, 19.5, 14.1. FT-IR (cm^{-1}): 3340, 2960, 2926, 2854, 2114, 1727, 1617, 1568, 1462, 1378, 1268, 1170, 1079. EI-MS (*m/z*): 633 $[M]^+$. EA (%) calculated for $C_{30}H_{48}Br_2O_4$: C, 56.97; H, 7.65; Br, 25.27. Found: C, 58.45; H, 7.59; Br, 25.17.

9.2.5. Synthesis of 3,6-bis(2-thienyl)-bis(2-undecanyl)phthalate (7)

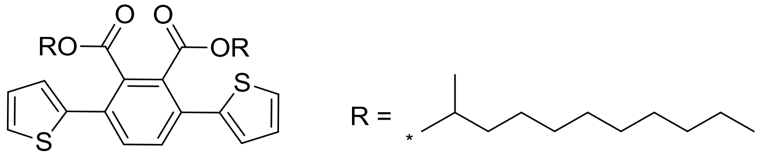

6 (2.00 g, 3.16 mmol), 2-(tributylstannyl)thiophene (2.94 g, 7.87 mmol) and $PdCl_2(PPh_3)_2$ (0.05 g, 0.07 mmol) added to a flask and degassed under argon. Dry toluene (20 mL) added, the flask degassed and heated at 110 °C for 24h. After cooling the flask to RT, the volatiles concentrated to obtain the product which purified by column chromatography *via* gradient (petroleum ether, 0-30% DCM) to afford a yellow solid product. The product further purified by recrystallisation from EtOH to obtain **7** as white crystals (1.50 g, 2.3 mmol, 74% yield)[5].

^1H NMR ($CDCl_3$, δ): 7.52 (s, 2H), 7.37 (dd, 2H, *J* = 1.00 Hz , 5.00 Hz), 7.12 (dd, 2H, *J* = 1.00 Hz, 3.50 Hz), 7.06 (dd, 2H, *J* = 3.50 Hz, 5.00 Hz), 4.86-4.95 (sextet, 2H), 1.40-1.53 (m, 4H), 1.23-1.38 (m, 24H), 1.22 (d, 6H, *J* = 6.00 Hz), 1.11 (dd, 4H, *J* = 6.00 Hz, 6.50 Hz), 0.90 (t, 6H, *J* = 7.00 Hz). ^{13}C NMR ($CDCl_3$, δ): 167.7, 140.4, 133.0, 132.3, 131.6, 127.5, 127.2, 126.4, 73.5, 35.5, 32.0, 29.6, 29.6, 29.5, 29.4, 24.9, 22.7, 19.1, 14.1. FT-IR (cm^{-1}): 2914, 2850, 1720, 1556, 1467, 1380, 1284, 1147, 1124, 1099, 1076. EI-MS (*m/z*): 638.4 $[M]^+$. EA (%) calculated for $C_{38}H_{54}O_4S_2$: C, 71.43; H, 8.52; S, 10.03. Found: C, 71.23; H, 8.72; S, 9.94.

9.2.6. Synthesis of 5,5′-dibromo-3,6-bis(2-thienyl)-bis(2-undecanyl)phthalate (8)

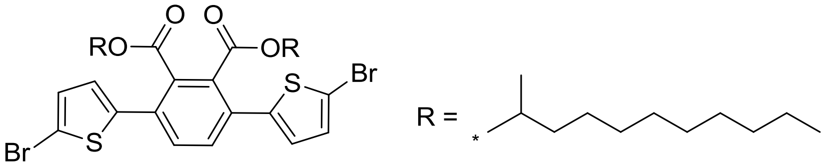

7 (0.68 g, 1.06 mmol) dissolved in $CHCl_3$ (15 mL) and glacial acetic acid (15 mL) in a flask. To this mixture, NBS (0.37 g, 2.12 mmol) added and stirred at RT for 24h. The solvent evaporated to obtain the product which purified by chromatography using $CHCl_3$ to afford the **8** as a yellow solid material. The yellow material further purified by recrystallisation from EtOH to obtain **8** as white crystals (0.65 g, 0.8 mmol, 77% yield)[6].

^{1}H NMR ($CDCl_3$, δ): 7.46 (s, 2H), 7.02 (d, 2H, *J* = 4.00 Hz), 6.86 (d, 2H, *J* = 4.00 Hz), 4.82-5.02 (sextet, 2H), 1.42-1.54 (m, 4H), 1.23-1.38 (m, 24H), 1.22 (d, 6H, *J* = 6.00 Hz), 1.16 (dd, 4H, *J* = 6.00 Hz, 12.00 Hz), 0.90 (t, 6H, *J* = 7.00 Hz). ^{13}C NMR ($CDCl_3$, δ): 167.2, 141.7, 133.1, 131.7, 131.5, 130.3, 127.6, 113.2, 73.9, 35.5, 32.0, 29.6, 29.6, 29.5, 29.3, 25.0, 22.7, 19.2, 14.1. FT-IR (cm^{-1}): 2921, 2850, 1715, 1556, 1467, 1375, 1279, 1116, 1056. EI-MS (*m/z*): 796.2 $[M]^+$. EA (%) calculated for $C_{38}H_{52}Br_2O_4S_2$: C, 57.28; H, 6.58; Br, 20.06; S, 8.05. Found: C, 58.19; H, 6.92; Br, 20.17; S, 7.83.

9.2.7. Synthesis of 2,7-dibromofluorene (27)

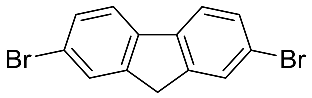

Fluorene (**26**) (10.00 g, 60.16 mmol) dissolved in $CHCl_3$ (32 mL) in a flask. To this mixture, bromine (22.27 g, 139.41 mmol) in $CHCl_3$ (8 mL) added dropwise and the mixture was covered by aluminium foil to avoid light and stirred at RT for 24h. The brown precipitate filtered and subsequently washed with $CHCl_3$ to yield the product which recrystallised from EtOH to give **27** as white crystals (15.00 g, 46.3 mmol, 77% yield)[7].

^{1}H NMR ($CDCl_3$, δ): 7.69 (s, 2H), 7.62 (d, 2H, *J* = 8.00 Hz), 7.52 (d, 2H, *J* = 8.00 Hz), 3.89 (s, 2H). ^{13}C NMR ($CDCl_3$, δ): 144.8, 139.7, 130.2, 128.3, 121.2, 121.0, 36.6. FT-IR (cm^{-1}): 3046, 2918, 2900, 1563, 1453, 1396, 1159, 1049. EI-MS (*m/z*): 323.9 $[M]^+$. EA (%) calculated for $C_{13}H_8Br_2$: C, 48.19; H, 2.49; Br, 49.32. Found: C, 48.04; H, 2.45; Br, 49.24.

9.2.8. Synthesis of 9,9-dimethyl-2,7-dibromofluorene (28)

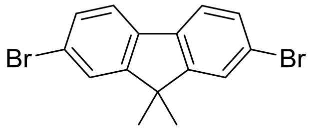

27 (15.00 g, 46.29 mmol), potassium hydroxide (10.30 g, 183.58 mmol) and potassium iodide (0.77 g, 4.63 mmol) combined in a flask. Before adding anhydrous DMSO (100 mL), the system degassed under argon. To this mixture, iodomethane (16.40 g, 115.54 mmol) added dropwise during 45 minutes and the reaction stirred at RT for 24h. Deionised water added and subsequently extracted with DCM. The organic phase dried over $MgSO_4$ and filtered. The solvent evaporated to obtain the product which purified by chromatography with DCM to afford **28** as pale yellow crystals (15.90 g, 45 mmol, 97% yield)[8].

^{1}H NMR ($CDCl_3$, δ): 7.53-7.61 (m, 4H), 7.48 (dd, 2H, *J* = 1.50 Hz, 8.00 Hz), 1.48 (s, 6H). ^{13}C NMR ($CDCl_3$, δ): 155.3, 137.2, 130.3, 126.2, 121.5, 121.5, 47.3, 26.9. FT-IR (cm^{-1}): 2960, 2921, 2858, 1864, 1726, 1595, 1446, 1258, 1123, 1081. EI-MS (*m/z*): 351.9 $[M]^+$. EA (%) calculated for $C_{15}H_{12}Br_2$: C, 51.17; H, 3.44; Br, 45.39. Found: C, 50.91; H, 3.27; Br, 44.56.

9.2.9. Synthesis of 9,9-dimethyl-2,7-bis(trimethylstannyl)fluorene (29)

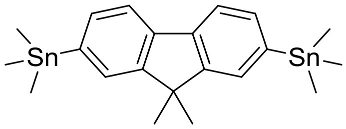

28 (3.25 g, 9.23 mmol) dissolved in anhydrous Et_2O (100 mL) in a flask. The flask cooled to –78 °C and *N*,*N*,*N'*,*N'*-tetramethylethylenediamine (2.63 g, 22.66 mmol) added. The system degassed under argon and *n*-BuLi (13.85 mL, 22.16 mmol) added to the mixture dropwise during 45 minutes. The reaction contents stirred at –78 °C for 1h and then at RT for 2h. The flask cooled to –78 °C and trimethyltin chloride (4.78 g, 23.98 mmol) which dissolved in anhydrous Et_2O (10 mL) added dropwise. The flask stirred overnight at RT. The mixture put into deionised H_2O and extracted with Et_2O. The organic layer separated and dried over anhydrous $MgSO_4$. The solvent concentrated to obtain the product. It purified by recrystallization from Et_2O to yield the **29** as white crystals (3.00 g, 5.8 mmol, 62% yield)[9].

^{1}H NMR ($CDCl_3$, δ): 7.73 (d, 2H, *J* = 7.50 Hz), 7.56 (s, 2H), 7.48 (d, 2H, *J* = 7.50 Hz), 1.53 (s, 6H), 0.35 (s, 18H). ^{13}C NMR ($CDCl_3$, δ): 153.0, 141.4, 139.5, 134.2, 129.8, 119.6, 46.9, 27.3, –7.5. FT-IR (cm^{-1}): 2971, 2914, 1457, 1393, 1254, 1191, 1070. EI-MS (*m/z*): 520 $[M]^+$. EA (%) calculated for $C_{21}H_{30}Sn_2$: C, 48.52; H, 5.82. Found: C, 48.98; H, 5.79.

9.2.10. Synthesis of 5,5'-bis(trimethylstannyl)-2,2'-bithiophene (34)

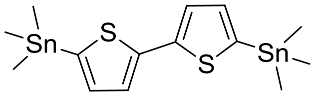

2,2'-Bithiophene (**33**) (2.00 g, 12.02 mmol) dissolved in dry THF (50 mL) in a flask and degassed under argon. The flask cooled to –78 °C and *n*-BuLi (12.00 mL, 30 mmol) added dropwise. The reaction contents stirred for 1h at –78 °C and 2h at RT. The flask cooled to –78 °C and trimethyltin chloride (30 mL, 30.00 mmol) added dropwise. The reaction contents stirred overnight at RT. The mixture quenched with deionised H_2O and subsequently extracted with *n*-hexane and the organic layer washed with NH_4Cl solution and deionised water. The organic layer separated and dried over $MgSO_4$. The solvent concentrated to obtain a product which recrystallised from (80:20, *n*-hexane: EtOH) to afford **34** as pale green crystals (4.20 g, 8.5 mmol, 71% yield)[10].

^{1}H NMR ($CDCl_3$, δ): 7.29 (d, 2H, *J* = 3.5 Hz), 7.10 (d, 2H, *J* = 3.5 Hz), 0.40 (s, 18H). ^{13}C NMR ($CDCl_3$, δ): 143.1, 137.1, 135.8, 124.9, –8.2. FT-IR (cm^{-1}): 3051, 2979, 2907, 1754, 1606, 1488, 1257, 1192, 1063. EI-MS (*m/z*): 492 [M]$^+$. EA (%) calculated for $C_{14}H_{22}S_2Sn_2$: C, 34.19; H, 4.51; S, 13.04. Found: C, 34.78; H, 4.34; S, 12.95.

9.2.11. Synthesis of 2,5-dibromothiophene (39)

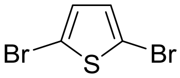

Thiophene (**38**) (25.00 g, 297.12 mmol) in DMF (250 mL) added to a flask and cooled to –15 °C. To this solution, NBS (110.00 g, 618.04 mmol) in DMF (300 mL) added dropwise in the dark and the reaction stirred overnight at RT. The reaction contents put into ice and DCM and subsequently extracted with DCM and the organic phase washed with deionised H_2O to a neutral pH. The organic layer collected and dried over $MgSO_4$ and the solvent concentrated to afford the product which purified by vacuum distillation and gave **39** as a yellow oil (59.30 g, 245 mmol, 82% yield)[11].

^{1}H NMR ($CDCl_3$, δ): 6.87 (s, 2H). ^{13}C NMR ($CDCl_3$, δ): 130.4, 111.6. FT-IR (cm^{-1}): 3096, 1726, 1516, 1410, 1200. EI-MS (*m/z*): 242 [M]$^+$. EA (%) calculated for $C_4H_2Br_2S$: C, 19.86; H, 0.83; Br, 66.06, S, 13.25. Found: C, 20.01; H, 0.85; Br, 65.02, S, 11.96.

9.2.12. Synthesis of 2,5-dibromo-3,4-dinitrothiophene (40)

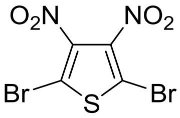

Concentrated H_2SO_4 (150 mL) and fuming H_2SO_4 (150 mL, 20% free SO_3) combined in a flask. This flask cooled to 0 °C and **39** (26.00 g, 107.46 mmol) was added dropwise. Concentrated nitric acid (125 mL) added dropwise and the reaction contents kept under 20 °C. During addition of nitric acid yellow precipitate formed quickly. The mixture stirred for 3h at 20-30 °C. Then, the mixture poured into ice and upon melting of the ice a yellow precipitate filtrated and washed thoroughly with deionised H_2O. The product recrystallised from methanol to afford **40** as yellow crystals (32.50 g, 98 mmol, 91% yield)[12].

^{13}C NMR ($CDCl_3$, δ): 140.7, 113.4. FT-IR (cm^{-1}): 2886, 2851, 2813, 1535, 1497, 1345, 1081. EI-MS (*m/z*): 332 [M]$^+$. EA (%) calculated for $C_4Br_2N_2O_4S$: C, 14.47; N, 8.44; S, 9.66; Br, 48.15. Found: C, 14.51; N, 7.91; S, 9.19; Br, 46.57.

9.2.13. Synthesis of 3′,4′-dinitro-2,2':5',2''-terthiophene (41)

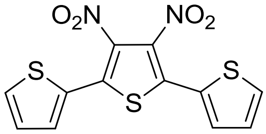

In a flask, **40** (9.90 g, 29.82 mmol), 2-(tributylstannyl)thiophene (27.82 g, 74.54 mmol) and $PdCl_2(PPh_3)_2$ (0.45 g, 0.64 mmol) added. The system degassed under argon and anhydrous toluene (100 mL) added and heated at 115 °C for 24h. The flask cooled to RT and the volatiles removed to obtain the product which purified by column chromatography with gradient (petroleum ether, 0-50% DCM) to obtain an orange solid and the product further purified by recrystallisation from methanol to afford **41** as orange crystals (9.10 g, 27 mmol, 90% yield)[13].

^{1}H NMR ($CDCl_3$, δ): 7.62 (dd, 2H, *J* = 1.0 Hz, 5.0 Hz), 7.56 (dd, 2H, *J* = 1.0 Hz, 4.0 Hz), 7.19 (dd, 2H, *J* = 4.0 Hz, 5.0 Hz). ^{13}C NMR ($CDCl_3$, δ): 135.9, 133.9, 131.3, 131.2, 128.4, 128.0. FT-IR (cm^{-1}): 3076, 1821, 1528, 1379, 1348, 1299, 1223, 1066. EI-MS (*m/z*): 338 [M]$^+$. EA (%) calculated for $C_{12}H_6N_2O_4S_3$: C, 42.60; H, 1.79; N, 8.28; S, 28.42. Found: C, 42.49; H, 1.66; N, 8.13; S, 28.16.

9.2.14. Synthesis of 3',4'-diamino-2,2':5,2''-terthiophene (42)

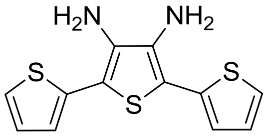

EtOH (31 mL) and HCl (62 mL, 35%) added to **41** (3.00 g, 8.86 mmol) in a flask. To this mixture, anhydrous tin(II) chloride (31.00 g, 163.50 mmol) in ethanol (62 mL) added and stirred at 30 °C for 24h. The mixture cooled to RT and put into cold NaOH. To this mixture, toluene added and then stirred vigorously and filtered through celite. The product extracted with toluene and the organic phases washed with NaCl and subsequently dried over $MgSO_4$. The solvent concentrated to obtain the **42** as a brown solid (2.40 g, 9 mmol, 97% yield)[14].

^{1}H NMR ($CDCl_3$, δ): 7.30 (d, 2H, *J* = 2.0 Hz), 7.27 (s, 2H), 7.09-7.14 (m, 2H), 3.76 (bs, 4H). ^{13}C NMR ($CDCl_3$, δ): 136.0, 133.6, 127.8, 124.0, 124.0, 110.1. FT-IR (cm^{-1}): 3371, 3298, 3224, 3182, 3096, 1631, 1615, 1573, 1528, 1509, 1441, 1336, 1294, 1070. EI-MS (*m/z*): 278 $[M]^+$. EA (%) calculated for $C_{12}H_{10}N_2S_3$: C, 51.77; H, 3.62; N, 10.06; S, 34.55. Found: C, 51.69; H, 3.54; N, 9.97; S, 34.78.

9.2.15. Synthesis of 4,6-bis(2-thienyl)-thieno[3,4-*c*][1,2,5]-thiadiazole (43)

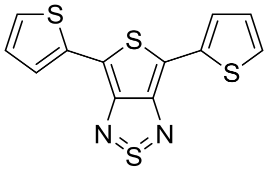

42 (1.67 g, 5.99 mmol) dissolved in dry pyridine (30 mL) in a flask and degassed under argon. To this mixture, *N*-thionylaniline (1.60 g, 11.49 mmol) added dropwise and chlorotrimethylsilane (4.50 g, 41.42 mmol) then added dropwise, resulting in a dark blue colour. The reaction contents stirred for 3h at RT and then put into DCM. The solution washed with HCl and with deionised water and extracted with DCM. The organic phase dried over anhydrous $MgSO_4$ and subsequently filtered. The solvent evaporated to afford the product which purified *via* chromatography with DCM to afford **43** as blue crystals (1.72 g, 6 mmol, 93% yield)[15].

^1H NMR ($CDCl_3$, δ): 7.59 (dd, 2H, $J = 1.0$ Hz, 3.5 Hz), 7.34 (dd, 2H, $J = 1.0$ Hz, 5.0 Hz), 7.12 (dd, 2H, $J = 3.5$ Hz, 5.0 Hz). ^{13}C NMR ($CDCl_3$, δ): 156.3, 135.0, 128.2, 125.4, 124.3, 112.4. FT-IR (cm^{-1}): 3102, 3073, 1797, 1525, 1483, 1365, 1223, 1137, 1047. EI-MS (*m/z*): 306 $[M]^+$. EA (%) calculated for $C_{12}H_6N_2S_4$: C, 47.04; H, 1.97; N, 9.14; S, 41.85. Found: C, 47.25; H, 2.18; N, 8.83; S, 39.16.

9.2.16. Synthesis of 4,7-di(thien-2-yl)-2,1,3-benzothiadiazole-5,6-dimethyl ester (44)

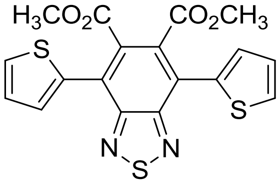

43 (1.86 g, 6.06 mmol) and dimethyl acetylenedicarboxylate (1.73 g, 12.17 mmol) combined in a flask. The system evacuated and refilled with argon for three cycles before anhydrous xylene (40 mL) added. The reaction contents refluxed for 24h. The flask cooled to RT and the solvent removed to afford the product which purified by column chromatography with gradient (petroleum ether, 0-50% DCM) to afford **44** as yellow crystals (2.37 g, 6 mmol, 94% yield)[16].

^{1}H NMR ($CDCl_3$, δ): 7.62 (dd, 2H, *J* = 1.0 Hz, 5.0 Hz), 7.44 (dd, 2H, *J* = 1.0 Hz, 3.5 Hz), 7.22 (dd, 2H, *J* = 3.5 Hz, 5.0 Hz), 3.78 (s, 6H). ^{13}C NMR ($CDCl_3$, δ): 168.1, 153.6, 135.1, 132.0, 129.7, 129.0, 127.3, 126.2, 53.1. FT-IR (cm^{-1}): 3109, 2975, 2932, 2900, 2865, 2159, 2031, 1971, 1730, 1513, 1460, 1318, 1283, 1198. EI-MS (*m/z*): 416 [M]$^+$. EA (%) calculated for $C_{18}H_{12}N_2O_4S_3$: C, 51.91; H, 2.90; N, 6.73; S, 23.09. Found: C, 51.86; H, 2.94; N, 6.61; S, 22.97.

9.2.17. Synthesis of 4,7-di(thien-2-yl)-2,1,3-benzothiadiazole-5,6-dicarboxylic acid (45)

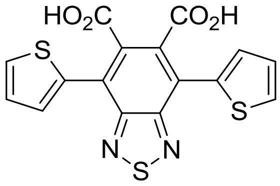

Sodium hydroxide (4.00 g, 100.00 mmol) dissolved in deionised water (30 mL) and added to a flask. To this solution, ethanol (200 mL) and **44** (2.27 g, 5.45 mmol) added and the reaction contents refluxed for 24h. The flask cooled to RT and deionised H_2O added. This mixture cooled to 0 °C and neutralised by HCl to precipitate the product. The precipitate filtered and subsequently washed with deionised H_2O. The precipitate dried under high vacuum to afford **45** as yellow solid (1.80 g, 5 mmol, 85% yield)[17].

^{1}H NMR (CD_3SOCD_3, δ): 7.86 (dd, 2H, *J* = 1.0 Hz, 5.0 Hz), 7.47 (dd, 2H, *J* = 1.0 Hz, 3.5 Hz), 7.25 (dd, 2H, *J* = 3.5 Hz, 5.0 Hz). ^{13}C NMR (CD_3SOCD_3, δ): 168.4, 152.5, 134.8, 133.0, 129.7, 129.3, 127.2, 123.8. FT-IR (cm^{-1}): 3106, broad (3300-2600), 2162, 2024, 1971, 1815, 1765, 1705, 1552, 1453, 1386, 1261, 1152, 1020. EI-MS (*m/z*): 387 [M-H]$^+$. EA (%) calculated for $C_{16}H_8N_2O_4S_3$: C, 49.48; H, 2.08; N, 7.21; S, 24.76. Found: C, 45.33; H, 2.70; N, 6.47; S, 21.35.

9.2.18. Synthesis of 4,7-di(thien-2-yl)-2,1,3-benzothiadiazole-5,6-dicarboxylic anhydride (46)

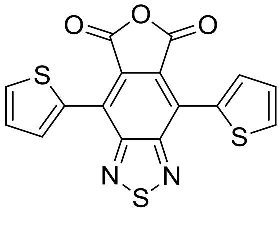

45 (1.15 g, 2.96 mmol) and anhydrous acetic anhydride (10.00 g, 97.95 mmol) combined in a flask. The system evacuated and refilled with argon for three cycles before anhydrous xylene (30 mL) added. The mixture heated at 130 °C for 6h. The mixture cooled to RT, the solvent evaporated to obtain **46** as red solid (1.06 g, 3 mmol, 97% yield)[18].

^{1}H NMR (CDCl$_3$, δ): 8.11 (dd, 2H, *J* = 1.0 Hz, 4.0 Hz), 7.82 (dd, 2H, *J* = 1.0 Hz, 5.0 Hz), 7.33 (dd, 2H, *J* = 4.0 Hz, 5.0 Hz). ^{13}C NMR (CD$_3$SOCD$_3$, δ): 162.0, 156.0, 134.3, 132.6, 131.4, 127.8, 127.6, 125.5. FT-IR (cm^{-1}): 3131, 3109, 3081, 1808, 1765, 1552, 1453, 1393, 1247, 1152, 1088. EI-MS (*m/z*): 370 [M]$^+$. EA (%) calculated for $C_{16}H_6N_2O_3S_3$: C, 51.88; H, 1.63; N, 7.56; S, 25.97. Found: C, 52.11; H, 2.00; N, 7.20; S, 24.55.

9.2.19. Synthesis of 4,7-di(thien-2-yl)-2,1,3-benzothiadiazole-5,6-*N*-(3,7-dimethyloctyl)dicarboxylic imide (47)

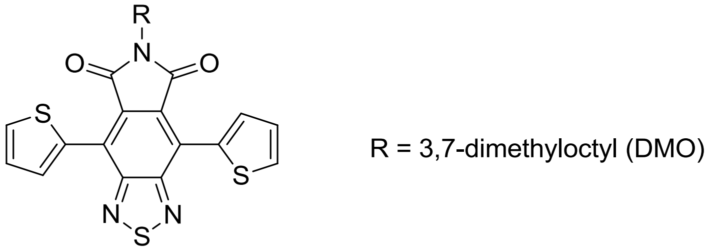

46 (1.00 g, 2.69 mmol), acetic acid (50 mL, 100%) and **54** (0.88 g, 5.59 mmol) combined in a flask. The system evacuated and refilled with argon for three cycles and heated at 110 °C overnight. The mixture cooled to RT, acetic anhydride (20 mL) added and heated at 110 °C for 6h. The mixture cooled to RT and the solvent concentrated to yield the product which purified by chromatography with (60:10, petroleum ether: ethyl acetate) to afford **47** as an orange solid (1.15 g, 2.3 mmol, 84% yield)[18].

^{1}H NMR (CDCl$_3$, δ): 7.91 (dd, 2H, *J* = 1.0 Hz, 3.5 Hz), 7.73 (dd, 2H, *J* = 1.0 Hz, 5.0 Hz), 7.30 (dd, 2H, *J* = 3.5 Hz, 5.0 Hz), 3.84-3.70 (m, 2H), 1.78-1.65 (m, 1H), 1.55-1.43 (m, 3H), 1.39-1.22 (m, 3H), 1.20-1.08 (m, 3H), 0.97 (d, 3H, *J* = 6.0 Hz), 0.86 (d, 6H, *J* = 6.0 Hz). ^{13}C NMR (CDCl$_3$, δ): 165.7, 156.5, 133.1, 131.5, 130.2, 127.0, 126.9, 126.7, 39.2, 37.2, 37.0, 35.2, 31.0, 27.9, 24.6, 22.7, 22.6, 19.4. FT-IR (cm^{-1}): 3439, 3102, 3074, 2953, 2925, 2865, 1804, 1751, 1694, 1549, 1453, 1364, 1226, 1162, 1056. EI-MS (*m/z*): 510.1 [MH]$^+$. EA (%) calculated for $C_{26}H_{27}N_3O_2S_3$: C, 61.27; H, 5.34; N, 8.24; S, 18.87. Found: C, 61.59; H, 5.56; N, 7.94; S, 16.79.

9.2.20. Synthesis of 4,7-di(thien-2-yl)-2,1,3-benzothiadiazole-5,6-*N*-octyl-dicarboxylic imide (48)

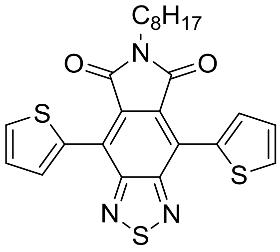

48 was prepared followed by the same procedure for synthesis of **47** except *N*-octylamine (1.20 g, 9.28 mmol) was used. **48** was obtained as an orange solid (1.20 g, 2.5 mmol, 93% yield)[18].

^{1}H NMR (CDCl$_3$, δ): 7.91 (dd, 2H , *J* = 1.0 Hz, 3.5 Hz), 7.73 (dd, 2H, *J* = 1.0 Hz, 5.0 Hz), 7.30 (dd, 2H, *J* = 3.5 Hz, 5.0 Hz), 3.74 (t, 2H, *J* = 7.5 Hz), 1.65-1.76 (m, 2H), 1.23–1.41 (m, 10H), 0.88 (t, 3H, *J* = 7.0 Hz). ^{13}C NMR (CDCl$_3$, δ): 165.8, 156.5, 133.1, 131.5, 130.2, 127.1, 126.9, 126.7, 39.0, 31.8, 29.1, 28.2, 27.0, 22.7, 14.0. FT-IR (cm^{-1}): 3443, 3102, 3070, 2918, 2854, 1808, 1754, 1694, 1556, 1457, 1364, 1226, 1169, 1098. EI-MS (*m/z*): 481.1 [M]$^+$. EA (%) calculated for $C_{24}H_{23}N_3O_2S_3$: C, 59.85; H, 4.81; N, 8.72; S, 19.97. Found: C, 59.91; H, 4.93; N, 8.70; S, 20.72.

9.2.21. Synthesis of 4,7-di(5-bromo-thien-2-yl)-2,1,3-benzothiadiazole-5,6-*N*-(3,7-dimethyloctyl)dicarboxylic imide (49)

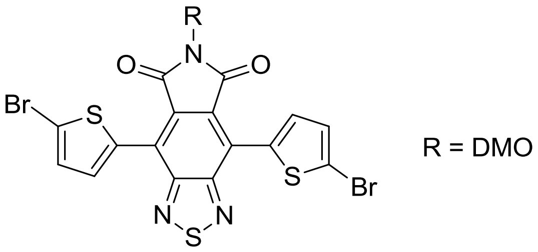

47 (1.00 g, 1.96 mmol) and THF (100 mL) combined in a flask. To this mixture, NBS (1.74 g, 9.77 mmol) added and stirred at RT overnight in the dark. The solvent evaporated to obtain the product as red solid, subsequently washed with cold CH$_3$OH, filtered and dried. The product purified *via* chromatography with DCM to yield **49** as red solid (1.28 g, 2 mmol, 98% yield)[17].

^{1}H NMR (CDCl$_3$, δ): 7.80 (d, 2H, *J* = 4.0 Hz), 7.24 (d, 2H, *J* = 4.0 Hz), 3.70-3.84 (m, 2H), 1.78-1.66 (m, 1H), 1.54-1.44 (m, 3H), 1.41-1.22 (m, 3H), 1.20-1.11 (m, 3H), 0.98 (d, 3H, *J* = 6.0 Hz), 0.87 (d, 6H, *J* = 6.5 Hz). ^{13}C NMR (CDCl$_3$, δ): 165.6, 155.9, 134.1, 133.0, 129.8, 126.4, 125.8, 118.7, 39.2, 37.3, 37.0, 35.2, 31.0, 27.9, 24.6, 22.7, 22.6, 19.4. FT-IR (cm^{-1}): 3429, 3120, 2957, 2918, 2865, 1747, 1691, 1563, 1460, 1364, 1283, 1073. EI-MS (*m/z*): 666.9 [M]$^+$. EA (%) calculated for $C_{26}H_{25}Br_2N_3O_2S_3$: C, 46.78; H, 3.78; Br, 23.94; N, 6.30; S, 14.41. Found: C, 46.61; H, 3.61; Br, 23.95; N, 6.29; S, 14.64.

9.2.22. Synthesis of 4,7-di(5-bromo-thien-2-yl)-2,1,3-benzothiadiazole-5,6-*N*-octyl-dicarboxylic imide (50)

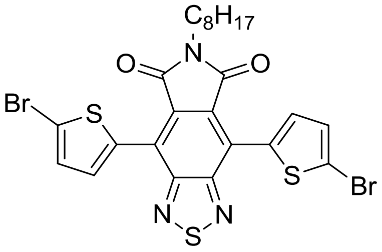

50 was prepared followed by the same procedure for synthesis of **49**.

48 (1.00 g, 2.07 mmol), THF (100 mL) and NBS (1.84 g, 10.33 mmol). **50** was obtained as red solid (1.27 g, 2 mmol, 96% yield)[17].

^{1}H NMR ($CDCl_3$, δ): 7.80 (d, 2H, *J* = 4.0 Hz), 7.24 (d, 2H, *J* = 4.0 Hz), 3.75 (t, 2H, *J* = 7.0 Hz,), 1.66-1.75 (m, 2H), 1.23–1.40 (m, 10H), 0.88 (t, 3H, *J* = 6.5 Hz,). ^{13}C NMR ($CDCl_3$, δ): 165.7, 156.0, 134.1, 133.0, 129.8, 126.4, 125.9, 118.7, 39.0, 31.8, 29.1, 28.3, 27.0, 22.6, 14.1. FT-IR (cm^{-1}): 3421, 3120, 2953, 2911, 2850, 1744, 1687, 1556, 1446, 1375, 1244, 1176. EI-MS (*m/z*): 638.9 [M]$^+$. EA (%) calculated for $C_{24}H_{21}Br_2N_3O_2S_3$: C, 45.08; H, 3.31; N, 6.57; S, 15.04; Br, 24.99. Found: C, 44.79; H, 3.41; N, 6.47; S, 15.74; Br, 28.80.

9.2.23. Synthesis of 3,7-dimethyloctyl bromide (52)

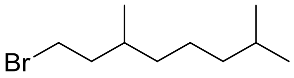

Triphenylphosphine (21.10 g, 80.44 mmol) added to a mixture of 3,7-dimethyloctyl alcohol (**51**) (12.61 g, 79.69 mmol) and dichloromethane (250 mL) and stirred in a flask. To this mixture, NBS (14.26 g, 80.14 mmol) added portionwise and stirred at RT for 90 min. The mixture washed with $NaHCO_3$ solution, dried over $MgSO_4$, filtered and the solvent evaporated. The substance stirred in petroleum ether for 1h at RT, filtered and the filtrate evaporated. The product purified by chromatography with petroleum ether to yield **52** as colourless oil (23.00 g, 59 mmol, 73% yield)[19].

^{1}H NMR ($CDCl_3$, δ): 3.55-3.37 (m, 2H), 1.96-1.83 (m, 1H), 1.77-1.61 (m, 2H), 1.60-1.49 (m, 1H), 1.41-1.24 (m, 3H), 1.22-1.11 (m, 3H), 0.82-0.94 (m, 9H). ^{13}C NMR ($CDCl_3$, δ): 40.1, 39.2, 36.7, 32.3, 31.7, 28.0, 24.6, 22.7, 22.6, 19.0. FT-IR (cm^{-1}): 2953, 2925, 2868, 1464, 1382, 1261, 1173. EI-MS (*m/z*): 222.1 [M]$^+$. EA (%) calculated for $C_{10}H_{21}Br$: C, 54.30; H, 9.57; Br, 36.13. Found: C, 55.04; H, 9.53; Br, 34.23.

9.2.24. Synthesis of *N*-(3,7-dimethyloctyl)phthalimide (53)

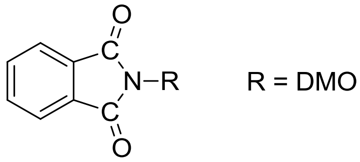

52 (4.07 g, 18.40 mmol) and anhydrous DMF (20 mL) added into a flask. To this mixture, potassium phthalimide (3.75 g, 20.27 mmol) added and the reaction contents heated to 90 °C for 17h. The mixture cooled to RT and put in deionised H_2O and the product subsequently extracted with DCM. The organic extracts combined, washed with KOH and deionised water. The organic phase dried over $MgSO_4$ and the solvent evaporated to obtain the product which purified *via* chromatography with dichloromethane to yield **53** as colourless oil (5.29 g, 18 mmol, 91% yield)[20].

^{1}H NMR ($CDCl_3$, δ): 7.85 (dd, 2H, *J* = 3.0 Hz, 5.5 Hz), 7.72 (dd, 2H, *J* = 3.0 Hz, 5.5 Hz), 3.80-3.66 (m, 2H), 1.77-1.66 (m, 1H), 1.53-1.43 (m, 3H), 1.41-1.25 (m, 3H), 1.20-1.11 (m, 3H), 0.98 (d, 3H, *J* = 6.5 Hz), 0.87 (d, 6H, *J* = 7.0 Hz). ^{13}C NMR ($CDCl_3$, δ): 168.4, 133.8, 132.2, 123.1, 39.2, 37.0, 36.3, 35.5, 30.7, 27.9, 24.5, 22.7, 22.6, 19.4. FT-IR (cm^{-1}): 2953, 2925, 2868, 1772, 1706, 1616, 1469, 1398, 1267, 1189, 1055. EI-MS (*m/z*): 288.2 [MH]$^+$. EA (%) calculated for $C_{18}H_{25}NO_2$: C, 75.22; H, 8.77; N, 4.87. Found: C, 72.17; H, 8.62; N, 4.43.

9.2.25. Synthesis of 3,7-dimethyl-1-octanamine (54)

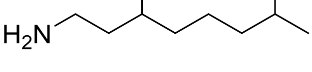

53 (6.03 g, 20.98 mmol), hydrazine hydrate (4.0 mL, 65.0 mmol, 51%) and methanol (100 ml) combined in a flask. The reaction contents refluxed until the starting material disappeared. Upon completion, excess HCl added and the mixture refluxed for 1h and then cooled to RT. The precipitate filtered and washed with water. The methanol concentrated and the residue diluted with dichloromethane. The organic layer washed with KOH and the product extracted with dichloromethane. The organic phase washed with NaCl, dried over $MgSO_4$ and the solvent concentrated to yield **54** as a brown oil (2.85 g, 18 mmol, 86% yield)[21].

^{1}H NMR ($CDCl_3$, δ): 2.82-2.62 (m, 2H), 1.60-1.43 (m, 3H), 1.35-1.22 (m, 4H), 1.20-1.06 (m, 3H), 0.88 (dd, 9H, *J* = 2.0 Hz, 6.5 Hz). ^{13}C NMR ($CDCl_3$, δ): 41.1, 40.1, 39.3, 37.3, 30.5, 28.0, 24.7, 22.7, 22.6, 19.6. FT-IR (cm^{-1}): 3521, 3375, 3219, 3021, 2953, 2925, 2868, 2155, 2028, 1978, 1598, 1464, 1382, 1166, 1063. EI-MS (*m/z*): 157.2 $[M]^+$. EA (%) calculated for $C_{10}H_{23}N$: C, 76.36; H, 14.74; N, 8.90. Found: C, 71.74; H, 13.51; N, 7.71.

9.2.26. Synthesis of 4,4'-dibromo-2,2'-dinitrobiphenyl (68)

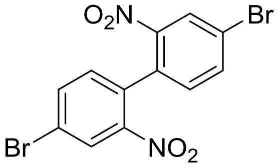

2,5-Dibromonitrobenzene (**67**) (50.00 g, 179.30 mmol) and Cu powder (25.00 g, 393.39 mmol) combined in a flask. The mixture evacuated and refilled with argon for three cycles before anhydrous DMF (230 mL) added and heated at 125 °C for 3h. The reaction contents cooled to RT and dissolved in toluene and filtered. $NaHCO_3$ solution added to the filtrate and the mixture extracted with toluene and the organic phases combined and washed with deionised H_2O several times until became neutral. The organic phase dried over anhydrous $MgSO_4$, filtered and the solvent evaporated to afford the product which recrystallised from isopropanol to yield **68** as yellow crystals (32.61 g, 162 mmol, 90% yield)[22].

^{1}H NMR ($CDCl_3$, δ): 8.40 (d, 2H, *J* = 2.0 Hz), 7.85 (dd, 2H, *J* = 2.0 Hz, 8.0 Hz), 7.18 (d, 2H, *J* = 8.0 Hz). ^{13}C NMR ($CDCl_3$, δ): 147.4, 136.6, 132.0, 132.0, 128.1, 123.0. FT-IR (cm^{-1}): 3085, 2847, 1598, 1332, 1276, 1152, 1098. EI-MS (*m/z*): 403 $[M]^+$. EA (%) calculated for $C_{12}H_6Br_2N_2O_4$: C, 35.85; N, 6.97; Br, 39.75; H, 1.50. Found: C, 35.55; N, 6.77; Br, 39.74; H, 1.59.

9.2.27. Synthesis of 4,4'-dibromobiphenyl-2,2'-diamine (69)

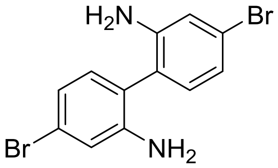

68 (6.00 g, 14.92 mmol), ethanol (74 mL) and HCl (43 mL, 32%) added to a flask. To this mixture, Sn (7.00 g, 58.96 mmol) added over 10 minutes and refluxed for 90 min. The reaction contents cooled to RT and another portion of Sn (7.00 g, 58.96 mmol) added and refluxed for 90 min. The flask cooled to RT and the mixture filtered and deionised water added to the filtrate. NaOH solution was added dropwise until pH became approximately 9. The mixture extracted with Et_2O and organic phase washed with NaCl, dried over $MgSO_4$ and then filtered. The solvent concentrated in obtain the **69** as brown crystals (3.58 g, 10.5 mmol, 70% yield)[23].

^1H NMR ($CDCl_3$, δ): 6.99-6.93 (m, 6H), 3.59 (bs, 4H). ^{13}C NMR ($CDCl_3$, δ): 145.4, 132.3, 122.7, 122.1, 121.7, 118.2. FT-IR (cm^{-1}): 3393, 3280, 3187, 1630, 1557, 1496, 1396, 1272, 1137, 1081. EI-MS (*m/z*): 341.9 $[M]^+$. EA (%) calculated for $C_{12}H_{10}Br_2N_2$: C, 42.14; N, 8.19; Br, 46.72; H, 2.95. Found: C, 41.74; N, 7.95; Br, 46.71; H, 2.93.

9.2.28. Synthesis of 4,4'-dibromo-2,2'-diiodobiphenyl (70)

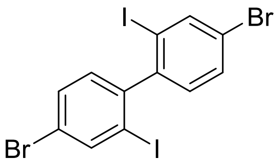

69 (5.00 g, 14.61 mmol), HCl (50 mL, 32 %), H_2O (200 mL) and acetonitrile (200 mL) combined in a flask and cooled to 0 °C. To this mixture, $NaNO_2$ (4.59 g, 66.53 mmol) dissolved in deionised H_2O (25 mL) added dropwise and stirred for 1h between –5 and –10 °C. KI (22.28 g, 134.21 mmol) dissolved in deionised H_2O (50 mL) and cooled to 0 °C and added dropwise whilst the reaction temperature maintained at –10 to –15 °C. After addition completed, the temperature raised to RT and then heated to 80 °C for 20h and cooled to RT. The mixture extracted with DCM, the collected organic layers washed with $Na_2S_2O_3$ solution, deionised water and NaCl solution. The collected organic layers dried over $MgSO_4$, filtered and the solvent concentrated to afford the product which purified *via* chromatography with petroleum ether. It further purified by recrystallisation from *n*-hexane to yield **70** as white crystals (4.23 g, 7.5 mmol, 51% yield)[24].

^1H NMR ($CDCl_3$, δ): 8.11 (d, 2H, $J = 2.0$ Hz), 7.57 (dd, 2H, $J = 2.0$ Hz, 8.0 Hz), 7.05 (d, 2H, $J = 8.0$ Hz). ^{13}C NMR ($CDCl_3$, δ): 146.8, 141.0, 131.4, 130.7, 122.5, 99.9. FT-IR (cm^{-1}): 3400, 3393, 3294, 3191, 1634, 1581, 1449, 1364, 1084. EI-MS (*m/z*): 563.7 $[M]^+$. EA (%) calculated for $C_{12}H_6Br_2I_2$: C, 25.56; H, 1.07; Br, 28.34; I, 45.02. Found: C, 25.47; H, 1.21; Br, 28.14; I, 45.23.

9.2.29. Synthesis of 2,7-dibromo-9,9-dioctyldibenzosilole (71)

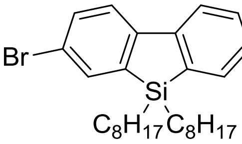

70 (4.20 g, 7.44 mmol) was added to a flask. Anhydrous THF (84 mL) added and the mixture cooled to –78 °C and then the system degassed under argon. To this mixture, *n*-BuLi (12.00 mL, 30.0 mmol) added dropwise over 2h. The reaction contents stirred for 1h Dichlorodioctylsilane (4.86 g, 14.95 mmol) added dropwise over 5 min and the temperature raised to RT and mixture stirred overnight. Deionised water added and the product extracted with Et_2O and organic layers collected and washed with brine. The organic layer dried over $MgSO_4$, filtered and the solvent concentrated to yield a product which purified using chromatography with PE to yield **71** as a colourless oil (3.80 g, 7 mmol, 90% yield)[25].

^{1}H NMR ($CDCl_3$, δ): 7.70 (d, 2H, *J* = 2.0 Hz), 7.65 (d, 2H, *J* = 8.0 Hz), 7.55 (dd, 2H, *J* = 2.0 Hz, 8.0 Hz), 1.08-1.47 (m, 28H), 0.90 (t, 6H, *J* = 2.0 Hz). ^{13}C NMR ($CDCl_3$, δ): 146.0, 140.5, 135.8, 133.1, 122.5, 122.2, 33.2, 31.8, 29.1, 29.0, 23.7, 22.6, 14.1, 11.99. FT-IR (cm^{-1}): 2957, 2921, 2858, 1552, 1446, 1382, 1237, 1141, 1070. EI-MS (*m/z*): 564.1 $[M]^+$. EA (%) calculated for $C_{28}H_{40}Br_2Si$: C, 59.57; H, 7.14; Br, 28.31. Found: C, 60.29; H, 7.60; Br, 24.72%.

9.2.30. Synthesis of 9,9-dioctyl-2,7-bis(4,4,5,5-tetramethyl-1,3,2-dioxaborolan-2-yl)-dibenzosilole (72)

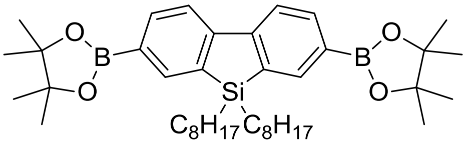

71 (1.51 g, 2.65 mmol), potassium acetate (1.56 g, 15.89 mmol), bis(pinacolato)diboron (2.36 g, 9.29 mmol) and $PdCl_2$(dppf) (0.12 g, 0.14 mmol, 5.54 mol%) combined in a flask and then the system degassed under argon. To this mixture, anhydrous DMF (30 mL) added and heated at 100 °C for 48h. The flask cooled to RT and the product extracted with Et_2O and organic phases washed with deionised H_2O. The organic layers separated and dried over $MgSO_4$, filtered and the solvent evaporated to obtain a product which recrystallised from methanol which passed through the basic alumina to remove the acidic protons to obtain **72** as brown crystals (0.92 g, 1.4 mmol, 53% yield)[26].

^{1}H NMR ($CDCl_3$, δ): 8.07 (s, 2H), 7.92-7.85 (m, 4H), 1.39 (s, 24H), 1.15-1.34 (m, 24H), 0.92-0.99 (m, 4H), 0.86 (t, 6H, *J* = 7.0 Hz). ^{13}C NMR ($CDCl_3$, δ): 151.0, 139.7, 137.5, 136.8, 120.5, 83.7, 33.4, 31.8, 29.2, 29.0, 24.9, 23.8, 22.6, 14.1, 12.3. FT-IR (cm^{-1}): 2975, 2921, 2854, 1595, 1460, 1343, 1272, 1137, 1091. EI-MS (*m/z*): 658.5 $[M]^+$. EA (%) calculated for $C_{40}H_{64}B_2O_4Si$: C, 72.94; H, 9.79. Found: C, 72.30; H, 9.42.

9.2.31. Synthesis of 1,4-dibromo-2-fluoro-5-nitrobenzene (81)

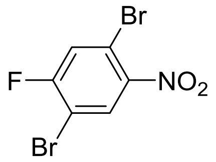

1,4-Dibromo-2-fluorobenzene (**80**) (25.00 g, 98.46 mmol) dissolved in DCM (75 mL), trifluoroacetic acid (75 mL) and trifluoroacetic anhydride (37.5 mL) in a flask and then cooled to 0 °C. To this mixture, ammonium nitrate (9.70 g, 121.17 mmol) added slowly and the mixture stirred overnight at RT. The reaction contents put into ice, deionised water added and the product extracted with DCM. The organic layer separated, dried over $MgSO_4$, filtered and the solvent evaporated to obtain the product. It purified by recrystallisation from EtOH to yield the **81** as yellow crystals (25.00 g, 84 mmol, 85% yield)[27].

^{1}H NMR ($CDCl_3$, δ): 8.20 (d, 1H, *J* = 6.5 Hz), 7.55 (d, 1H, *J* = 7.5 Hz). ^{13}C NMR ($CDCl_3$, δ): 161.9, 159.3, 130.9 (d, *J* = 2.0 Hz), 122.9 (d, *J* = 27.0 Hz), 114.9 (d, *J* = 9.0 Hz), 108.9 (d, *J* = 23.0 Hz). ^{19}F NMR ($CDCl_3$, δ): –97.2 (t, *J* = 7.0 Hz). FT-IR (cm^{-1}): 3092, 3017, 2865, 1762, 1584, 1464, 1286, 1222, 1070. EI-MS (*m/z*): 298.8 $[M]^+$. EA (%) calculated for $C_6H_2O_2FNBr_2$: C, 24.11; N, 4.69; Br, 53.47; H, 0.67. Found: C, 24.13; N, 4.72; Br, 52.99; H, 1.06.

9.2.32. Synthesis of 4,4'-dibromo-5,5'-difluoro-2,2'-dinitrobiphenyl (82)

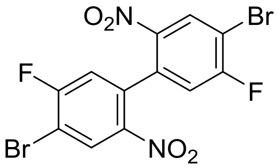

82 prepared followed by the same procedure for synthesis of **68**.

81 (19.00 g, 63.56 mmol), Cu powder (5.32 g, 83.71 mmol) and anhydrous DMF (95 mL). **82** was obtained as yellow crystals (10.63 g, 48.5 mmol, 76% yield)[28].

^{1}H NMR ($CDCl_3$, δ): 8.57 (d, 2H, *J* = 6.0 Hz), 7.09 (d, 2H, *J* = 8.0 Hz). ^{13}C NMR ($CDCl_3$, δ): 161.7 (d, *J* = 258.0 Hz), 142.9, 134.1 (d, *J* = 8.5 Hz), 131.2 (d, *J* = 2.0 Hz), 118.3 (d, *J* = 25.5 Hz), 110.4 (d, *J* = 23.0 Hz). ^{19}F NMR ($CDCl_3$, δ): –95.9 (t, *J* = 6.5 Hz). FT-IR (cm^{-1}): 3109, 3056, 2861, 1790, 1613, 1563, 1488, 1464, 1396, 1293, 1233, 1191, 1066. EI-MS (*m/z*): 400.1 $[M-2F]^+$. EA (%) calculated for $C_{12}H_4O_4F_2N_2Br_2$: C, 32.91; N, 6.40; Br, 36.49; H, 0.92. Found: C, 32.91; N, 6.44; Br, 36.16; H, 1.25.

9.2.33. Synthesis of 4,4'-dibromo-5,5'-difluorobiphenyl-2,2'-diamine (83)

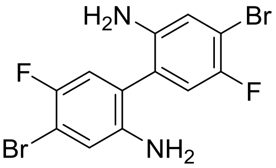

83 was prepared followed by the same procedure for synthesis of **69**.

82 (10.50 g, 23.97 mmol), ethanol (145 mL), HCl (45 mL, 35%) and Sn powder (22.76 g, 191.72 mmol). **83** was obtained as a brown solid (7.34 g, 19 mmol, 81% yield)[29].

^{1}H NMR ($CDCl_3$, δ): 6.99 (d, 2H, *J* = 6.0 Hz), 6.90 (d, 2H, *J* = 8.5 Hz), 3.74 (bs, 4H). ^{13}C NMR ($CDCl_3$, δ): 152.5 (d, *J* = 237.5 Hz), 141.0 (d, *J* = 2.0 Hz), 112.8 (d, *J* = 5.5 Hz), 119.7, 118.0 (d, *J* = 23.0 Hz), 109.4 (d, *J* = 22.0 Hz). ^{19}F NMR ($CDCl_3$, δ): –121.2 (t, *J* = 7.0 Hz). FT-IR (cm^{-1}): 3436, 3411, 3304, 3194, 1620, 1481, 1293, 1194, 1056. EI-MS (*m/z*): 377.9 $[M]^+$. EA (%) calculated for $C_{12}H_8Br_2F_2N_2$: C, 38.13; N, 7.41; Br, 42.28; H, 2.13. Found: C, 37.90; N, 7.09; Br, 45.95; H, 2.37.

9.2.34. Synthesis of 3,6-difluoro-2,7-dibromo-*9H*-carbazole (84)

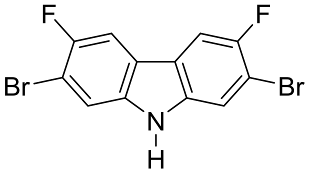

83 (6.60 g, 17.45 mmol) and H_3PO_4 (150 mL, 85%) combined in a flask and the mixture heated at 190 °C for 24h. The flask cooled to RT, filtered and washed with deionised H_2O. Subsequently, the precipitate dissolved in toluene, passed through flash column chromatography and washed with toluene. The solvent concentrated to afford the product which purified *via* recrystallisation from (10:1, toluene: hexane) to afford **84** as ivory crystals (5.00 g, 14 mmol, 79% yield)[30].

^{1}H NMR (CD_3COCD_3, δ): 10.67 (bs, 1H); 8.09 (d, 2H, *J* = 9.0 Hz); 7.85 (d, 2H, *J* = 6.0 Hz). ^{13}C NMR (CD_3COCD_3, δ): 152.9 (d, *J* = 235.0 Hz), 137.8, 122.2 (dd, *J* = 4.0 Hz, 8.5 Hz), 115.5, 107.2 (d, *J* = 5.5 Hz), 107.0 (d, *J* = 4.0 Hz). ^{19}F NMR (CD_3COCD_3, δ): –120.3 (dd, *J* = 5.5 Hz, 8.5 Hz). FT-IR (cm^{-1}): 3450, 3046, 1694, 1613, 1574, 1474, 1347, 1283, 1205, 1176, 1038. EI-MS (*m/z*): 360.9 [M]$^{+}$. EA (%) calculated for $C_{12}H_5Br_2F_2N$: C, 39.93; N, 3.88; Br, 44.27; H, 1.40. Found: C, 40.81; N, 3.87; Br, 43.59; H, 1.83.

9.2.35. Synthesis of heptadecan-9-ol (86)

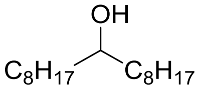

In a flask, Mg (6.68 g, 274.84 mmol) added and heated under high vacuum at 150 °C for 1h. The flask cooled to RT, degassed under argon before anhydrous THF (130 mL) and few crystals of iodine added and the mixture stirred until the colour of mixture changed from brown to colourless. The flask cooled to 0 °C before 1-bromooctane (**85**) (47.92 g, 248.18 mmol) in anhydrous THF (75 mL) added dropwise. After the addition completed, the colour of the solution became grey and the mixture refluxed for 2h at 60 °C to form *n*-octylmagnesium bromide. To this Grignard reagent, ethyl formate (**95**) (6.13 g, 82.81 mmol) in anhydrous THF (140 mL) added dropwise at –78 °C during 2h. The reaction contents stirred at RT overnight. Methanol and saturated NH_4Cl solution added, the product extracted with diethyl ether, the organic layer separated and washed with brine solution. The organic layer separated, dried over $MgSO_4$, filtered and the solvent evaporated to afford the **86** as a white solid (21.20 g, 82 mmol, 99% yield)[31].

^{1}H NMR ($CDCl_3$, δ): 3.64-3.56 (m, 1H), 1.54-1.25 (m, 28H), 0.90 (t, 6H, *J* = 7.0 Hz). ^{13}C NMR ($CDCl_3$, δ): 72.0, 37.5, 31.9, 29.7, 29.6, 29.3, 25.7, 22.7, 14.1. FT-IR (cm^{-1}): 3507-3021 (broad), 2953, 2918, 2854, 1467, 1379, 1130, 1088. EI-MS (*m/z*): 256.3 [M]$^{+}$. EA (%) calculated for $C_{17}H_{36}O$: C, 79.61; H, 14.15. Found: C, 79.94; H, 13.63.

9.2.36. Synthesis of 9-heptadecane-*p*-toluenesulfonate (87)

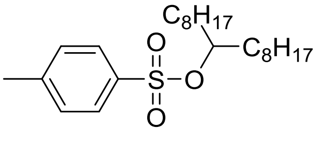

86 (20.00 g, 77.98 mmol), triethyl amine (27.1 mL, 194.29 mmol), trimethylammonium monohydrochloride (7.43 g, 77.74 mmol) and DCM (100 mL) combined in a flask and cooled to 0 °C. To this mixture, *p*-toluenesulfonyl chloride (22.26 g, 116.75 mmol) in

DCM (100 mL) added dropwise during 1h and then the mixture stirred for 3h. Deionised water added and the product extracted with DCM, organic layer was separated, washed with deionised H_2O and then with brine. The organic layer dried over $MgSO_4$, filtered and the solvent evaporated to afford the product. It purified *via* column chromatography using (90:10, petroleum ether: ethyl acetate) to obtain **87** as a colourless oil which was changed to white crystals within time (28.43 g, 69 mmol, 89% yield)[32].

^{1}H NMR ($CDCl_3$, δ): 7.81 (dd, 2H, J = 1.5 Hz, 6.5 Hz); 7.34 (dd, 2H, J = 0.5 Hz, 8.5 Hz); 4.62-4.51 (qt, 1H, J = 6.0 Hz); 2.47 (s, 3H); 1.69-1.51 (m, 4H); 1.38-1.11 (m, 24H); 0.89 (t, 6H, J = 7.0 Hz). ^{13}C NMR ($CDCl_3$, δ): 144.3, 134.8, 129.6, 127.7, 84.6, 34.1, 31.8, 29.7, 29.3 (d, J = 7.5 Hz), 29.2, 24.7, 22.7, 21.6, 14.1. FT-IR (cm^{-1}): 2953, 2925, 2854, 1602, 1467, 1354, 1169. EI-MS (*m/z*): 433 $[MNa]^+$. EA (%) calculated for $C_{24}H_{42}O_3S$: C, 70.20; S, 7.81; H, 10.31. Found: C, 70.35; S, 7.44; H, 10.03.

9.2.37. Synthesis of 3,6-difluoro-*N*-9'-heptadecanyl-2,7-dibromocarbazole (88)

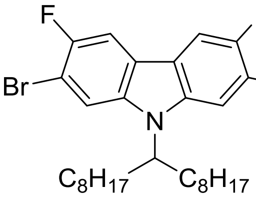

84 (2.00 g, 5.54 mmol) and KOH (1.76 g, 31.37 mmol) combined in a flask and then degassed under argon before anhydrous DMSO (40 mL) added. To this mixture, **87** (3.72 g, 9.05 mmol) was dissolved in anhydrous THF (40 mL) added dropwise and the resulting mixture heated at 45 °C overnight. The mixture cooled to RT and deionised water added. The product extracted with *n*-hexane and washed with saturated solution of brine. The organic phase separated, dried over $MgSO_4$ and filtered. The solvent evaporated to afford the product which purified *via* column chromatography using petroleum ether to obtain **88** as white crystals (2.51 g, 4 mmol, 76% yield)[33].

^{1}H NMR ($CDCl_3$, δ): 7.83-7.69 (bm, 2H); 7.58 (d, 2H, J = 4.0 Hz), 4.45-4.34 (m, 1H), 2.57-2.11 (bm, 2H), 1.97-1.84 (m, 2H), 1.39-1.07 (m, 20H), 1.04-0.91 (m, 4H), 0.85 (t, 6H, J = 7.0 Hz). ^{13}C NMR ($CDCl_3$, δ): 153.1, 139.5, 135.8, 122.7, 121.2, 115.6, 113.4, 107.6, 106.7, 57.3, 33.5, 31.7, 29.3, 29.1, 26.7, 22.6, 14.1. ^{19}F NMR ($CDCl_3$, δ): –118.8 (d, J = 196.5 Hz). FT-IR (cm^{-1}): 2957, 2918, 2850, 1701, 1598, 1467, 1336, 1244, 1191, 1038. EI-MS (*m/z*): 599.1 $[M]^+$. EA (%) calculated for $C_{29}H_{39}Br_2F_2N$: C, 58.11; Br, 26.66; N, 2.34; H, 6.56. Found: C, 58.33; Br, 26.01; N, 2.29; H, 6.66.

9.2.38. Synthesis of 3,6-difluoro-*N*-9'-heptadecanyl-2,7-bis(4,4,5,5-tetramethyl-1,3,2- dioxaborolan-2-yl)carbazole (89)

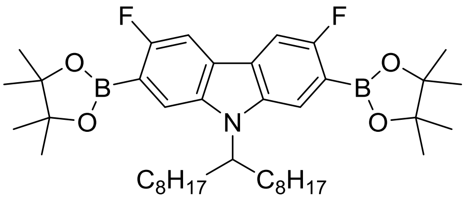

89 prepared followed by the same procedure for synthesis of **72**.

88 (1.00 g, 1.66 mmol), bis(pinacolato)diboron (1.48 g, 5.82 mmol), potassium acetate (0.98 g, 9.98 mmol), Pd(dppf)Cl_2 (0.08 g, 0.10 mmol) and anhydrous DMF (20 mL). **89** was obtained as brown crystals (0.79 g, 1 mmol, 69% yield)[34].

^{1}H NMR ($CDCl_3$, δ): 7.89 (bs, 1H); 7.75 (bs, 1H); 7.66 (bd, 2H, *J* = 7.0 Hz), 4.71-4.56 (m, 1H), 2.38-2.23 (m, 2H), 2.02-1.87 (m, 2H), 1.43 (s, 24H), 1.33-1.08 (m, 20H), 1.04-0.90 (m, 4H), 0.84 (t, 6H, *J* = 7.0 Hz). ^{13}C NMR ($CDCl_3$, δ): 160.8, 139.6, 136.0, 126.4, 124.9, 119.0, 116.5, 114.8, 106.1, 83.9, 56.6, 33.8, 31.7, 29.4, 29.3, 29.2, 26.6, 24.9, 22.6, 14.0. ^{19}F NMR ($CDCl_3$, δ): –116.28 (d, *J* = 163.0 Hz). FT-IR (cm^{-1}): 2978, 2925, 2854, 1609, 1566, 1442, 1332, 1293, 1141, 1066. EI-MS (*m/z*): 693.5 $[M]^+$. EA (%): calculated for $C_{41}H_{63}B_2NO_4F_2$: C, 71.00; N, 2.02; H, 9.16. Found: C, 70.94; N, 2.05; H, 8.90.

9.2.39. Synthesis of bis(3-thienyl)methanol (113)

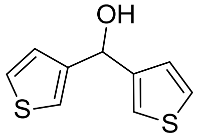

In a flask, 3-bromothiophene (**111**) (19.56 g, 119.97 mmol) added and then degassed under argon before anhydrous Et_2O (150 mL) added. The flask cooled to −78 °C and *n*-BuLi (48.00 mL, 120.00 mmol) added dropwise and stirred for 4h. To this mixture, thiophene-3-carboxaldehyde (**112**) (13.44 g, 119.83 mmol) added dropwise. The reaction contents stirred at −78 °C for 3h and the temperature raised to RT and stirred overnight. NH_4Cl solution added and the product extracted with $CHCl_3$. The organic layer separated and washed with NaCl solution. The combined organic layers dried over $MgSO_4$, filtered and the solvent evaporated to yield the product. It purified *via* column chromatography using (80:20, petroleum ether: ethyl acetate) to obtain **113** as yellow oil (20.00 g, 102 mmol, 85% yield)[35].

^{1}H NMR ($CDCl_3$, δ): 7.32 (dd, 2H, J = 3.0 Hz, 5.0 Hz), 7.25-7.23 (m, 2H), 7.07 (dd, 2H, J = 1.0 Hz, J = 5.0 Hz), 5.99 (d, 1H, J = 4.5 Hz), 2.22 (d, 1H, J = 4.5 Hz). ^{13}C NMR ($CDCl_3$, δ): 143.0, 126.8, 126.0, 122.4, 73.0. FT-IR (cm^{-1}): 3507-3131 (broad), 3099, 3081, 2900, 2865, 2109, 1410, 1304, 1283, 1137, 1077. EI-MS (*m/z*): 196.0 [M]$^+$. EA (%) calculated for $C_9H_8OS_2$: C, 55.07; H, 4.11; S, 32.67. Found: C, 56.68; H, 3.64; S, 34.12.

9.2.40. Synthesis of bis(2-iodo-3-thienyl)methanol (114)

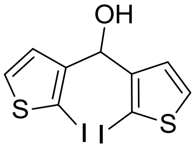

In a flask, **113** (10.00 g, 50.94 mmol) added and then degassed under argon before anhydrous Et_2O (50 mL) added. The flask cooled to −78 °C and *n*-BuLi (62.5 mL, 156.25 mmol) added dropwise at this temperature during 2h and stirred for 2h. The reaction contents stirred at RT for 2h. The mixture cooled to –78 °C and subsequently iodine (42.70 g, 168.24 mmol) dissolved in anhydrous Et_2O (250 mL) added dropwise. The reaction stirred at RT overnight. Sodium thiosulfate solution added and the product extracted with Et_2O. The organic layers separated and dried over $MgSO_4$ then filtered. The solvent concentrated to afford the product. It purified *via* chromatography using (70:30, petroleum ether: DCM) to afford **114** as cream-colored crystals (18.00 g, 40 mmol, 79% yield)[36].

^{1}H NMR ($CDCl_3$, δ): 7.46 (dd, 2H, J = 0.5 Hz, 5.5 Hz), 6.96 (d, 2H, J = 5.5 Hz), 5.80 (d, 1H, J = 3.5 Hz), 2.26 (d, 1H, J = 3.5 Hz). ^{13}C NMR ($CDCl_3$, δ): 146.7, 131.5, 126.9, 75.3, 71.8. FT-IR (cm^{-1}): 3507-3131 (broad), 3095, 3085, 2911, 1772, 1747, 1609, 1517, 1400, 1219, 1091. EI-MS (*m/z*): 447.8 [M]$^+$. EA (%) calculated for $C_9H_6I_2OS_2$: C, 24.13; H, 1.35; S, 14.31; I, 56.64. Found: C, 24.94; H, 1.28; S, 13.82; I, 57.17.

9.2.41. Synthesis of bis(2-iodo-3-thienyl)ketone (115)

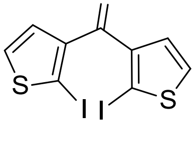

114 (6.64 g, 14.81 mmol), and DCM (150 mL) combined in a flask. To this mixture, pyridinium chlorochromate (4.79 g, 22.22 mmol) added and stirred at RT for 24h. The whole mixture passed through flash chromatography using DCM to afford the **115** as yellow crystals (6.40 g, 14 mmol, 97% yield)[37].

^{1}H NMR ($CDCl_3$, δ): 7.49 (d, 2H, *J* = 5.5 Hz), 7.08 (d, 2H, *J* = 5.5 Hz). ^{13}C NMR ($CDCl_3$, δ): 185.6, 143.2, 131.7, 129.8, 81.3. FT-IR (cm^{-1}): 3102, 3077, 1648, 1503, 1396, 1233, 1194, 1063. EI-MS (*m/z*): 445.8 $[M]^+$. EA (%) calculated for $C_9H_4I_2OS_2$: C, 24.23; H, 0.90; S, 14.37; I, 56.90. Found: C, 24.30; H, 0.75; S, 14.57, I, 57.09.

9.2.42. Synthesis of *4H*-cyclopenta[2,1-*b*:3,4-*b*']dithiophen-4-one (116)

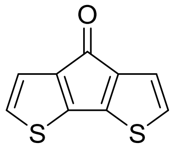

116 prepared followed by the same procedure for synthesis of **68**.

115 (3.50 g, 7.84 mmol), Cu powder (1.49 g, 23.44 mmol) and anhydrous DMF (25 mL). **116** was obtained as purple crystals (1.47 g, 8 mmol, 98% yield)[38].

^{1}H NMR ($CDCl_3$, δ): 7.06 (d, 2H, *J* = 5.0 Hz), 7.01 (d, 2H, *J* = 5.0 Hz). ^{13}C NMR ($CDCl_3$, δ): 182.7, 149.2, 142.5, 127.2, 121.8. FT-IR (cm^{-1}): 3386, 3102, 3085, 1705, 1354, 1233, 1081. EI-MS (*m/z*): 192.0 $[M]^+$. EA (%) calculated for $C_9H_4OS_2$: C, 56.23; H, 2.10; S, 33.35. Found: C, 55.94; H, 2.05; S, 33.13.

9.2.43. Synthesis of *4H*-cyclopenta[2,1-*b*:3,4-*b*']dithiophene (117)

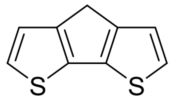

116 (2.47 g, 12.84 mmol), potassium hydroxide (2.47 g, 44.02 mmol) and hydrazine hydrate (15 mL, 64%) combined in a flask. The system evacuated and refilled with argon for three cycles before triethylene glycol (247 mL) added and heated at 180 °C for 17h. The flask cooled to RT and deionised H_2O added and the product extracted with diethyl ether. The organic layer washed with NH_4Cl solution. The organic layer dried over $MgSO_4$, filtered and the solvent concentrated to obtain the product. It purified *via* chromatography with petroleum ether to afford **117** as white crystals (1.83 g, 10 mmol, 80% yield)[39].

^{1}H NMR ($CDCl_3$, δ): 7.20 (d, 2H, *J* = 5.0 Hz), 7.11 (d, 2H, *J* = 5.0 Hz), 3.56 (s, 2H). ^{13}C NMR ($CDCl_3$, δ): 149.7, 138.7, 124.5, 123.0, 31.8. FT-IR (cm^{-1}): 3095, 3077, 2897, 2765, 1481, 1389, 1251, 1159, 1088. EI-MS (*m/z*): 178.0 $[M]^+$. EA (%) calculated for $C_9H_6S_2$: C, 60.64; H, 3.39; S, 35.97. Found: C, 60.46; H, 3.39; S, 35.95.

9.2.44. Synthesis of 4,4-bis(2-ethylhexyl)cyclopenta[2,1-*b*:3,4-*b*']dithiophene (118)

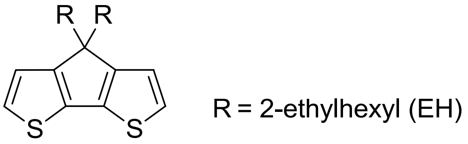

117 (0.25 g, 1.40 mmol), 2-ethylhexyl bromide (0.65 g, 3.36 mmol) and NaI (0.02 g, 0.13 mmol) combined in a flask. The system purged with three vacuum/argon cycles before anhydrous DMSO (8.5 mL) added and cooled to 0 °C. To this mixture, potassium hydroxide (0.31 g, 5.61 mmol) added and stirred for 17h at RT. Deionised H_2O added to the mixture and extracted with *n*-hexane. The organic phase separated, dried over anhydrous $MgSO_4$ and filtered. The solvent evaporated to obtain the product. It purified using chromatography with petroleum ether to afford **118** as yellow oil (0.50 g, 1 mmol, 89% yield)[40].

^1H NMR ($CDCl_3$, δ): 7.13 (d, 2H, *J* = 5.0 Hz), 6.96-6.92 (m, 2H), 1.96-1.82 (m, 4H), 1.10-0.83 (m, 18H), 0.77 (t, 6H, *J* = 7.0 Hz), 0.60 (t, 6H, *J* = 7.0 Hz). ^{13}C NMR ($CDCl_3$, δ): 157.6 (t, *J* = 4.0 Hz), 136.8, 124.0, 122.3 (t, 6H, *J* = 4.0 Hz), 53.2, 43.2, 35.0, 34.1, 28.6, 27.3, 22.7, 14.1, 10.6. FT-IR (cm^{-1}): 2953, 2921, 2858, 1460, 1379, 1081. EI-MS (*m/z*): 402.2 $[M]^+$. EA (%) calculated for $C_{25}H_{38}S_2$: C, 74.57; H, 9.51; S, 15.92. Found: C, 74.20; H, 9.14; S, 15.38.

9.2.45. Synthesis of 4,4-dioctylcyclopenta[2,1-*b*:3,4-*b*']dithiophene (119)

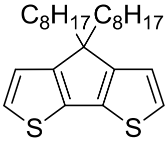

119 prepared followed by the same procedure for synthesis of **118**.

117 (0.65 g, 3.64 mmol), 1-bromooctane (**85**) (1.25 mL, 8.22 mmol), potassium iodide (0.06 g, 0.38 mmol), anhydrous DMSO (20 mL) and potassium hydroxide (0.81 g, 14.43 mmol). **119** was obtained as a yellow oil (1.33 g, 3 mmol, 91% yield)[40].

^1H NMR ($CDCl_3$, δ): 7.16 (d, 2H, *J* = 5.0 Hz,); 6.95 (d, 2H, *J* = 5.0 Hz,), 1.93-1.80 (m, 4H), 1.37-1.09 (m, 20H), 1.04-0.91 (m, 4H), 0.87 (t, 6H, *J* = 7.0 Hz,).^{13}C NMR ($CDCl_3$, δ): 158.1, 136.5, 124.4, 121.7, 53.3, 37.7, 31.8, 30.0, 29.4, 29.3, 24.5, 22.6, 14.1. FT-IR (cm^{-1}): 2957, 2921, 2850, 1457, 1379, 1081. EI-MS (*m/z*): 402.2 [M]$^+$. EA (%) calculated for $C_{25}H_{38}S_2$: C, 74.57; H, 9.51; S, 15.92. Found: C, 72.96; H, 9.20; S, 14.56.

9.2.46. Synthesis of 4,4-bis(2-ethylhexyl)-2,6-dibromocyclopenta[2,1-*b*:3,4-*b*']dithiophene (120)

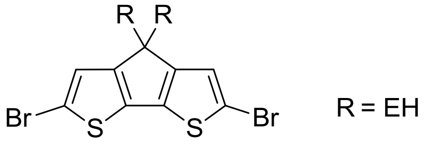

118 (1.07 g, 2.65 mmol) dissolved in DMF (25 mL) in a flask. To this mixture, NBS (0.94 g, 5.28 mmol) added and stirred at RT for 18h in the dark. Deionised water added to the mixture and extracted with Et_2O. The organic phase washed with deionised H_2O until the mixture became neutral. The organic layer separated, dried over $MgSO_4$ and filtered. The solvent concentrated to obtain the product. It purified using chromatography with petroleum ether to afford **120** as yellow oil (1.30 g, 2 mmol, 88% yield)[41].

^{1}H NMR ($CDCl_3$, δ): 6.95 (t, 2H, *J* = 3.5 Hz), 1.92-1.75 (m, 4H), 1.13-0.84 (m, 18H), 0.80 (t, 6H, *J* = 7.0 Hz), 0.64 (t, 6H, *J* = 7.5 Hz). ^{13}C NMR ($CDCl_3$, δ): 155.5 (t, *J* = 6.5 Hz), 136.6 (t, *J* = 3.5 Hz), 125.2 (t, *J* = 10.5 Hz), 110.7 (t, *J* = 5.0 Hz), 55.0, 43.0, 35.1, 34.0, 28.5, 27.4, 22.8, 14.1, 10.7. FT-IR (cm^{-1}): 2952, 2921, 2853, 1455, 1366, 1174. EI-MS (*m/z*): 560.1 [M]$^+$. EA (%) calculated for $C_{25}H_{36}Br_2S_2$: C, 53.57; H, 6.47; S, 11.44; Br, 28.51. Found: C, 53.44; H, 6.27; S, 11.50; Br, 28.41.

9.2.47. Synthesis of 4,4-dioctyl-2,6-dibromocyclopenta[2,1-*b*:3,4-*b*']dithiophene (121)

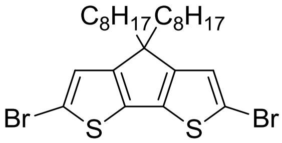

121 prepared followed by the same procedure for synthesis of **120**.

119 (1.23 g, 3.05 mmol), DMF (30 mL) and NBS (1.08 g, 6.06 mmol). **121** was obtained as a green oil (1.48 g, 3 mmol, 87% yield)[41].

^{1}H NMR ($CDCl_3$, δ): 6.94 (s, 2H), 1.82-1.71 (m, 4H), 1.36-1.10 (m, 20H), 0.97-0.89 (m, 4H), 0.87 (t, 6H, *J* = 7.0 Hz). ^{13}C NMR ($CDCl_3$, δ): 156.0, 136.3, 124.6, 111.1, 55.0, 37.5, 31.8, 30.0, 29.3, 29.3, 24.4, 22.6, 14.1. FT-IR (cm^{-1}): 2926, 2855, 1457, 1368. EI-MS (*m/z*): 560 $[M]^+$. EA (%) calculated for $C_{25}H_{36}Br_2S_2$: C, 53.57; H, 6.47; S, 11.44; Br, 28.51. Found: C, 54.00; H, 6.42; S, 11.19; Br, 26.83.

9.2.48. Synthesis of 4,4-bis(2-ethylhexyl)-2,6-bis(4,4,5,5-tetramethyl-1,3,2-dioxaboralan-2-yl)cyclopenta[2,1-*b*:3,4-*b*']dithiophene (122)

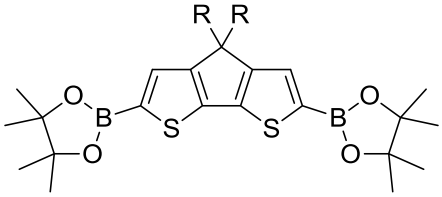

R = EH

122 was prepared followed by the same procedure for synthesis of **72**.

120 (0.38 g, 0.67 mmol), potassium acetate (0.39 g, 3.97 mmol), bis(pinacolato)diboron (0.51 g, 2.00 mmol), Pd(dppf)Cl_2 and anhydrous DMF (10 mL). **122** was obtained as red sticky oil (0.25 g, 0.4 mmol, 57% yield)[42].

^{1}H NMR ($CDCl_3$, δ): 7.46 (t, 2H, *J* = 6.5 Hz), 1.96-1.78 (m, 4H), 1.36 (s, 24H), 1.10-0.81 (m, 18H), 0.79-0.71 (m, 6H), 0.69-0.55 (m, 6H). ^{13}C NMR ($CDCl_3$, δ): 161.0, 144.1, 131.9, 84.2, 52.7, 43.4, 35.1, 34.1, 31.8, 28.5, 27.3, 25.0, 24.8, 22.8, 14.1, 10.6. FT-IR (cm^{-1}): 2962, 2923, 2862, 1375, 1264, 1139, 1121. EI-MS (*m/z*): 654.4 $[M]^+$. EA (%) calculated for $C_{37}H_{60}B_2O_4S_2$: C, 67.89; H, 9.24; S, 9.79. Found: C, 66.36; H, 8.92; S, 7.78.

9.2.49. Synthesis of 3,3',5,5'-tetrabromo-2,2'-bithiophene (138)

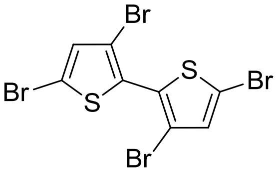

2,2'-Bithiophene (**33**) (1.81 g, 10.88 mmol) dissolved in glacial acetic acid (36 mL) and chloroform (27 mL) in a flask and cooled to 0 °C. To this mixture, bromine (1.20 mL, 23.27 mmol) in chloroform (22 mL) added dropwise during 1.5h. Second portion of bromine (1.20 mL, 23.27 mmol) in chloroform (22 mL) was added at RT over 1h. The mixture stirred overnight and refluxed for 24h. The reaction contents cooled to RT and the solvent removed to obtain the product which purified using recrystallisation from EtOH to afford **138** as green crystals (3.95 g, 8 mmol, 75% yield)[43].

^{1}H NMR ($CDCl_3$, δ): 7.07 (s, 2H). ^{13}C NMR ($CDCl_3$, δ): 133.0, 129.6, 114.8, 112.1. FT-IR (cm^{-1}): 3088, 1481, 1389, 1290, 1130. EI-MS (*m/z*): 481.6 $[M]^+$. EA (%) calculated for $C_8H_2Br_4S_2$: C, 19.94; H, 0.42; S, 13.31; Br, 66.33. Found: C, 19.91; H, 0.53; S, 13.27; Br, 66.43.

9.2.50. Synthesis of 3,3'-dibromo-2,2'-bithiophene (139)

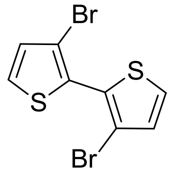

138 (3.75 g, 7.78 mmol) added to the refluxing mixture of zinc powder (1.96 g, 29.97 mmol) in ethanol (39 mL), deionised water (3.9 mL), glacial acetic acid (9.3 mL) and HCl (0.8 mL, 3.0 M) in a flask during 30 minutes. The reaction contents refluxed for 2h. The flask cooled to RT and filtered and the excess of zinc washed three times with ethanol. Deionised water added to the filtrate and extracted with diethyl ether. The organic phase washed with deionised H_2O, dried over $MgSO_4$ and the solvent evaporated to obtain the product. It purified *via* recrystallisation from *n*-hexane to afford **139** as white crystals (1.73 g, 5 mmol, 69% yield)[44].

^1H NMR ($CDCl_3$, δ): 7.43 (d, 2H, *J* = 5.5 Hz), 7.10 (d, 2H, *J* = 5.5 Hz). ^{13}C NMR ($CDCl_3$, δ): 130.8, 128.9, 127.5, 112.7. FT-IR (cm^{-1}): 3102, 3081, 1747, 1552, 1485, 1332, 1130, 1073. EI-MS (*m/z*): 323.8 $[M]^+$. EA (%) calculated for $C_8H_4Br_2S_2$: C, 29.65; H, 1.24; S, 19.79; Br, 49.32. Found: C, 29.70; H, 1.34; S, 19.89; Br, 48.37.

9.2.51. Synthesis of 4,4-dioctyl-dithieno[3,2-*b*:2',3'-*d*]silole (140)

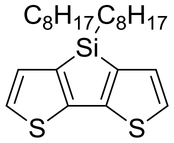

A flask purged with three vacuum/argon cycles. *n*-BuLi (9.76 mL, 24.4 mmol) added to anhydrous Et_2O (120 mL) and the mixture cooled to –78 °C. To this solution, **139** (3.97 g, 12.25 mmol) was dissolve in anhydrous THF (40 mL) added dropwise over 30 minutes with vigorous stirring and the mixture stirred at –78 °C for 3h. To this mixture, di-*n*-octyldichlorosilane (4.24 mL, 12.19 mmol) dissolved in anhydrous THF (80 mL) and added dropwise at –78 °C and stirred for 5h. Subsequently, the reaction contents stirred at RT overnight. NH_4Cl solution added to the reaction mixture, extracted with Et_2O. The organic phase washed with deionised H_2O and NaCl solution. The organic phase dried over $MgSO_4$ and the solvent was evaporated to obtain the product. It purified *via* chromatography with petroleum ether to afford **140** as yellow oil (3.10 g, 7 mmol, 60% yield)[45].

^{1}H NMR ($CDCl_3$, δ): 7.21 (d, 2H, J = 4.5 Hz), 7.07 (d, 2H, J = 4.5 Hz), 1.47–1.35 (m, 4H), 1.34–1.17 (m, 20H), 0.98–0.84 (m, 10H). ^{13}C NMR ($CDCl_3$, δ): 149.2, 141.6, 129.6, 124.9, 33.1, 31.9, 29.2, 29.2, 24.2, 22.6, 14.1, 11.9. FT-IR (cm^{-1}): 3063, 2953, 2918, 2854, 1460, 1375, 1251, 1173, 1084. EI-MS (*m/z*): 418.2 $[M]^+$. EA (%) calculated for $C_{24}H_{38}S_2Si$: C, 68.84; H, 9.15; S, 15.31. Found: C, 69.08; H, 8.96; S, 14.11.

9.2.52. Synthesis of 4,4-dioctyl-2,6-dibromo-dithieno[3,2-*b*:2',3'-*d*]silole (141)

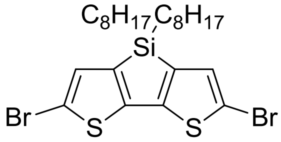

140 (0.84 g, 2.00 mmol) dissolved in DMF (20 mL) in a flask. To this mixture, NBS (0.87 g, 4.88 mmol) added and stirred at RT for 10 minutes in the dark. Deionised water added, extracted with $CHCl_3$ and the organic phase washed with deionised H_2O. The collected organic layers dried over $MgSO_4$, filtered and the solvent concentrated to obtain the product. It purified using chromatography with petroleum ether to afford **141** as yellow oil (0.65 g, 1 mmol, 56% yield)[46].

^{1}H NMR ($CDCl_3$, δ): 7.01 (s, 2H), 1.40–1.19 (m, 24H), 0.92–0.84 (m, 10H). ^{13}C NMR ($CDCl_3$, δ): 148.9, 141.0, 132.2, 111.4, 33.1, 31.8, 29.2, 29.1, 24.0, 22.7, 14.1, 11.6. FT-IR (cm^{-1}): 3081, 2957, 2914, 2843, 1684, 1460, 1375, 1247, 1166, 1006. EI-MS (*m/z*): 576.0 $[M]^+$. EA (%) calculated for $C_{24}H_{36}Br_2S_2Si$: C, 50.00; H, 6.29; S, 11.12, Br, 27.72. Found: C, 50.05; H, 6.37; S, 11.87; Br, 28.80.

9.2.53. Synthesis of 4,4-dioctyl-2,6-bis(trimethylstannyl)-dithieno[3,2-*b*:2',3'-*d*]silole (142)

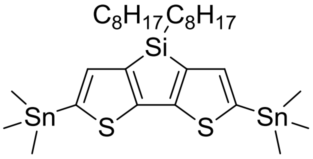

In a flask, **140** (0.25 g, 0.59 mmol) added and the system degassed under argon. Anhydrous *n*-hexane (7 mL) and tetramethylethylenediamine (0.26 mL, 1.73 mmol) added and cooled to –78 °C. To this solution, *n*-BuLi (0.59 mL, 1.49 mmol) added dropwise during 5 minutes and stirred for 3h. Trimethyltin chloride (0.31 g, 1.55 mmol) added quickly. The reaction stirred for 3h and then stirred at RT overnight. The mixture put into deionised H_2O and extracted with Et_2O. The combined organic phase washed with brine solution and organic phase dried over $MgSO_4$, filtered and the solvent evaporated to obtain the **142** as green sticky oil (0.36 g, 0. 5 mmol, 81% yield)[47].

^1H NMR ($CDCl_3$, δ): 7.10 (s, 2H), 1.38–1.48 (m, 4H), 1.20–1.37 (m, 20H), 0.84–0.96 (m, 10H), 0.40 (s, 18H). ^{13}C NMR ($CDCl_3$, δ): 155.0, 143.1, 137.7, 125.0, 33.2, 31.9, 29.3, 29.2, 24.3, 22.7, 14.1, 12.0, -8.0. FT-IR (cm^{-1}): 2957, 2921, 2854, 1457, 1379, 1254, 1176, 1077. EI-MS (*m/z*): 744.2 $[M]^+$. EA (%) calculated for $C_{30}H_{54}S_2SiSn_2$: C, 48.41; H, 7.31; S, 8.61. Found: C, 52.44; H, 7.89; S, 9.70.

9.3. Other Monomers Used

9.3.1. 9,9-Dioctylfluorene-2,7-diboronic acid bis(1,3-propanediol) ester (75)

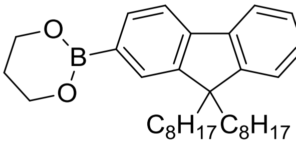

75 purchased from supplier.

9.3.2. 9-(Heptadecan-9-yl)-2,7-bis(4,4,5,5-tetramethyl-1,3,2-dioxaborolan-2-yl)carbazole (103)

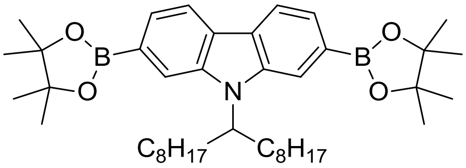

103 prepared by H. Yi in Iraqi group[31].

9.3.3. 9,10-Bis(4-(dodecyloxy)phenyl)-2,6-bis(4,4,5,5-tetramethyl-1,3,2-dioxaborolan-2-yl)anthracene (108)

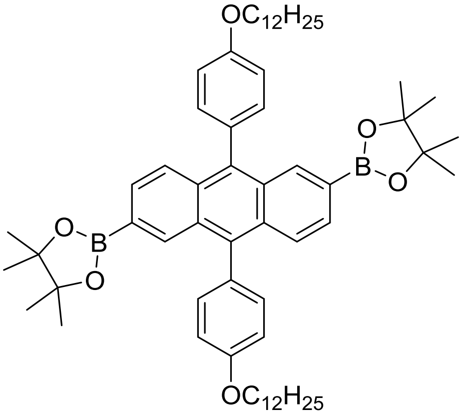

108 prepared by M. Almeataq in Iraqi group[48].

9.4. Synthetic procedures for the polymers

9.4.1. Synthesis of poly[2,2'-bithiophene-*alt*-(3',6'-bis(2-undecanyl)phthalate)] (35)

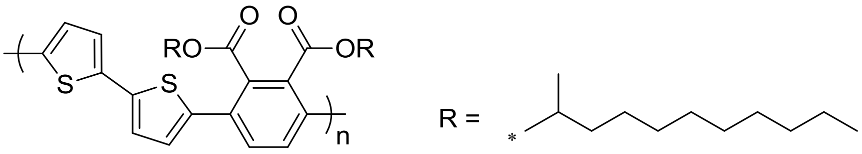

6 (400 mg, 0.60 mmol), **34** (290 mg, 0.60 mmol), $Pd_2(dba)_3$ (27.47 mg, 0.02 mmol) and $P(o\text{-tol})_3$ (54.78 mg, 0.18 mmol) added to a flask and degassed under argon. Anhydrous toluene (10 mL) added and the system degassed again and heated at 100 °C for 48h. The reaction contents cooled to RT and dissolved in chloroform (300 mL). NH_4OH solution (50 mL, 35% in H_2O) added and the mixture stirred overnight. The organic phase separated and washed with deionised H_2O. The organic phase reduced to around (50 mL) and put into methanol (300 mL) and stirred overnight. The mixture filtered and the polymer was cleaned using Soxhlet extraction with methanol (300 mL), acetone (300 mL) and hexane (300 mL). The hexane fraction concentrated to around (50 mL) and then put into methanol (300 mL). The mixture stirred overnight and the pure polymer recovered by filtration to obtain **35** as green powder (150 mg, 0.23 mmol, 39% yield)[49].

GPC: hexane fraction, M_n = 9600 g mol^{-1}, M_w = 13500 g mol^{-1}, PDI = 1.3 and Dp = 15. ^{1}H NMR (hexane fraction) ($CDCl_3$, δ): 7.55 (s, 2H), 7.13 (t, 2H, J = 4.0 Hz), 7.05 (d, 2H, J = 3.5 Hz), 5.11-4.90 (m, 2H), 1.70-1.47 (m, 4H), 1.45-1.34 (m, 2H), 1.32-1.08 (m, 32H), 0.96-0.82 (m, 6H). FT-IR (cm^{-1}): 3065, 2920, 2851, 1715, 1463, 1379, 1246, 1116, 1062. EA (%) calculated for $C_{38}H_{52}O_4S_2$: C, 71.66; H, 8.23; S, 10.07. Found: C, 68.28; H, 7.39; S, 12.90.

9.4.2. Synthesis of poly[2,2'-bithiophene-*alt*-5,5-(3',6'-bis(2-thienyl)-bis(2-undecanyl)phthalate)] (36)

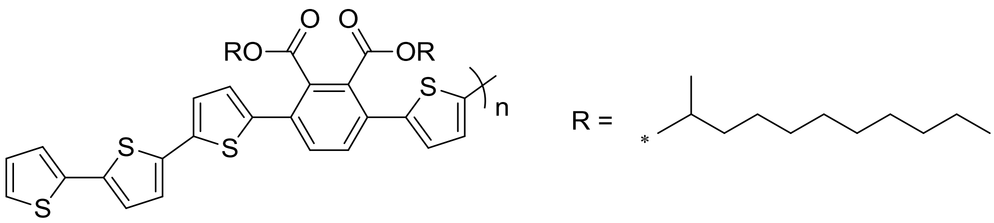

36 was prepared followed by the same procedure for synthesis of **35**.

8 (180 mg, 0.225 mmol), **34** (110 mg, 0.225 mmol), Pd(OAc)$_2$ (3.7 mg, 0.016 mmol), P(*o*-tol)$_3$ (10 mg, 0.032 mmol) and anhydrous toluene (10 mL). **36** was obtained as red powders (154 mg, 0.19 mmol, 87% yield)[49].

GPC: toluene fraction, M_n = 9500 g mol^{-1}, M_w = 14300 g mol^{-1}, PDI = 1.5 and Dp = 12. ^{1}H NMR (toluene fraction) ($C_2D_2Cl_4$, δ): 7.48 (s, 2H), 7.13-7.01 (bm, 6H), 6.99-6.91 (bm, 2H), 4.94-4.78 (bm, 2H), 1.47- 1.36 (m, 4H), 1.34-1.26 (bm, 4H), 1.22-0.98 (bm, 26H), 0.82-0.70 (bm, 6H). FT-IR (cm^{-1}): 3063, 2918, 2850, 1715, 1464, 1375, 1240, 1120, 1063. EA (%) calculated for $C_{46}H_{56}O_4S_4$: C, 68.96; H, 7.05; S, 16.01. Found: C, 67.76; H, 6.86; S, 15.45.

9.4.3. Synthesis of poly[9,9-dimethyl-2,7-fluorene-*alt*-5,5-(3',6'-bis(2-thienyl)-bis(2-undecanyl)phthalate)] (37)

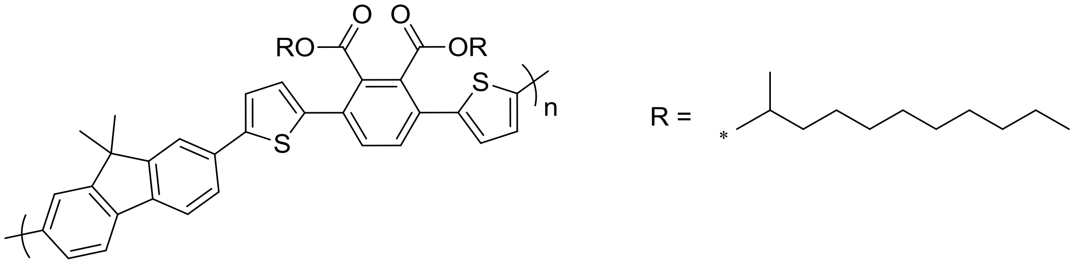

37 was prepared followed by the same procedure for synthesis of **35**.

8 (180 mg, 0.225 mmol), **29** (116 mg, 0.225 mmol), Pd(OAc)$_2$ (3.7 mg, 0.016 mmol), P(*o*-tol)$_3$ (10.22 mg, 0.03 mmol) and anhydrous toluene (6 mL). **37** was obtained as green powders (134 mg, 0.14 mmol, 64% yield)[49].

GPC: hexane fraction, M_n = 16400 g mol^{-1}, M_w = 30300 g mol^{-1}, PDI = 1.8 and Dp = 20. ^{1}H NMR (hexane fraction) ($CDCl_3$, δ): 7.76-7.61 (bm, 6H), 7.36 (bs, 2H), 7.15 (bs, 2H), 5.07-4.94 (bm, 2H), 1.70-1.48 (bm, 12H), 1.47-1.06 (bm, 34H), 0.93-0.79 (bm, 6H). FT-IR (cm^{-1}): 2921, 2854, 1719, 1460, 1375, 1293, 1116, 1063. EA (%) calculated for $C_{53}H_{64}O_4S_2$: C, 76.77; H, 7.78; S, 7.73. Found: C, 76.40; H, 7.65; S, 7.61.

9.4.4. Synthesis of poly[9,9-dioctyl-2,7-fluorene-*alt*-5,5-(4',7'-bis(2-thienyl)-2',1',3'-benzothiadiazole-5,6-*N*-(3,7-dimethyloctyl)dicarboxylic imide)] (76)

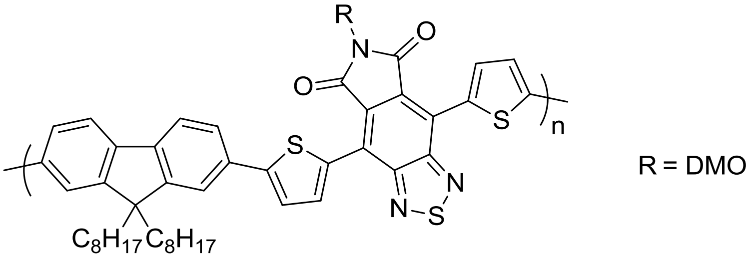

75 (125.4 mg, 0.224 mmol) and **49** (150 mg, 0.224 mmol) added to a flask and degassed under argon. Anhydrous THF (10 mL) followed by sodium hydrogen carbonate solution (2.5 mL, 5% wt, degassed) added and the system degassed again. To this mixture, $Pd(OAc)_2$ (3.7 mg, 0.0168 mmol) and $P(o\text{-tol})_3$ (10.2 mg, 0.0336 mmol) added, degassed and heated at 90 °C for 30 h. The flask cooled to RT, the polymer dissolved in $CHCl_3$ (200 mL) and an NH_4OH solution (50 mL, 35% in H_2O) added and the mixture stirred overnight. The organic phase separated and washed with deionised H_2O. The organic phase concentrated to around (50 mL) and put into methanol (300 mL) and stirred overnight. The mixture filtered and the polymer cleaned using Soxhlet extraction with methanol (300 mL), acetone (300 mL), hexane (300 mL) and then toluene (300 mL). The toluene fraction concentrated to around (50 mL) and then put into methanol (300 mL). The mixture stirred overnight and the pure polymer recovered by filtration to afford **76** as purple powders (170 mg, 0.18 mmol, 85% yield)[50].

GPC: toluene fraction, M_n = 16000 g mol^{-1}, M_w = 33000 g mol^{-1}, PDI = 2.0 and Dp = 18. ^1H NMR (toluene fraction) ($C_2D_2Cl_4$, δ): 8.02 (d, 2H, J = 3.5 Hz), 7.81-7.68 (bm, 6H), 7.52 (d, 2H, J = 3.5 Hz), 3.90-3.68 (bm, 2H), 2.20-1.99 (bm, 4H), 1.83-1.68 (bm, 1H), 1.61-1.47 (bm, 3H), 1.42-1.34 (bs, 6H), 1.23-1.04 (bm, 24H), 0.99 (d, 3H, J = 6.0 Hz), 0.86 (d, 6H, J = 6.5 Hz), 0.78 (t, 6H, J = 7.0 Hz). FT-IR (cm^{-1}): 2921, 2854, 1754, 1698, 1549, 1364, 1173, 1070. EA (%) calculated for $C_{55}H_{65}N_3O_2S_3$: C, 73.70; H, 7.31; N, 4.69; S, 10.73. Found: C, 72.52; H, 7.02; N, 4.60; S, 9.38.

9.4.5. Synthesis of poly[9,9-dioctyl-2,7-fluorene-*alt*-5,5-(4',7'-bis(2-thienyl)-2',1',3'-benzothiadiazole-5,6-*N*-octyl-dicarboxylic imide)] (77)

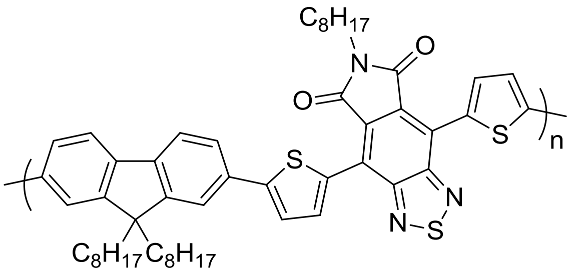

77 was prepared followed by the same procedure for synthesis of **76**.

75 (125.4 mg, 0.224 mmol) and **50** (143.2 mg, 0.224 mmol) were copolymerised for 24 h to afford **77** as purple powders. Toluene fraction (36 mg, 0.04 mmol, 18% yield), chloroform fraction (120 mg, 0.13 mmol, 60% yield) with total yield 78%[50].

GPC: toluene fraction M_n = 11200 g mol^{-1}, M_w = 29100 g mol^{-1}, PDI = 2.5 and Dp = 13; chloroform fraction, M_n = 24900 g mol^{-1}, M_w = 74400 g mol^{-1}, PDI = 2.9 and Dp = 29. ^{1}H NMR (toluene fraction) ($C_2D_2Cl_4$, δ): 8.02 (d, 2H, J = 3.5 Hz), 7.81-7.68 (bm, 6H), 7.52 (d, 2H, J = 3.5 Hz), 3.90-3.68 (bm, 2H), 2.20-1.99 (bm, 4H), 1.81-1.71 (bm, 2H), 1.44-1.24 (bm, 10H), 1.23-1.04 (bm, 24H), 0.88 (t, 3H, J = 7.0 Hz), 0.82-0.77 (bm, 6H). FT-IR (cm^{-1}): 2921, 2850, 1754, 1701, 1552, 1400, 1361, 1254, 1166, 1098. EA (%) calculated for $C_{53}H_{61}N_3O_2S_3$: C, 73.32; H, 7.08; N, 4.84; S, 11.08. Found: C, 72.70; H, 7.02; N, 4.77; S, 10.51.

9.4.6. Synthesis of poly[9,9-dioctyl-2,7-dibenzosilole-*alt*-5,5-(4',7'-bis(2-thienyl)-2',1',3'-benzothiadiazole-5,6-*N*-(3,7-dimethyloctyl)dicarboxylic imide)] (78)

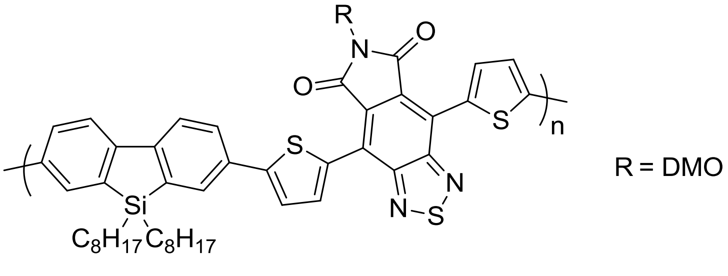

78 was prepared followed by the same procedure for synthesis of **76**.

72 (147.5 mg, 0.224 mmol) and **49** (150 mg, 0.224 mmol) were copolymerised for 21 h to afford **78** as purple powders. Toluene fraction (50 mg, 0.05 mmol, 22% yield), chloroform fraction (95 mg, 0.10 mmol, 46% yield) with total yield 68%[50].

GPC: toluene fraction, M_n = 9400 g mol^{-1}, M_w = 19400 g mol^{-1}, PDI = 2.0 and Dp = 10; chloroform fraction, M_n = 20000 g mol^{-1}, M_w = 44900 g mol^{-1}, PDI = 2.2 and Dp = 22. ^{1}H NMR (toluene fraction) ($C_2D_2Cl_4$, δ): 8.02 (d, 2H, *J* = 3.5 Hz), 7.96 (s, 2H), 7.87 (d, 2H, *J* = 11.0 Hz), 7.80 (d, 2H, *J* = 8.0 Hz), 7.50 (d, 2H, *J* = 3.0 Hz), 3.90-3.68 (bm, 2H), 1.89-1.67 (bm, 1H), 1.62-1.29 (bm, 9H), 1.28-1.12 (bm, 24H), 1.12-1.03 (bm, 4H), 1.03-0.95 (bm, 3H), 0.86 (d, 6H, *J* = 6.5 Hz), 0.84-0.79 (bm, 6H). FT-IR (cm^{-1}): 2953, 2918, 2850, 1754, 1698, 1556, 1432, 1364, 1254, 1173, 1063. EA (%) calculated for $C_{54}H_{65}N_3O_2S_3Si$: C, 71.09; H, 7.18; N, 4.61; S, 10.54. Found: C, 69.43; H, 7.00; N, 4.36; S, 10.08.

9.4.7. Synthesis of poly[9,9-dioctyl-2,7-dibenzosilole-*alt*-5,5-(4',7'-bis(2-thienyl)-2',1',3'-benzothiadiazole-5,6-*N*-octyl-dicarboxylic imide)] (79)

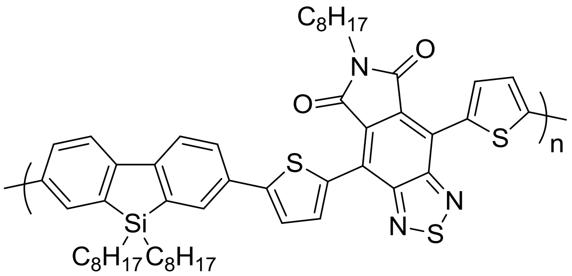

79 was prepared followed by the same procedure for synthesis of **76**.

72 (147.5 mg, 0.224 mmol) and **50** (143.2 mg, 0.224 mmol) were copolymerised for 22 h to afford **79** as purple powders. Toluene fraction (66 mg, 0.07 mmol, 33% yield), chloroform fraction (52 mg, 0.05 mmol, 26% yield) with total yield 59%[50].

GPC: toluene fraction, M_n = 10000 g mol^{-1}, M_w = 26200 g mol^{-1}, PDI = 2.6 and Dp = 11; chloroform fraction, M_n = 16100 g mol^{-1}, M_w = 38700 g mol^{-1}, PDI = 2.4 and Dp = 18. ^{1}H NMR (toluene fraction) ($C_2D_2Cl_4$, δ): 8.02 (d, 2H, *J* = 3.5 Hz), 7.96 (s, 2H), 7.87 (d, 2H, *J* = 11.0 Hz), 7.80 (d, 2H, *J* = 8.0 Hz), 7.50 (d, 2H, *J* = 3.0 Hz), 3.90-3.68 (bm, 2H), 1.81-1.69 (bm, 2H), 1.53-1.15 (bm, 34H), 1.12-1.03 (bm, 4H), 0.88 (t, 3H, *J* = 6.5 Hz), 0.85-0.80 (bm, 6H). FT-IR (cm^{-1}): 2950, 2921, 2854, 1758, 1701, 1556, 1428, 1364, 1254, 1166, 1003. EA (%) calculated for $C_{52}H_{61}N_3O_2S_3Si$: C, 70.63; H, 6.95; N, 4.75; S, 10.88. Found: C, 69.92; H, 6.85; N, 4.60; S, 10.22.

9.4.8. Synthesis of poly[*N*-9'-heptadecanyl-2,7-carbazole-*alt*-5,5-(4',7'-bis(2-thienyl)-2',1',3'-benzothiadiazole-5,6-*N*-(3,7-dimethyloctyl)-dicarboxylic imide)] (104)

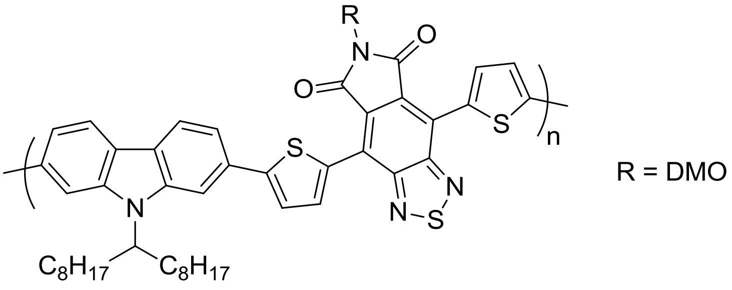

104 was prepared followed by the same procedure for synthesis of **76**.

103 (147 mg, 0.224 mmol) and **49** (150 mg, 0.224 mmol) were copolymerised for 30h to afford **104** as purple powders (150 mg, 0.16 mmol, 73% yield)[50].

GPC: toluene fraction, M_n = 12200 g mol^{-1}, M_w = 30400 g mol^{-1}, PDI = 2.4 and Dp = 13. ^{1}H NMR (toluene fraction) ($C_2D_2Cl_4$, δ): 8.12 (d, 2H, *J* = 8.0 Hz), 8.08 (s, 2H), 7.89-7.79 (bm, 2H), 7.63 (d, 2H, *J* = 8.0 Hz), 7.56 (s, 2H), 4.78-4.61 (bm, 1H), 3.90-3.72 (bm, 2H), 2.48-2.30 (bm, 2H), 2.16-2.00 (bm, 2H), 1.85-1.72 (bm, 1H), 1.66-1.48 (bm, 3H), 1.42-1.27 (bm, 6H), 1.24-1.13 (bm, 24H), 1.02 (d, 3H, *J* = 6.0 Hz), 0.88 (d, 6H, *J* = 6.0 Hz), 0.80 (t, 6H, *J* = 6.0 Hz). FT-IR (cm^{-1}): 2950, 2925, 2854, 1754, 1701, 1598, 1425, 1336, 1219, 1176, 1066. EA (%) calculated for $C_{55}H_{66}N_4O_2S_3$: C, 72.49; H, 7.30; N, 6.15; S, 10.55. Found: C, 70.83; H, 6.98; N, 5.92; S, 10.38.

9.4.9. Synthesis of poly[*N*-9'-heptadecanyl-2,7-carbazole-*alt*-5,5-(4',7'-bis(2-thienyl)-2',1',3'-benzothiadiazole-5,6-*N*-octyl-dicarboxylic imide)] (105)

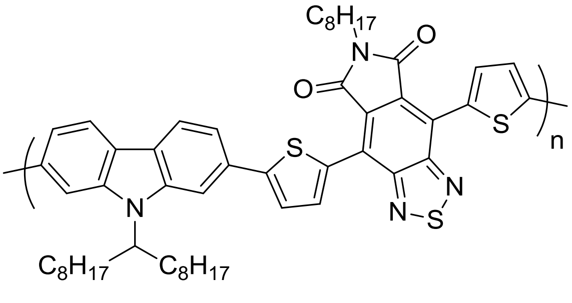

105 was prepared followed by the same procedure for synthesis of **76**.

103 (147 mg, 0.224 mmol) and **50** (143.2 mg, 0.224 mmol) were copolymerised for 24h to afford **105** as purple powders (170 mg, 0.19 mmol, 86% yield).[50]

GPC: chloroform fraction, M_n = 20500 g mol^{-1}, M_w = 65300 g mol^{-1}, PDI = 3.1 and Dp = 23. ^{1}H NMR (chloroform fraction) ($C_2D_2Cl_4$, δ): 8.12 (d, 2H, J = 8.0 Hz), 8.08 (s, 2H), 7.89-7.79 (bm, 2H,), 7.63 (d, 2H, J = 8.0 Hz), 7.56 (d, 2H, J = 3.5 Hz), 4.78-4.61 (bm, 1H), 3.90-3.72 (bm, 2H), 2.48-2.30 (bm, 2H), 2.16-2.00 (bm, 2H), 1.82-1.68 (bm, 2H), 1.45-1.25 (bm, 10H), 1.24-1.11 (bm, 24H), 0.88 (t, 3H, J = 7.0 Hz), 0.80 (t, 6H, J = 7.0 Hz). FT-IR (cm^{-1}): 2921, 2854, 1758, 1701, 1598, 1428, 1336, 1219, 1166, 1095. EA (%) calculated for $C_{53}H_{62}N_4O_2S_3$: C, 72.07; H, 7.08; N, 6.34; S, 10.89. Found: C, 70.92; H, 6.96; N, 6.15; S, 10.11.

9.4.10. Synthesis of poly[*N*-9'-heptadecanyl-3,6-difluoro-2,7-carbazole-*alt*-5,5-(4',7'-bis(2-thienyl)-2',1',3'-benzothiadiazole-5,6-*N*-(3,7-dimethyloctyl)dicarboxylic imide)] (106)

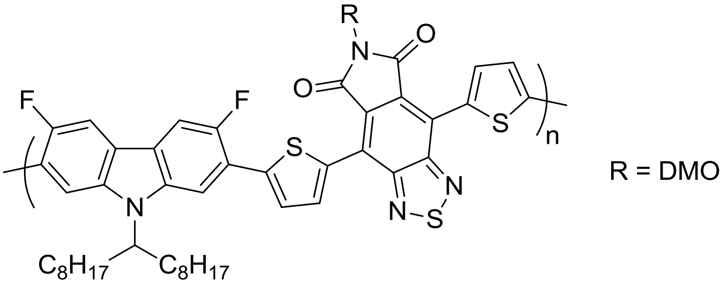

106 was prepared followed by the same procedure for synthesis of **76**.

89 (155.8 mg, 0.224 mmol) and **49** (150 mg, 0.224 mmol) were copolymerised for 48h to yield **106** as purple powders (214 mg, 0.22 mmol, 98% yield)^{50}.

GPC: toluene fraction, M_n = 8700 g mol^{-1}, M_w = 16300 g mol^{-1}, PDI = 1.8 and Dp = 9. ^{1}H NMR (toluene fraction) ($C_2D_2Cl_4$, δ): 8.06 (d, 2H, J = 3.5 Hz), 7.86-7.74 (bm, 4H), 7.67 (d, 2H, J = 3.5 Hz), 4.63-4.50 (bm, 1H), 3.86-3.70 (bm, 2H), 2.38-2.25 (bm, 2H), 2.09-1.93 (bm, 2H), 1.83-1.69 (bm, 1H), 1.62-1.48 (bm, 3H), 1.45-1.23 (bm, 6H), 1.22-1.12 (bm, 24H), 0.99 (d, 3H, J = 6.0 Hz), 0.85 (d, 6H, J = 6.0 Hz), 0.78 (t, 6H, J = 6.0 Hz). FT-IR (cm^{-1}): 2953, 2921, 2854, 1754, 1701, 1556, 1453, 1336, 1176, 1066. EA (%) calculated for $C_{55}H_{64}F_2N_4O_2S_3$: C, 70.19; H, 7.03; N, 5.74; S, 9.86. Found: C, 69.20; H, 6.72; N, 5.79; S, 9.97.

9.4.11. Synthesis of poly[*N*-9'-heptadecanyl-3,6-difluoro-2,7-carbazole-*alt*-5,5-(4',7'-bis(2-thienyl)-2',1',3'-benzothiadiazole-5,6-*N*-octyl-dicarboxylic imide)] (107)

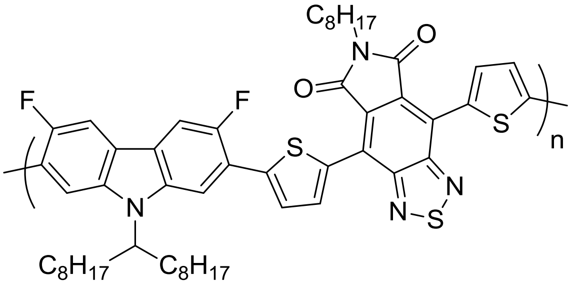

107 was prepared followed by the same procedure for synthesis of **76**.

89 (155.8 mg, 0.224 mmol) and **50** (143.2 mg, 0.224 mmol) were copolymerised for 24h to yield **107** as purple powders. Toluene fraction (90 mg, 0.10 mmol, 44% yield), chloroform fraction (50 mg, 0.05 mmol, 24% yield) with total yield 68%.[50]

GPC: toluene fraction, M_n = 8200 g mol^{-1}, M_w = 18400 g mol^{-1}, PDI = 2.2 and Dp = 9; chloroform fraction, M_n = 24200 g mol^{-1}, M_w = 46300 g mol^{-1}, PDI = 1.9 and Dp = 26. ^{1}H NMR (toluene fraction) ($C_2D_2Cl_4$, δ): 8.06 (d, 2H, *J* = 3.5 Hz), 7.86-7.74 (bm, 4H), 7.67 (d, 2H, *J* = 3.5 Hz), 4.78-4.61 (bm, 1H), 3.90-3.72 (bm, 2H), 2.48-2.30 (bm, 2H), 2.16-2.00 (bm, 2H), 1.82-1.68 (bm, 2H), 1.45-1.25 (bm, 10H), 1.24-1.11 (bm, 24H), 0.88 (t, 3H, *J* = 7.0 Hz), 0.83-0.75 (m, 6H). FT-IR (cm^{-1}): 2921, 2854, 1758, 1698, 1566, 1449, 1166, 1045. EA (%) calculated for $C_{53}H_{60}F_2N_4O_2S_3$: C, 69.25; H, 6.58; N, 6.09; S, 10.46. Found: C, 68.15; H, 6.45; N, 5.85; S, 9.98.

9.4.12. Synthesis of poly[9,10-bis(4-(dodecyloxy)phenyl)-2,6-anthracene-*alt*-5,5-(4',7'-bis(2-thienyl)-2',1',3'-benzothiadiazole-*N*-5,6-(3,7-dimethyloctyl)dicarboxylic imide)] (109)

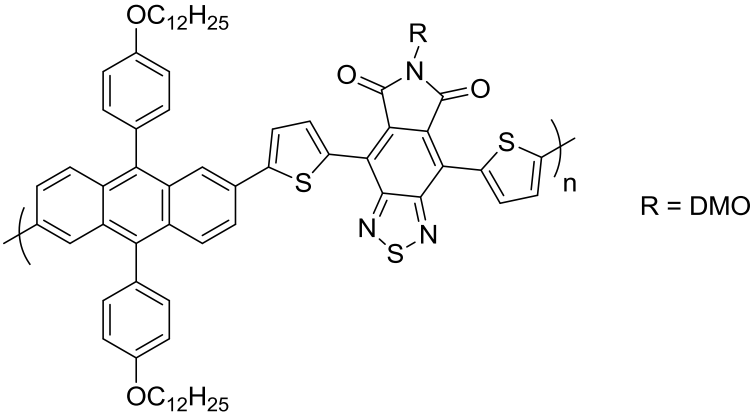

109 was prepared followed by the same procedure for synthesis of **76**.

108 (213.6 mg, 0.224 mmol) and **49** (150 mg, 0.224 mmol) were copolymerised for 23h to afford **109** as purple powders. Toluene fraction (82 mg, 0.07 mmol, 30% yield), chloroform fraction (180 mg, 0.15 mmol, 67% yield) with total yield 97%.[50]

GPC: toluene fraction, M_n = 6700 g mol^{-1}, M_w = 12600 g mol^{-1}, PDI = 1.8 and Dp = 6; chloroform fraction, M_n = 12700 g mol^{-1}, M_w = 22400 g mol^{-1}, PDI = 1.7 and Dp = 11. ^{1}H NMR (toluene fraction) ($C_2D_2Cl_4$, δ): 7.96-7.87 (bm, 2H), 7.71-7.61 (bm, 2H), 7.57-7.50 (bm, 4H), 7.30-7.05 (bm, 10H), 4.18-4.01 (bm, 4H), 3.81-3.61 (bm, 2H), 1.91-1.79 (bm, 4H), 1.78-1.64 (bm, 1H), 1.60-1.46 (bm, 8H), 1.43-1.21 (bm, 34H), 1.20-1.09 (bm, 3H), 1.00-0.90 (bm, 3H), 0.89-0.78 (bm, 12H). FT-IR (cm^{-1}): 2918, 2850, 1754, 1701, 1606, 1570, 1428, 1361, 1240, 1176, 1066. EA (%) calculated for $C_{76}H_{89}N_3O_4S_3$: C, 75.77; H, 7.45; N, 3.49; S, 7.98. Found: C, 73.30; H, 7.15; N, 3.27; S, 7.79.

9.4.13. Synthesis of poly[9,10-bis(4-(dodecyloxy)phenyl)-2,6-anthracene-*alt*-5,5-(4',7'-bis(2-thienyl)-2',1',3'-benzothiadiazole-5,6-*N*-octyl-dicarboxylic imide)] (110)

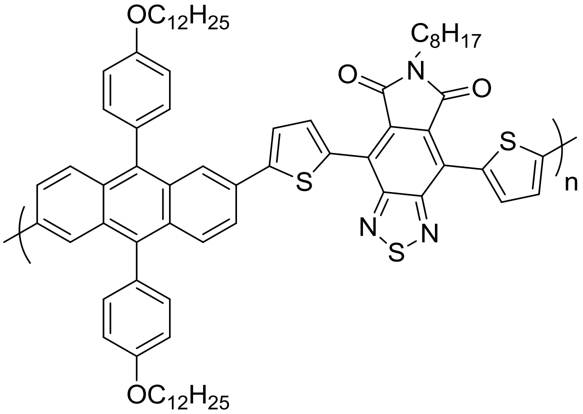

110 was prepared followed by the same procedure for synthesis of **76**.

108 (213.6 mg, 0.224 mmol) and **50** (143.2 mg, 0.224 mmol) were copolymerised for 24h to afford **110** as purple powders. Toluene fraction (65 mg, 0.05 mmol, 25% yield), chloroform fraction (190 mg, 0.16 mmol, 72% yield) with total yield 97%[50].

GPC: toluene fraction, M_n = 6000 g mol^{-1}, M_w = 11100 g mol^{-1}, PDI = 1.8 and Dp = 5; chloroform fraction, M_n = 12500 g mol^{-1}, M_w = 27400 g mol^{-1}, PDI = 2.1 and Dp = 11. ^{1}H NMR (toluene fraction) ($C_2D_2Cl_4$, δ): 7.96-7.87 (bm, 2H), 7.71-7.61 (bm, 2H), 7.57-7.50 (bm, 4H), 7.30-7.05 (bm, 10H), 4.18-4.01 (bm, 4H), 3.81-3.61 (bm, 2H), 1.91-1.79 (bm, 4H), 1.79-1.63 (bm, 2H), 1.60-1.48 (bm, 4H), 1.46-1.20 (bm, 42H), 0.92-0.79 (bm, 9H). FT-IR (cm^{-1}): 2921, 2850, 1751, 1701, 1606, 1574, 1432, 1364, 1244, 1173, 1031. EA (%) calculated for $C_{74}H_{85}N_3O_4S_3$: C, 75.54; H, 7.28; N, 3.57; S, 8.17. Found: C, 72.97; H, 7.05; N, 3.38; S, 7.58.

9.4.14. Synthesis of poly[4,4-bis(2-ethylhexyl)-2,6-cyclopenta[2,1-*b*:3,4-*b*']dithiophene-*alt*-5,5-(4',7'-bis(2-thienyl)-2',1',3'-benzothiadiazole-5,6-*N*-(3,7-dimethyloctyl) dicarboxylic imide)] (134)

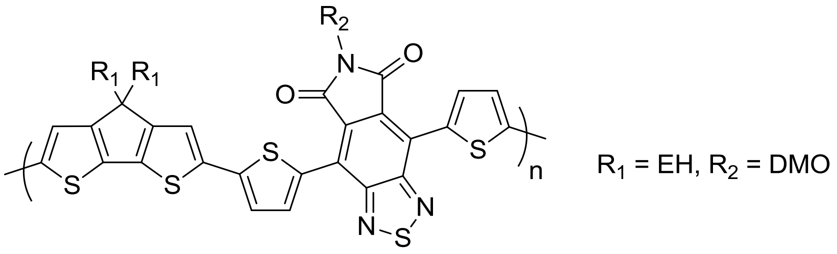

134 was prepared followed by the same procedure for synthesis of **76**.

122 (147.1 mg, 0.224 mmol) and **49** (150 mg, 0.224 mmol) were copolymerised for 48h to afford **134** as dark green powders (16 mg, 0.02 mmol, 8% yield)[50].

GPC: toluene fraction, M_n = 5200 g mol^{-1}, M_w = 10100 g mol^{-1}, PDI = 1.9 and Dp = 6. ^{1}H NMR (toluene fraction) ($C_2D_2Cl_4$, δ): 8.08 (d, 2H, *J* = 9.0 Hz), 7.52-7.16 (bm, 4H), 3.85-3.66 (bm, 2H), 2.01-1.83 (bm, 4H), 1.81-1.68 (bm, 1H), 1.61-1.48 (bm, 3H), 1.47-1.22 (bm, 12H), 1.20-0.92 (bm, 12H), 0.90-0.82 (bm, 9H), 0.81-0.72 (bm, 6H), 0.69 (t, 6H, *J* = 7.5 Hz). FT-IR (cm^{-1}): 3127, 3074, 2953, 2921, 2850, 1751, 1698, 1513, 1432, 1361, 1169, 1063.

9.4.14. Synthesis of poly[4,4-dioctyl-2,6-cyclopenta[2,1-*b*:3,4-*b*']dithiophene-*alt*-5,5-(4',7'-bis(2-thienyl)-2',1',3'-benzothiadiazole-5,6-*N*-(3,7-dimethyloctyl)-dicarboxylic imide)] (135)

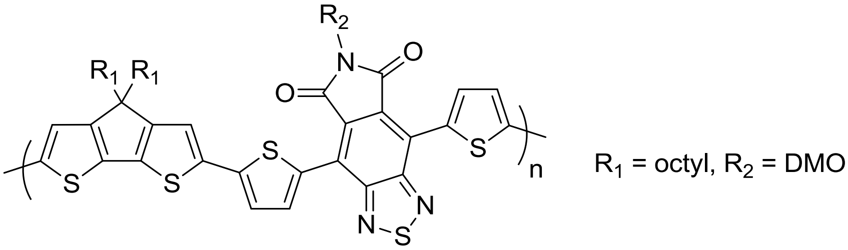

1st polymerisation

121 (109.9 mg, 0.196 mmol), **47** (100 mg, 0.196 mmol), $Pd_2(dba)_3.CHCl_3$ (6.2 mg, 0.005 mmol), P(*o*-MeOPh)$_3$ (8.4 mg, 0.023 mmol), PivOH (20 mg, 0.196 mmol) and Cs_2CO_3 (191.7 mg, 0.588 mmol) added to a top sealing tube and degassed under argon. Dry (toluene: DMF, 2 mL: 0.2 mL) added and the system degassed again and heated at 115 °C for 17h. The reaction contents cooled to RT, the polymer dissolved in $CHCl_3$ (300 mL) and an NH_4OH solution (50 mL, 35% in H_2O) added and stirred overnight. The organic phase separated and washed with deionised H_2O. The organic phase concentrated to around (50 mL) and put into methanol (300 mL). The mixture stirred overnight and filtered. The polymer purified by Soxhlet extraction with methanol (300 mL), acetone (300 mL), and hexane (300 mL) and finally toluene (300 mL). The toluene fraction concentrated to around (50 mL) and put into methanol (300 mL). The solution stirred overnight and the pure polymer recovered by filtration to yield **135** as dark green powders (170 mg, 0.19 mmol, 95% yield)[51].

GPC: toluene fraction, M_n = 7800 g mol^{-1}, M_w = 18100 g mol^{-1}, PDI = 2.3 and Dp = 9. ^1H NMR (toluene fraction) ($C_2D_2Cl_4$, δ): 8.04 (bm, 2H), 7.35-7.06 (bm, 4H), 3.83-3.69 (bm, 2H), 1.98-1.84 (bm, 4H), 1.80-1.67 (bm, 1H), 1.62-1.47 (bm, 3H), 1.45-1.13 (bm, 23H), 1.12-1.03 (bm, 3H), 1.01-0.93 (bm, 3H), 0.88-0.77 (bm, 16H). FT-IR (cm^{-1}): 3131, 3067, 2921, 2847, 1744, 1694, 1503, 1432, 1396, 1173, 1105, 1066. EA (%) calculated for $C_{51}H_{61}N_3O_2S_5$: C, 67.44; H, 6.77; N, 4.63; S, 17.65. Found: C, 61.10; H, 7.02; N, 3.98; S, 15.38.

2nd polymerisation

135 was prepared for the second time by the same procedure except the polymerisation was left for 72h. Toluene fraction (110 mg, 0.12 mmol, 62% yield), chloroform fraction (42 mg, 0.05 mmol, 24% yield) with total yield 86%[51].

GPC: toluene fraction, M_n = 10000 g mol^{-1}, M_w = 30900 g mol^{-1}, PDI = 3.0 and Dp = 11; chloroform fraction, M_n = 17400 g mol^{-1}, M_w = 61400 g mol^{-1}, PDI = 3.5 and Dp = 19.

9.4.16. Synthesis of poly[4,4-dioctyl-2,6-cyclopenta[2,1-*b*:3,4-*b*']dithiophene-*alt*-5,5-(4',7'-bis(2-thienyl)-2',1',3'-benzothiadiazole-5,6-*N*-octyl-dicarboxylic imide) (136)

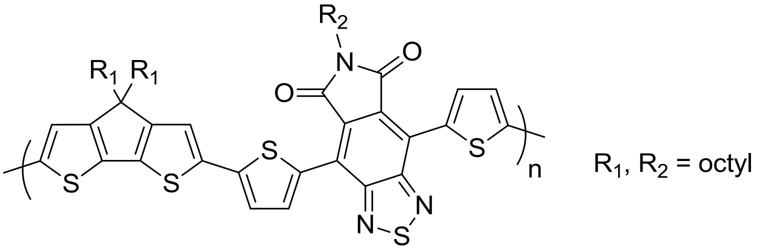

1st polymerisation

136 was prepared followed by the same procedure for synthesis of **135**.

121 (101.2 mg, 0.180 mmol) and **48** (86.9 mg, 0.180 mmol) were copolymerised in the presence of $Pd_2(dba)_3.CHCl_3$ (5.5 mg, 0.0053 mmol), P(*o*-MeOPh)$_3$ (7.6 mg, 0.0216 mmol), PivOH (18.4 mg, 0.180 mmol), Cs_2CO_3 (176.4 mg, 0.54 mmol) and anhydrous (toluene: DMF, 2 mL: 0.2 mL) for 51h to afford **136** as dark green powders (114 mg, 0.13 mmol, 72% yield)[51].

GPC: toluene fraction, M_n = 4900 g mol^{-1}, M_w = 20800 g mol^{-1}, PDI = 4.2 and Dp = 6. ^{1}H NMR (toluene fraction) ($C_2D_2Cl_4$, δ): 8.07 (bm, 2H), 7.35-7.18 (bm, 4H), 3.83-3.66 (bm, 2H), 1.98-1.83 (bm, 4H), 1.81-1.66 (bm, 2H), 1.48-1.04 (bm, 30H), 0.90-0.78 (bm, 13H). FT-IR (cm^{-1}): 3127, 3067, 2918, 2850, 1747, 1698, 1510, 1432, 1393, 1166, 1010. EA (%) calculated for $C_{49}H_{57}N_3O_2S_5$: C, 66.86; H, 6.53; N, 4.77; S, 18.21. Found: C, 67.23; H, 6.60; N, 4.41; S, 17.45.

2nd polymerisation

136 was prepared for the second time by the same procedure except the polymerisation was left for 96h. Toluene fraction (120 mg, 0.14 mmol, 76% yield)[51].

GPC: toluene fraction, M_n = 9100 g mol^{-1}, M_w = 18300 g mol^{-1}, PDI = 2.0 and Dp = 10.

9.4.17. Synthesis of poly[4,4-bis(2-ethylhexyl)-2,6-cyclopenta[2,1-*b*:3,4-*b*']dithiophene-*alt*-5,5-(4',7'-bis(2-thienyl)-2',1',3'-benzothiadiazole-5,6-*N*-octyl-dicarboxylic imide) (137)

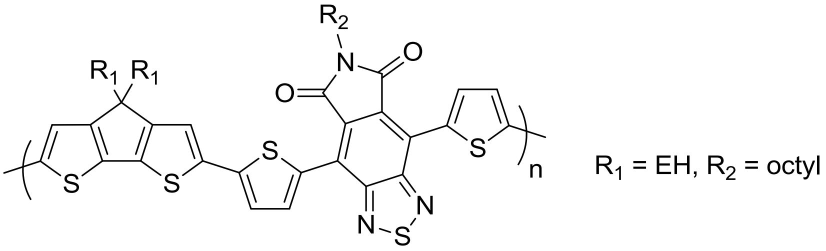

137 was prepared followed by the same procedure for synthesis of **135**.

120 (104 mg, 0.185 mmol) and **48** (89.3 mg, 0.185 mmol) were copolymerised in the presence of $Pd_2(dba)_3.CHCl_3$ (5.8 mg, 0.0056 mmol), P(*o*-MeOPh)$_3$ (7.8 mg, 0.022 mmol), PivOH (18 mg, 0.185 mmol), Cs_2CO_3 (180 mg, 0.55 mmol) and anhydrous (toluene: DMF, 2 mL: 0.2 mL) for 96h to afford **137** as dark green powders (118 mg, 0.13 mmol, 72% yield)[51].

GPC: toluene fraction, M_n = 15900 g mol^{-1}, M_w = 29700 g mol^{-1}, PDI = 1.8 and Dp = 18. ^{1}H NMR (toluene fraction) ($C_2D_2Cl_4$, δ): 8.15-8.02 (bm, 2H), 7.35-7.20 (bm, 4H), 3.83-3.66 (bm, 2H), 2.07-1.89 (bm, 4H), 1.81-1.70 (bm, 2H), 1.48-1.22 (bm, 18H), 1.17-0.97 (bm, 10H), 0.94-0.84 (bm, 3H), 0.83-0.76 (bm, 6H), 0.75-0.69 (bm, 6H). FT-IR (cm^{-1}): 3131, 3070, 2921, 2854, 1751, 1698, 1527, 1432, 1396, 1166, 1098. EA (%) calculated for $C_{49}H_{57}N_3O_2S_5$: C, 66.86; H, 6.53; N, 4.77; S, 18.21. Found: C, 67.09; H, 6.41; N, 4.57; S, 17.65.

9.4.18. Synthesis of poly[4,4-dioctyl-2,6-dithieno[3,2-*b*:2',3'-*d*]silole-*alt*-5,5-(4',7'-bis(2-thienyl)-2',1',3'-benzothiadiazole-5,6-*N*-(3,7-dimethyloctyl)-dicarboxylic imide) (144)

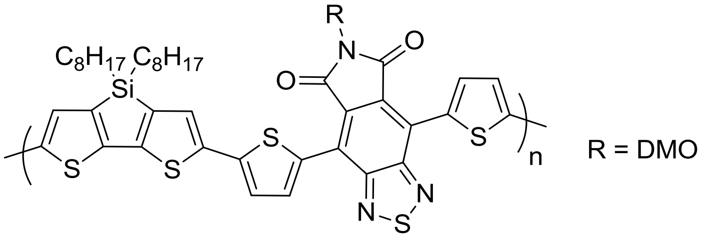

144 was prepared followed by the same procedure for synthesis of **35**.

142 (100 mg, 0.134 mmol) and **49** (89 mg, 0.134 mmol) were copolymerised using $Pd(OAc)_2$ (2.2 mg, 0.0097 mmol) and P(*o*-tol)$_3$ (6.1 mg, 0.020 mmol) in anhydrous toluene (5 mL) at 110 °C for 72h. **144** was obtained as dark blue powders. Toluene fraction (42 mg, 0.05 mmol, 34% yield), chloroform fraction (72 mg, 0.08 mmol, 58% yield) with total yield 92%^{52}.

GPC: Toluene fraction, M_n = 6200 g mol^{-1}, M_w = 20600 g mol^{-1}, PDI = 3.2 and Dp = 7; chloroform fraction, M_n = 14600 g mol^{-1}, M_w = 79900 g mol^{-1}, PDI = 5.4 and Dp = 16. ^{1}H NMR (toluene fraction) ($C_2D_2Cl_4$, δ): 8.16-8.01 (bm, 2H), 7.54-7.17 (bm, 4H), 3.87-3.65 (bm, 2H), 1.81-1.67 (bm, 1H), 1.60-1.50 (bm, 3H), 1.48-1.07 (bm, 33H), 1.05-0.94 (bm, 6H), 0.89-0.78 (bm, 10H). FT-IR (cm^{-1}): 3129, 3062, 2955, 2923, 2848, 1753, 1696, 1546, 1425, 1350, 1168, 1068. EA (%) calculated for $C_{50}H_{61}N_3O_2S_5Si$: C, 64.96; H, 6.65; N, 4.55; S, 17.34. Found: C, 63.29; H, 6.49; N, 4.74; S, 17.10.

9.4.19. Synthesis of poly[4,4-dioctyl-2,6-dithieno[3,2-*b*:2',3'-*d*]silole-*alt*-5,5-(4',7'-bis(2-thienyl)-2',1',3'-benzothiadiazole-5,6-*N*-octyl-dicarboxylic imide) (145)

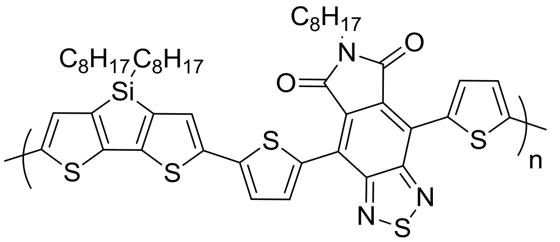

145 was prepared followed by the same procedure for synthesis of **35**.

142 (107 mg, 0.143 mmol) and **50** (91 mg, 0.143 mmol) were copolymerised using $Pd(OAc)_2$ (2.3 mg, 0.01 mmol) and P(*o*-tol)$_3$ (6.5 mg, 0.021mmol) in anhydrous toluene (5 mL) at 110 °C for 72h. **145** was obtained as blue powders (73 mg, 0.08 mmol, 57% yield)^{52}.

GPC: toluene fraction, M_n = 5700 g mol^{-1}, M_w = 14000 g mol^{-1}, PDI = 2.4 and Dp = 6. ^{1}H NMR (toluene fraction) ($C_2D_2Cl_4$, δ): 8.19-8.01 (bm, 2H), 7.55-7.20 (bm, 4H), 3.87-3.66 (bm, 2H), 1.841.64 (bm, 2H), 1.61-1.07 (bm, 34H), 1.06-0.92 (bm, 3H), 0.89-0.78 (bm, 10H). FT-IR (cm^{-1}): 3129, 3062, 2951, 2919, 2851, 1749, 1689, 1549, 1425, 1350, 1161, 1007. EA (%) calculated for $C_{48}H_{57}N_3O_2S_5Si$: C, 64.32; H, 6.41; N, 4.69; S, 17.88. Found: C, 63.09; H, 6.19; N, 5.11; S, 17.63.

References

1. X. Guo, F. S. Kim, S. A. Jenekhe and M. D. Watson, *Journal of the American Chemical Society*, 2009, **131**, 7206-7207.
2. N. Eleya, T. Patonay, A. Villinger and P. Langer, *Helvetica Chimica Acta*, 2013, **96**, 408-413.
3. D. Albanese, M. Benaglia, D. Landini, A. Maia, V. Lupi and M. Penso, *Industrial & Engineering Chemistry Research*, 2002, **41**, 4928-4935.
4. M. Helgesen, M. Bjerring, N. C. Nielsen and F. C. Krebs, *Chemistry of Materials*, 2010, **22**, 5617-5624.
5. J. Y. Lee, S. M. Lee, K. W. Song and D. K. Moon, *European Polymer Journal*, 2012, **48**, 532-540.
6. J. Y. Lee, K. W. Song, J. R. Ku, T. H. Sung and D. K. Moon, *Solar Energy Materials and Solar Cells*, 2011, **95**, 3377-3384.
7. Q. Li, H. Guo, L. Ma, W. Wu, Y. Liu and J. Zhao, *Journal of Materials Chemistry*, 2012, **22**, 5319-5329.
8. V. Singh, S. Wang and E. T. Kool, *Journal of the American Chemical Society*, 2013, **135**, 6184-6191.
9. P. Chen, R. A. Lalancette and F. Jäkle, *Journal of the American Chemical Society*, 2011, **133**, 8802-8805.
10. D. S. Chung, J. W. Park, S.-O. Kim, K. Heo, C. E. Park, M. Ree, Y.-H. Kim and S.-K. Kwon, *Chemistry of Materials*, 2009, **21**, 5499-5507.
11. S. Ponomarenko, A. Muzafarov, O. Borshchev, E. Vodopyanov, N. Demchenko and V. Myakushev, *Russian Chemical Bulletin*, 2005, **54**, 684-690.
12. L. Wen and S. C. Rasmussen, *Journal of Chemical Crystallography*, 2007, **37**, 387-398.
13. R. L. Schwiderski and S. C. Rasmussen, *The Journal of Organic Chemistry*, 2013, **78**, 5453-5462.
14. H. Hailu, B. Atsbeha, S. Admassie, W. Mammo, V. Raju and Y. Chebude, *Bulletin of the Chemical Society of Ethiopia*, 2011, **25**.
15. M. R. Delgado, V. Hernandez, J. L. Navarrete, S. Tanaka and Y. Yamashita, *Journal of Physical Chemistry B*, 2004, **108**, 2516-2526.
16. L. Wang, D. Cai, Q. Zheng, C. Tang, S.-C. Chen and Z. Yin, *ACS Macro Letters*, 2013, **2**, 605-608.

17. C. B. Nielsen, R. S. Ashraf, N. D. Treat, B. C. Schroeder, J. E. Donaghey, A. J. White, N. Stingelin and I. McCulloch, *Advanced Materials*, 2015, **27**, 948-953.
18. L. Lan, Z. Chen, Y. Li, L. Ying, F. Huang and Y. Cao, *Polymer Chemistry*, 2015, **6**, 7558-7569.
19. Y. Matsueda, S. Xu and E.-i. Negishi, *Tetrahedron Letters*, 2015, **56**, 3346-3348.
20. A. Thomson, S. O’Connor, B. Knuckley and C. P. Causey, *Bioorganic & Medicinal Chemistry*, 2014, **22**, 4602-4608.
21. W. Yue, Y. Zhao, S. Shao, H. Tian, Z. Xie, Y. Geng and F. Wang, *Journal of Materials Chemistry*, 2009, **19**, 2199-2206.
22. G. Lu, H. Usta, C. Risko, L. Wang, A. Facchetti, M. A. Ratner and T. J. Marks, *Journal of the American Chemical Society*, 2008, **130**, 7670-7685.
23. J. Yang, N. Sun, J. Huang, Q. Li, Q. Peng, X. Tang, Y. Dong, D. Ma and Z. Li, *Journal of Materials Chemistry C*, 2015, **3**, 2624-2631.
24. C. W. Keyworth, K. L. Chan, J. G. Labram, T. D. Anthopoulos, S. E. Watkins, M. McKiernan, A. J. White, A. B. Holmes and C. K. Williams, *Journal of Materials Chemistry*, 2011, **21**, 11800-11814.
25. H. Usta, G. Lu, A. Facchetti and T. J. Marks, *Journal of the American Chemical Society*, 2006, **128**, 9034-9035.
26. K. L. Chan, M. J. McKiernan, C. R. Towns and A. B. Holmes, *Journal of the American Chemical Society*, 2005, **127**, 7662-7663.
27. C. Du, W. Li, Y. Duan, C. Li, H. Dong, J. Zhu, W. Hu and Z. Bo, *Polymer Chemistry*, 2013, **4**, 2773-2782.
28. P. K. Kundu, A. Lerner, K. Kučanda, G. Leitus and R. Klajn, *Journal of the American Chemical Society*, 2014, **136**, 11276-11279.
29. M. Nakamura, K. Yamabuki, T. Oishi and K. Onimura, *Polymer Journal*, 2014, **46**, 94-103.
30. M. Sonntag and P. Strohriegl, *Chemistry of Materials*, 2004, **16**, 4736-4742.
31. N. Blouin, A. Michaud and M. Leclerc, *Advanced Materials*, 2007, **19**, 2295-2300.
32. W. Bao, M. Reddy Billa, K. Kassireddy, M. Haro, M. J. Kelly, S. P. Kitney, M. S. Al Kalifah, P. Wei, D. Dong and M. O'Neill, *Liquid Crystals*, 2010, **37**, 1289-1303.
33. E. Zhou, S. Yamakawa, K. Tajima, C. Yang and K. Hashimoto, *Chemistry of Materials*, 2009, **21**, 4055-4061.

34. J. Jo, C. Chi, S. Höger, G. Wegner and D. Y. Yoon, *Chemistry–A European Journal*, 2004, **10**, 2681-2688.
35. G. L. Gibson, T. M. McCormick and D. S. Seferos, *Journal of the American Chemical Society*, 2011, **134**, 539-547.
36. C.-H. Chen, C.-H. Hsieh, M. Dubosc, Y.-J. Cheng and C.-S. Hsu, *Macromolecules*, 2009, **43**, 697-708.
37. B. Pal, W.-C. Yen, J.-S. Yang, C.-Y. Chao, Y.-C. Hung, S.-T. Lin, C.-H. Chuang, C.-W. Chen and W.-F. Su, *Macromolecules*, 2008, **41**, 6664-6671.
38. W. C. Yen, B. Pal, J. S. Yang, Y. C. Hung, S. T. Lin, C. Y. Chao and W. F. Su, *Journal of Polymer Science Part A: Polymer Chemistry*, 2009, **47**, 5044-5056.
39. R. Li, J. Liu, N. Cai, M. Zhang and P. Wang, *The Journal of Physical Chemistry B*, 2010, **114**, 4461-4464.
40. P. Coppo, D. C. Cupertino, S. G. Yeates and M. L. Turner, *Macromolecules*, 2003, **36**, 2705-2711.
41. A. P. Zoombelt, S. G. Mathijssen, M. G. Turbiez, M. M. Wienk and R. A. Janssen, *Journal of Materials Chemistry*, 2010, **20**, 2240-2246.
42. C.-Y. Yu and C.-Y. Wu, *Dyes and Pigments*, 2014, **106**, 81-86.
43. E. Khor, S. C. Ng, H. C. Li and S. KHOR, *Heterocycles*, 1991, **32**, 1805-1812.
44. J. A. Letizia, M. R. Salata, C. M. Tribout, A. Facchetti, M. A. Ratner and T. J. Marks, *Journal of the American Chemical Society*, 2008, **130**, 9679-9694.
45. P. M. Beaujuge, H. N. Tsao, M. R. Hansen, C. M. Amb, C. Risko, J. Subbiah, K. R. Choudhury, A. Mavrinskiy, W. Pisula and J.-L. Brédas, *Journal of the American Chemical Society*, 2012, **134**, 8944-8957.
46. R. Grisorio, G. P. Suranna, P. Mastrorilli, G. Allegretta, A. Loiudice, A. Rizzo, G. Gigli, K. Manoli, M. Magliulo and L. Torsi, *Journal of Polymer Science Part A: Polymer Chemistry*, 2013, **51**, 4860-4872.
47. H. Medlej, H. Awada, M. Abbas, G. Wantz, A. Bousquet, E. Grelet, K. Hariri, T. Hamieh, R. C. Hiorns and C. Dagron-Lartigau, *European Polymer Journal*, 2013, **49**, 4176-4188.
48. A. Abdulaziz, *Chemical Communications*, 2013, **49**, 2252-2254.
49. Z. Zhu, D. Waller, R. Gaudiana, M. Morana, D. Mühlbacher, M. Scharber and C. Brabec, *Macromolecules*, 2007, **40**, 1981-1986.
50. H. Yi, S. Al-Faifi, A. Iraqi, D. C. Watters, J. Kingsley and D. G. Lidzey, *Journal of Materials Chemistry*, 2011, **21**, 13649-13656.
51. M. Wakioka, Y. Kitano and F. Ozawa, *Macromolecules*, 2013, **46**, 370-374.

52. J. Hou, H.-Y. Chen, S. Zhang, G. Li and Y. Yang, *Journal of the American Chemical Society*, 2008, **130**, 16144-16145.

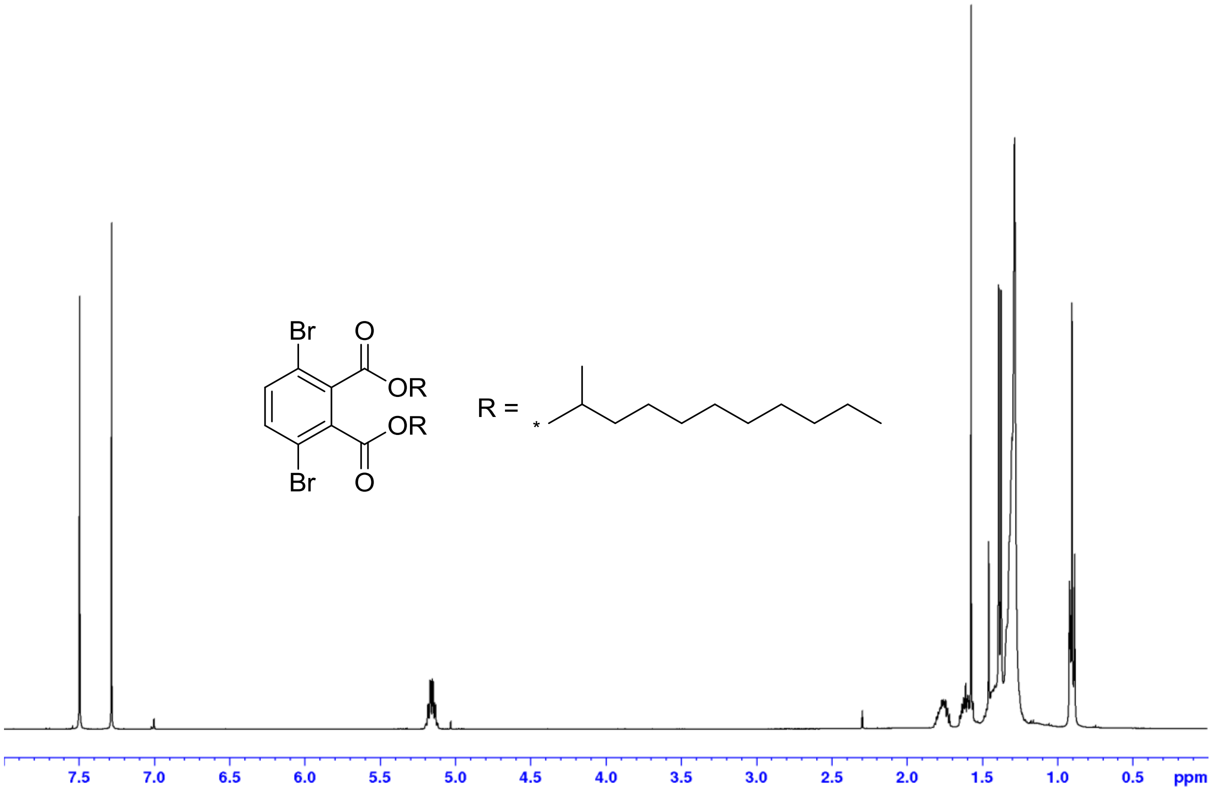

Figure 10.1: ^{1}H NMR spectrum of **6** in $CDCl_3$

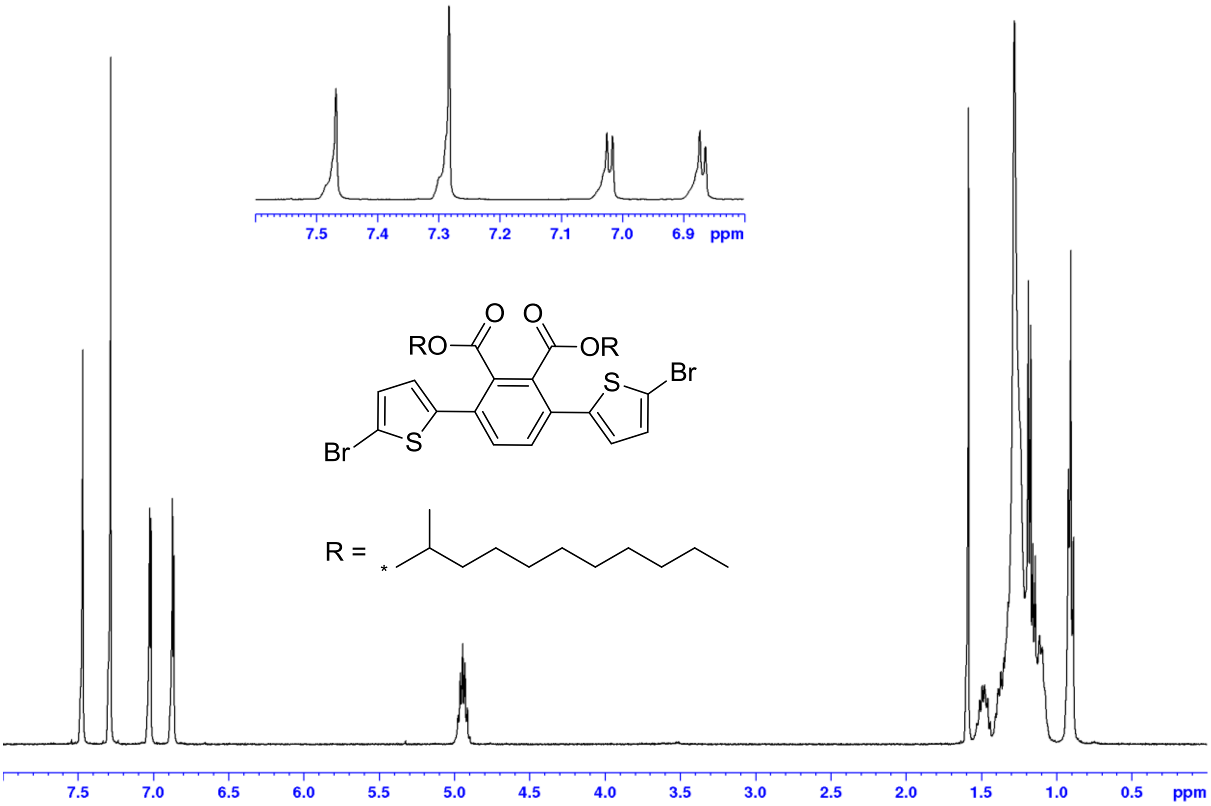

Figure 10.2: ^{1}H NMR spectrum of **8** in $CDCl_3$

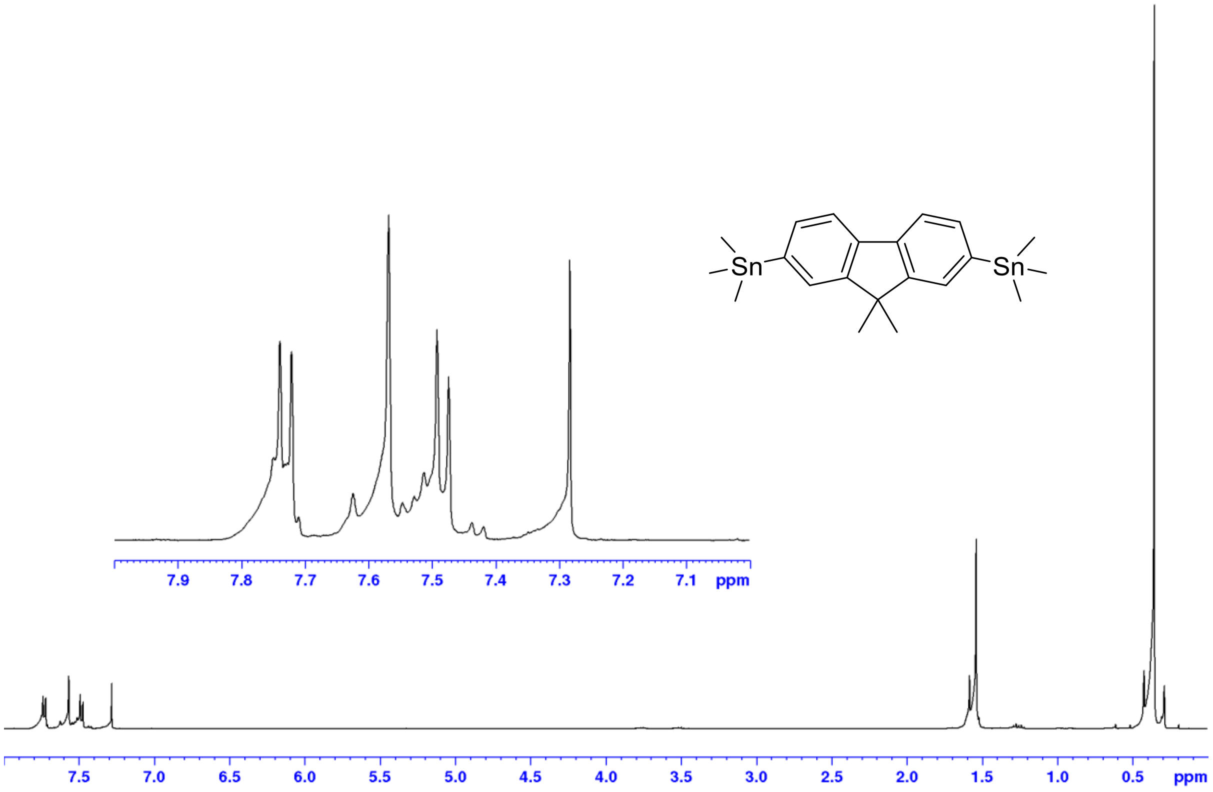

Figure 10.3: ^{1}H NMR spectrum of **29** in $CDCl_3$

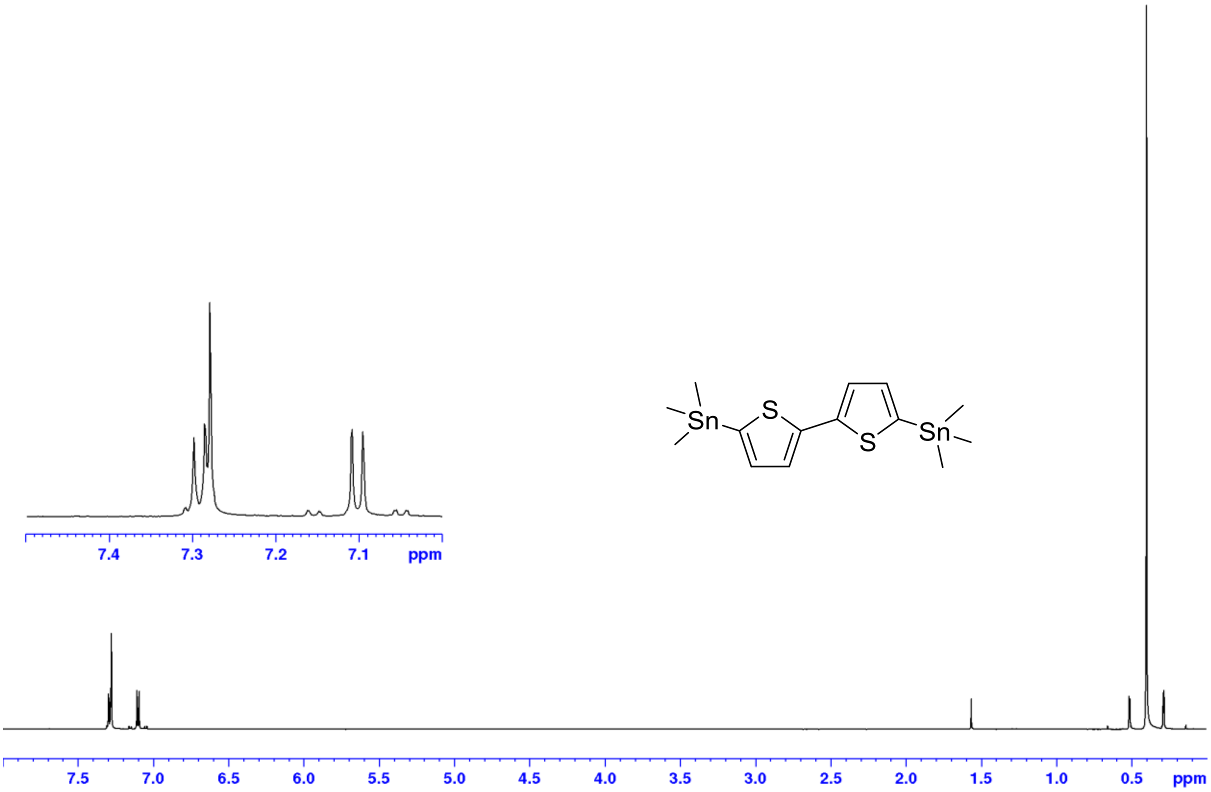

Figure 10.4: ^{1}H NMR spectrum of **34** in $CDCl_3$

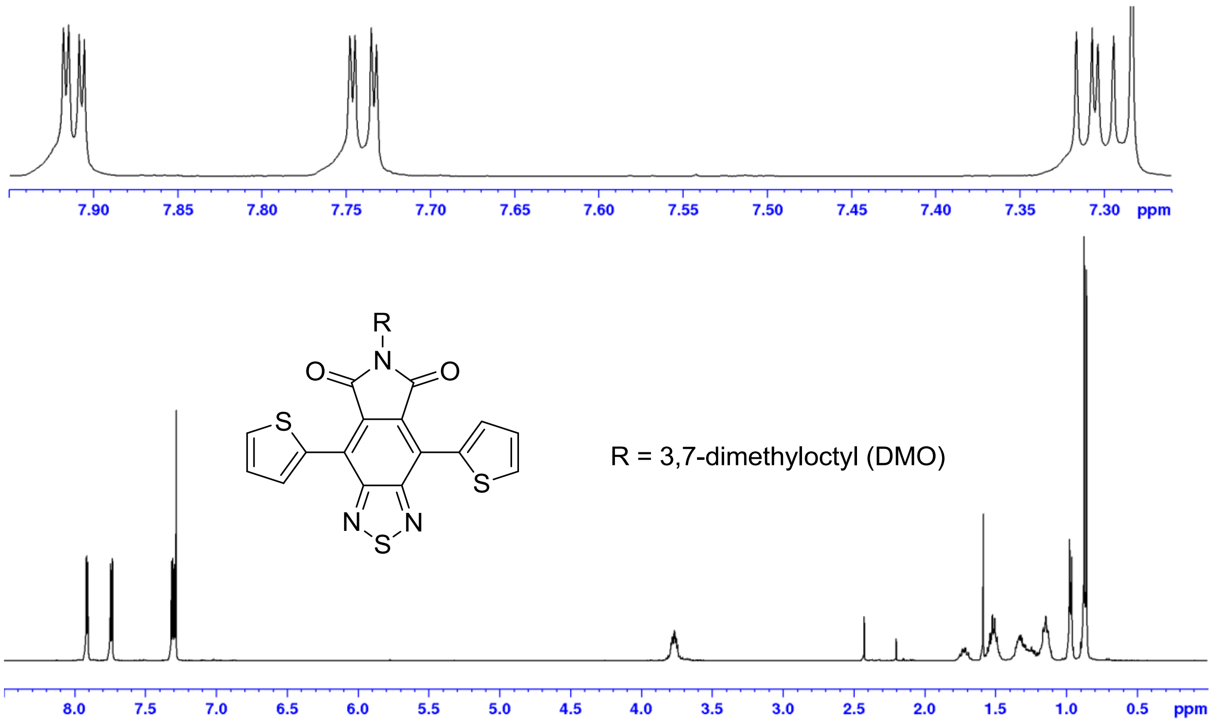

Figure 10.5: ^{1}H NMR spectrum of **47** in $CDCl_3$

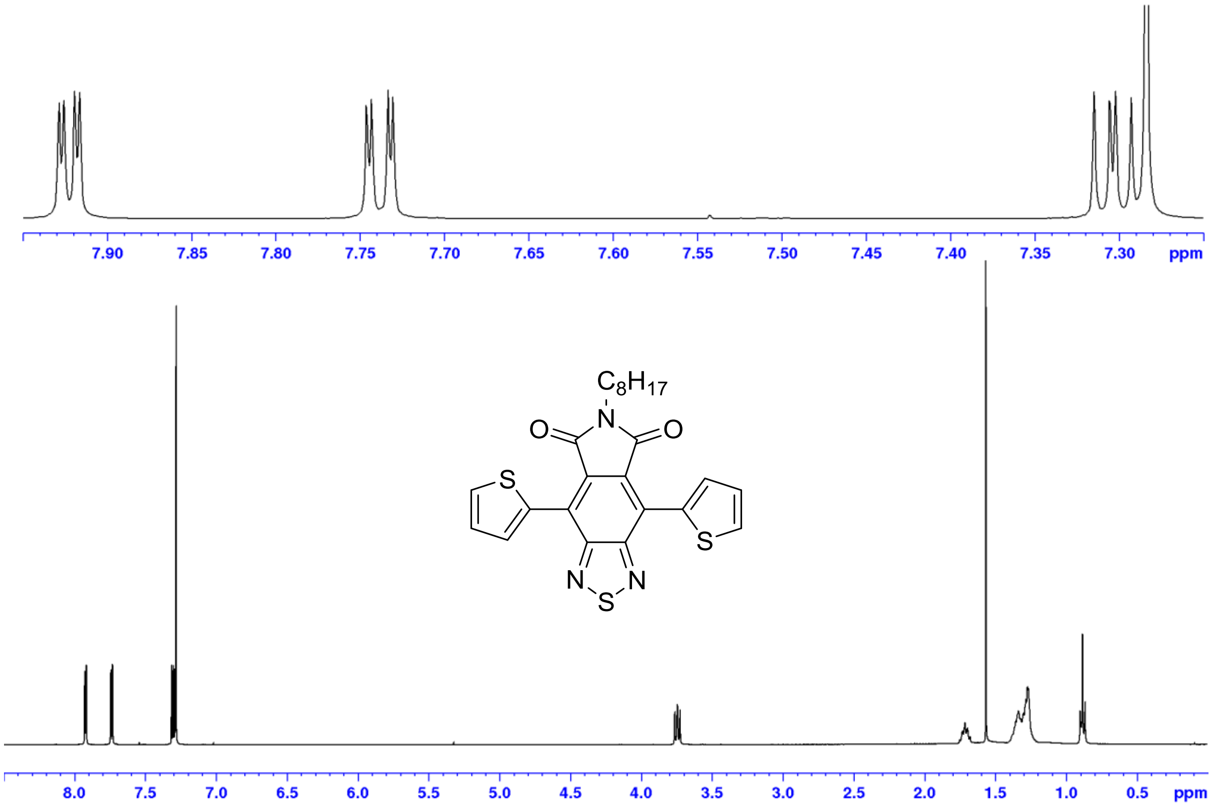

Figure 10.6: ^{1}H NMR spectrum of **48** in $CDCl_3$

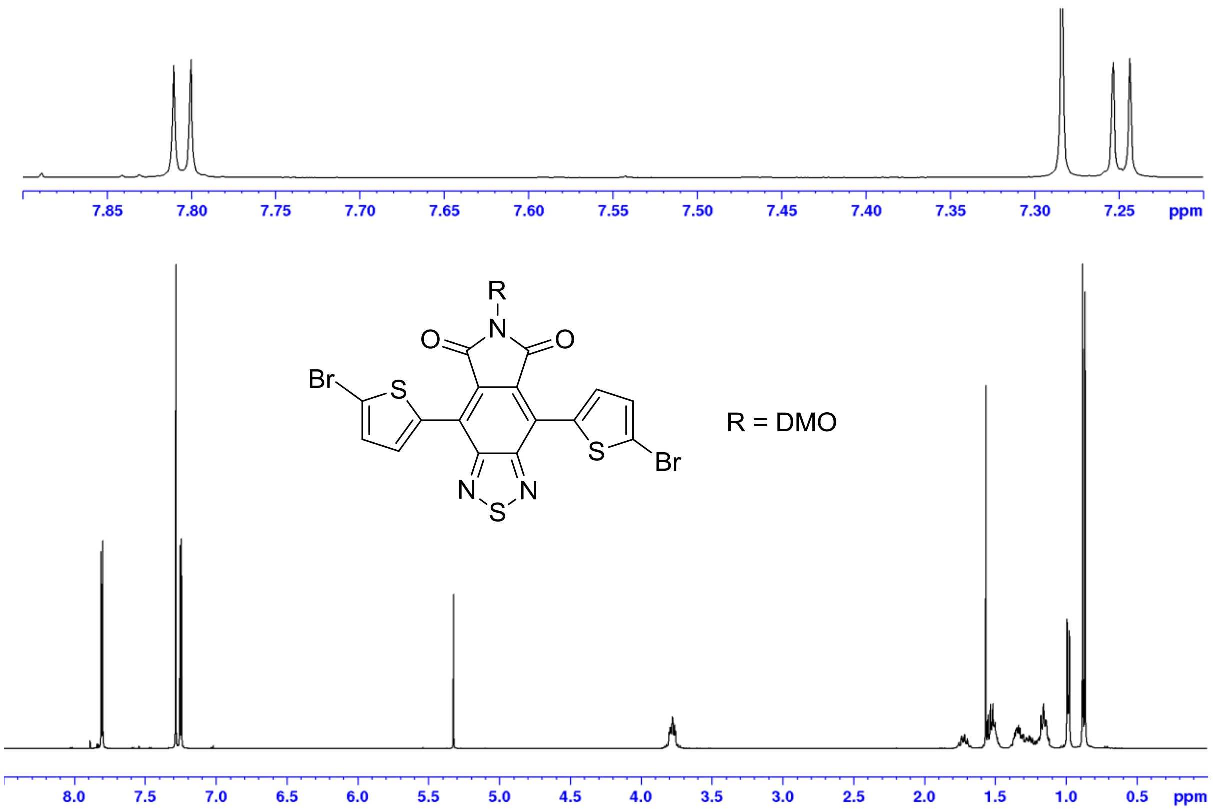

Figure 10.7: ^{1}H NMR spectrum of **49** in $CDCl_3$

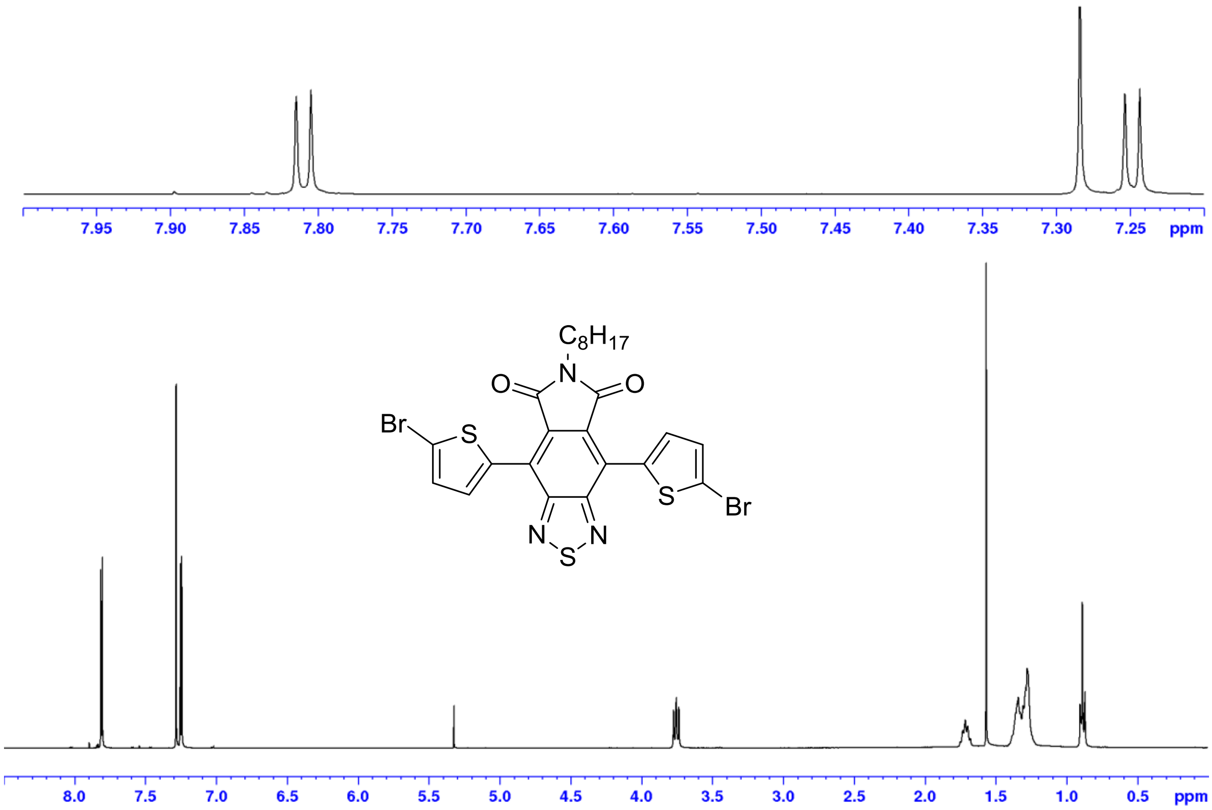

Figure 10.8: ^{1}H NMR spectrum of **50** in $CDCl_3$

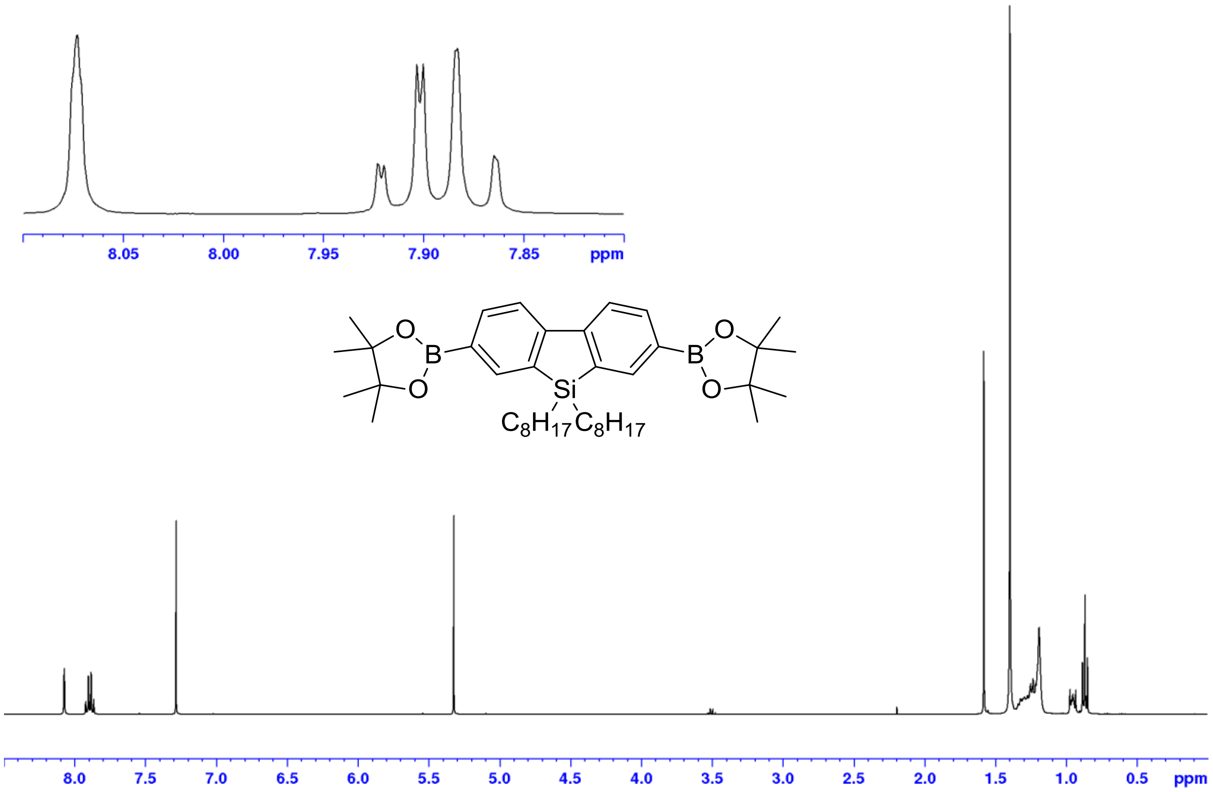

Figure 10.9: ^{1}H NMR spectrum of **72** in $CDCl_3$

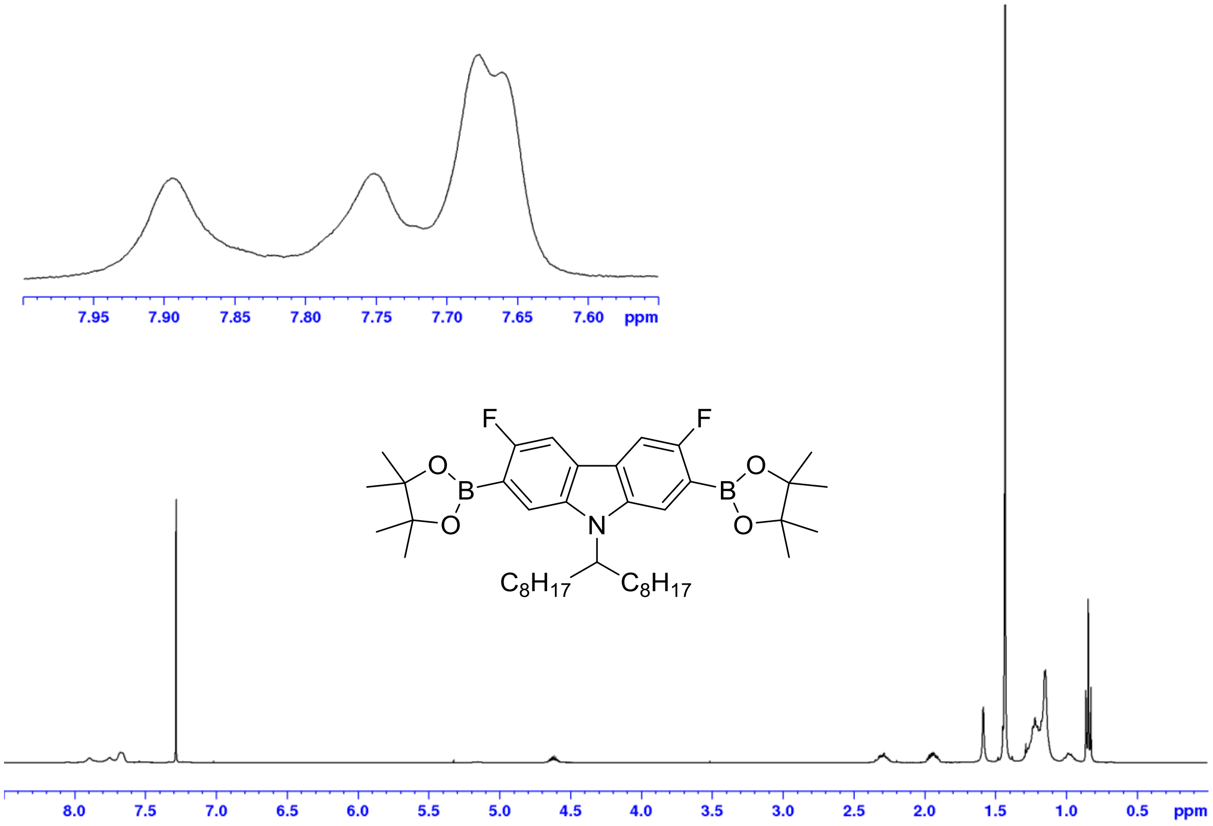

Figure 10.10: ^{1}H NMR spectrum of **89** in $CDCl_3$

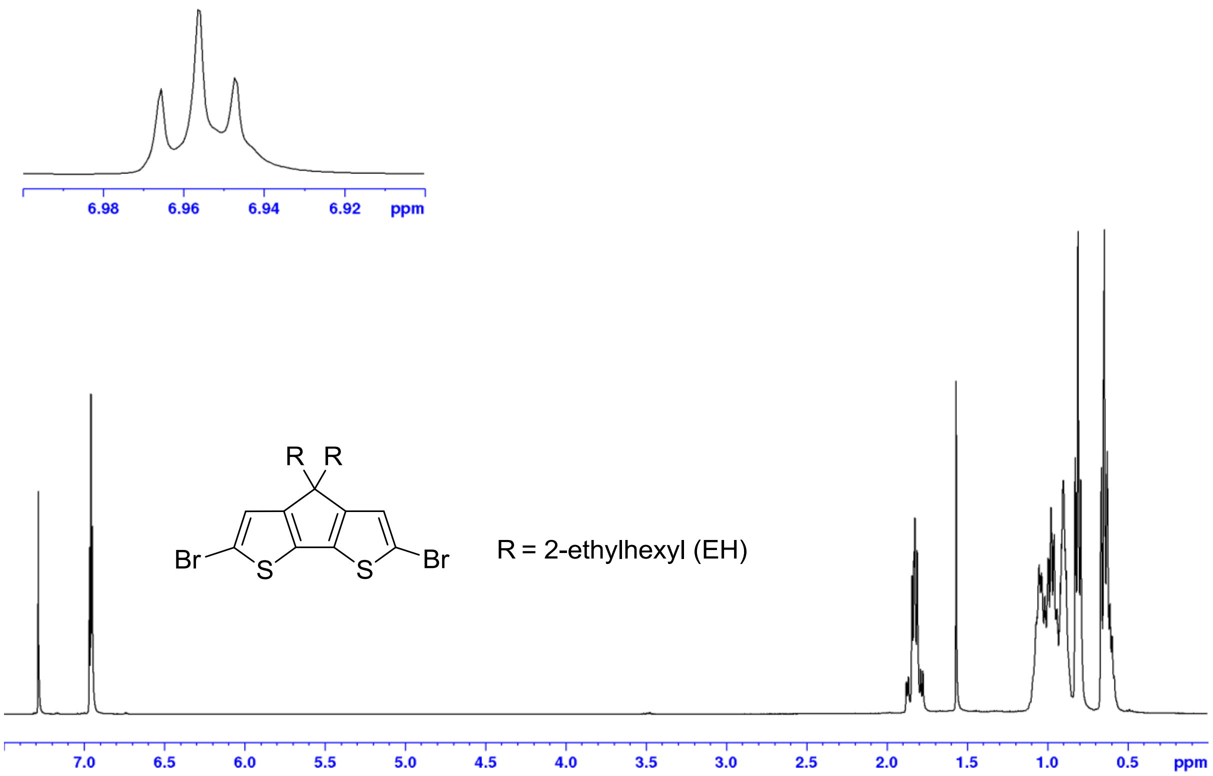

Figure 10.11: ^{1}H NMR spectrum of **120** in $CDCl_3$

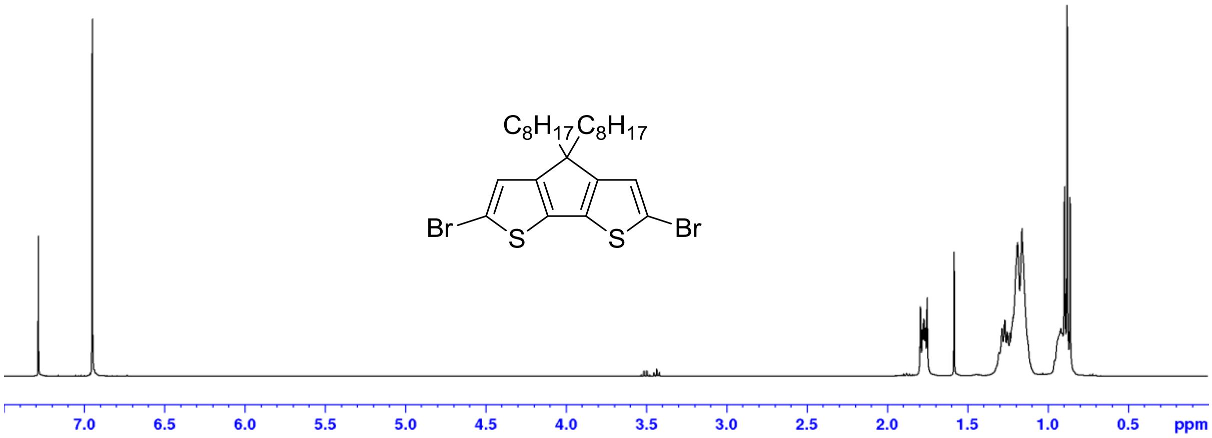

Figure 10.12: ^{1}H NMR spectrum of **121** in $CDCl_3$

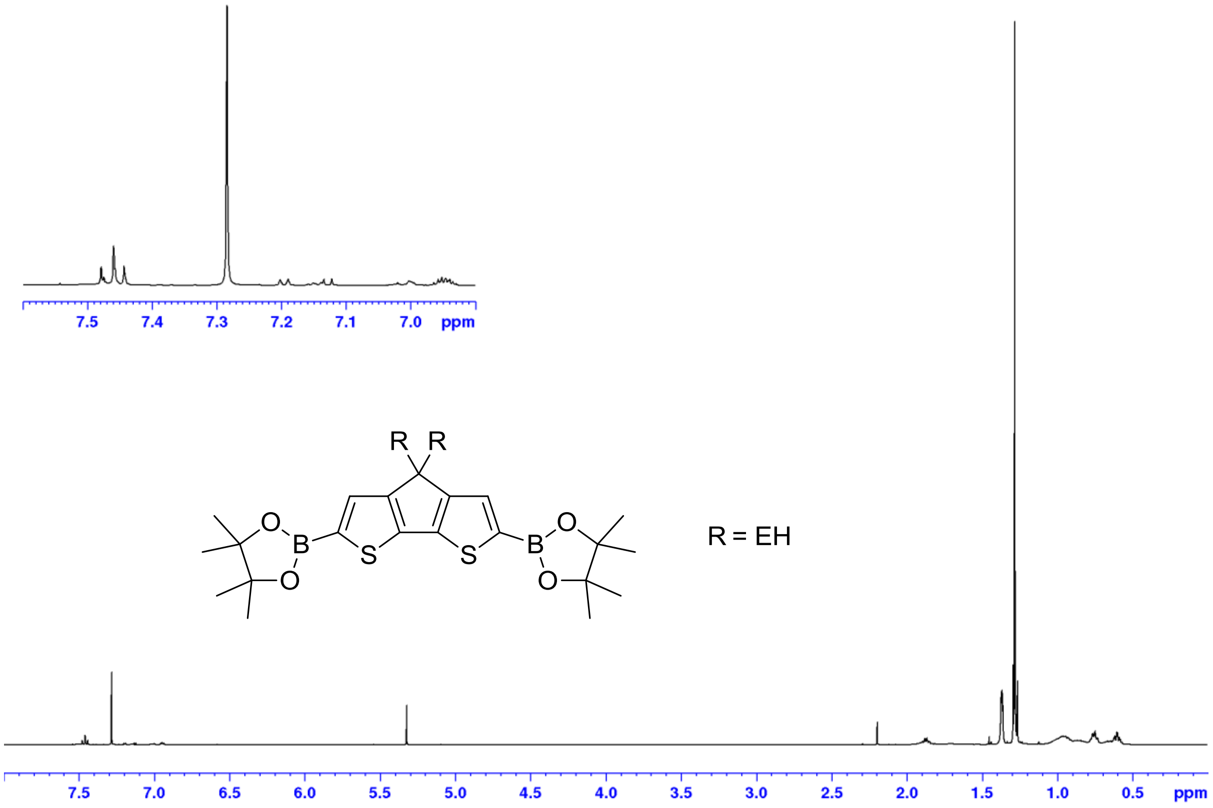

Figure 10.13: ^{1}H NMR spectrum of **122** in $CDCl_3$

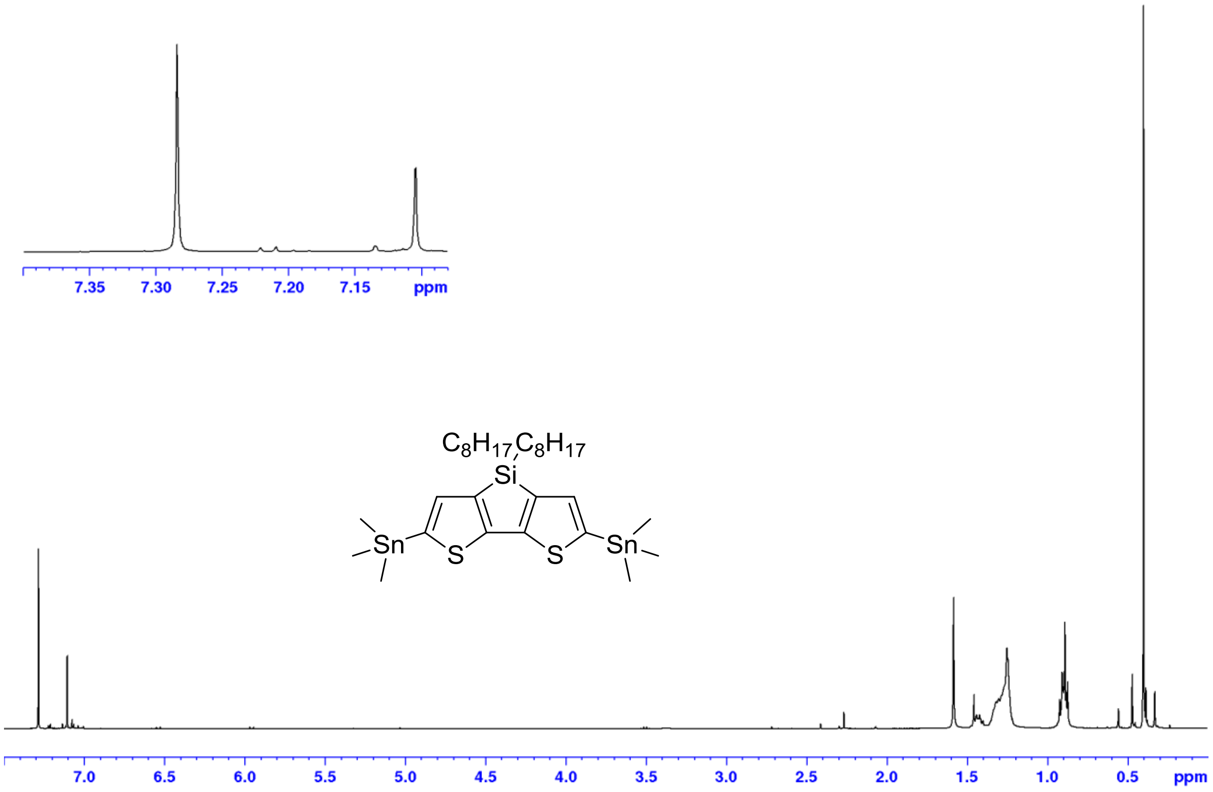

Figure 10.14: ^{1}H NMR spectrum of **142** in $CDCl_3$

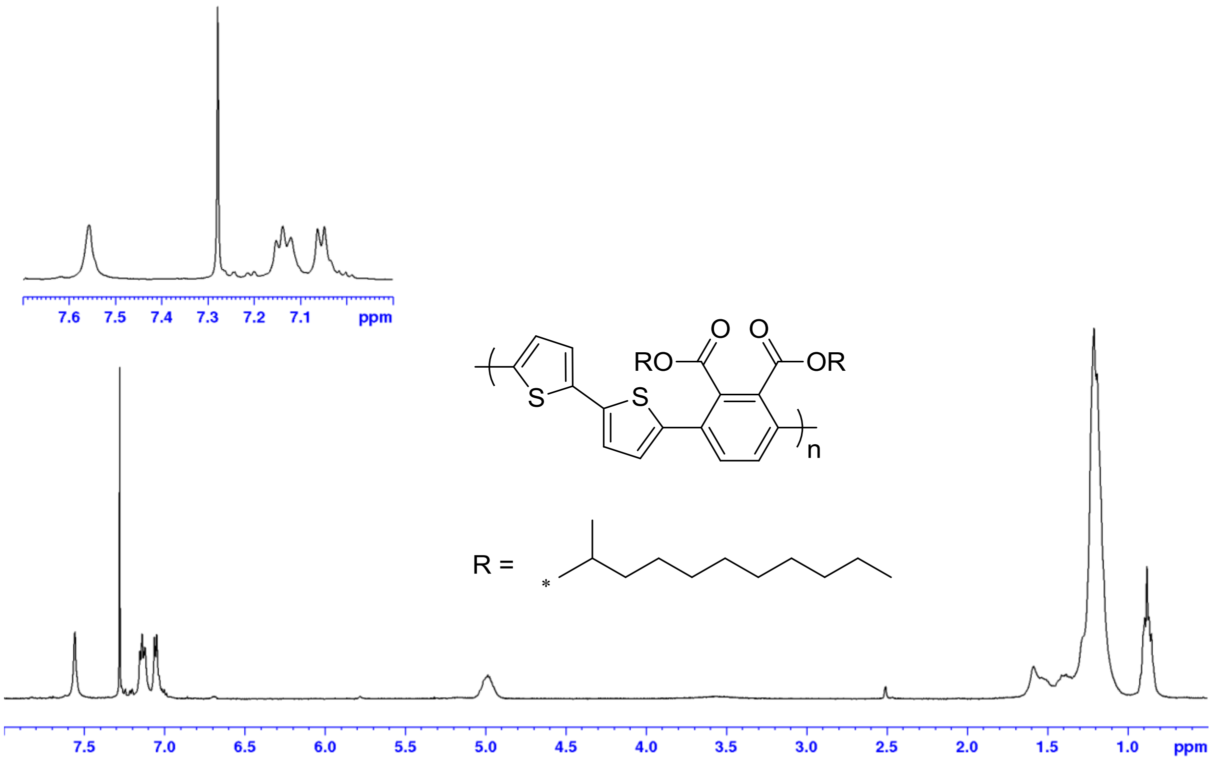

Figure 10.15: ^{1}H NMR spectrum of **35** in $CDCl_3$

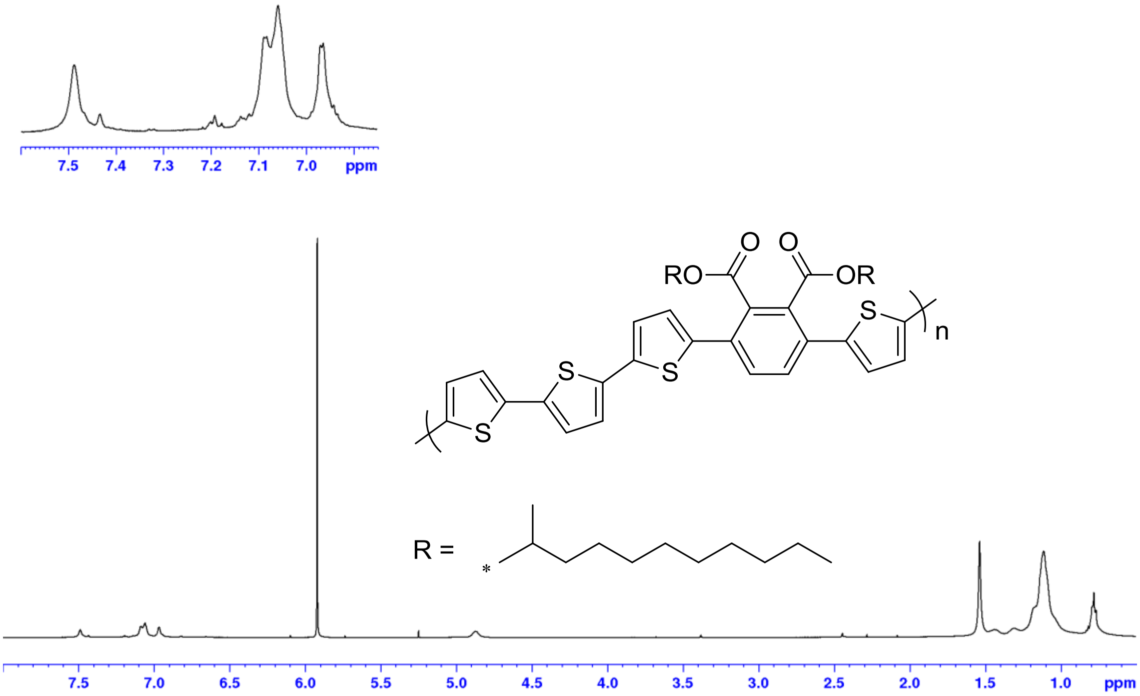

Figure 10.16: ^{1}H NMR spectrum of **36** in $C_2D_2Cl_4$ at 100 °C

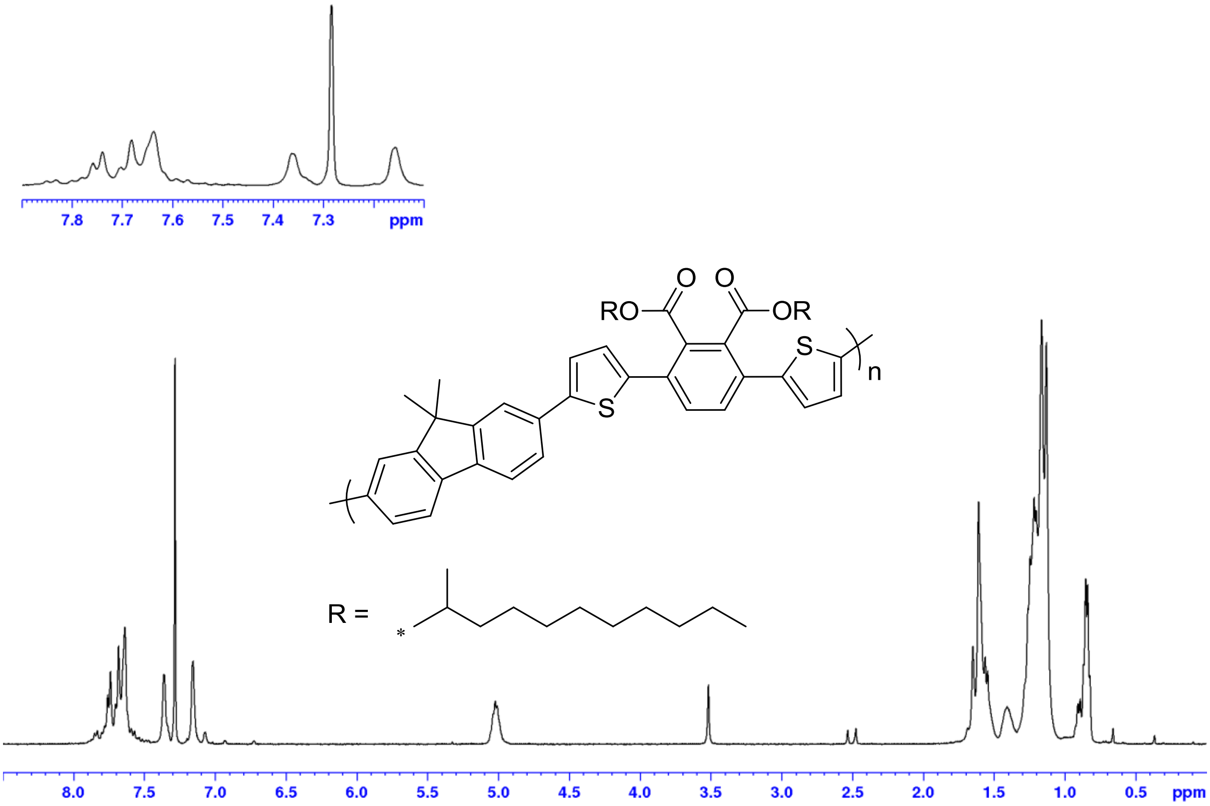

Figure 10.17: ^{1}H NMR spectrum of **37** in $CDCl_3$

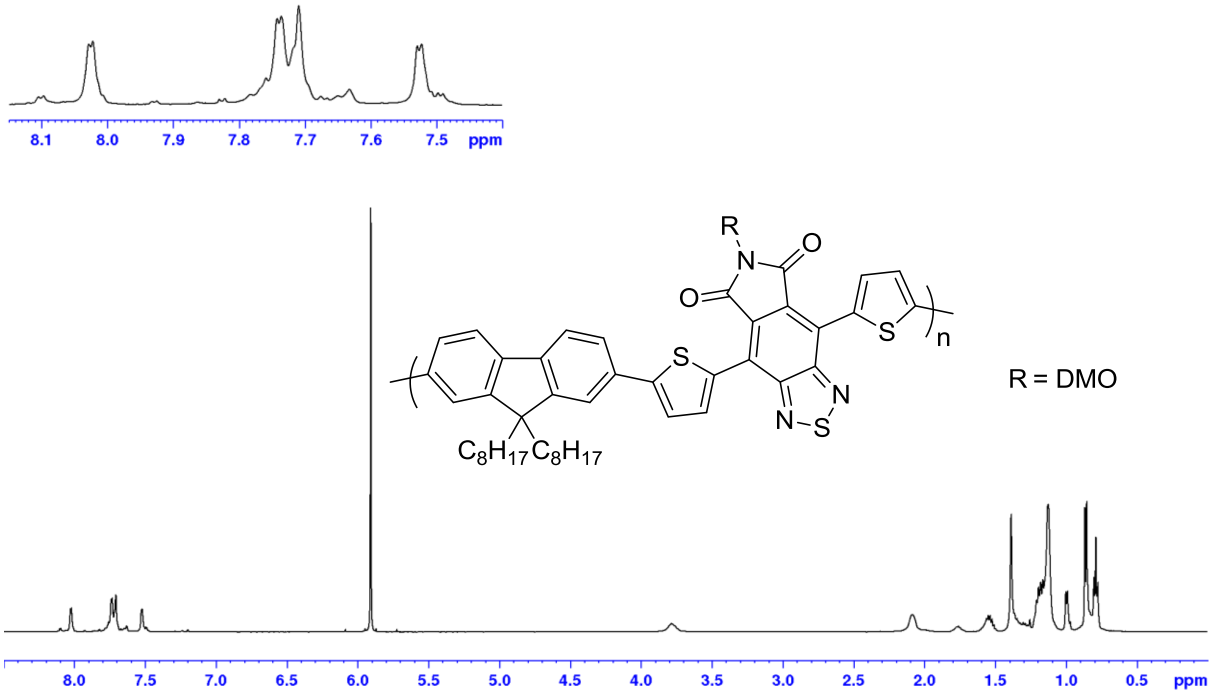

Figure 10.18: ^{1}H NMR spectrum of **76** in $C_2D_2Cl_4$ at 100 °C

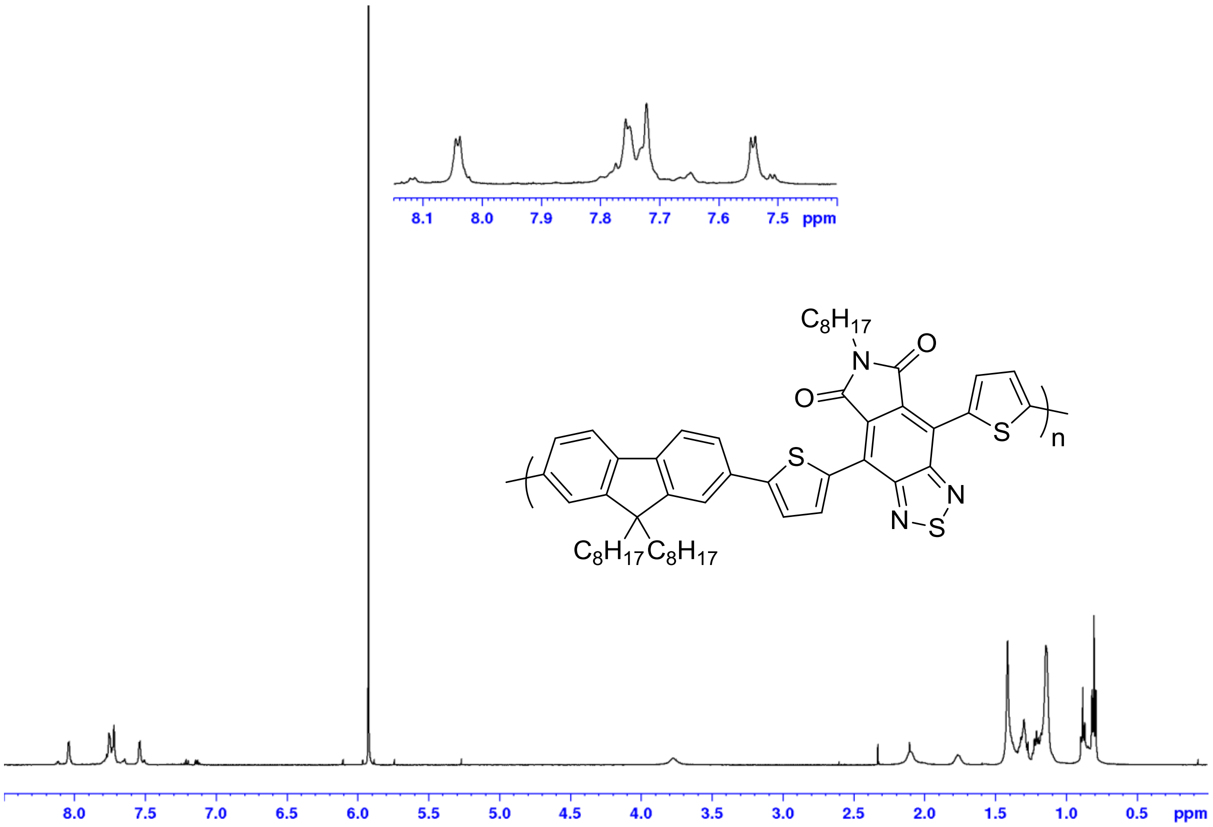

Figure 10.19: ^{1}H NMR spectrum of **77** in $C_2D_2Cl_4$ at 100 °C

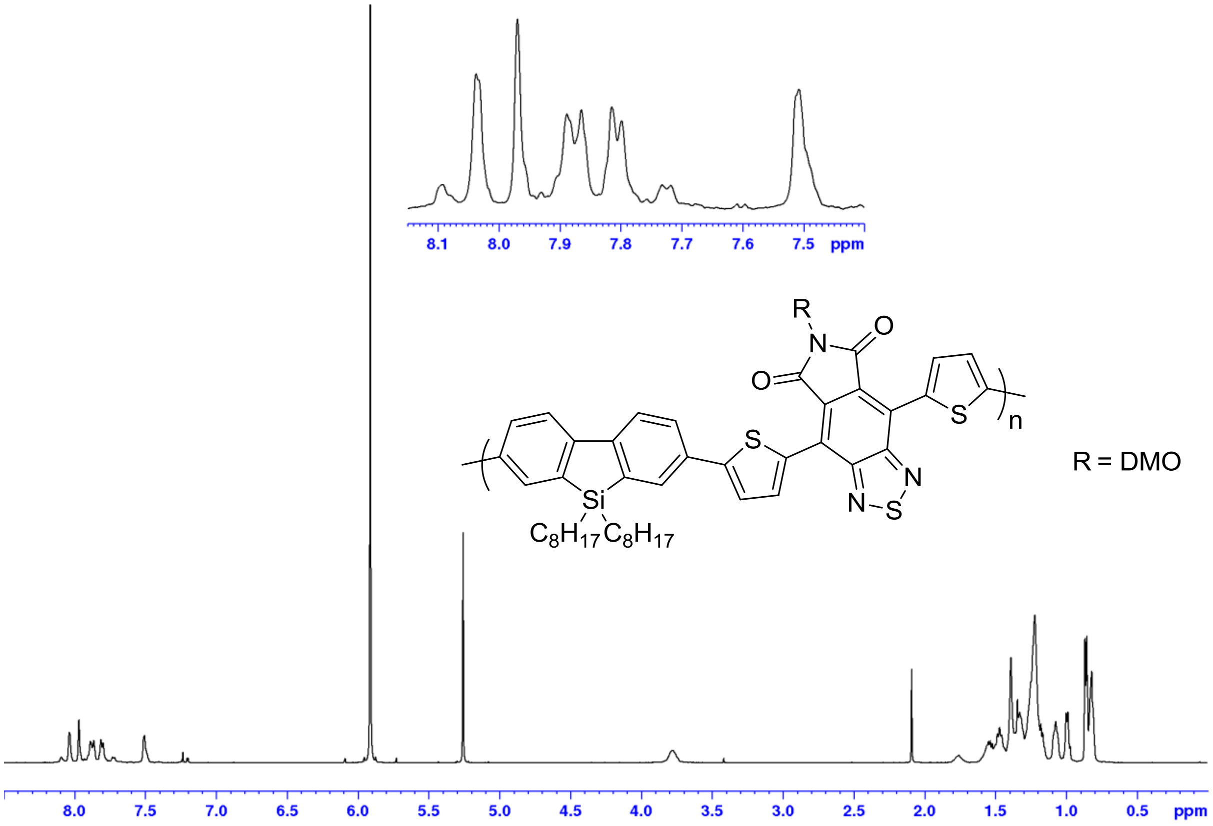

Figure 10.20: ^{1}H NMR spectrum of **78** in $C_2D_2Cl_4$ at 100 °C

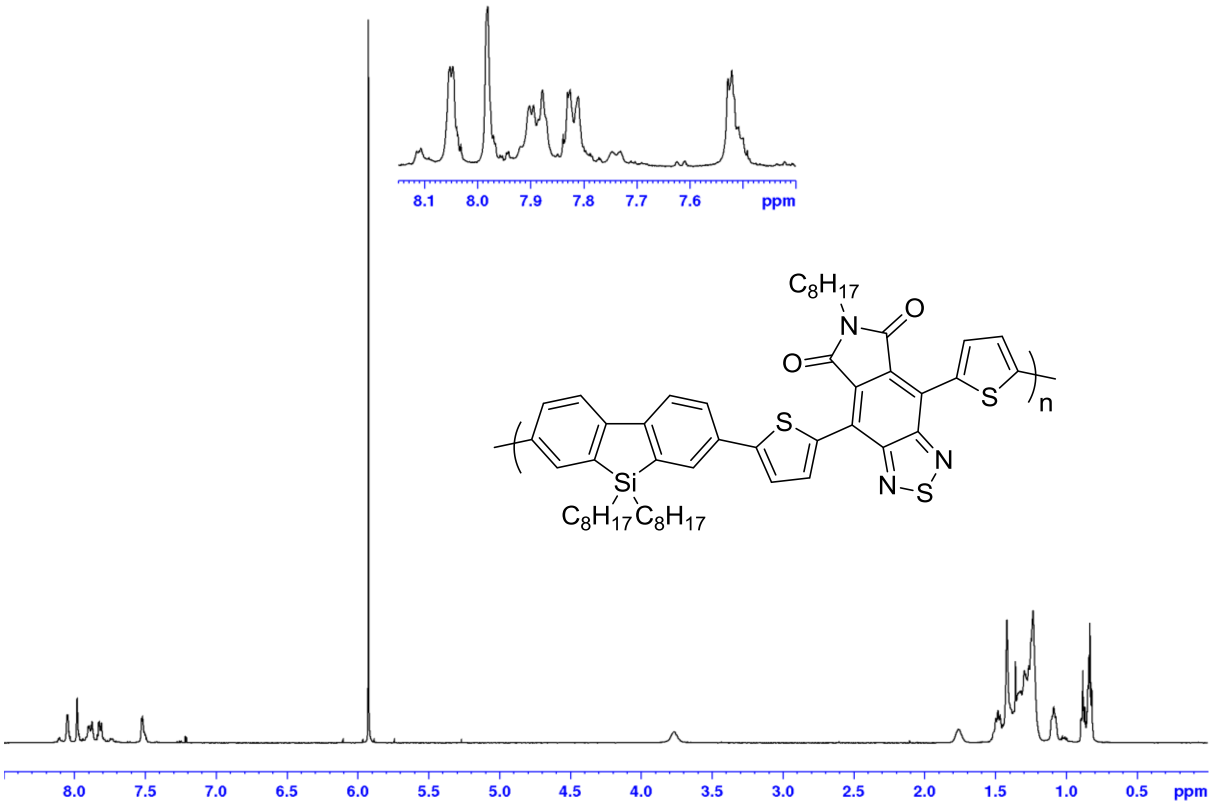

Figure 10.21: ^{1}H NMR spectrum of **79** in $C_2D_2Cl_4$ at 100 °C

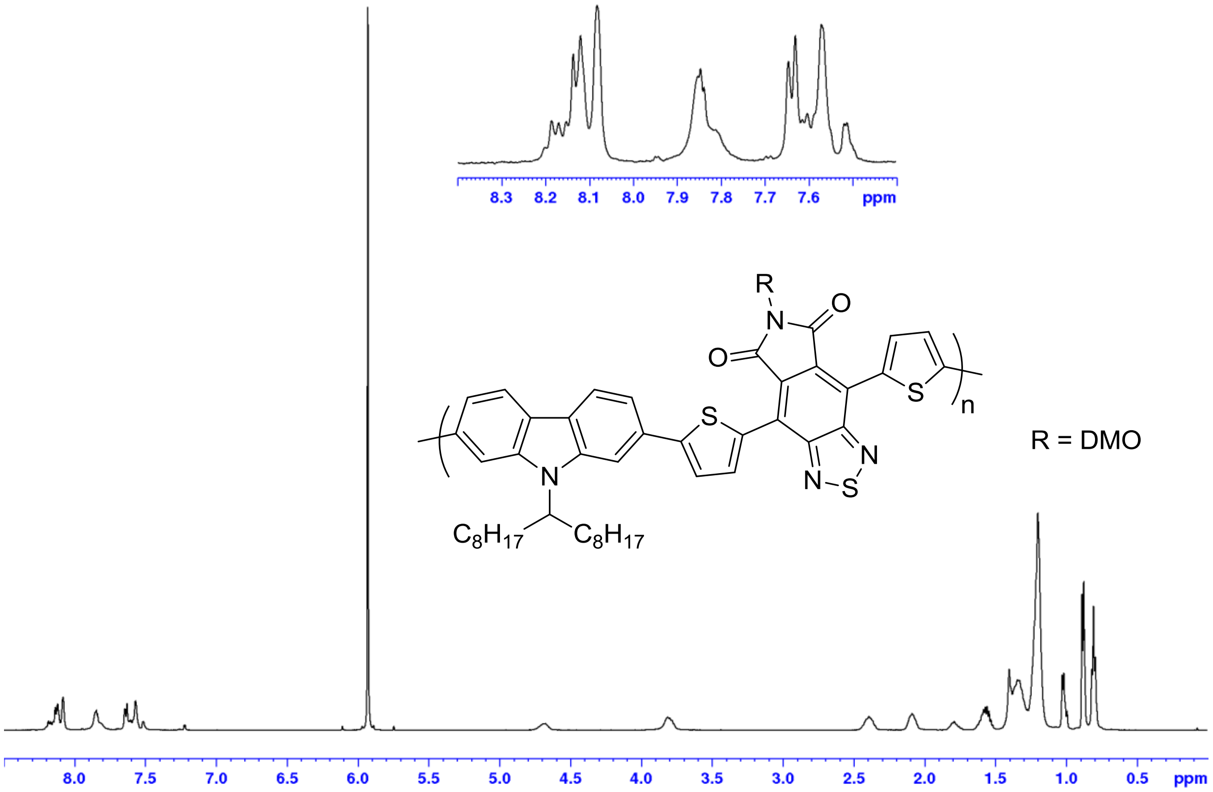

Figure 10.22: ^{1}H NMR spectrum of **104** in $C_2D_2Cl_4$ at 100 °C

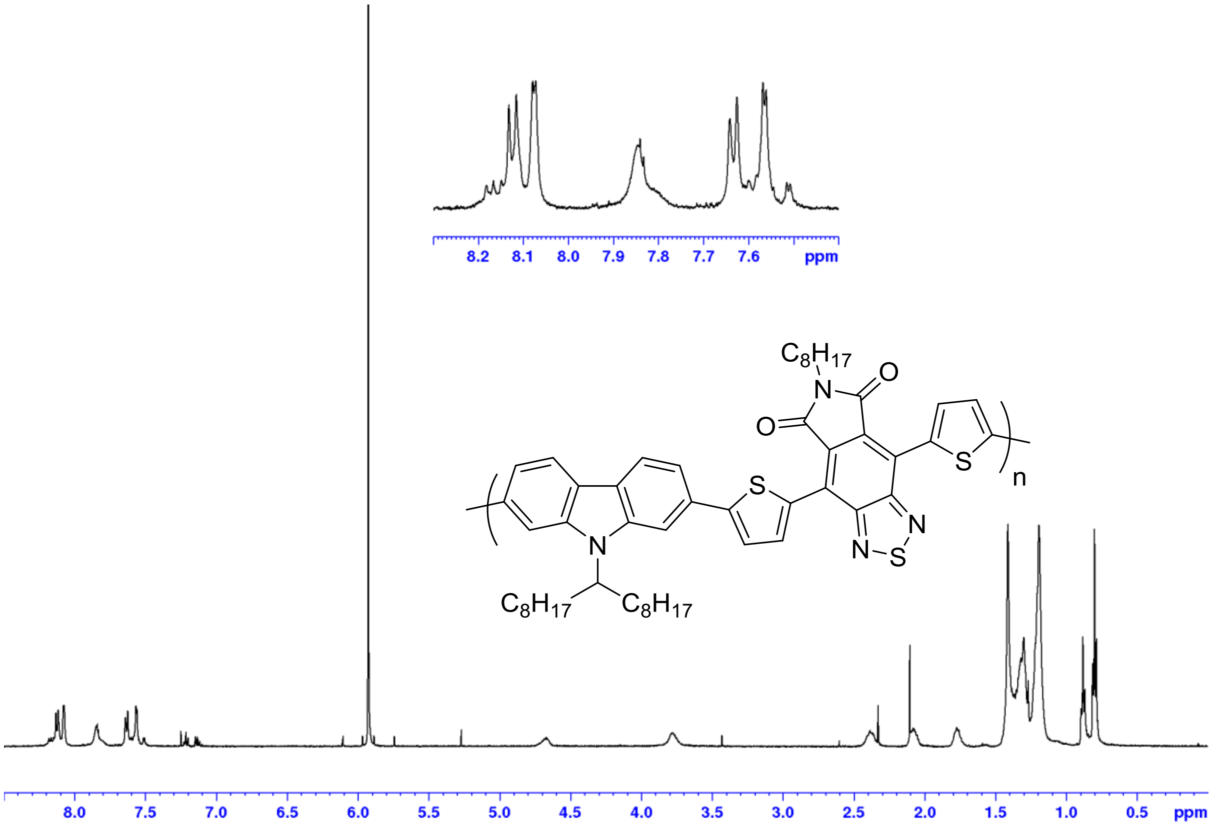

Figure 10.23: ^{1}H NMR spectrum of **105** in $C_2D_2Cl_4$ at 100 °C

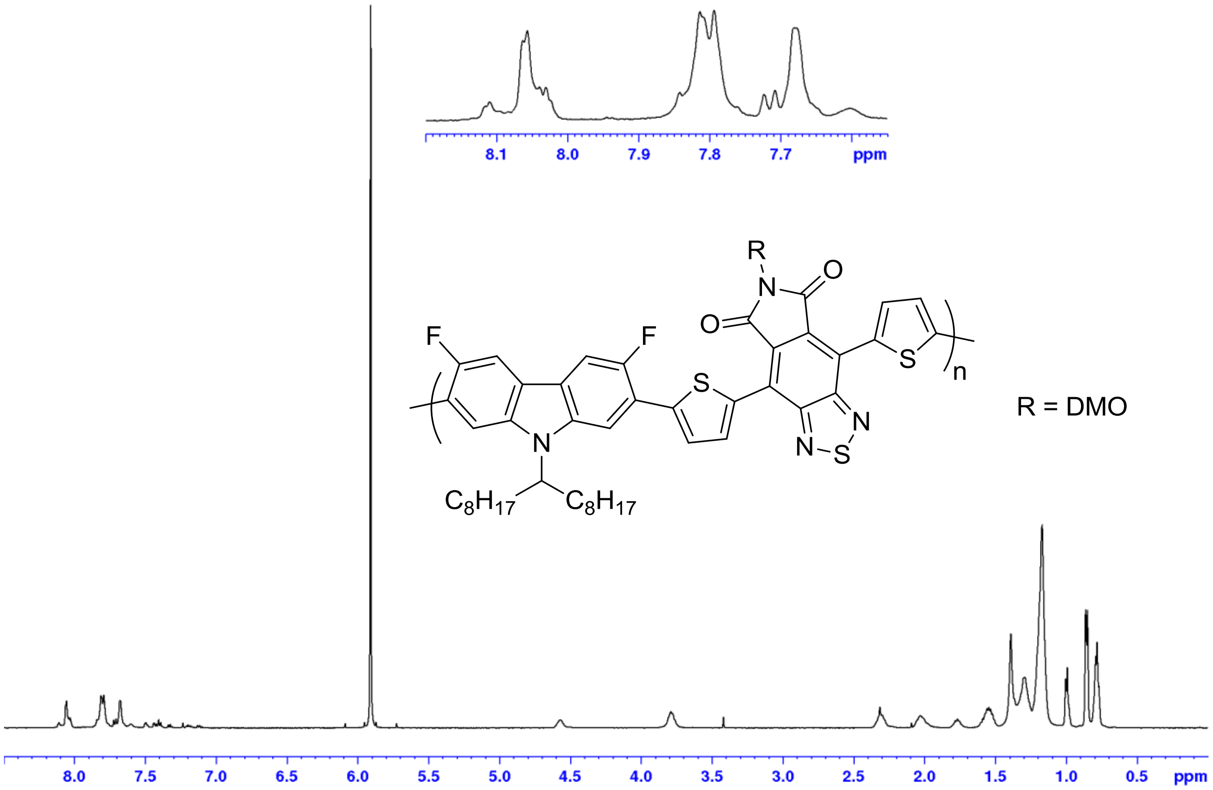

Figure 10.24: ^{1}H NMR spectrum of **106** in $C_2D_2Cl_4$ at 100 °C

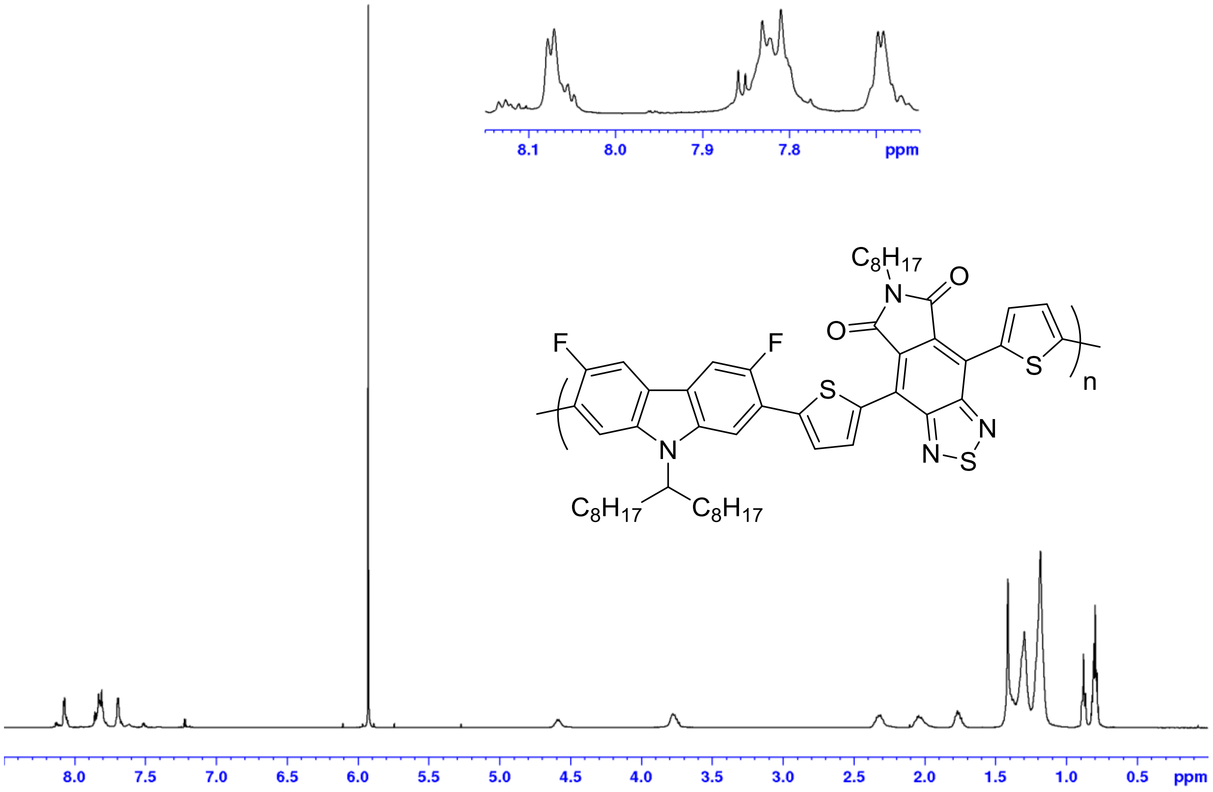

Figure 10.25: ^{1}H NMR spectrum of **107** in $C_2D_2Cl_4$ at 100 °C

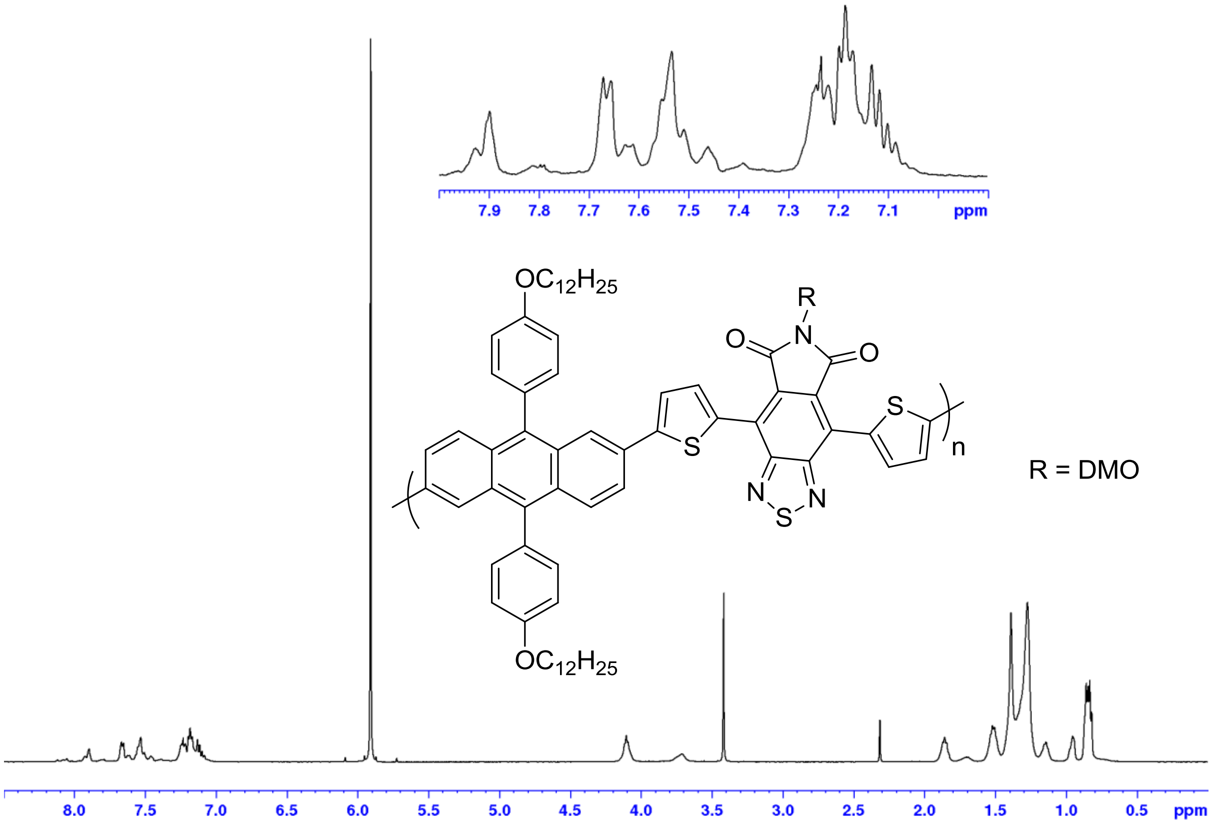

Figure 10.26: ^{1}H NMR spectrum of **109** in $C_2D_2Cl_4$ at 100 °C

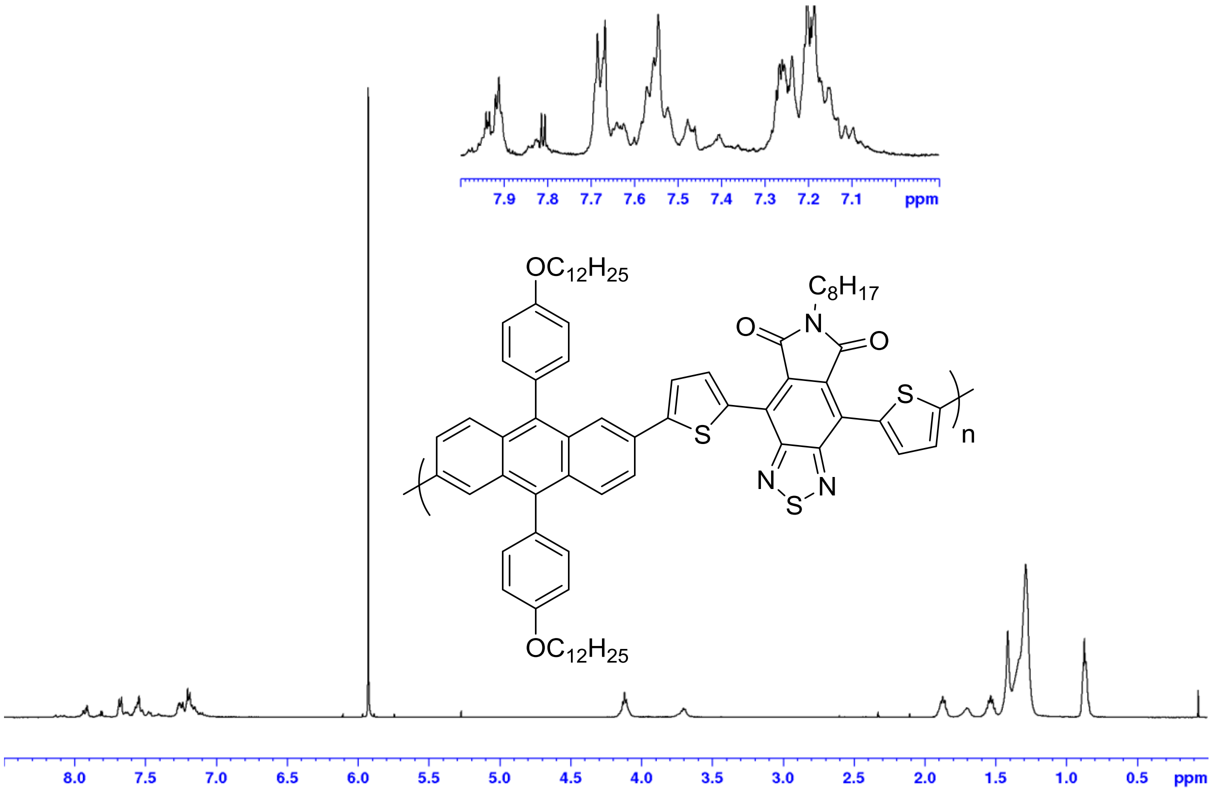

Figure 10.27: ^{1}H NMR spectrum of **110** in $C_2D_2Cl_4$ at 100 °C

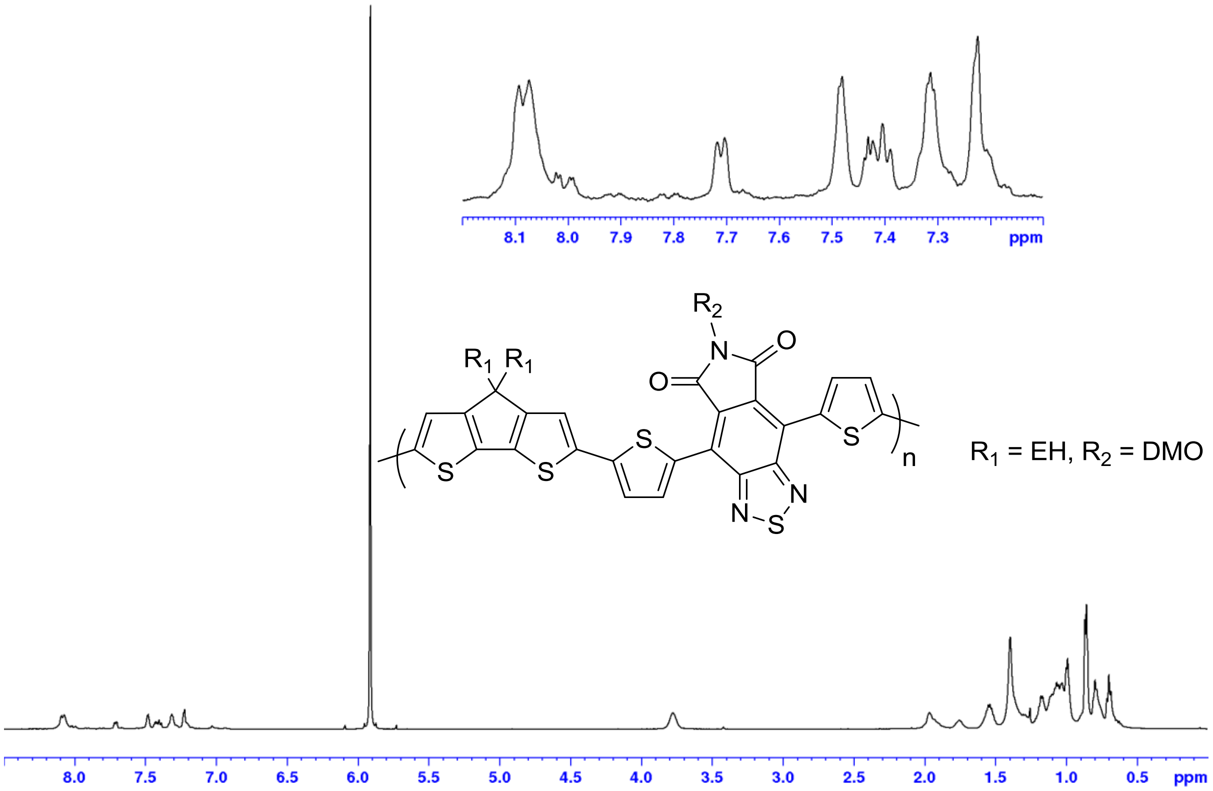

Figure 10.28: ^{1}H NMR spectrum of **134** in $C_2D_2Cl_4$ at 100 °C

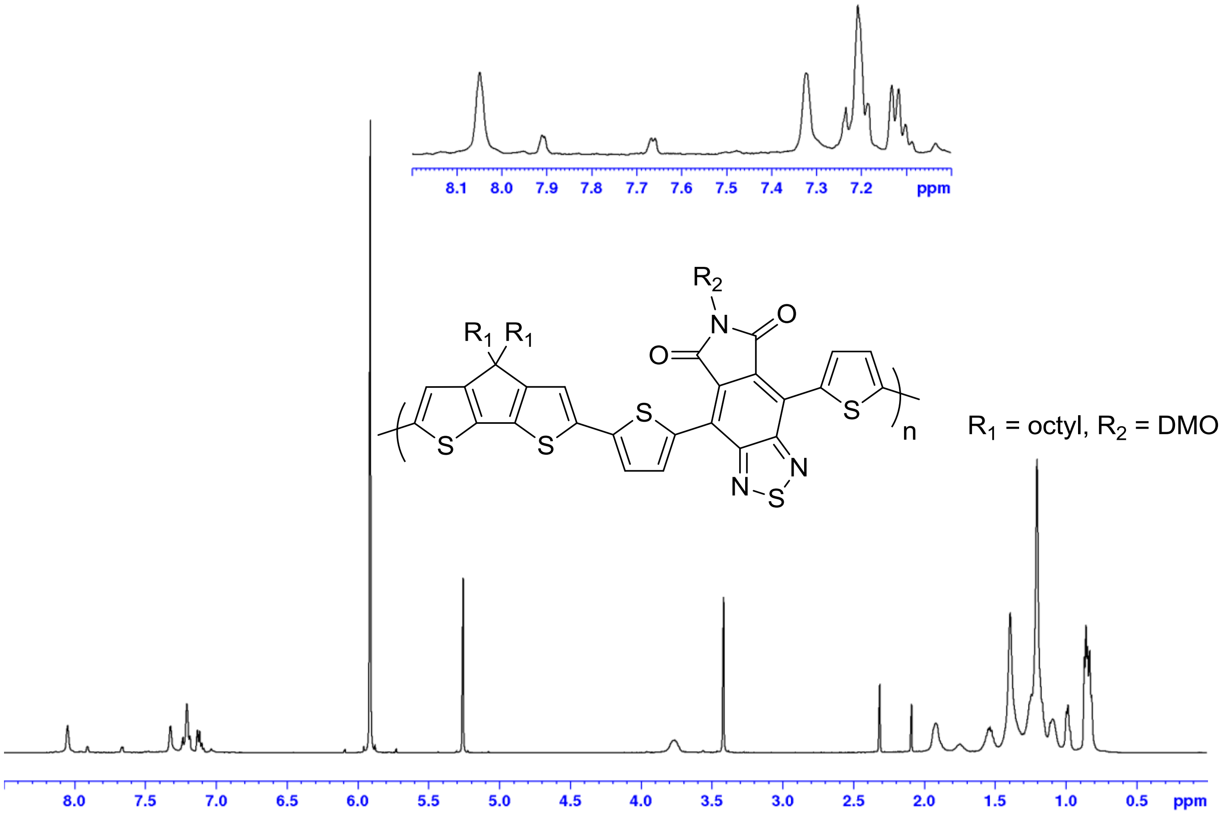

Figure 10.29: ^{1}H NMR spectrum of **135** in $C_2D_2Cl_4$ at 100 °C

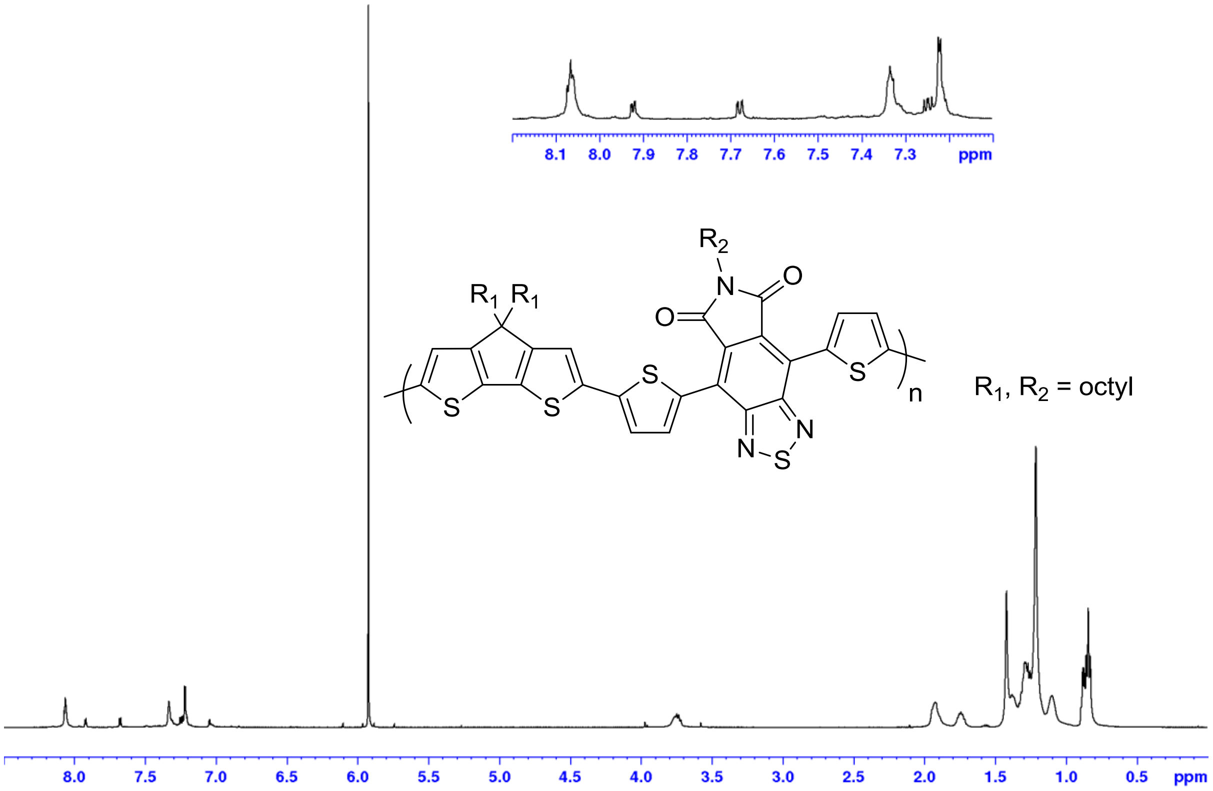

Figure 10.30: ^{1}H NMR spectrum of **136** in $C_2D_2Cl_4$ at 100 °C

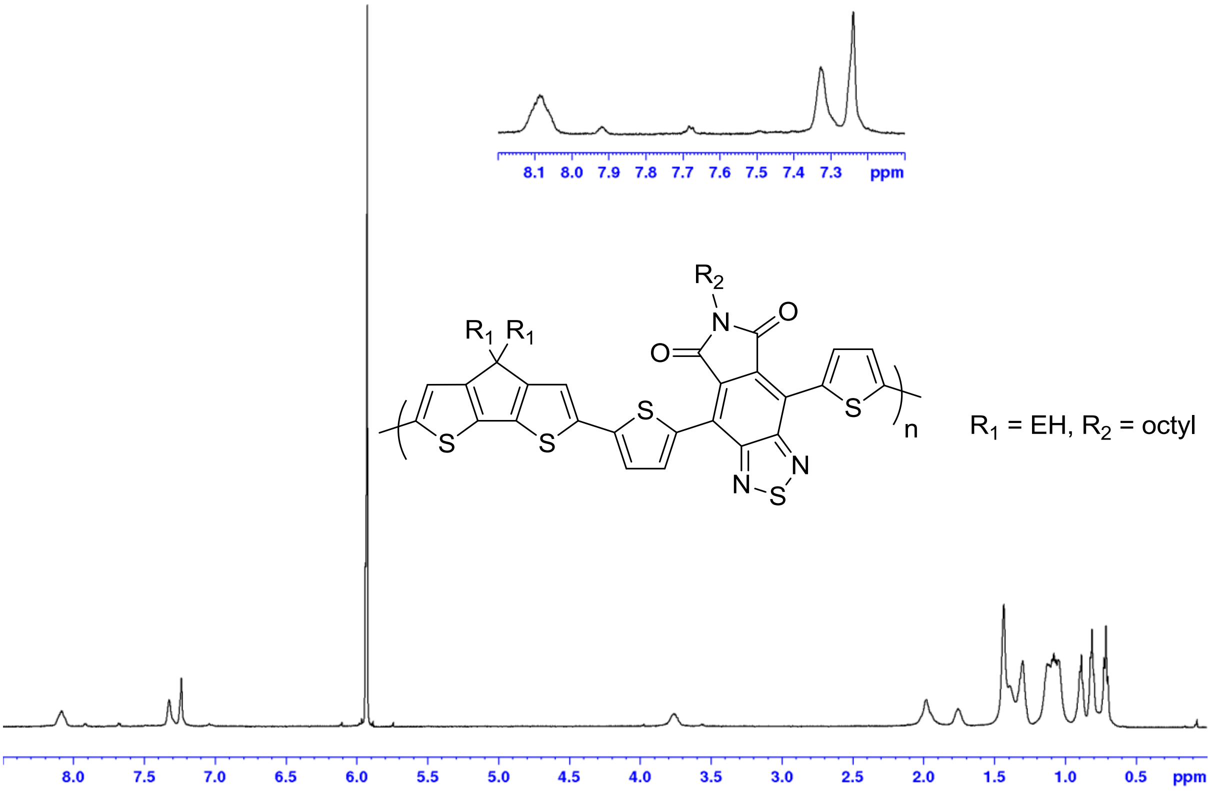

Figure 10.31: ^{1}H NMR spectrum of **137** in $C_2D_2Cl_4$ at 100 °C

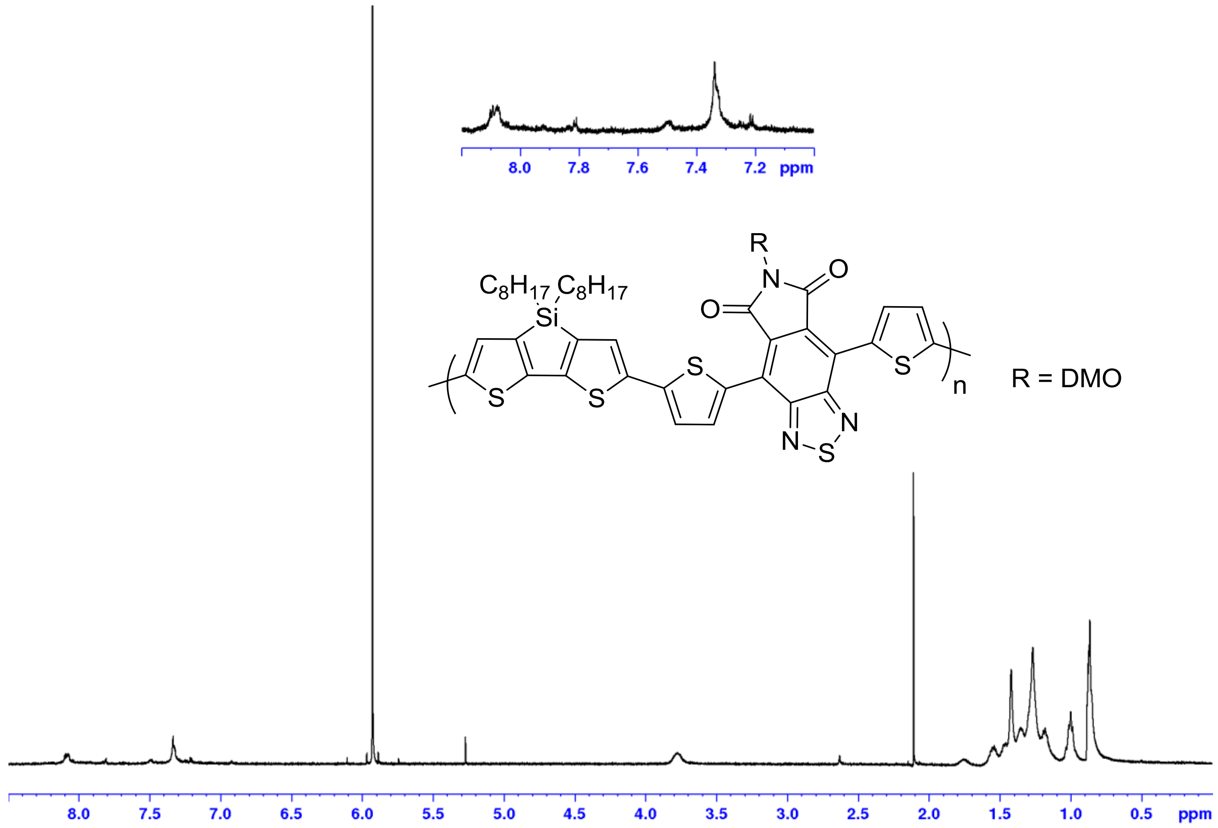

Figure 10.32: ^{1}H NMR spectrum of **144** in $C_2D_2Cl_4$ at 100 °C

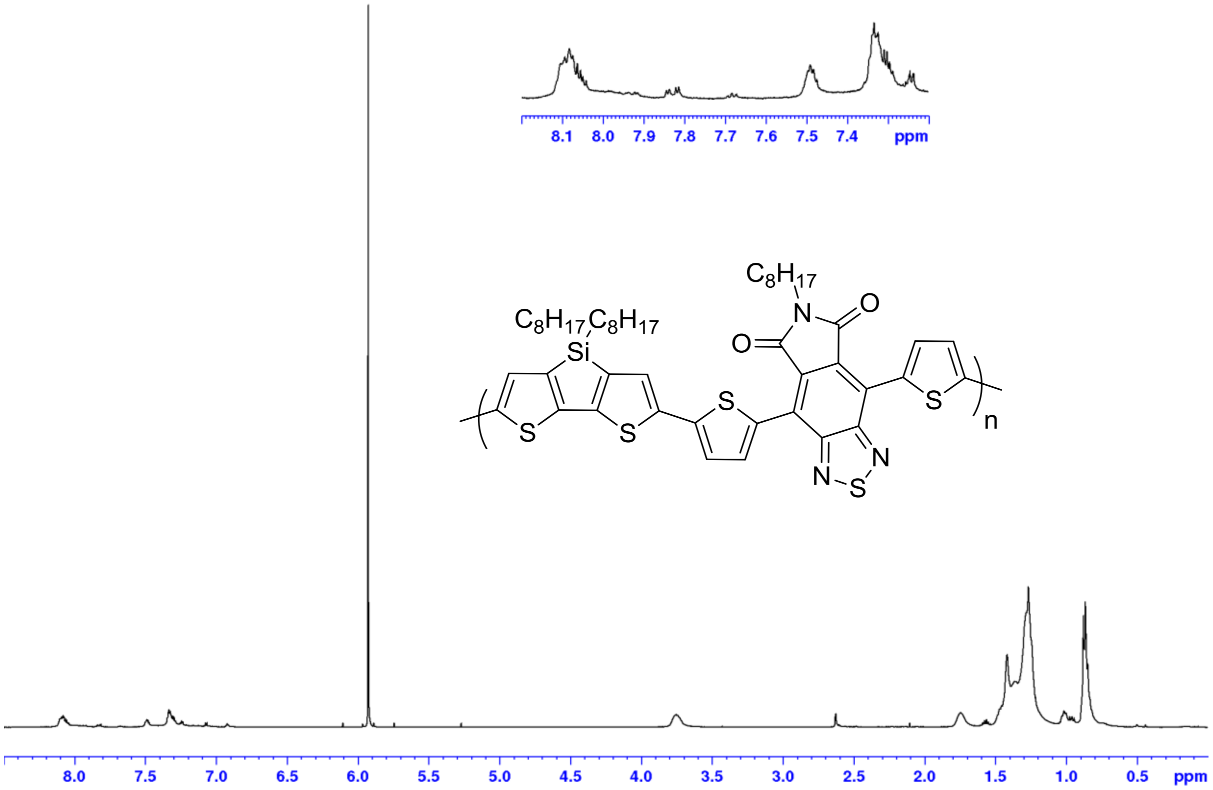

Figure 10.33: ^{1}H NMR spectrum of **145** in $C_2D_2Cl_4$ at 100 °C